A GOLDEN AGE FOR STRONTIUM ISOTOPE RESEARCH? CURRENT ADVANCES IN PALEOECOLOGICAL AND ARCHAEOLOGICAL RESEARCH

EDITED BY: Brooke Crowley, Clement Pierre Bataille, Kate Britton, Joshua H. Miller and Matthew Wooller

PUBLISHED IN: Frontiers in Ecology and Evolution

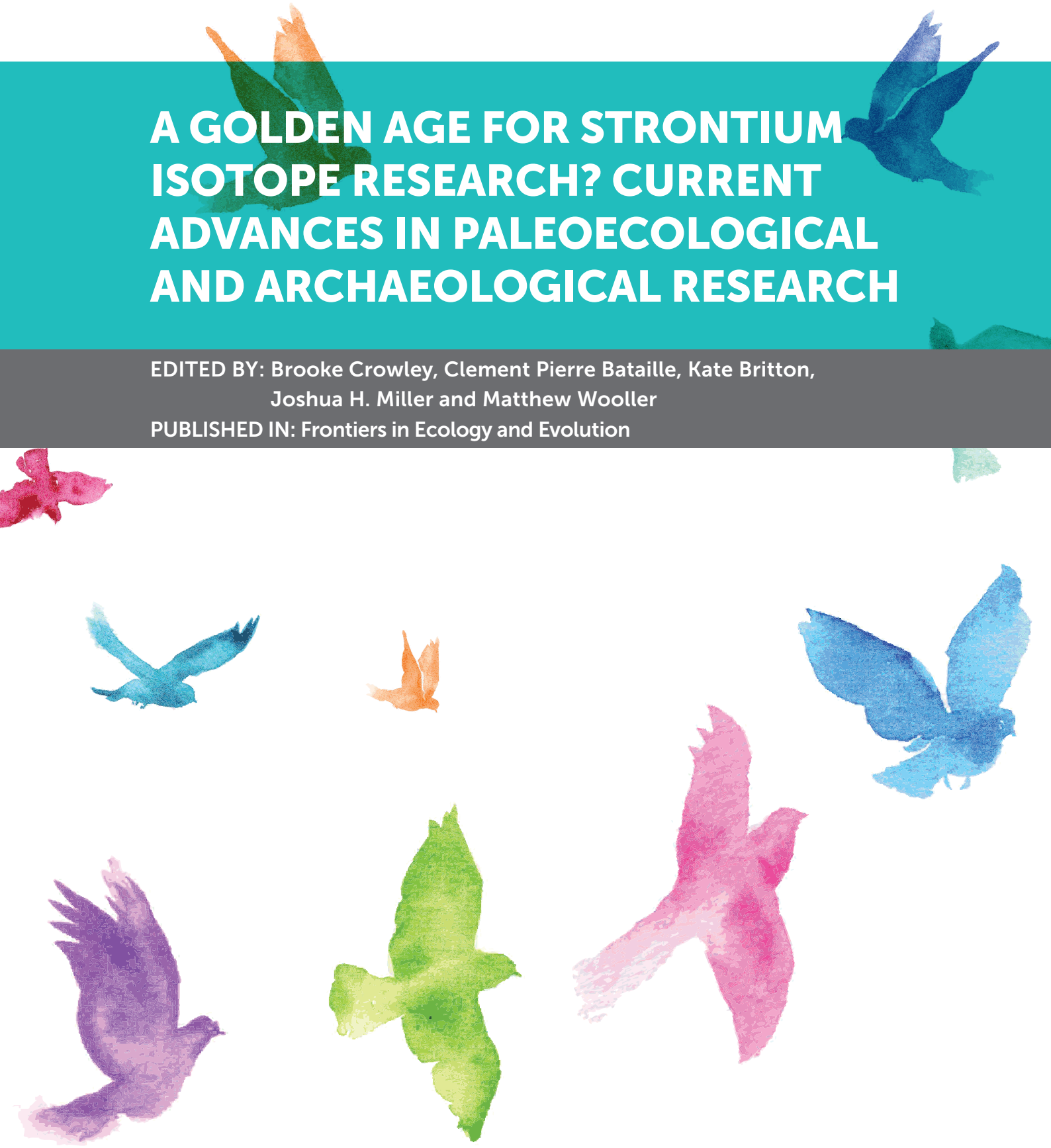

frontiers Research Topics

ISSN 1664-8714
ISBN 978-2-88974-441-1
DOI 10.3389/978-2-88974-441-1

About Frontiers

Frontiers is more than just an open-access publisher of scholarly articles: it is a pioneering approach to the world of academia, radically improving the way scholarly research is managed. The grand vision of Frontiers is a world where all people have an equal opportunity to seek, share and generate knowledge. Frontiers provides immediate and permanent online open access to all its publications, but this alone is not enough to realize our grand goals.

Frontiers Journal Series

The Frontiers Journal Series is a multi-tier and interdisciplinary set of open-access, online journals, promising a paradigm shift from the current review, selection and dissemination processes in academic publishing. All Frontiers journals are driven by researchers for researchers; therefore, they constitute a service to the scholarly community. At the same time, the Frontiers Journal Series operates on a revolutionary invention, the tiered publishing system, initially addressing specific communities of scholars, and gradually climbing up to broader public understanding, thus serving the interests of the lay society, too.

Dedication to Quality

Each Frontiers article is a landmark of the highest quality, thanks to genuinely collaborative interactions between authors and review editors, who include some of the world's best academicians. Research must be certified by peers before entering a stream of knowledge that may eventually reach the public - and shape society; therefore, Frontiers only applies the most rigorous and unbiased reviews.
Frontiers revolutionizes research publishing by freely delivering the most outstanding research, evaluated with no bias from both the academic and social point of view. By applying the most advanced information technologies, Frontiers is catapulting scholarly publishing into a new generation.

What are Frontiers Research Topics?

Frontiers Research Topics are very popular trademarks of the Frontiers Journals Series: they are collections of at least ten articles, all centered on a particular subject. With their unique mix of varied contributions from Original Research to Review Articles, Frontiers Research Topics unify the most influential researchers, the latest key findings and historical advances in a hot research area! Find out more on how to host your own Frontiers Research Topic or contribute to one as an author by contacting the Frontiers Editorial Office: frontiersin.org/about/contact

A GOLDEN AGE FOR STRONTIUM ISOTOPE RESEARCH? CURRENT ADVANCES IN PALEOECOLOGICAL AND ARCHAEOLOGICAL RESEARCH

Topic Editors:
Brooke Crowley, University of Cincinnati, United States
Clement Pierre Bataille, University of Ottawa, Canada
Kate Britton, University of Aberdeen, United Kingdom
Joshua H. Miller, University of Cincinnati, United States
Matthew Wooller, University of Alaska Fairbanks, United States

Citation: Crowley, B., Bataille, C. P., Britton, K., Miller, J. H., Wooller, M., eds. (2022). A Golden Age for Strontium Isotope Research? Current Advances in Paleoecological and Archaeological Research. Lausanne: Frontiers Media SA. doi: 10.3389/978-2-88974-441-1

Table of Contents

frontiers in Ecology and Evolution

EDITORIAL
published: 13 January 2022
doi: 10.3389/fevo.2021.820295

Editorial: A Golden Age for Strontium Isotope Research? Current Advances in Paleoecological and Archaeological Research

Kate Britton[1,2]*, *Brooke E. Crowley*[3,4], *Clément P. Bataille*[5,6], *Joshua H. Miller*[3] and *Matthew J. Wooller*[7,8]

[1] Department of Archaeology, University of Aberdeen, Aberdeen, United Kingdom, [2] Department of Human Evolution, Max-Planck-Institute for Evolutionary Anthropology, Leipzig, Germany, [3] Department of Geology, University of Cincinnati, Cincinnati, OH, United States, [4] Department of Anthropology, University of Cincinnati, Cincinnati, OH, United States, [5] Department of Earth and Environmental Sciences, University of Ottawa, Ottawa, ON, Canada, [6] Department of Biology, University of Ottawa, Ottawa, ON, Canada, [7] Alaska Stable Isotope Facility, University of Alaska Fairbanks, Fairbanks, AK, United States, [8] Department of Marine Biology, University of Alaska Fairbanks, Fairbanks, AK, United States

Keywords: mobility, provenance, migrations, landscape use, $^{87}Sr/^{86}Sr$

Editorial on the Research Topic

A Golden Age for Strontium Isotope Research? Current Advances in Paleoecological and Archaeological Research

Building from a session we chaired at the 2019 International Union for Quaternary Research Congress in Dublin, this Research Topic explores advances and new applications in strontium isotope research across paleoecology, archaeology, and allied fields. These contributions encompass the range of current research, the latest developments, and future potentials of this rapidly advancing research area. With authors from the fields of archaeology, anthropology, geology, geochemistry, and ecology, the multi-disciplinary relevance of modern strontium isotope analyses of biological materials is clear. The scope of the papers is also vast, with international research teams presenting work from Madagascar, the USA, Canada, the Peruvian and Southern Andes, China, the Levant, Western Europe and Scandinavia, and a temporal range spanning from the Neolithic up to the present.

Papers by Weber et al. and Snoeck et al. present novel experimental studies *sensu stricto*: A controlled feeding study using rodents, and the evaluation of artificially-treated wood samples, respectively. In their study, Weber et al. found differences in the time it took for cohorts of rats to reach tissue equilibrium after a dietary switch, as well as time-lags along the growth axis of their teeth. They also found inter-specific differences in equilibration time when individuals were fed new diets. There was a measurable influence of both drinking water and kaolin dust on rodent enamel, shifting enamel strontium isotope ratios ($^{87}Sr/^{86}Sr$) toward these additive sources. These authors go on to speculate that some diet-tissue $^{87}Sr/^{86}Sr$ differences may reflect bioavailable components of diet differing from bulk $^{87}Sr/^{86}Sr$—an idea supported by subsequent acid leaching tests on food samples designed to mimic the rodents' digestive tracts. These findings contribute significantly to our understanding of bioavailable $^{87}Sr/^{86}Sr$ assimilation and complement the few previous controlled feeding studies (e.g., Lewis et al., 2017; Anders et al., 2019).

Despite a small number of successful applications (e.g., English et al., 2001; Rich et al., 2016; Hajj et al., 2017), strontium-based wood provenance research in archaeology remains controversial. Archaeological wood is often either waterlogged or has been treated in some way, and the impact

OPEN ACCESS

Edited and reviewed by:
Franco Biondi,
University of Nevada, United States

***Correspondence:**
Kate Britton
k.britton@abdn.ac.uk

Specialty section:
This article was submitted to Paleoecology, a section of the journal Frontiers in Ecology and Evolution

Received: *22 November 2021*
Accepted: *21 December 2021*
Published: *13 January 2022*

Citation:
Britton K, Crowley BE, Bataille CP, Miller JH and Wooller MJ (2022) Editorial: A Golden Age for Strontium Isotope Research? Current Advances in Paleoecological and Archaeological Research. Front. Ecol. Evol. 9:820295. doi: 10.3389/fevo.2021.820295

of these processes on $^{87}Sr/^{86}Sr$ has not been well-characterised. In their experimental study, Snoeck et al. artificially waterlogged wood in salt-water, or treated them with pitch, and found that these both altered wood $^{87}Sr/^{86}Sr$. The authors then explored the efficacy of various pre-treatments for removing this exogenous strontium, concluding that waterlogged samples may be unsuitable for $^{87}Sr/^{86}Sr$ analyses with any of the current pre-treatment protocols. Conversely, for pitch-treated samples, organic solvents proved effective in removing contaminants, but that aqueous-based acid-base-acid pre-treatment removed significant amounts of endogenous strontium as well. These findings underpin the need for continued caution in the use of $^{87}Sr/^{86}Sr$ in wood provenance studies, particularly in the case of waterlogged wood.

Hu et al. provide a useful field experimental dataset from the multi-isotope, intra-strand analysis of human hair from an individual with known (and considerable) movement history. They measured and compared carbon, hydrogen, and strontium isotopes with expected isotope profiles using the individual's travel history and existing databases of isotope values in human hair. They demonstrate that hydrogen and, to a lesser extent, carbon isotopes faithfully record expectations when the individual travelled to isotopically-distinct regions and for periods longer than a couple of weeks. Unfortunately, they also demonstrate that the $^{87}Sr/^{86}Sr$ profile for this individual's hair does not record travel history. Instead, it displays a constant ratio similar to the $^{87}Sr/^{86}Sr$ of the last location of residence. This finding corroborates previous laboratory experiments (e.g., Tipple et al., 2013; Hu et al., 2020) showing that strontium exchanges rapidly with water when wetted. This study underlines that more work is required to understand how strontium integrates in organic tissues, particularly those for which it is not a structural component and is only present in trace amounts (e.g., keratin, cellulose). In these tissues, contamination from exogenous sources can rapidly modify $^{87}Sr/^{86}Sr$ and complicate interpretations.

Many papers in this Research Topic revolve around the central issue of how we use underlying $^{87}Sr/^{86}Sr$ variability within landscapes to interpret mobility in the past, reflecting a current preoccupation of the field. In their contributions, both Andreasen and Thomsen and Thomsen et al. explored how anthropogenic activities can modify bioavailable $^{87}Sr/^{86}Sr$. Specifically, they investigated how widespread farming and agricultural liming can impact local bioavailable $^{87}Sr/^{86}Sr$, which in turn affects our ability to use modern isotope baselines in assessments of past human mobility. To assess the impacts of agricultural liming, Andreasen and Thomsen took advantage of a site in Denmark that was previously subjected to large additions of lime. Five years after liming, the authors analysed soil geochemistry to quantify the modification of strontium concentration and strontium mobility within the profile. They determined that strontium is highly mobile and estimate that after only 5 years, the majority of strontium added by the liming experiment had escaped the shallow soil profiles, likely flowing into the underlying groundwater. They further found that surface water at the experimental site has similar $^{87}Sr/^{86}Sr$ to agricultural lime (and lower than nearby surface waters). These findings suggest that agricultural liming has the potential to impact local strontium geochemistry, particularly in soils with naturally low strontium concentrations. They conclude that evaluating the $^{87}Sr/^{86}Sr$ of archaeological specimens using isoscapes (maps of environmental $^{87}Sr/^{86}Sr$) that incorporate agriculturally "contaminated" data will likely lead to overestimating the mobility of past human populations. However, in a commentary to this article, Frei (2021) caution that the mass balance calculations used by Andreasen and Thomsen do not account for the historical additions of strontium over the past century and that they subsequently overestimate the role of recent lime additions to the bioavailable $^{87}Sr/^{86}Sr$ pool.

Building on this theme, Thomsen et al. evaluated $^{87}Sr/^{86}Sr$ variability in Denmark both as a function of underlying Quaternary geology (different glacial tills) as well as agricultural activity. They show that the overall range of water $^{87}Sr/^{86}Sr$ in this region is higher than previous studies have suggested (e.g., Frei et al., 2019), and also that it varies across small geographical areas and geological boundaries. They also show that, within a region, surface waters from areas influenced by agricultural lime have lower $^{87}Sr/^{86}Sr$ than those from neighbouring areas without agricultural influence. In light of these findings, the authors re-evaluate multiple Bronze and Viking age archaeological burials whose $^{87}Sr/^{86}Sr$ had been previously shown to be too high to be locally sourced. The authors conclude that, in light of their new data, the $^{87}Sr/^{86}Sr$ for many of these individuals and textiles is actually consistent with naturally occurring bioavailable $^{87}Sr/^{86}Sr$ within Denmark.

Other papers in this Research Topic address the different factors that influence bioavailability within landscapes and, ultimately, how these can shape and influence how we build isoscapes. This includes the generation of new and refined isoscapes from parts of South America and Europe. Barberena et al. and Scaffidi et al. both developed new isoscapes for different regions of South America—a continent apt for $^{87}Sr/^{86}Sr$-based geolocation studies given both its geological diversity and importance from an archaeological standpoint. Barberena et al. apply an existing mapping framework (Bataille et al., 2018, 2020) and combine machine learning and remote sensing data to generate bioavailable $^{87}Sr/^{86}Sr$ isoscapes for paleo-applications in the Southern Andes. The authors amassed a dataset of $^{87}Sr/^{86}Sr$ in plants and soils to calibrate a regional bioavailable $^{87}Sr/^{86}Sr$ isoscape. They used the calibrated isoscape for a preliminary archaeological study on human remains, where they argue for a pulse of migration in AD 1280–1420. This study emphasises the need to generate large bioavailable datasets for calibrating high-resolution regional bioavailable $^{87}Sr/^{86}Sr$ isoscapes.

Taking a different mapping approach, Scaffidi et al. used a large dataset of $^{87}Sr/^{86}Sr$ in water to calibrate a regional isoscape in South America. The use of water as a mapping substrate rather than plants or soils brings up some interesting questions that are also discussed in Frei (2021). While drinking water is not a dominant strontium source for osseous tissues in human (or other animals), water integrates strontium sources at a larger scale than soils and plants. As such, the authors speculate whether water might better represent the bioavailable $^{87}Sr/^{86}Sr$ that is available to humans because humans often consume food

from regional sources. Using a kriging approach, Scaffidi et al. produce a robust map of $^{87}Sr/^{86}Sr$ in rivers and reiterate that the question of bioavailable substrate choice for archaeological study remains debated.

The study by Britton, et al. also focuses on isoscape reconstruction and the selection of substrate choice using an approach that compares $^{87}Sr/^{86}Sr$ signatures from soils, different plant types, and land snails in order to assess how much variation in estimations of environmental $^{87}Sr/^{86}Sr$ is introduced by the different materials researchers select. The study targets a region of south-west France and includes biological samples collected across 17 sampling locations spanning six lithological units. While the authors found a broad correspondence of plant and snail $^{87}Sr/^{86}Sr$ with lithological unit and previously-published soil $^{87}Sr/^{86}Sr$ data (Willmes et al., 2014, 2018), there is a closer relationship between plant and soil $^{87}Sr/^{86}Sr$ than between snails and soils. However, plants growing on heterogeneous substrates (e.g., granite) also had more variable $^{87}Sr/^{86}Sr$ than those on more homogeneous lithologies (e.g., limestone) echoing the findings of other $^{87}Sr/^{86}Sr$ bioavailability studies (e.g., Sillen et al., 1998; Hartman and Richards, 2014; Willmes et al., 2018; Aguzzoni et al., 2019). An influence of proximity to water on bioavailable $^{87}Sr/^{86}Sr$ was also determined, likely reflecting the origin of rivers on bedrocks with elevated $^{87}Sr/^{86}Sr$. These results highlight the importance of analysing biological samples to complement, inform and refine strontium isoscape models, and the authors outline practical recommendations for environmental sampling. The authors also discuss the potential for $^{87}Sr/^{86}Sr$ differences among plants with different rooting depths to be passed on to different herbivore guilds (e.g., grazers, browsers, and frugivores), emphasising the need for ongoing research into dietary selection and physiology on the $^{87}Sr/^{86}Sr$ of mineralized mammalian tissues.

Four papers in this Research Topic are dedicated to case studies, both archaeological (Tütken et al.; Wang et al.) and (paleo-)ecological (Crowley and Godfrey; Miller et al.). Tütken et al. used strontium and oxygen isotopes to identify the origin of marine fish teeth (sharks and seabream) from Iron Age deposits from the City of David in the Southern Levant. The authors generated novel baseline data for modern marine and freshwater fish from Egypt and Israel and compared these data to their archaeological samples. Isotope data for seabream were similar to the modern marine fish, indicating they may have originated from the Mediterranean Sea or the hypersaline Bardawil Lagoon, Egypt. However, isotope data for the shark teeth did not match the modern reference dataset and were more compatible with seawater during the Late Cretaceous. Additional analyses confirm a fossil origin, and several of the identifiable teeth belong to Cretaceous taxa. The authors propose that these teeth were brought to the city as a cultural commodity. This study is particularly significant because it demonstrates how dual isotope analysis can not only trace the geographical origins of animal foods exploited in the past but also distinguish contemporary and fossil specimens—making this distinction is critical for understanding human behaviour in the past.

In their archaeological study, Wang et al. re-analysed previously published tooth enamel $^{87}Sr/^{86}Sr$ for domestic fauna, including pigs, cows, sheep/goats, horses, and dogs from a range of Neolithic and Western Zhou Dynasty sites in China and used Bayesian methods to build an isoscape to explore differences in the movement of domestic fauna and/or their primary products among sites and through time. The authors determined a large diversity of origins for animals (particularly sheep and cattle) from the Late Neolithic onwards, and argue that these data demonstrate that wider circulation networks (evidenced by greater diversity in faunal strontium isotope ratios) replaced more local economies during this period. This study highlights both the potential for strontium isotope approaches to reveal social and economic changes through time, and the power of bringing together larger datasets from multiple sources.

In an ecological application, Crowley and Godfrey determined variability in $^{87}Sr/^{86}Sr$ for co-occurring extant and extinct lemur genera in Madagascar to test the hypothesis that extinct, large-bodied lemurs were relatively sedentary and had small home ranges similar to smaller-bodied still-extant lemurs. Low $^{87}Sr/^{86}Sr$ variability for all genera supports low mobility for extinct lemurs. The authors conclude that low metabolisms and activity levels appear to be shared traits within Lemuriformes that may have evolved in response to the harsh environments that characterise Madagascar. This paper highlights the interactions between paleobiology, strontium isotope geochemistry, and modern conservation ecology.

Miller et al. take advantage of the ecological and taphonomic opportunities of antler accumulations (Miller, 2012; Miller et al., 2013) in their historical ecology case study. Using antler $^{87}Sr/^{86}Sr$, they reconstruct historical migrations for two herds of North American caribou, the Central Arctic and Porcupine Caribou Herds, which currently calve on the Coastal Plain of the Arctic National Wildlife Refuge, Alaska (USA). The authors evaluated patterns of summer landscape use for both herds and found that while the Porcupine Herd show continuity in patterns of summer landscape use, the Central Arctic Herd indicate a shift in summer range after the late 1970s. This study highlights the detailed historical ecological data available from skeletal accumulations and the value of integrating historical perspectives into our evaluations of how animal populations are responding to modern environmental, climatic, and anthropogenic perturbations.

Finally, this Research Topic includes two perspective pieces on the past development and future directions of the field by Sillen and Britton et al. Sillen, a pioneer in the field, reviews the advent of $^{87}Sr/^{86}Sr$ analysis, both in terms of initial research into radioactive isotopes in the food chain in the 1960s, and the unintended consequence, the initial applications to ancient human and faunal remains. He also evaluates the current field and encourages the continued and ongoing development of the techniques themselves, arguing that fundamental studies, such as controlled feeding experiments, tissue formation and diagenesis research, modelling, and ecosystem mapping necessitate thoughtful funders as well as interdisciplinary teams. Britton et al. also reflect on the value of controlled feeding

experiments and appraise important recent developments in computational modelling and isoscape mapping in the field. They too emphasise the strengths of cross-disciplinarity and multi-proxy approaches, calling for both theoretical as well as methodological innovation in the field. As highlighted by many of the papers in this Research Topic, these calls are beginning to be answered—we are truly now entering a golden age for strontium isotope research.

AUTHOR CONTRIBUTIONS

KB and BC planned out the editorial. KB wrote the initial draft with input from BC. All authors made written contributions, comments, and edits.

FUNDING

KB thanks the Leverhulme Trust for support during the production of this editorial (PLP-2019-284).

ACKNOWLEDGMENTS

We thank everyone who contributed to this Research Topic. MW would like to acknowledge that, at Fairbanks, he is working on the ancestral land of Troth Yeddha', home of the Lower Tanana people. He would also like to acknowledge that the lands on which he does his work are the ancestral lands of the Dené people who stewarded those lands for thousands of years and continue to steward those lands, further he would like to thank them and respects their enduring relationship to their homelands.

REFERENCES

Aguzzoni, A., Bassi, M., Robatscher, P., Scandellari, F., Tirler, W., and Tagliavini, M. (2019). Intra- and intertree variability of the 87Sr/86Sr ratio in apple orchards and its correlation with the soil 87Sr/86Sr ratio. *J. Agric. Food Chem.* 67, 5728–5735. doi: 10.1021/acs.jafc.9b01082

Anders, D., Osmanovic, A., and Vohberger, M. (2019). Intra- and inter-individual variability of stable strontium isotope ratios in hard and soft body tissues of pigs. *Rap. Commun. Mass Spectromet.* 33, 281–290. doi: 10.1002/rcm.8350

Bataille, C. P., Crowley, B. E., Wooller, M. J., and Bowen, G. J. (2020). Advances in global bioavailable strontium isoscapes. *Palaeogeogr. Palaeoclimatol. Palaeoecol.* 555:109849. doi: 10.1016/j.palaeo.2020.109849

Bataille, C. P., von Holstein, I. C. C., Laffoon, J. E., Willmes, M., Liu, X.-M., and Davies, G. R. (2018). A bioavailable strontium isoscape for Western Europe: a machine learning approach. *PLOS ONE* 13:e0197386. doi: 10.1371/journal.pone.0197386

English, N. B., Betancourt, J. L., Dean, J. S., and Quade, J. (2001). Strontium isotopes reveal distant sources of architectural timber in Chaco Canyon, New Mexico. *Proc. Natl. Acad. Sci. U.S.A.* 98, 11891–11896. doi: 10.1073/pnas.211305498

Frei, K. M., Bergerbrant, S., Sjögren, K.-G., Jørkov, M. L., Lynnerup, N., Harvig, L., et al. (2019). Mapping human mobility during the third and second millennia BC in present-day Denmark. *PLOS ONE* 14:e0219850. doi: 10.1371/journal.pone.0219850

Frei, R. (2021). Commentary: strontium is released rapidly from agricultural lime–implications for provenance and migration studies. *Front. Ecol. Evol.* 9:681896. doi: 10.3389/fevo.2021.681896

Hajj, F., Poszwa, A., Bouchez, J., and Guérold, F. (2017). Radiogenic and "stable" strontium isotopes in provenance studies: a review and first results on archaeological wood from shipwrecks. *J. Archaeol. Sci.* 86, 24–49. doi: 10.1016/j.jas.2017.09.005

Hartman, G., and Richards, M. (2014). Mapping and defining sources of variability in bioavailable strontium isotope ratios in the Eastern Mediterranean. *Geochim. Cosmochim. Acta* 126, 250–264. doi: 10.1016/j.gca.2013.11.015

Hu, L., Fernandez, D. P., Cerling, T. E., and Tipple, B. J. (2020). Fast exchange of strontium between hair and ambient water: implication for isotopic analysis in provenance and forensic studies. *PLoS ONE* 15:e0233712. doi: 10.1371/journal.pone.0233712

Lewis, J., Pike, A. W. G., Coath, C. D., and Evershed, R. P. (2017). Strontium concentration, radiogenic (87Sr/86Sr) and stable (δ88Sr) strontium isotope systematics in a controlled feeding study. *STAR Sci. Technol. Archaeol. Res.* 3, 45–57. doi: 10.1080/20548923.2017.1303124

Miller, J. H. (2012). Spatial fidelity of skeletal remains: elk wintering and calving grounds revealed by bones on the yellowstone landscape. *Ecology* 93, 2474–2482. doi: 10.1890/12-0272.1

Miller, J. H., Druckenmiller, P., and Bahn, V. (2013). Antlers on the Arctic Refuge: capturing multi-generational patterns of calving ground use from bones on the landscape. *Proc. R. Soc. B* 280:20130275. doi: 10.1098/rspb.2013.0275

Rich, S., Manning, S. W., Degryse, P., Vanhaecke, F., and Van Lerberghe, K. (2016). Provenancing East Mediterranean cedar wood with the 87 Sr/86 Sr strontium isotope ratio. *Archaeol. Anthropol. Sci.* 8, 467–476. doi: 10.1007/s12520-015-0242-7

Sillen, A., Hall, G., Richardson, S., and Armstrong, R. (1998). $^{87}Sr/^{86}Sr$ ratios in modern and fossil food-webs of the sterkfontein valley: implications for early hominid habitat preference. *Geochim. Cosmochim. Acta* 62, 2463–2478. doi: 10.1016/S0016-7037(98)00182-3

Tipple, B. J., Chau, T., Chesson, L. A., Fernandez, D. P., and Ehleringer, J. R. (2013). Isolation of strontium pools and isotope ratios in modern human hair. *Anal. Chim. Acta* 798, 64–73. doi: 10.1016/j.aca.2013.08.054

Willmes, M., Bataille, C. P., James, H. F., Moffat, I., McMorrow, L., Kinsley, L., et al. (2018). Mapping of bioavailable strontium isotope ratios in France for archaeological provenance studies. *Appl. Geochem.* 90, 75–86. doi: 10.1016/j.apgeochem.2017.12.025

Willmes, M., McMorrow, L., Kinsley, L., Armstrong, R., Aubert, M., Eggins, S., et al. (2014). The IRHUM (isotopic reconstruction of human migration) database - bioavailable strontium isotope ratios for geochemical fingerprinting in France. *Earth Syst. Sci. Data* 6, 117–122. doi: 10.5194/essd-6-117-2014

Conflict of Interest: The authors declare that the research was conducted in the absence of any commercial or financial relationships that could be construed as a potential conflict of interest.

Publisher's Note: All claims expressed in this article are solely those of the authors and do not necessarily represent those of their affiliated organizations, or those of the publisher, the editors and the reviewers. Any product that may be evaluated in this article, or claim that may be made by its manufacturer, is not guaranteed or endorsed by the publisher.

frontiers in Ecology and Evolution

ORIGINAL RESEARCH
published: 20 December 2019
doi: 10.3389/fevo.2019.00490

Strontium Isotopes Support Small Home Ranges for Extinct Lemurs

Brooke Erin Crowley[1,2]* *and Laurie Rohde Godfrey*[3]

[1] Department of Geology, University of Cincinnati, Cincinnati, OH, United States, [2] Department of Anthropology, University of Cincinnati, Cincinnati, OH, United States, [3] Department of Anthropology, University of Massachusetts, Amherst, MA, United States

Among mammals, including anthropoid primates, the primary factors that affect mobility are body size (larger-bodied species move more than smaller ones), diet (frugivores and trophic omnivores are more mobile than folivores), and habit (terrestrial taxa have larger home ranges than arboreal ones). If similar factors hold for Lemuriformes, we would expect large-bodied (particularly frugivorous) extinct lemurs to have been more mobile than smaller-bodied (particularly folivorous) extant species. Yet multiple lines of evidence (e.g., low Retzius Periodicities, small semicircular canal size, small relative brain size) suggest that extinct lemurs were relatively inactive. If so, they may have had relatively small home ranges, perhaps on par with smaller-bodied extant lemurs. We used strontium isotopes ($^{87}Sr/^{86}Sr$), which vary spatially primarily as a function of geology, to compare mobility for eight lemur genera: *Eulemur*, *Lemur*, *Lepilemur,* and *Propithecus* (extant), and *Archaeolemur*, *Megaladapis*, *Pachylemur,* and *Palaeopropithecus* (extinct). Subfossils came from two sites: Ankilitelo/Mikoboka, a series of sinkholes in a limestone plateau, and Ampasambazimba, a wetland underlain by a variety of igneous and metamorphic rocks. Within either site, we expected more mobile taxa to exhibit more variable $^{87}Sr/^{86}Sr$, reflecting larger movement across a diversity of geologies. We found no differences in median $^{87}Sr/^{86}Sr$ or variance between extinct and extant lemurs at either site (Wilcoxon and Bartlett $p > 0.05$ for all comparisons). There were apparent but insignificant differences among genera (Kruskal-Wallis and Bartlett $p > 0.05$). Isotopic variability was greater at Ampasambazimba than at Ankilitelo/Mikoboka, reflecting differences in the underlying geology. One *Palaeopropithecus* from Ankilitelo/Mikoboka and one *Eulemur* from Ampasambazimba had unusually elevated $^{87}Sr/^{86}Sr$. Both of these individuals could have been deposited at their respective sites by a predatory bird. These results demonstrate the value of $^{87}Sr/^{86}Sr$ for testing hypotheses related to the behavior of now-extinct species. Strontium isotopes support low mobility for extinct lemurs, and suggest that Lemuriformes as a whole differ from anthropoids in having relatively depressed basal metabolic rates and reduced activity levels. These traits reduce energetic expenditure, and likely developed in response to Madagascar's harsh environments. However, small home ranges also make lemurs more vulnerable to extinction.

Keywords: $^{87}Sr/^{86}Sr$, mobility, energy conservation, seed dispersal, Madagascar

OPEN ACCESS

Edited by:
Pasquale Raia,
University of Naples Federico II, Italy

Reviewed by:
Marina Melchionna,
University of Naples Federico II, Italy
Gina Marie Semprebon,
Bay Path University, United States

***Correspondence:**
Brooke Erin Crowley
brooke.crowley@uc.edu

Specialty section:
This article was submitted to Paleoecology, a section of the journal Frontiers in Ecology and Evolution

Received: *19 September 2019*
Accepted: *03 December 2019*
Published: *20 December 2019*

Citation:
Crowley BE and Godfrey LR (2019) Strontium Isotopes Support Small Home Ranges for Extinct Lemurs. Front. Ecol. Evol. 7:490. doi: 10.3389/fevo.2019.00490

INTRODUCTION

Madagascar is well-known for its diversity of plants and animals, including its endemic primates, the lemurs. Over 100 living species of extant lemur are now recognized, and an additional 17 species went extinct in the Late Holocene (Burney et al., 2004; Crowley, 2010). Thanks to decades of multi-disciplinary research, a wealth of information is now available for Madagascar's extinct lemurs. All were larger-bodied than their extant relatives (ca. 12 to >100 kg vs. <100 g to <8 kg; Smith and Jungers, 1997; Jungers et al., 2008; Mittermeier et al., 2008), and we have a reasonably good understanding of what they ate and the kinds of environments that they inhabited (e.g., Jungers et al., 2002; Schwartz et al., 2002; Godfrey et al., 2006, 2012, 2016a; Crowley et al., 2012). However, we do not yet have a clear idea of how much they may have moved among habitats or across landscapes. Gaining further insight into movement patterns for these species would contribute to our understanding of ecological roles (e.g., their importance as seed-dispersers), which in turn could help inform conservation and biodiversity management decisions on Madagascar.

Among mammals, including anthropoid primates, there are a number of factors that affect home ranges. The primary control appears to be body size; smaller-bodied species tend to have smaller home ranges than larger-bodied species (Milton and May, 1976; Harvey and Clutton-Brock, 1981; Lindstedt et al., 1986; Ofstad et al., 2016; Crowley et al., 2017). Beyond this, terrestrial taxa tend to have larger home ranges than arboreal ones, frugivores tend to have larger home ranges than folivores, omnivores and faunivores have larger home ranges than herbivores, and animals living in open habitats tend to have larger home ranges than those living in denser habitats (Milton and May, 1976). These variables are correlated; for example, body size and diet are both tied to metabolism, and range size is related to the distribution and abundance of preferred resources, in addition to body size (Milton and May, 1976). On the basis of this evidence, we might expect the large-bodied (particularly frugivorous and terrestrial) extinct lemurs to have been more mobile than smaller-bodied (particularly folivorous and arboreal) extant species. This would be especially true for *Archaeolemur*, which has been reconstructed as one of the most terrestrial and frugivorous of the extinct lemurs (e.g., Tattersall, 1973; Jungers et al., 2002; Godfrey et al., 2005).

Yet multiple lines of evidence suggest that the extinct lemurs were relatively inactive. First, none of the giant lemurs have postcranial characteristics suggestive of high agility. Most were arboreal with adaptations for deliberate climbing, and some had adaptations for below-branch suspension (converging on sloths); none were saltatory and none were cursorial (Walker, 1974; Jouffroy and Lessertisseur, 1978; Godfrey et al., 1997; Jungers et al., 2002; Shapiro et al., 2005). Second, small semicircular canals, which are balance organs within the inner ear, also suggest low agility for all of the extinct taxa (Walker et al., 2008). Third, periodicity in the striae of Retzius is low in all measured extinct lemurs (Hogg et al., 2015; Schwartz and Rahantaharivao, unpublished data on *Pachylemur*). These striae are lamellar growth bands in tooth enamel related to biological rhythms, such as the Havers-Halberg Oscillation (HHO), which modulate life-history related traits like brain and body size, age at first reproduction, and activity levels (Bromage et al., 2012). Because Retzius Periodicity (RP) intervals correlate strongly with body size in most mammals, including anthropoid primates, we would expect the larger-bodied extinct taxa to have longer intervals than smaller-bodied extant lemurs. However, this is not the case; all lemuriforms, including the giant lemurs, have relatively low values for RP (Hogg et al., 2015). *Archaeolemur* has a slightly higher RP value than other taxa (4 vs. 2 or 3), but this value is still quite low in comparison to anthropoids of similar body size, such as *Theropithecus*, the gelada (RP = 7), with which *Archaeolemur* has been compared. Hogg et al. (2015) hypothesized that low RP relates to constraints on energy expenditure in lemurs (i.e., selection for risk-averse life histories), which could impact mobility and thus home-range size. Lastly, extinct lemurs had relatively small brains (Catlett et al., 2010), which further suggests low basal metabolic rate, low energy expenditure, and in turn low activity levels. On the basis of this collective body of evidence, we might expect that extinct lemurs had relatively small home-ranges, perhaps as small as those of much smaller-bodied extant lemurs.

Strontium isotope ratios ($^{87}Sr/^{86}Sr$) in tooth enamel and bone may be able to detect mobility differences among co-occurring extinct and extant taxa. Strontium ions leached from rocks are taken up by plants, and subsequently into animal tissues with negligible fractionation (Capo et al., 1998; Bentley, 2006; Lewis et al., 2017). Because biologically available (bioavailable) $^{87}Sr/^{86}Sr$ is closely tied to geology, it varies spatially. Madagascar is well-suited for this type of geochemical approach. Its rocks preserve nearly three billion years of our planet's history (reviewed in Crowley and Sparks, 2018), and consequently, the island's geology is extraordinarily diverse (Roig et al., 2012). Within any given site, more mobile taxa should exhibit more variable $^{87}Sr/^{86}Sr$, reflecting larger movement across a diversity of geologies.

We used strontium isotopes to compare mobility for extant and extinct lemur genera that are reasonably well-represented in subfossil deposits and fill much of the spectrum of variation in diet and locomotor habits (**Table 1**): *Eulemur*, *Lemur*, *Lepilemur* and *Propithecus* (extant), and *Archaeolemur*, *Megaladapis*, *Pachylemur,* and *Palaeopropithecus* (extinct). *Eulemur* is one of the more frugivorous of extant lemurids and an important seed disperser, *Lemur* is more folivorous but still an important seed disperser, *Propithecus* is yet more folivorous and more of a seed predator than a seed disperser, and *Lepilemur* is a specialized folivore. These taxa vary in their preferred locomotor habits; *Eulemur, Lemur,* and *Propithecus* spend time both on the ground and in the trees while *Lepilemur* is primarily arboreal. The extinct genera that we sampled also run the gamut from the frugivorous and seed dispersing *Pachylemur* to the specialized folivore *Megaladapis*. *Archaeolemur* and *Palaeopropithecus* had more intermediate diets and were likely seed predators (especially *Archaeolemur*). *Pachylemur*, *Megaladapis* and *Palaeopropithecus*

TABLE 1 | Body mass, diet, and locomotion, for taxa included in this study.

Genus	Body Mass Range (kg)	Sources[a]	Diet	Sources[b]	Locomotion	Sources[c]	SCR (mm)[d]	RP (days)[e]	ECV (cc)	Sources[f]
EXTANT										
Eulemur	1.1–2.4	1–3	Primarily fruit	1, 2	Arboreal, quadrupedal, climbing, and leaping	1	2.2–2.3	3	20.17–26.23	1
Lemur	2.2	1	Primarily fruit	1–3	Primarily arboreal, quadrupedal with some leaping	1	2.1	2–3	22.90	1
Lepilemur	∼0.5–1.0	1	Leaves	1, 2	Vertical clinging and leaping	1	1.8	–	6.87–9.56	1
Propithecus	3.0–6.3	1, 2	Primarily leaves	1, 2	Vertical clinging and leaping, some hanging	1	2.3–2.7	2–3	26.21–39.80	1
EXTINCT										
Archaeolemur	18.2–26.5	4	Primarily fruit, seeds, hard objects	2, 4–6	Semi-terrestrial. non-cursorial	1–3	3.0	4	93	2
Megaladapis	46.5–85.1	4	Leaves	2, 4–6	Primarily arboreal, likely slow, and deliberate vertical climbing	1–3	2.3	3	137	2
Pachylemur	11.5–13.4	4	Primarily fruit	2, 6	Primarily arboreal quadruped, some hind-limb suspension	1, 3	–	3	40–46	3
Palaeopropithecus	25.8–45.8	4, 5	Primarily leaves	2, 6, 7	Primarily arboreal and suspensory	1–3	1.9	2	80	2

[a] *Body Mass Sources: 1, Smith and Jungers (1997); 2, Gordon (2006); 3, Isler et al. (2008); 4, Jungers et al. (2008); 5, Jungers et al. (2002).*
[b] *Diet Sources: 1, Godfrey et al. (2004a); 2, Godfrey et al. (2012); 3, Gould (2006); 4, Godfrey et al. (2005); 5, Scott et al. (2009); 6, Muchlinski et al. (2011); 7, Godfrey et al. (2004b).*
[c] *Locomotion Sources: 1, Walker (1974); 2, Jungers et al. (2002); 3, Shapiro et al. (2005).*
[d] *All semicircular canal radius (SCR) data are from Spoor et al. (2007). Measurements for Archaeolemur and Palaeopropithecus are based on single species (A. edwardsi and P. ingens, respectively).*
[e] *All Retzius periodicity (RP) data are from Hogg et al. (2015) with the exception of Pachylemur; unpublished Pachylemur data from Noromamy Rahantaharivao and Gary Schwartz (personal communication).*
[f] *Endocranial volume (ECV) sources: 1, Isler et al. (2008); 2, Catlett et al. (2010); 3, unpublished data for Pachylemur from Noromamy Rahantaharivao (personal communication). Measurements for extinct taxa are based on single species (Archaeolemur majori, Megaladapis edwardsi, Palaeopropithecus ingens, and Pachylemur insignis).*

have anatomical adaptations suggesting they were primarily arboreal while *Archaeolemur* was likely semi-terrestrial.

MATERIALS AND METHODS

Site Description

Because bioavailable $^{87}Sr/^{86}Sr$ is spatially variable, differences in mobility among taxa can only be examined within single sites or regions (i.e., among co-occurring taxa exposed to the same baseline conditions). We sampled Holocene subfossil material from two localities that have relatively abundant and robust preservation: Ankilitelo/Mikoboka and Ampasambazimba (Crowley, 2010; Muldoon, 2010; Crowley et al., 2012, 2017; Goodman et al., 2013; Godfrey et al., 2016a; **Figure 1**). Ankilitelo/Mikoboka is a series of sinkholes in a plateau in southwestern Madagascar composed of Eocene limestone, oolitic limestone, and sandstone (Roig et al., 2012). Ampasambazimba is a wetland in Central Madagascar underlain by a variety of

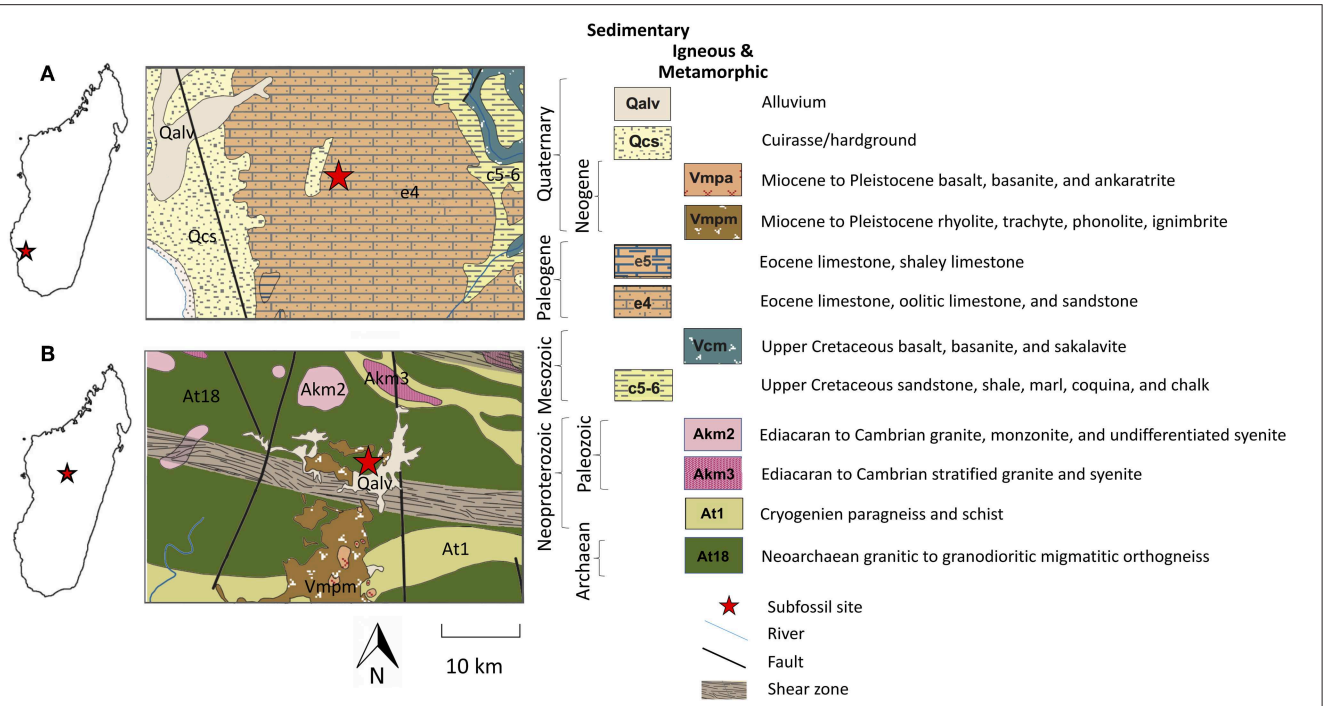

FIGURE 1 | Maps showing the location of our two study sites in Madagascar, as well as the geology at Ankilitelo/Mikoboka **(A)**, and Ampasambazimba **(B)**. Geologic maps were modified from Roig et al. (2012).

igneous and metamorphic rocks dating to the Neoarchean through the Tertiary (Roig et al., 2012).

Sample Acquisition, Preparation, and Analysis

We acquired bones and teeth from previously collected, curated material housed at a variety of museum and university collections, including the University of Antananarivo, the University of Massachusetts Amherst, and the Division of Fossil Primates at the Duke Lemur Center (**Supplementary Table 1**). In total, we were able to include 25 specimens from Ampasambazimba and 30 specimens from Ankilitelo/Mikoboka.

Specimen surfaces were cleaned using a tooth brush or a rotary Dremel tool equipped with a dental drill bit. We then removed 10–20 mg of powder from each sample using the Dremel or by pulverizing fragments with an agate mortar and pestle. Bone and enamel carbonate were isolated chemically (following Crowley and Wheatley, 2014; Baumann and Crowley, 2015; Crowley et al., 2018). Organics were removed by soaking samples in 30% H_2O_2 at room temperature. Enamel samples were soaked for 24 h; bone samples were allowed to react for 72 h, and liquid was replaced between 24 and 48 h. Samples were rinsed 5x with ultrapure water and then reacted for 24 h in 1 M calcium-buffered acetic acid at 4°C. They were again rinsed 5x with ultrapure water, and freeze dried. During both chemical pretreatment steps, samples were agitated regularly to help ensure consistent reaction.

Pretreated samples were sent to the Multicollector Inductively Coupled Plasma Mass Spectrometry (MC-ICPMS) Laboratory in the Geology Department at the University of Illinois Urbana-Champaign for $^{87}Sr/^{86}Sr$ analysis. Three to five mg of each sample were dissolved in 3N HNO_3 and filtered through 0.2 mL of Eichrom Sr spec resin (100–150 mm) packed into Teflon ion-exchange columns. Samples were then eluted with a combination of ultrapure water and 0.05 N HNO_3 into 4-mL Teflon autosampler vials for analysis. Samples were analyzed on a Nu plasma High Resolution MC-ICPMS (Nu Instruments Ltd, Wrexham, Wales, UK). Data were normalized using SRM-987 (accepted $^{87}Sr/^{86}Sr = 0.710255$), and the quality of resulting corrected data was checked using two independent internal standards—South China Sea Coral ($^{87}Sr/^{86}Sr = 0.70918$) and "E&A" ($^{87}Sr/^{86}Sr = 0.70804$). Reported precision for the lab is ± 0.00005.

Data Analysis

At each site, we compared strontium isotope ratios among genera and between extinct and extant lemurs (combining genera). Because we have small and uneven sample sizes, we used non-parametric Wilcoxon and Kruskal-Wallis analyses. We assessed homoscedasticity using Bartlett tests. For all analyses, we used JMP Pro 14.0 with significance set at $\alpha = 0.05$.

One *Palaeopropithecus* from Ankilitelo/Mikoboka and one *Eulemur* from Ampasambazimba had unusually elevated $^{87}Sr/^{86}Sr$ compared to other individuals at the same sites

(**Figures 2**, **3**). The *Palaeopropithecus* was not a statistical outlier for extinct lemurs but was a statistical outlier for this genus at Ankilitelo/Mikoboka. Conversely, the *Eulemur* was a statistical outlier for extant lemurs but was not an outlier for this genus at Ampasambazimba. There was nothing unusual about either of these samples (either in terms of preservation or analysis), which suggests that these data are real. We ran all statistical analyses both including and excluding these two individuals.

RESULTS

There were no differences in median $^{87}Sr/^{86}Sr$ or isotopic variance between extinct and extant lemurs at either Ankilitelo/Mikoboka or Ampasambazimba (**Figures 2**, **3**). These results were consistent whether or not we included the outliers at each site (Wilcoxon and Bartlett $p > 0.05$ for all comparisons). There were small apparent differences in median $^{87}Sr/^{86}Sr$ among individual genera at both sites, but these were not significant (Kruskal-Wallis $p > 0.05$; **Figures 2**, **3**). Likewise, differences in variance among genera at either site were insignificant (Bartlett $p > 0.05$; **Figure 4**). Excluding the outlier individuals, variance was reasonably consistent among taxa at both sites, although *Palaeopropithecus* had considerably smaller variability in $^{87}Sr/^{86}Sr$ than other taxa at both Ankilitelo and Ampasambazimba (**Figure 4**). Including the outliers did not affect the significance of these results, although there were some apparent changes. Specifically, *Palaeopropithecus* had apparently larger variance than all other taxa, including *Eulemur*, at Ankilitelo/Mikiboka, while variance for *Eulemur* was roughly two times larger than *Archaeolemur*, and four times larger than *Palaeopropithecus* at Ampasambazimba (**Figure 4**).

DISCUSSION

We set out to compare mobility of sympatric extinct and extant lemurs using strontium isotopes. Variability in $^{87}Sr/^{86}Sr$ exhibited by both extant and extinct lemurs was greater at Ampasambazimba than at Ankilitelo/Mikoboka (**Figures 2**–**4**). This likely reflects differences in the underlying geology of the two regions (**Figure 1**; Crowley et al., 2015). While Ampasambazimba is situated in Quaternary sediments, it is surrounded by Neogene volcanics. There are also outcrops of Ediacaran to Cambrian granites, and very old metamorphic complexes in close proximity to the site, including both Cryogenian paragneiss and schist and Neoarchaean orthogneiss (Roig et al., 2012). Typically, geologic heterogeneity is beneficial for detecting differences in mobility among individuals; however, this degree of geologic complexity may, in fact, hamper our ability to identify differences in mobility among taxa at Ampasambazimba (**Figures 2**, **4**). Even the *Eulemur* with an elevated Sr isotope ratio could easily have spent much of its life foraging on one or more of these older geologies before meeting its demise at Ampasambazimba. It may have moved to the site on its own, or have been deposited by a predator, such as the crowned eagle (*Stephanoaetus mahery*), which has previously been implicated in the accumulation of lemur remains at the site (Goodman, 1994).

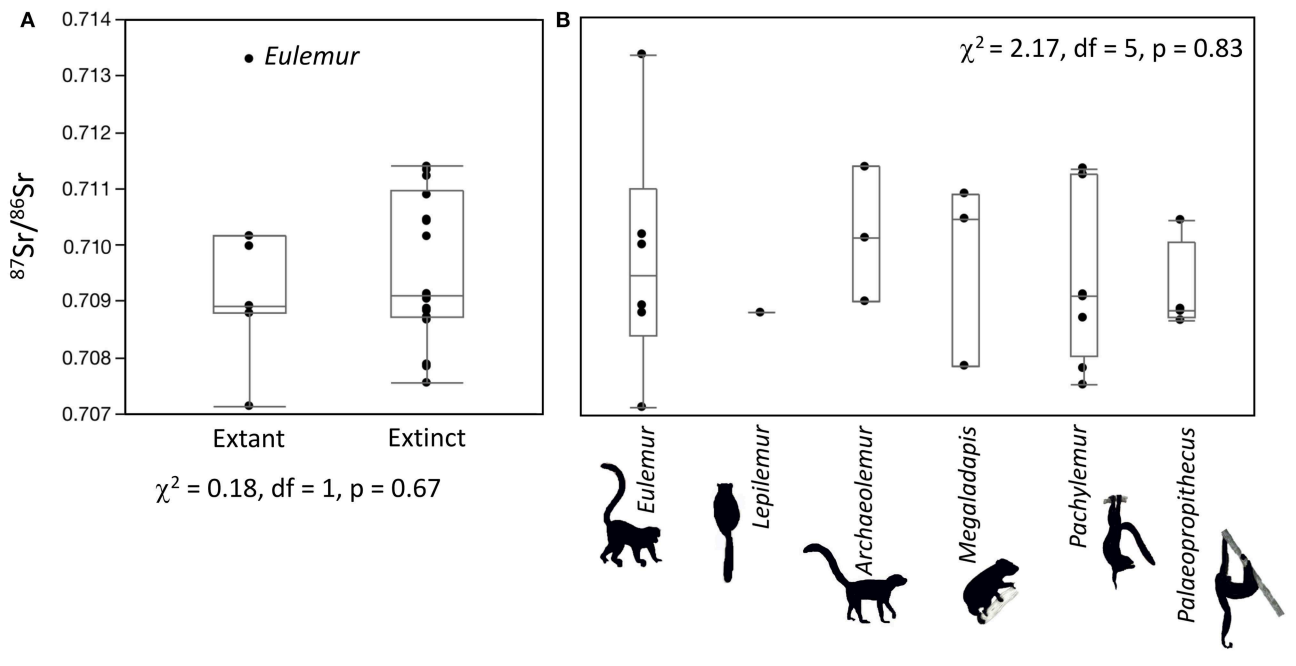

FIGURE 2 | Box plots comparing extinct and extant lemurs **(A)** and all genera **(B)** at Ampasambazimba. Statistical results do not change if the outlier *Eulemur* is excluded ($\chi^2 = 0.51$, df = 1, $p = 0.47$, and $\chi^2 = 9.75$, df = 6, $p = 0.14$, respectively).

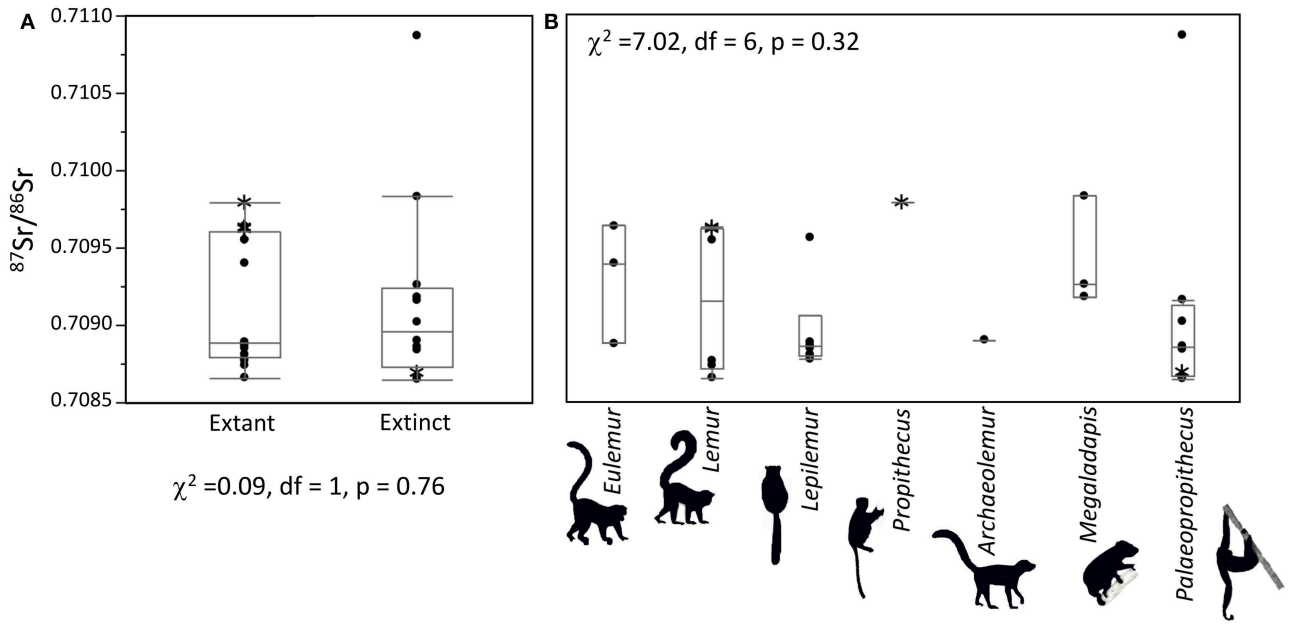

FIGURE 3 | Box plots comparing extinct and extant lemurs **(A)** and all genera **(B)** at Ankilitelo/Mikoboka. Statistical results do not change if the outlier *Palaeopropithecus* is excluded ($\chi^2 = 1.14$, df = 1, $p = 0.29$, and $\chi^2 = 2.95$, df = 5, $p = 0.71$, respectively). Asterisks (*) indicate material from non-Ankilitelo sinkholes on the Mikoboka plateau.

The story at Ankilitelo/Mikoboka is rather different. Here, the geology is much more homogenous, and overall variability in $^{87}Sr/^{86}Sr$ is quite low (**Figures 3**, **4**). Curiously, the distribution of strontium isotope ratios at Ankilitelo/Mikoboka is apparently bimodal. This is most obvious for extant lemurs, but it also holds for *Megaladapis* and *Palaeopropithecus*. Small apparent isotopic differences may reflect resource partitioning. Extant sympatric lemurs do this by feeding at different times or heights within the forest canopy, or targeting different species of plants (e.g., Ganzhorn, 1988; Wright et al., 2011). Today the habitat surrounding both Ankilitelo and Ampasambazimba is degraded and ruderal vegetation dominates. However, this is likely a relatively recent phenomenon. On the basis of faunal comparisons, Muldoon (2010) argued that vegetation at Ankilitelo during the Late Holocene was similar to succulent woodland or spiny thicket (both of which are native biomes in the region today; Burgess et al., 2004). This type of vegetation would have made it challenging for larger-bodied arboreal folivores, like *Megaladapis* and *Palaeopropithecus*, to feed at different canopy heights. However, it seems quite likely that they would have targeted different food species, as extant folivores do today (Ganzhorn, 1988; Warren, 1997; Thalmann, 2006). They may also have spatially segregated where they foraged. Either of these scenarios could result in isotopic differences between lemur taxa. First, co-occurring species of trees may have slightly different $^{87}Sr/^{86}Sr$ due to differences in rooting depth and nutrient cycling (Poszwa et al., 2004). Second, although the geology of the Mikoboka Plateau is relatively homogenous, there is still some lithologic variability. For example, the primary geology is Eocene limestone ("e4"; **Figure 1**), but sandstone is also present within this stratigraphic unit (Roig et al., 2012). Moreover, there is a mapped outcrop of Quaternary hardground (Qcs) not far from Ankilitelo (**Figure 1**), and it is highly likely that additional unmapped smaller outcrops are present in the vicinity of the sinkholes. Both sandstone and Qcs would be expected to have higher $^{87}Sr/^{86}Sr$ than Eocene limestone given that they are comprised of sediments derived from a variety of sources (Crowley et al., 2015). Strontium isotope ratios <0.708 would be consistent with foraging on Eocene limestone (Mcarthur et al., 2001), while ratios larger than this likely reflect input from either sandstone or Quaternary deposits.

Given that multiple lines of evidence suggest sloth lemurs had small ranges, it seems unlikely that the individual *Palaeopropithecus* with an elevated $^{87}Sr/^{86}Sr$ moved a great distance before meeting its demise at Ankilitelo. There are at least two explanations that would not necessarily require long distance ranging for this individual. First, the ratio for this individual (0.71085) could be consistent with foraging on local Quaternary sediments (e.g., Qcs). Yet if this were the case, we might expect at least some other individuals to also have similarly elevated $^{87}Sr/^{86}Sr$. Second, like the *Eulemur* from Ampasambazimba, it is possible that this *Palaeopropithecus* was transported to Ankilitelo by a predatory bird. Raptors are among the most common taxa represented in the subfossil material from Ankilitelo, and it has been suggested that the sinkhole was used as a roosting and nesting location (Goodman et al., 2013). Most of the remains recovered belong to smaller-bodied hawks, kites, and owls that would not be able to carry a

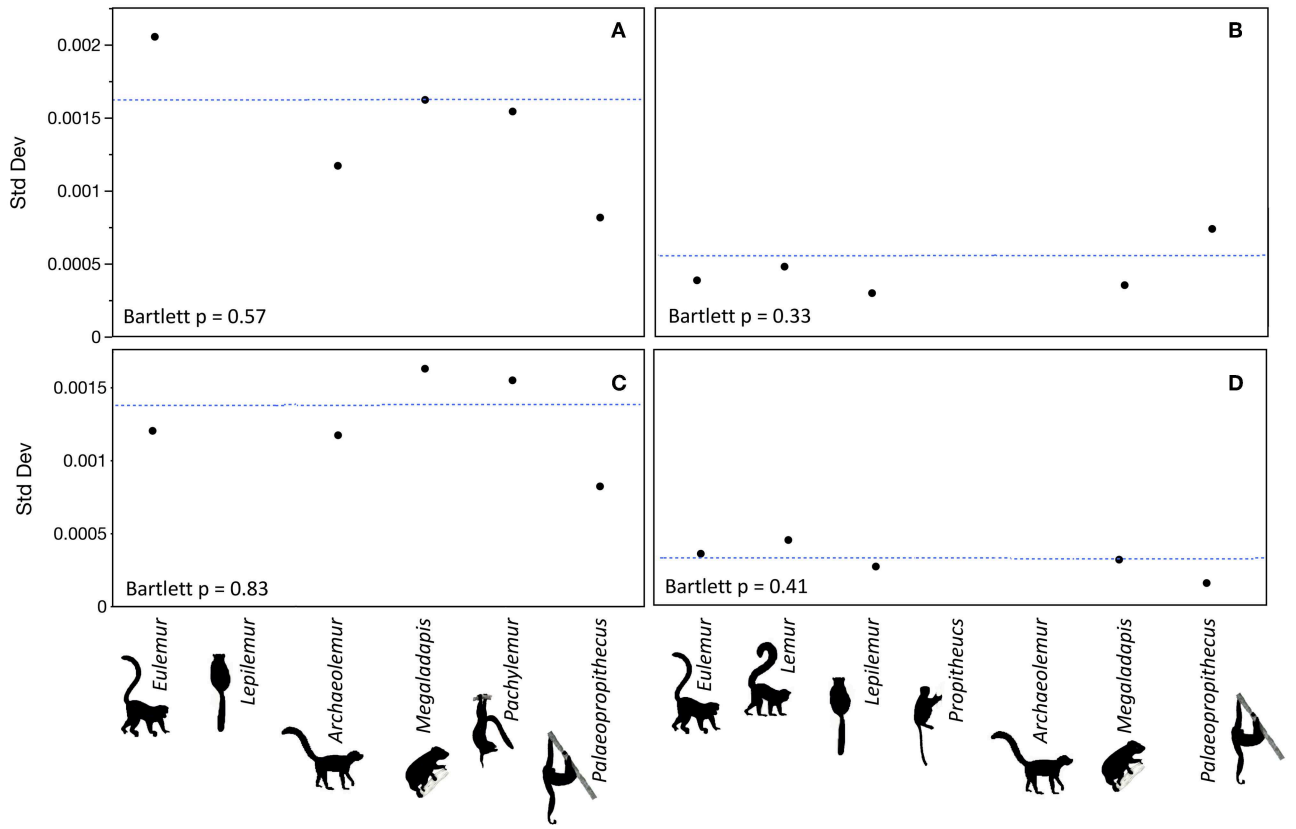

FIGURE 4 | Standard deviations of $^{87}Sr/^{86}Sr$ for each genus at Ampasambazimba **(A)** and **(C)** and Ankilitelo/Mikoboka **(B)** and **(D)**. The dashed blue lines in each panel indicate the average for all taxa. Outliers are included in **(A)** and **(C)** and excluded in **(B)** and **(D)**.

quarry as large as *Palaeopropithecus*. However, remains of at least one extinct crowned eagle (*Stephanoaetus mahery*) have also been recovered from Ankilitelo (Goodman and Muldoon, 2016). This species was considerably larger than still-extant raptors, and likely larger than its living congener, the African crowned eagle, which regularly predates primates up to ca. 12 kg (Goodman, 1994; Mitani et al., 2001; Mcgraw, 2006). Although *S. mahery* likely preferred taxa <25 kg, taphonomic evidence indicates that it was capable of eating extinct lemurs as large as *Megaladapis edwardsi* (the second largest extinct lemur; Meador et al., 2019).

In summary, $^{87}Sr/^{86}Sr$ data support comparable mobility for extinct and extant lemurs. This finding contradicts expectations based on body size, but is compatible with other lines of evidence that suggest these extinct taxa were relatively anchored (e.g., Walker et al., 2008; Hogg et al., 2015). Compared to like-sized anthropoids, the extinct lemurs have considerably smaller semi-circular canals, endocranial volume, and lower Retzius Periodicity (Walker et al., 2008; Catlett et al., 2010; Hogg et al., 2015).

Palaeopropithecus, in particular, is thought to have been very slow and sloth like (reviewed in Walker et al., 2008). Elongated forelimbs and curved phalanges demonstrate that it was skilled at below-the-branch quadrupedal suspension (Jungers et al., 2002; Godfrey et al., 2016b) and its semicircular canal radius is comparable to *Lepilemur* (an animal that weighs ∼1 kg). If we exclude the single *Palaeopropithecus* at Ankilitelo/Mikoboka with an elevated $^{87}Sr/^{86}Sr$, we note that this genus has apparently smaller variance than co-occurring taxa at both sites, perhaps on par with *Lepilemur* (**Figures 2**, **3**).

What Are the Consequences of Small Home Ranges?

Both living and extinct Lemuriformes appear to differ from anthropoid primates in their relatively depressed basal metabolism, small brains, low Retzius Periodicity, and reduced activity levels. Collectively, this suite of traits serves to reduce energetic expenditure, and likely developed so lemurs can cope with living in the harsh environments that characterize Madagascar (Wright, 1999; Godfrey et al., 2006; Hogg et al., 2015).

Unfortunately, these same traits may make lemurs more vulnerable to extinction. Home range size is often used as a parameter in evaluating extinction risk for a species. Specifically, species with limited mobility are more threatened by habitat fragmentation than species with greater mobility, and large-bodied species are more threatened by habitat fragmentation than small-bodied ones (Haskell et al., 2002). However, diet,

resource density and resource distribution also play a role. Frugivores are more vulnerable than folivores because of differences in the distribution of preferred food resources; indeed, folivore population density may even increase following low- or medium-level disturbances such as cyclones, because young foliage tends to increase as pioneer species fill light gaps caused by the destruction of older fruit-producing trees (Johns and Skorupa, 1987).

Given this, it is, perhaps, unsurprising that larger-bodied and frugivorous lemurs are the ones to have disappeared first. Unfortunately, their extinction has reverberating consequences. Globally, the loss of large-seed dispersal services is one of the most challenging problems facing conservationists in the wake of recent megafaunal extinctions (Corlett, 2013), and this is particularly challenging in places like Madagascar, where these services may have been marginal prior to the loss of the largest-bodied species. The size of the primate frugivore guild on Madagascar is small (Fleagle and Reed, 1996; Goodman and Ganzhorn, 1997). Climatic unpredictability and hypervariability have been posited as contributing to this (Wright, 1999; Wright et al., 2005; Dewar and Richard, 2007). Madagascar also has extended dry or lean seasons which can result in erratic fruiting, and a high frequency of cyclones, which can be extremely destructive to older fruiting trees. Furthermore, at any single point in time, fruit is generally less abundant in Madagascar than it is in other places that are home to many primate species (Federman et al., 2017). Additionally or alternatively, it appears that low levels of fruit nitrogen are responsible for the poor representation of frugivores in Madagascar's primate community (Ganzhorn et al., 2009; Donati et al., 2017; Federman et al., 2017). This argument is grounded in the observations, not merely that the fruits of Madagascar have low nitrogen content, but also that such fruits cannot meet the protein requirements of primates during critical times of the year such as the reproductive season.

What is less clear is the extent to which large, fruit-bearing trees and their seed dispersers were better represented in the recent past, the degree to which they face disproportionate extinction risk in the future, and the degree to which that risk depends on the survival of primates. Although Madagascar today has an unusually low number of plant species that disperse their seeds via endozoochory, most of those that do rely on endozoochory have adaptations to attract primates rather than birds (Albert-Daviaud et al., 2018). This is particularly the case for trees with large seeds (Razafindratsima et al., 2018). Thus, the primate frugivore guild plays a very important role in seed dispersal. Threats to plant communities in Madagascar are compounded by the facts that: (1) the primate frugivore guild on Madagascar is increasingly dominated by species too small to disperse large seeds (Richard and Dewar, 1991; Federman et al., 2016); and (2) still-extant seed-dispersing lemurs (i.e., those more likely to pass seeds whole and undamaged through the gut; Dew and Wright, 1998; Razafindratsima and Martinez, 2012) have small seed-dispersal distances in comparison to like-sized frugivores on other continents (Razafindratsima et al., 2014). When seed dispersers have limited home ranges, the plant community as a whole may be more vulnerable to habitat disturbance, and therefore at greater risk of entering into an extinction vortex. The problem is not merely that the loss of key seed dispersers may result in an increase in the number of "orphaned" plants (those lacking seed dispersers; Bollen et al., 2004; Godfrey et al., 2008; Crowley et al., 2011; Buerki et al., 2015; Albert-Daviaud et al., 2018), but also that the plant species most likely to become orphaned are the trees with the highest above-ground biomass, and therefore the greatest capacity to store carbon. They are precisely the trees that contribute the most to climate stability and the health of the entire ecosystem (Razafindratsima et al., 2018). With this in mind, it is imperative that remaining forest cover be protected and that connectivity among fragments be improved.

DATA AVAILABILITY STATEMENT

The dataset analyzed for this study can be found in **Supplementary Table 1**.

AUTHOR CONTRIBUTIONS

BC and LG conceived of the project. BC prepared samples and conducted the data analysis. Both authors wrote the manuscript.

FUNDING

Funding was provided by NSF BCS-1749676 to BC and NSF BCS-1750598 to LG.

ACKNOWLEDGMENTS

We thank Gideon Bartov, Gregg Gunnell, Ian Macadam, Tom Johnson, Catherine Riddle, and Jani Sparks for technical and logistical assistance. This is Duke Lemur Center publication #1448.

SUPPLEMENTARY MATERIAL

The Supplementary Material for this article can be found online at: https://www.frontiersin.org/articles/10.3389/fevo.2019.00490/full#supplementary-material

REFERENCES

Albert-Daviaud, A., Perillo, S., and Stuppy, W. (2018). Seed dispersal syndromes in the Madagascan flora: the unusual importance of primates. *Oryx* 52, 418–426. doi: 10.1017/S0030605317001600

Baumann, E., and Crowley, B. E. (2015). Stable isotopes reveal ecological differences amongst now-extinct proboscideans from the Cincinnati region, USA. *Boreas* 44, 240–254. doi: 10.1111/bor.12091

Bentley, R. A. (2006). Strontium isotopes from the Earth to the archaeological skeleton: a review. *J. Archaeol. Method Th.* 13, 135–187. doi: 10.1007/s10816-006-9009-x

Bollen, A., Elsacker, L. V., and Ganzhorn, J. U. (2004). Relations between fruits and disperser assemblages in a Malagasy littoral forest: a community-level approach. *J. Trop. Ecol.* 20, 599–612. doi: 10.1017/S0266467404001853

Bromage, T. G., Hogg, R. T., Lacruz, R. S., and Hou, C. (2012). Primate enamel evinces long period biological timing and regulation of life history. *J. Theor. Biol.* 305, 131–144. doi: 10.1016/j.jtbi.2012.04.007

Buerki, S., Callmander, M. W., Bachman, S., Moat, J., Labat, J.-N., and Forest, F. (2015). Incorporating evolutionary history into conservation planning in biodiversity hotspots. *Philos. Trans. Royal Soc. B* 370:20140014. doi: 10.1098/rstb.2014.0014

Burgess, N. D., D'amico Hales, J., Underwood, E. C., Dinerstein, E., Olson, D., Itoua, I., et al. (2004). *Terrestrial Ecoregions of Africa and Madagascar: A Conservation Assessment*. Washington, DC: Island Press.

Burney, D. A., Burney, L. P., Godfrey, L. R., Jungers, W. L., Goodman, S. M., Wright, H. T., et al. (2004). A chronology for late prehistoric Madagascar. *J. Hum. Evol.* 47, 25–63. doi: 10.1016/j.jhevol.2004.05.005

Capo, R. C., Stewart, B. W., and Chadwick, O. A. (1998). Strontium isotopes as tracers of ecosystem processes: theory and methods. *Geoderma* 82, 197–225. doi: 10.1016/S0016-7061(97)00102-X

Catlett, K. K., Schwartz, G. T., Godfrey, L. R., and Jungers, W. L. (2010). "Life History Space": a multivariate analysis of life history variation in extant and extinct Malagasy lemurs. *Am. J. Phys. Anthropol.* 142, 391–404. doi: 10.1002/ajpa.21236

Corlett, R. T. (2013). The shifted baseline: prehistoric defaunation in the tropics and its consequences for biodiversity conservation. *Biol. Conserv.* 163, 13–21. doi: 10.1016/j.biocon.2012.11.012

Crowley, B. E. (2010). A refined chronology of prehistoric Madagascar and the demise of the megafauna. *Quat. Sci. Rev.* 29, 2591–2603. doi: 10.1016/j.quascirev.2010.06.030

Crowley, B. E., Castro, I., Soarimalala, V., and Goodman, S. M. (2018). Isotopic evidence for niche partitioning and the influence of anthropogenic disturbance on endemic and introduced rodents in central Madagascar. *Sci. Nat.* 105:44. doi: 10.1007/s00114-018-1564-y

Crowley, B. E., Godfrey, L. R., Bankoff, R. J., Perry, G. H., Culleton, B. J., Kennett, D. J., et al. (2017). Island-wide aridity did not trigger recent megafaunal extinctions in Madagascar. *Ecography* 40, 901–912. doi: 10.1111/ecog.02376

Crowley, B. E., Godfrey, L. R., Guilderson, T. P., Zermeño, P., Koch, P. L., and Dominy, N. J. (2012). Extinction and ecological retreat in a community of primates. *Proc. Royal Soc. Lond. B.* 279, 3597–3605. doi: 10.1098/rspb.2012.0727

Crowley, B. E., Godfrey, L. R., and Irwin, M. T. (2011). A glance to the past: subfossils, stable isotopes, seed dispersal, and lemur species loss in southern Madagascar. *Am. J. Primatol.* 73, 25–37. doi: 10.1002/ajp.20817

Crowley, B. E., Slater, P. A., Muldoon, K. M., and Godfrey, L. R. (2015). Reconstructing the mobility of Madagascar's fauna using strontium isotopes: results and implications for management and conservation. *Am. J. Phys. Anthropol.* 156:252.

Crowley, B. E., and Sparks, J. A. (2018). "Geology," in *Les Aires Protégées Terrestres de Madagascar: Leur Histoire, Description et Biote / The Terrestrial Protected Areas of Madagascar: Their History, Description, and Biota*, eds S. M. Goodman, M. J. Raherilalao, and S. Wolhauser (Antananarivo: Association Vahatra), 169–180.

Crowley, B. E., and Wheatley, P. V. (2014). To bleach or not to bleach? Comparing treatment methods for isolating biogenic carbonate. *Chem. Geol.* 381, 234–242. doi: 10.1016/j.chemgeo.2014.05.006

Dew, J. L., and Wright, P. C. (1998). Frugivory and seed dispersal by four species of primates in Madagascar's eastern rain forest. *Biotropica* 30, 425–437. doi: 10.1111/j.1744-7429.1998.tb00076.x

Dewar, R. E., and Richard, A. F. (2007). Evolution in the hypervariable environment of Madagascar. *Proc. Natl. Acad. Sci. U.S.A.* 103, 13723–13727. doi: 10.1073/pnas.0704346104

Donati, G., Santini, L., Eppley, T. M., Arrigo-Nelson, S. J., Balestri, M., Boinski, S., et al. (2017). Low levels of fruit nitrogen as drivers for the evolution of Madagascar's primate communities. *Sci. Rep.* 7:14406. doi: 10.1038/s41598-017-13906-y

Federman, S., Dornburg, A., Daly, D. C., Downie, A., Perry, G. H., Yoder, A. D., et al. (2016). Implications of lemuriform extinctions for the Malagasy flora. *Proc. Natl. Acad. Sci. U.S.A.* 113, 5041–5046. doi: 10.1073/pnas.1523825113

Federman, S., Sinnott-Armstrong, M., Baden, A. L., Chapman, C. A., Daly, D. C., Richard, A. R., et al. (2017). The paucity of frugivores in Madagascar may not be due to unpredictable temperatures or fruit resources. *PLoS ONE* 12:e0168943. doi: 10.1371/journal.pone.0168943

Fleagle, J. G., and Reed, K. E. (1996). Comparing primate communities: a multivariate approach. *J. Hum. Evol.* 30, 489–510. doi: 10.1006/jhev.1996.0039

Ganzhorn, J. U. (1988). Food partitioning among Malagasy primates. *Oecologia* 75, 436–450. doi: 10.1007/BF00376949

Ganzhorn, J. U., Arrigo-Nelson, S. J., Boinski, S., Bollen, A., Carrai, V., Derby, A., et al. (2009). Possible fruit protein effects on primate communities in Madagascar and the Neotropics. *PLoS ONE* 4:e8253. doi: 10.1371/journal.pone.0008253

Godfrey, L. R., Crowley, B. E., Muldoon, K. M., Kelley, E. A., King, S. J., Best, A. W., et al. (2016a). What did *Hadropithecus* eat, and why should paleoanthropologists care? *Am. J. Primatol.* 78, 1098–1112. doi: 10.1002/ajp.22506

Godfrey, L. R., Granatosky, M. C., and Jungers, W. L. (2016b). "The hands of subfossil lemurs," in *The Evolution of the Primate Hand: Anatomical, Developmental, Functional, and Paleontological Evidence,* eds T. L. Kivell, P. Lemelin, B. G. Richmond, and D. Schmitt (New York, NY: Springer Science), 421–453. doi: 10.1007/978-1-4939-3646-5_15

Godfrey, L. R., Jungers, W. L., and Schwartz, G. T. (2006). "Ecology and extinction of Madagascar's subfossil lemurs," in *Lemurs: Ecology and Adapaptation,* eds L. Gould and M. L. Sauther (New York, NY: Springer), 41–64. doi: 10.1007/978-0-387-34586-4_3

Godfrey, L. R., Jungers, W. L., Schwartz, G. T., and Irwin, M. T. (2008). "Ghosts and orphans: Madagascar's vanishing ecosystems," in *Elwyn Simons: A Search for Origins,* eds J. G. Fleagle and C. C. Gilbert (New York, NY: Springer), 361–395. doi: 10.1007/978-0-387-73896-3_24

Godfrey, L. R., Samonds, K. E., Jungers, W. L., Sutherland, M. R., and Irwin, M. T. (2004a). Ontogenetic correlates of diet in Malagasy lemurs. *Am. J. Phys. Anthropol.* 123, 250–276. doi: 10.1002/ajpa.10315

Godfrey, L. R., Semprebon, G., Schwartz, G. T., Burney, D. A., Jungers, W. L., Flanagan, E. K., et al. (2005). New insights into old lemurs: the trophic adaptations of the Archaeolemuridae. *Int. J. Primatol.* 26, 825–854. doi: 10.1007/s10764-005-5325-3

Godfrey, L. R., Semprebon, G. M., Jungers, W. L., Sutherland, M. R., Simons, E. L., and Solounias, N. (2004b). Dental use wear in extinct lemurs: evidence of diet and niche differentiation. *J. Hum. Evol.* 47, 145–169. doi: 10.1016/j.jhevol.2004.06.003

Godfrey, L. R., Winchester, J. M., King, S. J., Boyer, D. M., and Jernvall, J. (2012). Dental topography indicates ecological contraction of lemur communities. *Am. J. Phys. Anthropol.* 148, 215–227. doi: 10.1002/ajpa.21615

Godfrey, L. R., Wunderlich, R. E., and Richmond, B. C. (1997). Reappraisal of the postrcranium of *Hadropithecus* (Primates, Indroidea). *Am. J. Phys. Anthropol.* 103, 529–56. doi: 10.1002/(SICI)1096-8644(199708)103:4<529::AID-AJPA9>3.0.CO;2-H

Goodman, S. M. (1994). Description of a new species of subfossil eagle from Madagascar, *Stephanoaetus* (Aves, Falconiformes) from the deposits of Ampasambazimba. *Proc. Biol. Soc. Washington* 107, 421–428.

Goodman, S. M., and Ganzhorn, J. U. (1997). Rarity of figs (*Ficus*) on Madagascar and its relationship to a depauperate frugivore community. *Rev. Ecol. Terr. Vie* 52, 321–329.

Goodman, S. M., and Muldoon, K. M. (2016). A new subfossil locality for the extinct large Malagasy eagle *Stephanoaetus mahery* (Aves: Falconiformes): implications for time of extinction and ecological specificity. *Holocene* 26, 985–989. doi: 10.1177/0959683615622554

Goodman, S. M., Raherilalao, M. J., and Muldoon, K. M. (2013). Bird fossils from Ankilitelo Cave: inference about Holocene environmental changes in Southwestern Madagascar. *Zootaxa* 5, 534–548. doi: 10.11646/zootaxa.3750.5.6

Gordon, A. D. (2006). Scaling of size and dimorphism in primates II: macroevolution. *Int. J. Primatol.* 27, 63–105. doi: 10.1007/s10764-005-9004-1

Gould, L. (2006). "*Lemur catta* ecology: what we know and what we need to know," in *Lemurs: Ecology and Adaptation,* eds L. Gould and M. L. Sauther (Boston, MA: Springer), 255–274. doi: 10.1007/978-0-387-34586-4_12

Harvey, P. H., and Clutton-Brock, T. H. (1981). Primate home-range size and metabolic needs. *Behav. Ecol. Sociobiol.* 8, 151–155. doi: 10.1007/BF00300828

Haskell, J. P., Ritchie, M. E., and Olff, H. (2002). Fractal geometry predicts varying body size scaling relationships for mammal and bird home ranges. *Nature* 418, 527–530. doi: 10.1038/nature00840

Hogg, R. T., Godfrey, L. R., Schwartz, G. T., Dirks, W., and Bromage, T. G. (2015). Lemur biorhythms and life history evolution. *PLoS ONE* 10:e0134210. doi: 10.1371/journal.pone.0134210

Isler, K., Kirk, E. C., Miller, J. M., Albrecht, G. A., Gelvin, B. R., and Martin, R. D. (2008). Endocranial volumes of primate species: scaling analyses using a comprehensive and reliable data set. *J. Hum. Evol.* 55, 967–978. doi: 10.1016/j.jhevol.2008.08.004

Johns, A. D., and Skorupa, J. P. (1987). Responses of rain-forest primates to habitat disturbance: a review *Int. J. Primatol.* 8, 157–191. doi: 10.1007/BF02735162

Jouffroy, F. K., and Lessertisseur, J. (1978). Etude ecomorphologique des proportions des members des primates et specialement des prosimiens. *Annal. Sci. Nat. Zool.* 20, 99–128.

Jungers, W. L., Demes, B., and Godfrey, L. R. (2008). "How big were the "giant extinct lemurs of Madagascar?," in *Elwyn Simons: A Search for Origins,* eds J. G. Fleagle and C. C. Gilbert (New York, NY: Springer), 343–360. doi: 10.1007/978-0-387-73896-3_23

Jungers, W. L., Godfrey, L. R., Simons, E. L., Wunderlich, R. E., Richmond, B. G., and Chatrath, P. S. (2002). "Ecomorphology and behavior of giant extinct lemurs from Madagascar," in *Reconstructing Behavior in the Primate Fossil Record,* eds J. M. Plavcan, R. F. Kay, W. L. Jungers, and C. P. Van Schaik (New York, NY: Kluwer Academic/Plenum), 371–411. doi: 10.1007/978-1-4615-1343-8_10

Lewis, J., Pike, A. W. G., Coath, C. D., and Evershed, R. P. (2017). Strontium concentration, radiogenic ($^{87}Sr/^{86}Sr$) and stable ($\delta^{88}Sr$) strontium isotope systematics in a controlled feeding study. *STAR* 3, 45–57. doi: 10.1080/20548923.2017.1303124

Lindstedt, S. L., Miller, B. J., and Buskirk, S. W. (1986). Home range, time, and body size in mammals. *Ecology* 67, 413–418. doi: 10.2307/1938584

Mcarthur, J. M., Howarth, R. J., and Bailey, T. R. (2001). Strontium isotope stratigraphy: LOWESS Version 3: best fit to the marine Sr-isotope curve for 0–509 Ma and accompanying look-up table for deriving numerical age. *Geology* 109, 155–170. doi: 10.1086/319243

Mcgraw, W. S. (2006). Primate remains from African crowned eagle (*Stephanoaetus coronatus*) nests in Ivory Coast's Tai Forest: implications for primate predation and early hominid taphonomy in South Africa. *Am. J. Phys. Anthropol.* 131, 151–165. doi: 10.1002/ajpa.20420

Meador, L. R., Godfrey, L. R., Rakotondramavo, J. C., Ranivoharimanana, L., Zamora, A., Sutherland, M. R., et al. (2019). *Cryptoprocta spelea* (Carnivora: Eupleridae): what did it eat and how do we know? *J. Mamm. Evol.* 26, 237–251. doi: 10.1007/s10914-017-9391-z

Milton, K., and May, M. L. (1976). Body weight, diet and home range area in primates. *Nature* 259, 459–462. doi: 10.1038/259459a0

Mitani, J. C., Sanders, W. J., Lwanga, J. S., and Windfelder, T. L. (2001). Predatory behavior of crowned hawkeagles (*Stephanoaetus coronatus*) in Kibale National Park, Uganda. *Behav. Ecol. Sociobiol.* 49, 187–195. doi: 10.1007/s002650000283

Mittermeier, R. A., Ganzhorn, J. U., Konstant, W. R., Glander, K., Tattersall, I., Groves, C. P., et al. (2008). Lemur diversity in Madagascar. *Int. J. Primatol.* 29, 1607–1656. doi: 10.1007/s10764-008-9317-y

Muchlinski, M. N., Godfrey, L. R., Muldoon, K. M., and Tongasoa, L. (2011). Evidence for dietary niche separation based on infraorbital foramen size variation among subfossil lemurs. *Folia Primatol.* 81, 330–345. doi: 10.1159/000323277

Muldoon, K. M. (2010). Paleoenvironment of Ankilitelo Cave (late Holocene, southwestern Madagascar): implications for the extinction of the giant lemurs *J. Hum. Evol.* 58, 338–352. doi: 10.1016/j.jhevol.2010.01.005

Ofstad, E. G., Herfindal, I., Solberg, E. J., and Sæther, B. E. (2016). Home ranges, habitat and body mass: simple correlates of home range size in ungulates. *Proc. Royal Soc. Lond. B* 283:20161234. doi: 10.1098/rspb.2016.1234

Poszwa, A., Ferry, B., Dambrine, E., Pollier, B., Wickman, T., Loubet, M., et al. (2004). Variations of bioavailable Sr concentration and $^{87}Sr/^{86}Sr$ ratio in boreal forest ecosystems. Role of biocycling, mineral weathering and depth of root uptake. *Biogeochemistry* 67, 1–20. doi: 10.1023/B:BIOG.0000015162.12857.3e

Razafindratsima, O. H., Brown, K. A., Carvalho, F., Johnson, S. E., Wright, P. C., and Dunham, A. E. (2018). Edge effects on components of diversity and above-ground biomass in a tropical rainforest. *J. Appl. Ecol.* 55, 977–985. doi: 10.1111/1365-2664.12985

Razafindratsima, O. H., Jones, T. A., and Dunham, A. E. (2014). Patterns of movement and seed dispersal by three lemur species. *Am. J. Primatol.* 76, 84–96. doi: 10.1002/ajp.22199

Razafindratsima, O. H., and Martinez, B. T. (2012). Seed dispersal by red-ruffed lemurs: seed size, viability, and beneficial effect on seedling growth. *Ecotropica* 18, 15–26.

Richard, A. F., and Dewar, R. E. (1991). Lemur ecology. *Annu. Rev. Ecol. Syst.* 22, 145–175. doi: 10.1146/annurev.es.22.110191.001045

Roig, J. Y., Tucker, R. D., Delor, C., Peters, S. G., and Théveniaut, H. (2012). *Carte Géologique de la République de Madagascar à 1/1,000,000*. Antananarivo, République de Madagascar: Ministère des Mines, Programme de Gouvernance des Ressources Minérales.

Schwartz, G. T., Samonds, K. E., Godfrey, L. R., Jungers, W. L., and Simons, E. L. (2002). Dental microstructure and life history in subfossil Malagasy lemurs. *Proc. Natl. Acad. Sci. U.S.A.* 99, 6124–6129. doi: 10.1073/pnas.092685099

Scott, J. R., Godfrey, L. R., Jungers, W. L., Scott, R. S., Simons, E. L., Teaford, M. F., et al. (2009). Dental microwear texture analysis of two families of subfossil lemurs from Madagascar. *J. Hum. Evol.* 54, 405–416. doi: 10.1016/j.jhevol.2008.11.003

Shapiro, L. J., Seiffert, C. V., Godfrey, L. R., Jungers, W. L., Simons, E. L., and Randria, G. F. (2005). Morphometric analysis of lumbar vertebrae in extinct Malagasy strepsirrhines. *Am. J. Phys. Anthropol.* 128, 823–839. doi: 10.1002/ajpa.20122

Smith, R. J., and Jungers, W. L. (1997). Body mass in comparative primatology. *J. Hum. Evol.* 32, 523–559. doi: 10.1006/jhev.1996.0122

Spoor, F., Garland, T., Krovitz, G., Ryan, T. M., Silcox, M. T., and Walker, A. (2007). The primate semicircular canal system and locomotion. *Proc. Natl. Acad. Sci. U.S.A.* 104, 10808–10812. doi: 10.1073/pnas.0704250104

Tattersall, I. (1973). Cranial anatomy of the Archaeolemurinae (Lemuroidea, Primates). *Anthropol. Papers Am. Mus. Nat. Hist.* 52, 1–110.

Thalmann, U. (2006). "Behavioral and ecological adaptations in two small folivorous lemurs with different social organization: *Avahi* and *Lepilemur*," in *Lemurs: Ecology and Adaptation,* eds L. Gould and M. L. Sauther (Boston, MA: Springer), 327–352. doi: 10.1007/978-0-387-34586-4_15

Walker, A., Ryan, T. M., Silcox, M. T., Simons, E. L., and Spoor, F. (2008). The semicircular canal system and locomotion: the case of extinct lemuroids and lorisoids. *Evol. Anthropol.* 17, 135–145. doi: 10.1002/evan.20165

Walker, A. C. (1974). "Locomotor adaptations in past and present prosimian primates," in *Primate Locomotion,* ed F.A. Jenkins Jr. (New York, NY; London: Academic Press), 349–381. doi: 10.1016/B978-0-12-384050-9.50016-7

Warren, R. D. (1997). Habitat use and support preference of two free-ranging saltatory lemurs (*Lepilemur edwardsi* and *Avahi occidentalis*). *J. Zool.* 241, 325–341. doi: 10.1111/j.1469-7998.1997.tb01963.x

Wright, P. C. (1999). Lemur traits and Madagascar ecology: coping with an island environment. *Yearb. Phys. Anthropol.* 42, 31–72.

Wright, P. C., Razafindratsita, V. R., Pochron, S. T., and Jernvall, J. (2005). "The key to Madagascar frugivores," in *Tropical Fruits and Frugivores,* eds J. L. Dew and J. P. Boubli (New York, NY: Springer).

Wright, P. C., Tecot, S. R., Erhart, E. M., Baden, A. L., King, S. J., and Grassi, C. (2011). Frugivory in four sympatric lemurs: implications for the future of Madagascar's forests. *Am. J. Primatol.* 73, 585–602. doi: 10.1002/ajp.20936

Conflict of Interest: The authors declare that the research was conducted in the absence of any commercial or financial relationships that could be construed as a potential conflict of interest.

frontiers in Ecology and Evolution

ORIGINAL RESEARCH
published: 15 September 2020
doi: 10.3389/fevo.2020.568943

Assessing the Reliability of Mobility Interpretation From a Multi-Isotope Hair Profile on a Traveling Individual

Lihai Hu†, Michelle M. G. Chartrand, Gilles St-Jean, Madenn Lopes and Clément P. Bataille**

Department of Earth and Environmental Sciences, University of Ottawa, Ottawa, ON, Canada

OPEN ACCESS

Edited by:
Gael Le Roux, UMR 5245 Laboratoire Ecologie Fonctionnelle et Environnement (ECOLAB), France

Reviewed by:
Christine Lehn, Ludwig Maximilian University of Munich, Germany
George Kamenov, University of Florida, United States

***Correspondence:**
Lihai Hu
lihai.hu@uottawa.ca
Clément P. Bataille
cbataill@uottawa.ca

†ORCID:
Lihai Hu
orcid.org/0000-0003-2044-0524

Specialty section:
This article was submitted to Paleoecology, a section of the journal Frontiers in Ecology and Evolution

Received: *02 June 2020*
Accepted: *24 August 2020*
Published: *15 September 2020*

Citation:
Hu L, Chartrand MMG, St-Jean G, Lopes M and Bataille CP (2020) Assessing the Reliability of Mobility Interpretation From a Multi-Isotope Hair Profile on a Traveling Individual. Front. Ecol. Evol. 8:568943. doi: 10.3389/fevo.2020.568943

Forensic practitioners, archeologists, and ecologists increasingly use hair isotope profiles and isotope databases and maps to reconstruct the life history of unidentified individuals. Relationships between hair isotope profiles with travel history have been primarily investigated through controlled laboratory experiments. However, those controlled studies do not reflect the complex life history of modern individuals who often travel between multiple locations over different periods. Here, we collect one bundle of hairs from a volunteer whose primary residence is in Ottawa (Canada) but who traveled to multiple destinations over a period of 18 months. Those travels include multi-week trips to distant locations and multi-day trips to more local areas. We use multi-isotope profiles on the individual's hairs coupled with isotope databases across the world to reconstruct travel history at sub-monthly temporal resolution. We compare the isotopic interpretation of mobility with the recorded travel history. A prominent shift in δ^2H values is interpreted as a westward movement toward central Canada, which corresponds to a month-long road-trip to the Prairie. We observed a marked negative excursion in $\delta^{13}C$ values along the hairs profile, which was related to a multi-week-long trip to several countries in Europe. Except for an exceptionally variable interval likely driven by health issues, $\delta^{15}N$ values show very little fluctuation across the entire profile, indicating consumption of consistent amounts of animal or marine-based protein at different locations. The isotopic shifts in the proximal part of the hair reveal a clearer picture of traveling destinations than the shifts in the distal part, which have larger uncertainty in terms of timing and amplitude. Except for the last couple of months before collection, $^{87}Sr/^{86}Sr$ ratios show little variation throughout the profile likely due to recent exchange with Ottawa tap water during bathing or showering. The different $^{87}Sr/^{86}Sr$ ratios in the month preceding collection appear to partially preserve the $^{87}Sr/^{86}Sr$ ratio of the volunteer's diet. This study demonstrates the interest of using multi-isotope systems and large isotopic databases to reconstruct individual mobility. This study also underlines the challenges in linking isotope data to mobility, particularly in rapidly growing keratinous tissues.

Keywords: stable isotopes, strontium, hair, mobility, 87Sr/86Sr, isoscape, travel history, multi-isotope

INTRODUCTION

The isotopic values of different elements (e.g., hydrogen, oxygen, and strontium) in foods and water vary geographically (Ehleringer et al., 2008; Bowen, 2010; Bataille and Bowen, 2012; Chesson et al., 2012). Such variation can be integrated into human and animal tissues, from which the isotopic values may be used to identify their regions of origin (West et al., 2010; Valenzuela et al., 2011; Hobson et al., 2012; Chesson et al., 2020). Some keratinous tissues, like hair and nail, preserve the regional isotopic values in time sequence, and may thus be used to reconstruct the travel history of individuals (Fraser et al., 2006; O'Brien and Wooller, 2007; Hobson et al., 2010; Remien et al., 2014). With increasingly available isoscapes—"isotope land-scapes" or the maps of the spatial isotopic variation of the material(s) of interest (e.g., West et al., 2010)—for more elements and more regions, studies on the isotopic profiles of multiple elements are getting more attention in forensic sciences, archeology, and ecology (Lehn et al., 2011, 2015a,b, 2019; Thompson et al., 2014; Meier-Augenstein, 2019).

Although there are isotopic fractionations between hair and local water, the hydrogen and oxygen isotope compositions (reported as δ^2H and $\delta^{18}O$ values, respectively) in hair have largely a linear relationship with local water (Fraser and Meier-Augenstein, 2007). For example, one study found that the δ^2H profile in elephant hair had similar patterns with the change of δ^2H values of local water (Cerling et al., 2009). Large-scale prediction maps have also been established for the average δ^2H and $\delta^{18}O$ values in the human hair in the United States based mainly on the geographical distributions of the δ^2H and $\delta^{18}O$ values of the tap water, respectively (Ehleringer et al., 2008). Therefore, it has been proposed to use hydrogen and oxygen isotope analysis of hair to help forensic human identification (Fraser and Meier-Augenstein, 2007). There have been successful forensic applications where sequential isotopic analysis of hydrogen and oxygen along hair strands provided key information to help solve cold cases (e.g., Ehleringer et al., 2010). The oxygen and hydrogen isotope analyses in animal keratinous tissues have also been very useful to reconstruct the mobility of modern fauna (Rubenstein and Hobson, 2004; Bowen et al., 2005; Wunder, 2012). Similarly, δ^2H and $\delta^{18}O$ values in hair, skeleton, and tooth enamel were used to identify diet or geographic origins of ancient humans in archeological applications (Sharp et al., 2003; Buzon et al., 2011; Lightfoot and O'Connell, 2016).

The carbon and nitrogen isotope compositions (reported as $\delta^{13}C$ and $\delta^{15}N$ values, respectively) in hair are primarily related to diet, nutritional status, and metabolic status (Mekota et al., 2006; Petzke et al., 2010). Feeding experiments have shown that dietary change could cause fluctuation of $\delta^{13}C$ and $\delta^{15}N$ profiles in hair (Cerling et al., 2007; Huelsemann et al., 2009). Despite globalization trends, there are still considerable population-wide isotope differences even between the industrialized regions like Western Europe and the United States due to heterogeneity in the food resources (Valenzuela et al., 2012). Because of the link between diet history and the $\delta^{13}C$ and $\delta^{15}N$ values in hair, archeological studies have applied the carbon and nitrogen isotope analyses of keratin samples to reveal paleodietary information (e.g., trophic level and C_3/C_4 food proportion) of ancient fauna and humans (White, 1993; Macko et al., 1999b; Thompson et al., 2005; Hedges and Reynard, 2007; White et al., 2009; Webb et al., 2013; Knudson et al., 2015). However, other studies also showed that, along with dietary habits, $\delta^{13}C$ and $\delta^{15}N$ profiles in elephant tail hair could be used to show the migration patterns of individual elephants (Cerling et al., 2006). Therefore, $\delta^{13}C$ and $\delta^{15}N$ values may be useful for the identification of the geographical movements associated with major changes in diet or health that can cause significant isotopic fluctuations.

Strontium isotope analysis is an emerging tool to identify the regions of origin of biological samples in archeology, paleoecology, and forensics (Font et al., 2012; Frei et al., 2015; Vautour et al., 2015; Chau et al., 2017; Chesson et al., 2020). It has the advantage of no detectable isotopic fractionation (of $^{87}Sr/^{86}Sr$ ratios) during biological processes, comparing to the light elements like carbon and oxygen (Bentley, 2006). Therefore, the $^{87}Sr/^{86}Sr$ ratios in tissues can be directly compared to the sources to identify the geographic origins as shown in the studies on archeological bone and enamel samples (Bentley, 2006). Studies have demonstrated the potential of using $^{87}Sr/^{86}Sr$ ratios in keratinous tissues to identify local versus non-local signal for humans (Font et al., 2012; Vautour et al., 2015), to identify migration paths and breeding sites for birds (Font et al., 2007), and to reconstruct travel history of horses (Chau et al., 2017). The $^{87}Sr/^{86}Sr$ ratios in hair samples may also be used in archeological studies to identify the travel history of buried human remains (Frei et al., 2015, 2017; Lugli et al., 2018). Similarly, the provenance of ancient textiles could be identified using strontium isotope analysis in wool (Frei et al., 2009). Cerling et al. (2018) also demonstrated that $^{87}Sr/^{86}Sr$ ratios in rhino hair are related to local geological bedrock while the $\delta^{13}C$ and $\delta^{15}N$ values are good indicators of food sources for black rhinos (*Diceros bicornis*) in Kenya. However, unlike major elements that can mostly ignore contamination influence in their isotopic profiles in hair, strontium in hair can be easily contaminated, which will alter its $^{87}Sr/^{86}Sr$ ratios (Hu et al., 2020). The co-existent endogenous and exogenous Sr in hair thus make the $^{87}Sr/^{86}Sr$ profile in hair complicated to interpret (Chesson et al., 2020).

Despite those promising studies and applications, there is still no universal criterion of using isotopes in hair to determine local versus non-local origin (Reynard et al., 2016). The isotopic variability in hair should also be considered for geolocation and dietary studies. Such limitation calls for more real-world studies on the use of the isotopic values of multiple elements in hair for a better understanding of travel history reconstruction. Here, we measured the isotopic values of multiple elements (H, C, N, and Sr) along hair strands which were collected from an individual with complex travel history. Based on the travel history, we compiled the ranges of expected isotopic variations in hair of the traveled locations from an existing isotopic database and the literature. We then used those data and a single exponential best-fit turnover model to reconstruct the expected isotopic profile for each element. We compared the predicted isotopic profiles with the measured isotopic values of the traveling individual. We conclude on the ability of different isotopic systems to provide

information about the travel history of a mobile individual at different temporal scales.

MATERIALS AND METHODS

Ethics Statement

The research procedure was approved by the Office of Research Ethics and Integrity of the University of Ottawa (Ethics File number: H10-17-10). Specifically, all sampling and analytical methods used were in accordance with relevant guidelines from the Office of Research Ethics and Integrity of the University of Ottawa. Written consents were obtained from all participants in accordance with and maintained under regulations from the Office of Research Ethics and Integrity of the University of Ottawa.

Travel History of the Volunteer

The hair sample was collected from a volunteer in on November 20, 2010. The travel history of the volunteer is shown in **Table 1**. The volunteer primarily resided in Ottawa, Canada and traveled to several distant locations during the timeframe of this study (May 2009 to November 2010). The four major trips longer than a week were (1) a trip to the Prairie provinces of Canada between June 30 and July 27, 2010; (2) a trip to Europe between May 2 and May 17, 2010; (3) a trip to Cuba between January 29 and February 5, 2010; and (4) a trip to the Eastern provinces of Canada between June 15 and July 24, 2009. **Figure 1** shows the regions of four major trips of the individual outside Ontario on a world map.

Hair Preparation

One bundle of approximately 80 hairs was provided by the volunteer to the lab. It was cut with metal scissor near the root of hair on November 20, 2010.

∼50 individual hairs were aligned by the root and were taped on weighing paper. The aligned hairs were cut every half centimeter using an in-house built cutting apparatus. The 0–0.5 cm segment was kept with the adhesive tape that was used to hold the orientation of the hair bundle. But the adhesive tape residue and the trapped dust may contaminate isotope analysis. Thus the 0–0.5 cm segment was not analyzed. 38 samples were obtained from the hair of ∼19.5 cm long. Each hair sample was washed for 15 min with gentle agitation in a 2:1 chloroform/methanol (v/v) solution to remove surface contamination (Font et al., 2012; Tipple et al., 2018). After drying, each sample was analyzed for $\delta^{13}C$, $\delta^{15}N$, and $\delta^{2}H$. An aliquot of each sample was saved for $^{87}Sr/^{86}Sr$ analysis. Sr abundance was too low for $^{87}Sr/^{86}Sr$ analysis at half-centimeter resolution. Consequently, we combined at least two 0.5 cm segments into one sample.

Isotopic Analyses of Carbon, Nitrogen, and Hydrogen

For $\delta^{13}C$ and $\delta^{15}N$ analysis, the hair segment samples and isotope standards (approximately 400 μg each) were weighed into tin capsules and loaded onto an Elemental Analyser (Vario EL III, Elementar, Germany) interfaced with a ConFlo III (Thermo, Germany) to an isotope ratio mass spectrometer (IRMS, Delta^{Plus} Advantage, Thermo, Germany). One tin capsule was analyzed for each sample. Internal standards used for calibration were a mix of ammonium sulfate and sucrose ($\delta^{13}C_{VPDB}$, −11.94‰; $\delta^{15}N_{AIR}$, 16.58‰), nicotinamide ($\delta^{13}C_{VPDB}$, −22.95‰; $\delta^{15}N_{AIR}$, 0.07‰), and caffeine ($\delta^{13}C_{VPDB}$, −28.53‰; $\delta^{15}N_{AIR}$, −3.98‰). All $\delta^{15}N$ and $\delta^{13}C$ values are reported versus AIR and V-PDB, respectively. Analytical precision is based on an internal QC sample (glutamic acid, which is not used for normalization) and is usually better than ±0.2‰ for both $\delta^{13}C$ and $\delta^{15}N$.

For $\delta^{2}H$ analysis, the hair segment samples and isotope standards (approximately 300 μg each) were weighed into silver capsules and loaded onto a Pyrolysis Elemental Analyser with a zero-blank autosampler (TC/EA, Thermo, Germany) interfaced with a ConFlo IV (Thermo, Germany) to an IRMS (Delta^{Plus} XP, Thermo, Germany). Due to exchangeable hydrogen in the cut hair samples, an exchange experiment was performed on the cut hair segments to determine the "true" $\delta^{2}H$ value, following the procedure in Meier-Augenstein et al. (2011). This procedure requires two aliquots of the same hair sample, one equilibrated in isotopically "light" water ($\delta^{2}H_{VSMOW,}$ -398‰), and the other in isotopically "heavy" water ($\delta^{2}H_{VSMOW,}$ + 15.6 ‰). The segmented hair samples were normalized to two materials with non-exchangeable H: IAEA-CH-7 ($\delta^{2}H_{VSMOW}$, −100.3‰), and an in-house kaolinite ($\delta^{2}H_{VSMOW}$, −58.0‰). Four ground human hair samples were used as QC (Meier-Augenstein et al., 2011): AND ($\delta^{2}H_{VSMOW}$, −71.6‰), COL ($\delta^{2}H_{VSMOW}$, −87.9‰), CAL/CAN ($\delta^{2}H_{VSMOW}$, −106.4‰) and CAL/SAL ($\delta^{2}H_{VSMOW}$, −101.2‰). All reported $\delta^{2}H$ values are reported to the international scale VSMOW. Analytical precision for $\delta^{2}H$ was ±2.0‰. For all $\delta^{2}H$ hair analyses, the production of HCN was not accounted for Gehre et al. (2015).

Isotopic Analysis of Strontium

All samples (approximately 2 mg each) for $^{87}Sr/^{86}Sr$ analysis were digested in 7 mL cleaned Xpress Teflon vials using a mixture of 200 μL hydrogen peroxide ≥ 30% (for trace analysis Grade; Sigma-Aldrich, Italy) and 3 mL concentrated nitric acid (HNO_3) (TraceMetal^{TM} Grade; Fisher Chemical, Canada) for 15 min at 150°C using the CEM MARS 5 Microwave Accelerated Reaction System. After digestion, the solutions were dried on a hot plate at 100°C in a laminar flow fume hood. When there is only a drop left, each vial was removed from the hotplate and the bottom of the vial was observed to check if the liquid was limpid. If there were still white particles, suggesting uncompleted digestion, further digestion was done by adding hydrogen peroxide to digest all the organic residue. If there was no more particle in the final drop of solution, 1 mL concentrated HNO_3 was added to each vial and then transferred to a 7 mL Savillex PTFE vial. An aliquot of 50 μL of the solution from each Savillex vial was pipetted to a Labcon MetalFree^{TM} centrifuge tubes and diluted with 2 mL of 2% v/v HNO_3. The diluted solution was then centrifuged for 10 min before Sr concentration analysis. Sr concentration analysis was performed by Inductively Coupled Plasma Mass Spectrometry (ICP-MS) (Agilent 8800 triple quadrupole mass spectrometer) at the Department of Earth

TABLE 1 | Travel history of the volunteer and the isotope ranges for each location and region.

Date	Place	δ^2H (‰)		$\delta^{13}C$ (‰)		$\delta^{15}N$ (‰)		$^{87}Sr/^{86}Sr$	
		Min	Max	Min	Max	Min	Max	Min	Max
2010 November 20	Hail sampling								
2010 October 9–II	Sudbury, ON, Canada	−92	−82[a]	−18.4	−17.5[a]	8.5	9.6[a]	0.7162	0.7164[b]
2010 August 20–21	Killbear Provincial Park, ON, Canada	−85	−76[a]	−18.2	−17.1[a]	9.1	9.3[a]	0.7092	0.7094[b]
2010 August 18–19	Toronto, ON, Canada	−89	−76[a]	−19.4	−17.8[a]	8.8	10.0[a]	0.7093	0.7095[b]
2010 August 15–17	Niagara Falls, ON, Canada	−84	−76[a]	−18.0	−17.9[a]	9.3	9.4[a]	0.7093	0.7095[b]
2010 June 30–July 27	Canadian Prairies (MB, SK, AB)	−114	−79[a#]	−19.6	−17.3[a#]	7.6	10.5[a#]	0.7073	0.7242[b#]
2010 June 26–28	Montreal, QC, Canada	−88	−75[a]	−19.2	−18.3[a]	8.5	9.4[d]	0.7093	0.7099[b]
2010 June 4–6	Sudbury, ON, Canada	−92	−82[a]	−18.4	−17.5[a]	8.5	9.6[d]	0.7162	0.7164[b]
2010 May 17	Vienna, Austria	−94	−73[c]	−21.6	−19.8[d]	8.0	9.6[d]	0.7090	0.7100[f]
2010 May 15–16	Zurich, Switzerland	−89	−68[c]	−21.6	−19.8[d]	8.0	9.6[d]	0.7101	0.7110[g]
2010 May 14	Basel. Switzerland	−89	−68[c]	−21.6	−19.8[d]	8.0	9.6[d]	0.7101	0.7110[g]
2010 May 12–13	Zurich, Switzerland	−89	−68[c]	−21.6	−19.8[d]	8.0	9.6[d]	0.7101	0.7110[g]
2010 May 9–11	Lyon, France	−69	−56[c]	−20.9	−19.7[d]	8.5	9.9[d]	0.7101	0.7110[g]
2010 May 2–8	Vienna, Austria	−94	−73[c]	−21.6	−19.8[d]	8.0	9.6[d]	0.7090	0.7100[f]
2010 April 30	Brighton, ON, Canada	−80	−78[a]	−17.9	−17.7[a]	9.0	9.2[a]	0.7087	0.7093[b]
2010 April 10–15	Washington, DC, United States	−94	−90[e]	−18.8	−16.4[d]	8.0	9.8[d]	0.7111	0.7113[h]
2010 January 29 – February 5	Cuba	−68	−51[c]	−19.9	−17.7[d]	8.4	10.0[d]	0.7083	0.7087[g]
2009 June 15 – July 24	Eastern Canada (PEI, NL, QC, NB, NS)	−100	−68[a#]	20.2	−16.8[a#]	8.1	10.8[a#]	0.7058	0.7291[b#]
2009 June 7	Toronto, ON, Canada	−89	−76[a]	−19.4	−17.8[a]	8.8	10.0[a]	0.7093	0.7095[b]
Other time	Ottawa, ON, Canada	−78	−75[a]	−18.6	−18.6[a]	9.2	10.2[a]	0.7126	0.7128[b]

*The estimates of isotope ranges for each location are discussed in section "Estimate isotope ranges from the Forensic Attribution Database and the literature." Data sources: [a]Ranges of stable isotope values of local residents' hair samples from CBRNE project (Chartrand and St-Jean, 2015; Bataille et al., 2020a). [b]Ranges of strontium isotope ratios of tap water samples from CBRNE project (Chartrand and St-Jean, 2015). [c]Ranges of Austria, Switzerland, France, and Cuba hair isotope values calculated from Lehn et al. (2015b) using mean value ± SD. [d]Ranges of Austria, Switzerland, France, United States, and Caribbean hair isotope values calculated from Hülsemann et al. (2015) using weighted mean value ± variance. [e]Data from graph reading of Fig.3 (hair samples) from Ehleringer et al. (2008). [f]Ranges of strontium isotope ratios of surface water samples in Marchfeld, Austria from Voerkelius et al. (2010). [g]Ranges of strontium isotope ratios of river water samples from Bataille et al. (2020b). [h]Strontium isotope ratio of the tap water sample in Washington, DC ± 0.0001 from Chesson et al. (2012). [#]Detailed daily ranges during the two trips to Canadian Prairies and Eastern Canada can be found in **Supplementary Tables S1, S2** in the **Supplementary Material**, respectively.*

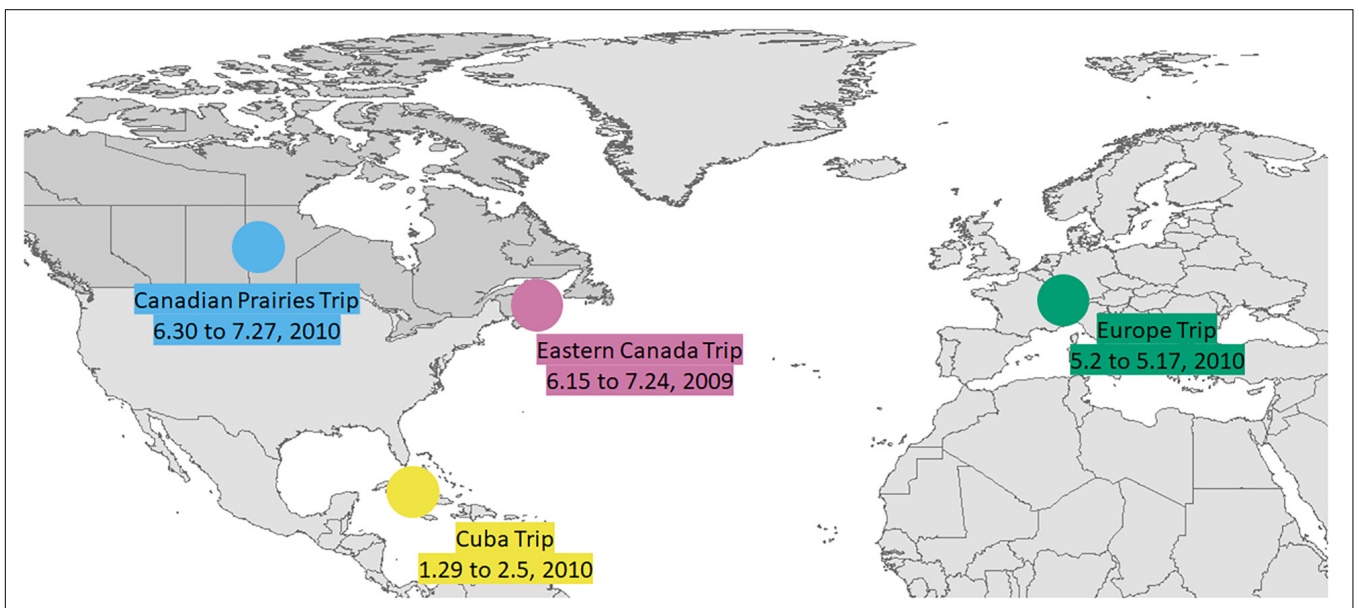

FIGURE 1 | Map showing four major trips.

and Environmental Sciences, University of Ottawa. Calibration standards were prepared using single element certified standards purchased from SCP Science (Montreal, Canada).

The remaining ∼1 mL aliquot of the sample in the 7 mL Savillex PTFE vial was dried down and re-dissolved in 1 mL 6 M HNO_3. The separation of Sr was processed in 100 μL microcolumn loaded with Sr-spec Resin^{TM} (100–150 μm; Eichrom Technologies, LLC). The matrix was rinsed out using 6 M HNO_3. The Sr was collected with 0.05 M HNO_3. After separation, the eluates were dried and re-dissolved in 200 μL 2% v/v HNO_3 for $^{87}Sr/^{86}Sr$ analysis. The $^{87}Sr/^{86}Sr$ analysis was performed at the Isotope Geochemistry and Geochronology Research Centre, Carleton University using a Thermo Scientific^{TM} Neptune^{TM} high-resolution multi-collector inductively coupled plasma mass spectrometer (MC-ICP-MS; Thermo Fisher Scientific, Bremen, Germany). Sample solutions in 2% v/v HNO_3 were introduced using a micro*FAST* MC single-loop system (Elemental Scientific). The loading volume was 200 μL and the injecting rate was 30 μL/min. The solution was aspirated using a PFA nebulizer, a double-pass quartz spray chamber, quartz torch, and nickel sample and skimmer cones. Isotopes ^{82}Kr, ^{83}Kr, ^{84}Sr, ^{85}Rb, ^{86}Sr, ^{87}Sr, and ^{88}Sr were simultaneously measured in L4, L3, L2, L1, C, H1, and H2 Faraday cups, respectively. Measurements of samples were made using a static multi-collector routine that consisted of one block of 75 cycles with an integration time of 4.194 s/cycle. ^{84}Sr and ^{86}Sr have isobaric interferences from ^{84}Kr and ^{86}Kr, respectively. ^{87}Sr has an isobaric interference from ^{87}Rb. The interferences of ^{84}Sr and ^{86}Sr were corrected by subtracting the amount of ^{84}Kr and ^{86}Kr corresponding to the ^{83}Kr signal. The interference of ^{87}Sr was corrected by subtracting the amount of ^{87}Rb corresponding to the ^{85}Rb signal. Instrumental mass fractionation was corrected by normalizing $^{86}Sr/^{88}Sr$ to 0.1194 using the exponential law. Strontium isotope compositions are reported as $^{87}Sr/^{86}Sr$ ratios. The long-term reproducibility of the $^{87}Sr/^{86}Sr$ measurement for NIST SRM987 is 0.71025 ± 0.00004 (1 SD, n = 16). A 100 ng/g pure Sr standard was measured along with the sample as the in-house standard (0.70823 ± 0.00005, 1 SD, n = 4). The long-term reproducibility of the in-house standard is (0.70822 ± 0.00004, 1 SD, n = 106).

Estimate Isotope Ranges From the Forensic Attribution Database and the Literature

We compiled the ranges of δ^2H values, $\delta^{13}C$ values, $\delta^{15}N$ values, and $^{87}Sr/^{86}Sr$ ratios of each location from our database, the Forensic Attribution Database (FAD; Chartrand and St-Jean, 2015; Bataille et al., 2020a), completed by literature data (**Table 1**). The FAD gathers isotope data in hair from 600 Canadian hair donors and tap water samples collected across Canada (Chartrand and St-Jean, 2015; Bataille et al., 2020a). In this study, we compiled those isotopic ranges from hair samples of the locations (or the nearest locations) visited by our volunteer from May 1, 2009 to Nov 20, 2010.

We estimated the isotopic ranges of H, C, and N in Canadian locations from the hair samples in the FAD. To estimate the isotopic ranges of H, C, and N in the locations visited in Europe, Cuba, and the United States, we used existing compilations of isotope data for hair (Ehleringer et al., 2008; Hülsemann et al., 2015; Lehn et al., 2015b) (**Table 1**).

For Sr, we have not yet measured the $^{87}Sr/^{86}Sr$ of the hair samples in the FAD. Data from the literature are also too sparse to characterize the $^{87}Sr/^{86}Sr$ of the traveled locations either. Therefore, we cannot directly estimate the range of hair $^{87}Sr/^{86}Sr$ for the studied individual. Theoretically, we could use the $^{87}Sr/^{86}Sr$ range of local food to estimate the possible $^{87}Sr/^{86}Sr$ profile, considering more than 90% of Sr in mammal's body is from food (Lewis et al., 2017). However, because of the complexity of the modern supermarket diet, it is almost impossible to compile the $^{87}Sr/^{86}Sr$ ranges of local foods from all traveled locations. As previous studies have shown that the hair samples usually have the same $^{87}Sr/^{86}Sr$ as the local tap water (Tipple et al., 2019; Ammer et al., 2020), we chose the $^{87}Sr/^{86}Sr$ ratios of the tap water samples in the FAD (Chartrand and St-Jean, 2015) and the river or tap water samples in the literature (Voerkelius et al., 2010; Chesson et al., 2012; Bataille et al., 2020b) to estimate the range of hair $^{87}Sr/^{86}Sr$ for the studied individual. The assumption behind such estimation, that the $^{87}Sr/^{86}Sr$ profile in hair followed the $^{87}Sr/^{86}Sr$ of the local water, is not ideal, but it is the best we can do in this study.

The isotopic ranges compiled in **Table 1** are unlikely to cover the entire range of isotopic variability at each of the visited locations but they provided a strong empirical basis to approximate these values.

Isotopic Profile Prediction Based on Travel History

In this study, we know both the travel history of the studied individual and the ranges of the isotopic values of hair samples from local residents at each traveling location (**Table 1**). We aim to use those data to reconstruct the expected isotopic variations in the hair of the traveling individual. One issue, however, is that the stable isotope signal of the newly grown hair segment does not reflect 100% of the local foods and drinks, because there are different metabolic pools with different turnover rates. For example, Ayliffe et al. (2004) found that, following a dietary change from C3 to C4 food, ∼41% of carbon isotope signal of the horse tail hair was from a pool (probably from the new diet) with a very fast turnover rate (half-life of ∼0.5 days), ∼15% from a pool with an intermediate turnover rate (half-life of ∼4 days), and ∼44% from a pool with very slow turnover rate (half-life of ∼140 days). In our case study, as an individual moves on the landscape, the isotopic composition of the diet is constantly changing, which complicates the reconstruction of the expected isotopic variations in the hair profile.

Several methods can be used to account for isotope turnover in hair. Traditionally, researchers used a single exponential best-fit model to describe isotope turnover in biological tissues (Podlesak et al., 2005). Since fitting data to an exponential function cannot ascertain the possibility of multiple turnover pools, Cerling et al. (2007) introduced the reaction progress model to determine the turnover rate. It has been shown that some elements have

multiple turnover pools in the body, and their isotopic profiles in hair can be better reconstructed with a reaction progress model (Cerling et al., 2007; Podlesak et al., 2008). However, constructing a multiple-pool model requires a highly controlled feeding experiment and high-resolution isotopic analysis of hair to calibrate the parameters. As far as we know, there has not been such a feeding experiment on human beings. In this study, we do not have sufficiently accurate dietary and metabolic information to calibrate this type of multiple pool model. In addition, the temporal resolution in this study (∼2 weeks for hydrogen, carbon, nitrogen and ∼4 weeks for strontium) was much less precise than the dietary studies with short sampling interval (∼1 day or less) (e.g., Cerling et al., 2007). Lastly, because we were looking at a bundle of hairs growing at different rates and different phases (LeBeau et al., 2011), it can lead to further noise in the turnover rate modeling, which we cannot address in our model. Therefore, we assume that a single exponential best-fit model is a good-enough first-order approximation to predict isotopic variations in the hair profile. We represented isotope turnover time using the following equation of an exponential decay function (Cerling et al., 2007):

$$\frac{\delta_A^t - \delta_A^{eq}}{\delta_A^{init} - \delta_A^{eq}} = e^{-\lambda t}$$

where δ_A^{init}, δ_A^{eq}, and δ_A^t are the δ-values of element A at the initial time (t = 0), at equilibrium (t = infinity), and at time t, respectively. We calculated the λ value for this equation using existing data from the literature for hydrogen isotopes (Ehleringer et al., 2008) and we obtain a λ value of 0.04 day $^{-1}$ (half-life of 17.3 days), which was comparable to the first-stage 19 days half-life measured on woodrats (*Neotoma cinerea*) hair (Podlesak et al., 2008). We use this calibrated λ value for all the isotopic systems used in this study. While it is likely that different elements have different λ values, changing the λ value within a reasonable range has little influence on the general pattern and the interpretation of the isotopic profiles. Please see the sensitivity analysis in the **Supplementary Material** for more information.

Once calibrated, we used this λ value and the isotope forensic attribution database to reconstruct the isotopic variations in the hair through time. We use the following equation to calculate the expected isotope variations in the hair of the traveling individual at daily resolution:

$$\frac{\delta_{\text{hair predicted}}^{\text{day (n)}} - \delta_{\text{local value}}^{\text{day (n)}}}{\delta_{\text{local value}}^{\text{day (n−1)}} - \delta_{\text{local value}}^{\text{day (n)}}} = e^{-\lambda \cdot (1\ \text{day})}$$

where δ is the isotopic value of hydrogen (δ^2H), carbon (δ^{13}C), or nitrogen (δ^{15}N).

For ^{87}Sr/^{86}Sr ratios, this equation becomes:

$$\frac{R_{\text{hair predicted}}^{\text{day (n)}} - R_{\text{local value}}^{\text{day (n)}}}{R_{\text{local value}}^{\text{day (n−1)}} - R_{\text{local value}}^{\text{day (n)}}} = e^{-\lambda \cdot (1\ \text{day})}$$

where R is the isotopic ratio of strontium, ^{87}Sr/^{86}Sr. As discussed in the last section, we did not have the ranges of hair ^{87}Sr/^{86}Sr in the traveled locations. We predicted the hair ^{87}Sr/^{86}Sr profile using the ranges of ^{87}Sr/^{86}Sr of tap water or river water samples in the traveled locations. The impact of such approach is evaluated in the discussion.

The minimum and maximum of isotopic values for every day is calculated from May 1, 2009 to Nov 20, 2010.

RESULTS

Stable Isotope Compositions Along the Hair Profile

The δ^2H, δ^{13}C, and δ^{15}N values of the hair segments are shown in **Table 2**. The δ^2H values in the hair ranged from −85 to −75‰. Except for four hair segments between A8 (Sample ID) and A11, the majority of the segments fall between −80 to −75‰. The δ^{13}C values in the hair ranged from −18.4 to −17.0‰. While most of the δ^{13}C values of the segments from A10 to A38 were relatively stable, the δ^{13}C value of the segment A16 was much lower (−18.4‰) than the rest of the hair. The δ^{13}C values of the segments from A1 to A9 were higher than the rest of the hair. The δ^{15}N values in the hair ranged from 8.8 to 11.9 ‰. The first 13 cm of the hair (from A1 to A26) had a relatively narrow range of δ^{15}N values (9.6–10.1‰) except for the segment A1 (10.5‰), A22 (10.5‰), and A25 (10.4‰), which contained slightly higher δ^{15}N values. The remaining hair (A27–A38) had a much larger variation of δ^{15}N value (**Table 2**).

Strontium Isotope Composition Along the Hair Profile

The Sr concentrations ([Sr]) and isotopic ratios (^{87}Sr/^{86}Sr) of the hair segments are shown in **Table 3**. The [Sr] increases from the root to the tip of the hair from 1.6 mg/kg to 12.4 mg/kg. The ^{87}Sr/^{86}Sr ratios in the segments range from 0.7110 to 0.7119. The segment B10 was lost during the isotope analysis and is thus not reported. The first two segments (B1 and B2) had lower ^{87}Sr/^{86}Sr ratios than all other segments.

Determining the Age Model of the Observed Isotopic Profiles

A prerequisite prior to comparing the observed and modeled hair isotopic profiles is to convert hair length into time. Hair growth rate can vary a lot among individuals. The average growth rate of human scalp hair is about 1 cm/month but can range from 0.6 to 2.2 cm/month (Pötsch, 1996). As it is difficult to determine the growth rate of an individual after hair collection, we matched the most prominent δ^2H peaks between the observed and predicted hair profiles. We found a growth rate of 1.5 cm per 30 days provided the best fit between observed and predicted peaks for δ^2H values but also for δ^{13}C values. However, the growth rate chosen in this study may not be suitable for other studies. We also added 0.8 cm to the distance of the hair segment to the hair root (**Tables 2**, **3**) to make up the ∼0.5 cm of hair remaining at the scalp during cutting (LeBeau et al., 2011; Lehn et al., 2019) and ∼0.3 cm of hair residue left in the hair follicle (Jimenez et al., 2011). The "distance from hair root" is then used

TABLE 2 | Stable isotope values of hair segments.

Sample ID	Hair segment (distance from cutting end)	Distance from hair root (cm)*	$\delta^{2}H$ (‰)	$\delta^{13}C$ (‰)	$\delta^{15}N$ (‰)
A1	0.5–1 cm	1.55 (0.75 + 0.8)		−17.5	10.5
A2	1–1.5 cm	2.05	−77	−17.3	10.0
A3	1.5–2 cm	2.55	−77	−17.4	9.8
A4	2–2.5 cm	3.05	−78	−17.3	10.0
A5	2.5–3 cm	3.55	−78	−17.1	9.7
A6	3–3.5 cm	4.05	−78	−17.2	9.9
A7	3.5–4 cm	4.55	−79	−17.0	9.8
A8	4–4.5 cm	5.05	−81	−17.0	9.7
A9	4.5–5 cm	5.55	−84	−17.3	9.7
A10	5–5.5 cm	6.05	−85	−17.7	9.9
A11	5.5–6 cm	6.55	−81	−17.7	10.0
A12	6–6.5 cm	7.05	−78	−17.5	9.8
A13	6.5–7 cm	7.55	−77	−17.6	10.0
A14	7–7.5 cm	8.05	−77	−17.6	9.9
A15	7.5–8 cm	8.55	−78	−17.8	9.7
A16	8–8.5 cm	9.05	−76	−18.4	9.8
A17	8.5–9 cm	9.55	−78	−17.9	9.6
A18	9–9.5 cm	10.05	−79	−17.7	9.7
A19	9.5–10 cm	10.55	−79	−17.8	10.1
A20	10–10.5 cm	11.05	−79	−17.7	9.7
A21	10.5–11 cm	11.55	−77	−17.8	9.6
A22	11–11.5 cm	12.05	−76	−17.9	10.5
A23	11.5–12 cm	12.55	−77	−18.0	10.0
A24	12–12.5 cm	13.05	−77	−17.9	9.8
A25	12.5–13 cm	13.55	−77	−18.0	10.4
A26	13–13.5 cm	14.05	−75	−18.0	10.1
A27	13.5–14 cm	14.55	−76	−17.9	11.9
A28	14–14.5 cm	15.05	−76	−17.9	9.9
A29	14.5–15 cm	15.55	−77	−17.9	11.0
A30	15–15.5 cm	16.05	−78	−17.9	9.6
A31	15.5–16 cm	16.55	−77	−17.9	9.8
A32	16–16.5 cm	17.05	−78	−17.8	9.6
A33	16.5–17 cm	17.55	−80	−17.9	8.9
A34	17–17.5 cm	18.05	−79	−17.9	9.1
A35	17.5–18 cm	18.55	−80	−17.8	9.7
A36	18–18.5 cm	19.05	−80	−17.9	8.8
A37	18.5–19 cm	19.55	−80	−17.5	9.0
A38	19–19.5 cm	20.05	−78	−17.6	10.0

**"Distance from hair root" equals the "distance from cutting end" plus 0.8 cm, which accounts for the distance between the cutting end and the root (discussion in the section "Determining the age model of the observed isotopic profiles").*

for the comparison between the measured and the predicted isotope profiles.

DISCUSSION

Uncertainty of Intra-Individual Hair Growth Rate

In this study, we used a bundle of hair to measure isotopic variations in the hair profile of the volunteer. As mentioned above, we assumed that all hair in the bundle had a constant growth rate of 1.5 cm per 30 days. In reality, scalp hairs of the same individual have different growth rates as well as different growth phases (Hayashi et al., 1991; LeBeau et al., 2011). The isotopic variability measured on multiple hairs will become progressively attenuated due to the mixing of hair segments from slightly different life periods. This issue was underlined by Remien et al. (2014) who compared the isotopic signal measured in a single hair with that of multiple hairs and found that the signal was progressively blurred and difficult to use for provenance applications. Consequently, in our study, the isotopic variations identified close to the base of the hair are likely more representative of the true isotopic variability of the water or diet. Isotopic variations identified in the distal portion of the hair have larger uncertainty in terms of timing and amplitude.

TABLE 3 | [Sr] and $^{87}Sr/^{86}Sr$ ratios in hair segments.

Sample ID	Hair segment (distance from cutting end)	Distance from hair root (cm)*	[Sr] (mg/kg)	$^{87}Sr/^{86}Sr$		2 SD
B1	0.5–1.5 cm	1.8 (1 + 0.8)	1.6	0.7110	±	0.0002
B2	1.5–2.5 cm	2.8	2.0	0.7112	±	0.0002
B3	2.5–3.5 cm	3.8	2.1	0.7117	±	0.0002
B4	3.5–4.5 cm	4.8	3.9	0.7116	±	0.0001
B5	4.5–5.5 cm	5.8	2.7	0.7116	±	0.0001
B6	5.5–6.5 cm	6.8	4.8	0.7116	±	0.0001
B7	6.5–7.5 cm	7.8	5.9	0.7114	±	0.0001
B8	7.5–8.5 cm	8.8	5.4	0.7117	±	0.0001
B9	8.5–9.5 cm	9.8	6.5	0.7115	±	0.0001
B10	9.5–10.5 cm	10.8	6.9			
B11	10.5–11.5 cm	11.8	5.6	0.7119	±	0.0001
B12	11.5–12.5 cm	12.8	7.3	0.7116	±	0.0001
B13	12.5–13.5 cm	13.8	7.9	0.7117	±	0.0001
B14	13.5–14.5 cm	14.8	9.9	0.7114	±	0.0001
B15	14.5–15.5 cm	15.8	7.7	0.7115	±	0.0001
B16	15.5–16.5 cm	16.8	11.3	0.7115	±	0.0001
B17	16.5–17.5 cm	17.8	11.6	0.7115	±	0.0001
B18	17.5–19 cm	19.05	12.4	0.7113	±	0.0001

*"Distance from hair root" equals the "distance from cutting end" plus 0.8 cm, which accounts for the distance between the cutting end and the root (discussion in the section "Determining the age model of the observed isotopic profiles").

Interestingly, Lehn et al. (2019) have found that the change of isotope signal on bundled hair profile is usually provoked by the fastest-growing hairs in the hair bundle because those fast-growing single hairs tend to be thicker and heavier thus their isotopic signals outweigh the others. Considering a commonly used mean hair growth rate of 1.1 cm/month and a proposed ± 30% intra-individual variability in single hair growth rate, they found that the growth rate of 1.4 cm per 30 days may be the best approach to calculate the exact dates of the isotopic shifts along the hair profile. Therefore, although our chosen value of 1.5 cm per 30 days is the best estimate for the hair growth rate that was used to interpret the isotope profiles, it is likely to represent the fastest growth rate, instead of the average hair growth rate, of the studied individual. Lehn et al. (2019) included the uncertainty of intra-individual hair growth rate in their calculation for the expected $\delta^{13}C$ values along the hair strands. In this study, we calculate the predicted isotope values using a fixed growth rate and discuss the impact of the uncertainty of growth rate on our results in the following section.

Comparing the Predicted Isotopic Profile and the Measured Isotopic Values of Hydrogen

The majority of the measured δ^2H values in the hair profile of the individual falls within a tight range between −75 and −78‰ (**Figure 2**). Those values are within the range of observed δ^2H values for human hair in the Ottawa region (**Table 1**). This relatively constant isotopic composition is found during periods when the volunteer was residing in the Ottawa region. This limited variability demonstrates that in the absence of large movements the δ^2H values remain relatively stable and are within the expected range from the city.

We observed a major shift in δ^2H values between July and September 2010 (**Figure 2**). This shift matches well with the predicted isotopic variations and corresponds to the 4 weeks long road trip to the Prairie provinces (Manitoba, Saskatchewan, and Alberta). The Prairie provinces are located inland in comparison with Ottawa, and tap waters in those regions have much lower δ^2H values (Bowen, 2010). As the δ^2H value in hair mostly (∼80%) reflects the food (Topalov et al., 2019), the remarkably low δ^2H value (as low as −114‰) in the hair of Prairie residents (**Table 1**) indicates a distinctly low δ^2H signal in the local diet. As the volunteer ate local food and drank local water this isotopic difference is transmitted to the hair. We notice that the amplitude of the observed δ^2H shift is slightly attenuated in comparison with the predicted values (**Figure 2**) which likely reflects signal attenuation associated with combining multiple strands of hair.

The volunteer also traveled to central Europe in May 2010 for 17 days and this trip is reflected in the measured isotopic profile. The volunteer traveled to Washington, DC for 6 days during mid-April 2010. Because of the distinct low δ^2H values in Washington, DC (−94 to −90‰) compared to Ottawa (**Table 1**), a sharp negative shift of δ^2H value is shown in the predicted profile. A similar negative shift of δ^2H is shown in the measured profile near 11–12 cm from the hair root (**Figure 2**), which is about 2 weeks earlier than the April shift in the predicted profile. As mentioned above, signals of the hair bundle distant from the hair root will be attenuated, and their timing will be more uncertain due to the differential growth rate of hair (Hayashi et al., 1991; LeBeau et al., 2011; Remien et al., 2014).

The volunteer traveled to Cuba for 7 days in January and February 2010. This trip is associated with a prominent positive

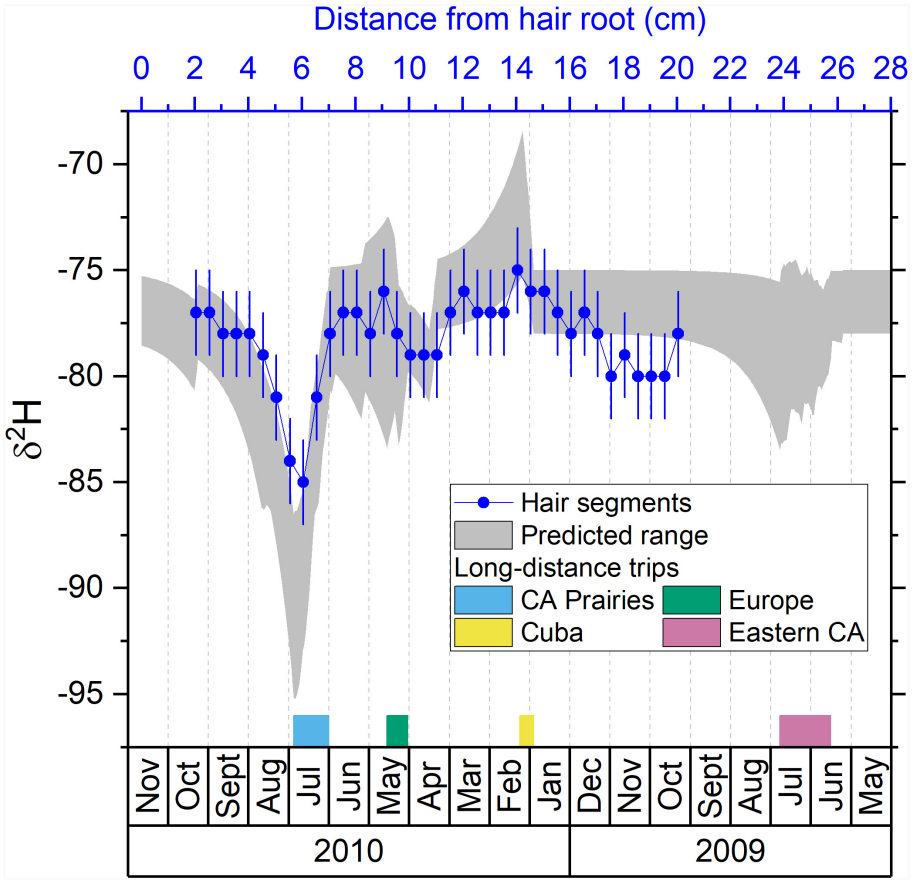

FIGURE 2 | Comparison between the predicted isotopic profile and the measured isotopic values in hair segments for hydrogen. Blue dots are the measured δ^2H values in hair segments versus their distances from the hair root **(top axis)**. The shaded area is the predicted range of δ^2H values in hair versus the date **(bottom axis)**. The periods of the four major trips are marked with colored bars next to the bottom axis.

shift in δ^2H values in the predicted profile but only a small increase in the observed profile (**Figure 2**). The amplitude of the measured isotopic signal is attenuated in comparison with the predicted values. However, the increase of the lower limit of the predicted δ^2H profile during the Cuba trip was not as prominent as its upper limit, allowing the possibility of a small increase of the observed δ^2H values in hair. We note that signals found in bundle hair > 10 cm can still provide some indication of travel.

During summer 2009, the volunteer traveled to the Eastern provinces (New Brunswick, Newfoundland and Labrador, Nova Scotia, Prince Edward Island, and Quebec) for about 40 days. The Eastern provinces have lower δ^2H values than Ottawa as reflected by the predicted δ^2H values. The measured δ^2H values progressively decrease toward the Eastern isotopic values. However, such decrease is longer and does not match well with the timing of travel as shown in the predicted profile (**Figure 2**). This signal in distal part of hair has a high uncertainty in terms of timing (Lehn et al., 2019) and thus is probably highly attenuated by the isotopic signal from Ottawa.

As the turnover rate was calculated based on the measured δ^2H values in hair from Ehleringer et al. (2008), the pattern matching of δ^2H profiles seems to be the best among all four isotopic systems in this study. The trip to the Prairie provinces significantly decreased the δ^2H values by about 10 ‰, which is shown in both measured and predicted profiles (**Figure 2**). The increase around January and February 2010 during Cuba trip and the decrease around March and April in 2010 during the Washington DC trip are also shown in both profiles. This suggests that hydrogen isotope analysis of hair may be helpful to reconstruct the travel history of highly mobile individuals for forensic applications of modern fauna and human, when the traveled locations have distinct δ^2H values (Ehleringer et al., 2008; Mant et al., 2016).

When using a hair bundle, quantitative geolocation is possible for an isotopic signal located close to the base of the hair (<10 cm). For isotopic signal located in a more distal portion of the hair, we suggest that only qualitative interpretation of travel can be provided as the timing and attenuation become significant issues. As the forward hair bundle model in Remien et al. (2014) shows and the isotope data along human hair strands in Lehn et al. (2019) show, the uncertainty of timing in the distal portion of hair can be ±2 months or more. Keratinous tissues can be preserved for thousands of years, however, using δ^2H values in archeological samples requires additional caution as δ^2H values

may be altered by exchanging hydrogen with the depositional environment (e.g., Saul, 2017; Kootker et al., 2020).

Comparing the Predicted Isotopic Profile and the Measured Isotopic Values of Carbon

The majority of the measured $\delta^{13}C$ values in the hair profile of the individual falls within a tight range between −18 to −17.5‰, except for the segment A16 and the segments A2–A9 (**Table 2**). Interestingly, none of the measured $\delta^{13}C$ values falls inside the predicted profile, although the measured and predicted profiles share very similar patterns (**Figure 3**). There is a relatively constant 1.5‰ offset between the measured and predicted $\delta^{13}C$ profiles. For example, during the time of October to December 2009 when the volunteer stayed at Ottawa, the measured $\delta^{13}C$ was around −17.9‰ compared with the Ottawa local range of −18.9 to −18.6‰ (**Table 1**). Such offset demonstrates the existence of individual variability of hair $\delta^{13}C$ values from the local ranges, which may be caused by personal dietary preference (Hobson and Clark, 1992; Mekota et al., 2006; Petzke et al., 2010). The high $\delta^{13}C$ values in the hair of this study may indicate a higher intake of animal or marine-based protein in the diet. Such discrepancy between measured and predicted individual value suggests that the absolute $\delta^{13}C$ values in hair are unreliable to identify local versus non-local samples because $\delta^{13}C$ values in hair can be largely influenced by individual preferences of certain foods or special diets. However, the strong correspondence between the measured and predicted profiles also suggest that $\delta^{13}C$ values are useful to assess mobility. For example, the large, negative excursion in $\delta^{13}C$ values in the predicted profile associated with the trip to Europe in May 2010 matches well with the negative shift of the measured profile in the hair segment A16 (**Table 2** and **Figure 3**). The difference in $\delta^{13}C$ values in food consumed in Europe and North America is well-established (Valenzuela et al., 2012; Hülsemann et al., 2015). Foods in North America, including livestock, tend to have much higher $\delta^{13}C$ values than those of Europe because of the higher proportion of C_4 plant such as corn or cane sugar (with higher $\delta^{13}C$ value) within food systems. In Europe, livestock are primarily fed with C_3 plants (with lower $\delta^{13}C$ value) and the lower $\delta^{13}C$ baseline of food system propagate within the population (Valenzuela et al., 2012; Hülsemann et al., 2015). Movement from the US to Europe usually leads to a significant decrease of $\delta^{13}C$ value in hair (McCullagh et al., 2005). Therefore, the negative shifts of $\delta^{13}C$ value in both the measured and the predicted profile of the volunteer correspond to a change in the isotopic baseline values in food consumed during the trip to Europe in May 2010.

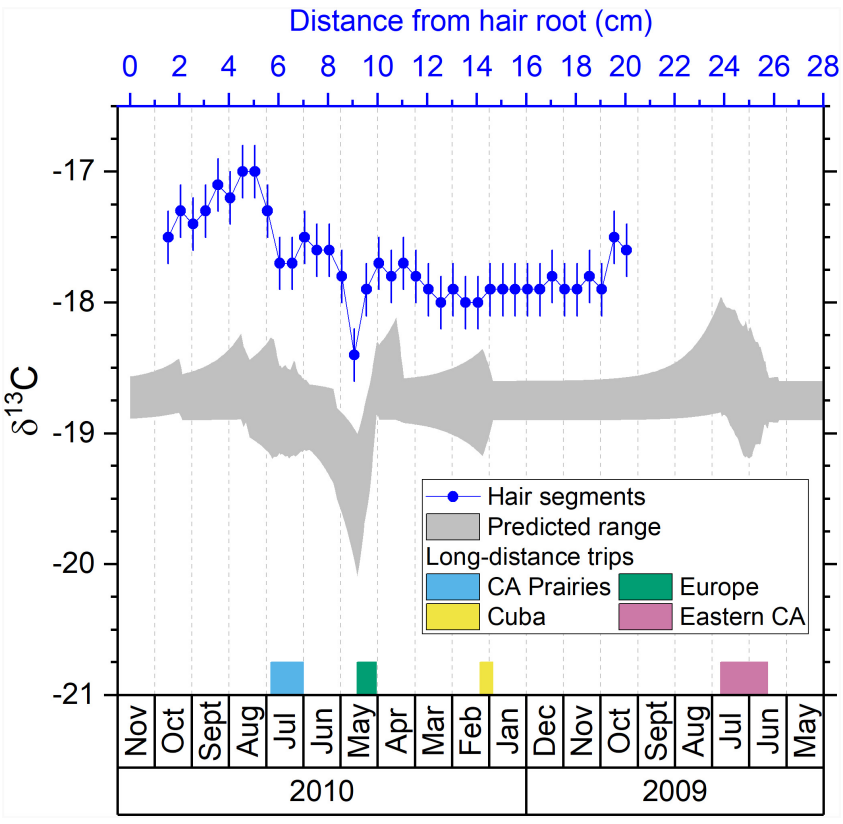

FIGURE 3 | Comparison between the predicted isotopic profile and the measured isotopic values in hair segments for carbon. Blue dots are the measured $\delta^{13}C$ values in hair segments versus their distances from the hair root **(top axis)**. The shaded area is the predicted range of $\delta^{13}C$ values in hair versus the date **(bottom axis)**. The periods of the four major trips are marked with colored bars next to the bottom axis.

While the European trip is easily identifiable in the measured and predicted $\delta^{13}C$ profiles, other multi-week trips show some significant variations. The trip to the Prairie provinces between June and July 2010 is associated with a negative shift of measured $\delta^{13}C$ values around 6–7 cm in the hair (A10–A11) (**Figure 3**) as some locations in the Prairie provinces have as low as −19.6‰ of the $\delta^{13}C$ value (**Supplementary Table S1**), lower than the Ottawa range (−18.9 to −18.6‰) (**Table 1**). Again, this difference is associated with different isotopic baseline in food systems with western provinces growing and incorporating more C_3 crops. For this trip to western provinces, the amplitude of the shift in $\delta^{13}C$ values is less marked than the shift of $\delta^{2}H$ values (**Figure 2**). However, the combined use of $\delta^{13}C$ and $\delta^{2}H$ values can strongly help constrain the location of travel within Canada. The trip to Cuba in early 2010 did not cause significant fluctuation of $\delta^{13}C$ values in the measured or predicted profile because the $\delta^{13}C$ values in Cuba, although wider range, have similar average value as Ottawa (**Table 1**). There is an increase in $\delta^{13}C$ values observed in the last two segments toward the tip of the volunteer's hair which likely correspond to the trip to the Eastern provinces as shown in the predicted profile (**Figure 3**). As observed for $\delta^{2}H$ value, there is a mismatch between the timing of the observed and predicted shifts for the trip to Eastern provinces because those isotopic signals are located in the distal portion of the hair.

There is also an increase of measured $\delta^{13}C$ value in the hair segments A2–A9 (**Table 2**), which is not predicted by the model (**Figure 3**). This increase of measured $\delta^{13}C$ values might be related to a change in dietary habit of the volunteer which was not recorded in our study. Another possible reason for the increase of measured $\delta^{13}C$ value is that the volunteer took a series of short trips to southern Ontario during that period (Niagara Falls, Toronto, and Killbear Provincial Park in August, and Sudbury in October 2010) where the $\delta^{13}C$ values can be much higher (−17.1‰) than Ottawa (−18.9 to −18.6‰) (**Table 1**). The predicted profile did not show an increasing $\delta^{13}C$ value associated with those trips because they were too short to cause a significant shift in the predicted profile. Adoption of a more accurate hair growth model like the reaction progress model (Cerling et al., 2007) might improve the prediction and reduce such discrepancy between the measured and the predicted profiles.

We suggest that while $\delta^{13}C$ values in hair likely respond to dietary preferences, they can provide further geolocation constraints for modern individuals. For example, the $\delta^{13}C$ and $\delta^{15}N$ values of human hair were used to identify the recent migrants in a rural community in SW England (Bol et al., 2007), and could also be used, along with collagen samples, to identify the migrants from Ireland to 19th century London during the Great Irish Famine (1845–1852) (Beaumont et al., 2013). As the isotopic $\delta^{13}C$ baseline from different countries and regions become well established (Hülsemann et al., 2015), we suggest that $\delta^{13}C$ value could be added to provide a qualitative assessment of mobility and constrain $\delta^{2}H$ values. Similar applications could be envisioned for archeological applications as far as the $\delta^{13}C$ variations in food systems of different regions at the studied time are established. Early studies have shown that the ancient mummies from different locations (Egypt, Chile, and Oetztaler Alps) have different $\delta^{13}C$ and $\delta^{15}N$ values in hair likely due to dietary differences of C_3 and C_4 food as a carbon source, and marine food as a nitrogen source (Macko et al., 1999a,b). A later study demonstrated the use of $\delta^{13}C$ and $\delta^{15}N$ values in archeological human hairs from Northern Chile to reconstruct the travel history of the individual moving between the coast and highlands (Knudson et al., 2012). Paleomobility studies would thus be further benefited from the $\delta^{13}C$ hair analysis if the paleo-isoscape of food sources (e.g., $\delta^{13}C$ variation due to C_3/C_4 proportion) could be established like the modern isoscapes (West et al., 2010).

Comparing the Predicted Isotopic Profile and the Measured Isotopic Values of Nitrogen

The predicted $\delta^{15}N$ profile has little fluctuation (**Figure 4**) despite the long-distance travel of the volunteer. The majority of the measured $\delta^{15}N$ values in the hair profile of the individual falls within a tight range of 9.5–10.25‰ (**Figure 4**). These values are in the upper range of other Canadians in the FAD (Chartrand and St-Jean, 2015; Bataille et al., 2020a), suggesting, as $\delta^{13}C$ values do, that our volunteer had a specific diet, possibly high intake of animal or marine-based protein (O'Connell and Hedges, 1999; Petzke et al., 2005b, 2010). Most of the values are within the predicted range except for a few outliers. The segment A1 has a $\delta^{15}N$ value of 10.5‰ (**Table 2**), slightly higher than the upper limit of the predicted range (**Figure 4**), which might reflect a change of nutritional or metabolic status of the individual (Mekota et al., 2006; Petzke et al., 2010). We can also see several outliers in the hair segments A22–A29, with the highest $\delta^{15}N$ value of 11.9‰ in the segment A27 (**Table 2** and **Figure 4**).

Studies have shown that $\delta^{15}N$ value in hair can be affected by both diet and nutritional stress (O'Connell and Hedges, 1999; Fuller et al., 2005; Mekota et al., 2006; Petzke et al., 2005a, 2010). Therefore, the drastic change of $\delta^{15}N$ value measured in the segment A27 and A29 of the volunteer's hair might be related to a severe illness reported by the volunteer during and post Cuba trip. This disease could have led to metabolic stress causing a change of nutritional stress or diet, as reported by the volunteer. However, the timing of the $\delta^{15}N$ excursions in the measured profile does not match exactly the timing of the Cuba trip: one of the $\delta^{15}N$ excursion (A29) occurs a month before the Cuba trip (**Figure 4**). As discussed before, it is possible that because these isotopic signals are located in the distal portion of the hair, their timing are more uncertain. We also notice some rapid $\delta^{15}N$ fluctuations (8.8–9.7‰) in the hair segments A33–A37 (**Table 2** and **Figure 4**). These variations do not match any travel and are likely influence by physiological or dietary factors.

In general, $\delta^{15}N$ value in hair may not be a good tool to identify geographical movements because of its geographical invariability. $\delta^{15}N$ values mainly depend on the protein source in the individual's diet. As evidenced by previous studies, $\delta^{15}N$ value in hair can be potentially a powerful tool to identify the change of diet, nutritional stress, or metabolic status of the subject

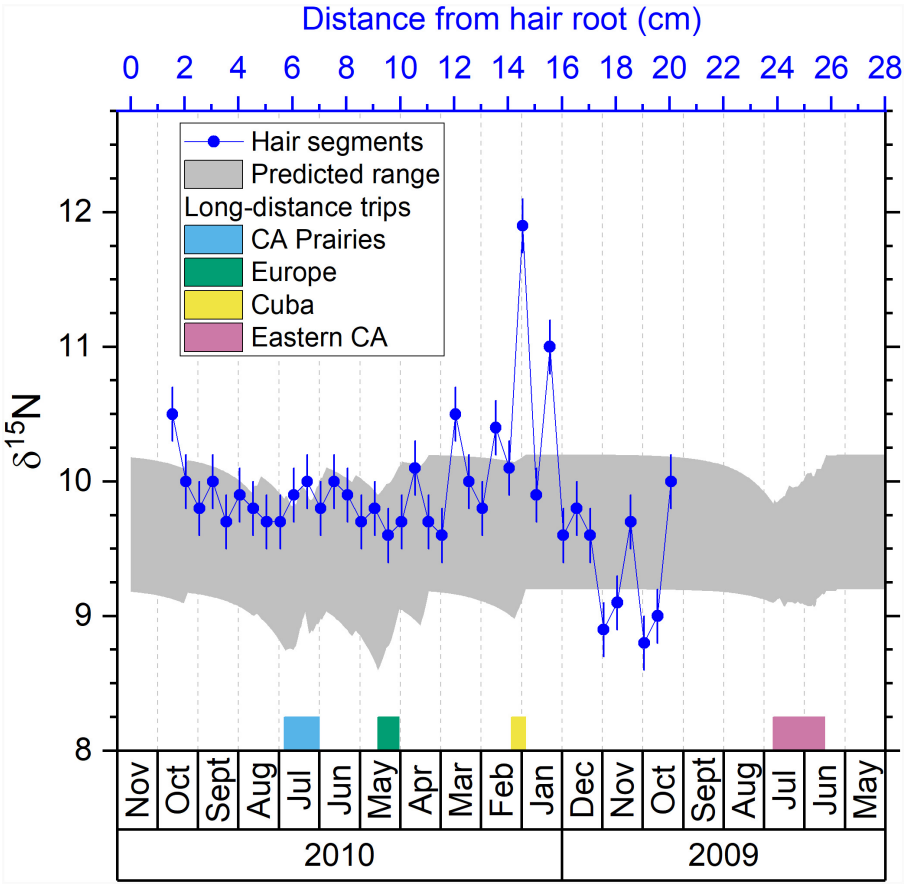

FIGURE 4 | Comparison between the predicted isotopic profile and the measured isotopic values in hair segments for nitrogen. Blue dots are the measured $\delta^{15}N$ values in hair segments versus their distances from the hair root **(top axis)**. The shaded area is the predicted range of $\delta^{15}N$ values in hair versus the date **(bottom axis)**. The periods of the four major trips are marked with colored bars next to the bottom axis.

(Fuller et al., 2004, 2005; Mekota et al., 2006; Huelsemann et al., 2009; Petzke et al., 2010).

Comparing the Predicted Isotopic Profile and the Measured Isotopic Values of Strontium

Previous studies demonstrated that the $^{87}Sr/^{86}Sr$ ratios in hair are strongly related to the $^{87}Sr/^{86}Sr$ ratio of local tap water (Tipple et al., 2018, 2019; Ammer et al., 2020). If the hair of the volunteer recorded the $^{87}Sr/^{86}Sr$ ratios of tap water at traveled locations by drinking the tap water and incorporating its $^{87}Sr/^{86}Sr$ ratio into hair through the bloodstream like the light stable isotope systems, we would expect large $^{87}Sr/^{86}Sr$ variations throughout the predicted profile shown in **Figure 5**. However, the measured $^{87}Sr/^{86}Sr$ ratios display a low range of $^{87}Sr/^{86}Sr$ variations remaining around 0.7115 (0.7110–0.7119) which is much smaller than the expected range from the predicted profile (0.7100–0.7143) (**Figure 5**). A possible explanation for this discrepancy is that Sr in hair has a much long turnover time than hydrogen isotopes used to calibrate the hair age model (Cohn et al., 1962; Kitchings et al., 1976). A more likely reason is that hair incorporates Sr from tap water through surface contamination during bathing or showering instead of drinking (Tipple et al., 2018; Hu et al., 2020). As shown in previous studies, exogenous Sr can be rapidly incorporated into hair keratin after the eruption from the scalp (Chittleborough, 1980; Kempson and Lombi, 2011), and the $^{87}Sr/^{86}Sr$ ratios in human keratinous tissues can rapidly inherit the $^{87}Sr/^{86}Sr$ of bathing or showering water (Mancuso and Ehleringer, 2018; Tipple et al., 2018; Hu et al., 2020). Therefore, we would expect the $^{87}Sr/^{86}Sr$ ratios in the hair of the volunteer to incorporate exogenous Sr from the last location where the volunteer resided and/or from the location where the volunteer resided the longest (Hu et al., 2018, 2020; Tipple et al., 2018, 2019). Indeed, the $^{87}Sr/^{86}Sr$ ratios in the hair of the volunteer (0.7110–0.7119) fall close to the $^{87}Sr/^{86}Sr$ ratios of tap water in Ottawa, the last city where the volunteer resided (0.7126–0.7128) (**Table 1**). The slight difference between measured $^{87}Sr/^{86}Sr$ ratios in hair and that of Ottawa tap water may reflect seasonal variations of the $^{87}Sr/^{86}Sr$ ratio in tap water originated from the Ottawa river, with $^{87}Sr/^{86}Sr$ ratios of ~0.711 in Spring and ~0.712 in Fall from Telmer (1998). This hypothesis of exogenous incorporation is consistent with the longitudinal increase of Sr concentration ([Sr]) in the hair profile of the

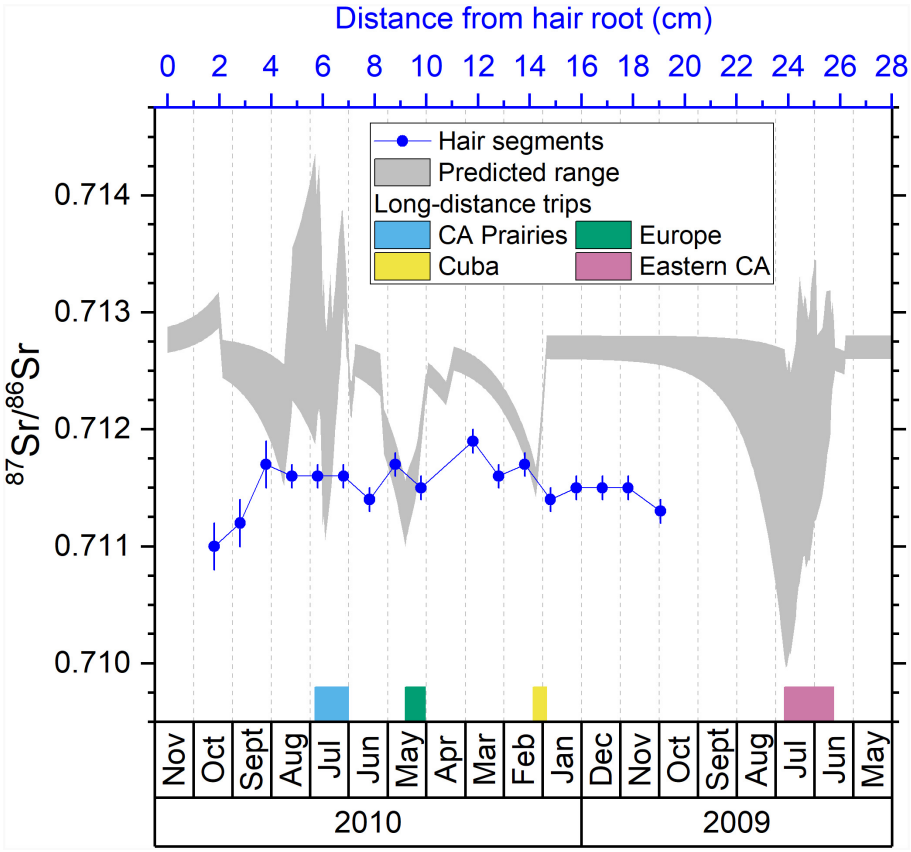

FIGURE 5 | Comparison between the predicted isotopic profile and the measured isotopic ratios in hair segments for strontium. Blue dots are the measured $^{87}Sr/^{86}Sr$ ratios in hair segments versus their distances from the hair root **(top axis)**. The shaded area is the predicted range of $^{87}Sr/^{86}Sr$ ratios in hair versus the date **(bottom axis)**. The periods of the four major trips are marked with colored bars next to the bottom axis.

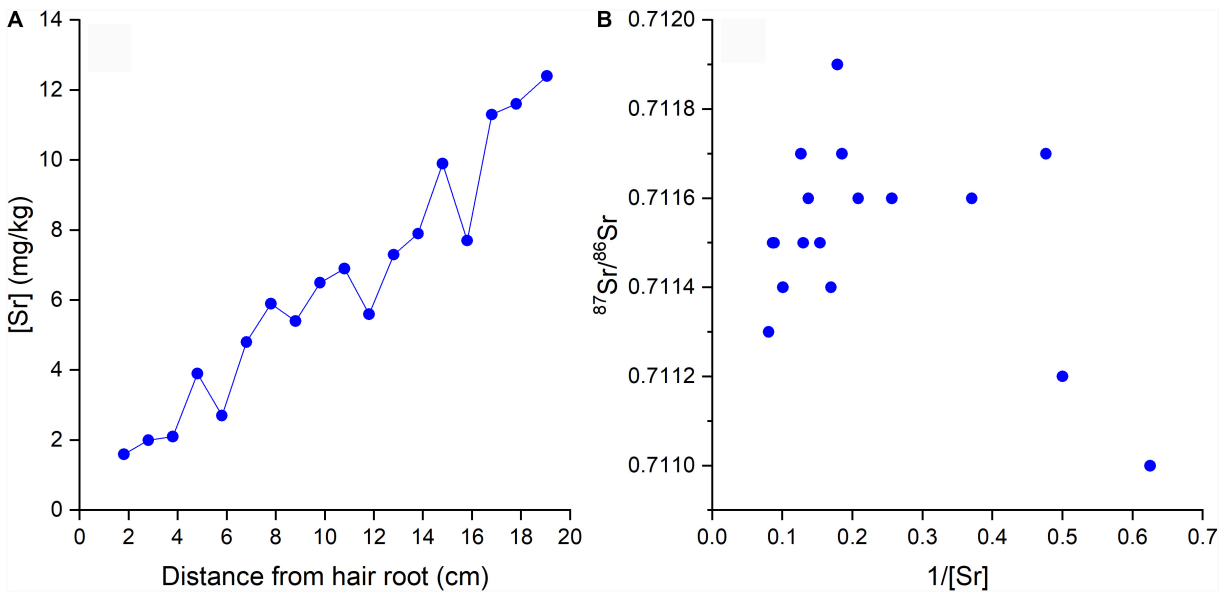

FIGURE 6 | (A) [Sr] in hair segments versus the distance from hair root; **(B)** $^{87}Sr/^{86}Sr$ versus 1/[Sr] in hair segments.

volunteer (**Figure 6A**) and the convergence of the hair $^{87}Sr/^{86}Sr$ ratios toward an end-member of ∼0.7112 (**Figure 6B**), equal to Ottawa river $^{87}Sr/^{86}Sr$ ratio in Spring (Telmer, 1998).

However, we also notice that the measured $^{87}Sr/^{86}Sr$ ratios in the two first hair segments (B1 and B2, **Table 3**) were quite lower (0.7110 and 0.7112) than the rest of the hair profile and sit on the bottom-right corner of **Figure 6B**, suggesting another source of Sr for segment B1 and B2. Both hair segments are the most recently grown, and as evidenced by their lower Sr concentrations (**Figure 6A**) they have incorporated less exogeneous Sr through bathing or showering. Young hair tends to be less damaged, thus limiting water diffusion during bathing. Consequently, the most proximal portion of the hair may preserve, in part, endogenous $^{87}Sr/^{86}Sr$ ratio. This is supported by the distinct isotopic ratios of these segments relative to the rest of the hair where Sr is overprinted or exchanged with exogenous Sr from Ottawa tap water. This endogenous Sr must come primarily from dietary sources and not from tap water and is incorporated into hair through blood (Lewis et al., 2017). The volunteer had a typical supermarket diet and most of the food items consumed while residing in Ottawa came from a variety of regional, national, and international sources with variable $^{87}Sr/^{86}Sr$ ratios. This complex food sourcing makes it challenging to characterize the integrated dietary $^{87}Sr/^{86}Sr$ ratio. However, it is likely that the $^{87}Sr/^{86}Sr$ ratios of the food consumed by the volunteer in Ottawa differ from that of the local tap water explaining the isotopic difference between the young and older hair segments.

Although studies have been trying to use $^{87}Sr/^{86}Sr$ ratios in hair for forensic and archeologic applications (Font et al., 2012; Frei et al., 2015; Vautour et al., 2015), it has been shown that hair can exchange Sr with the ambient water, either in modern environment during bathing or showering (Tipple et al., 2018; Hu et al., 2020), or in post-mortem environment (Gordon et al., 2019). Our result generally agrees that the Sr in modern human hair above 3 cm from scalp is mostly replaced by the exogenous signal. However, the initial 3 cm of hair (segments B1 and B2) in this study contained different $^{87}Sr/^{86}Sr$ ratios from the rest of the hair, indicating the preservation of the most recent endogenous $^{87}Sr/^{86}Sr$ ratios. Therefore, the proximal end (root) of hair could preserve endogenous Sr signal which can be useful for provenance applications and archeological applications allowing in particular to verify if an individual recently moved or if human remains were displaced.

CONCLUSION

In this study, we analyzed the isotopic compositions of four elements (hydrogen, carbon, nitrogen, and strontium) along the ∼20 cm hair profile of a volunteer. This volunteer was a resident of Ottawa, who had traveled to several distant locations over a period of 2 years. We used the existing isotope database, detailed travel history, and a single exponential best-fit model to predict the isotopic profile for each of these isotopic systems. We compared the measured isotopic values in hair with the predicted profiles to evaluate the ability to reconstruct the life history of a mobile individual with different isotopic systems. Our results demonstrate that no single isotopic system can show all major travel events. The measured δ^2H profile faithfully recorded a 2 months trip to the Prairie Provinces, thus a good tool to identify travel events of which the original location and the destination have substantial δ^2H difference, in this case ∼10‰. The absolute values of the measured $\delta^{13}C$ and $\delta^{15}N$ profiles do not match the predicted profiles, suggesting that dietary and/or physiological factors could control the overall isotopic compositions. For example, there is a relatively constant ∼1.5‰ offset between the measured and predicted $\delta^{13}C$ profiles. However, the patterns of $\delta^{13}C$ variations in the measured and predicted profiles are very similar which both properly recorded a 2 weeks trip in Europe, indicating that $\delta^{13}C$ in hair can be a good indicator of mobility when traveling between countries with distinct $\delta^{13}C$ signatures in the food systems. Nitrogen isotope compositions in the hair of the volunteer are generally on the upper limit of predicted ranges, indicating the consumption of consistent amounts of animal or marine-based protein at the different locations. The spikes of $\delta^{15}N$ values in the measured profile are likely caused by the severe illness of the individual associated with a trip to Cuba, indicating its potential to identify the change of physiological status. From the stable isotope results, we found that the isotopic shifts in the proximal part of the hair bundle (<10 cm) are likely more representative of the true isotopic variability, while the isotopic shifts in the distal part (>10 cm) have larger uncertainty in terms of timing and amplitude. Lastly, strontium isotope composition in the volunteer's hair was mostly affected by the exogenous Sr signal incorporated during environmental contamination, which mainly reflects the most recent residential signal. However, we also notice that the root of the hair may have preserved at least partial endogenous signal from the diet. Therefore, while the $^{87}Sr/^{86}Sr$ profile in the distal part of hair may not be used to reconstruct travel history, the $^{87}Sr/^{86}Sr$ ratio in the proximal part of hair may be used for dietary studies.

DATA AVAILABILITY STATEMENT

All datasets generated for this study are included in the article/**Supplementary Material**.

ETHICS STATEMENT

The studies involving human participants were reviewed and approved by the University of Ottawa Research Ethics Board. The patients/participants provided their written informed consent to participate in this study.

AUTHOR CONTRIBUTIONS

LH, CB, GS-J, and MC designed the project. MC, LH, and ML analyzed the datasets. CB and LH performed the interpretation and model development steps. LH and CB led the writing of

the manuscript. All the authors contributed to the article and approved the submitted version.

FUNDING

CB and LH acknowledge funding from Canadian Security and Safety Program Targeted Investment (CSSP-2018-TI-2385). GS-J and MC acknowledge funding from the Chemical, Biological, Radiological and Nuclear Research & Technology Initiative (CRTI 08-0116RD).

SUPPLEMENTARY MATERIAL

The Supplementary Material for this article can be found online at: https://www.frontiersin.org/articles/10.3389/fevo.2020.568943/full#supplementary-material

REFERENCES

Ammer, S. T. M., Kootker, L. M., Bartelink, E. J., Anderson, B. E., Cunha, E., and Davies, G. R. (2020). Comparison of strontium isotope ratios in Mexican human hair and tap water as provenance indicators. *Forensic Sci. Int.* 314:110422. doi: 10.1016/j.forsciint.2020.110422

Ayliffe, L. K., Cerling, T. E., Robinson, T., West, A. G., Sponheimer, M., Passey, B. H., et al. (2004). Turnover of carbon isotopes in tail hair and breath CO2 of horses fed an isotopically varied diet. *Oecologia* 139, 11–22. doi: 10.1007/s00442-003-1479-x

Bataille, C. P., and Bowen, G. J. (2012). Mapping 87Sr/86Sr variations in bedrock and water for large scale provenance studies. *Chem. Geol.* 304–305, 39–52. doi: 10.1016/j.chemgeo.2012.01.028

Bataille, C. P., Chartrand, M. M. G., Raposo, F., and St-Jean, G. (2020a). Assessing geographic controls of hair isotopic variability in human populations: a case-study in Canada. *PLoS One* 15:e0237105. doi: 10.1371/journal.pone.0237105

Bataille, C. P., Crowley, B. E., Wooller, M. J., and Bowen, G. J. (2020b). Advances in global bioavailable strontium isoscapes. *Palaeogeogr. Palaeoclimatol. Palaeoecol.* 555:109849. doi: 10.1016/j.palaeo.2020.109849

Beaumont, J., Geber, J., Powers, N., Wilson, A., Lee-Thorp, J., and Montgomery, J. (2013). Victims and survivors: stable isotopes used to identify migrants from the Great Irish Famine to 19th century London. *Am. J. Phys. Anthropol.* 150, 87–98. doi: 10.1002/ajpa.22179

Bentley, R. A. (2006). Strontium Isotopes from the Earth to the archaeological skeleton: a review. *J. Archaeol. Method Theory* 13, 135–187. doi: 10.1007/s10816-006-9009-x

Bol, R., Marsh, J., and Heaton, T. H. E. (2007). Multiple stable isotope (18O, 13C, 15N and 34S) analysis of human hair to identify the recent migrants in a rural community in SW England. *Rapid. Commun. Mass Spectrom.* 21, 2951–2954. doi: 10.1002/rcm.3168

Bowen, G. J. (2010). Isoscapes: spatial pattern in isotopic biogeochemistry. *Annu. Rev. Earth Planet. Sci.* 38, 161–187. doi: 10.1146/annurev-earth-040809-152429

Bowen, G. J., Wassenaar, L. I., and Hobson, K. A. (2005). Global application of stable hydrogen and oxygen isotopes to wildlife forensics. *Oecologia* 143, 337–348. doi: 10.1007/s00442-004-1813-y

Buzon, M. R., Conlee, C. A., and Bowen, G. J. (2011). Refining oxygen isotope analysis in the Nasca region of Peru: an investigation of water sources and archaeological samples. *Int. J. Osteoarchaeol.* 21, 446–455. doi: 10.1002/oa.1151

Cerling, T. E., Andanje, S. A., Gakuya, F., Kariuki, J. M., Kariuki, L., Kingoo, J. W., et al. (2018). Stable isotope ecology of black rhinos (*Diceros bicornis*) in Kenya. *Oecologia* 187, 1095–1105. doi: 10.1007/s00442-018-4185-4

Cerling, T. E., Ayliffe, L. K., Dearing, M. D., Ehleringer, J. R., Passey, B. H., Podlesak, D. W., et al. (2007). Determining biological tissue turnover using stable isotopes: the reaction progress variable. *Oecologia* 151, 175–189. doi: 10.1007/s00442-006-0571-4

Cerling, T. E., Wittemyer, G., Ehleringer, J. R., Remien, C. H., and Douglas-Hamilton, I. (2009). History of animals using isotope records (HAIR): a 6-year dietary history of one family of African elephants. *Proc. Natl. Acad. Sci. U.S.A.* 106:8093. doi: 10.1073/pnas.0902192106

Cerling, T. E., Wittemyer, G., Rasmussen, H. B., Vollrath, F., Cerling, C. E., Robinson, T. J., et al. (2006). Stable isotopes in elephant hair document migration patterns and diet changes. *Proc. Natl. Acad. Sci. U.S.A.* 103, 371–373. doi: 10.1073/pnas.0509606102

Chartrand, M., and St-Jean, M. G. (2015). *Forensic Attribution of CBRNE Materials: A Chemical Fingerprint Database*. Ottawa: Defence Research and Development Canada.

Chau, T. H., Tipple, B. J., Hu, L., Fernandez, D. P., Cerling, T. E., Ehleringer, J. R., et al. (2017). Reconstruction of travel history using coupled δ18O and 87Sr/86Sr measurements of hair. *Rapid Commun. Mass Spectrom.* 31, 583–589. doi: 10.1002/rcm.7822

Chesson, L. A., Meier-Augenstein, W., Berg, G. E., Bataille, C. P., Bartelink, E. J., and Richards, M. P. (2020). "Basic principles of stable isotope analysis in humanitarian forensic science," in *Forensic Science and Humanitarian Action: Interacting with the Dead and the Living*, eds R. C. Parra, S. C. Zapico, and D. H. Ubelaker (Hoboken, NJ: John Wiley & Sons, Ltd), 285–310. doi: 10.1002/9781119482062.ch20

Chesson, L. A., Tipple, B. J., Mackey, G. N., Hynek, S. A., Fernandez, D. P., and Ehleringer, J. R. (2012). Strontium isotopes in tap water from the coterminous USA. *Ecosphere* 3, 1–17. doi: 10.1890/ES12-00122.1

Chittleborough, G. (1980). A chemist's view of the analysis of human hair for trace elements. *Sci. Total Environ.* 14, 53–75. doi: 10.1016/0048-9697(80)90126-6

Cohn, S. H., Spencer, H., Samachson, J., and Robertson, J. S. (1962). The turnover of strontium-85 in man as determined by whole-body counting. *Radiat. Res.* 17, 173–185. doi: 10.2307/3571307

Ehleringer, J. R., Bowen, G. J., Chesson, L. A., West, A. G., Podlesak, D. W., and Cerling, T. E. (2008). Hydrogen and oxygen isotope ratios in human hair are related to geography. *Proc. Natl. Acad. Sci. U.S.A.* 105, 2788–2793. doi: 10.1073/pnas.0712228105

Ehleringer, J. R., Thompson, A. H., Podlesak, D. W., Bowen, G. J., Chesson, L. A., Cerling, T. E., et al. (2010). "A framework for the incorporation of isotopes and isoscapes in geospatial forensic investigations," in *Isoscapes: Understanding Movement, Pattern, and Process on Earth through Isotope Mapping*, eds J. B. West, G. J. Bowen, T. E. Dawson, and K. P. Tu (Netherlands: Springer), 357–387. doi: 10.1007/978-90-481-3354-3_17

Font, L., Nowell, G. M., Graham Pearson, D., Ottley, C. J., and Willis, S. G. (2007). Sr isotope analysis of bird feathers by TIMS: a tool to trace bird migration paths and breeding sites. *J. Anal. At. Spectrom.* 22, 513–522. doi: 10.1039/B616328A

Font, L., van der Peijl, G., van Wetten, I., Vroon, P., van der Wagt, B., and Davies, G. (2012). Strontium and lead isotope ratios in human hair: investigating a potential tool for determining recent human geographical movements. *J. Anal. At. Spectrom.* 27, 719–732. doi: 10.1039/c2ja10361c

Fraser, I., and Meier-Augenstein, W. (2007). Stable 2H isotope analysis of modern-day human hair and nails can aid forensic human identification. *Rapid Commun. Mass Spectrom.* 21, 3279–3285. doi: 10.1002/rcm.3209

Fraser, I., Meier-Augenstein, W., and Kalin, R. M. (2006). The role of stable isotopes in human identification: a longitudinal study into the variability of isotopic signals in human hair and nails. *Rapid Commun. Mass Spectrom.* 20, 1109–1116. doi: 10.1002/rcm.2424

Frei, K. M., Frei, R., Mannering, U., Gleba, M., Nosch, M. L., and Lyngstrøm, H. (2009). Provenance of ancient textiles—a pilot study evaluating the strontium isotope system in wool. *Archaeometry* 51, 252–276. doi: 10.1111/j.1475-4754.2008.00396.x

Frei, K. M., Mannering, U., Kristiansen, K., Allentoft, M. E., Wilson, A. S., Skals, I., et al. (2015). Tracing the dynamic life story of a bronze age female. *Sci. Rep.* 5:10431. doi: 10.1038/srep10431

Frei, K. M., Villa, C., Jørkov, M. L., Allentoft, M. E., Kaul, F., Ethelberg, P., et al. (2017). A matter of months: high precision migration chronology of a bronze age female. *PLoS One* 12:e0178834. doi: 10.1371/journal.pone.0178834

Fuller, B. T., Fuller, J. L., Sage, N. E., Harris, D. A., O'Connell, T. C., and Hedges, R. E. M. (2004). Nitrogen balance and δ15N: why you're not what you eat during pregnancy. *Rapid Commun. Mass Spectrom.* 18, 2889–2896. doi: 10.1002/rcm.1708

Fuller, B. T., Fuller, J. L., Sage, N. E., Harris, D. A., O'Connell, T. C., and Hedges, R. E. M. (2005). Nitrogen balance and δ15N: why you're not what you eat during nutritional stress. *Rapid Commun. Mass Spectrom.* 19, 2497–2506. doi: 10.1002/rcm.2090

Gehre, M., Renpenning, J., Gilevska, T., Qi, H., Coplen, T. B., Meijer, H. A. J., et al. (2015). On-line hydrogen-isotope measurements of organic samples using elemental chromium: an extension for high temperature elemental-analyzer techniques. *Anal. Chem.* 87, 5198–5205. doi: 10.1021/acs.analchem.5b00085

Gordon, G., Saul, T., Steadman, D., Knudson, K., Anbar, A. D., and Wescott, D. (2019). *Isotopic Taphonomy of Human Remains (NIJ document No. 252506)*. Washington, DC: U.S. Department of Justice.

Hayashi, S., Miyamoto, I., and Takeda, K. (1991). Measurement of human hair growth by optical microscopy and image analysis. *Br. J. Dermatol.* 125, 123–129. doi: 10.1111/j.1365-2133.1991.tb06058.x

Hedges, R. E. M., and Reynard, L. M. (2007). Nitrogen isotopes and the trophic level of humans in archaeology. *J. Archaeol. Sci.* 34, 1240–1251. doi: 10.1016/j.jas.2006.10.015

Hobson, K. A., Barnett-Johnson, R., and Cerling, T. (2010). "Using isoscapes to track animal migration," in *Isoscapes: Understanding Movement, Pattern, and Process on Earth through Isotope Mapping*, eds J. B. West, G. J. Bowen, T. E. Dawson, and K. P. Tu (Springer: Netherlands), 273–298. doi: 10.1007/978-90-481-3354-3_13

Hobson, K. A., and Clark, R. G. (1992). Assessing avian diets using stable isotopes ii: factors influencing diet-tissue fractionation. *Condor* 94, 189–197. doi: 10.2307/1368808

Hobson, K. A., Van Wilgenburg, S. L., Wassenaar, L. I., Powell, R. L., Still, C. J., and Craine, J. M. (2012). A multi-isotope (δ13C, δ15N, δ2H) feather isoscape to assign Afrotropical migrant birds to origins. *Ecosphere* 3:art44. doi: 10.1890/ES12-00018.1

Hu, L., Fernandez, D. P., and Cerling, T. E. (2018). Longitudinal and transverse variation of trace element concentrations in elephant and giraffe hair: implication for endogenous and exogenous contributions. *Environ. Monit. Assess.* 190:644. doi: 10.1007/s10661-018-7038-z

Hu, L., Fernandez, D. P., Cerling, T. E., and Tipple, B. J. (2020). Fast exchange of strontium between hair and ambient water: implication for isotopic analysis in provenance and forensic studies. *PLoS One* 15:e0233712. doi: 10.1371/journal.pone.0233712

Huelsemann, F., Flenker, U., Koehler, K., and Schaenzer, W. (2009). Effect of a controlled dietary change on carbon and nitrogen stable isotope ratios of human hair. *Rapid Commun. Mass Spectrom.* 23, 2448–2454. doi: 10.1002/rcm.4039

Hülsemann, F., Lehn, C., Schneiders, S., Jackson, G., Hill, S., Rossmann, A., et al. (2015). Global spatial distributions of nitrogen and carbon stable isotope ratios of modern human hair. *Rapid Commun. Mass Spectrom.* 29, 2111–2121. doi: 10.1002/rcm.7370

Jimenez, F., Izeta, A., and Poblet, E. (2011). Morphometric analysis of the human scalp hair follicle: practical implications for the hair transplant surgeon and hair regeneration studies. *Dermatol. Surg.* 37, 58–64. doi: 10.1111/j.1524-4725.2010.01809.x

Kempson, I. M., and Lombi, E. (2011). Hair analysis as a biomonitor for toxicology, disease and health status. *Chem. Soc. Rev.* 40, 3915–3940. doi: 10.1039/c1cs15021a

Kitchings, T., DiGregorio, D., and Van Voris, P. (1976). *Review of the Ecological Parameters of Radionuclide Turnover in Vertebrate Food Chains*. Ultimo, NSW: Halsted Press.

Knudson, K. J., Pestle, W. J., Torres-Rouff, C., and Pimentel, G. (2012). Assessing the life history of an andean traveller through biogeochemistry: stable and radiogenic isotope analyses of archaeological human remains from Northern Chile. *Int. J. Osteoarchaeol.* 22, 435–451. doi: 10.1002/oa.1217

Knudson, K. J., Peters, A. H., and Cagigao, E. T. (2015). Paleodiet in the paracas necropolis of Wari Kayan: carbon and nitrogen isotope analysis of keratin samples from the south coast of Peru. *J. Archaeol. Sci.* 55, 231–243. doi: 10.1016/j.jas.2015.01.011

Kootker, L. M., von Holstein, I. C. C., Broeders, J., Wescott, D. J., Davies, G. R., and Mickleburgh, H. L. (2020). The effects of decomposition and environment on antemortem H-Pb-Sr isotope compositions and degradation of human scalp hair: actualistic taphonomic observations. *Forensic Sci. Int.* 312:110336. doi: 10.1016/j.forsciint.2020.110336

LeBeau, M. A., Montgomery, M. A., and Brewer, J. D. (2011). The role of variations in growth rate and sample collection on interpreting results of segmental analyses of hair. *Forensic Sci. Int.* 210, 110–116. doi: 10.1016/j.forsciint.2011.02.015

Lehn, C., Kalbhenn, E. M., Rossmann, A., and Graw, M. (2019). Revealing details of stays abroad by sequential stable isotope analyses along human hair strands. *Int. J. Legal Med.* 133, 935–947. doi: 10.1007/s00414-018-1866-9

Lehn, C., Lihl, C., and Roßmann, A. (2015a). Change of geographical location from Germany (Bavaria) to USA (Arizona) and its effect on H–C–N–S stable isotopes in human hair. *Isotopes Environ. Health Stud.* 51, 68–79. doi: 10.1080/10256016.2014.995645

Lehn, C., Rossmann, A., and Graw, M. (2015b). Provenancing of unidentified corpses by stable isotope techniques – presentation of case studies. *Sci. Justice* 55, 72–88. doi: 10.1016/j.scijus.2014.10.006

Lehn, C., Mützel, E., and Rossmann, A. (2011). Multi-element stable isotope analysis of H, C, N and S in hair and nails of contemporary human remains. *Int. J. Legal Med.* 125, 695–706. doi: 10.1007/s00414-011-0595-0

Lewis, J., Pike, A. W. G., Coath, C. D., and Evershed, R. P. (2017). Strontium concentration, radiogenic (87Sr/86Sr) and stable (δ88Sr) strontium isotope systematics in a controlled feeding study. *STAR Sci. Technol. Archaeol. Res.* 3, 45–57. doi: 10.1080/20548923.2017.1303124

Lightfoot, E., and O'Connell, T. C. (2016). On the use of biomineral oxygen isotope data to identify human migrants in the archaeological record: intra-sample variation, statistical methods and geographical considerations. *PLoS One* 11:e0153850. doi: 10.1371/journal.pone.0153850

Lugli, F., Cipriani, A., Tavaglione, V., Traversari, M., and Benazzi, S. (2018). Transhumance pastoralism of roccapelago (Modena, Italy) early-modern individuals: inferences from Sr isotopes of hair strands. *Am. J. Phys. Anthropol.* 167, 470–483. doi: 10.1002/ajpa.23643

Macko, S. A., Engel, M. H., Andrusevich, V., Lubec, G., O'Connell, T. C., and Hedges, R. E. (1999a). Documenting the diet in ancient human populations through stable isotope analysis of hair. *Philos. Trans. R. Soc. Lond. B. Biol. Sci.* 354, 65–76. doi: 10.1098/rstb.1999.0360

Macko, S. A., Lubec, G., Teschler-Nicola, M., Andrusevich, V., and Engel, M. H. (1999b). The Ice Man's diet as reflected by the stable nitrogen and carbon isotopic composition of his hair. *FASEB J.* 13, 559–562. doi: 10.1096/fasebj.13.3.559

Mancuso, C. J., and Ehleringer, J. R. (2018). Strontium isotope ratios (87Sr/86Sr) of human fingernail clippings reveal multiple location signals. *Rapid Commun. Mass Spectrom.* 32, 1922–1930. doi: 10.1002/rcm.8270

Mant, M., Nagel, A., and Prowse, T. (2016). Investigating residential history using stable hydrogen and oxygen isotopes of human hair and drinking water. *J. Forensic Sci.* 61, 884–891. doi: 10.1111/1556-4029.13066

McCullagh, J. S. O., Tripp, J. A., and Hedges, R. E. M. (2005). Carbon isotope analysis of bulk keratin and single amino acids from British and North American hair. *Rapid Commun. Mass Spectrom.* 19, 3227–3231. doi: 10.1002/rcm.2150

Meier-Augenstein, W. (2019). Forensic stable isotope signatures: comparing, geo-locating, detecting linkage. *WIREs Forensic Sci.* 1:e1339. doi: 10.1002/wfs2.1339

Meier-Augenstein, W., Chartrand, M. M. G., Kemp, H. F., and St-Jean, G. (2011). An inter-laboratory comparative study into sample preparation for both reproducible and repeatable forensic 2H isotope analysis of human hair by continuous flow isotope ratio mass spectrometry. *Rapid Commun. Mass Spectrom.* 25, 3331–3338. doi: 10.1002/rcm.5235

Mekota, A.-M., Grupe, G., Ufer, S., and Cuntz, U. (2006). Serial analysis of stable nitrogen and carbon isotopes in hair: monitoring starvation and recovery phases of patients suffering from anorexia nervosa. *Rapid Commun. Mass Spectrom.* 20, 1604–1610. doi: 10.1002/rcm.2477

O'Brien, D. M., and Wooller, M. J. (2007). Tracking human travel using stable oxygen and hydrogen isotope analyses of hair and urine. *Rapid Commun. Mass Spectrom.* 21, 2422–2430. doi: 10.1002/rcm.3108

O'Connell, T. C., and Hedges, R. E. M. (1999). Investigations into the effect of diet on modern human hair isotopic values. *Am. J. Phys. Anthropol* 108, 409–425. doi: 10.1002/(SICI)1096-8644(199904)108:4<409::AID-AJPA3>3.0.CO;2-E

Petzke, K. J., Boeing, H., Klaus, S., and Metges, C. C. (2005a). Carbon and nitrogen stable isotopic composition of hair protein and amino acids can be used as biomarkers for animal-derived dietary protein intake in humans. *J. Nutr.* 135, 1515–1520. doi: 10.1093/jn/135.6.1515

Petzke, K. J., Boeing, H., and Metges, C. C. (2005b). Choice of dietary protein of vegetarians and omnivores is reflected in their hair protein 13C and 15N abundance. *Rapid Commun. Mass Spectrom.* 19, 1392–1400. doi: 10.1002/rcm.1925

Petzke, K. J., Fuller, B. T., and Metges, C. C. (2010). Advances in natural stable isotope ratio analysis of human hair to determine nutritional and metabolic status. *Curr. Opin. Clin. Nutr. Metab. Care* 13, 532–540. doi: 10.1097/MCO.0b013e32833c3c84

Podlesak, D. W., McWilliams, S. R., and Hatch, K. A. (2005). Stable isotopes in breath, blood, feces and feathers can indicate intra-individual changes in the diet of migratory songbirds. *Oecologia* 142, 501–510. doi: 10.1007/s00442-004-1737-6

Podlesak, D. W., Torregrossa, A.-M., Ehleringer, J. R., Dearing, M. D., Passey, B. H., and Cerling, T. E. (2008). Turnover of oxygen and hydrogen isotopes in the body water. CO2, hair, and enamel of a small mammal. *Geochim. Cosmochim. Acta* 72, 19–35. doi: 10.1016/j.gca.2007.10.003

Pötsch, L. (1996). A discourse on human hair fibers and reflections on the conservation of drug molecules. *Int. J. Legal Med.* 108, 285–293. doi: 10.1007/BF02432122

Remien, C. H., Adler, F. R., Chesson, L. A., Valenzuela, L. O., Ehleringer, J. R., and Cerling, T. E. (2014). Deconvolution of isotope signals from bundles of multiple hairs. *Oecologia* 175, 781–789. doi: 10.1007/s00442-014-2945-3

Reynard, L. M., Burt, N., Koon, H. E. C., and Tuross, N. (2016). Limits and possibilities in the geolocation of humans using multiple isotope ratios (H, O, N, C) of hair from east coast cities of the USA. *Isotopes Environ. Health Stud.* 52, 498–512. doi: 10.1080/10256016.2016.1143821

Rubenstein, D. R., and Hobson, K. A. (2004). From birds to butterflies: animal movement patterns and stable isotopes. *Trends Ecol. Evol.* 19, 256–263. doi: 10.1016/j.tree.2004.03.017

Saul, T. B. (2017). *An Exploration of the Effects of Taphonomy on Isotope Ratios of Human Hair*. PhD dissertation, University of Tennessee, Knoxville, TN.

Sharp, Z. D., Atudorei, V., Panarello, H. O., Fernández, J., and Douthitt, C. (2003). Hydrogen isotope systematics of hair: archeological and forensic applications. *J. Archaeol. Sci.* 30, 1709–1716. doi: 10.1016/S0305-4403(03)00071-2

Telmer, K. H. (1998). *Biogeochemistry and Water Balance of the Ottawa River Basin*. Ottawa: University of Ottawa, doi: 10.20381/ruor-10233

Thompson, A. H., Richards, M. P., Shortland, A., and Zakrzewski, S. R. (2005). Isotopic palaeodiet studies of ancient egyptian fauna and humans. *J. Archaeol. Sci.* 32, 451–463. doi: 10.1016/j.jas.2004.11.004

Thompson, A. H., Wilson, A. S., and Ehleringer, J. R. (2014). "Hair as a geochemical recorder: ancient to modern," in *Treatise on Geochemistry*, 2nd Edn, eds H. D. Holland and K. K. Turekian (Oxford: Elsevier), 371–393. doi: 10.1016/B978-0-08-095975-7.01227-4

Tipple, B. J., Valenzuela, L. O., Chau, T. H., Hu, L., Bataille, C. P., Chesson, L. A., et al. (2019). Strontium isotope ratios of human hair from the United States: patterns and aberrations. *Rapid Commun. Mass Spectrom.* 33, 461–472. doi: 10.1002/rcm.8378

Tipple, B. J., Valenzuela, L. O., and Ehleringer, J. R. (2018). Strontium isotope ratios of human hair record intra-city variations in tap water source. *Sci. Rep.* 8:3334. doi: 10.1038/s41598-018-21359-0

Topalov, K., Schimmelmann, A., Polly, P. D., Sauer, P. E., and Viswanathan, S. (2019). Stable isotopes of H, C and N in mice bone collagen as a reflection of isotopically controlled food and water intake. *Isotopes Environ. Health Stud.* 55, 129–149. doi: 10.1080/10256016.2019.1580279

Valenzuela, L. O., Chesson, L. A., Bowen, G. J., Cerling, T. E., and Ehleringer, J. R. (2012). Dietary heterogeneity among western industrialized countries reflected in the stable isotope ratios of human hair. *PLoS One* 7:e34234. doi: 10.1371/journal.pone.0034234

Valenzuela, L. O., Chesson, L. A., O'Grady, S. P., Cerling, T. E., and Ehleringer, J. R. (2011). Spatial distributions of carbon, nitrogen and sulfur isotope ratios in human hair across the central United States. *Rapid Commun. Mass Spectrom.* 25, 861–868. doi: 10.1002/rcm.4934

Vautour, G., Poirier, A., and Widory, D. (2015). Tracking mobility using human hair: what can we learn from lead and strontium isotopes? *Sci. Justice* 55, 63–71. doi: 10.1016/j.scijus.2014.10.001

Voerkelius, S., Lorenz, G. D., Rummel, S., Quétel, C. R., Heiss, G., Baxter, M., et al. (2010). Strontium isotopic signatures of natural mineral waters, the reference to a simple geological map and its potential for authentication of food. *Food Authent. Traceability* 118, 933–940. doi: 10.1016/j.foodchem.2009.04.125

Webb, E., White, C., and Longstaffe, F. (2013). Dietary shifting in the Nasca Region as inferred from the carbon- and nitrogen-isotope compositions of archaeological hair and bone. *J. Archaeol. Sci.* 40, 129–139. doi: 10.1016/j.jas.2012.08.020

West, J. B., Bowen, G. J., Dawson, T. E., and Tu, K. P. (2010). *Isoscapes: Understanding Movement, Pattern, and Process on Earth Through Isotope Mapping*. Dordrecht: Springer.

White, C. D. (1993). Isotopic determination of seasonality in diet and death from nubian mummy hair. *J. Archaeol. Sci.* 20, 657–666. doi: 10.1006/jasc.1993.1040

White, C. D., Nelson, A. J., Longstaffe, F. J., Grupe, G., and Jung, A. (2009). Landscape bioarchaeology at pacatnamu, peru: inferring mobility from δ13C and δ15N values of hair. *J. Archaeol. Sci.* 36, 1527–1537. doi: 10.1016/j.jas.2009.03.008

Wunder, M. B. (2012). Determining geographic patterns of migration and dispersal using stable isotopes in keratins. *J. Mammal.* 93, 360–367. doi: 10.1644/11-MAMM-S-182.1

Conflict of Interest: The authors declare that the research was conducted in the absence of any commercial or financial relationships that could be construed as a potential conflict of interest.

frontiers in Ecology and Evolution

ORIGINAL RESEARCH
published: 29 September 2020
doi: 10.3389/fevo.2020.00281

Drinking Locally: A Water $^{87}Sr/^{86}Sr$ Isoscape for Geolocation of Archeological Samples in the Peruvian Andes

Beth K. Scaffidi[1], Tiffiny A. Tung[2], Gwyneth Gordon[3], Aleksa K. Alaica[4], Luis Manuel González La Rosa[5], Sara J. Marsteller[6], Allisen Dahlstedt[6], Emily Schach[7] and Kelly J. Knudson[6]*

[1] Department of Anthropology and Heritage Studies, University of California, Merced, Merced, CA, United States, [2] Bioarchaeology and Stable Isotope Research Laboratory, Department of Anthropology, Vanderbilt University, Nashville, TN, United States, [3] Metals, Environmental and Terrestrial Analytical Laboratory, School of Earth and Space Exploration, Arizona State University, Tempe, AZ, United States, [4] Department of Anthropology, University of Toronto, Toronto, ON, Canada, [5] Archaeology Centre, University of Toronto, Toronto, ON, Canada, [6] Center for Bioarchaeological Research, School of Human Evolution and Social Change, Arizona State University, Tempe, AZ, United States, [7] Department of Anthropology, University of California, Santa Cruz, Santa Cruz, CA, United States

OPEN ACCESS

Edited by:
Clement Pierre Bataille, University of Ottawa, Canada

Reviewed by:
Ramiro Barberena, CONICET Mendoza, Argentina
Alejandro Serna, National University of La Plata, Argentina

***Correspondence:**
Beth K. Scaffidi
cscaffidi@ucmerced.edu

Specialty section:
This article was submitted to Paleoecology, a section of the journal Frontiers in Ecology and Evolution

Received: *04 June 2020*
Accepted: *10 August 2020*
Published: *29 September 2020*

Citation:
Scaffidi BK, Tung TA, Gordon G, Alaica AK, González La Rosa LM, Marsteller SJ, Dahlstedt A, Schach E and Knudson KJ (2020) Drinking Locally: A Water $^{87}Sr/^{86}Sr$ Isoscape for Geolocation of Archeological Samples in the Peruvian Andes. Front. Ecol. Evol. 8:281. doi: 10.3389/fevo.2020.00281

The analysis of $^{87}Sr/^{86}Sr$ has become a robust tool for identifying non-local individuals at archeological sites. The $^{87}Sr/^{86}Sr$ in human bioapatite reflects the geological signature of food and water consumed during tissue development. Modeling relationships between $^{87}Sr/^{86}Sr$ in human environments, food webs, and archeological human tissues is critical for moving from identifying non-locals to determining their likely provenience. In the Andes, obstacles to sample geolocation include overlapping $^{87}Sr/^{86}Sr$ of distant geographies and a poor understanding of mixed strontium sources in food and drink. Here, water is investigated as a proxy for bioavailable strontium in archeological human skeletal and dental tissues. This study develops a water $^{87}Sr/^{86}Sr$ isoscape from 262 samples (220 new and 42 published samples), testing the model with published archeological human skeletal $^{87}Sr/^{86}Sr$ trimmed of probable non-locals. Water $^{87}Sr/^{86}Sr$ and prediction error between the predicted and measured $^{87}Sr/^{86}Sr$ for the archeological test set are compared by elevation, underlying geology, and watershed size. Across the Peruvian Andes, water $^{87}Sr/^{86}Sr$ ranges from 0.7049 to 0.7227 (M = 0.7081, SD = 0.0027). Water $^{87}Sr/^{86}Sr$ is higher in the highlands, in areas overlying older bedrock, and in larger watersheds, characteristics which are geographically correlated. Spatial outliers identified are from canals, wells, and one stream, suggesting those sources could show non-representative $^{87}Sr/^{86}Sr$. The best-fit water $^{87}Sr/^{86}Sr$ isoscape achieves prediction errors for archeological samples ranging from 0.0017 – 0.0031 (M = 0.0012, n = 493). The water isoscape explains only 7.0% of the variation in archeological skeletal $^{87}Sr/^{86}Sr$ (R^2 = 0.07), but 90.0% of archeological skeleton $^{87}Sr/^{86}Sr$ fall within the site isoscape prediction ± site prediction standard error. Due to lower sampling density and higher geological variability in the highlands, the water $^{87}Sr/^{86}Sr$ isoscape is more useful for ruling out geographic origins for lowland

dwellers than for highlanders. Baseline studies are especially needed in the highlands and poorly sampled regions. Because the results demonstrate that a geostatistical water model is insufficient for fully predicting human $^{87}Sr/^{86}Sr$ variation, future work will incorporate additional substrates like plants, fauna, soils, and dust, aiming to eventually generate a regression and process-based mixing model for the probabilistic geolocation of Andean samples.

Keywords: pre-Hispanic Andes, strontium isotope analysis, geostatistical analysis, isoscape, archeological geolocation

INTRODUCTION

Over the past few decades, the analysis of radiogenic strontium isotopes ($^{87}Sr/^{86}Sr$) in skeletal and dental tissues has become a robust tool for identifying probable non-local individuals among archeological samples and for geo-locating them by matching sample $^{87}Sr/^{86}Sr$ to landscape $^{87}Sr/^{86}Sr$. While mass-dependent isotopic fractionation does occur between dietary and water sources of strontium as they are processed by the human body, the effects of fractionation are negligible after laboratory normalization (Graustein, 1989, p. 492; Beard and Johnson, 2000; Knudson et al., 2010, p. 2; Lewis et al., 2017; Bataille et al., 2020). Due to this small magnitude of diet-body offset of strontium isotopes, the $^{87}Sr/^{86}Sr$ in animal tissues reflect the geological signature of underlying bedrock, which is incorporated into the mixed sources of food, water, and atmospheric elements in the food chain that are consumed and imbibed throughout the course of tissue development (Graustein, 1989; Bentley, 2006; Grimstead et al., 2017; Bataille et al., 2020). Strontium isotope analysis is typically employed by archeologists to examine questions of past migration and mobility: identifying first-generation migrants in a skeletal sample, constraining areas of possible provenience for those non-locals, and assessing the proportion of geologically local to non-local individuals in skeletal assemblages (e.g., Ericson, 1985; Price et al., 1994, 2002, 2015; Evans et al., 2006; Knudson and Price, 2007; Slovak et al., 2009; Montgomery, 2010; Tung and Knudson, 2011; Frei and Price, 2012; Knudson et al., 2012b). Assuming mostly local foods were consumed, individuals with $^{87}Sr/^{86}Sr$ that differs from most other individuals in a sample, or from the measured $^{87}Sr/^{86}Sr$ of the local environmental baseline, were likely non-local during the period when the sampled tissue was developing.

Understanding how much difference in $^{87}Sr/^{86}Sr$ across the sample is required for a non-local designation and then reconstructing the likely provenience of those suspected non-locals depends on accurately characterizing the $^{87}Sr/^{86}Sr$ expected throughout the region(s) where they might have lived or traveled. Methods for defining the expected local $^{87}Sr/^{86}Sr$ range have shifted over the last few decades from statistically parsing human skeletal $^{87}Sr/^{86}Sr$ around the sample mean (e.g., Wright, 2005; Slovak et al., 2009; Price et al., 2015) to testing archeological and modern fauna with small home ranges (Price et al., 2002, 2007; Evans and Tatham, 2004; Hedman et al., 2009, 2018; Knudson and Tung, 2011). More recently, many scholars have argued that the only reliable way to determine the local $^{87}Sr/^{86}Sr$ range is by analyzing the bioavailable strontium in local environmental reference or baseline materials like soils, plants, and local fauna, and then aggregating those reference $^{87}Sr/^{86}Sr$ to geological units, soil units, or statistical groupings of baseline and/or skeletal materials (Valentine et al., 2008; Evans et al., 2010; Maurer et al., 2012; Knudson et al., 2014; Kootker et al., 2016; Grimstead et al., 2017; Willmes et al., 2018; Barberena et al., 2019; Pacheco-Forés et al., 2020; Snoeck et al., 2020). Unfortunately, because underlying bedrock geology is highly variable even at a short distance, and because rock weathers unevenly throughout catchments, these methods do not enable the sourcing of a sample to any location beyond the immediate vicinity of the sampling location. This is in part because the geological units the isotopic catchments are aggregated to are themselves models of the underlying bedrock that do not account for uncertainty error. Furthermore, because mammalian tissues derive their strontium content from the mixing of plants, fauna, water, and atmospheric particles ingested from the diet, sampling any one reference material or overreliance on bedrock geology will inevitably fail to capture the mixing of strontium in the human diet or in the diets of other animal end-members (Bentley, 2006; Grupe et al., 2011; Bataille et al., 2012; Burton and Price, 2013; Grimstead et al., 2017).

Because the $^{87}Sr/^{86}Sr$ of mixed-source isotopic catchments vary predictably across the landscape, models of baseline or reference landscape $^{87}Sr/^{86}Sr$ have become essential for reconstructing movements across the landscape throughout human history (Fisher et al., 2010; Frei and Frei, 2011; Laffoon et al., 2012; Knudson et al., 2014; Grupe et al., 2017a,b; Bataille et al., 2018; Willmes et al., 2018; Adams et al., 2019; Hoogewerff et al., 2019; Lengfelder et al., 2019; Scaffidi and Knudson, 2020). Isoscapes are spatially explicit models of isotope variability (Bowen, 2010; Ehleringer et al., 2010; Wunder, 2010; West et al., 2014; Pellegrini et al., 2016). Archeological and anthropological isoscapes have most commonly utilized a geostatistical kriging method to model isotopic variability across the landscape, which relies on underlying spatial auto-correlation in GPS-located isotope measurements to predict isotope values at unsampled locations (Copeland et al., 2016; Pellegrini et al., 2016; Wang et al., 2018; Willmes et al., 2018; Adams et al., 2019; Scaffidi and Knudson, 2020). Geostatistical models have been improved on in recent years by process-based isoscapes that rely on regression or machine learning methods to predict isotope variability as a function of environmental variables (Bataille and Bowen, 2012; Bataille et al., 2014, 2020; Hoogewerff et al., 2019)—these are rare in archeological and anthropological applications but are becoming more common (Bataille et al., 2012, 2018;

Hoogewerff et al., 2019; Zimmer-Dauphinee et al., 2020). In either case, when predictive isoscapes are generated from samples reflecting the bioavailable strontium in the dietary catchment rather than bedrock outcroppings or soils containing weathered bedrock, they have the distinct advantage of capturing and predicting the mix of foods, water, and dust at every geographic location. This is important since studies have generally found that soil and bedrock $^{87}Sr/^{86}Sr$ alone are poor predictors for human tissue $^{87}Sr/^{86}Sr$ (Price et al., 2002, pp. 120–122; Knudson et al., 2014; Grimstead et al., 2017; Snoeck et al., 2020). Establishing accurate isoscapes of bioavailable $^{87}Sr/^{86}Sr$ variation in the natural environment and understanding what proxy materials best reflect human $^{87}Sr/^{86}Sr$ are prerequisites for accurately identifying non-locals in archeological assemblages and constraining their likely geographic origins to the most probable locations.

Isoscape modeling is notoriously tricky in mountainous landscapes due to their highly variable geology, hydrology, weather, and climate patterns (Bowen and Revenaugh, 2003; Yamanaka et al., 2015). In the Andes Mountains, seismic activity, droughts, flooding, landslides, and intensive mining and agricultural practices are additional factors that alter $^{87}Sr/^{86}Sr$ distributions around the landscape. This is expected to contribute to high heterogeneity of $^{87}Sr/^{86}Sr$ in higher-elevation zones. The study region of southern Peru is located in the Central Volcanic Zone of the Andes, where lava flows across a broad geographic area tap the same magma sources, homogenizing surface materials across regions within the volcanic arc (Scott et al., 2018). Similarly, recent findings by Serna et al. (2020, p. 10) confirm that in volcanic zones of Northern Patagonia are influenced away from bedrock $^{87}Sr/^{86}Sr$ by the deposition and mixing of "unradiogenic volcanic tephra"... and "reworked loess mixing Quaternary and Jurassic volcaniclastic sediments." Serna et al. (2020) conclude that dust and sediment reworking processes dominate the geomorphology of bioavailable Sr in some volcanic zones—sampling in these areas is critical for correctly characterizing expected $^{87}Sr/^{86}Sr$.

Another obstacle to accurate geolocation that is particularly pronounced in the Andes is the problem of equifinality (Price et al., 2002)—the fact that $^{87}Sr/^{86}Sr$ of geographically distant regions are often identical, so that samples with the same $^{87}Sr/^{86}Sr$, recovered from the same location, may have actually originated in distinct places. For example, the recent meta-analysis of published $^{87}Sr/^{86}Sr$ from Andean archeological sites by Scaffidi and Knudson (2020) show that archeological human and animal tissue $^{87}Sr/^{86}Sr$ ranges from 0.7038 to 0.7239. The upper and lower ends of the human and animal range are slightly higher than the theoretical Andean range based on bedrock, where $^{87}Sr/^{86}Sr$ = 0.7050 to 0.7200 (Knudson et al., 2014). Variation follows an east-west gradient corresponding to increasing elevation, longitude, and distance from the coast, so that locally born individuals from similar longitudes might display identical $^{87}Sr/^{86}Sr$ even though they grew up thousands of miles apart latitudinally (Scaffidi and Knudson, 2020). Yet another obstacle is that the mixing of geological strontium sources in Andean food webs prior to their incorporation into human tissues—between soils, crops, fertilizers, animal protein, different water sources, dust, and sea spray—is poorly understood, both in the past and the present.

There is considerable debate over the use of relatively simplistic geostatistical kriging models for predicting $^{87}Sr/^{86}Sr$ variability across the landscape. Kriging assumes data are normally distributed, continuous, stationary, and spatially auto-correlated—nearer points should be more similar than farther points (Cressie, 1993; Oliver and Webster, 2014, 2015). Because bedrock units are discrete blocks, Sr reservoirs are not continuous in $^{87}Sr/^{86}Sr$ across the landscape and $^{87}Sr/^{86}Sr$ are often non-normally distributed. Therefore, geostatistical methods "can give ambiguous and inaccurate results due to the challenges of incorporating non-normal and skewed distributions" which limit the utility of kriged isoscapes for determining provenience (Bataille et al., 2014, 2020, p. 8). Process and regression-based methods are ultimately necessary for developing high-resolution models of human $^{87}Sr/^{86}Sr$ variability (Hoogewerff et al., 2019; Bataille et al., 2020; Serna et al., 2020). Notwithstanding these limitations, kriging has been used to develop coarse, preliminary predictions of bioavailable $^{87}Sr/^{86}Sr$ for hydrological (e.g., Varouchakis et al., 2012; Johnson et al., 2018) and anthropological and archeological applications (Frei and Frei, 2011; Copeland et al., 2016; Wang et al., 2018; Willmes et al., 2018; Adams et al., 2019). Published bedrock and volcanic tephra $^{87}Sr/^{86}Sr$ are abundant throughout the Andes (Mamani et al., 2008; Scott et al., 2018), but these samples are limited in various parts of the Peruvian Andes, which limits the accuracy of existing bedrock $^{87}Sr/^{86}Sr$ models (e.g., Schenk et al., 1999). Therefore, this paper argues that modeling a geostatistical isoscape of bioavailable $^{87}Sr/^{86}Sr$ is appropriate as an initial step to characterizing $^{87}Sr/^{86}Sr$ variability in these sparsely sampled regions, an effort which will be improved on by subsequent sampling campaigns and future regression-based models.

This paper follows recent ecological and archeological studies to argue that because water averages strontium from throughout the dietary catchment (Frei and Frei, 2011; Bataille and Bowen, 2012; Frei and Frei, 2013; Zitek et al., 2015; Crowley et al., 2017), imbibed water from the dietary catchment may contribute to a portion of $^{87}Sr/^{86}Sr$ variation in archeological skeletal tissues. We report 220 new water $^{87}Sr/^{86}Sr$ from GPS-located water samples throughout the Peruvian Andes. We plot these together with 46 published Peruvian water $^{87}Sr/^{86}Sr$ (Flusche et al., 2005; Alaica et al., 2020), and generate a geostatistical water $^{87}Sr/^{86}Sr$ isoscape from this dataset trimmed of spatial outlier values (n = 249). We then test the validity of the model for geolocating previously compiled human archeological samples considered local to their burial location (from Scaffidi and Knudson, 2020)[1]. Ultimately, a mismatch (beyond the model error range) between the model predictions and a measured archeological sample will enable that individual to be identified as non-local during the time of tissue development and allow archeologists and other researchers in the Andes to constrain possible provenience matches along the modeled $^{87}Sr/^{86}Sr$ gradient.

[1]This study focuses on predicting human $^{87}Sr/^{86}Sr$ from water $^{87}Sr/^{86}Sr$ measurements, but the water model could also be applied to flora and non-human fauna if the water physiology and strontium biogeochemistry of those organisms is well-understood.

MATERIALS AND METHODS

Strontium Isotopes in the Andes: From Dietary Catchments to the Human Skeleton

Strontium enters the body through food and water consumed, and then substitutes for Ca ions in the bioapatite crystals of bone and enamel. While diet-body fractionation throughout the process of digestion and tissue incorporation is minimal, a trophic level effect called biopurification has been well documented throughout ecological systems. The Sr/Ca is reduced by approximately a factor of five in each trophic level, so that plants contain lower Sr/Ca ratios than soils, but higher Sr/Ca than meat (Comar et al., 1957a,b; Wasserman et al., 1958; Sillen and Kavanagh, 1982; Burton and Wright, 1995; Bentley, 2006). Because strontium follows calcium pathways into skeletal tissues, calcium-enriched foods like salt and seafood can be disproportionately reflected in tissue $^{87}Sr/^{86}Sr$, which could override the signature of the isotopic catchment for individuals with significantly more consumption of salty or marine foods (Sillen and Kavanagh, 1982; Hodell et al., 2004; Slovak et al., 2009; Knudson et al., 2010). Thus, the Sr/Ca ratio and related $^{87}Sr/^{86}Sr$ in human body tissues are largely impacted by the proportion and types of foods in the diet. Assuming these foods were mostly locally procured, skeletal $^{87}Sr/^{86}Sr$ reflects the geological $^{87}Sr/^{86}Sr$ of the dietary catchment of residence during the period of tissue formation (Ericson, 1985; Price et al., 1994, 2002; Montgomery, 2010).

The $^{87}Sr/^{86}Sr$ in the food chain at a given sampling location is a mix of weathered bedrock eroded and mixed into soils, surface and groundwater carrying strontium from different weathered sources, atmospheric sources of strontium like sea spray, ash, and dust, and faunal and plant strontium reservoirs (Bentley, 2006; Bataille et al., 2020). The proportion of these different sources varies across the landscape, and is best understood by localized, multi-source mixing models (Montgomery et al., 2007; Bataille et al., 2012, 2018, 2020; Willmes et al., 2018). In the Andes, $^{87}Sr/^{86}Sr$ baseline data from plants, fauna, and water are relatively limited compared to other world regions (but see Barberena et al., 2017, 2019). Expectations for catchment $^{87}Sr/^{86}Sr$ are primarily derived from models based on bedrock outcroppings. Bedrock models illustrate that patterns in $^{87}Sr/^{86}Sr$ in the Peruvian Andes are influenced by the age and lithology of the two sub-ranges: the Cordillera Occidental (Western Cordillera), which rises sharply out of the coastal plain into a lower-elevation range, and the Cordillera Oriental (Eastern Cordillera), which is the highest elevation range to the east that gradually descends into the Amazonian basin (**Figure 1**). Coastal areas throughout the north and south of Peru are comprised by Quaternary sediments with contributions from various alluvial flows from the highlands (Bellido et al., 1956; Schenk et al., 1999), and thus, bioavailable $^{87}Sr/^{86}Sr$ is expected to be relatively heterogeneous at the country scale. The near-coastal Cordillera Occidental is comprised of late Cenozoic volcanic rocks, which are older in the south-central Andes than in the north-central Andes. For example, bedrock outcropping $^{87}Sr/^{86}Sr$ in this front range varies from a mean of 0.7043 in Ecuador, to 0.7074 in Arequipa, to 0.7065 in northern Chile (see summary in Knudson et al., 2014, p. 206). In contrast, in the Cordillera Oriental, bedrock is dominated by Paleozoic andesites with more radiogenic (higher) $^{87}Sr/^{86}Sr$, although bedrock has not been well-sampled in this region. In areas between the two ranges, like Lake Titicaca, $^{87}Sr/^{86}Sr$ should reflect a mix of alluvial deposits from both ranges, but again, bedrock samples are lacking (see summary in Knudson et al., 2014, pp. 206–207). Finally, the Amazon basin is comprised of Precambrian-Devonian sediments and alluvial contributions from the Cordillera Oriental (Bellido et al., 1956; Schenk et al., 1999). To the far east, Amazonian rivers show a broad range of $^{87}Sr/^{86}Sr$, from 0.7056 to 0.7438, which reflect drainage of highly variable highland geologies in the eastern sub-range (Santos et al., 2015).

At present, it is unclear how bedrock $^{87}Sr/^{86}Sr$ variability is integrated into the human dietary catchment in the Andes. Generally, bedrock has broader $^{87}Sr/^{86}Sr$ ranges than the catchment-averaged bioavailable $^{87}Sr/^{86}Sr$ from biological substrates (Bataille et al., 2020), and of those substrates, omnivorous skeletons show broader ranges than soils, herbivorous fauna, and plants (Valentine et al., 2008; Ladegaard-Pedersen et al., 2020). However, in geologically active areas in the highlands like those around Cusco, Knudson et al. (2014) found wider $^{87}Sr/^{86}Sr$ variability in soils than in published bedrock. In coastal locations, soil $^{87}Sr/^{86}Sr$ matched bedrock $^{87}Sr/^{86}Sr$ but very few coastal bedrock samples were available for comparison. This study shows promise for establishing local bioavailable $^{87}Sr/^{86}Sr$ expectations through soil analysis but is limited by its geographic coverage—soils were tested from only 17 locations (n = 114), all but three of which were coastal. Knudson et al. (2014) also found that archeological human and faunal samples were consistently offset from soil $^{87}Sr/^{86}Sr$ in many locations. This makes sense since soils and rocks are generally not directly consumed, although rock contributions to the diet might be nominal in groups that process food with grinding stones (Johnson et al., 2019), practice geophagy, or consume geological materials as digestive aids—all were done in the ancient Andes (Johns, 1990). These inconsistencies between bedrock, soil, and skeletal $^{87}Sr/^{86}Sr$ could be due to differential weathering of bedrock throughout the steep Andes and/or the overall paucity of bedrock and soil samples from the region; nonetheless, this illustrates the need for a deeper examination of different substrates for the analysis of bioavailable Sr in the region.

Indeed, across the globe, researchers have debated which environmental baseline materials incorporated into the food web are the best proxy for human tissue $^{87}Sr/^{86}Sr$. Baseline studies have accordingly varied in their reference material of focus according to the different landscapes of archeological study locations. Using small modern or archeological fauna to establish a baseline was the earliest approach, which remains one of the most common approaches. Because small animals tend to have small homes ranges, they should average many of the same elements of the isotopic catchment as human end members do (Price et al., 2002; Bentley and Knipper, 2005; Hedman et al., 2009; Kootker et al., 2016; Fernández-Crespo

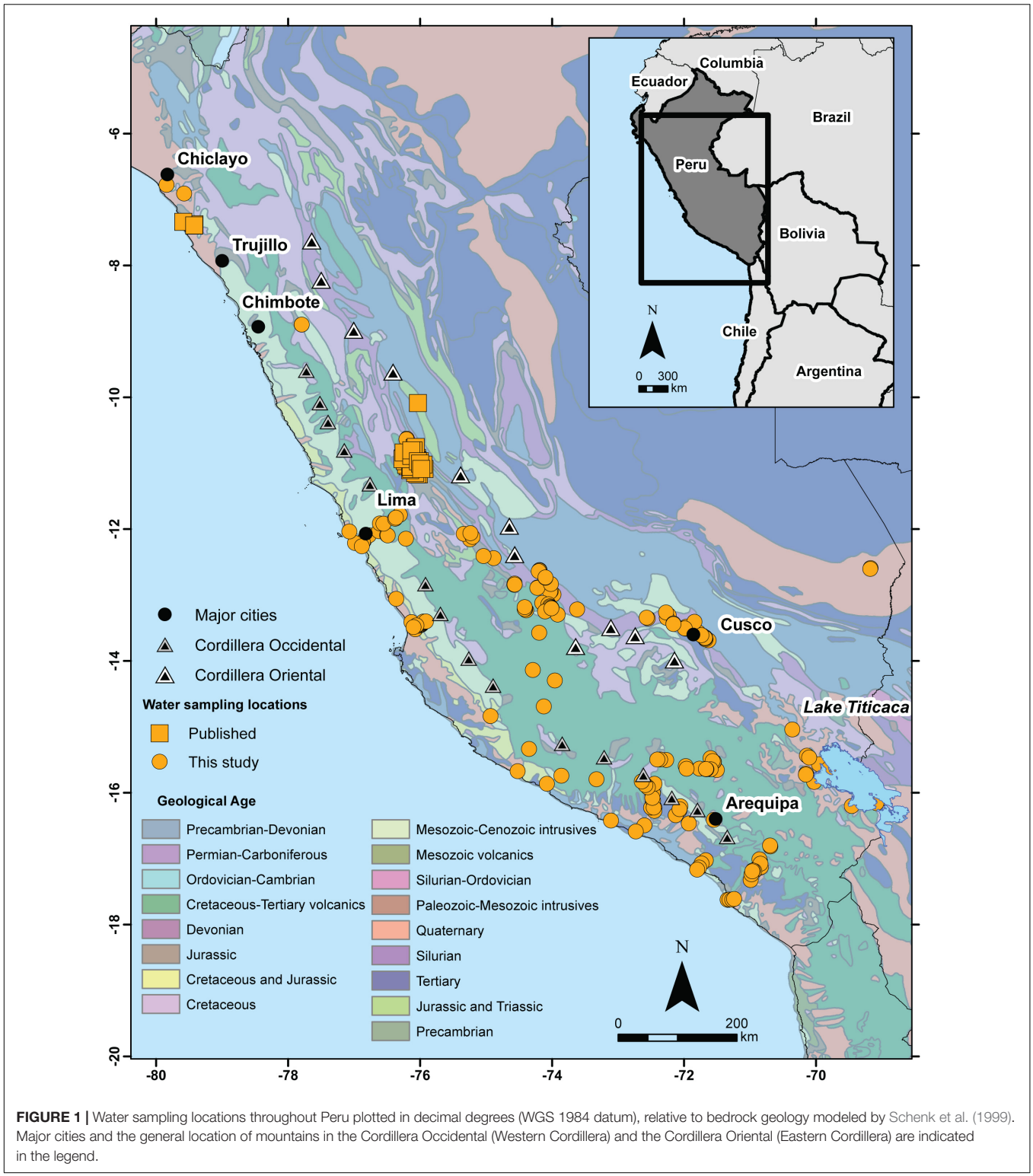

FIGURE 1 | Water sampling locations throughout Peru plotted in decimal degrees (WGS 1984 datum), relative to bedrock geology modeled by Schenk et al. (1999). Major cities and the general location of mountains in the Cordillera Occidental (Western Cordillera) and the Cordillera Oriental (Eastern Cordillera) are indicated in the legend.

et al., 2020). However, fauna may not be local at all, and this is especially true for livestock (Knudson et al., 2012a; Grimstead et al., 2016). Furthermore, the home ranges of small animals can be larger than expected and may crosscut discrete $^{87}Sr/^{86}Sr$ catchments (Copeland et al., 2010). Or, faunal substrate animals may have consumed non-local food, especially when they fed at or near archeological settlements that relied to some extent on imported or fertilized foods. Furthermore, animal behavior and physiology can also lead to results that do not represent the dietary catchment well; for example, land snails burrow

into discrete geological pockets (Thornton, 2011) and have an extraordinarily high rainwater contribution to their shell (Evans et al., 2009, 2010), leading to abnormal $^{87}Sr/^{86}Sr$ compared to other fauna or plants from the same area.

Plants are another common reference material for bioavailable strontium. When sampled from various root depths, they can provide a more representative mix of the dietary catchment (Åberg, 1995; Knipper et al., 2012; Grimstead et al., 2017), but caution still must be exercised when relying on plants for several reasons. First due to the process of biopurification, $^{87}Sr/^{86}Sr$ can vary throughout different plant organs and according to plant age (Bailey et al., 1996; Drouet et al., 2005; Drouet and Herbauts, 2008). Second, different species can also show distinct $^{87}Sr/^{86}Sr$ from the same location, due in part to their root systems accessing discrete pockets of strontium in the soil (Dijkstra, 2003; Poszwa et al., 2004). Third, differential contributions from sea spray and the acidity or other molecular differences of the microhabitat can cause plant $^{87}Sr/^{86}Sr$ to differ even when the same organ and species are sampled from the same location (Snoeck et al., 2020). A fourth complicating factor is the use of non-local fertilizers in either modern or ancient times, which can contribute a non-local geological signature to plant and soil samples (Bentley et al., 2004; Bentley, 2006; Evans et al., 2012; Thomsen and Andreasen, 2019). Sea bird guano (Julien et al., 1985; Szpak et al., 2012) and manure (Finucane, 2007) were commonly applied to agricultural fields throughout the pre-Hispanic Andes. Avoiding sampling from fertilized fields is therefore essential for accurately characterizing local bioavailable strontium throughout pre-Hispanic Andes (Knudson et al., 2014). However, in many parts of the Andes, unfertilized fields are rare to non-existent, so that systematic sampling of soils and plants to avoid contamination can be challenging if not impossible. Knudson et al.'s (2014) study suggests there is much more localized variability in bioavailable Sr that could be captured through systematic sampling of plants and other reference materials in the geologically and hydrologically complex dietary catchments of the Andes.

To that end, efforts are currently underway to develop local baseline models from environmental reference materials in discrete parts of the Andes, by a variety of research teams (e.g., Barberena et al., 2017; Barberena et al., 2019, *inter alia*; Serna et al., 2020). However, these efforts are largely localized to sub-regions of the Andes and constrained to sampling locations near targeted archeological sites. The only supra-regional analysis of Andean $^{87}Sr/^{86}Sr$ for archeological provenience published as of June 2020 is that of the Andean Paleomobility Unification (APU) project directed by Scaffidi and Knudson (2020). Arguing that humans provide the ultimate mixing model for $^{87}Sr/^{86}Sr$ in dietary catchments, this research shows that at a supra-regional scale, archeological tissue $^{87}Sr/^{86}Sr$ alone can be used to distinguish provenience between nearby areas, provided that suspected mobility routes are between discrete isoscape areas, along an east-west or coastal-highland gradient. However, this archeological isoscape does not handle equifinality well, given that people living at a similar distance from the coast but at different latitudes show similar $^{87}Sr/^{86}Sr$. Therefore, the ongoing aims of the APU project include developing broader regional coverage and exploring variability in different $^{87}Sr/^{86}Sr$ substrates to further refine expected local baselines in the Andes.

Skeletal tissue $^{87}Sr/^{86}Sr$ at a sampling location reflects the averaging of plant and animal foods I the diet. In prehistoric communities, these are assumed to have been mostly locally procured, with the plant portion of the diet dominating the $^{87}Sr/^{86}Sr$ in the tissues of omnivorous humans (Beard and Johnson, 2000; Montgomery, 2010). In the pre-Hispanic Andes, however, the local food assumption may not hold true, and may not hold true uniformly across different individual's diets within a community. As far back as the Preceramic, reciprocal exchange of maritime products and highland grains was practiced over robust long-distance trade networks throughout the Andes (Quilter and Stocker, 1983; Hastorf, 2003; see contributions in Dillehay, 2011; Cuéllar, 2013). Particularly with the rise of the first Andean states and empires, distinct diets developed between elites and subelites, so that access to imported foods varied between individuals in communities where social inequality was manifested through differential food consumption (Hastorf and Johannessen, 1993; Hastorf, 2003; Cuéllar, 2013). For communities or individuals with access to imported foods, diet-derived $^{87}Sr/^{86}Sr$ of human tissues might depart significantly from local plant, animal, and soil inputs. Therefore, it would not be surprising for archeological human $^{87}Sr/^{86}Sr$ in the Andes to deviate substantially from any mixed model of local soil, plant, and faunal $^{87}Sr/^{86}Sr$. However, given that the human body is up to 60% water, with up to 31% of skeletal tissues comprised by water (Mitchell et al., 1945), the $^{87}Sr/^{86}Sr$ of imbibed water may also contribute significantly to skeletal tissues. If this is the case, local drinking water $^{87}Sr/^{86}Sr$ analysis could help diminish the effect of imported foods. Therefore, this paper examines the potential for water $^{87}Sr/^{86}Sr$ to predict $^{87}Sr/^{86}Sr$ in archeological human tissues, comparing water $^{87}Sr/^{86}Sr$ and measured vs. predicted $^{87}Sr/^{86}Sr$ between samples from different elevations, watershed sizes, and underlying geologies.

Assessing Water as a Proxy for Local Skeletal $^{87}Sr/^{86}Sr$

Water is influential in the $^{87}Sr/^{86}Sr$ of a dietary catchment and varies somewhat predictably throughout watersheds and flowing surface water networks (Aubert et al., 2002; Bataille and Bowen, 2012; Frei and Frei, 2013; Bataille et al., 2014; Zitek et al., 2015; Crowley et al., 2017). Because the Sr/Ca entering food chains in the form of plants are directly related to the Sr/Ca of the water they consume (Sillen and Kavanagh, 1982), dissolved strontium in surface and groundwater heavily influences plant and faunal $^{87}Sr/^{86}Sr$ (Beard and Johnson, 2000; Bentley, 2006; Bataille and Bowen, 2012). Fast-flowing rivers might be suspected to carry a greater proportion of strontium from distant rocks and soils relative to slower-moving rivers, but the $^{87}Sr/^{86}Sr$ of river water has repeatedly been observed as consistent regardless of flow rate (see summary in Bentley, 2006, p. 8), seasonal, or long-term temporal variation (Voerkelius et al., 2010). In geologically active, higher elevations or during seasons of low discharge, flowing water $^{87}Sr/^{86}Sr$ is higher (more radiogenic), reflecting faster weathering of higher $^{87}Sr/^{86}Sr$ rock from higher elevation water

sources throughout the watershed's headwaters, depositing high-altitude sediments on floodplains (Bentley, 2006). The $^{87}Sr/^{86}Sr$ of these sediments is then mixed into the waters consumed throughout the dietary catchment at a given sampling location (see summary in Bataille et al., 2020, pp. 5–6). Hodell et al. (2004) report that water body depth also influences $^{87}Sr/^{86}Sr$—locations with shallower water tables reflect upstream mixing, while locations with deeper water tables reflect more of the underlying bedrock signature. Watershed size also influenced $^{87}Sr/^{86}Sr$ variability, with larger watersheds leading to more homogenized $^{87}Sr/^{86}Sr$ in rivers (Brennan et al., 2019).

There are several limitations to using water $^{87}Sr/^{86}Sr$ as a reference material. First, sampling locations low in a watershed might also have greater pollution levels from upstream agricultural runoff, so higher elevation waters more closely reflect the weathering of underlying bedrock (Buhl et al., 1991; Tricca et al., 1999; Eikenberg et al., 2001; Thomsen and Andreasen, 2019). However, a recent study of Danish surface waters (Frei et al., 2020) shows that much of agricultural lime is retained by soils, so agricultural contamination may not influence surface water $^{87}Sr/^{86}Sr$ as much as previously thought. Second, proximity to the ocean also impacts water $^{87}Sr/^{86}Sr$. Because modern ocean water is uniform across the planet ($^{87}Sr/^{86}Sr = 0.7092$) (Veizer, 1989), sea spray and brackish water can drive up otherwise low $^{87}Sr/^{86}Sr$ in coastal plains (Whipkey et al., 2000; Bentley, 2006; Snoeck et al., 2020), particularly for water samples closest to the ocean. This can lead $^{87}Sr/^{86}Sr$ in coastal regions to deviate from expectations based on bedrock. Third, Sr concentrations are generally low in global surface waters (0.06 ppm on average) (Capo et al., 1998), so water samples can be difficult to measure. Finally, at a global scale, river water $^{87}Sr/^{86}Sr$ is less variable than other substrates (Peucker-Ehrenbrink and Fiske, 2019; Bataille et al., 2020), which may average out some of the $^{87}Sr/^{86}Sr$ variability needed for identifying non-locals in zones with homogeneous bedrock geology.

Notwithstanding these potential drawbacks, surficial and groundwaters have been used as $^{87}Sr/^{86}Sr$ reference materials for provenience human samples. The earliest approach involved testing $^{87}Sr/^{86}Sr$ of water sources and comparing those to people known or suspected to reside at those locations. Over four decades ago, Nixon and Helsby (1976) showed a relationship between strontium concentrations of tap water in 12 English towns and tooth enamel of their human residents. However, a more recent study found no relationship with modern tooth enamel $^{87}Sr/^{86}Sr$ and tap water $^{87}Sr/^{86}Sr$ throughout the Netherlands (Kootker et al., 2020). In another study, Tipple et al. (2018) found that modern human hair $^{87}Sr/^{86}Sr$ reflected tap water $^{87}Sr/^{86}Sr$. They analyzed 41 student hair samples alongside 99 tap water samples collected from sites around three schools in Salt Lake City, Utah, and found that only 6 hair samples fell outside of the tap water ranges for those locations (Tipple et al., 2018, p. 4, inferred from **Figure 4**). However, all tap water and hair $^{87}Sr/^{86}Sr$ fell within 0.0070 of each other (inferred from **Figure 4**), and the three schools shared overlapping $^{87}Sr/^{86}Sr$, so that without known provenience data it would be impossible to distinguish between origin sites for all but individuals with the highest $^{87}Sr/^{86}Sr$. In contrast with the Nixon and Helsby (1976) enamel study, the Tipple et al. (2018) study shows that $^{87}Sr/^{86}Sr$ in hair reflects uptake from bathing waters rather than from imbibed water.

Recent studies suggest that dietary Sr dominates human skeletal tissue $^{87}Sr/^{86}Sr$ rather than drinking water or atmospheric contributions. For example, a recent porcine controlled feeding study (Lewis et al., 2017) shows that there is little correlation between drinking water $^{87}Sr/^{86}Sr$ and skeletal $^{87}Sr/^{86}Sr$ compared to high correlations between dietary $^{87}Sr/^{86}Sr$ and skeletal $^{87}Sr/^{86}Sr$. However, this study is limited by a small sample size (n = 19 pigs) and the assumption that human water metabolism is like that of pigs. Similarly, a large study of French children (Glorennec et al., 2016) shows that Sr concentrations are dominated by dietary Sr contributions rather than drinking water or atmospheric dust. However, this study is limited in that tissues were not directly tested for $^{87}Sr/^{86}Sr$—instead, dietary Sr concentrations were estimated from known values of foods reported in national survey data. Furthermore, the sources of water were not controlled for. Bottled water was widely consumed by study participants, so the Sr concentrations may not reflect local water. Lewis et al. (2017) further clarify that drinking water can, in fact, contribute to skeletal $^{87}Sr/^{86}Sr$ in animals that drink frequently or in landscapes with Sr-rich waters. Additional testing of human tissues relative to known food and water sources is needed to further clarify how much water $^{87}Sr/^{86}Sr$ is integrated into human bioapatite relative to dietary sources in Andean landscapes.

The potential of using water $^{87}Sr/^{86}Sr$ for archeological skeleton provenience has varied according to study location and approach. Many baseline studies including water do not directly compare water and archeological human $^{87}Sr/^{86}Sr$ (Hodell et al., 2004; Bentley and Knipper, 2005; Frei and Frei, 2011, 2013; Lengfelder et al., 2019; Ladegaard-Pedersen et al., 2020; Pacheco-Forés et al., 2020), although some incorporate water into a mixed or predictive model and evaluate archeological data points against that model (e.g., Montgomery et al., 2007; Snoeck et al., 2020). Among studies in mountainous regions comparing skeletal $^{87}Sr/^{86}Sr$ directly to local water measurements, a relationship is reported between water elevation, sample variability, and fit of archeological samples to local water. In the Rhine Valley of the Alps, Hoogewerff et al. (2001) found that high elevation stream water $^{87}Sr/^{86}Sr$ in an area comprised of old, high Rb/Sr gneisses the river's headwaters matched historic skeletal $^{87}Sr/^{86}Sr$ better than waters overlying younger, lower Rb/Sr limestone. After excluding outlier archeological pig $^{87}Sr/^{86}Sr$, Bentley and Knipper (2005) report a similar finding for Rhine Valley sites—archeological samples overlapped with water $^{87}Sr/^{86}Sr$ from published studies, and showed more variability in the uplands than the lowlands. So far, direct comparisons of water and archeological $^{87}Sr/^{86}Sr$ have not been published for the Andes, but similar highland vs. lowland trends are to be expected for the similarly geologically complex river valleys of the Andes mountains.

The second approach to water $^{87}Sr/^{86}Sr$ sourcing involves testing water $^{87}Sr/^{86}Sr$ throughout a region, generating an isoscape predicting $^{87}Sr/^{86}Sr$ at unmeasured regions, and then validating that model with $^{87}Sr/^{86}Sr$ measurements from tissue

samples. Testing how well a water strontium isoscape for the United States derived from bedrock weathering projections and river $^{87}Sr/^{86}Sr$ measurements (Bataille and Bowen, 2012) predicts mammalian body tissues, Crowley et al. (2017) found that that large-bodied mammalian tissues were more accurately predicted by the surface water model than vegetation and fish skeletons. They also report that the surface water model predicted mammalian tissues better for small, relatively non-complex watersheds than for larger watersheds. Frei and Frei (2011) found that surface water $^{87}Sr/^{86}Sr$ predictions in Denmark were consistently 15% higher in modern snail shell and soil leachates than in water samples from the same location, but modern sheep wool coincided with water $^{87}Sr/^{86}Sr$. Lengfelder et al. (2019) used water $^{87}Sr/^{86}Sr$ in the Alps to construct an environmental mixing model which predicted $^{87}Sr/^{86}Sr$ $^{87}Sr/^{86}Sr$ in 70% (80/115) zooarchaeological samples. Lengfelder et al. (2019) considered the prediction matching if it fell within the isoscape prediction ± (2 SD + mean offset between water and archeological fauna, which was ∼0.001 for their study area). These appear to be the only studies that validate predictive models based on water $^{87}Sr/^{86}Sr$ for modern mammalian or archeological tissues. It is important to note that none of these studies tested water $^{87}Sr/^{86}Sr$ models with human skeletal $^{87}Sr/^{86}Sr$; in light of this and recent feeding studies critiqued above (Glorennec et al., 2016; Lewis et al., 2017), understanding how much water contributes to skeletal $^{87}Sr/^{86}Sr$ is an ongoing research question.

In the present study, water was selected as a potential baseline proxy for the bioavailable strontium in archeological human tissues for several reasons. First, water samples are relatively quick to process (as described in section "Sample Collection and Strontium Isotope Analysis Methods" below). Unlike for stable oxygen isotope analysis, which is impacted by evaporation and storage of water samples, there is no evidence that $^{87}Sr/^{86}Sr$ is impacted by water storage and evaporation, so old, un-parafilmed samples can still be analyzed. Second, agricultural fields in many parts of the Andes are rarely planted up to the river line, to secure crops from seasonal flooding. Due to this, water samples from rivers are suspected to be less likely than plants or soils to be contaminated by non-local fertilizer (although this may not be the case for stationary water bodies). Third, unlike foods that were sometimes exchanged across great distances in the prehistoric Andes, water was difficult to transport and would have been largely imbibed from local sources. Particularly in dry coastal valleys of the Peruvian Andes, settlements were located within walking distance of rivers, which comprised some of the only sources of drinking water in many places[2]. While the composition and geographic origin of diets often varied within and between neighboring archeological sites due to social status differences, gender, occupation, or other social identities, drinking water should have been sourced mostly from the same nearby locations. Finally, surface water provides an inherently mixed model of local and upriver bioavailable strontium catchments that averages bedrock weathering, soil runoff, atmospheric, and upriver water contributions as it moves throughout the watershed. When local foods are consumed, the overall contribution of local water to the human diet may be further amplified—i.e., directly imbibed water is disproportionately represented in human tissues, and in the tissues of local plants and animals consumed. Based on the studies above, it is hypothesized that $^{87}Sr/^{86}Sr$ will vary according to elevation, watershed size, and underlying geological age. It is also hypothesized that homogenous water at lower elevations will better predict human archeological $^{87}Sr/^{86}Sr$ compared to geologically complex higher elevation zones.

Sample Collection and Strontium Isotope Analysis Methods

Water samples were collected by co-authors and collaborators[3] during the North American summer and early fall of the 2009–2019 field seasons that comprise the drier months of the Austral winter and spring (**Supplementary Table S1**). We focused on collecting surface water from Southern Peru, where the majority of the co-authors' archeological samples were excavated. Because lakes, rivers, and streams would have been the most commonly used drinking water sources for archeological communities, we focused our collection on flowing surface water near archeological sites, far from fertilized fields (following the prior methods of BSIRL and APU described in Zimmer-Dauphinee et al., 2020). Since much of the municipal water stores in Peru come from diverted surficial water, we also tested tap and fountain water samples to understand how accurately they reflect surface water $^{87}Sr/^{86}Sr$, following Chesson et al.'s (2012) investigation of tap water in the United States. Between 15 and 50 mL of sediment-free water was collected from each location and each was categorized as surface water (rivers, streams/tributaries, lakes/ponds), ground or subsurface water (springs/wells), or man-made storage or diversion of surface water (reservoirs, canals, tap water/fountains). Non-acid washed collection vials were parafilmed to prevent contamination.

The geographic coordinates, water temperature, speed, location of sampling within the water body were collected by APU collaborators in a database developed by Scaffidi using the cloud-based and collaborative Collector app (ESRI) deployed on mobile devices equipped with Bad Elf precision GPS receivers accurate to within 2 m. Coordinates collected by the ACL and BSIRL were collected with consumer to technical grade GPS receivers ranging from 10 m to 1 m in locational accuracy, and limited hydrological data was collected from sampling sites.

[2]Water management practices in the pre-Hispanic Andes were intensive—coastal and highland regions utilized expansive irrigation systems to divert water into agricultural fields and settlements (Netherly, 1984; Denevan, 2001; Billman, 2002; Lane, 2014) or to tap underground water sources (see discussion of Nasca coastal aqueducts and well systems in Schreiber and Lancho Rojas, 2003). Regardless of this hydraulic expertise, in many areas, much of diverted water would have been sourced from local surface or groundwater. Thus, even if ancient Peruvians consumed most of their water from irrigation-fed fountains, water $^{87}Sr/^{86}Sr$ should largely reflect local drinking water sources.

[3]As reflected in **Supplementary Table S1**, samples were collected by researchers from the Archaeological Chemistry Laboratory (Center for Bioarchaeological Research, School of Human Evolution and Social Change, Arizona State University), the Vanderbilt University Bioarchaeological and Stable Isotope Research Laboratory (Department of Anthropology), and the Andean Paleomobility Unification Project directed by the first author, in collaboration with both laboratories.

Finally, a literature search for published water $^{87}Sr/^{86}Sr$ in the Andes was completed. Several publications list $^{87}Sr/^{86}Sr$ for water sources in and around the Andes (Coudrain et al., 2002; Grove et al., 2003; Santos et al., 2015), but only one study published sample collection coordinates necessary for addition to this study's database (Flusche et al., 2005). Coordinates were determined for published water $^{87}Sr/^{86}Sr$ points from the North Coast of Peru (Alaica et al., 2020). Sampling locations are illustrated relative to the bedrock geological units modeled by Schenk et al. (1999) in **Figure 1**.

Water samples were prepared for analysis in the Archaeological Chemistry Laboratory (Center for Bioarchaeological Research) at Arizona State University following established protocols (Pacheco-Forés et al., 2020). Water was strained into metal-free vials through a 2.5 μm pore size filter paper and acidified with 5% HCl to prevent microbial growth. In the Metals, Environmental, and Terrestrial Analytical Laboratory (METAL Lab) at Arizona State University, water was evaporated and precipitates were re-dissolved in concentrated nitric acid and diluted to a 2 M stock solution. From the stock, a 1 mL aliquot was measured for elemental concentrations on the Thermo Fisher Scientific iCAP quadrupole inductively coupled plasma mass spectrometer (Q-ICP-MS). Strontium was separated through ion chromatography using a Sr-Ca ion exchange resin either with manual columns using Eichrom brand Sr Spec resin (Horwitz et al., 1992) or TODGA resin on the prepFAST automated low pressure chromatography system (Pourmand and Dauphas, 2010; Romaniello et al., 2015). For samples separated on the prepFAST system, elemental concentrations were compared for sample aliquots taken before and after strontium separation, to verify consistent yields were achieved. After separation, the strontium-containing sample was completely evaporated in a Teflon beaker and refluxed with concentrated nitric acid and 30% hydrogen peroxide to oxidize organic complexes eluted from the resin. Samples were then evaporated and reconstituted with 0.32 M nitric acid. Finally, samples were diluted with 0.32 M nitric acid in the amount necessary to achieve a concentration of 50 ppb Sr, based on the elemental concentrations of each sample from analysis on the Q-ICP-MS.

Strontium isotope ratios were measured on the Thermo-Finnigan Neptune multicollector inductively coupled plasma mass spectrometer (MC-ICP-MS) using an Apex sample introduction system. Measurements were made after on-peak blank correction, rejection of voltage outliers greater than 2 standard deviations outside the mean and normalization of $^{87}Sr/^{86}Sr$ ratios to $^{86}Sr/^{88}Sr$ of 0.1194 (Romaniello et al., 2015). Prior to any sample analysis, a sequence of SRM 987 from five to 50 ppb was analyzed to ensure measured $^{87}Sr/^{86}Sr$ was accurate within 0.00002 over the entire range. The analytical sequence included bracketing concentration-matched SRM 987 standard every six samples, and frequent secondary check standards. The SRM 987 bracketing standard was measured as 0.710247 ± 0.000019 (2 *SD*, n = 63) with a standard error of 0.000001. Purified IAPSO seawater gave an accurate value of 0.709169 compared to the known value of 0.709187 (Romaniello et al., 2015). A secondary check standard was created to simulate a sample with poor chemical recovery, SRM 987 run at 50% of the concentration of the bracketing standard and doped with calcium ICP solution to a Ca/Sr ratio of 500. This provided both an accurate and precise value of 0.710231 ± 0.00004 (2 *SD*, n = 28) with a standard error of 0.000004. In addition to these analytical check standards, NIST 1400 was purified and measured in parallel to samples to evaluate user and laboratory accuracy and precision. Aliquots of NIST 1400 similar in amount to samples was processed with each batch of samples; over the course of this project, the measured value was 0.713118 ± 0.000053 (2 *SD*, n = 10) with a standard error of 0.000008. This was in good agreement with the GeoREM value of 0.71314 (Romaniello et al., 2015).

$^{87}Sr/^{86}Sr$ was rounded to four decimal places before spatial and statistical analyses, as this has been found to be sufficient for discriminating between origins for human tissues (Bentley, 2006; Knudson et al., 2016). Then, point values were divided into subgroupings for statistical analysis. Following prior work (Scaffidi and Knudson, 2020), groups were assigned to geo-ecological zones of Pulgar Vidal (1981): coastal (0 – 500 masl), *yunga* (500 – 2300 masl) and highland (2300+ masl). Point values were also divided into subgroups by geological era (Cenozoic, Mesozoic, and Paleozoic). Finally, point values were divided into groups based on watershed size, which was arbitrarily defined as small (<500,000 ha), medium (500,000 – 1 million ha), and large (>1 million ha). Because $^{87}Sr/^{86}Sr$ and the residuals were non-normally distributed according to Shapiro–Wilks tests and could not be transformed into normal distributions (see results), the non-parametric Kruskal–Wallis test was used to compare central tendencies and variability between three subgroupings. Mann–Whitney *U* was used to compare central tendencies between two subgroupings.

Spatial Analysis and Geostatistical Methods

All spatial and geostatistical analysis was completed with the Geostatistical Analyst tools in ArcMap 10.6.2 following prior Andean isoscape modeling methods (Scaffidi and Knudson, 2020; Zimmer-Dauphinee et al., 2020). Sampling location points (n = 263) recorded in degrees, minutes, seconds, or UTM were projected to decimal degrees (WGS, 1984) as a common coordinate space. One sample was from the Maipo Valley in Chile, and due to its distance from the main geographic focus area, it was excluded from geostatistical analysis, leaving 262 Peruvian samples. Points were plotted in ArcMap 10.6.2 and projected to the Albers Equal Area Conic coordinate system, which is necessary for accurate modeling of metric distances with the least distortion possible at the regional scale in South America. The name, distance in meters, and type of the nearest surface water body (i.e., primary river, secondary river, or lake/pond) was determined using the near tool in ArcMap. Following Scaffidi and Knudson (2020, p. 6), elevation at each sampling location was extracted from the 250 m resolution Aster Digital Elevation Model (version 2) (Tachikawa et al., 2011) and coded as coastal (0–500 masl), *yunga* (mid-elevation, 500–2300 masl), or highland (2300 masl and higher).

Finally, each sampling location was spatially joined to DEM-derived drainage basins/watershed boundaries created by the HydroSHEDS project (Lehner and Grill, 2013), primary rivers (Instituto Geográfico Nacional de Perú, 2015), and the bedrock geology model of Schenk et al. (1999).

Before generating the isoscape, an analysis for suspected aberrant $^{87}Sr/^{86}Sr$ values was carried out. This is important, as a high percentage of the highland Colca Valley samples were collected from puquios or wells made with non-local cements and/or quarried stone. Furthermore, some highland samples were collected from canals flowing from higher to lower field terraces, or from areas with a history of mining contamination. These factors contributed to suspicion of non-representative $^{87}Sr/^{86}Sr$ in some parts of the highlands, necessitating analytical scrutiny. In order to assess the dataset for the possibility of contamination, following prior archeological isoscape studies (Pellegrini et al., 2016; Scaffidi and Knudson, 2020), spatial outliers identified as high-low or low-high clusters were screened for with the Anselin Local Moran's I statistic in ArcMap and were trimmed from the dataset prior to generating the isoscape.

Because the trend analysis tool in ArcMap identified a strong east-west trend from less to more radiogenic, Universal Kriging with first order trend removal was used to detrend the dataset, model the residuals, and add the trend back in to the final model. Due to the non-normal distribution (see results), $^{87}Sr/^{86}Sr$ was modeled using *trans*-Gaussian kriging and first transformed with the arcsin transformation. The best fit model was selected based on the following criteria: lowest mean standard error between predicted and measured $^{87}Sr/^{86}Sr$, a root-mean square and average standard error closest to each other, a mean standardized error closest to 0, and a root-mean-square standardized error closest to 1 (Oliver and Webster, 1990; Oliver and Webster, 2014, 2015). Coincidental points were not averaged before kriging and **Supplementary Table S2** presents the parameters used to achieve the best fit model.

The best fit model was assessed in two ways. First, a random 20% subset of the water measurement points was removed, the remaining 80% training subset was modeled on the same parameters as the best fit model and measured vs. predicted $^{87}Sr/^{86}Sr$ was cross-validated for the 20% test subset. Second, the models were tested with published $^{87}Sr/^{86}Sr$ archeological human tissue measurements at known geographic coordinates from the archeological meta-analysis compiled by Scaffidi and Knudson (2020). The archeological test set was limited to 12 sites spanning the coast, *yunga,* and highlands, with samples of 10 or more individuals. Trophy heads and sacrificial victims were excluded, given the likelihood that they represented non-local individuals. The archeological dataset was also limited to sites with a low proportion of inter-quartile range (IQR) outliers relative to the sample size analyzed (see Scaffidi and Knudson, 2020); specifically, sites with an IQR outlier proportion more than 10.0%[4] were excluded (n = 493 archeological human $^{87}Sr/^{86}Sr$). Each site's IQR outliers were trimmed from the archeological test dataset prior to plotting the points and extracting predicted $^{87}Sr/^{86}Sr$ from the kriged isoscape raster, elevation, geological units, and watershed size at each site.

Cross-validation and model tests produced two metrics that are emphasized here: prediction error, which is the difference between measured and predicted $^{87}Sr/^{86}Sr$ at a given location, and prediction standard error (PSE or uncertainty) at each sampling location or archeological site. Linear regressions were also used to assess the fit between measured water and predicted $^{87}Sr/^{86}Sr$ and between measured archeological $^{87}Sr/^{86}Sr$ from the Scaffidi and Knudson (2020) dataset and water isoscape predicted $^{87}Sr/^{86}Sr$. The $^{87}Sr/^{86}Sr$ at each site was considered a match if it fell within the isoscape $^{87}Sr/^{86}Sr$ prediction $\pm$ prediction standard error at that location. Kruskal–Wallis tests were then used to compare $^{87}Sr/^{86}Sr$ prediction standard errors between site groupings based on elevation, geology, and watershed characteristics. Finally, Chi-squared was used to compare the proportions of archeological samples falling within and beyond the geostatistical prediction standard error at each site to understand whether higher prediction rates were associated with an elevational zone.

RESULTS

Andean Water $^{87}Sr/^{86}Sr$ Is Related to Elevation, Bedrock Geology, and Watershed Size

Plotting water sampling locations (n = 262)[5] demonstrates that water was collected from a wide range of watersheds and underlying geologies. Water was collected from 31 distinct watersheds, reflecting sampling coverage of approximately one-quarter (24.4%) of the 127 watersheds within Peru (**Figure 2**). The geographic coordinates, elevation, and watershed characteristics of sampling locations are reported in **Supplementary Tables S1, S4**. Water was collected from locations corresponding to 10 bedrock geological age units (according to the Schenk et al., 1999 model), reflecting sampling coverage of approximately two-thirds (66.7%) of the 15 bedrock age units in Peru.

Elemental concentrations of ^{88}Sr are sufficient to measure $^{87}Sr/^{86}Sr$ in all samples, ranging from 0.0001 – 0.0113 (M = 0.0007, SD = 0.0019, n = 220) (**Supplementary Table S3**). New $^{87}Sr/^{86}Sr$ from this study (n = 220) are reported in **Supplementary Table S4**. Throughout the entire sample water $^{87}Sr/^{86}Sr$ ranges from 0.7049 to 0.7227 (M = 0.7081, SD = 0.0027, n = 262). Water $^{87}Sr/^{86}Sr$ and residuals are non-normally distributed according to Shapiro–Wilk, $W(261) = 0.672$, $p < 0.001$. Trend analysis in ArcMap shows a strong east-west trend where $^{87}Sr/^{86}Sr$ increases longitudinally with elevation and distance from the coast. Water $^{87}Sr/^{86}Sr$ is lowest near the coasts of Lima, Moquegua, and Nasca. Water $^{87}Sr/^{86}Sr$ increases to the highest (most radiogenic) around the eastern portion of Lake

[4]Sites with high proportions of IQR outliers include places like the Inca site of Machu Picchu, where studies have shown high variation in $^{87}Sr/^{86}Sr$ because they were settled by people from diverse geographic origins (Turner et al., 2009; see discussion in Scaffidi and Knudson, 2020). Samples from settlements comprised of a high relative proportion of probable first-generation migrants would not be expected to match the local environmental baseline as communities comprised of mostly locally born individuals, and were thus excluded from the archeological test set.

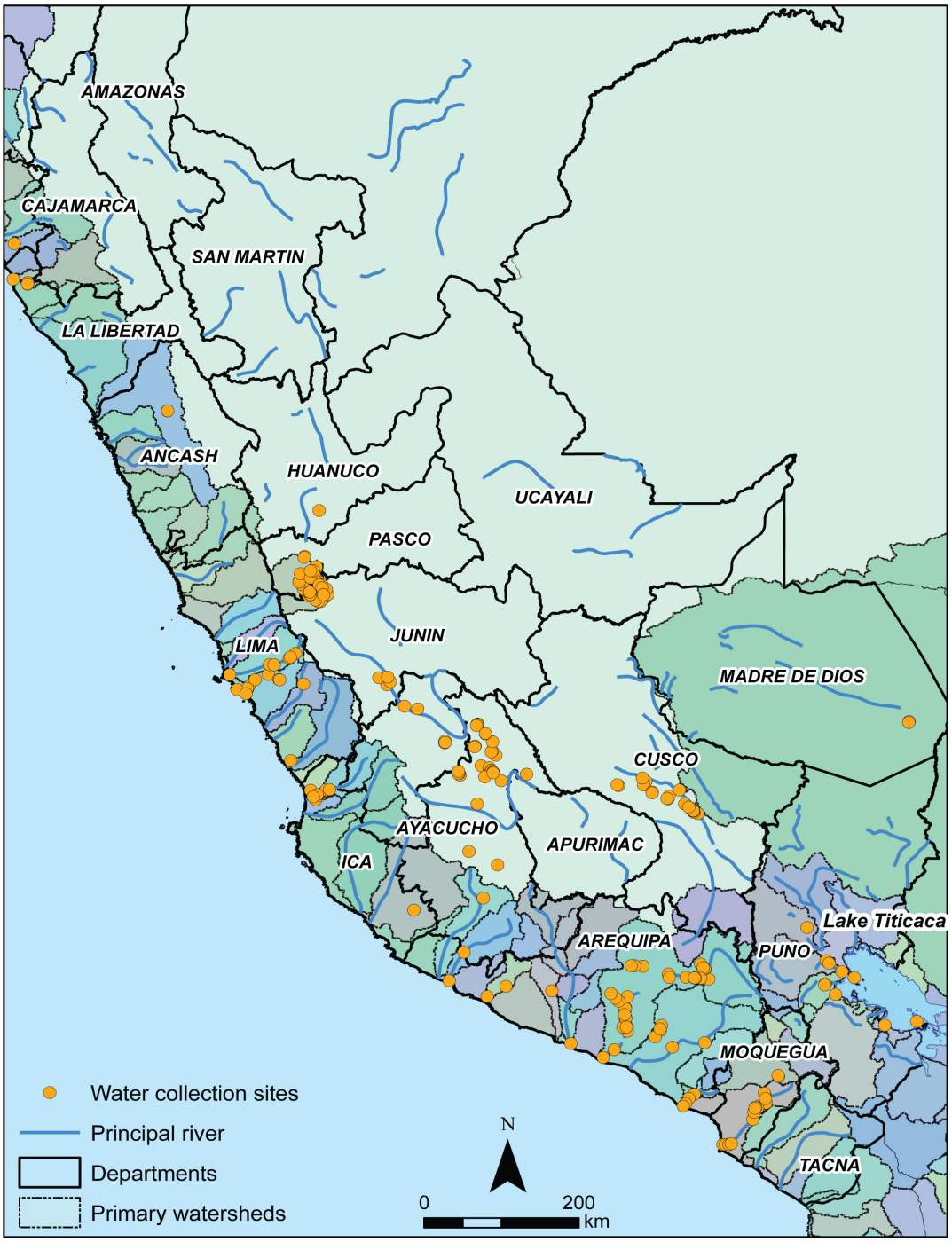

FIGURE 2 | Water sampling locations (n = 262) throughout Peruvian departments (labeled with solid outline) relative to principal rivers and primary watersheds (colored fill with dashed outline).

Junín, the eastern Ayacucho Basin, and the northwestern part of the Cusco Valley near Machu Picchu (**Figure 3**).

Water $^{87}Sr/^{86}Sr$ varies according to elevation, watershed size, and underlying bedrock geological age. Highland samples show a significantly different median $^{87}Sr/^{86}Sr$ (*Median* = 0.7080, *SD* = 0.0031, n = 162) than those from the coast (*Median* = 0.7067, *SD* = 0.0016, n = 56) and *yunga* (*Median* = 0.7068, *SD* = 0.0013, n = 44), Kruskal–Wallis $H(2) = 35.97$, $p < 0.001$ (**Figure 4A**). Similarly, larger watersheds show significantly higher and more variable $^{87}Sr/^{86}Sr$ (*Median* = 0.7080, *SD* = 0.0029, n = 135) than small ones (*Median* = 0.7067, *SD* = 0.0011, n = 62) and medium ones [*Median* = 0.7070, *SD* = 0.0029, n = 65,

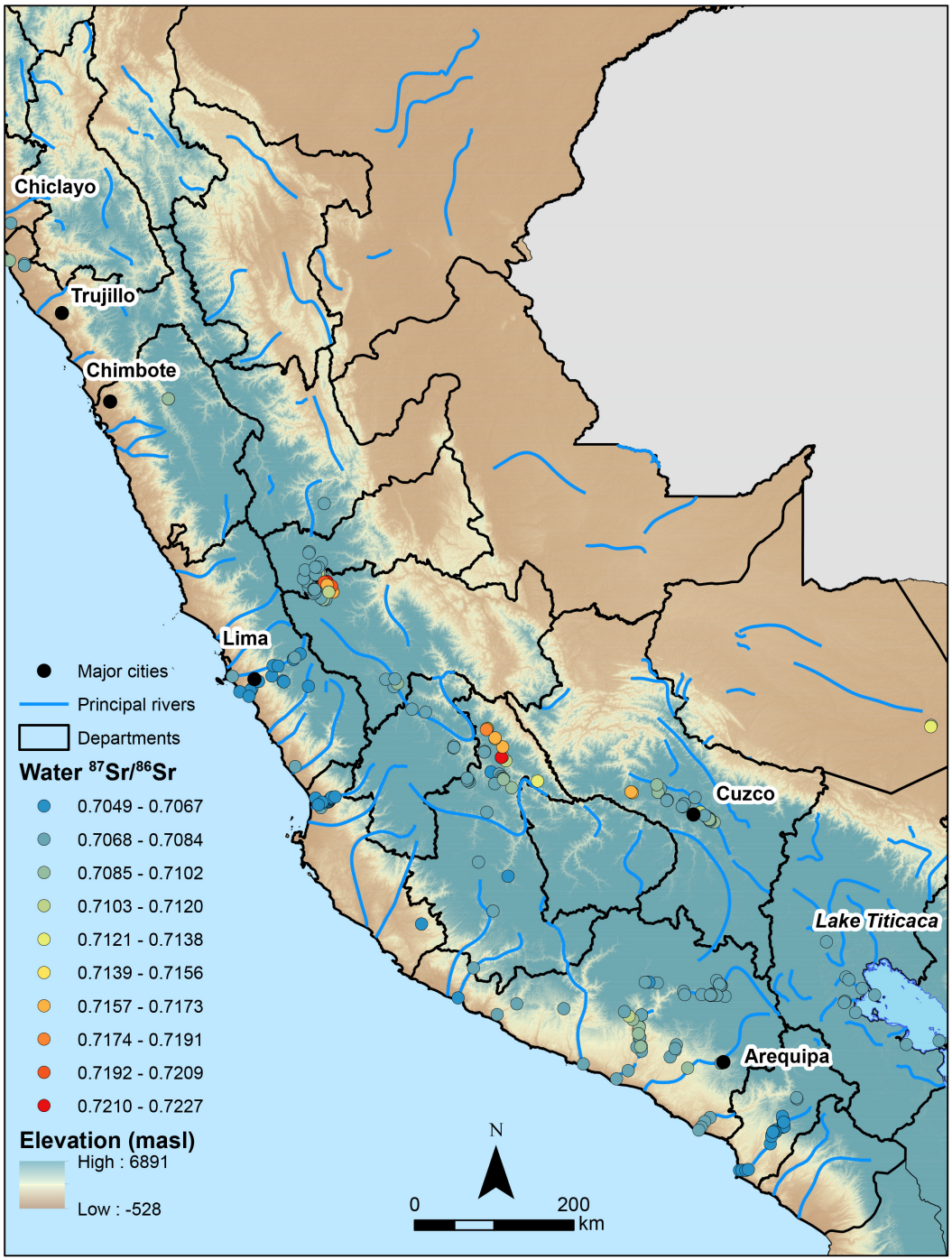

FIGURE 3 | Peruvian water $^{87}Sr/^{86}Sr$ results, arbitrarily divided into 10 equally sized bins, relative to the locations of major cities, rivers, and elevation at sampling locations (n = 262).

Kruskal–Wallis $H(2) = 50.47$, $p < 0.001$] (**Figure 4B**). Watershed size (hectares) accounts for nearly 60% of the variability in water $^{87}Sr/^{86}Sr$ (Adjusted R^2 = 0.60); as watershed size increases, so does the standard deviation within the watershed. Watershed size accounts for 43.6% of $^{87}Sr/^{86}Sr$ variation (SD) across a watershed (Adjusted R^2 = 0.42). These differences in water $^{87}Sr/^{86}Sr$ also correspond to the geological age of the underlying bedrock geological units (**Supplementary Table S5**). Water overlying units deposited in the most distant past, the Paleozoic, are significantly more radiogenic (*Median* = 0.7087, *SD* = 0.0034, n = 31) compared to those from the Mesozoic (*Median* = 0.7076, *SD* = 0.0027, n = 134) and the most recent

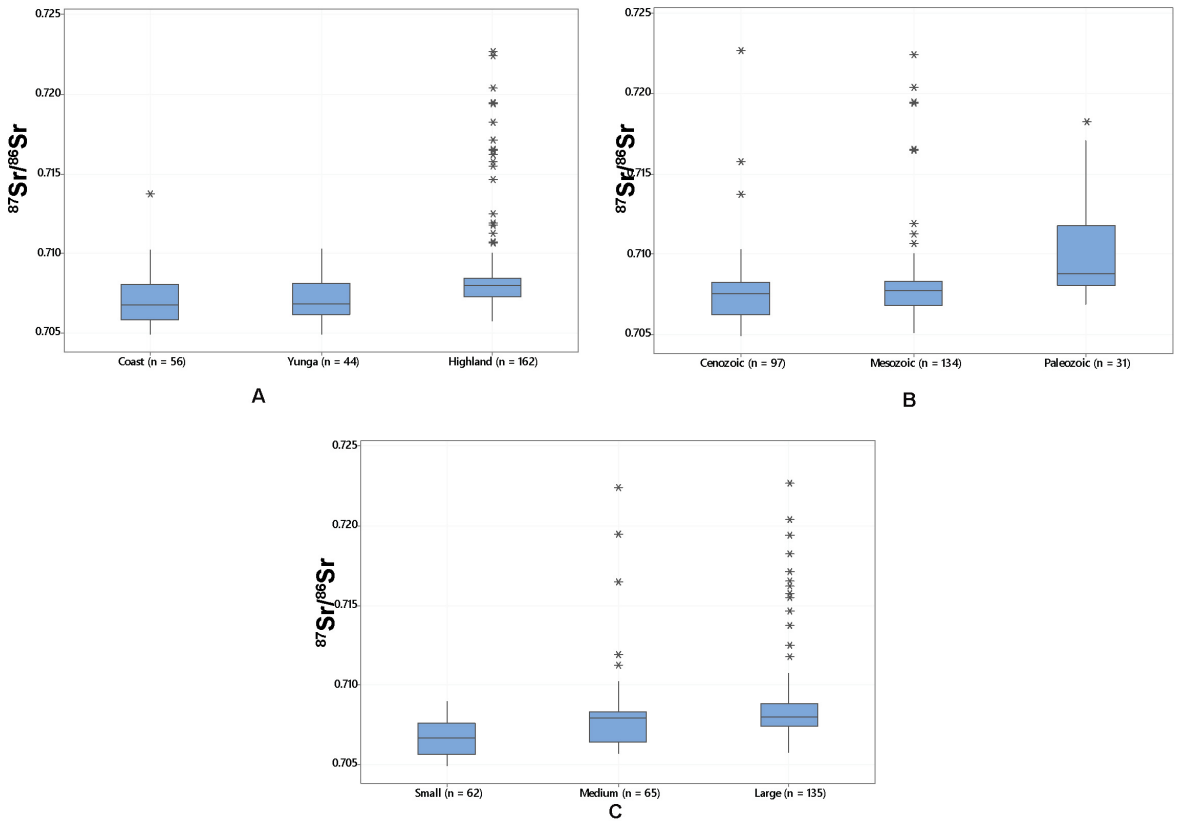

FIGURE 4 | (A) Boxplot of $^{87}Sr/^{86}Sr$ (n = 262) from coastal, *yunga*, and highland elevations; **(B)** Boxplot of $^{87}Sr/^{86}Sr$ from small, medium, and large watersheds (hectares); and **(C)** Boxplot of water $^{87}Sr/^{86}Sr$ overlying geological units from the Cenozoic, Mesozoic, and Paleozoic eras (from most recently to oldest deposited bedrock).

Cenozoic [*Median* = 0.7076, *SD* = 0.0022, n = 97, Kruskal–Wallis $H(2) = 26.45$, $p < 0.001$].

Anselin Local Moran's I test generates 13 spatial outlier $^{87}Sr/^{86}Sr$ that were excluded from the isoscape model, since they were suspected to reflect contamination from agricultural runoff or storage in non-native stone wells at those sampling locations. Of these outliers, nine are low $^{87}Sr/^{86}Sr$ surround by abnormally high $^{87}Sr/^{86}Sr$. One of these is an abnormally low value from a high-elevation (3900 masl) stream in the Ayacucho Basin. The remaining eight abnormally low $^{87}Sr/^{86}Sr$ are from around the western and northern Lake Junín area collected by the Flusche et al. (2005) study. There are also four points with abnormally high $^{87}Sr/^{86}Sr$ surrounded by more typical low $^{87}Sr/^{86}Sr$. Three of these are from the high-elevation Colca Valley of the Department of Arequipa—one is from a natural spring, and two are from man-made irrigation canals. The final high-low outlier is from a stream in Lucanas in the Ayacucho Basin. Interestingly, none of the tap water samples (n = 5) are outliers relative to surrounding sample $^{87}Sr/^{86}Sr$, and none of the larger surface water bodies—rivers (n = 133) and lakes (n = 34)—produced spatial outliers.

Geostatistical Water $^{87}Sr/^{86}Sr$ Model

The trimmed $^{87}Sr/^{86}Sr$ model (n = 249, **Figure 5A**) shows a range of $^{87}Sr/^{86}Sr$ = 0.7049 – 0.7227. Leave-one-out validation of the best-fit isoscape achieves a mean error = < 0.0001 (other model parameters and metrics are reported in **Supplementary Table S2**). Measured water $^{87}Sr/^{86}Sr$ explains 99.1% of the variability in predicted $^{87}Sr/^{86}Sr$ (Adjusted R^2 = 0.99, n = 249). As anticipated, the 80% training model (n = 199) performs more poorly, with the random 20% test set (n = 50) of measured $^{87}Sr/^{86}Sr$ explaining only 31.0% (R^2 = 0.31) of the variability in predicted $^{87}Sr/^{86}Sr$ at corresponding locations. The model semivariogram (**Figure 5B**) shows no spatial autocorrelation of water $^{87}Sr/^{86}Sr$ beyond pairwise distances of approximately 10 km apart.

Prediction errors for the model range from $^{87}Sr/^{86}Sr$ = 0.0004 to 0.0052 (**Supplementary Table S6**; prediction standard error is illustrated in **Figure 5C**). The geographic distribution shows a lower prediction standard error at highland sites in Cusco, Ayacucho, and Huancavelica, as well as around the Lima coast (**Supplementary Table S6**). The geographic distribution of prediction standard errors is partially a function of sampling coverage, with lowest errors in the well-sampled Department of Arequipa and neighboring departments in southern Peru (**Figure 5B**). There are no statistically significant differences in the measured-predicted $^{87}Sr/^{86}Sr$ errors between groupings based on watershed size, elevational zone, or underlying bedrock geology age.

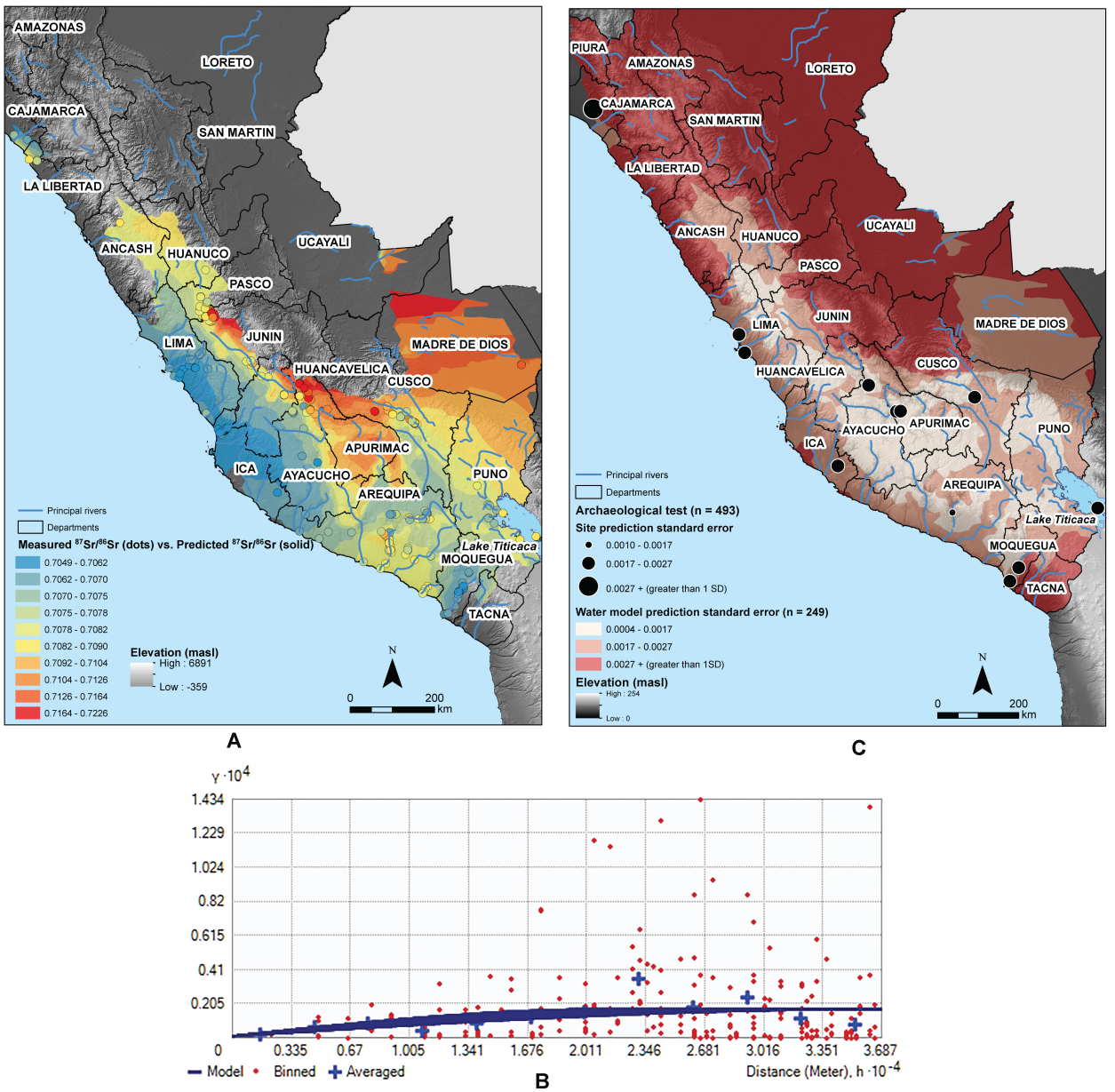

FIGURE 5 | (A) Predictive $^{87}Sr/^{86}Sr$ isoscape of the trimmed water dataset (n = 249) (solid fill) compared to measured water $^{87}Sr/^{86}Sr$ (points in graduated colors), clipped to areas where the prediction standard error is less than 1 SD of the dataset (SD = 0.0027), with digital elevation model (250 m ASTER) for reference. Data values are arbitrarily classified into 10 equal bins. **(B)** The kriging semivariogram shows the absence of spatial autocorrelation between points further away from each other than 10 km. **(C)** Solid fill indicates error between predicted vs. measured $^{87}Sr/^{86}Sr$ at water sampling sites (n = 249). Predicted vs. measured $^{87}Sr/^{86}Sr$ is illustrated by increasing point size at the 12 archaeological test sites (n = 493 test points trimmed of IQR outliers).

Testing the isoscape with the archeological samples from 12 sites trimmed of IQR outliers (n = 493) shows mediocre performance of the surface water-only model, explaining about one-tenth (7.0%) of the variation in human skeletal tissue $^{87}Sr/^{86}Sr$ (Adjusted R^2 = 0.07) (**Supplementary Table S7**). Error between the isoscape predicted and measured $^{87}Sr/^{86}Sr$ for the archeological test set ranges from 0.0000 – 0.0089 (M = 0.0012, n = 493, see **Supplementary Table S7**). Prediction standard error (uncertainty) at each site ranges from 0.0001 – 0.0052. The only site with a prediction standard error larger than 1 SD (SD = 0.0027) is the north coast Moche settlement of Huaca Colorada (PSE = 0.0031, n = 16).

Yunga archeological samples have a significantly smaller prediction error (*Median* = 0.0007, n = 103) than coastal (*Median* = 0.0012, n = 251) and highland (*Median* = 0.0014, n = 139) archeological samples according to a Kruskal–Wallis test $H(2)$ = 8.42, p = 0.015 (**Figure 6**). Prediction error is also significantly lower for samples from sites in large

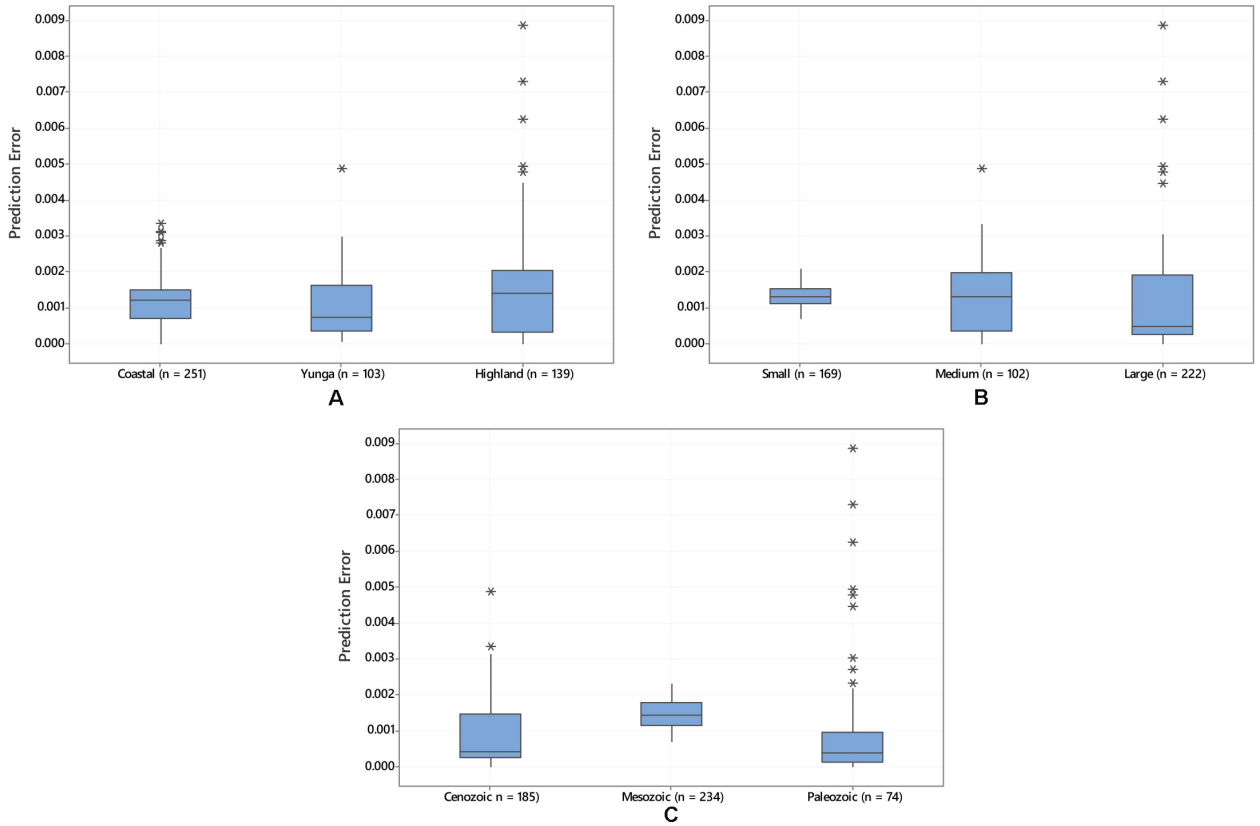

FIGURE 6 | (A) Boxplot of predicted-measured error in $^{87}Sr/^{86}Sr$ for archeological samples from coastal, *yunga*, and highland elevations; **(B)** Boxplot of predicted-measured error in $^{87}Sr/^{86}Sr$ for archeological samples from small, medium, and large watersheds (in hectares); and **(C)** predicted-measured error in $^{87}Sr/^{86}Sr$ for archeological samples overlying geological units dating to the Cenozoic, Mesozoic, and Paleozoic eras (from most recently to oldest deposited bedrock). The predicted-measured errors plotted are from 493 published archeological samples trimmed of IQR outliers.

watersheds (*Median* = 0.0004, n = 222) than for samples from medium (*Median* = 0.0013, n = 102) and small watersheds (*Median* = 0.0013, n = 169), according to Kruskal–Wallis [$H(2) = 30.35$, $p < 0.001$] (**Figure 6**). Prediction error is also lower for samples from sites with more recent underlying bedrock deposition dating to the Cenozoic (*Median* = 0.0004, n = 185) and Paleozoic (*Median* = 0.0004, n = 74) than for samples with underlying Mesozoic bedrock (*Median* = 0.0014, n = 234) according to a Kruskal–Wallis, [$F(2) = 112.68$, $p < 0.001$] (**Figure 6**).

The archeological $^{87}Sr/^{86}Sr$ (trimmed of their IQR outliers) are within the site's prediction standard error of the water $^{87}Sr/^{86}Sr$ isoscape prediction for 90.0% (451/493) of the test samples (**Supplementary Table S8**). More archeological samples from the coast (248/251 = 98.9%) fall within their site's prediction standard error range of the water isoscape than *yunga* (87/103 = 84.5%) or highland samples (117/139 = 84.2%), and this difference is statistically significant, $X^2(2) = 35.081$, $p < 0.001$, n = 493. One highland site has a particularly low proportion of skeletal $^{87}Sr/^{86}Sr$ within the model uncertainty range—none of the nine samples from Turpo fall within the prediction of 0.7092 ± 0.0019 (they are all less radiogenic than expected based on the isoscape prediction) (**Supplementary Table S8**).

DISCUSSION

Overall, the water isoscape mirrors the east-west distribution of $^{87}Sr/^{86}Sr$ from less to more radiogenic illustrated by the Scaffidi and Knudson (2020) archeological isoscape, as well as the bedrock geology model of Schenk et al. (1999). Both this water model and the Scaffidi and Knudson (2020) archeological isoscape lack adequate sampling coverage in the north coast and highlands, all rainforest departments (e.g., Loreto, Ucayali, and most of the Madre de Dios), and within regions in between major cities in Peru. Nonetheless, the water $^{87}Sr/^{86}Sr$ isoscape illustrates important points about the heterogeneity of water in the highlands compared to coastal and *yunga* water, which has critical implications for understanding the suitability of sampling likely drinking water sources as a reference material for $^{87}Sr/^{86}Sr$ geolocation of archeological individuals.

Water $^{87}Sr/^{86}Sr$ Varies According to Elevation, Watershed Size, and Geology

Measured water $^{87}Sr/^{86}Sr$ fits with expectations from previous water studies in mountainous zones that show more variable

$^{87}Sr/^{86}Sr$ at higher elevations (Frei and Frei, 2011; Bataille and Bowen, 2012; Crowley et al., 2017). The isoscape predictions vary from less to more radiogenic from east to west, with a few areas of highly radiogenic predictions around the highlands of Junín, Cusco, the north coast of La Libertad, and around the northern jungles of the Madre de Dios. The lowest $^{87}Sr/^{86}Sr$ is predicted for the Lima, Nasca, and Moquegua desert coasts (**Figure 5A**). Pockets of the highest and lowest projected $^{87}Sr/^{86}Sr$ are a function of poor sampling in some regions (e.g., the north coast, the Eastern slopes and the jungle, and the central and northern highlands), and should be ground-truthed by future sampling in those areas. Indeed, the isoscape is not reliable in areas where the prediction standard error is higher than the SD of the water samples (SD = 0.0027, **Figure 5B**). Furthermore, the fact that the water model only explains 30% of the variance in measured water $^{87}Sr/^{86}Sr$ on cross-validation demonstrates that sampling coverage should be further improved, and also that geostatistical methods may not produce accurate models in these hydrogeologically complex mountainous areas.

Notwithstanding the poor cross-validation results, important patterns emerge that can inform our understanding of bioavailable $^{87}Sr/^{86}Sr$ in Andean waters. Highland water samples displayed distinct $^{87}Sr/^{86}Sr$ than those from mid-elevation (*yunga*) and coastal zones, which demonstrates the homogenization of water strontium sources as rivers drain into the Pacific Ocean. Heterogeneity in water $^{87}Sr/^{86}Sr$ increases with watershed size, a finding that differs from the findings of Brennan et al. (2019). In the Andes, the largest watersheds are located along the eastern slopes of the Andes and the Amazon Rainforest (**Figure 2**). These watersheds drain some of the oldest and most variable Precambrian-Devonian geologies (**Figure 1**) from the Cordillera Oriental, which produce highly variable $^{87}Sr/^{86}Sr$ water. This is important for several reasons. First, according to this isoscape, $^{87}Sr/^{86}Sr$ in the Amazon Rainforest should not be homogenous, as has been often suggested by archeologists contemplating $^{87}Sr/^{86}Sr$ results for items traded into communities from Amazonian groups. In fact, and consistent with recent hydrological analyses that report distinct $^{87}Sr/^{86}Sr$ for Amazonian rivers (Bouchez et al., 2010; Santos et al., 2015), this study suggests that $^{87}Sr/^{86}Sr$ signatures are likely to be more heterogeneous on the eastern slopes of the Andes than on the western slopes. On the other hand, these water $^{87}Sr/^{86}Sr$ results suggest that within smaller watersheds, river and stream water averages strontium from fewer distinct headwaters, so that mixed, large water bodies of lower elevation watersheds should be better proxies for local $^{87}Sr/^{86}Sr$ than the higher elevation, large watersheds. Of course, it is most prudent to generate localized and mixed models for any region, but this study shows that care should be taken to systematically sample the hydrological system particularly, in the Andean highlands and in the largest watersheds.

Water type should also be considered carefully when devising baseline sampling campaigns. As other studies have argued, it is critical to sample the most likely drinking water sources for a given archeological site (Hodell et al., 2004; Montgomery et al., 2007; Pacheco-Forés et al., 2020; Snoeck et al., 2020). This study's examination of spatial outlier water $^{87}Sr/^{86}Sr$ generally agrees with this proposition. Of the 13 spatial outliers detected with possibly aberrant $^{87}Sr/^{86}Sr$, none were large water bodies like rivers and lakes. Most were canals and one small stream, which may have been contaminated with fertilizer from agricultural runoff, as some studies have shown (Frei and Frei, 2013; Thomsen and Andreasen, 2019). However, a more recent study by Frei et al. (2020) shows that Danish waters were not contaminated by agricultural liming, and fertilizers were fully contained in the soils. Modern and ancient Peruvian fertilization practices and their impact on soil and water $^{87}Sr/^{86}Sr$ need to be studied in-depth to understand whether this impacts the local baseline. The other spatial outliers in the present study were from natural springs or man-made wells. Springs might reflect distinct groundwater $^{87}Sr/^{86}Sr$, while stored waters from wells or stone-lined canals may take on the geological signature of their containers, which may themselves not be local. The fact that these outliers were all from highland locations could reflect the intensity of agriculture and the proximity of fields to water sources in the highlands that make them more likely to be contaminated. Mining contamination is certainly another factor that could contribute to abnormal $^{87}Sr/^{86}Sr$ around Lake Junín (Rodbell et al., 2014), although it does not explain the unusually high $^{87}Sr/^{86}Sr$ in the Colca Canyon. Spatial outlier analysis suggests that springs, wells, and canals could reflect non-representative $^{87}Sr/^{86}Sr$. However, it is possible that seemingly abnormal well and canal $^{87}Sr/^{86}Sr$ represents true variability of bedrock strontium contributions—these areas need to be more systematically sampled to understand the complexity of the local geohydrological system.

The fact that none of the five tap water samples were spatial outliers demonstrates that tap-derived drinking water $^{87}Sr/^{86}Sr$ is close to that of the source waters they are diverted from. This pattern may have been different if tap waters from very large cities like Lima, Arequipa, and Trujillo were sampled, but in Chiclayo, Chincha, and Cusco, tap samples are within the range of nearby river $^{87}Sr/^{86}Sr$ variation. Because there were no archeological samples in the archeological test dataset that were directly comparable at the tap water sampling sites, it remains unclear whether tap water could be useful for geolocation of human skeletons. A thorough understanding of Peruvian water management practices and water transportation materials would be necessary to conduct a large-scale tap water provenience study like those conducted in the US by Chesson et al. (2012) and Tipple et al. (2018). Another consideration is that wild animals would likely have consumed primarily water from rivers or lakes, and not the tap water, smaller streams, springs, and canals closer to human settlements. Therefore, it is suspected that water contributions of wild faunal protein sources in the human food web would be better reflected by preferentially sampling large water bodies outside of anthropogenically altered settlements. Further testing of different modern and ancient drinking water sources throughout the Andes is needed to assess the utility of these dietary substrates for provenience human skeletons.

Peruvian Water $^{87}Sr/^{86}Sr$ Isoscape Predicts One-Tenth of the Variation in Archeological Human Tissues

At a broad scale, the variation in water $^{87}Sr/^{86}Sr$ from the Peruvian Andes is similar to that observed in the meta-analysis of human archeological tissues across the Andes by Scaffidi and Knudson (2020). The median $^{87}Sr/^{86}Sr$ of the water samples from this study (*Median* = 0.7077, n = 262) is not statistically distinct from the archeological human $^{87}Sr/^{86}Sr$ from the Andes aggregated by Scaffidi and Knudson (2020) [*Median* = 0.7077, n = 1390, Mann–Whitney U $W(1)$, p = 0.315]. The present study is limited as it does not model rainwater in areas with significant precipitation, or groundwater or fog-water $^{87}Sr/^{86}Sr$, which may have been the source of a significant amount of imbibed water in arid coastal regions where rivers frequently run dry or underground. The water-only isoscape performs well overall at predicting archeological $^{87}Sr/^{86}Sr$—archeological $^{87}Sr/^{86}Sr$ falls within the water isoscape prediction ± prediction standard error for 90% of the IQR-outlier-trimmed archeological samples. This 90% prediction accuracy exceeds the 70% reported by Lengfelder et al. (2019) for a mixing model in the Alps based on soil, dust, groundwater, drinking water, vegetation, and fauna. The high prediction accuracy of the water-only model makes sense given that the drinking water from riverine sources reflects a mix of upstream bedrock weathering, soil and alluvial runoff, and atmospheric strontium (Whipkey et al., 2000; Hodell et al., 2004; Bentley, 2006; Bataille and Bowen, 2012; Crowley et al., 2017). However, the poor correlation between the measured and predicted $^{87}Sr/^{86}Sr$ still leaves most of the variation in human archeological $^{87}Sr/^{86}Sr$ to be accounted for from dietary sources of strontium.

Since R^2 values rarely approach a one-to-one correlation when modeling complex human phenomena, it is informative that $^{87}Sr/^{86}Sr$ alone accounts for nearly one-tenth of the variation in the archeological human test set $^{87}Sr/^{86}Sr$ trimmed of IQR outliers. The poor test performance could be explained by the fact that the water model accounts for 30% of the variation in water $^{87}Sr/^{86}Sr$ across the landscape when cross-validated with random water points in the 20% validation set. These low R^2 values are undoubtedly influenced by shortcomings of the geostatistical approach for modeling bioavailable strontium, including its reliance on Euclidean distances to predict $^{87}Sr/^{86}Sr$ (Bataille et al., 2018, 2020). However, it is important to note that the fit of isoscapes to archeological or human data is always assessed based on an interval from the prediction—linear fit statistics (R^2) are generally not reported for human studies. This is because, as Lengfelder et al. (2019, p. 246) discuss with respect to assessing the fit between isoscape predictions and archeological values, "isotopes in bioarchaeology will always remain proxy data and how much of this 'noise' can be tolerated depends on the specific hypothesis." Nonetheless, regression-based methods are necessary to improve higher accuracy predictions than are allowed by geostatistical models (Bataille et al., 2018, 2020; Hoogewerff et al., 2019). Predicting a continuous surface from linear features like rivers is also problematic, as spatial autocorrelation is constrained by distance to those rivers (Brennan et al., 2016). Particularly in the *yunga* and coastal Andes where settlements were constrained to river valleys, methods that constrain predictions to networks within specific watersheds (Bataille et al., 2014; Brennan et al., 2016, 2019) would likely improve prediction accuracy for sites located within a walking-distance proximity to the river networks accessed by archeological human residents.

The model will also be improved with the incorporation of bioavailable $^{87}Sr/^{86}Sr$ from faunal and plant sources in local food webs that were likely consumed by inhabitants at different sites, as well as collection of baseline data from under-sampled areas. Care must be used in modeling animal and plant strontium sources, however, given that non-local plants and animals likely played an important role in many Andean groups with access to far-reaching and complex exchange networks. In particular, camelids like alpacas and llamas are common protein sources in the Andes—and many of these moved from the highlands to the coast and/or vice-versa throughout their lifetimes (Núñez and Dillehay, 1979; Browman, 1980; Thornton et al., 2011; deFrance et al., 2016; Tripcevich and Capriles, 2016; Mader et al., 2018), so that individuals with diets high in camelid protein might demonstrate correspondingly complex $^{87}Sr/^{86}Sr$ that does not necessarily echo the landscape $^{87}Sr/^{86}Sr$ of origin for human end-members. Similarly, marine proteins like dried fish were often exchanged over great distances into mid-elevations and highlands (Lynch, 1983; Quilter and Stocker, 1983; Hastorf, 2003), which could drive radiogenic isotope signatures upwards in communities with sustained and significant access to coastal exchange routes. Even in places with access to traded foods, though, community members may not have uniformly consumed those imported goods. Furthermore, communities may have altered their local production and import of different foods based on cultural or environmental conditions. In other words, faunal distributions and subsistence practices in many parts of the Andes varied at different temporal resolutions: seasonally, from year to year, or over many generations. At present, macrobotanical and stable isotopic reconstructions of local diets are limited from the 12 archeological test sites. To more accurately model the bioavailable Sr of local dietary catchments, it is critical that archeological evidence-based local food webs and water sources are identified, sampled, and integrated into multi-scalar models. In practice, this means that future efforts at $^{87}Sr/^{86}Sr$ mixing models in the Andes will best be achieved through local and collaborative, supra-regional scale process-based models, informed and contextualized by combining ethnohistoric and archeological information on diets with geological and hydrological data. While beyond the scope of this study, multiple stable isotope data points are essential for developing appropriately weighted $^{87}Sr/^{86}Sr$ models of past dietary catchments for addressing bioarchaeological and zooarchaeological questions about mobility practices.

The water $^{87}Sr/^{86}Sr$ isoscape improves equifinality in well-sampled regions that look homogeneous in the archeological isoscape, like within Arequipa, Cusco, and the Lake Titicaca areas (Scaffidi and Knudson, 2020, p. 13). In particular, the model has a low uncertainty (**Figure 5B**) and a low prediction standard error (**Supplementary Tables S7, S8**) for samples at Beringa in

the Majes Valley, and at Chokepukio in Cusco, where both the number of archeological samples and water samples are high. In these areas, water $^{87}Sr/^{86}Sr$ and the model predictions can be relied on to identify non-locals, but in areas with uncertainty higher than the water $^{87}Sr/^{86}Sr$ standard deviation (**Figure 5B**), the model cannot be relied on for this and further sampling is needed. The high uncertainty in most of the Andes reflects the absence of sampling throughout areas that are more difficult to access and beyond the research focus of this study's authors in southern Peru. Due to this high uncertainty, it is emphasized here that this preliminary model cannot be relied on for geolocation, and future models will seek to incorporate additional dietary proxies for bioavailable Sr, increased the geographic scope sampling, and incorporate regression-based methods to improve the model.

The fit between archeological samples and the water isoscape prediction is better in coastal and *yunga* regions than in the highlands. *Yunga* waters show the lowest prediction standard error (**Supplementary Table S6**) due to homogenized, well-mixed water and high sample numbers at these elevations. Coastal water is also well-mixed, but sea-spray contributions and the preponderance of salt-rich seafood in diets may have masked local drinking water signatures in several communities (Sillen and Kavanagh, 1982; Bentley, 2006). At the coastal settlements of Ancón and Huaca Colorada where a few individuals show $^{87}Sr/^{86}Sr$ not within the site prediction standard error range (**Supplementary Tables S7, S8**), reliance on seafood may have driven human $^{87}Sr/^{86}Sr$ higher than the local drinking water prediction. Indeed, carbon and nitrogen data from Ancón show they consumed primarily marine proteins (Slovak and Paytan, 2011). Carbon and nitrogen data are not yet published for Huaca Colorada, but given iconographic evidence for reliance of north coastal Moche people on seafood (Donnan and McClelland, 1999; see, e.g., Bourget and Jones, 2009), it is likely that Huaca Colorada's inhabitants relied heavily on marine products, just as other coastal people did (Knudson et al., 2007, 2015; Slovak and Paytan, 2011). In contrast, at the coastal site of Armatambo, all of the human samples fell within the isoscape prediction ± prediction standard error, even though they consumed a high proportion of marine foods (Marsteller et al., 2017). At Armatambo, measured $^{87}Sr/^{86}Sr$ have a mean error of 0.0012 more radiogenic than the drinking water prediction, which may reflect a uniform elevation of $^{87}Sr/^{86}Sr$ consistent with greater consumption of marine products with $^{87}Sr/^{86}Sr$ around 0.7092. Reliance on water storage and underground aquifers may also have contributed to higher $^{87}Sr/^{86}Sr$ at these sites. Since coastal sites are generally located along arid desert seashores with little year-round freshwater, coastal and desert-dwelling people often relied on stored water or used underground wells or aqueducts (Netherly, 1984; Denevan, 2001; Schreiber and Lancho Rojas, 2003; Lane, 2014; Scaffidi, 2019). Furthermore, the use of guano fertilizers at might have driven $^{87}Sr/^{86}Sr$ up. Differences in the proportion of marine foods, and/or guano, and/or variable amounts of sea spray could contribute to prediction error, and these factors should be examined in future models.

Highland waters have the highest prediction error rates (**Supplementary Table S6**), which likely reflects true heterogeneity in the $^{87}Sr/^{86}Sr$ of water and underlying geology. At Ch'isi on Lake Titicaca, the fact that all archeological samples were within the isoscape prediction ± prediction standard error could confirm that most people obtained drinking water from the lake. In contrast, the failure of the water isoscape to predict any of the archeological samples from the highland site of Turpo in Andahuaylas might reflect that these people consumed water primarily from a spring or small lake that deviates from the local river system. The poor fit is to be expected when there were no water samples from this area, but the limits of geostatistical modeling and the absence of dietary substrate materials in the model are also likely at play. Overall, the higher variability of highland water $^{87}Sr/^{86}Sr$ and the potential of high-$^{87}Sr/^{86}Sr$ seafood masking to impact coastal $^{87}Sr/^{86}Sr$ demonstrates that localized conditions and diets must be modeled alongside of supra-regional patterns in bioavailable substrates. Given their greater variability, localized highland water models have immense potential to discriminate between different geographic origins if geo-hydrological systems, other isotopic proxies for diet are analyzed, and likely drinking water sources are understood and systematically sampled.

Sample Collection and $^{87}Sr/^{86}Sr$ Mixing Model Development in the Andes

Systematic sampling and coordinating data collected in different coordinate systems with varying techniques remain the most significant deficiencies in baseline isoscape modeling in the Andes. Particularly along Andean coastal valleys, it is often impossible to travel in a grid, sampling at every 500 km^2, as recommended by prior studies (Garrett et al., 1990; Fordyce et al., 1993). Furthermore, modern roads do not always pass where ancient ones like the Qhapaq Ñan (the Inca and pre-Inca road system) did, which makes many archeological sites and their isotopic catchments difficult to access. Due to these factors, more accessible archeological sites around larger cities are disproportionately well-sampled compared to more remote sites (**Figure 1**).

To advance regional and localized baseline models, a unified, cloud-based approach would maximize efficiency in the data collection and data aggregation phases and predictive accuracy of the isoscape products. One challenge to this project was aggregating spreadsheets from multiple field sampling excursions which collected different types of locational attributes in different coordinate systems and at different spatial resolutions—points not collected in the APU relational database required manual spreadsheet consolidation, which amplified opportunities for error. Another challenge is that environmental co-variates that could be analyzed for process-based modeling, such as temperature, soil type, or contamination levels, were not collected. Widespread adoption of a single cloud-based, collaborative database with environmental co-variates suitable for the region, such as the APU database generated by Scaffidi with the ArcCollector app (ESRI), is one excellent option for multi-user collection. With an inexpensive external GPS receiver, this database can be deployed on mobile IOS and Android devices, standardizing data collection and aggregation. Data is uploaded to the cloud whenever a wi-fi signal is detected, so

users can plan routes around extant points. The 2019 APU team found that even if base maps were not downloaded, Peruvian cellular data enabled sufficient bandwidth for caching base map tiles. Data is stored in a web map at ArcGIS Online, which can be viewed, edited, and downloaded by users with institutional ESRI subscriptions. The APU water sampling map can be viewed at: https://arcg.is/1bj4CT; prospective users can be added to the web map by emailing Scaffidi. Collaborative databases like those developed in other world regions (Salesse et al., 2018; Willmes et al., 2018; Hermann et al., 2020) are absolutely critical for fully characterizing isotopic variability in this difficult-to-traverse region.

This study shows that a water $^{87}Sr/^{86}Sr$ isoscape is useful at a coarse scale for discerning between samples from highland, mid-elevation, and coastal provenience in the Peruvian Andes—particularly when known trade and migration networks are in well-sampled areas, pass between elevational zones, and are implicated by the research question of a given study. The greater variability in highland locations and larger watersheds calls for proportionally more baseline sampling when investigating archeological populations from these geo-hydrologically complex high-elevation zones. This study demonstrates the need for a mixing model to explain the other nine-tenths of variation in archeological human $^{87}Sr/^{86}Sr$, and the need for standardized, collaborative sampling and data sharing. It also demonstrates the importance of analyzing environmental materials alongside paleodietary evidence to understand dietary-driven deviance from the environmental baseline. Future research will analyze bioavailable strontium from plant and faunal baselines throughout the Peruvian Andes, with the eventual goal of incorporating these multiple bioavailable strontium sources into a new, process-based mixing model for the probabilistic geolocation of archeological human $^{87}Sr/^{86}Sr$.

DATA AVAILABILITY STATEMENT

All datasets presented in this study are included in the article/**Supplementary Material**.

AUTHOR CONTRIBUTIONS

BS funded (through grants to BS and to BS, TT, and KK) and analyzed the majority of the samples, collected the samples, and wrote the manuscript. TT collected the samples and revised the manuscript. GG assisted with isotopic analysis and contributed paragraphs on analytical and instrument methods. AA and LG funded (through a grant to AA) and analyzed the some samples. AA revised the manuscript. SM, AD, and ES collected the samples and revised the manuscript. All authors contributed to the article and approved the submitted version.

FUNDING

The National Science Foundation SBE Postdoctoral Fellowship (award # 18090470) to BS funded collection and isotopic analysis of water samples. A Vanderbilt University Research Scholar Grant to TT funded additional field collection of samples. A Collaborative Research Grant from the Center for Bioarchaeological Research at Arizona State University to BS, TT, and KK funded analysis of a portion of the water samples. The analysis of seven other samples was supported by the Wenner-Gren Dissertation Fieldwork Grant to AA (award # 9580). The collection of Ilo Valley samples was funded by the Graduate and Professional Student Association Graduate Research Support Program Grant at Arizona State University to ES. Finally, the open access fee was funded by BS, KK, and TT.

ACKNOWLEDGMENTS

Water sample collection and analysis was supported primarily by: a National Science Foundation SBE Postdoctoral Fellowship to BS (award number 1809470), a Collaborative Research Grant from the Center for Bioarchaeological Research at Arizona State University to BS, TT, and KK, and a Vanderbilt University Research Scholar Grant to TT. The analysis of seven samples was supported by the Wenner-Gren Dissertation Fieldwork Grant to AA (award number 9580). The collection of Ilo Valley samples was funded by the Graduate and Professional Student Association Graduate Research Support Program Grant at Arizona State University to ES. Vanderbilt University BSIRL and Natasha Vang facilitated a great deal of the sample collection, organization, and shipping to Scaffidi for analysis. In addition to BSIRL, ACL, and APU students, the following individuals also graciously assisted with water sampling: Manuel Mamaní Calloapaza, Jacob Bongers, Dave Reid, Jake Dean, Alex Menaker, Matt Biwer, Donna Nash, and Kirk Costion. Furthermore, the following individuals allowed us to use their archeological research projects as home bases for sample collection: Rebecca Bria, Véronique Bélisle, Willy Yépez Álvarez, Justin Jennings, and Donna Nash. We thank researchers at the METAL Laboratory at Arizona State University for assisting with instrumentation and data processing: Trevor Martin, Tyler Goepfert, and Natasha Zolotova. Andrew Zipkin of the Archaeological Chemistry Laboratory at Arizona State University was a limitless source of feedback about chemical and spatial analysis of strontium, and the SPATIAL short course (Isotopes in Spatial Systems) from the Inter-university Training for Continental-scale Ecology group at the University of Utah provided isoscape training for Scaffidi. Michael Scaffidi assisted with figure creation. Finally, we appreciate the invitation to participate in this special edition; we also thank the two reviewers and the editors for their feedback which greatly improved the manuscript.

SUPPLEMENTARY MATERIAL

The Supplementary Material for this article can be found online at: https://www.frontiersin.org/articles/10.3389/fevo.2020.00281/full#supplementary-material

REFERENCES

Åberg, G. (1995). The use of natural strontium isotopes as tracers in environmental studies. *Water Air Soil Pollut.* 79, 309–322. doi: 10.1007/BF01100444

Adams, S., Grün, R., McGahan, D., Zhao, J. X., Feng, Y., Nguyen, A., et al. (2019). A strontium isoscape of north-east Australia for human provenance and repatriation. *Geoarchaeology* 34, 231–251. doi: 10.1002/gea.21728

Alaica, A. K., González La Rosa, L. M., and Knudson, K. J. (2020). Creating a body-subject in the Late Moche Period (CE 650-850). Bioarchaeological and biogeochemical analyses of human offerings from Huaca Colorada, Jequetepeque Valley, Peru. *World Archaeol.* 52, 49–70. doi: 10.1080/00438243.2019.1743205

Aubert, D., Probst, A., Stille, P., and Viville, D. (2002). Evidence of hydrological control of Sr behavior in stream water (Strengbach catchment, Vosges mountains, France). *Appl. Geochem.* 17, 285–300. doi: 10.1016/S0883-2927(01)00080-4

Bailey, S. W., Hornbeck, J. W., Driscoll, C. T., and Gaudette, H. E. (1996). Calcium inputs and transport in a base-poor forest ecosystem as interpreted by Sr isotopes. *Water Resourc. Res.* 32, 707–719. doi: 10.1029/95WR03642

Barberena, R., Durán, V. A., Novellino, P., Winocur, D., Benítez, A., Tessone, A., et al. (2017). Scale of human mobility in the southern Andes (Argentina and Chile): a new framework based on strontium isotopes. *Am. J. Phys. Anthropol.* 164, 305–320. doi: 10.1002/ajpa.23270

Barberena, R., Tessone, A., Cagnoni, M., Gasco, A., Durán, V., Winocur, D., et al. (2019). Bioavailable strontium in the Southern Andes (Argentina and Chile): a tool for tracking human and animal movement. *Environ. Archaeol.* doi: 10.1080/14614103.2019.1689894

Bataille, C. P., and Bowen, G. J. (2012). Mapping 87Sr/86 Sr variations in bedrock and water for large scale provenance studies. *Chem. Geol.* 304, 39–52. doi: 10.1016/j.chemgeo.2012.01.028

Bataille, C. P., Brennan, S. R., Hartmann, J., Moosdorf, N., Wooller, M., and Bowen, G. J. (2014). A geostatistical framework for predicting variations in strontium concentrations and isotope ratios in Alaskan rivers. *Chem. Geol.* 389, 1–15. doi: 10.1016/j.chemgeo.2014.08.030

Bataille, C. P., Crowley, B. E., Wooller, M. J., and Bowen, G. J. (2020). Advances in global bioavailable strontium isoscapes. *Palaeogeogr. Palaeoclimatol. Palaeoecol.* 2020:109849. doi: 10.1016/j.palaeo.2020.109849

Bataille, C. P., Laffoon, J., and Bowen, G. J. (2012). Mapping multiple source effects on the strontium isotopic signatures of ecosystems from the circum-Caribbean region. *Ecosphere* 3, 1–24. doi: 10.1890/ES12-00155.1

Bataille, C. P., von Holstein, I. C., Laffoon, J. E., Willmes, M., Liu, X.-M., and Davies, G. R. (2018). A bioavailable strontium isoscape for Western Europe: a machine learning approach. *PLoS One* 13:e0197386. doi: 10.1371/journal.pone.0197386

Beard, B., and Johnson, C. (2000). Strontium isotope composition of skeletal material can determine the birth place and geographic mobility of humans and animals. *J. Forensic Sci.* 45, 1049–1061. doi: 10.1520/JFS14829J

Bellido, B. E., Navarez, S., and Simons, F. D. (1956). *Mapa Geológica del Perú*. Lima: La Sociedad Geológica del Peru.

Bentley, R. A. (2006). Strontium isotopes from the earth to the archaeological skeleton: a review. *J. Archaeol. Method Theory* 13, 135–187. doi: 10.1007/s10816-006-9009-x

Bentley, R. A., and Knipper, C. (2005). Geographical patterns in biologically available strontium, carbon and oxygen isotope signatures in prehistoric SW Germany. *Archaeometry* 47, 629–644. doi: 10.1111/j.1475-4754.2005.00223.x

Bentley, R. A., Price, T. D., and Stephan, E. (2004). Determining the 'local'87Sr/86Sr range for archaeological skeletons: a case study from Neolithic Europe. *J. Archaeol. Sci.* 31, 365–375. doi: 10.1016/j.jas.2003.09.003

Billman, B. R. (2002). Irrigation and the origins of the southern Moche state on the north coast of Peru. *Latin Am. Antiq.* 13, 371–400. doi: 10.2307/972222

Bouchez, J., Lajeunesse, E., Gaillardet, J., France-Lanord, C., Dutra-Maia, P., and Maurice, L. (2010). Turbulent mixing in the Amazon River: the isotopic memory of confluences. *Earth Planet. Sci. Lett.* 290, 37–43. doi: 10.1016/j.epsl.2009.11.054

Bourget, S., and Jones, K. L. (2009). *The Art and Archaeology of the Moche: An Ancient Andean Society of the Peruvian North Coast*. Austin, TX: University of Texas Press.

Bowen, G. (2010). Isoscapes: spatial patterns in isotopic biogeochemistry. *Annu. Rev. Earth Planet. Sci.* 38, 161–187. doi: 10.1146/annurev-earth-040809-152429

Bowen, G. J., and Revenaugh, J. (2003). Interpolating the isotopic composition of modern meteoric precipitation. *Water Resour. Res.* 39, 1–13. doi: 10.1029/2003WR002086

Brennan, S. R., Schindler, D. E., Cline, T. J., Walsworth, T. E., Buck, G., and Fernandez, D. P. (2019). Shifting habitat mosaics and fish production across river basins. *Science* 364, 783–786. doi: 10.1126/science.aav4313

Brennan, S. R., Torgersen, C. E., Hollenbeck, J. P., Fernandez, D. P., Jensen, C. K., and Schindler, D. E. (2016). Dendritic network models: improving isoscapes and quantifying influence of landscape and in-stream processes on strontium isotopes in rivers. *Geophys. Res. Lett.* 43, 5043–5051. doi: 10.1002/2016GL068904

Browman, D. L. (1980). Tiwanaku expansion and altiplano economic patterns. *Estud. Arqueológ.* 5, 107–120.

Buhl, D., Neuser, R., Richter, D., Riedel, D., Roberts, B., Strauss, H., et al. (1991). Nature and nurture: environmental isotope story of the river Rhine. *Naturwissenschaften* 78, 337–346. doi: 10.1007/BF01131605

Burton, J. H., and Price, T. D. (2013). "Seeking the local 87Sr/86Sr ratio to determine geographic origins of humans," in *Across the Alps in Prehistory*, eds R. A. Armitage and J. H. Burton (Cham: Spring), 27–48. doi: 10.1021/bk-2013-1147.ch018

Burton, J. H., and Wright, L. E. (1995). Nonlinearity in the relationship between bone Sr/Ca and diet: paleodietary implications. *Am. J. Phys. Anthropol.* 96, 273–282. doi: 10.1002/ajpa.1330960305

Capo, R. C., Stewart, B. W., and Chadwick, O. A. (1998). Strontium isotopes as tracers of ecosystem processes: theory and methods. *Geoderma* 82, 197–225. doi: 10.1016/S0016-7061(97)00102-X

Chesson, L. A., Tipple, B. J., Mackey, G. N., Hynek, S. A., Fernandez, D. P., and Ehleringer, J. R. (2012). Strontium isotopes in tap water from the coterminous USA. *Ecosphere* 3, 1–17. doi: 10.1890/ES12-00122.1

Comar, C., Russell, R. S., and Wasserman, R. (1957a). Strontium-calcium movement from soil to man. *Science* 126, 485–492. doi: 10.1126/science.126.3272.485

Comar, C., Wasserman, R., Ullberg, S., and Andrews, G. (1957b). Strontium metabolism and strontium-calcium discrimination in man. *Proc. Soc. Exper. Biol. Med.* 95, 386–391. doi: 10.3181/00379727-95-23231

Copeland, S. R., Cawthra, H. C., Fisher, E. C., Lee-Thorp, J. A., Cowling, R. M., Le Roux, P. J., et al. (2016). Strontium isotope investigation of ungulate movement patterns on the pleistocene paleo-agulhas plain of the greater cape floristic region, South Africa. *Q. Sci. Rev.* 141, 65–84. doi: 10.1016/j.quascirev.2016.04.002

Copeland, S. R., Sponheimer, M., Lee-Thorp, J. A., de Ruiter, D. J., le Roux, P. J., Grimes, V., et al. (2010). Using strontium isotopes to study site accumulation processes. *J. Taphon.* 8, 115–127.

Coudrain, A., Loubet, M., Condom, T., Talbi, A., Ribstein, P., Pouyaud, B., et al. (2002). Données isotopiques (8786/Sr) et changements hydrologiques depuis 15 000 ans sur l'Altiplano andin. *Hydrol. Sci. J.* 47, 293–306. doi: 10.1080/02626660209492931

Cressie, N. (1993). *Statistics for Spatial Data*. New York, NY: John Wiley and Sons, Inc. doi: 10.1002/9781119115151

Crowley, B. E., Miller, J. H., and Bataille, C. P. (2017). Strontium isotopes (87Sr/86Sr) in terrestrial ecological and palaeoecological research: empirical efforts and recent advances in continental-scale models. *Biol. Rev. Camb. Philos. Soc.* 92, 43–59. doi: 10.1111/brv.12217

Cuéllar, A. M. (2013). The archaeology of food and social inequality in the Andes. *J. Archaeol. Res.* 21, 123–174. doi: 10.1007/s10814-012-9061-x

deFrance, S. D., Capriles, J. M., and Tripcevich, N. (2016). "Pastoralism through time in Southern Peru," in *The Archaeology of Andean Pastoralism*, eds J. M. Capriles and N. Tripcevich (Albuquerque, NM: University of New Mexico Press), 119–138.

Denevan, W. M. (2001). *Cultivated Landscapes of Native Amazonia and the Andes*. Oxford: Oxford University Press.

Dijkstra, F. A. (2003). Calcium mineralization in the forest floor and surface soil beneath different tree species in the northeastern US. *For. Ecol. Manag.* 175, 185–194. doi: 10.1016/S0378-1127(02)00128-7

Dillehay, T. D. (2011). *From Foraging to Farming in the Andes: New Perspectives on Food Production and Social Organization*. Cambridge: Cambridge University Press. doi: 10.1017/CBO9780511793790

Donnan, C. B., and McClelland, D. (1999). *Moche Fineline Painting: Its Evolution and Its Artists*. Los Angeles, CA: University of California Los Angeles Fowler Museum Publications.

Drouet, T., and Herbauts, J. (2008). Evaluation of the mobility and discrimination of Ca, Sr and Ba in forest ecosystems: consequence on the use of alkaline-earth element ratios as tracers of Ca. *Plant Soil* 302, 105–124. doi: 10.1007/s11104-007-9459-2

Drouet, T., Herbauts, J., Gruber, W., and Demaiffe, D. (2005). Strontium isotope composition as a tracer of calcium sources in two forest ecosystems in Belgium. *Geoderma* 126, 203–223. doi: 10.1016/j.geoderma.2004.09.010

Ehleringer, J. R., Thompson, A. H., Podlesak, D. W., Bowen, G. J., Chesson, L. A., Cerling, T. E., et al. (2010). "A framework for the incorporation of isotopes and isoscapes in geospatial forensic investigations," in *Isoscapes*, eds G. J. Bowen and J. B. West (New York, NY: Springer), 357–387. doi: 10.1007/978-90-481-3354-3_17

Eikenberg, J., Tricca, A., Vezzu, G., Stille, P., Bajo, S., and Ruethi, M. (2001). 228Ra/226Ra/224Ra and 87Sr/86Sr isotope relationships for determining interactions between ground and river water in the upper Rhine valley. *J. Environ. Radioact.* 54, 133–162. doi: 10.1016/S0265-931X(00)00171-5

Ericson, J. E. (1985). Strontium isotope characterization in the study of prehistoric human ecology. *J. Hum. Evol.* 14, 503–514. doi: 10.1016/S0047-2484(85)80029-4

Evans, J. A., Chenery, C. A., and Fitzpatrick, A. P. (2006). Bronze Age childhood migration of individuals near Stonehenge, revealed by strontium and oxygen isotope tooth enamel analysis. *Archaeometry* 48, 309–321. doi: 10.1111/j.1475-4754.2006.00258.x

Evans, J. A., Chenery, C. A., and Montgomery, J. (2012). A summary of strontium and oxygen isotope variation in archaeological human tooth enamel excavated from Britain. *J. Analyt. Atom. Spectrom.* 27, 754–764. doi: 10.1039/c2ja10362a

Evans, J. A., Montgomery, J., and Wildman, G. (2009). Isotope domain mapping of 87Sr/86Sr biosphere variation on the Isle of Skye, Scotland. *J. Geol. Soc.* 166, 617–631. doi: 10.1144/0016-76492008-043

Evans, J. A., Montgomery, J., Wildman, G., and Boulton, N. (2010). Spatial variations in biosphere 87Sr/86Sr in Britain. *J. Geol. Soc.* 167, 1–4. doi: 10.1144/0016-76492009-090

Evans, J. A., and Tatham, S. (2004). Defining 'local signature'in terms of Sr isotope composition using a tenth-to twelfth-century Anglo-Saxon population living on a Jurassic clay-carbonate terrain, Rutland, UK. *Geol. Soc. Lond. Spec. Public.* 232, 237–248. doi: 10.1144/GSL.SP.2004.232.01.21

Fernández-Crespo, T., Snoeck, C., Ordoño, J., de Winter, N., Czermak, A., Mattielli, N., et al. (2020). Multi-isotope evidence for the emergence of cultural alterity in Late Neolithic Europe. *Sci. Adv.* 6:eaay2169. doi: 10.1126/sciadv.aay2169

Finucane, B. C. (2007). Mummies, maize, and manure: multi-tissue stable isotope analysis of late prehistoric human remains from the Ayacucho Valley, Peru. *J. Archaeol. Sci.* 34, 2115–2124. doi: 10.1016/j.jas.2007.02.006

Fisher, E. C., Bar-Matthews, M., Jerardino, A., and Marean, C. W. (2010). Middle and Late Pleistocene paleoscape modeling along the southern coast of South Africa. *Q. Sci. Rev.* 29, 1382–1398. doi: 10.1016/j.quascirev.2010.01.015

Flusche, M. A., Seltzer, G., Rodbell, D., Siegel, D., and Samson, S. (2005). Constraining water sources and hydrologic processes from the isotopic analysis of water and dissolved strontium, Lake Junin, Peru. *J. Hydrol.* 312, 1–13. doi: 10.1016/j.jhydrol.2005.02.021

Fordyce, F. M., Green, P., and Simpson, P. (1993). Simulation of regional geochemical survey maps at variable sample density. *J. Geochem. Explor.* 49, 161–175. doi: 10.1016/0375-6742(93)90043-L

Frei, K. M., and Frei, R. (2011). The geographic distribution of strontium isotopes in Danish surface waters-A base for provenance studies in archaeology, hydrology and agriculture. *Appl. Geochem.* 26, 326–340. doi: 10.1016/j.apgeochem.2010.12.006

Frei, K. M., and Price, T. D. (2012). Strontium isotopes and human mobility in prehistoric Denmark. *Archaeol. Anthropol. Sci.* 4, 103–114. doi: 10.1007/s12520-011-0087-7

Frei, R., and Frei, K. M. (2013). The geographic distribution of Sr isotopes from surface waters and soil extracts over the island of Bornholm (Denmark)-A base for provenance studies in archaeology and agriculture. *Appl. Geochem.* 38, 147–160. doi: 10.1016/j.apgeochem.2013.09.007

Frei, R., Frei, K. M., and Jessen, S. (2020). Shallow retardation of the strontium isotope signal of agricultural liming-implications for isoscapes used in provenance studies. *Sci. Total Environ.* 706:135710. doi: 10.1016/j.scitotenv.2019.135710

Garrett, R. G., Banville, R. M., and Adcock, S. W. (1990). Regional geochemical data compilation and map preparation, Labrador, Canada. *J. Geochem. Explor.* 39, 91–116. doi: 10.1016/0375-6742(90)90070-Q

Glorennec, P., Lucas, J.-P., Mercat, A.-C., Roudot, A.-C., and Le Bot, B. (2016). Environmental and dietary exposure of young children to inorganic trace elements. *Environ. Int.* 97, 28–36. doi: 10.1016/j.envint.2016.10.009

Graustein, W. C. (1989). "87Sr/86Sr ratios measure the sources and flow of strontium in terrestrial ecosystems," in *Stable Isotopes in Ecological Research*, eds P. Rundle, J. Ehleringer, and K. Nagy (New York, NY: Springer-Verlag), 491–512. doi: 10.1007/978-1-4612-3498-2_28

Grimstead, D. N., Nugent, S., and Whipple, J. (2017). Why a standardization of strontium isotope baseline environmental data is needed and recommendations for methodology. *Adv. Archaeol. Pract.* 5, 184–195. doi: 10.1017/aap.2017.6

Grimstead, D. N., Quade, J., and Stiner, M. C. (2016). Isotopic evidence for long-distance mammal procurement, chaco canyon, New Mexico, USA. *Geoarchaeology* 31, 335–354. doi: 10.1002/gea.21545

Grove, M. J., Baker, P. A., Cross, S. L., Rigsby, C. A., and Seltzer, G. O. (2003). Application of strontium isotopes to understanding the hydrology and paleohydrology of the Altiplano, Bolivia-Peru. *Palaeogeogr. Palaeoclimatol. Palaeoecol.* 194, 281–297. doi: 10.1016/S0031-0182(03)00282-7

Grupe, G., Hölzl, S., Kocsis, B., Kröger, P., Mauder, M., Mayr, C., et al. (2017a). "Isotopic mapping and migration research based on bioarchaeological finds," in *ResourceCultures: Sociocultural Dynamics and the Use of Resources – Theories, Methods, and Perspectives*, eds A. Scholz, M. Bartleheim, R. Hardenberg, and J. Staecker (Tübingen: University of Tübingen), 195–208.

Grupe, G., Hölzl, S., Mayr, C., and Söllner, F. (2017b). "The concept of isotopic landscapes: modern ecogeochemistry versus bioarchaeology," in *Across the Alps in Prehistory*, eds G. Grupe, A. Grigat, and G. McGlynn (Cham: Springer), 27–48. doi: 10.1007/978-3-319-41550-5_2

Grupe, G., von Carnap-Bornheim, C., and Söllner, F. (2011). Stable strontium isotope mapping for provenance studies in archaeology: different material, different signals. *Bull. Soc. Suisse Anthropol.* 17, 67–76.

Hastorf, C. A. (2003). Andean luxury foods: special food for the ancestors, deities and the élite. *Antiquity* 77, 545–554. doi: 10.1017/S0003598X00092607

Hastorf, C. A., and Johannessen, S. (1993). Pre-Hispanic political change and the role of maize in the Central Andes of Peru. *Am. Anthropol.* 95, 115–138. doi: 10.1525/aa.1993.95.1.02a00060

Hedman, K. M., Curry, B. B., Johnson, T. M., Fullagar, P. D., and Emerson, T. E. (2009). Variation in strontium isotope ratios of archaeological fauna in the Midwestern United States: a preliminary study. *J. Archaeol. Sci.* 36, 64–73. doi: 10.1016/j.jas.2008.07.009

Hedman, K. M., Slater, P. A., Fort, M. A., Emerson, T. E., and Lambert, J. M. (2018). Expanding the strontium isoscape for the American midcontinent: identifying potential places of origin for Cahokian and Pre-Columbian migrants. *J. Archaeol. Sci. Rep.* 22, 202–213. doi: 10.1016/j.jasrep.2018.09.027

Hermann, A., Forkel, R., McAlister, A., Cruickshank, A., Golitko, M., Kneebone, B., et al. (2020). Pofatu, a curated and open-access database for geochemical sourcing of archaeological materials. *Sci. Data* 7, 1–9. doi: 10.1038/s41597-020-0485-8

Hodell, D. A., Quinn, R. L., Brenner, M., and Kamenov, G. (2004). Spatial variation of strontium isotopes (87Sr/86Sr) in the Maya region: a tool for tracking ancient human migration. *J. Archaeol. Sci.* 31, 585–601. doi: 10.1016/j.jas.2003.10.009

Hoogewerff, J., Papesch, W., Kralik, M., Berner, M., Vroon, P., Miesbauer, H., et al. (2001). The last domicile of the Iceman from Hauslabjoch: a geochemical approach using Sr, C and O isotopes and trace element signatures. *J. Archaeol. Sci.* 28, 983–989. doi: 10.1006/jasc.2001.0659

Hoogewerff, J. A., Reimann, C., Ueckermann, H., Frei, R., Frei, K. M., Van Aswegen, T., et al. (2019). Bioavailable 87Sr/86Sr in European soils: a baseline for provenancing studies. *Sci. Total Environ.* 672, 1033–1044. doi: 10.1016/j.scitotenv.2019.03.387

Horwitz, P., Chiarizia, R., and Dietz, M. L. (1992). A novel strontium-selective extraction chromatographic resin. *Solvent Extract. Ion Exchang.* 10, 313–336. doi: 10.1080/07366299208918107

Instituto Geográfico Nacional de Perú (2015). *Información Hidrográfica de Perú*. Perú: Instituto Geográfico Nacional de Perú.

Johns, T. (1990). *With Bitter Herbs They Shall Eat It: Chemical Ecology and the Origins of Human Diet and Medicine*. Tucson, AZ: University of Arizona Press.

Johnson, C. D., Nandi, A., Joyner, T. A., and Luffman, I. (2018). Iron and manganese in groundwater: using Kriging and GIS to locate high concentrations in Buncombe County, North Carolina. *Groundwater* 56, 87–95. doi: 10.1111/gwat.12560

Johnson, L., Montgomery, J., Evans, J., and Hamilton, E. (2019). Contribution of strontium to the human diet from querns and millstones: an experiment in digestive strontium isotope uptake. *Archaeometry* 61, 1366–1381. doi: 10.1111/arcm.12485

Julien, C. J., Shozo, M., Isumi, S., and Craig, M. (1985). "Guano and resource control in sixteenth-century Arequipa," in *Andean Ecology and Civilization*, eds S. Masuda and M. C. Shimada (Tokyo: University of Tokyo Press), 185–231.

Knipper, C., Maurer, A.-F., Peters, D., Meyer, C., Brauns, M., Galer, S. J., et al. (2012). "Mobility in thuringia or mobile thuringians: a strontium isotope study from early Medieval central Germany," in *Population Dynamics in Prehistory and Early History: New Approaches Using Stable Isotopes and Genetics*, eds E. Kaiser, J. Burger, and W. Schier (Berlin: de Gruyter), 287–310.

Knudson, K. J., Aufderheide, A. E., and Buikstra, J. E. (2007). Seasonality and paleodiet in the Chiribaya polity of southern Peru. *J. Archaeol. Sci.* 34, 451–462. doi: 10.1016/j.jas.2006.07.003

Knudson, K. J., Gardella, K. R., and Yaeger, J. (2012a). Provisioning Inka feasts at tiwanaku, bolivia: the geographic origins of camelids in the pumapunku complex. *J. Archaeol. Sci.* 39, 479–491. doi: 10.1016/j.jas.2011.10.003

Knudson, K. J., O'Donnabhain, B., Carver, C., Cleland, R., and Price, T. D. (2012b). Migration and Viking Dublin: paleomobility and paleodiet through isotopic analyses. *J. Archaeol. Sci.* 39, 308–320. doi: 10.1016/j.jas.2011.09.014

Knudson, K. J., Peters, A. H., and Cagigao, E. T. (2015). Paleodiet in the Paracas Necropolis of Wari Kayan: carbon and nitrogen isotope analysis of keratin samples from the south coast of Peru. *J. Archaeol. Sci.* 55, 231–243. doi: 10.1016/j.jas.2015.01.011

Knudson, K. J., and Price, T. D. (2007). Utility of multiple chemical techniques in archaeological residential mobility studies: case studies from Tiwanaku-and Chiribaya-affiliated sites in the Andes. *Am. J. Phys. Anthropol.* 132, 25–39. doi: 10.1002/ajpa.20480

Knudson, K. J., Stanish, C., Lozada, M. C., Faull, K. M., and Tantaleán, H. (2016). Intra-individual variability and strontium isotope measurements: a methodological study using 87 Sr/86 Sr data from Pampa de los Gentiles, Chincha Valley, Peru. *J. Archaeol. Sci. Rep.* 5, 590–597. doi: 10.1016/j.jasrep.2016.01.016

Knudson, K. J., and Tung, T. A. (2011). Investigating regional mobility in the southern hinterland of the Wari Empire: biogeochemistry at the site of Beringa, Peru. *Am. J. Phys. Anthropol.* 145, 299–310. doi: 10.1002/ajpa.21494

Knudson, K. J., Webb, E., White, C., and Longstaffe, F. J. (2014). Baseline data for Andean paleomobility research: a radiogenic strontium isotope study of modern Peruvian agricultural soils. *Archaeol. Anthropol. Sci.* 6, 205–219. doi: 10.1007/s12520-013-0148-1

Knudson, K. J., Williams, H. M., Buikstra, J. E., Tomczak, P. D., Gordon, G. W., and Anbar, A. D. (2010). Introducing δ88/86 Sr analysis in archaeology: a demonstration of the utility of strontium isotope fractionation in paleodietary studies. *J. Archaeol. Sci.* 37, 2352–2364. doi: 10.1016/j.jas.2010.04.009

Kootker, L., Plomp, E., Ammer, S., Hoogland, V., and Davies, G. (2020). Spatial patterns in 87Sr/86Sr ratios in modern human dental enamel and tap water from the Netherlands: implications for forensic provenancing. *Sci. Total Environ.* 729:138992. doi: 10.1016/j.scitotenv.2020.138992

Kootker, L. M., van Lanen, R. J., Kars, H., and Davies, G. R. (2016). Strontium isoscapes in the Netherlands: Spatial variations in 87 Sr/86 Sr as a proxy for palaeomobility. *J. Archaeol. Sci. Rep.* 6, 1–13. doi: 10.1016/j.jasrep.2016.01.015

Ladegaard-Pedersen, P., Achilleos, M., Dörflinger, G., Frei, R., Kristiansen, K., and Frei, K. M. (2020). A strontium isotope baseline of Cyprus. Assessing the use of soil leachates, plants, groundwater and surface water as proxies for the local range of bioavailable strontium isotope composition. *Sci. Total Environ.* 708:134714. doi: 10.1016/j.scitotenv.2019.134714

Laffoon, J. E., Davies, G. R., Hoogland, M. L., and Hofman, C. L. (2012). Spatial variation of biologically available strontium isotopes (87 Sr/86 Sr) in an archipelagic setting: a case study from the Caribbean. *J. Archaeol. Sci.* 39, 2371–2384. doi: 10.1016/j.jas.2012.02.002

Lane, K. (2014). "Water technology in the Andes," in *Encyclopaedia of the History of Science, Technology, and Medicine in Non-Western Cultures*, ed. H. Selin (Dordrecht: Springer), 1–24. doi: 10.1007/978-94-007-3934-5_10182-1

Lehner, B., and Grill, G. (2013). Global river hydrography and network routing: baseline data and new approaches to study the world's large river systems. *Hydrol. Process.* 27, 2171–2186. doi: 10.1002/hyp.9740

Lengfelder, F., Grupe, G., Stallauer, A., Huth, R., and Söllner, F. (2019). Modelling strontium isotopes in past biospheres-assessment of bioavailable 87Sr/86Sr ratios in local archaeological vertebrates based on environmental signatures. *Sci. Total Environ.* 648, 236–252. doi: 10.1016/j.scitotenv.2018.08.014

Lewis, J., Pike, A., Coath, C., and Evershed, R. (2017). Strontium concentration, radiogenic (87Sr/86Sr) and stable (δ 88Sr) strontium isotope systematics in a controlled feeding study. *Sci. Technol. Archaeol. Res.* 3, 45–57. doi: 10.1080/20548923.2017.1303124

Lynch, T. F. (1983). Camelid pastoralism and the emergence of Tiwanaku civilization in the south-central Andes. *World Archaeol.* 15, 1–14. doi: 10.1080/00438243.1983.9979881

Mader, C., Hölzl, S., Heck, K., Reindel, M., and Isla, J. (2018). The llama's share: highland origins of camelids during the Late Paracas period (370 to 200 BCE) in south Peru demonstrated by strontium isotope analysis. *J. Archaeol. Sci. Rep.* 20, 257–270. doi: 10.1016/j.jasrep.2018.04.032

Mamani, M., Tassara, A., and Wörner, G. (2008). Composition and structural control of crustal domains in the central Andes. *Geochem. Geophys. Geosyst.* 9:2007GC001925. doi: 10.1029/2007GC001925

Marsteller, S. J., Zolotova, N., and Knudson, K. J. (2017). Investigating economic specialization on the central Peruvian coast: a reconstruction of Late Intermediate Period Ychsma diet using stable isotopes. *Am. J. Phys. Anthropol.* 162, 300–317. doi: 10.1002/ajpa.23117

Maurer, A.-F., Galer, S. J., Knipper, C., Beierlein, L., Nunn, E. V., Peters, D., et al. (2012). Bioavailable 87Sr/86Sr in different environmental samples—Effects of anthropogenic contamination and implications for isoscapes in past migration studies. *Sci. Total Environ.* 433, 216–229. doi: 10.1016/j.scitotenv.2012.06.046

Mitchell, H., Hamilton, T., Steggerda, F., and Bean, H. (1945). The chemical composition of the adult human body and its bearing on the biochemistry of growth. *J. Biol. Chem.* 158, 625–637.

Montgomery, J. (2010). Passports from the past: investigating human dispersals using strontium isotope analysis of tooth enamel. *Ann. Hum. Biol.* 37, 325–346. doi: 10.3109/03014461003649297

Montgomery, J., Evans, J. A., and Cooper, R. E. (2007). Resolving archaeological populations with Sr-isotope mixing models. *Appl. Geochem.* 22, 1502–1514. doi: 10.1016/j.apgeochem.2007.02.009

Netherly, P. J. (1984). The management of late Andean irrigation systems on the north coast of Peru. *Am. Antiq.* 49, 227–254. doi: 10.2307/280017

Nixon, G., and Helsby, C. (1976). The relationship between strontium in water supplies and human tooth enamel. *Arch. Oral. Biol.* 21, 691–695. doi: 10.1016/0003-9969(76)90144-8

Núñez, L., and Dillehay, T. (1979). *Movilidad Giratoria, Armonía y Desarrollo en los Andes Meridionales, Patrones de tráfico e Interacción Económica, Dirección General de Investigaciones Tecnológicas*. Antofagasta: Universidad del Norte.

Oliver, M., and Webster, R. (2014). A tutorial guide to geostatistics: computing and modelling variograms and kriging. *Catena* 113, 56–69. doi: 10.1016/j.catena.2013.09.006

Oliver, M. A., and Webster, R. (1990). Kriging: a method of interpolation for geographical information systems. *Intern. J. Geograp. Inform. Syst.* 4, 313–332. doi: 10.1080/02693799008941549

Oliver, M. A., and Webster, R. (2015). *Basic Steps in Geostatistics: The Variogram and Kriging*. Cham: Springer Nature. doi: 10.1007/978-3-319-15865-5

Pacheco-Forés, S. I., Gordon, G. W., and Knudson, K. J. (2020). Expanding radiogenic strontium isotope baseline data for central Mexican paleomobility studies. *PLoS One* 15:e0229687. doi: 10.1371/journal.pone.0229687

Pellegrini, M., Pouncett, J., Jay, M., Pearson, M. P., and Richards, M. P. (2016). Tooth enamel oxygen "isoscapes" show a high degree of human mobility in prehistoric Britain. *Sci. Rep.* 6:34986. doi: 10.1038/srep34986

Peucker-Ehrenbrink, B., and Fiske, G. J. (2019). A continental perspective of the seawater 87Sr/86Sr record: a review. *Chem. Geol.* 510, 140–165. doi: 10.1016/j.chemgeo.2019.01.017

Poszwa, A., Ferry, B., Dambrine, E., Pollier, B., Wickman, T., Loubet, M., et al. (2004). Variations of bioavailable Sr concentration and 87 Sr/86 Sr ratio in boreal forest ecosystems. *Biogeochemistry* 67, 1–20. doi: 10.1023/B:BIOG.0000015162.12857.3e

Pourmand, A., and Dauphas, N. (2010). Distribution coefficients of 60 elements on TODGA resin: application to Ca, Lu, Hf, U and Th isotope geochemistry. *Talanta* 81, 741–753. doi: 10.1016/j.talanta.2010.01.008

Price, T. D., Burton, J. H., and Bentley, R. A. (2002). The characterization of biologically available strontium isotope ratios for the study of prehistoric migration. *Archaeometry* 44, 117–135. doi: 10.1111/1475-4754.00047

Price, T. D., Burton, J. H., Fullagar, P. D., Wright, L. E., Buikstra, J. E., and Tiesler, V. (2015). "Strontium isotopes and the study of human mobility among the ancient Maya," in *Archaeology and Bioarchaeology of Population Movement Among the Prehispanic Maya*, ed. A. Cucina (New York, NY: Springer), 119–132. doi: 10.1007/978-3-319-10858-2_11

Price, T. D., Burton, J. H., and Stoltman, J. B. (2007). Place of origin of prehistoric inhabitants of Aztalan, Jefferson Co., Wisconsin. *Am. Antiq.* 72, 524–538. doi: 10.2307/40035859

Price, T. D., Johnson, C. M., Ezzo, J. A., Ericson, J., and Burton, J. H. (1994). Residential mobility in the prehistoric southwest United States: a preliminary study using strontium isotope analysis. *J. Archaeol. Sci.* 21, 315–330. doi: 10.1006/jasc.1994.1031

Pulgar Vidal, J. (1981). *Geografiìa del Perú: Las Ocho Regiones Naturales del Perú*. Lima: PUCP- Fondo Editorial.

Quilter, J., and Stocker, T. (1983). Subsistence economies and the origins of Andean complex societies. *Am. Anthropol.* 85, 545–562. doi: 10.1525/aa.1983.85.3.02a00030

Rodbell, D. T., Delman, E. M., Abbott, M. B., Besonen, M. T., and Tapia, P. M. (2014). The heavy metal contamination of Lake Junín National Reserve, Peru: an unintended consequence of the juxtaposition of hydroelectricity and mining. *GSA Today* 24, 4–10. doi: 10.1130/GSATG200A.1

Romaniello, S., Field, M., Smith, H., Gordon, G., Kim, M., and Anbar, A. (2015). Fully automated chromatographic purification of Sr and Ca for isotopic analysis. *J. Analyt. Atom. Spectrom.* 30, 1906–1912. doi: 10.1039/C5JA00205B

Salesse, K., Fernandes, R., de Rochefort, X., Brůžek, J., Castex, D., and Dufour, É (2018). IsoArcH. eu: an open-access and collaborative isotope database for bioarchaeological samples from the Graeco-Roman world and its margins. *J. Archaeol. Sci. Rep.* 19, 1050–1055. doi: 10.1016/j.jasrep.2017.07.030

Santos, R. V., Sondag, F., Cochonneau, G., Lagane, C., Brunet, P., Hattingh, K., et al. (2015). Source area and seasonal 87Sr/86Sr variations in rivers of the Amazon basin. *Hydrol. Process.* 29, 187–197. doi: 10.1002/hyp.10131

Scaffidi, B. K. (2019). Spatial paleopathology: a geographic approach to the etiology of cribrotic lesions in the prehistoric Andes. *Intern. J. Paleopathol.* 29, 102–116. doi: 10.1016/j.ijpp.2019.07.002

Scaffidi, B. K., and Knudson, K. J. (2020). An archaeological strontium isoscape for the prehistoric Andes: understanding population mobility through a geostatistical meta-analysis of archaeological 87Sr/86Sr values from humans, animals, and artifacts. *J. Archaeol. Sci.* 117, 105–121. doi: 10.1016/j.jas.2020.105121

Schenk, C. J., Viger, R. J., and Anderson, C. P. (1999). *Maps Showing Geology, Oil and Gas Fields, and Geological Provinces of South America: U.S. Geological Survey Open-File Report 97-470-D*. Available online at: https://pubs.er.usgs.gov/publication/ofr97470D doi: 10.3133/ofr97470D (accessed May 1, 2020).

Schreiber, K., and Lancho Rojas, J. (2003). *Irrigation and Society in the Peruvian Desert: The Puquios of Nasca*. Lanham, MD: Lexington Books.

Scott, E. M., Allen, M. B., Macpherson, C. G., McCaffrey, K. J. W., Davidson, J. P., Saville, C., et al. (2018). Andean surface uplift constrained by radiogenic isotopes of arc lavas. *Nat. Commun.* 9, 969–977. doi: 10.1038/s41467-018-03173-4

Serna, A., Prates, L., Mange, E., Salazar-García, D. C., and Bataille, C. P. (2020). Implications for paleomobility studies of the effects of quaternary volcanism on bioavailable strontium: a test case in North Patagonia (Argentina). *J. Archaeol. Sci*. 121:105198. doi: 10.1016/j.jas.2020.105198

Sillen, A., and Kavanagh, M. (1982). Strontium and paleodietary research: a review. *Am. J. Phys. Anthropol.* 25, 67–90. doi: 10.1002/ajpa.1330250505

Slovak, N. M., and Paytan, A. (2011). Fisherfolk and farmers: carbon and nitrogen isotope evidence from Middle Horizon Ancón, Peru. *Intern. J. Osteoarchaeol.* 21, 253–267. doi: 10.1002/oa.1128

Slovak, N. M., Paytan, A., and Wiegand, B. A. (2009). Reconstructing Middle Horizon mobility patterns on the coast of Peru through strontium isotope analysis. *J. Archaeol. Sci.* 36, 157–165. doi: 10.1016/j.jas.2008.08.004

Snoeck, C., Ryan, S., Pouncett, J., Pellegrini, M., Claeys, P., Wainwright, A. N., et al. (2020). Towards a biologically available strontium isotope baseline for Ireland. *Sci. Total Environ.* 712:136248. doi: 10.1016/j.scitotenv.2019.136248

Szpak, P., Millaire, J.-F., White, C. D., and Longstaffe, F. J. (2012). Influence of seabird guano and camelid dung fertilization on the nitrogen isotopic composition of field-grown maize (Zea mays). *J. Archaeol. Sci.* 39, 3721–3740. doi: 10.1016/j.jas.2012.06.035

Tachikawa, T., Hato, M., Kaku, M., and Iwasaki, A. (2011). "Characteristics of ASTER GDEM version 2," in *Proceedings of the 2011 IEEE International Geoscience and Remote Sensing Symposium (IGARSS): Institute of Electrical and Electronics Engineers*, Piscataway, NJ. doi: 10.1109/IGARSS.2011.6050017

Thomsen, E., and Andreasen, R. (2019). Agricultural lime disturbs natural strontium isotope variations: implications for provenance and migration studies. *Sci. Adv.* 5, 1–11. doi: 10.1126/sciadv.aav8083

Thornton, E. K. (2011). Reconstructing ancient Maya animal trade through strontium isotope (87Sr/86Sr) analysis. *J. Archaeol. Sci.* 38, 3254–3263. doi: 10.1016/j.jas.2011.06.035

Thornton, E. K., Defrance, S. D., Krigbaum, J., and Williams, P. R. (2011). Isotopic evidence for Middle Horizon to 16th century camelid herding in the Osmore Valley, Peru. *Intern. J. Osteoarchaeol.* 21, 544–567. doi: 10.1002/oa.1157

Tipple, B. J., Valenzuela, L. O., and Ehleringer, J. R. (2018). Strontium isotope ratios of human hair record intra-city variations in tap water source. *Sci. Rep.* 8, 1–10. doi: 10.1038/s41598-018-21359-0

Tricca, A., Stille, P., Steinmann, M., Kiefel, B., Samuel, J., and Eikenberg, J. (1999). Rare earth elements and Sr and Nd isotopic compositions of dissolved and suspended loads from small river systems in the Vosges mountains (France), the river Rhine and groundwater. *Chem. Geol.* 160, 139–158. doi: 10.1016/S0009-2541(99)00065-0

Tripcevich, N., and Capriles, J. M. (2016). *The Archaeology of Andean Pastoralism*. Albuquerque: University of New Mexico Press.

Tung, T. A., and Knudson, K. J. (2011). Identifying locals, migrants, and captives in the Wari heartland: a bioarchaeological and biogeochemical study of human remains from Conchopata, Peru. *J. Anthropol. Archaeol.* 30, 247–261. doi: 10.1016/j.jaa.2011.06.005

Turner, B. L., Kamenov, G. D., Kingston, J. D., and Armelagos, G. J. (2009). Insights into immigration and social class at Macchu Picchu, Peru, based on oxygen, strontium, and lead isotopic analysis. *J. Archaeol. Sci.* 36, 317–332. doi: 10.1016/j.jas.2008.09.018

Valentine, B., Kamenov, G. D., and Krigbaum, J. (2008). Reconstructing Neolithic groups in Sarawak, Malaysia through lead and strontium isotope analysis. *J. Archaeol. Sci.* 35, 1463–1473. doi: 10.1016/j.jas.2007.10.016

Varouchakis, E., Hristopulos, D., and Karatzas, G. (2012). Improving kriging of groundwater level data using nonlinear normalizing transformations—a field application. *Hydrol. Sci. J.* 57, 1404–1419. doi: 10.1080/02626667.2012.717174

Veizer, J. (1989). Strontium isotopes in seawater through time. *Annu. Rev. Earth Planet. Sci.* 17, 141–167. doi: 10.1146/annurev.ea.17.050189.001041

Voerkelius, S., Lorenz, G. D., Rummel, S., Quétel, C. R., Heiss, G., Baxter, M., et al. (2010). Strontium isotopic signatures of natural mineral waters, the reference to a simple geological map and its potential for authentication of food. *Food Chem.* 118, 933–940. doi: 10.1016/j.foodchem.2009.04.125

Wang, X., Tang, Z., and Dong, X. (2018). Distribution of strontium isotopes in river waters across the Tarim Basin: a map for migration studies. *J. Geol. Soc.* 175, 967–973. doi: 10.1144/jgs2018-074

Wasserman, R., Lengemann, F., and Comar, C. (1958). Comparative metabolism of calcium and strontium in lactation. *J. Dairy Sci.* 41, 812–821. doi: 10.3168/jds.S0022-0302(58)91004-X

West, A., February, E., and Bowen, G. (2014). Spatial analysis of hydrogen and oxygen stable isotopes ("isoscapes") in ground water and tap water across South Africa. *J. Geochem. Explorat.* 145, 213–222. doi: 10.1016/j.gexplo.2014.06.009

Whipkey, C., Capo, R., Chadwick, O., and Stewart, B. (2000). The importance of sea spray to the cation budget of a coastal Hawaiian soil: a strontium

isotope approach. *Chem. Geol.* 168, 37–48. doi: 10.1016/S0009-2541(00)00187-X

Willmes, M., Bataille, C. P., James, H. F., Moffat, I., McMorrow, L., Kinsley, L., et al. (2018). Mapping of bioavailable strontium isotope ratios in France for archaeological provenance studies. *Appl. Geochem.* 90, 75–86. doi: 10.1016/j.apgeochem.2017.12.025

Wright, L. (2005). Identifying immigrants to Tikal, Guatemala: defining local variability in strontium isotope ratios of human tooth enamel. *J. Archaeol. Sci.* 32, 555–566. doi: 10.1016/j.jas.2004.11.011

Wunder, M. B. (2010). "Using isoscapes to model probability surfaces for determining geographic origins," in *Isoscapes: Understanding Movement, Pattern, and Process on Earth Through Isotope Mapping*, eds J. B. West, G. J. Bowen, T. E. Dawson, and K. P. Tu (Dordrecht: Springer), 251–270. doi: 10.1007/978-90-481-3354-3_12

Yamanaka, T., Makino, Y., Wakiyama, Y., Kishi, K., Maruyama, K., Kano, M., et al. (2015). How reliable are modeled precipitation isoscapes over a high-relief mountainous region? *Hydrol. Res. Lett.* 9, 118–124. doi: 10.3178/hrl.9.118

Zimmer-Dauphinee, J., Scaffidi, B., and Tung, T. (2020). "Finding family using forensic isoscapes: The application of stable oxygen isotope analysis in Peru," in *Humanitarian Forensic Science: Interacting with the Dead and the Living*, eds D. Ubelaker and R. Parra (Hoboken, NJ: John Wiley & Sons), 311–329. doi: 10.1002/9781119482062.ch21

Zitek, A., Tchaikovsky, A., Irrgeher, J., Waidbacher, H., and Prohaska, T. (2015). "The 87Sr/86Sr river water isoscape of the Danube catchment," in *Joint Danube Survey 3: A Comprehensive Analysis of Danube Water Quality*, eds I. Liška, F. Wagner, M. Sengl, K. Deutsch, and J. Slobodnik (Vienna: ICPDR - International Commission for the Proteccion of the Danube River), 349–354.

Conflict of Interest: The authors declare that the research was conducted in the absence of any commercial or financial relationships that could be construed as a potential conflict of interest.

frontiers in Ecology and Evolution

ORIGINAL RESEARCH
published: 07 December 2020
doi: 10.3389/fevo.2020.569940

Strontium Uptake and Intra-Population $^{87}Sr/^{86}Sr$ Variability of Bones and Teeth—Controlled Feeding Experiments With Rodents (*Rattus norvegicus, Cavia porcellus*)

Michael Weber[1], Théo Tacail[1,2], Federico Lugli[3], Marcus Clauss[4], Katrin Weber[1], Jennifer Leichliter[1], Daniela E. Winkler[1,5], Regina Mertz-Kraus[1] and Thomas Tütken[1]*

[1] Institute of Geosciences, Johannes Gutenberg University, Mainz, Germany, [2] Bristol Isotope Group, School of Earth Sciences, University of Bristol, Bristol, United Kingdom, [3] Department of Cultural Heritage, University of Bologna, Ravenna, Italy, [4] Clinic for Zoo Animals, Exotic Pets and Wildlife, Vetsuisse Faculty, University of Zürich, Zurich, Switzerland, [5] Center of Natural History, University of Hamburg, Hamburg, Germany

OPEN ACCESS

Edited by:
Brooke Crowley,
University of Cincinnati, United States

Reviewed by:
Anneke Janzen,
The University of Tennessee, Knoxville, United States
Robert S. Feranec,
New York State Museum, United States
Rachel Reid,
Virginia Tech, United States

***Correspondence:**
Michael Weber
michael.weber@uni-mainz.de

Specialty section:
This article was submitted to Paleoecology, a section of the journal Frontiers in Ecology and Evolution

Received: 05 June 2020
Accepted: 12 November 2020
Published: 07 December 2020

Citation:
Weber M, Tacail T, Lugli F, Clauss M, Weber K, Leichliter J, Winkler DE, Mertz-Kraus R and Tütken T (2020) Strontium Uptake and Intra-Population $^{87}Sr/^{86}Sr$ Variability of Bones and Teeth—Controlled Feeding Experiments With Rodents (Rattus norvegicus, Cavia porcellus). Front. Ecol. Evol. 8:569940. doi: 10.3389/fevo.2020.569940

Strontium isotopes in biogenic apatite, especially enamel, are widely employed to determine provenance and track migration in palaeontology and archaeology. Body tissues record the $^{87}Sr/^{86}Sr$ of bioavailable Sr of ingested food and water. To identify non-local individuals, knowledge of the $^{87}Sr/^{86}Sr$ of a non-migratory population is required. However, varying factors such as tissue turnover rates, feeding selectivity, Sr content, digestibility of food, and the ingestion of mineral dust can influence body tissue $^{87}Sr/^{86}Sr$. To evaluate the Sr contribution of diet and water to mammalian hard tissues $^{87}Sr/^{86}Sr$, controlled feeding studies are necessary. Here we present $^{87}Sr/^{86}Sr$ from controlled feeding experiments with two rodent species (*Rattus norvegicus, Cavia porcellus*). Due to the continuous and fast incremental growth of rat and guinea pig incisors (~0.1 – 0.5 mm/day), their enamel is expected to record isotopic dietary changes. For Experiment-1: Diet Switch, animals were switched from their respective supplier food to a pelleted experimental diet containing either insect-, plant-, or meat-meal and a staggered-sampling approach was used to monitor the $^{87}Sr/^{86}Sr$ changes in rat incisor enamel and bone over the course of the experiment. In Experiment-2: Basic Diets, separated cohorts ($n = 6$) of rats and guinea pigs were fed one of the three pelleted diets and received tap water for 54 days. While the rat incisors showed a complete tissue turnover, the slower-growing guinea pig incisors partially retained supplier diet-related isotopic compositions. In addition, one group of rats fed plant-meal pellets received Sr-rich mineral water, demonstrating that drinking water can be an important Sr source in addition to diet. Additionally, a leaching experiment showed that only a small fraction of diet-related Sr is bioavailable. Finally, in Experiment-3: Dust Addition, guinea pigs were fed pellets with and without addition of 4% of isotopically distinct dust (loess or kaolin). Animals that received kaolin-containing pellets displayed increased enamel $^{87}Sr/^{86}Sr$. Intra-population $^{87}Sr/^{86}Sr$ variability within each feeding

group was small and thus we conclude that it should not affect interpretations of $^{87}Sr/^{86}Sr$ in provenance studies. However, the differences between bulk food and leachate $^{87}Sr/^{86}Sr$ highlight the importance of Sr bioavailability for provenance studies and Sr isoscapes.

Keywords: strontium isotopes, rodents, population variability, enamel, bioavailability, bone, feeding study, faeces

INTRODUCTION

The number of studies dealing with the radiogenic Sr isotope ratio ($^{87}Sr/^{86}Sr$) have substantially increased within the past decades, and it has become an important tool in many scientific fields, such as petrology, palaeoclimatology, forensics and food traceability, especially in combination with light stable isotopes (e.g., McArthur et al., 2001, 2012; Kelly et al., 2005; Kimura and Chang, 2012; Marchionni et al., 2016; Weber et al., 2018b). The $^{87}Sr/^{86}Sr$ of bones and tooth enamel is commonly used in archaeological and palaeontological applications, mainly for the reconstruction of mobility and provenance of populations and individuals, as well as for reconstructing the life histories of animals and humans (e.g., Balasse et al., 2002; Outridge et al., 2002; Bentley, 2006; Copeland et al., 2011; Gregoricka, 2014; Lugli et al., 2017a). The mineral composition of bone and tooth enamel is hydroxylapatite [$Ca_5(PO_4)_3(OH)$], and the Ca^{2+} in the hydroxylapatite is substituted by Sr^{2+} in trace amounts due to their similar chemical behavior (Comar et al., 1957), making the determination of Sr isotope ratios in these materials feasible. Observed differences in $^{87}Sr/^{86}Sr$ in nature are related to differences in the relative abundance of the radiogenic ^{87}Sr vs. the stable ^{86}Sr, due to the decay of the radioactive parent isotope ^{87}Rb in geological materials (Banner, 2004). Therefore, different geographical regions with distinct bedrock geologies will yield different $^{87}Sr/^{86}Sr$ ratios (Faure and Mensing, 2005). The isotopic composition of the locally bioavailable Sr enters the food chain via Sr-bearing nutrients from ingested water and plants (Carr et al., 1962; Capo et al., 1998; Blum et al., 2000). After digestive assimilation, radiogenic Sr is incorporated into body tissues without any observed isotopic variation. There are apparently no biotic or abiotic factors affecting radiogenic Sr isotopes (Flockhart et al., 2015), while non-radiogenic stable Sr isotopes ($^{88}Sr/^{86}Sr$ expressed as $\delta^{88/86}Sr$) show a trophic level effect caused by biologically induced and mass-dependent fractionation (Knudson et al., 2010; Lewis et al., 2017). For radiogenic Sr ($^{87}Sr/^{86}Sr$), natural mass-dependent fractionation (Urey, 1947), as well as fractionation during mass spectrometric Sr isotope analysis are corrected for after normalization to a constant $^{88}Sr/^{86}Sr$ of 8.375209 during data reduction (Meija et al., 2016).

Differences in the formation time of vertebrate hard tissues allow the reconstruction of individual movements during an animal's lifetime from Sr isotope analysis of teeth and bones that form at different ontogenetic stages. While tooth enamel $^{87}Sr/^{86}Sr$ is not altered after its complete maturation (Hillson, 2005), bones undergo a continuous remodeling throughout life, depending on bone type and ontogenetic age (Jowsey et al., 1971). Therefore, tooth enamel of diphyodont mammals without ever-growing teeth reflects the $^{87}Sr/^{86}Sr$ during different phases of the animal's early life, while bones reflect an average of dietary $^{87}Sr/^{86}Sr$ ratios over the last years or the whole life of an animal, depending on the animals age and longevity (Knipper, 2004; Tütken, 2010). The differences in the timing of formation and turnover (or lack thereof in the case of teeth) of these tissues have led to extensive use of bone-tooth pairs to reconstruct the mobility and life history of animals and humans using radiogenic Sr isotopes (Müller et al., 2003; Schweissing and Grupe, 2003; Bentley, 2006; Scheeres et al., 2013). However, relatively little is known about the natural intra-population variability of Sr isotopes, which in turn may potentially influence the interpretation of differences in tooth-bone or tooth-tooth pairs, which are important to identify local vs. non-local values in comparison to Sr isoscapes (Bataille et al., 2020). Some studies evaluated intra- and/or inter-individual Sr isotope variability in archaeological sites (Gregoricka, 2014; Knudson et al., 2016). However, Sr sources and life histories are often poorly resolved in many archaeological populations, so the results of these studies potentially overestimate true intra-population variability. Therefore, feeding experiments with controlled diet/water Sr inputs and analyses of tissues formed during the experimental period are necessary to properly quantify intra- and/or inter-individual Sr isotope variability. Lewis et al. (2017) performed such a controlled feeding experiment on domestic pigs over two generations to evaluate the influence of marine resources on Sr/Ca, $^{87}Sr/^{86}Sr$, and $\delta^{88/86}Sr$. Analyzed materials included diet, tooth enamel, bones and faeces. The authors determined that the $^{87}Sr/^{86}Sr$ of the animals reflected the diet they received, in that the Sr/Ca ratio increased with increasing marine portion of the food. In addition, they showed a depletion of $\delta^{88/86}Sr$ of 0.322 ± 0.060 ‰ between diet and tooth enamel. Anders et al. (2019) used $^{87}Sr/^{86}Sr$ to study the locally bioavailable Sr isotope composition and characterize variability in different tissue types of pigs (tooth enamel, bones, bristles, meat, organs and blood). They observed a high intra- and inter-individual variability, as well as tissue-specific patterns. Tissues with higher turnover rates, such as soft tissues and blood, were found to have the highest variability in $^{87}Sr/^{86}Sr$. The authors suggested that only tissues with slow turnover, thus allowing for sufficient time averaging of the Sr isotope signal should be used for estimating local bioavailable Sr isotope ranges.

Rodent incisors are ever growing, which makes them an ideal, continuously recording archive in which to study the incorporation of isotopic signals into a hard tissue from diet and water sources. Additionally, enamel is frequently well-preserved

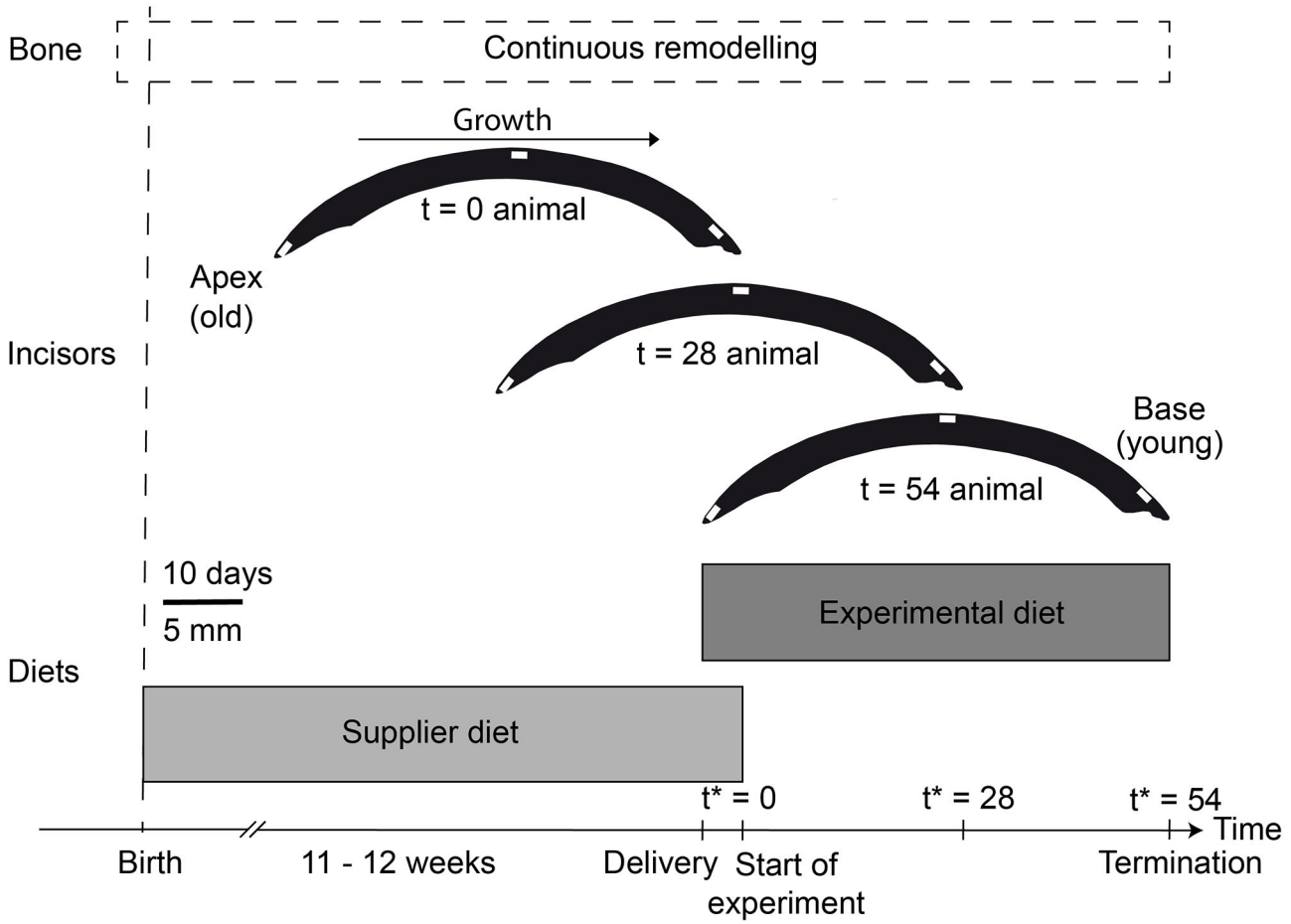

FIGURE 1 | Experimental overview for this study with the approximate growth phases of bone (dashed box) and (rat) incisor enamel (schematic illustration). The base of the incisors consist of the youngest enamel, while the apex is the oldest part of the incisor. We assumed a growth rate of 0.3 – 0.5 mm/day for the rodent incisors (Law et al., 2003; Müller et al., 2015). Feeding duration for each diet type is indicated by the two gray boxes (note the brief overlap between the supplier diet and the experimental diet during the acclimatization phase of the animals for 5 days, where both diets were provided). The white lines within the incisors indicate the sampling locations for LA-MC-ICP-MS Sr isotope analyses (see also **Supplementary Figure 1**). *Timing (*t*) is always relative to the start of the experiment (i.e., the consumption of experimental food only).

in the archaeological and palaeontological record (Copeland et al., 2010; Kirsanow and Tuross, 2011; Gehler et al., 2012). Newly formed tooth enamel and dentine is constantly produced at the basal end of the incisor (Leblond and Warshawsky, 1979), while older enamel is worn away and lost due to regular abrasion. This allows for a continuous monitoring of the Sr isotope composition, using high-resolution sampling techniques, such as micro-milling or *in-situ* laser ablation. While metabolically active soft tissues (e.g., liver or kidney) which turn over rapidly, reflect only the Sr isotopic compositions of the diet most recently consumed, tooth enamel remains unchanged after its maturation, making rodent incisor enamel a well-suited focal tissue in controlled feeding studies. With a growth rate of 0.5 mm/day for rats (Law et al., 2003) and 0.1 – 0.3 mm/day for guinea pigs (Müller et al., 2015), a typical rat or guinea pig incisor (∼2.6 – 3 cm total length) reflects up to the last 60 days of life (**Figure 1**). By measuring the $^{87}Sr/^{86}Sr$ along the rodent incisor, a time-resolved Sr isotope incorporation can be monitored. In addition, the analysis of bone material allows for a direct comparison between a fast (incisor enamel) and slow growing (bone) hard tissue with different turnover times.

Here we present radiogenic Sr isotope data from three controlled feeding experiments with two rodent species: the omnivorous, opportunistic feeding rat (*Rattus norvegicus* forma domestica) and the herbivorous guinea pig (*Cavia procellus*). In two of the experiments, both rats and guinea pigs received different meat-, insect-, or plant-meal based pelleted diets (25 – 56 wt%, see **Supplementary Table 1** for diet formula), while in the third experiment animals received pelleted diets with and without the addition of 4 wt% dust. In a first experiment (Experiment-1: Diet Switch), a staggered-sampling approach was used to determine the timing of dietary $^{87}Sr/^{86}Sr$ incorporation into the enamel and bone of rats after a diet switch from the supplier diet. For a second experiment (Experiment-2: Basic

Diets), rats and guinea pigs were fed with the three different pelleted diets described above for 54 days, resulting in a (near) complete growth of the incisors during the experimental duration (**Figure 1**). Due to the slower remodeling of bone, $^{87}Sr/^{86}Sr$ did not reach dietary equilibrium with the diets. Additionally, one group of rats was provided with Sr-rich mineral water. In a third experiment (Experiment-3: Dust Addition), guinea pigs were fed with a plant-based pelleted diet, supplemented with two different silt to clay sized natural and isotopically distinct mineral dusts (loess and kaolin) at a 4 wt% level, to simulate ingestion of soil components and assess its influence on the Sr isotope composition of an animal. Diet, water, teeth (all experiments), bones (Experiments-1: Diet Switch and−2: Basic Diets) as well as faeces samples (Experiment-2: Basic Diets) were analyzed for $^{87}Sr/^{86}Sr$ to evaluate the timing of the dietary overturn in the ever-growing incisors. A leaching experiment of the pelleted diets was performed to assess their differences in bioavailability of Sr from the different diets.

MATERIALS AND METHODS

Controlled Feeding Experiments

The controlled feeding experiments were approved by the Cantonal Veterinary Office in Zurich, Switzerland (license no. ZH135/16) and performed at the University of Zurich between July and October 2017. Adult female WISTAR (RjHan:WI) rats (11 – 12 weeks old at the beginning of the experiment, $n = 46$) and Dunkin Hartley (HsdDhl:DH) guinea pigs (3 – 5 weeks old at the beginning of the experiment, $n = 36$) were housed in groups of six individuals in separate indoor enclosures with water and food provided for *ad libitum* consumption. Animals were prevented from gnawing on the enclosure or other materials during the experiment to avoid unnecessary mechanical abrasion of tooth enamel. Prior to the experiments (from birth until arrival in Zurich), the animals received a standard pelleted diet (formula 2040 Teklad Global Guinea Pig Diet, for guinea pigs and formula 2018S Teklad Global 18% Protein Rodent Diet, for rats) at the supplier facility. All animals were provided with the supplier diet together with the experimental diet for 5 days to allow acclimatization to the new diet, before switching entirely to the experimental diet. For guinea pigs (which cannot synthesize vitamin C), drinking water was supplemented with vitamin C at a concentration of 200 mg/L. After the experiments, the animals were euthanized with CO_2 and dissected to sample soft- and hard-tissues for isotope analysis. Lower mandibular incisors and distal tibias were chosen for all analyses during this study. Additionally, faeces were collected during Experiment-2: Basic Diets after at least 20 days on the experimental diet.

In total, three different experimental setups were used in the framework of this study: (1) Diet Switch (three groups of rats; (2) Basic Diets (four groups of rats, including water enrichment, and three groups of guinea pigs; (3) Dust Addition (three groups of guinea pigs).

In the Diet Switch experiment, a staggered-sampling approach was performed, in which rats were euthanized after 0 – 40 days on the experimental diet ($n = 7$ for insect- and plant diets each, and $n = 8$ for meat based diet), to study Sr incorporation into enamel and bone after the switch from the supplier to the experimental diet (**Table 1**). Each plant-based diet also included either a plant (lucerne, *Medicago sativa*, 56 wt%), insect (Protix Insect Protein of soldier fly larvae, *Hermetia illucens*, 26 wt%), or mammalian meat (lamb, *Ovis aries*, 25 wt%, potentially with minor contribution of bone) meal ingredient to simulate different feeding categories (i.e., herbivore, insectivore, or carnivore, see **Supplementary Table 1** for the exact ingredients for each diet).

For the Basic Diets experiment, groups of six rats and six guinea pigs were each fed with the experimental diet for 54 days. Each feeding group received local Zurich tap water, with the exception of one group of rats, which received a commercially available Ca-Sr-rich mineral water (spring in Sersheim, Germany). Individuals from each group from the Basic Diets experiment Diets (excluding the rats provided the Sr-rich mineral water) were also kept in isolation in metabolic cages for 4 days after at least 20 days on the experimental diet to measure differences in food intake for each diet, and for individual fecal collection ($\geq$20 g/ individual). For each diet group, one fecal sample (25 – 50 mg) was analyzed.

In the third Dust Addition experiment, three groups of guinea pigs were fed, in groups of six, for 23 – 29 days with a standard plant pelleted diet (71 wt% lucerne meal) with and without 4% dust added. Dust additives included loess and kaolin, both of which have distinctively higher $^{87}Sr/^{86}Sr$ from the standard plant pelleted diet. These pellets were produced from a ground, pelleted diet (formula 2820 Granovit AG, Kaiseraugst, Switzerland) into which 4 wt% of loess or kaolin, respectively, were mixed. The mixture was then re-pelleted and fed to the animals to assess the influence of external, clay-to-silt-sized mineral dust particles on dental wear (see Winkler et al., 2020 for further details and the influence of the external abrasives on dental microwear texture). For Experiment-3: Dust Addition, only incisor enamel was sampled using LA-MC-ICP-MS.

Leaching Experiment

A leaching protocol was applied to all pelleted diets (each 2.5 – 3 g of whole pellets, see section "Controlled feeding experiment" for detailed description of the pellets) to evaluate potential differences in Sr chemical availability of Sr bearing phases. While the usual total bulk dissolution protocol involves a treatment with concentrated nitric acid overnight on a hot plate, the leaching experiment was performed with two dilutions of ultrapure hydrochloric acid for 3 h at 38°C to mimic conditions in a rodent stomach. For rats, we assumed a stomach pH value of 3 and a volume of 6 mL (Mcconnell et al., 2008) and for guinea pigs a pH of 3 and a volume of 15 mL (Merchant et al., 2011). To mimic stomach conditions intermediate between those of both animals, we selected a volume of 10 mL and a HCl concentration of 0.001 mol/L (pH 3). In addition, a second experiment was performed with a lower pH of 1 and acid concentration (0.1 mol/L HCl) to evaluate different dissolution conditions. After the experiment, the supernatant was separated from the undissolved solid remains by centrifugation at 6,000 min^{-1} for 5 min and evaporated to dryness. Afterwards, the supernatants of the leached pellet samples were treated as described in the section "Sample preparation."

TABLE 1 | Overview of the three controlled feeding experiments.

Animals	Experiment	Feeding group	Acclimatization [days]	Experimental duration [days]	No. of samples
Rats	1) Diet Switch	Supplier pellet	5	0	$n = 3$
Rats	1) Diet Switch	Plant pellet	5	6, 10, 20, 24, 28, 32, 40	Each $n = 1$
Rats	1) Diet Switch	Insect pellet	5	10, 16, 20, 24, 28, 32, 40	Each $n = 1$
Rats	1) Diet Switch	Meat pellet	5	6, 10, 16, 20, 24, 28, 32, 40	Each $n = 1$
Rats & guinea pigs	2) Basic diets	Plant pellet	5	54	$n = 6$
Rats & guinea pigs	2) Basic diets	Insect pellet	5	54	$n = 6$
Rats & guinea pigs	2) Basic diets	Meat pellet	5	54	$n = 6$
Rats	2) Basic diets	Plant pellet + Sr-rich water	5	54	$n = 6$
Guinea pigs	3) Dust Addition	Standard pellet	5	23, 26, 29	$n = 6$
Guinea pigs	3) Dust Addition	Standard pellet + 4% loess	5	23, 26, 29	$n = 6$
Guinea pigs	3) Dust Addition	Standard pellet + 4% kaolin	5	23, 26, 29	$n = 6$

During the 5-days acclimatization period, the animals were provided with both the supplier as well as the experimental diet. Afterwards, the animals were only provided with the experimental diet. All animals received tap water, except for one group which received Sr-rich mineral water. Rats and guinea pigs were held in separated enclosures without any mixing between different groups.

Sample Preparation

Bone (distal tibia) and enamel (sampled from the central part of the lower mandibular incisor) samples (1 – 5 mg) were used for solution-mode MC-ICP-MS Sr isotope analyses and digested using 500 µL of distilled trace metal grade concentrated nitric acid (Slovak and Paytan, 2012). Ball-milled food and fecal samples (25 – 50 mg) were digested in 4 mL of concentrated nitric acid and 1 mL of concentrated H_2O_2 (trace metal grade). All samples were placed in closed PFA screw-cap vials on a hot plate at 120°C overnight. This procedure removes the organic fraction of the foods prior to chemical separation (Eisenhauer et al., 2019). After digestion, samples were evaporated to dryness and re-dissolved in 2 mol/L HNO_3. Water samples were acidified using concentrated nitric acid until a concentration of 2 mol/L HNO_3 was reached.

Separation of Sr

For the separation of the Sr fraction, we used a prep*FAST* MC (ESI Elemental Scientific). The prep*FAST* is a low-pressure ion exchange chromatographic system (Romaniello et al., 2015) and is housed in a clean room at the Institute of Geosciences, University of Mainz. We slightly modified the default 1 mL Sr-Ca column (CF-MC-SrCa-1000) Sr-Ca separation protocol provided by ESI, by reducing the elution volume for the Sr fraction to 5 mL of 6 mol/L HNO_3. We find that this reduction prevents the potential elution of Ca into the Sr fraction during Sr elution steps. After sample purification, sample aliquots were evaporated to dryness and re-dissolved in 250 µL concentrated HNO_3 and 100 µL concentrated H_2O_2 to digest any potential organic remains (Eisenhauer et al., 2019). The samples were again evaporated to dryness and re-dissolved in 0.8 mol/L HNO_3, in preparation for Sr isotope analysis.

Solution-Based MC-ICP-MS Sr Isotope Analyses

Analysis of bulk samples for Sr isotopes was performed at the Institute of Geosciences, University of Mainz, using a Thermo Neptune Plus MC-ICP-MS systems coupled to either a CETAC Aridus 3 or an ESI Apex Omega HF desolvating system. All solutions were prepared in 0.8 mol/L HNO_3 with a Sr concentration of ∼10 ng/g. Sample introduction was performed using a 100 µL/min nebuliser and a Jet-X-interface. The following ion beams were monitored during analysis: ^{82}Kr, ^{83}Kr, ^{84}Sr, ^{85}Rb, ^{86}Sr, ^{87}Sr, and ^{88}Sr. A static multi-collection mode was applied to record all signals simultaneously within a single block of 50 cycles with 4.2 s integration time. Samples were bracketed and normalized to NIST SRM 987 (reference $^{87}Sr/^{86}Sr = 0.710248$, McArthur et al., 2001). Analysis of NIST SRM 987 yielded a longterm average $^{87}Sr/^{86}Sr$ of 0.71028 ± 0.00003 (2 SD, $n = 452$). The methods closely follow Weber et al. (2018a), where the data evaluation is described in detail. Data evaluation was performed offline, using an in-house R script (R Core Team, 2013). Krypton correction was performed iteratively using the natural $^{86}Kr/^{83}Kr$ of 1.505657. All $^{87}Sr/^{86}Sr$ ratios from solution-based analyses are mean values with their respective 2 SE (standard error, see Weber et al., 2017 for details).

In-situ LA-MC-ICP-MS Sr Isotope Analysis

In situ analysis of samples for $^{87}Sr/^{86}Sr$ was performed by LA-MC-ICP-MS (laser ablation multi-collector inductively coupled plasma mass spectrometry) at the Institute of Geosciences, University of Mainz. Incisors were cleaned with ethanol and placed on a glass slide to ablate the outer enamel surface. We chose sampling areas in the base, middle and apex of each incisor, in order to evaluate enamel that formed at different times during the experiment (**Figure 1**).

A Neptune Plus (Thermo Scientific) MC-ICP-MS was coupled to an ArF Excimer 193 nm laser system (ESI NWR193), equipped with a TwoVol^2 ablation cell. In addition, a CETAC Aridus 3 desolvating system was coupled to the sample line to introduce N_2 and Ar and to enhance sensitivity. Further details about the instrumentation are given in **Supplementary Table 2**. The methods generally follow Weber et al. (2017) and are only briefly described here. Nine faraday cups were used to monitor signal

intensities of the following m/z: ^{82}Kr, ^{83}Kr, ^{84}Sr, ^{85}Rb, ^{86}Sr, ^{87}Sr, and ^{88}Sr, as well as the doubly charged half-masses of ^{167}Er and ^{171}Yb. Due to their small signals, Rb, Er, and Yb were monitored using Faraday cups equipped with 10^{13} Ω resistors, while all other signals were monitored with Faraday cups equipped with 10^{11} Ω resistors. For the laser ablation analysis, line scans of 500 µm length were applied with a circular spot size of 110 µm, a translation speed of 5 µm/s, a repetition rate of 50 Hz and a resulting fluence of 5 J/m^2. Data evaluation and processing followed the methods described in Weber et al. (2017) and was performed using an in-house script in the statistical software R (R Core Team, 2013). Signals were corrected for Kr using the on-peak baseline technique and measuring a 30 s background without the laser firing prior to each analysis. Instrumental mass bias was corrected by applying the exponential law and an ^{88}Sr/^{86}Sr ratio of 8.375209. To correct ^{87}Sr for ^{87}Rb, we applied the mass bias correction factor and used the constant ^{87}Rb/^{85}Rb of 0.3857. We used a modern marine shark tooth as reference material to monitor drift during each analytical session. The long-term average for this shark tooth during this study yielded a ^{87}Sr/^{86}Sr of 0.70918 ± 0.00007 (2 SD, $n = 96$), in agreement with the modern-day seawater value of 0.70918 (McArthur et al., 2001). In addition, we used several bioapatite in-house reference materials (horse, elephant and shark teeth, human deciduous tooth, **Supplementary Table 3**), as well as internationally available apatite (bone ash NIST SRM 1400 and bone meal NIST SRM 1486) and carbonate (JCp-1, JCp-1, and NanoSr) reference materials (Okai et al., 2002; Inoue et al., 2004; Galler et al., 2007; Ohno and Hirata, 2007; Weber et al., 2018a, 2020). All results for ^{87}Sr/^{86}Sr are presented as the mean of each analysis with its corresponding 2 SE (standard error, see Weber et al., 2017 for further details).

Quantification of Sr Concentration

The Sr concentrations of water samples were determined using a Spectro CIROS Vision ICP-OES (inductively coupled plasma optical emission spectrometry) system at the Institute of Geosciences, University of Mainz.

Three rat incisors from the Diet Switch experiment with plant diet and three guinea pig incisors from each feeding group from the Basic Diet experiment were analyzed for their Sr/Ca ratio by *in-situ* LA-ICP-MS at the Institute of Geosciences, Mainz. An ArF Excimer 193 nm laser system (ESI NWR193), equipped with a TwoVol^2 ablation cell, was coupled to an Agilent 7500ce ICP-MS. NIST SRM 612 was used for calibration purposes, while NIST SRM 610, USGS BCR-2G and Durango Apatite were used as quality control materials (**Supplementary Table 4**). Spot analyses with a circular spot size of 100 µm were employed, using a repetition rate of 10 Hz and a fluence of 3.5 J/cm^2. Background time was set to 15 s, followed by 60 s of ablation. Data reduction was performed using an in-house spreadsheet based on Jochum et al. (2007). Details of the applied calculations are given in Mischel et al. (2017). The calcium isotope ^{43}Ca was used as internal standard element. Results for the quality control materials are presented in **Supplementary Table 4**. The investigated rat incisors include animals euthanized after 0, 32, and 40 days on the experimental plant pellet (after initial 5 days of acclimatization, see section "Controlled feeding experiments," **Table 1** and **Figure 1**). The guinea pig incisors include animals from the Basic Diets experiment which received the experimental diet for the complete experimental duration of 54 days.

Strontium concentrations for pellets and their leachates were determined using a Thermo Neptune Plus MC-ICP-MS at the Institute of Geosciences, Mainz. The NIST SRM 987 was diluted to three different concentrations (1, 5, and 10 ng/g) for quantification of the sample Sr concentration. Sample introduction was performed according to the methods described for the solution MC-ICP-MS Sr isotope analysis.

Statistics

Data evaluation and statistical analyses for Sr isotopes were performed using the statistical software R (R Core Team, 2013). Processing of the data followed Weber et al. (2017). After interference correction, we performed a 2 SD outlier test for the mean of all individual ^{87}Sr/^{86}Sr ratios within one measurement and calculated a corresponding 2 SE uncertainty (standard error, SE = SD / $\sqrt{n}$), both for solution based and laser ablation analyses. For the estimation of statistical significance, we used the implemented R function "wilcox.test" (Mann-Whitney-*U*-Test).

Water-Food Sr Mixing Models

In order to discuss the Sr isotope compositions measured in rat and guinea pig teeth and bones in relation to their dietary intake of Sr, we built a series of mixing models, to estimate the ranges of ^{87}Sr/^{86}Sr ratios as assimilated by the organisms and resulting from the mixing of Sr from drinking water and solid food. The basic principle consists of writing the mass balance of the contribution of water and food to the Sr eventually assimilated by the organism, also referred to as bioavailable Sr, expressed as follows:

$$m_{tot}^{Sr^*} = m_{wt}^{Sr*} + m_{fd}^{Sr*}$$

where $m_{tot}^{Sr^*}$, $m_{wt}^{Sr^*}$ and $m_{fd}^{Sr^*}$ correspond to the daily mass of bioavailable Sr in total, from water and solid food, respectively. We consider a fractional assimilation of Sr from water to the blood f_{wt}, and from food to the blood f_{fd} referred to as bioavailability values and defined for both water and food as the proportion of Sr actually available for assimilation by the organism. We can thus express the total mass of daily bioavailable Sr as follows:

$$m_{tot}^{Sr*} = f_{wt}\, m_{wt}^{Sr} + f_{fd}\, m_{fd}^{Sr}$$

where m_{wt}^{Sr} and m_{fd}^{Sr} correspond to the daily ingested mass of Sr from water and food, respectively. The mass balance for Sr then dictates the following relation for the isotope composition of the total daily bioavailable Sr:

$$\left(\frac{^{87}Sr}{^{86}Sr}\right)_{tot}^{*} = \frac{f_{wt}\ m_{wt}^{Sr}}{m_{tot}^{Sr^*}} \left(\frac{^{87}Sr}{^{86}Sr}\right)_{wt}^{*} + \frac{f_{fd}\ m_{fd}^{Sr}}{m_{tot}^{Sr^*}} \left(\frac{^{87}Sr}{^{86}Sr}\right)_{fd}^{*}$$

where $\left(\frac{^{87}Sr}{^{86}Sr}\right)^{*}$ corresponds to the radiogenic isotope composition of the bioavailable Sr in total (*tot*), water (*wt*),

TABLE 2 | Sr isotope composition and Sr concentration for all diets (including leachates) and waters provided to the animals in this study.

Type of diet	$^{87}Sr/^{86}Sr$	$^{87}Sr/^{86}Sr$ uncertainty	Sr [μg/g]	Sr [μg/g] 2 SD
Supplier pellet rats	0.70891	± 0.00001 (2 SE, $n = 1$)	4.8	± 0.1
Leachate pH 3	0.71131	± 0.00002 (2 SE, $n = 1$)	NA	NA
Leachate pH 1	0.70942	± 0.00002 (2 SE, $n = 1$)	NA	NA
Supplier pellet guinea pigs	0.70944	± 0.00002 (2 SE, $n = 1$)	NA	NA
Leachate pH 3	0.70980	± 0.00002 (2 SE, $n = 1$)	NA	NA
Leachate pH 1	0.70950	± 0.00002 (2 SE, $n = 1$)	NA	NA
Insect pellet*	0.70878	± 0.00005 (2 SD, $n = 9$)	11.7	± 0.1
Leachate pH 3	0.70878	± 0.00001 (2 SE, $n = 1$)	0.54	± 0.01
Leachate pH 1	0.70884	± 0.00001 (2 SE, $n = 1$)	1.2	± 0.04
Plant pellet*	0.70944	± 0.00019 (2 SD, $n = 9$)	19.6	± 0.9
Leachate pH 3	0.70782	± 0.00001 (2 SE, $n = 1$)	0.64	± 0.02
Leachate pH 1	0.70822	± 0.00001 (2 SE, $n = 1$)	1.04	± 0.03
Meat pellet*	0.70821	± 0.00007 (2 SD, $n = 9$)	26.4	± 1.2
Leachate pH 3	0.70863	± 0.00001 (2 SE, $n = 1$)	0.35	± 0.02
Leachate pH 1	0.70847	± 0.00002 (2 SE, $n = 1$)	1.07	± 0.03
Standard pellet	0.71032	± 0.00001 (2 SE, $n = 1$)	20.0	± 0.7
Leachate pH 3	0.70860	± 0.00002 (2 SE, $n = 1$)	NA	NA
Leachate pH 1	0.70876	± 0.00002 (2 SE, $n = 1$)	NA	NA
Standard pellet + 4% loess	0.71034	± 0.00002 (2 SE, $n = 1$)	31.1	± 1.0
Leachate pH 3	0.70837	± 0.00002 (2 SE, $n = 1$)	NA	NA
Leachate pH 1	0.70887	± 0.00001 (2 SE, $n = 1$)	NA	NA
Standard pellet + 4% kaolin	0.71147	± 0.00001 (2 SE, $n = 1$)	21.2	± 0.7
Leachate pH 3	0.70882	± 0.00002 (2 SE, $n = 1$)	NA	NA
Leachate pH 1	0.70902	± 0.00002 (2 SE, $n = 1$)	NA	NA
Zurich tap water	0.70910	± 0.00004 (2 SD, $n = 14$)	0.29	± 0.02
Sr-rich water (REWE mineral water)	0.70828	± 0.00002 (2 SD, $n = 2$)	8.6	± 0.6

The 2 SE (standard error) and 2 SD (standard deviation) uncertainty for single analyses and Sr concentration, respectively, are the analytical uncertainties during the measurement. For those samples where n > 1, several aliquots were analyzed.

**During the experiment, several bags (all produced in one large batch) of the pelleted diets were fed to the animals. We observed only slight isotopic differences (<0.0002) among different bags.*

and food (*fd*). This relation can also be expressed using the Sr concentration ($[Sr]_{wt}$, $[Sr]_{fd}$) and daily ingested mass (m_{wt}, m_{fd}) of water and food:

$$\left(\frac{^{87}Sr}{^{86}Sr}\right)^{*}_{tot} = \frac{f_{wt}\ [Sr]_{wt}\ m_{wt}}{m_{tot}^{Sr*}}\left(\frac{^{87}Sr}{^{86}Sr}\right)^{*}_{wt} + \frac{f_{fd}\ [Sr]_{fd}\ m_{fd}}{m_{tot}^{Sr*}}\left(\frac{^{87}Sr}{^{86}Sr}\right)^{*}_{fd}$$

This mixing equation was then used to draw maps of the total bioavailable Sr isotope composition in the 2D space of daily intake of water and food, as these values vary with time, between individuals and from one species to another. A map was drawn for each pellet type and for each measured isotope composition of pellet leachates (which were taken as food bioavailable Sr end-member values). Two sets of maps are presented in the main text and **Supplementary Information**, one with distinct bioavailability values for water and food Sr and another with equal bioavailability values for both (assuming no differential assimilation of Sr from water and food). The calculations and plots were performed using the statistical software R (R Core Team, 2013).

RESULTS

Food and Water

An overview of the Sr isotope ratios, as well as the Sr concentration of each diet and water are given in **Table 2**. Supplier diets for the two rodent species differed, with a $^{87}Sr/^{86}Sr$ of 0.70944 ± 0.00002 (2 SE, here and in the following if not specified otherwise) for the guinea pigs and 0.70891 ± 0.00001 for the rats. During their time at the breeder facilities, the animals received de-mineralised drinking water with Sr concentrations below the quantification limit of the ICP-OES system. Therefore, the contribution of the Sr isotope composition of supplier water is not considered to have influence on body tissues $^{87}Sr/^{86}Sr$ while the animals were at the breeding facilities.

The Zurich tap water showed slight seasonal variation in $^{87}Sr/^{86}Sr$, ranging from 0.70907 ± 0.00003 to 0.70914 ± 0.00003, with an average value of 0.70910 ± 0.00004 (2 SD). In contrast, the Sr-rich mineral water yielded a much lower $^{87}Sr/^{86}Sr$ of

0.70828 ± 0.00002 (2 SD), with a Sr concentration ca. 30 times higher than the Zurich tap water. The supplemental vitamin C received by the guinea pigs did not yield Sr concentrations above the blank level after sample preparation, and can therefore be ruled out as a factor influencing $^{87}Sr/^{86}Sr$ in these animals.

The insect, plant and meat diets differed distinctively in their Sr isotope composition (**Table 2**). Analyses of ball-milled, powdered samples of the pellets which were completely digested with concentrated HNO_3 yielded different results compared to the leaching experiment. In HNO_3 bulk digested samples, the meat pellet had the lowest $^{87}Sr/^{86}Sr$ of 0.70821 ± 0.00007 and the plant pellet the highest $^{87}Sr/^{86}Sr$ of 0.70944 ± 0.00019 (2 SD). An intermediate ratio was observed for the insect diet, with an average $^{87}Sr/^{86}Sr$ of 0.70878 ± 0.00005 (2 SD). In the leaching experiment, the plant diet leachate yielded distinctively lower $^{87}Sr/^{86}Sr$ of 0.70782 ± 0.00001 at pH 3 and 0.70822 ± 0.00001 at pH 1 than for the fully digested pellet. The meat diet leachate yielded slightly higher ratios compared to the HNO_3 digested pellet ($^{87}Sr/^{86}Sr$ of 0.70863 ± 0.00001 at pH 3 and 0.70847 ± 0.00001 at pH 1), while the insect diet showed similar values for the leaching experiment as for the completely dissolved pellets with $^{87}Sr/^{86}Sr$ of 0.70878 ± 0.00001 at pH 3 and 0.70884 ± 0.00001 at pH 1.

The completely dissolved rat supplier pellet yielded a much lower $^{87}Sr/^{86}Sr$ (0.70891 ± 0.00001) than both leachates at pH 3 (0.71131 ± 0.00002) and pH 1 (0.70942 ± 0.00002). In contrast, the bulk solution of the guinea pig supplier pellet yielded a lower $^{87}Sr/^{86}Sr$ (0.70944 ± 0.00002) than both leachates (0.70980 ± 0.00002 at pH 3 and 0.70950 ± 0.00002 at pH 1).

The highest bulk ratios of $^{87}Sr/^{86}Sr$ were obtained from the experiment in which mineral dust (loess and kaolin) was added into the standard pellet (0.71032 ± 0.00001). While the addition of 4 wt% loess did not change the $^{87}Sr/^{86}Sr$ notably (0.71034 ± 0.00002), the addition of 4 wt% kaolin shifted the Sr isotope ratio to a higher ratio of 0.71147 ± 0.00001 (**Table 2**). All leachates from these three pellets from the Dust Addition experiment yielded lower $^{87}Sr/^{86}Sr$ than their bulk solutions, where the leachates at pH 1 were generally higher in $^{87}Sr/^{86}Sr$ than at pH 3 (**Table 2**).

Strontium Isotope Incorporation Over Time (Experiment-1: Diet Switch)

To establish baseline values for the initial Sr isotope composition (i.e., supplier food derived $^{87}Sr/^{86}Sr$) of the rats, three animals were euthanized after the initial 5 days acclimatization period. The Sr isotope compositions of their hard tissues are therefore only influenced by the food and the water supplied by the breeder. Two animals had very similar bone and enamel $^{87}Sr/^{86}Sr$, however, one individual, despite a similar bone $^{87}Sr/^{86}Sr$ (between 0.70918 ± 0.00001 and 0.70924 ± 0.00001), had a higher enamel $^{87}Sr/^{86}Sr$, especially in the apex and middle part of the incisor (up to 0.71024 ± 0.00009, **Figure 2**, i.e., the older parts of the incisor). It is therefore necessary to take this initial variability in $^{87}Sr/^{86}Sr$ into consideration when interpreting data from the Diet Switch experiment. However, the observed $^{87}Sr/^{86}Sr$ of those animals (independent on tissue type) fall within the range of the rat supplier pellet when considering bulk and leachate data (**Figure 2** and **Table 2**), indicating that this variability is caused by the diet.

The temporal evolution of $^{87}Sr/^{86}Sr$ in the hard tissues of rats euthanized at different time points during the experiment ($n = 8$ for insect and plant group, $n = 9$ for meat group, as well as $n = 6$ for each group with full experimental duration) is shown in **Figure 3**. Day 0 is designated as the 1st day that animals received only the experimental diet (i.e., after the initial 5 days acclimatization period). At the beginning of the experiment, all rats display similar bone $^{87}Sr/^{86}Sr$ starting values of 0.7091–0.7093. This is slightly higher than the value expected based on the bulk rat supplier diet (∼0.7089), but lower than the leachate at pH 1 (∼0.7094). Over the course of the experiment, the bone values show a linear trend ($R > 0.9$, **Figure 3**) toward lower ratios, which differed slightly among the diet groups (see section below for further details). In all groups, the incisor enamel $^{87}Sr/^{86}Sr$ tends to lower ratios at the base (i.e., the youngest part, grown later in the experiment, compared to the apex, which grew in the beginning of the experiment). The base usually reaches a plateau value by the middle of the tooth. Some spikes of higher $^{87}Sr/^{86}Sr$ are visible, particularly in the apex. This part of the incisor is formed earliest and this mainly reflects supplier food which had high $^{87}Sr/^{86}Sr$ values in the leachate. These spikes are most prominent in the animals that were fed the insect diet. The $^{87}Sr/^{86}Sr$ obtained for animals that received an experimental diet for the full 54 days duration of the Basic Diets experiment does not necessarily agree with the bulk diet $^{87}Sr/^{86}Sr$ (i.e., when digested with concentrated nitric acid) obtained for the pellets. For instance, the incisor enamel $^{87}Sr/^{86}Sr$ of the rats receiving the plant diet have much lower ratios than their diet and somewhat lower values than their drinking water. The enamel $^{87}Sr/^{86}Sr$ of those on the insect diet largely match the Sr isotope composition of their food. Overall, the rats fed with the meat diet have $^{87}Sr/^{86}Sr$ above their diet, but below their drinking water. The incisors show a better agreement with their respective experimental foods when compared to the diet Sr isotope data obtained in the leaching experiment (**Figure 3**).

Evolution of the Sr/Ca Ratio From the Supplier Toward the Experimental Diet (Experiments-1: Diet Switch and 2: Basic Diets)

Rats from the Diet Switch experiment show variable trends in their Sr/Ca ratio (**Figure 7**). These animals received the plant diet for 0, 32, and 40 days. The rat euthanized at $t = 0$ (**Figure 7**) has the lowest Sr/Ca of $8.2 \times 10^{-5} \pm 1.3 \times 10^{-5}$. The animal euthanized at $t = 32$ days shows increasing Sr/Ca toward the base (**Figure 7**), up to a ratio of $\sim 4 \times 10^{-5}$. The initial values at the apex agree with the individual on the supplier diet ($Sr/Ca \sim 8 \times 10^{-5}$). A plateau value (discounting the last base measurements) for Sr/Ca is reached for the most recently grown ∼30% of the total incisor enamel length. The rat euthanized

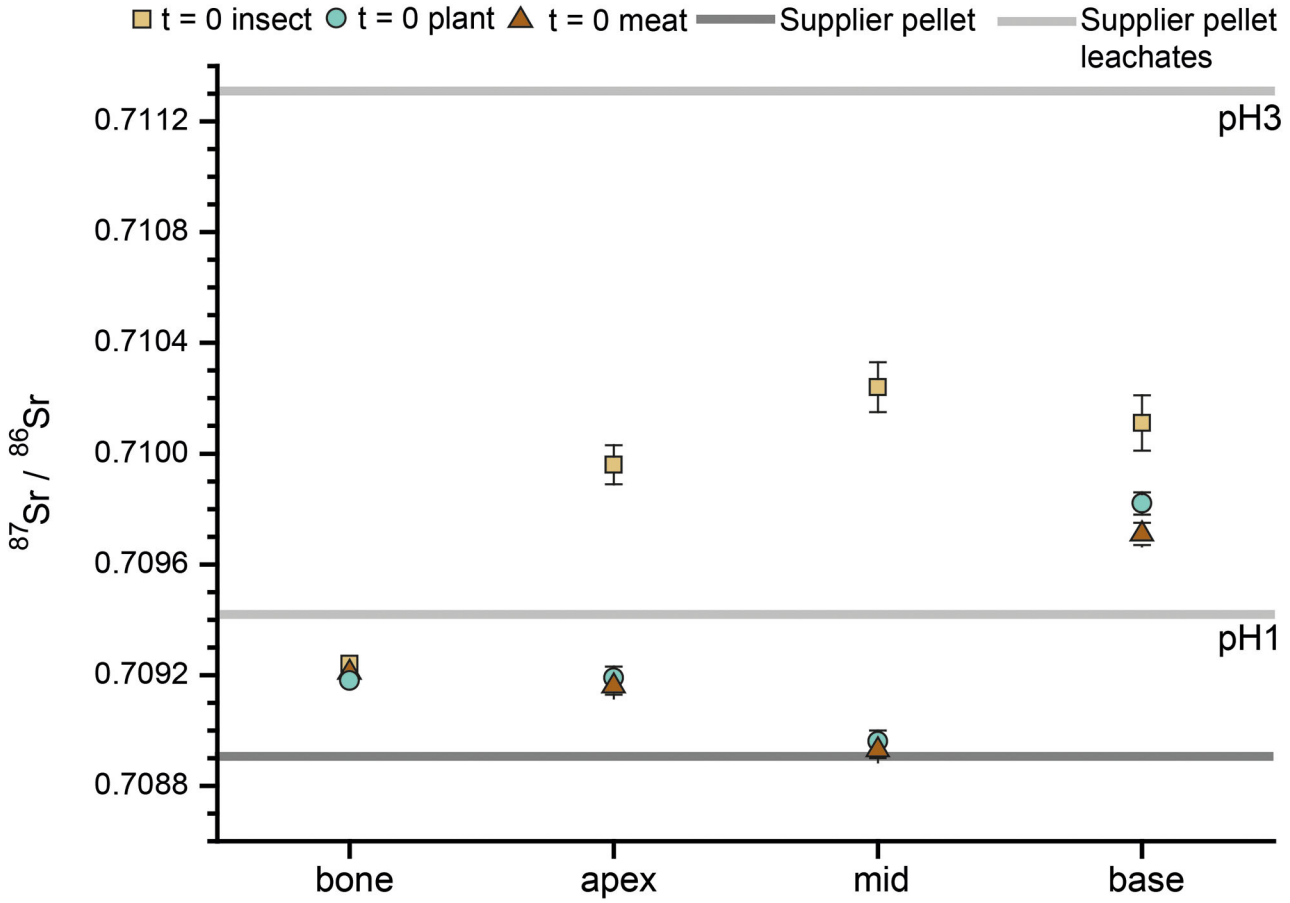

FIGURE 2 | Incisor enamel $^{87}Sr/^{86}Sr$ of three rats from $t = 0$ of the Diet Switch experiment. The dark gray line represents the $^{87}Sr/^{86}Sr$ from the supplier pellet, which the animals received during their entire life, post-weaning. The leachates (pH 3 and pH 1) of the supplier pellet are shown as light gray lines. For the last 5 days before euthanization, the animals were provided with both, supplier and experimental pelleted diets. Values for apex, middle and base were obtained by laser ablation, the bone and pellets were analyzed by solution mode MC-ICP-MS.

at $t = 40$ (**Figure 7**) shows a pattern similar to the individual fed for 32 days. The starting value is slightly higher than the ones for day 0 and day 32 individuals (1.0×10^{-4}) and a plateau of $\sim 2.8 \times 10^{-4}$ is reached at 50% of the total incisor enamel length.

In the guinea pigs from the Basic Diets experiment, the animal that received the plant diet shows the highest Sr/Ca (7.8×10^{-4}) with slightly increasing values toward the base (**Figure 7**). The animal fed the meat diet starts with a value similar to that of the guinea pig on the plant pellet at the apex and then this value progressively decreases to a minimum of $\sim 5 \times 10^{-4}$ in the middle of the incisor. Toward the base (i.e., the ontogenetically youngest part of the incisor), the Sr/Ca for the individual on the meat pellet progressively increases again (**Figure 7**). The enamel of the guinea pig that received the insect diet starts at a lower Sr/Ca than the two other individuals and decreases to a value similar to that of the meat diet specimen. Afterwards, the Sr/Ca increases again toward the base to a Sr/Ca that is similar to the two other individuals (**Figure 7**).

Sr Isotope Composition of Bones and Teeth After the Full Experimental Duration (Experiment-2: Basic Diets)

For the $^{87}Sr/^{86}Sr$ of the rats fed with the three basic diets for the full experimental duration (5 + 54 days), the bone values are similar across and within the feeding groups, except for one individual in the insect diet group (**Figure 4**). The $^{87}Sr/^{86}Sr$ obtained by LA-MC-ICP-MS for the incisors display a larger variability in comparison to the bones. However, the $^{87}Sr/^{86}Sr$ generally tends to have lower ratios toward the base of the incisor. The middle and base part of the incisors usually show similar results, while the apex (oldest) showed (some) higher $^{87}Sr/^{86}Sr$. Interestingly, the $^{87}Sr/^{86}Sr$ from the middle of incisors obtained by solution-based MC-ICP-MS are distinctively lower than the LA values by 0.0003 ± 0.0001 (1 SD) on average. As described in section "Strontium isotope incorporation over time (Experiment-1: Diet Switch)," enamel $^{87}Sr/^{86}Sr$ deviate from bulk pellet $^{87}Sr/^{86}Sr$ values and instead better agree with the data from the pellet leachates. The $^{87}Sr/^{86}Sr$ of rat fecal samples ($n = 3$) differ from those of the bulk pellet values (**Figure 4**). The rats that

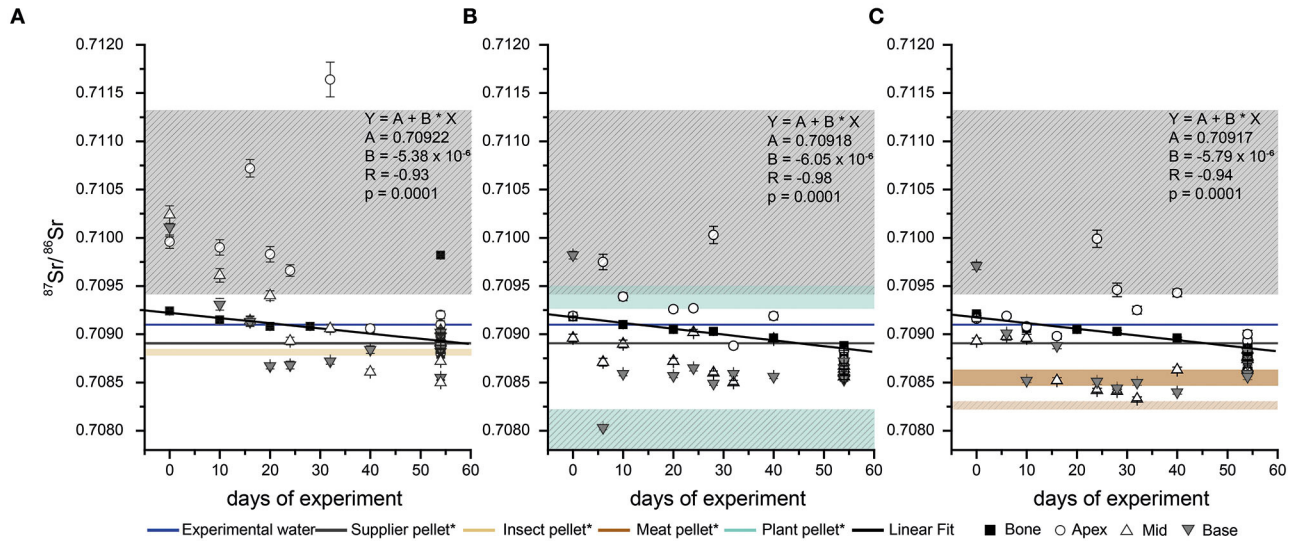

FIGURE 3 | Temporal evolution of the $^{87}Sr/^{86}Sr$ from different parts of the rat incisors and the bone during the Diet Switch experiment. For each feeding group, supplier pellet (which animals received prior to the experiment) and Zurich tap water (supplied during the feeding experiment) values are indicated by horizontal lines. Each x-axis value represents a single individual. The coloured boxes indicate the $^{87}Sr/^{86}Sr$ range, derived from the leaching of the pelleted diets: **(A)** insect pellet (beige) **(B)** plant pellet (cyan) **(C)** meat pellet (brown) and **(A–C)** supplier pellet (gray). All values were obtained by laser ablation, except for the bone values. The error bars indicate the analytical uncertainty for each data point. *The hatched boxes for the meat, plant and supplier diet represent the $^{87}Sr/^{86}Sr$ from the completely dissolved pellets. For the insect pellets, the $^{87}Sr/^{86}Sr$ overlap for both digestion types. The bone turnover shows a linear trend (black line) with the given R and *p*-values for each diet group.

received the Sr-rich mineral water and the plant diet have lower $^{87}Sr/^{86}Sr$ than the rats that received the tap water. Both the bone and the incisor values are lower and shifted toward the $^{87}Sr/^{86}Sr$ of the Sr-rich mineral water (**Figure 4**).

In general, the changes in $^{87}Sr/^{86}Sr$ described for the rats are also observed in the guinea pigs (**Figure 5**). All animals have higher $^{87}Sr/^{86}Sr$ in enamel in the apex of the incisor, even exceeding the values measured for bone. This is most likely related to the higher $^{87}Sr/^{86}Sr$ ratios of ∼0.7094 (pH 1 and 3 leachates at ∼0.7095 and ∼0.7098, respectively) of the guinea pig supplier food and the slower growth rate of guinea pig incisors (0.1 – 0.3 mm/day) compared to rats (0.5 mm/day). For some individuals, especially those fed the insect diet, we observed higher values in the middle part compared to the base, which mineralised just prior to the termination of the experiment.

In summary, bone and enamel $^{87}Sr/^{86}Sr$ in the insect group are higher than those of the two other groups. Values for guinea pigs fed in the plant group do not reflect the $^{87}Sr/^{86}Sr$ of the completely dissolved pellets, but do approach the values measured in the leachate of these same pellets. Guinea pig faeces from the plant and meat diet groups show higher $^{87}Sr/^{86}Sr$ than rat faeces from animals fed the same diets, while faeces from the insect fed guinea pigs and rats are very similar (**Figure 5**).

Influence of External Dust Sources (Experiment-3: Dust Addition)

Guinea pigs fed the standard diet are compared with guinea pigs fed the exact same standard diet, but with the addition of 4 wt% of loess and kaolin (for 23 – 29 days, **Figure 6**). In the apex, the $^{87}Sr/^{86}Sr$ of the three different feeding groups largely overlap, with two outliers (2 SD outlier test) at either side of the range, both of which are animals fed the standard pellet. While the enamel toward the middle of the incisor is characterized by a larger scatter and overlap in $^{87}Sr/^{86}Sr$, toward the incisor base the $^{87}Sr/^{86}Sr$ decreases progressively. Here, a difference between the animals that received the kaolin pellet and those that received the loess or standard pellet was observed. The guinea pigs fed the standard pellet show a large variation, covering nearly the entire $^{87}Sr/^{86}Sr$ range of all base samples. All incisor $^{87}Sr/^{86}Sr$ are distinctively lower than the $^{87}Sr/^{86}Sr$ of their respective food pellets, indicating that a fraction of (radiogenic) Sr from the pelleted diet was not bioavailable to the animals. Instead, values are similar to those of the drinking water and the leachates at pH 1.

DISCUSSION

Isotopic Homogeneity of Food and Water and Sr Bioavailability Assessed by Leaching

The variability of the $^{87}Sr/^{86}Sr$ of the pelleted diets among bags of the same batch was negligible for meat and insect pellets (2 SD = 0.00007 and 0.00005, respectively, each $n = 9$), when entirely dissolved in concentrated nitric acid. However, the plant pellets showed a two to four times higher variability of 2 SD = 0.00019 ($n = 9$). The seasonal variability of the Zurich tap water was low (2 SD = 0.00004 over a period of 1.5 years, $n = 14$) and is therefore also considered to be negligible since each

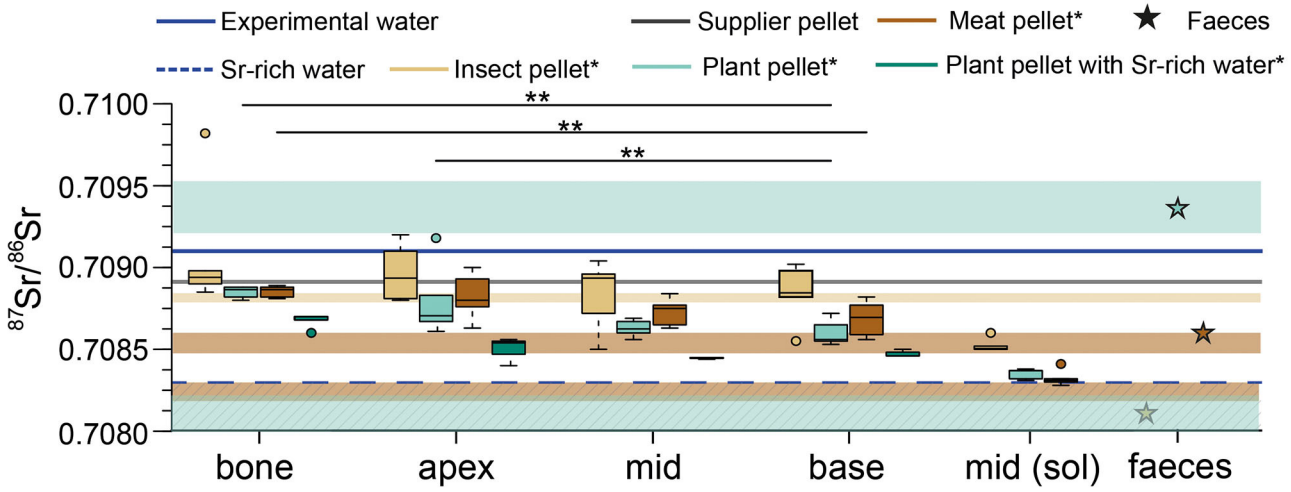

FIGURE 4 | Strontium isotope ratios as boxplots after the full experimental duration (54 + 5 days) for the different feeding groups of rats from the Basic Diets experiment. The $^{87}Sr/^{86}Sr$ of the supplier pellet and the experimental water supply is indicated by the horizontal lines. The coloured boxes indicate the $^{87}Sr/^{86}Sr$ range of the food pellets, derived from the leaching of the pellets: insect pellet (beige), plant pellet (cyan), meat pellet (redbrown Sr isotope ratios for apex, mid and base of the incisor were obtained by laser ablation. For each basic feeding group one fecal sample was analyzed. Apex, middle and base values were obtained by laser ablation. *The hatched boxes for the meat and the plant pellet show the $^{87}Sr/^{86}Sr$ ratios for the completely dissolved pellets. For the insect pellets, the $^{87}Sr/^{86}Sr$ overlap for both types of dissolution. The leachates for the supplier pellet are not shown due to better clarity (see **Figure 2**). Significance levels are presented as stars between bone and base (plant and meat group), as well as for apex – base pairs of the plant group).

experiment only lasted about 2 months. Therefore, the Sr isotope input from both food and water supply seem to have been mostly homogeneous and provided an isotopically constant Sr source during the controlled feeding experiment.

The $^{87}Sr/^{86}Sr$ measured in totally digested basic food pellets and the HCl leaching experiments at the two different pH levels (pH 1 and 3) yielded different $^{87}Sr/^{86}Sr$ ratios. While no distinct differences between the $^{87}Sr/^{86}Sr$ of the leachate and the whole food for the insect diet were observed, this difference seemed relevant for the meat diet, and was particularly large for the plant diet. These differences were however, in opposite directions, with the $^{87}Sr/^{86}Sr$ values of the leachates higher than the bulk meat diet, and lower for the plant diet. For the formulation of the pellets, which were produced specifically for our feeding experiments, different components were mixed, resulting in potentially different Sr bearing phases displaying varying $^{87}Sr/^{86}Sr$ end-member values and Sr bioavailabilites (see **Supplementary Table 1** for pellet ingredients). The different chemical environments of the Sr bearing phases are likely to induce a differential bioavailability of Sr to the animal. While Sr from some of the ingredients is highly available during the biological processing of food (e.g., digestion, metabolization), Sr from other ingredients may not have been as bioavailable. This is supported by the leaching data. The weaker acid (0.001 mol/L HCl) used for the leaching experiment, designed to mimic rodent stomach conditions, released Sr from Sr bearing phases where it is more bioavailable to the animals during digestion. This causes the pellet leachate $^{87}Sr/^{86}Sr$ to converge on a $^{87}Sr/^{86}Sr$ value ranging between 0.7082 and 0.7088. This range matches the range observed in the incisor data well (**Figures 4**, **5**). We therefore assume that the diet $^{87}Sr/^{86}Sr$ data obtained from the leaching experiments best reflects the Sr bioavailable to the animals.

Incorporation of Sr in the Ever-Growing Incisor Enamel (Experiment-1: Diet Switch)

The ever-growing incisors of rodents allow us to temporally constrain the incorporation of Sr into enamel. It is especially important to precisely determine which regions of the incisor were completely equilibrated with the experimental diet in order to further investigate the influence or the experimental diet on the isotopic composition of the dental hard tissues. We performed both Sr/Ca and Sr isotopic analyses on the incisors of rats which underwent a diet switch from a supplier diet to one of our custom designed diets in our controlled feeding experiment. The Sr/Ca of the rat that only received the supplier pellet (**Figure 7**) showed no clear trend, with only a slight increase in value toward the most proximal part at the base (i.e., the youngest part at a very early enamel mineralisation state). In comparison, the rats fed one of the experimental diets for 32 or 40 days showed an increase in Sr/Ca. While the individual that received the plant diet for 32 days had a value of Sr/Ca at the apex similar to the $t = 0$ animal, the individual fed for 40 days displayed a slightly higher apex Sr/Ca ratio. The transition to higher values in Sr/Ca ratios corresponds with the experimental diet thus appears to be phase shifted from $t = 32$ to $t = 40$ as expected. However, this difference is small and only based on this single individual. We therefore cannot rule out the possibility that this difference is simply the result of natural variability among individuals. Nevertheless, based on this observation, we propose that even the oldest part of the incisor (up to 60 days, see **Figure 1**), which grew for about 10 days prior

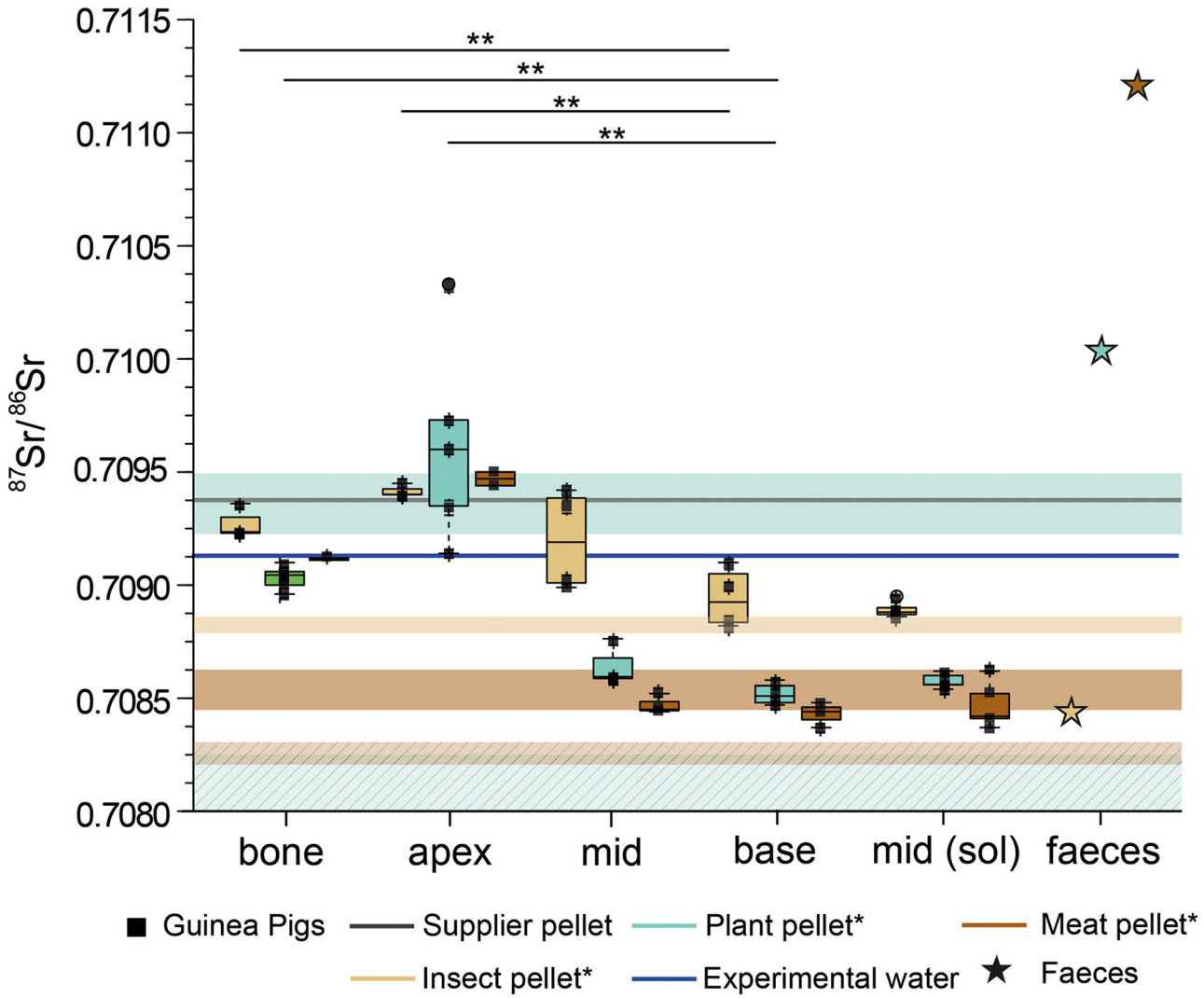

FIGURE 5 | Strontium isotope ratios as boxplots with underlying data points after the full experimental duration (54 + 5 days) for the different feeding groups of guinea pigs from the Basic Diets experiment. The $^{87}Sr/^{86}Sr$ of the supplier pellet and the drinking water during the experiment is provided. The coloured boxes indicate the $^{87}Sr/^{86}Sr$ range of the food pellets, derived from the leaching of the pellets: insect pellet (beige), plant pellet (cyan), meat pellet (brown). Strontium isotope ratios for apex, mid and base of the incisor have been obtained by laser ablation. For each basic feeding group one fecal sample was analyzed. *The hatched boxes for the meat and the plant pellet show the $^{87}Sr/^{86}Sr$ from the completely dissolved pellets. For the insect pellets, the $^{87}Sr/^{86}Sr$ overlap for all types of dissolution. Significance levels are presented as stars between bone and base, as well as for apex – base pairs.

to the start of the feeding experiment, was slightly influenced by the composition of the experimental diet. This observation can be explained by the enamel maturation process. Rodent enamel can be divided into three distinct zones of immature, maturing and mature enamel (Leblond and Warshawsky, 1979), and the chemical composition of enamel changes through the addition and maturation of bioapatite until the final maturation stage (i.e., full mineralisation of enamel) is reached. The whole process of enamel formation (∼1.5 days of pre-secretion, ∼7 days of secretion, and ∼20 days of maturation) can take up to 30 days (Leblond and Warshawsky, 1979). After the initial secretory stage of enamel formation, the maturing enamel remains an open system and can be influenced by dietary changes occurring after the initial secretory stage, resulting in the phase-shifting of time-dependent chemical signals (Passey and Cerling, 2002). This process also explains why there is no sharp transition in chemical composition from supplier to experimental diet, but rather a smooth one toward a plateau of Sr/Ca (**Figure 7**). Indeed, in addition to the phase-shifting, maturation of enamel also induces a dampening of time-dependent chemical signals. This plateau was reached for the last ∼30% of the incisor length for the rat fed for 32 days, while in the rat fed for 40 days this plateau comprised the full lower 50% of the incisor length (**Figure 7**), indicating the progression of the maturation front toward the apex because of the longer period of incisor growth and maturation.

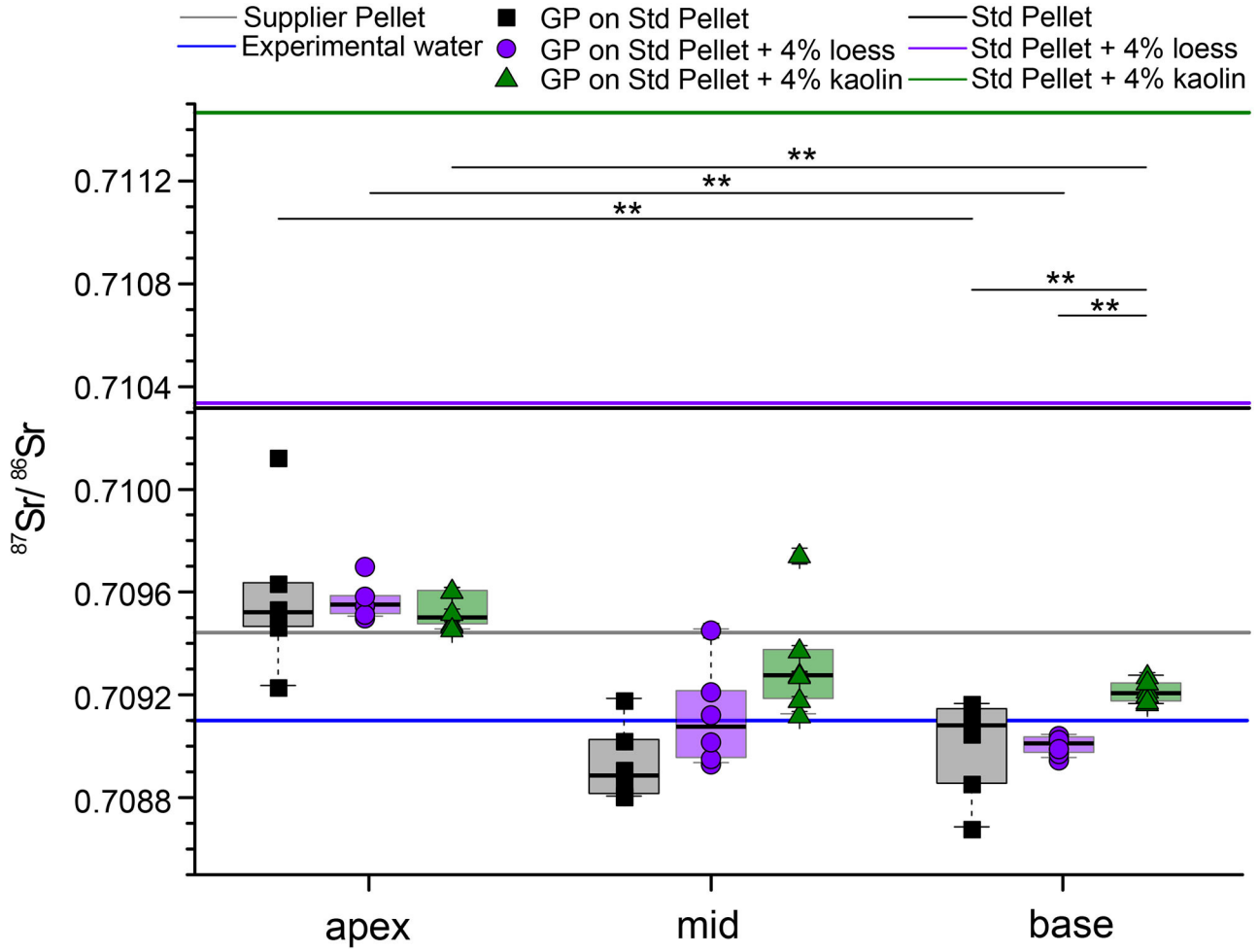

FIGURE 6 | Strontium isotope ratios of incisors from guinea pigs fed for up to 29 days on a standard pelleted diet with and without addition of 4 wt% loess or 4 wt% kaolin, respectively (Dust Addition experiment). The $^{87}Sr/^{86}Sr$ of the supplier pellet and the Zurich tap water supply is plotted for comparison, as well as the $^{87}Sr/^{86}Sr$ of the three different pelleted diets. All enamel $^{87}Sr/^{86}Sr$ were determined by LA-MC-ICP-MS. Significance levels are presented as stars between apex and base pairs, as well as within the base among different feeding groups.

Similar patterns were also recorded in the Sr isotope composition of the rat incisors during the Diet Switch experiment (**Figure 3**). Generally, isotopic turnover induced by the diet switch is fastest at the base, since it is the youngest-forming part of the incisors and reflects the most recent Sr input incorporated into the enamel by secretion and maturation. However, the three feeding groups differed slightly in terms of when they reached equilibrium with the bioavailable $^{87}Sr/^{86}Sr$ in the experimental diet in the base part. While the animals fed the plant diet reached $^{87}Sr/^{86}Sr$ values that reflected bioavailable $^{87}Sr/^{86}Sr$ from the experimental diet after just 10 days, the rats that received the insect diet needed at least 20 days to reach this value. The rats fed the meat diet were more variable. The observed differences in the timing of equilibrium may either be caused by intra-individual variability, or by the differences in $^{87}Sr/^{86}Sr$ between supplier diet and experimental diets. This difference is largest between supplier and plant pellet (leachates), indicating that the corresponding turnover signal might be enhanced due to the offset. Interestingly, while the individual that received the meat diet for 10 days seemed to have already reached a diet-related $^{87}Sr/^{86}Sr$, the individual fed the same diet for 16 days, had an elevated $^{87}Sr/^{86}Sr$. Here it is important to note, that each point in time is represented by a different individual ($n = 1$), which may have contributed to inter-individual bias due to slight differences in individual metabolism and feeding behavior. Similarly, a distinct time point at which a diet-related $^{87}Sr/^{86}Sr$ equilibrium is reached cannot be detected in the middle part of the rat incisor. The animals fed the meat diet had lower $^{87}Sr/^{86}Sr$ in the middle of the incisor in comparison to the base between 16 and 32 days of experiment, which were both lower than the $^{87}Sr/^{86}Sr$ after the full experimental duration of 54 days. The oldest part of the incisor (apex) always lagged distinctively behind the trend visible in the younger incisor parts. In addition, pronounced radiogenic Sr spikes (i.e., $^{87}Sr/^{86}Sr$ increases up to 0.002) are

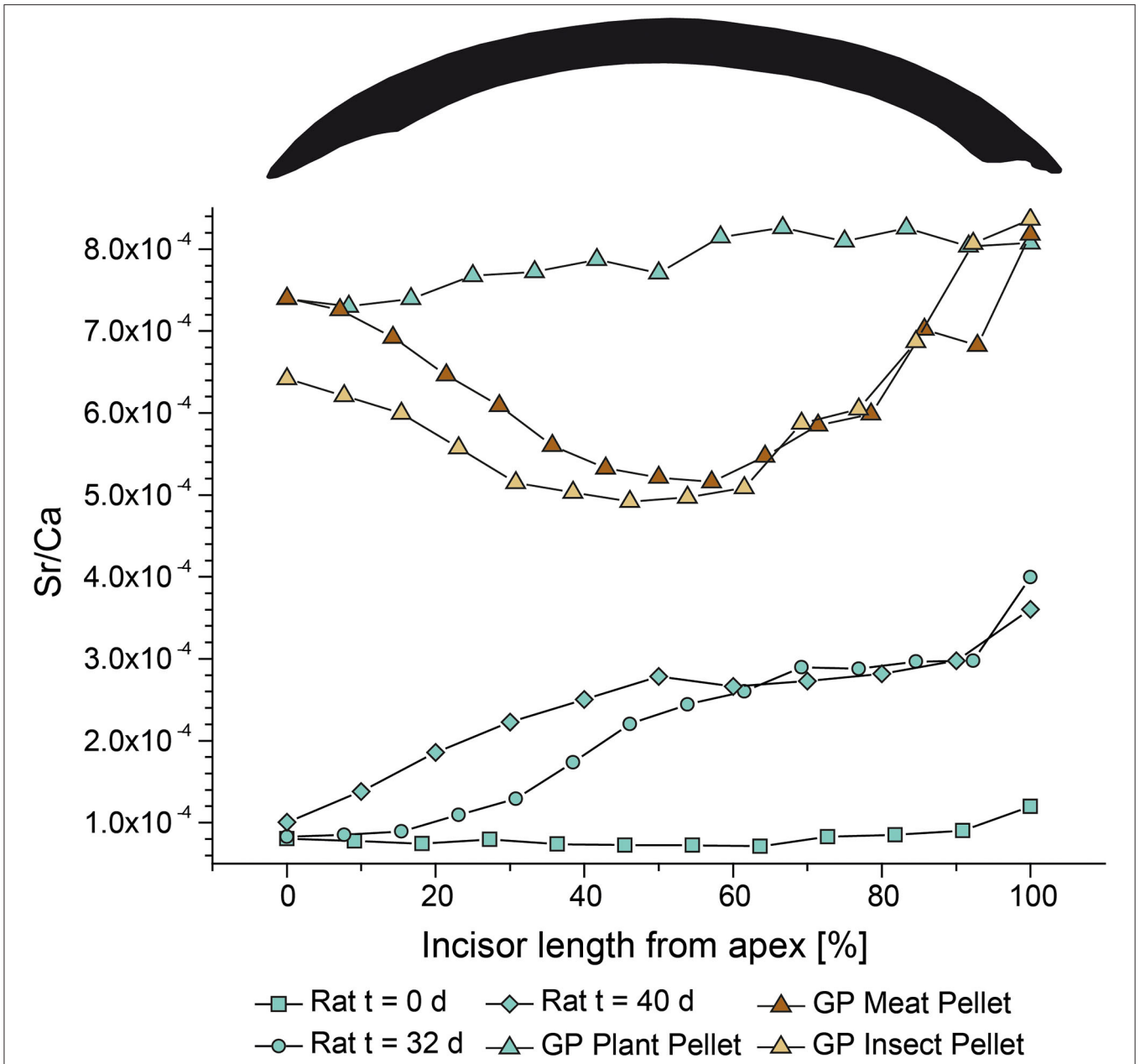

FIGURE 7 | Enamel incisor Sr/Ca of rats (each $n = 1$) from different points in time during the Diet Switch experiment. Rats were fed with the plant pellet for 0 days (cyan squares), 32 days (cyan circles), or 40 days (cyan diamonds). The Sr concentrations of the supplier and experimental plant diet are given in **Table 2**. Enamel incisors Sr/Ca for guinea pigs (each $n = 1$) from the Basic Diets experiment which were fed for the full experimental duration (54 + 5 days) with the three different pelleted diets based on insect (beige triangles), plant (cyan triangles), and meat meal (brown triangles), respectively.

detected in every feeding group, but were most prominent in the rats fed the insect diet. However, most of these spikes toward higher $^{87}Sr/^{86}Sr$ occurred in the apex, likely representing enamel that mostly mineralised before the start of the experiment. Therefore, these radiogenic inputs occurred during the supplier period, beyond the scope of the feeding experiment. As the supplier diet (the supplier water was demineralized and thus nearly Sr-free) did not yield high $^{87}Sr/^{86}Sr$, the source of these high values can only be explained by the bioavailable leachate values of the rat supplier pellet, reaching a $^{87}Sr/^{86}Sr$ as high as ~0.7113 at pH 3.

The guinea pigs fed for the whole experimental duration show distinct Sr/Ca patterns among the feeding groups (**Figure 7**). While the Sr/Ca was similar in the apex region for all three individuals (still reflecting a remnant supplier food-related value), toward the middle part, the Sr/Ca clearly diverged.

While the animals fed with plant pellets showed an increasing value similar to that seen in rats, guinea pigs fed the insect and meat diets had decreasing Sr/Ca ratios. This agrees with literature data showing that in general, Sr/Ca decreases with increasing trophic level due to Ca-biopurification processes (e.g., Elias et al., 1982; Burton and Wright, 1995; Burton et al., 1999; Blum et al., 2000; Balter et al., 2002). However, toward the base, the Sr/Ca of all three individuals increased and converged again, producing an *U*-shaped pattern for the two animals fed with animal-based (insect and meat) diets, while the plant diet individual is characterized by a similar Sr/Ca throughout the feeding period (**Figure 7**). This pattern could be an artifact of (i) the lower mineralisation state and lower Ca content of the base (Leblond and Warshawsky, 1979; Hillson, 2005), or (ii) an increased portion of dentin sampled during laser ablation, which typically has a higher Sr concentration in comparison to enamel (Kohn et al., 2013). However, the data seem to show that during secretion, there is more selectivity for Sr than during the maturation phase. The differences in the Sr/Ca ratio at the base of the incisor between rats and guinea pigs could also indicate that the area of progressively maturing enamel is spread across a larger portion of the incisor base in the latter compared to the former.

Our data suggests that a complete turnover of the Sr incorporated in the incisor enamel takes about 2 months for rats and a similar or longer time for guinea pigs. This difference might be related to the different incisor growth rates, as well as the difference in size of the animals. While the rats (11 – 12 weeks old) started at 197 ± 12 g ($n = 24$) and did not exceed a body weight of 300 g (**Supplementary Figure 5**), the guinea pigs (3 – 5 weeks) started at 398 ± 17 g ($n = 18$) and reached a final body weight of up to >700 g (**Supplementary Figure 7**). In the guinea pigs, therefore, one could speculate that incisors were not only growing for replacement of tissue lost by gnawing, but were also growing allometrically as a function of overall body size increase.

In contrast to the larger $^{87}Sr/^{86}Sr$ variability visible in the fast and continuously growing enamel, we observed a linear trend of $^{87}Sr/^{86}Sr$ in bone for the Basic Diets experiment ($R > 0.9$). Bone values at the start of the experiment reflect those of the supplier diet while those toward the end of the experiment reflect to the experimental diet. All animals from the three feeding groups on the three different diets started with a bone $^{87}Sr/^{86}Sr$ of ∼0.7092 and gradually moved toward lower $^{87}Sr/^{86}Sr$ values. After the full 54 days, bones reached a final $^{87}Sr/^{86}Sr$ between 0.7088 and 0.7090. This was slightly higher than the $^{87}Sr/^{86}Sr$ of the bioavailable Sr leached from the pellets during the leaching experiments. However, the enamel $^{87}Sr/^{86}Sr$ was slightly shifted toward higher values, possibly due to the additional influence of drinking water on an animal's Sr-uptake. In contrast to the incisor enamel, bone is a tissue with a much lower tissue turnover rate (Bryant and Loutit, 1964; Dahl et al., 2001). Therefore, the Sr isotope composition of bone averages the $^{87}Sr/^{86}Sr$ of the body water pool over a much longer time period than the ever-growing incisors.

Bioavailability of Sr From the Pelleted Diet (Experiment-2: Basic Diets)

It is generally accepted that the $^{87}Sr/^{86}Sr$ recorded in teeth and bones represents the locally bioavailable Sr isotopic signature at the basis of a local food chain (e.g., Blum et al., 2000; Slovak and Paytan, 2012; Flockhart et al., 2015; Lewis et al., 2017). The hard tissues, bones and incisor enamel, from animals of all three different feeding groups that fed the same basic diets for the full experimental duration did not reflect the $^{87}Sr/^{86}Sr$ of their respective, completely dissolved pellets. For bone it is expected that, due to its slow turnover rate, equilibrium with the experimental diet is not reached after a relatively short experimental duration (i.e., 54 days, **Figure 1**). A full turnover would take longer, and it is reasonable to assume that most of the Sr stored in the bones still derives from food consumed during the period the animals spent at the supplier facility. However, the ever-growing enamel of the incisors was expected to record the bioavailable Sr input from the diet and drinking water entirely toward the end of the experimental duration, especially the most recently grown and mineralised parts (i.e., the base and the middle area). Nevertheless, we observed distinct differences between the $^{87}Sr/^{86}Sr$ of the diets and the enamel. In addition, the $^{87}Sr/^{86}Sr$ obtained by LA-MC-ICP-MS were higher than those obtained by solution-based MC-ICP-MS by up to 0.0005 (**Figures 4**, **5**). This is a common observation for Sr isotope analyses by LA-MC-ICP-MS and is usually explained by unresolved interferences (Rb, Kr, REEs, Ca argides and dimers, CaPO for apatites) which influence the *in-situ* measurements (Copeland et al., 2008, 2010; Horstwood et al., 2008; Simonetti et al., 2008; Lewis et al., 2014). The effect was more pronounced for the rat samples, since these incisors had a much lower Sr/Ca (∼3×10^{-4}, **Figure 7**) than the guinea pig incisors (up to 8×10^{-4}, **Figure 7**) and are thus, due to their lower Sr content, more prone to such interferences. However, we tried to minimize this effect by adding nitrogen to the sample gas flow, as N_2 is known to reduce potential interferences (Zhang et al., 2018), using a desolvator system, and monitored the accuracy of the $^{87}Sr/^{86}Sr$ using several matrix-matched tooth samples with known $^{87}Sr/^{86}Sr$ (Willmes et al., 2016). By plotting the accuracy of $^{87}Sr/^{86}Sr$ vs. $1/^{88}Sr$ [V] (**Supplementary Figure 2**), one would expect a strong linear correlation if polyatomic interferences on $m/z = 87$ ($^{40}Ca^{31}P^{16}O$) will affect the $^{87}Sr/^{86}Sr$ (Horstwood et al., 2008; Lugli et al., 2017b). However, we did not observe such a correlation, which most likely excludes this explanation. Due to the low Sr concentration of the rodent incisors, it was necessary to employ a large spot size and repetition rate to increase the test portion mass (see method section) to achieve a sufficient signal intensity during LA-MC-ICP-MS acquisition for reliable Sr isotope analysis (usually >1 V for ^{88}Sr, e.g., Müller and Anczkiewicz, 2016; Weber et al., 2018a). This may have resulted in ablation of both enamel and the underlying dentin during laser ablation (see **Supplementary Figure 1**). There is a time lag between enamel and dentin formation in mammals (Hillson, 2005) which could, if dietary input changes temporally, potentially lead to differences in the $^{87}Sr/^{86}Sr$ of both dental tissues. As dentin forms prior to enamel, it will therefore have

incorporated higher $^{87}Sr/^{86}Sr$ (in our case Sr input from the supplier feeding period), as demonstrated by the analyses of individuals from the Diet Switch experiment. Most recently formed enamel shows lower $^{87}Sr/^{86}Sr$, since the source of its Sr is already shifted further toward the experimental diets. This could explain the differences between the *in-situ* and solution-based $^{87}Sr/^{86}Sr$ analyses, since for the latter the enamel was carefully separated from the dentin prior to the digestion and purification of Sr for solution-based $^{87}Sr/^{86}Sr$ analyses. Interestingly, the average guinea pig $^{87}Sr/^{86}Sr$ are generally higher by 0.0002 when compared to the rats, although both rodent groups received the same diets and water, potentially due to an increased absorption of water-derived Sr for the guinea pigs. In addition, the rodent incisor enamel $^{87}Sr/^{86}Sr$ does not record either the bulk ingested pellet nor the leachates of the pellets $^{87}Sr/^{86}Sr$ values (although they do plot closer to the leachates values, **Figures 4**, **5**). Every diet item, whether a designed pellet or a plant or animal food in the natural habitat, contains more or less bioavailable mineral components. The main difference between our experiment and a natural habitat is not that the individual sub-components of diet items vary in Sr availability, but rather that in natural habitats, all these different Sr-compounds have similar Sr isotope ratios. This occurs because most sub-components originate from the same habitat, and thus share the same baseline Sr values [though isotopic differences in bioavailable Sr have been observed even under such conditions (Maurer et al., 2012)]. In contrast, in our designed diets, items with variable Sr availability also differ in their individual Sr isotope ratios, because they derive from different ingredients produced in different regions and setting. In other words, whereas in the natural habitat, differences in Sr availability will not affect Sr isotope values, because the different Sr compounds all have similar Sr isotope composition, differences in Sr availability will distinctively affect the Sr isotopic signal in a pelleted diet in which the individual ingredients originate from different regions with different Sr isotope compositions. This becomes obvious by comparing the $^{87}Sr/^{86}Sr$ from the leachate of the pellets with the completely dissolved pellets (**Figures 3**–**5** and **Table 2**). The composition of the pellets causes differences in the bioavailability of Sr from the different ingredients of the pellets. Some components are more easily dissolved, while others can only be accessed using stronger acids and/or higher digestion temperatures. Of note, the insect diet showed the same $^{87}Sr/^{86}Sr$, regardless of which dissolution process was used, indicating better bioavailability of Sr in this type of pellet [i.e., in its main bioavailable component(s)], in comparison to the plant diet. These yielded much lower $^{87}Sr/^{86}Sr$ when digested in weaker acids and at lower temperatures, indicating a weak dissolution of the main plant matter and the preferential intake of Sr from a more easily accessible source within the pellet.

For the calculation of the mixing between water and diet (**Figure 8**, **Supplementary Figures 3**, **4**), we used the known daily food consumption of the rats and guinea pigs, obtained from metabolic cages. Rats consumed 15 – 20 g of pellets per day on average, while guinea pigs consumed 20 – 50 g per day. Water consumption was not monitored during the experiments but was assumed to be 10 mL/day per 100 g body weight (Sharp and Villano, 2012; Suckow et al., 2012). Generally, not all Sr ingested from food and water is absorbed during digestion. Values for Sr (International Commission on Radiological Protection, 1994; Kohn et al., 2013) and Ca absorption (Guéguen and Pointillart, 2000; Rozenberg et al., 2016), which is better documented in comparison to Sr (as a non-essential trace element), but has generally similar chemical behavior, range between 15 and 45%, typically 30%. We therefore used an absorption of 30% for both food water for the experimental data, independent of the animal model, even though there is reason to assume that guinea pig absorb a higher proportion of dietary Sr than rats, due to the similarity between Sr and Ca in biological systems, and the generally higher Ca digestibility in rabbits or guinea pigs as compared to rats (Cheeke and Amberg, 1973; Hagen et al., 2015). Note that we used the Sr concentration and $^{87}Sr/^{86}Sr$ ratios as measured in the leachates at pH 1 and 3 for the calculations. Since guinea pigs were roughly twice as heavy as the rats, their water consumption is estimated to be in the range of 50 – 100 mL/day, while we used a range of 10 – 40 mL/day for the rats. The mixing lines using the Sr isotope ratios and concentrations obtained from the completely dissolved pellet did not match the observed $^{87}Sr/^{86}Sr$ in the incisors, except for the insect pellet and the laser ablation data from the base of the rat incisors (**Supplementary Figure 3**). However, the leachates of the different pellets agreed much better with the incisor data, but still do not always match the observed $^{87}Sr/^{86}Sr$ incisor values (**Figure 8**). Nevertheless, especially for the plant pellet, we can see a much better agreement with the data from the leaching experiment, indicating a lower availability of Sr from the plant material (lucerne). The contribution of water in this feeding group appears to considerably contribute to the Sr budget, as mixing calculations agree well with the tissue values (**Figure 8**).

For future studies using Sr isotopes as provenance proxy, the careful assessment of $^{87}Sr/^{86}Sr$ from both the skeletal and dental remains, as well as the underlying geology and vegetation is necessary. We show that bulk food $^{87}Sr/^{86}Sr$ can largely differ from the bioavailable fraction and thus, may not necessarily reflect the $^{87}Sr/^{86}Sr$ recorded in the animal hard tissues. This effect should be considered when comparing hard tissue $^{87}Sr/^{86}Sr$ with local geology and potential Sr isotope isoscapes.

Strontium Isotope Variability Within the Feeding Groups (Experiment-2: Basic Diets)

The time-resolved analyses of the Sr isotope ratios from different time points in the experiment indicated that the full experimental duration of 54 days (and 5 days of acclimatization) was sufficient to reach diet-related $^{87}Sr/^{86}Sr$ for large parts of the ever-growing rodent incisors (entirely for rats, but not in the apex region for guinea pigs), but not for bone. However, most of the feeding groups display inter-individual $^{87}Sr/^{86}Sr$ differences among animals fed the same diet, even if only the base part of the incisor is considered (**Figures 4**, **5**). For the rat Basic Diets experiment, differences in $^{87}Sr/^{86}Sr$ intra-feeding group variability can be observed, even within different parts of the incisor enamel. Typical inter-individual variability ranged from

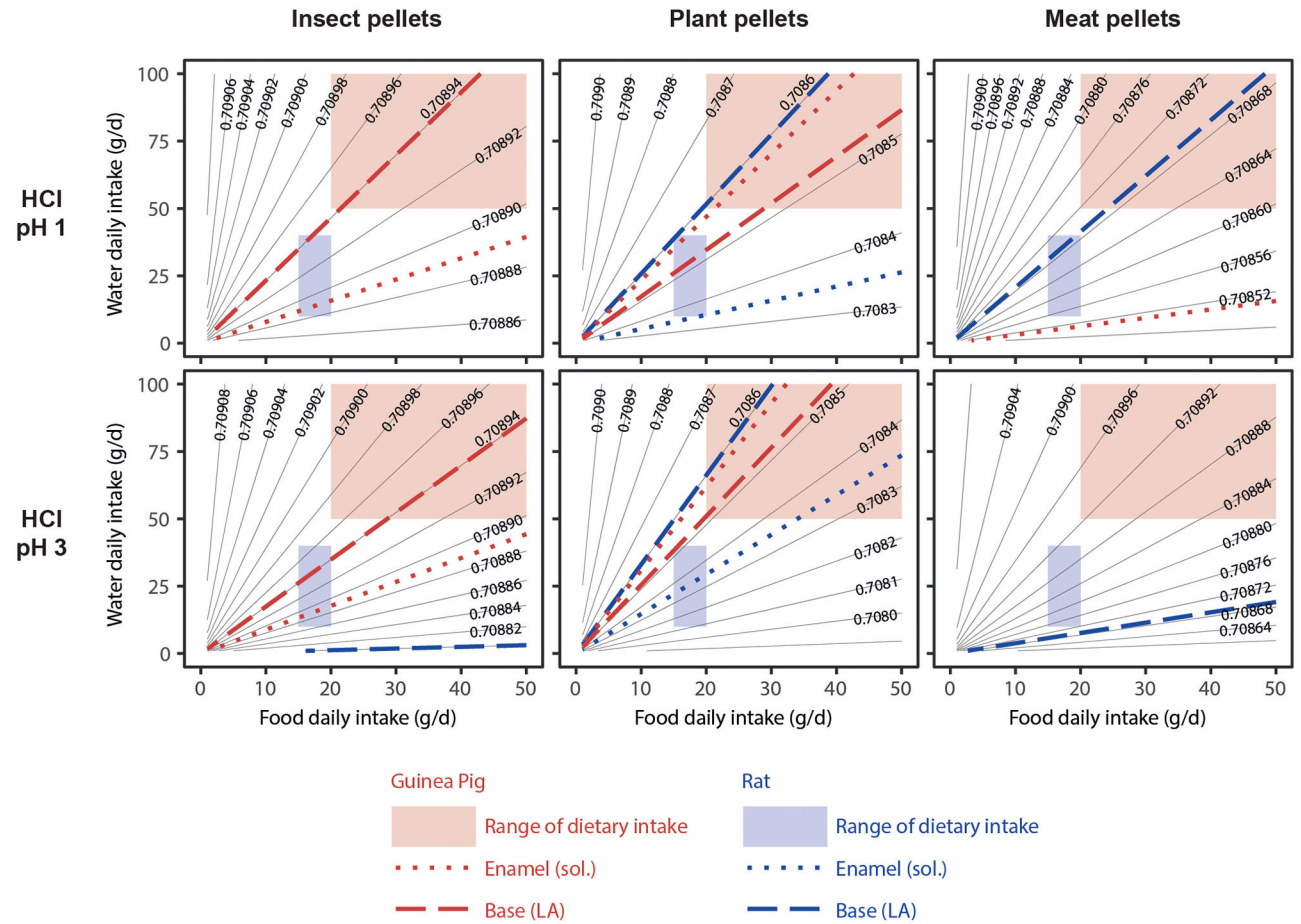

FIGURE 8 | Mixing calculations for the three insect, plant, and meat pelleted diets and the experimental tap water for $^{87}Sr/^{86}Sr$. We used bioavailable $^{87}Sr/^{86}Sr$ for the different pellet feeding groups, depending on the leachate values of the pellets leached at pH 1 and 3. For both food and water, a bioavailable component of 30% of the Sr was assumed as intake (International Commission on Radiological Protection, 1994; Guéguen and Pointillart, 2000; Rozenberg et al., 2016). Strontium isotope ratios and concentrations used for the mixing calculations are shown in **Table 2**. Rat (blue) and guinea pig (red) $^{87}Sr/^{86}Sr$ ratios for the enamel from laser ablation and solution MC-ICP-MS analyses are shown as dashed and stippled lines, respectively.

0.0001 to 0.0005, and this variability tended to decrease toward the younger base of the incisor (**Figure 9**). This trend is due to the fact that the animals received the experimental diet for longer and thus incorporated diet-related $^{87}Sr/^{86}Sr$ for longer, whereas in the (ontogenetically oldest) apex area, high $^{87}Sr/^{86}Sr$ spikes inherited from the supplier feeding period produce more scatter in enamel $^{87}Sr/^{86}Sr$. The main reason for this pattern is the continuous exchange between immature enamel and the bioavailable Sr pools in the body, i.e. the diet and the resorbed bone fraction (Johnson et al., 1968; Jowsey et al., 1971; Neiman and Eisenmann, 1975; Boyde and Reith, 1981; Montgomery et al., 2010). Bone (i.e., the skeleton) usually contains up to 99% of all body Sr (Schroeder et al., 1972; Sugihira and Suzuki, 1991). Thus, an important contribution of Sr in the blood originates from "old" Sr pool (incorporated into the bone at the supplier facility where animals were raised and then released from the bone during remodeling) that is incorporated in incisor enamel during the maturation process (Leblond and Warshawsky, 1979), which thus has a higher $^{87}Sr/^{86}Sr$ than the $^{87}Sr/^{86}Sr$ ingested during experimental conditions. While the bone $^{87}Sr/^{86}Sr$ slowly shifts toward the incisor value, the influence of the Sr fraction resorbed from the bones on the $^{87}Sr/^{86}Sr$ of new forming (hard)tissue is reduced. The same trend was also visible in the guinea pigs. The apex of the guinea pig incisors likely does not completely reflect the experimental diet, enhancing the inter-, as well as the intra-individual (i.e., intra-incisor) variability. For the guinea pigs fed the plant diet, the inter-individual $^{87}Sr/^{86}Sr$ variability was as high as 0.001 for the apex part and therefore an order of magnitude higher than within most other guinea pig groups, but also two to 10 times higher than for the rats (**Figure 9**). This variability is rather high for a population of small animals of the same species, sex, age, and feeding on the same diet and water sources. Typically, a $^{87}Sr/^{86}Sr$ cut-off value of 0.001 between bone and enamel of an individual is used in archaeological studies to differentiate between local and non-local individuals within one human population (e.g., Grupe et al., 1997; Price et al., 2004;

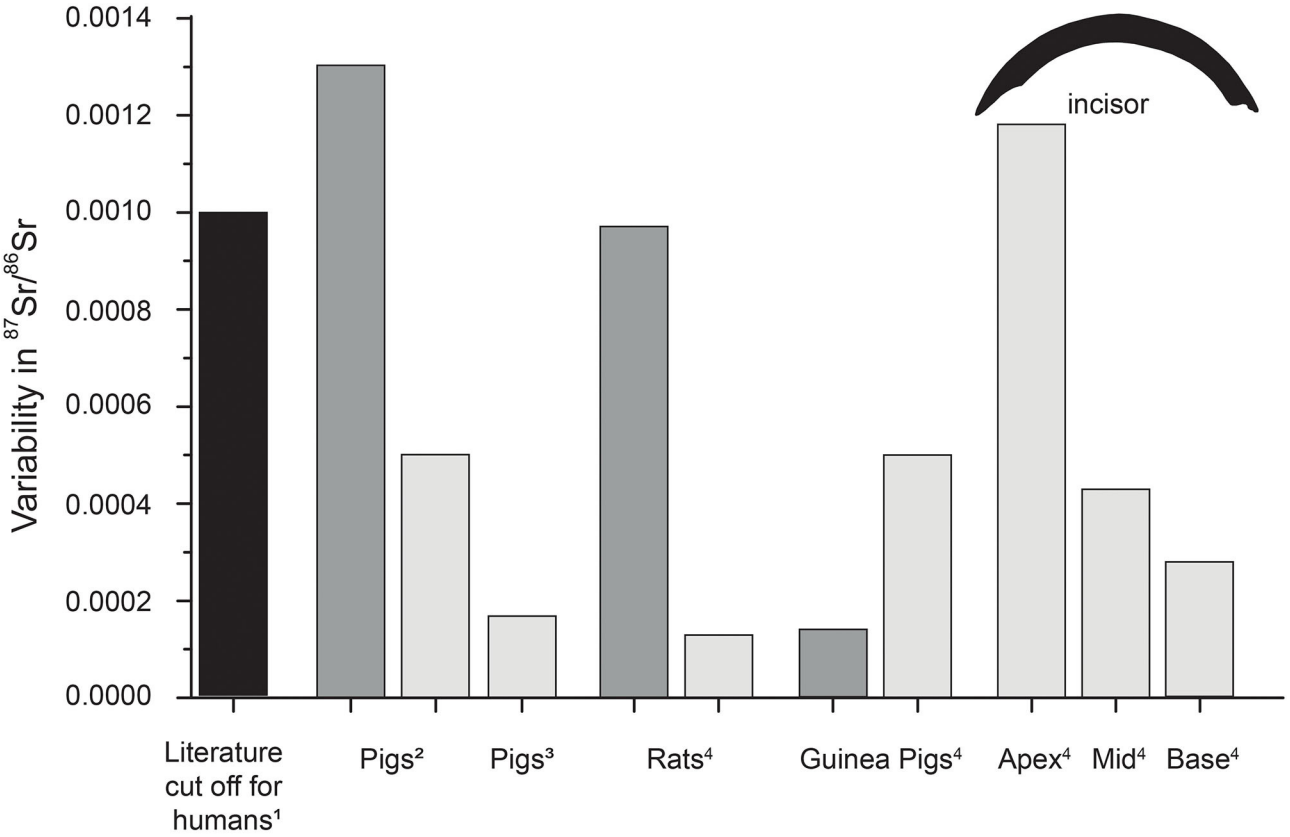

FIGURE 9 | Typical literature $^{87}Sr/^{86}Sr$ cut-off value for humans (1, e.g., Grupe et al., 1997; Price et al., 2004; Burton and Price, 2013; Knudson et al., 2016), as well as intra-population variability of $^{87}Sr/^{86}Sr$ in bones (dark gray) and teeth (light gray) of pigs (Lewis et al., 2017; Anders et al., 2019) and rats and guinea pigs (4, this study). Incisor variability reflects the largest variability observed in the respective part for both animal groups. For humans often a difference of 0.001 in $^{87}Sr/^{86}Sr$ between bones and tooth enamel is used to distinguish between local and non-local individuals.

Knudson et al., 2016). Other controlled feeding experiments, however, detected even higher inter-individual Sr isotope ranges of up to 0.002 for pigs raised on local derived diets (Anders et al., 2019). We observe a much lower variability in our study, and the high guinea pig variability is likely related to the influence of bone-resorption derived Sr. In addition, the sampling strategy using LA-MC-ICP-MS is more prone to a higher $^{87}Sr/^{86}Sr$ variability in comparison to solution-based analyses, due to the potential influence of interferences during data acquisition.

Besides the inter-individual variability, another important aspect for future Sr isotope studies is the observed intra-individual variability. Depending on the type of tooth or bone, differences in $^{87}Sr/^{86}Sr$ might be detected, due to differences in bone turnover rates reflecting different time averaging of isotopically distinct intake sources (Gregoricka, 2014; Knudson et al., 2016; Anders et al., 2019). Here only one type of bone (distal tibia) was investigated, and we did not compare the incisor enamel $^{87}Sr/^{86}Sr$ with those of the molar enamel of rats and/or guinea pigs. However, since molars of rats are not ever-growing, their $^{87}Sr/^{86}Sr$ will likely reflect the Sr ingested during their time at the supplier facility and therefore differ from our pelleted experiment diet. This is evident in the rat incisor $^{87}Sr/^{86}Sr$ of individuals that were euthanized prior to entering the feeding experiment (**Figure 2**). It highlights the importance of the adequate choice of teeth for Sr isotope analysis and the knowledge of tooth formation and maturation times to constrain accurately diet-related $^{87}Sr/^{86}Sr$ and hence modern or past mobility patterns. Interestingly, the intra-incisor variability rarely exceeds 0.0001, indicating a much lower intra-individual variability than suggested by Anders et al. (2019), who found a $^{87}Sr/^{86}Sr$ variability of 0.0005 for tooth and 0.0013 for bone samples (**Figure 9**).

The overall observed Sr isotope variability of both rodent species is small and does not exceed the cut off values typically employed in $^{87}Sr/^{86}Sr$ in provenance studies. Some incisor Sr isotope values from the apex (oldest part), especially for the guinea pigs, showed a higher Sr isotope variability than the other, ontogenetically younger parts of the incisor (**Figure 9**). This is an artifact of the feeding experiment, where the oldest part of the guinea pig incisors is still influenced by the supplier diet and thus, does not reflect a natural feeding behavior where an individual feeds only from local and similar food sources. Since the rat incisors grow faster than the guinea pig incisors (0.5 mm/day vs. 0.1 – 0.3 mm/day), even their oldest part (apex) mainly reflects

the experimental diet and is suited for Sr isotope variability estimation of animals feeding constantly on the same diet.

Influence of Water (Experiment-2: Basic Diets) and External Dust Sources on Tissue Sr Isotope Composition (Experiment-3: Dust Addition)

The rats that received the plant diet and Sr-enriched mineral water showed significantly lower $^{87}Sr/^{86}Sr$ (0.0001) than the group receiving the same pelleted diet but the less Sr-rich Zurich tap water for bone ($p < 0.01$), as well as for all parts of the incisors ($p < 0.02$). This shows that the high Sr concentration of the Ca- and Sr-enriched mineral water from a limestone aquifer had a significant influence on the incisor $^{87}Sr/^{86}Sr$. While the Sr concentration in natural freshwater water sources is often below 1 mg/L (Voerkelius et al., 2010), this Sr-enriched water had a Sr concentration of 8.6 mg/L and thus significantly influenced the $^{87}Sr/^{86}Sr$ of the hard tissues.

Although silicate minerals are usually not digested (Van Soest and Jones, 1968) and hence elements derived from them are not bioavailable, the small particle size and intra-layer bound cations (of the clay mineral kaolinite) bear the potential for some Sr uptake from the kaolin and the silt-sized carbonate fraction of loess, which makes up 20% of the 4 wt%. However, due to the relatively short experimental duration of up to 29 days, only the base of the incisor yielded the diet-related (i.e., potentially mineral dust-influenced) values (**Figure 1**). A significant difference, exceeding the analytical uncertainty between the animals feeding on the kaolin and the loess pellets was observed in the base part (**Figure 6**, $p < 0.01$) with the former having slightly higher values than the latter and also clearly different from the bulk diet values. While the bulk pellets yielded $^{87}Sr/^{86}Sr > 0.710$, all $^{87}Sr/^{86}Sr$ obtained from the enamel of the base area were <0.7093. Again, the Sr bioavailability of the different ingredients of the diets differ from the completely dissolved pellet. This is especially crucial for the silicate minerals, which are non-digestible. As described for the other pelleted diets, the leachates better reflect the bioavailable Sr fraction, especially those at pH 1. Furthermore, the pellet into which the mineral dust was admixed consisted of lucerne, from which Sr was shown to be less bioavailable. Nevertheless, enamel $^{87}Sr/^{86}Sr$ differences among incisors of the three feeding groups (mineral-dust-free, loess-containing, and kaolin-containing pellets) are visible.

CONCLUSION

Our controlled feeding experiment offered a unique possibility to evaluate the timing of Sr incorporation in tooth enamel, as well as the influence of diet-derived Sr (including water and mineral dust) on the $^{87}Sr/^{86}Sr$ of hard tissues (i.e., bone, enamel) of rodents. Intra-population variability in $^{87}Sr/^{86}Sr$ was lower (<0.001) than previously reported for other mammals, potentially due to the high degree of experimental control. Therefore, our data provide a minimum estimate of the $^{87}Sr/^{86}Sr$ variability within a (small mammal) population, and highlight the importance of proper sampling strategies in building local isotopic baselines using rodents. We also determined that the inter-individual variability is generally low and thus likely does not affect provenance studies based on radiogenic Sr isotopes. Mixing model calculations further support the importance of differential bioavailability of Sr in the diet (including both food and water). In addition, we observed differences in isotopic and elemental variability between bone and incisor enamel. While the bone showed slow and incomplete turnover over the course of the experiment, the incisors exhibited much higher variability. We demonstrated that a complete turnover of the rat incisors occurred after 54 days, while the guinea pig incisors still retained remnant isotopic signals from supplier food in the oldest part of their incisors. This indicates that we can estimate a minimum period of roughly 2 months, before the new, diet-related $^{87}Sr/^{86}Sr$ is recorded in enamel throughout the full length of the incisor. This information must be taken into consideration in human provenance studies which frequently use rodents' teeth to characterize locally bioavailable Sr isotope ranges. In addition, the leachates of the pelleted diets clearly demonstrate the effect of differences in Sr bioavailability on $^{87}Sr/^{86}Sr$, and should also be considered in Sr isoscapes studies. Furthermore, we observed an offset in $^{87}Sr/^{86}Sr$ between rats and guinea pigs feeding on the exact same diet, indicating taxon-specific absorption coefficients for Sr, especially from the drinking water.

DATA AVAILABILITY STATEMENT

The original contributions presented in the study are included in the article/**Supplementary Materials**, further inquiries can be directed to the corresponding author/s.

ETHICS STATEMENT

The animal study was reviewed and approved by Cantonal Veterinary Office Zurich, Switzerland (license no. ZH135/16).

AUTHOR CONTRIBUTIONS

MW, TTü, and MC designed the study. DW and MC performed the animal experiments. MW performed the solution-based MC-ICP-MS analyses, evaluated the data, performed the analyses, and wrote the manuscript. MW and RMK developed the LA-MC-ICP-MS methods. KW performed the LA-ICP-MS measurements and evaluated the *in-situ* Sr concentration data. TTü performed the ICP-OES measurements. MW, KW, JL, and DW prepared the samples prior to analysis. TTa did the mixing calculations. TTü, MC, TTa, FL, and KW improved the manuscript. MW, TTü, TTa, FL, and MC designed the leaching experiment. JL proof-read the English language. All authors discussed the results and commented on the manuscript.

FUNDING

This project received funding from the European Research Council (ERC) under the European Union's Horizon 2020

research and innovation programme, grant agreement No. 681450.

ACKNOWLEDGMENTS

We thank D. Codron for assistance during the setup of the study, M. Großkopf and J. Klose for their assistance in the laboratory and L. Martin, N. Schmid, K. Zbinden, D. Codron, and S. Heldstab for taking care of the animals during the experiments. The help of the student assistants in Mainz is greatly acknowledged. We also thank D. Scholz for the access to the laboratories at the Institute of Geosciences, University of Mainz. The comments and suggestions of three independent reviewers and the Editor Brooke E. Crowley helped to improve the study and are greatly acknowledged.

SUPPLEMENTARY MATERIAL

The Supplementary Material for this article can be found online at: https://www.frontiersin.org/articles/10.3389/fevo.2020.569940/full#supplementary-material

REFERENCES

Anders, D., Osmanovic, A., and Vohberger, M. (2019). Intra-and inter-individual variability of stable strontium isotope ratios in hard and soft body tissues of pigs. *Rapid Commun. Mass Spectrometry* 33, 281–290. doi: 10.1002/rcm.8350

Balasse, M., Ambrose, S. H., Smith, A. B., and Price, T. D. (2002). The seasonal mobility model for prehistoric herders in the south-western cape of south africa assessed by isotopic analysis of sheep tooth enamel. *J. Archaeol. Sci.* 29, 917–932. doi: 10.1006/jasc.2001.0787

Balter, V., Bocherens, H., Person, A., Labourdette, N., Renard, M., and Vandermeersch, B. (2002). Ecological and physiological variability of Sr/Ca and Ba/Ca in mammals of West European mid-Würmian food webs. *Palaeogeogr. Palaeoclimatol. Palaeoecol.* 186, 127–143. doi: 10.1016/S0031-0182(02)00448-0

Banner, J. L. (2004). Radiogenic isotopes: systematics and applications to earth surface processes and chemical stratigraphy. *Earth Sci. Rev.* 65, 141–194. doi: 10.1016/S0012-8252(03)00086-2

Bataille, C. P., Crowley, B. E., Wooller, M. J., and Bowen, G. J. (2020). Advances in global bioavailable strontium isoscapes. *Palaeogeogr. Palaeoclimatol. Palaeoecol.* 555:109849. doi: 10.1016/j.palaeo.2020.109849

Bentley, R. A. (2006). Strontium isotopes from the earth to the archaeological skeleton: a review. *J. Archaeol. Method Theory* 13, 135–187. doi: 10.1007/s10816-006-9009-x

Blum, J. D., Taliaferro, E. H., Weisse, M. T., and Holmes, R. T. (2000). Changes in Sr/Ca, Ba/Ca and $^{87}Sr/^{86}Sr$ ratios between trophic levels in two forest ecosystems in the northeastern USA. *Biogeochemistry* 49, 87–101. doi: 10.1023/A:1006390707989

Boyde, A., and Reith, E. J. (1981). Display of maturation cycles in rat incisor enamel with tetracycline labelling. *Histochemistry* 72, 551–561. doi: 10.1007/BF00493275

Bryant, F. J., and Loutit, J. F. (1964). The entry of strontium-90 into human bone. *Proc. R. Soc. Lond. Series B Biol. Sci.* 159, 449–465. doi: 10.1098/rspb.1964.0013

Burton, J. H., and Price, T. D. (2013). "Seeking the local $^{87}Sr/^{86}Sr$ ratio to determine geographic origins of humans," in *Archaeological chemistry VIII*, eds R. A. Armitage and J. H. Burton (Washington, DC: American Chemical Society), 309–320.

Burton, J. H., Price, T. D., and Middleton, W. D. (1999). Correlation of bone Ba/Ca and Sr/Ca due to biological purification of calcium. *J. Archaeol. Sci* 26, 609–616. doi: 10.1006/jasc.1998.0378

Burton, J. H., and Wright, L. E. (1995). Nonlinearity in the relationship between bone Sr/Ca and diet: paleodietary implications. *Am. J. Phys. Anthropol.* 96, 273–282. doi: 10.1002/ajpa.1330960305

Capo, R. C., Stewart, B. W., and Chadwick, O. A. (1998). Strontium isotopes as tracers of ecosystem processes: theory and methods. *Geoderma* 82, 197–225. doi: 10.1016/S0016-7061(97)00102-X

Carr, T. E. F., Harrison, G. E., Loutit, J. F., and Sutton, A. (1962). Movement of strontium in the human body. *Br. Med. J.* 2, 773–775. doi: 10.1136/bmj.2.5307.773

Cheeke, P. R., and Amberg, J. W. (1973). Comparative calcium excretion by rats and rabbits. *J. Anim. Sci* 37, 450–454. doi: 10.2527/jas1973.372450x

Comar, C. L., Russell, R. S., and Wasserman, R. H. (1957). Strontium-calcium movement from soil to man. *Science* 126, 485–492. doi: 10.1126/science.126.3272.485

Copeland, S. R., Sponheimer, M., De Ruiter, D. J., Lee-Thorp, J. A., Codron, D., Le Roux, P. J., et al. (2011). Strontium isotope evidence for landscape use by early hominins. *Nature* 474, 76–78. doi: 10.1038/nature10149

Copeland, S. R., Sponheimer, M., Le Roux, P. J., Grimes, V., Lee-Thorp, J. A., De Ruiter, D. J., et al. (2008). Strontium isotope ratios ($^{87}Sr/^{86}Sr$) of tooth enamel: a comparison of solution and laser ablation multicollector inductively coupled plasma mass spectrometry methods. *Rapid Commun. Mass Spectrom.* 22, 3187–3194. doi: 10.1002/rcm.3717

Copeland, S. R., Sponheimer, M., Lee-Thorp, J. A., Le Roux, P. J., De Ruiter, D. J., and Richards, M. P. (2010). Strontium isotope ratios in fossil teeth from South Africa: assessing laser ablation MC-ICP-MS analysis and the extent of diagenesis. *J. Archaeol. Sci.* 37, 1437–1446. doi: 10.1016/j.jas.2010.01.003

Dahl, S. G., Allain, P., Marie, P. J., Mauras, Y., Boivin, G., Ammann, P., et al. (2001). Incorporation and distribution of strontium in bone. *Bone* 28, 446–453. doi: 10.1016/S8756-3282(01)00419-7

Eisenhauer, A., Müller, M., Heuser, A., Kolevica, A., Glüer, C. C., Both, M., et al. (2019). Calcium isotope ratios in blood and urine: a new biomarker for the diagnosis of osteoporosis. *Bone Rep.* 10:100200. doi: 10.1016/j.bonr.2019.100200

Elias, R. W., Hirao, Y., and Patterson, C. C. (1982). The circumvention of the natural biopurification of calcium along nutrient pathways by atmospheric inputs of industrial lead. *Geochim. Cosmochim. Acta* 46, 2561–2580. doi: 10.1016/0016-7037(82)90378-7

Faure, G., and Mensing, T. M. (2005). *Isotopes: Principles and Applications*. (Hoboken: John Wiley & Sons Inc), 928.

Flockhart, D. T. T., Kyser, T. K., Chipley, D., Miller, N. G., and Norris, D. R. (2015). Experimental evidence shows no fractionation of strontium isotopes ($^{87}Sr/^{86}Sr$) among soil, plants, and herbivores: implications for tracking wildlife and forensic science. *Isotopes Environ. Health Stud.* 51, 372–381. doi: 10.1080/10256016.2015.1021345

Galler, P., Limbeck, A., Boulyga, S. F., Stingeder, G., Hirata, T., and Prohaska, T. (2007). Development of an on-line flow injection Sr/matrix separation method for accurate, high-throughput determination of Sr isotope ratios by multiple collector-inductively coupled plasma-mass spectrometry. *Anal. Chem.* 79, 5023–5029. doi: 10.1021/ac070307h

Gehler, A., Tütken, T., and Pack, A. (2012). Oxygen and carbon isotope variations in a modern rodent community–implications for palaeoenvironmental reconstructions. *PLoS ONE* 7:e49531. doi: 10.1371/journal.pone.0049531

Gregoricka, L. A. (2014). Assessing life history from commingled assemblages: the biogeochemistry of inter-tooth variability in Bronze Age Arabia. *J. Archaeol. Sci.* 47, 10–21. doi: 10.1016/j.jas.2014.04.004

Grupe, G., Price, T. D., Schröter, P., Söllner, F., Johnson, C. M., and Beard, B. L. (1997). Mobility of Bell Beaker people revealed by strontium isotope ratios of tooth and bone: a study of southern Bavarian skeletal remains. *Appl. Geochem.* 12, 517–525. doi: 10.1016/S0883-2927(97)00030-9

Guéguen, L., and Pointillart, A. (2000). The bioavailability of dietary calcium. *J. Am. College Nutr.* 19, 119S−136S. doi: 10.1080/07315724.2000.10718083

Hagen, K. B., Tschudin, A., Liesegang, A., Hatt, J. M., and Clauss, M. (2015). Organic matter and macromineral digestibility in domestic rabbits (*Oryctolagus cuniculus*) as compared to other hindgut fermenters. *J. Anim. Physiol. Anim. Nutr.* 99, 1197–1209. doi: 10.1111/jpn.12323

Hillson, S. (2005). *Teeth.* (Cambride, UK: Cambridge University Press), 388.

Horstwood, M. S. A., Evans, J. A., and Montgomery, J. (2008). Determination of Sr isotopes in calcium phosphates using laser ablation inductively coupled plasma mass spectrometry and their application to archaeological tooth enamel. *Geochim. Cosmochim. Acta* 72, 5659–5674. doi: 10.1016/j.gca.2008.08.016

Inoue, M., Nohara, M., Okai, T., Suzuki, A., and Kawahata, H. (2004). Concentrations of trace elements in carbonate reference materials coral JCp-1 and giant clam JCt-1 by inductively coupled plasma-mass spectrometry. *Geostand. Geoanalytical. Res.* 28, 411–416. doi: 10.1111/j.1751-908X.2004.tb00759.x

International Commission on Radiological Protection, C. (1994). *ICRP Publication 67: Age-dependent Doses to Members of the Public from Intake of Radionuclides: Part 2 Ingestion Dose Coefficients* (Oxford: Elsevier Health Sciences).

Jochum, K. P., Stoll, B., Herwig, K., and Willbold, M. (2007). Validation of LA-ICP-MS trace element analysis of geological glasses using a new solid-state 193 nm Nd : YAG laser and matrix-matched calibration. *J. Anal. At. Spectrom.* 22, 112–121. doi: 10.1039/B609547J

Johnson, A. R., Armstrong, W. D., and Singer, L. (1968). The incorporation and removal of large amounts of strontium by physiologic mechanisms in mineralized tissues of the rat. *Calcif. Tissue Res* 2, 242–252. doi: 10.1007/BF02279212

Jowsey, J., Gordon, G., and Bourne, G. H. (1971). Bone turnover and osteoporosis. *Biochem. Physiol. Bone* 3, 201–238. doi: 10.1016/B978-0-12-119203-7.50013-1

Kelly, S., Heaton, K., and Hoogewerff, J. (2005). Tracing the geographical origin of food: The application of multi-element and multi-isotope analysis. *Trends Food Sci. Technol.* 16, 555–567. doi: 10.1016/j.tifs.2005.08.008

Kimura, J. I., and Chang, Q. (2012). Origin of the suppressed matrix effect for improved analytical performance in determination of major and trace elements in anhydrous silicate samples using 200 nm femtosecond laser ablation sector-field inductively coupled plasma mass spectrometry. *J. Anal. At. Spectrom.* 27, 1549–1559. doi: 10.1039/c2ja10344c

Kirsanow, K., and Tuross, N. (2011). Oxygen and hydrogen isotopes in rodent tissues: Impact of diet, water and ontogeny. *Palaeogeogr. Palaeoclimatol. Palaeoecol.* 310, 9–16. doi: 10.1016/j.palaeo.2011.03.022

Knipper, C. (2004). Die Strontiumisotopenanalyse: eine naturwissenschaftliche Methode zur Erfassung von Mobilität in der Ur-und Frühgeschichte. *Jahrbuch des Römisch-Germanischen Zentralmuseums Mainz* 51, 589–686. doi: 10.11588/jrgzm.2004.2.21081

Knudson, K. J., Stanish, C., Cerna, M. C. L., Faull, K. F., and Tantaleán, H. (2016). Intra-individual variability and strontium isotope measurements: a methodological study using $^{87}Sr/^{86}Sr$ data from Pampa de los Gentiles, Chincha Valley, Peru. *J. Archaeol. Sci. Rep.* 5, 590–597. doi: 10.1016/j.jasrep.2016.01.016

Knudson, K. J., Williams, H. M., Buikstra, J. E., Tomczak, P. D., Gordon, G. W., and Anbar, A. D. (2010). Introducing $\delta^{88}/^{86}Sr$ analysis in archaeology: a demonstration of the utility of strontium isotope fractionation in paleodietary studies. *J. Archaeol. Sci.* 37, 2352–2364. doi: 10.1016/j.jas.2010.04.009

Kohn, M. J., Morris, J., and Olin, P. (2013). Trace element concentrations in teeth–a modern Idaho baseline with implications for archeometry, forensics, and palaeontology. *J. Archaeol. Sci.* 40, 1689–1699. doi: 10.1016/j.jas.2012.11.012

Law, K.-T., Lee, C.-K., King, N. M., and Rabie, A.-B. M. (2003). The relationship between eruption and length of mandibular incisors in young rats. *Med. Sci. Monitor* 9, BR47–BR53.

Leblond, C. P., and Warshawsky, H. (1979). Dynamics of enamel formation in the rat incisor tooth. *J. Dent. Res.* 58, 950–979. doi: 10.1177/00220345790580024901

Lewis, J., Coath, C. D., and Pike, A. W. G. (2014). An improved protocol for $^{87}Sr/^{86}Sr$ by laser ablation multi-collector inductively coupled plasma mass spectrometry using oxide reduction and a customised plasma interface. *Chem. Geol.* 390, 173–181. doi: 10.1016/j.chemgeo.2014.10.021

Lewis, J., Pike, A. W. G., Coath, C. D., and Evershed, R. P. (2017). Strontium concentration, radiogenic ($^{87}Sr/^{86}Sr$) and stable ($\delta^{88}Sr$) strontium isotope systematics in a controlled feeding study. *STAR: Sci. Technol. Archaeol. Res.* 3, 53–65. doi: 10.1080/20548923.2017.1303124

Lugli, F., Cipriani, A., Arnaud, J., Arzarello, M., Peretto, C., and Benazzi, S. (2017a). Suspected limited mobility of a Middle Pleistocene woman from Southern Italy: strontium isotopes of a human deciduous tooth. *Sci. Rep.* 7:8615. doi: 10.1038/s41598-017-09007-5

Lugli, F., Cipriani, A., Peretto, C., Mazzucchelli, M., and Brunelli, D. (2017b). In situ high spatial resolution $^{87}Sr/^{86}Sr$ ratio determination of two Middle Pleistocene (c.a. 580 ka) Stephanorhinus hundsheimensis teeth by LA–MC–ICP–MS. *Int. J. Mass Spectrometry* 412, 38–48. doi: 10.1016/j.ijms.2016.12.012

Marchionni, S., Buccianti, A., Bollati, A., Braschi, E., Cifelli, F., Molin, P., et al. (2016). Conservation of $^{87}Sr/^{86}Sr$ isotopic ratios during the winemaking processes of 'Red'wines to validate their use as geographic tracer. *Food Chem.* 190, 777–785. doi: 10.1016/j.foodchem.2015.06.026

Maurer, A.-F., Galer, S. J. G., Knipper, C., Beierlein, L., Nunn, E. V., Peters, D., et al. (2012). Bioavailable $^{87}Sr/^{86}Sr$ in different environmental samples—effects of anthropogenic contamination and implications for isoscapes in past migration studies. *Sci. Total Environ.* 433, 216–229. doi: 10.1016/j.scitotenv.2012.06.046

McArthur, J. M., Howarth, R. J., and Bailey, T. R. (2001). Strontium Isotope Stratigraphy: LOWESS version 3: best fit to the marine Sr-isotope curve for 0–509 Ma and accompanying look-up table for deriving numerical age. *J. Geol.* 109, 155–170. doi: 10.1086/319243

McArthur, J. M., Howarth, R. J., and Shields, G. A. (2012). Strontium isotope stratigraphy. *Geol. Time Scale* 1, 127–144. doi: 10.1016/B978-0-444-59425-9.00007-X

Mcconnell, E. L., Basit, A. W., and Murdan, S. (2008). Measurements of rat and mouse gastrointestinal pH, fluid and lymphoid tissue, and implications for *in-vivo* experiments. *J. Pharm. Pharmacol.* 60, 63–70. doi: 10.1211/jpp.60.1.0008

Meija, J., Coplen, T. B., Berglund, M., Brand, W. A., De Bièvre, P., Gröning, M., et al. (2016). Isotopic compositions of the elements 2013 (IUPAC technical Report). *Pure Appl. Chem.* 88, 293–306. doi: 10.1515/pac-2015-0503

Merchant, H. A., Mcconnell, E. L., Liu, F., Ramaswamy, C., Kulkarni, R. P., Basit, A. W., et al. (2011). Assessment of gastrointestinal pH, fluid and lymphoid tissue in the guinea pig, rabbit and pig, and implications for their use in drug development. *Eur. J. Pharm. Sci.* 42, 3–10. doi: 10.1016/j.ejps.2010.09.019

Mischel, S. A., Mertz-Kraus, R., Jochum Klaus, P., and Scholz, D. (2017). TERMITE: An R script for fast reduction of laser ablation inductively coupled plasma mass spectrometry data and its application to trace element measurements. *Rapid Commun. Mass Spectrom.* 31, 1079–1087. doi: 10.1002/rcm.7895

Montgomery, J., Evans, J. A., and Horstwood, M. S. A. (2010). Evidence for long-term averaging of strontium in bovine enamel using TIMS and LA-MC-ICP-MS strontium isotope intra-molar profiles. *Environ. Archaeol.* 15, 32–42. doi: 10.1179/146141010X12640787648694

Müller, J., Clauss, M., Codron, D., Schulz, E., Hummel, J., Kircher, P., et al. (2015). Tooth length and incisal wear and growth in guinea pigs (*Cavia porcellus*) fed diets of different abrasiveness. *J. Anim. Physiol. Anim. Nutr.* 99, 591–604. doi: 10.1111/jpn.12226

Müller, W., and Anczkiewicz, R. (2016). Accuracy of laser-ablation (LA)-MC-ICPMS Sr isotope analysis of (bio) apatite–a problem reassessed. *J. Anal. At. Spectrom.* 31, 259–269. doi: 10.1039/C5JA00311C

Müller, W., Fricke, H., Halliday, A. N., Mcculloch, M. T., and Wartho, J.-A. (2003). Origin and migration of the alpine iceman. *Science* 302, 862–866. doi: 10.1126/science.1089837

Neiman, A., and Eisenmann, D. R. (1975). The effect of strontium, cobalt and fluoride on rat incisor enamel formation. *Anat. Rec.* 183, 303–321. doi: 10.1002/ar.1091830207

Ohno, T., and Hirata, T. (2007). Simultaneous determination of mass-dependent isotopic fractionation and radiogenic isotope variation of strontium in geochemical samples by multiple collector-ICP-mass spectrometry. *Anal. Sci.* 23, 1275–1280. doi: 10.2116/analsci.23.1275

Okai, T., Suzuki, A., Kawahata, H., Terashima, S., and Imai, N. (2002). Preparation of a new geological survey of japan geochemical reference material: coral JCp-1. *Geostand. Geoanalytical. Res.* 26, 95–99. doi: 10.1111/j.1751-908X.2002.tb00627.x

Outridge, P., Chenery, S., Babaluk, J., and Reist, J. (2002). Analysis of geological Sr isotope markers in fish otoliths with subannual resolution using laser ablation-multicollector-ICP-mass spectrometry. *Environ. Geol.* 42, 891–899. doi: 10.1007/s00254-002-0596-x

Passey, B. H., and Cerling, T. E. (2002). Tooth enamel mineralization in ungulates: implications for recovering a primary isotopic time-series. *Geochim. Cosmochim. Acta* 66, 3225–3234. doi: 10.1016/S0016-7037(02)00933-X

Price, T. D., Knipper, C., Grupe, G., and Smrcka, V. (2004). Strontium isotopes and prehistoric human migration: the Bell Beaker period in central Europe. *Eur. J. Archaeol.* 7, 9–40. doi: 10.1177/1461957104047992

Romaniello, S. J., Field, M. P., Smith, H. B., Gordon, G. W., Kim, M. H., and Anbar, A. D. (2015). Fully automated chromatographic purification of Sr and Ca for isotopic analysis. *J. Anal. At. Spectrom.* 30, 1906–1912. doi: 10.1039/C5JA00205B

Rozenberg, S., Body, J.-J., Bruyere, O., Bergmann, P., Brandi, M. L., Cooper, C., et al. (2016). Effects of dairy products consumption on health: benefits and beliefs—a commentary from the belgian bone club and the european society for clinical and economic aspects of osteoporosis, osteoarthritis and musculoskeletal diseases. *Calcif. Tissue Int.* 98, 1–17. doi: 10.1007/s00223-015-0062-x

Scheeres, M., Knipper, C., Hauschild, M., Schönfelder, M., Siebel, W., Vitali, D., et al. (2013). Evidence for "Celtic migrations"? strontium isotope analysis at the early La Tène (LT B) cemeteries of Nebringen (Germany) and Monte Bibele (Italy). *J. Archaeol. Sci.* 40, 3614–3625. doi: 10.1016/j.jas.2013.05.003

Schroeder, H. A., Tipton, I. H., and Nason, A. P. (1972). Trace metals in man: strontium and barium. *J. Chronic Dis.* 25, 491–517. doi: 10.1016/0021-9681(72)90150-6

Schweissing, M. M., and Grupe, G. (2003). Stable strontium isotopes in human teeth and bone: a key to migration events of the late Roman period in Bavaria. *J. Archaeol. Sci.* 30, 1373–1383. doi: 10.1016/S0305-4403(03)00025-6

Sharp, P., and Villano, J. S. (2012). *The Laboratory Rat.* (Boca Raton: CRC press), 393. doi: 10.1201/b13862

Simonetti, A., Buzon, M. R., and Creaser, R. A. (2008). *In-situ* elemental and Sr isotope investigation of human tooth enamel by Laser Ablation-(MC-)ICP-MS: Successes and pitfalls. *Archaeometry* 50, 371–385. doi: 10.1111/j.1475-4754.2007.00351.x

Slovak, N. M., and Paytan, A. (2012). "Applications of Sr isotopes in archaeology," in *Handbook of Environmental Isotope Geochemistry*, ed M. Baskaran (Berlin: Springer), 743–768. doi: 10.1007/978-3-642-10637-8_35

Suckow, M. A., Stevens, K. A., and Wilson, R. P. (2012). *The Laboratory Rabbit, Guinea Pig, Hamster, and Other Rodents*. (San Diego: Academic Press), 1288.

Sugihira, N., and Suzuki, K. T. (1991). Discrimination between strontium and calcium in suckling rats. *Biol. Trace Elem. Res.* 29, 1–10. doi: 10.1007/BF03032669

R Core Team (2013). *R: A Language and Environment for Statistical Computing*. Vienna: R Foundation for Statistical Computing. Available online at: https://www.R-project.org/

Tütken, T. (2010). Die Isotopenanalyse fossiler Skelettreste – Bestimmung der Herkunft und Mobilität von Menschen und Tieren. Anthropologie, Isotopie und DNA -biografische Annäherung an namenlose vorgeschichtliche Skelette. *Tagungsband* 2, 33–51.

Urey, H. C. (1947). The thermodynamic properties of isotopic substances. *J. Chem. Soc.* 562–581. doi: 10.1039/jr9470000562

Van Soest, P. J., and Jones, L. H. P. (1968). Effect of silica in forages upon digestibility. *J. Dairy Sci.* 51, 1644–1648. doi: 10.3168/jds.S0022-0302(68)87246-7

Voerkelius, S., Lorenz, G. D., Rummel, S., Quétel, C. R., Heiss, G., Baxter, M., et al. (2010). Strontium isotopic signatures of natural mineral waters, the reference to a simple geological map and its potential for authentication of food. *Food Chem.* 118, 933–940. doi: 10.1016/j.foodchem.2009.04.125

Weber, M., Lugli, F., Hattendorf, B., Scholz, D., Mertz-Kraus, R., Guinoiseau, D., et al. (2020). NanoSr–a new carbonate microanalytical reference material for in situ strontium isotope analysis. *Geostand. Geoanalytical. Res.* 44, 69–83. doi: 10.1111/ggr.12296

Weber, M., Lugli, F., Jochum, K. P., Cipriani, A., and Scholz, D. (2018a). Calcium carbonate and phosphate reference materials for monitoring bulk and microanalytical determination of Sr isotopes. *Geostand. Geoanalytical. Res.* 42, 77–89. doi: 10.1111/ggr.12191

Weber, M., Scholz, D., Schröder-Ritzrau, A., Deininger, M., Spötl, C., Lugli, F., et al. (2018b). Evidence of warm and humid interstadials in central Europe during early MIS 3 revealed by a multi-proxy speleothem record. *Quat. Sci. Rev.* 200, 276–286. doi: 10.1016/j.quascirev.2018.09.045

Weber, M., Wassenburg, J. A., Jochum, K. P., Breitenbach, S. F. M., Oster, J., and Scholz, D. (2017). Sr-isotope analysis of speleothems by LA-MC-ICP-MS: High temporal resolution and fast data acquisition. *Chem. Geol.* 468, 63–74. doi: 10.1016/j.chemgeo.2017.08.012

Willmes, M., Kinsley, L., Moncel, M. H., Armstrong, R. A., Aubert, M., Eggins, S., et al. (2016). Improvement of laser ablation in situ micro-analysis to identify diagenetic alteration and measure strontium isotope ratios in fossil human teeth. *J. Archaeol. Sci.* 70, 102–116. doi: 10.1016/j.jas.2016.04.017

Winkler, D. E., Tütken, T., Schulz-Kornas, E., Kaiser, T. M., Müller, J., Leichliter, J., et al. (2020). Shape, size, and quantity of ingested external abrasives influence dental microwear texture formation in guinea pigs. *Proc. Natl. Acad. Sci. U.S.A.* 117, 22264–22273. doi: 10.1073/pnas.2008149117

Zhang, W., Hu, Z., Liu, Y., Wu, T., Deng, X., Guo, J., et al. (2018). Improved in situ Sr isotopic analysis by a 257 nm femtosecond laser in combination with the addition of nitrogen for geological minerals. *Chem. Geol.* 479, 10–21. doi: 10.1016/j.chemgeo.2017.12.018

Conflict of Interest: The authors declare that the research was conducted in the absence of any commercial or financial relationships that could be construed as a potential conflict of interest.

frontiers in Ecology and Evolution

ORIGINAL RESEARCH
published: 15 December 2020
doi: 10.3389/fevo.2020.579473

Sampling Plants and Malacofauna in $^{87}Sr/^{86}Sr$ Bioavailability Studies: Implications for Isoscape Mapping and Reconstructing of Past Mobility Patterns

Kate Britton[1,2†], Mael Le Corre[1†], Malte Willmes[3,4], Ian Moffat[5,6], Rainer Grün[5,7], Marcello A. Mannino[2,8], Stephen Woodward[9] and Klervia Jaouen[2,10]*

[1] Department of Archaeology, University of Aberdeen, Aberdeen, United Kingdom, [2] Department of Human Evolution, Max-Planck-Institute for Evolutionary Anthropology, Leipzig, Germany, [3] Institute of Marine Sciences, University of California, Santa Cruz, Santa Cruz, CA, United States, [4] Southwest Fisheries Science Center, National Marine Fisheries Service, Santa Cruz, CA, United States, [5] Research School of Earth Sciences, The Australian National University, Canberra, ACT, Australia, [6] Archaeology, College of Humanities, Arts and Social Sciences, Flinders University, Bedford Park, SA, Australia, [7] Australian Research Centre for Human Evolution, Griffith University, Nathan, QLD, Australia, [8] Department of Archaeology, School of Culture and Society, Aarhus University, Højbjerg, Denmark, [9] School of Biological Sciences, University of Aberdeen, Aberdeen, United Kingdom, [10] Géosciences Environnement Toulouse, Observatoire Midi Pyrénées, Université de Toulouse III Paul Sabatier, Toulouse, France

OPEN ACCESS

Edited by:
T. Douglas Price, Retired, Madison, WI, United States

Reviewed by:
Kelly Knudson, Arizona State University, United States
David Meiggs, Rochester Institute of Technology, United States

***Correspondence:**
Kate Britton
k.britton@abdn.ac.uk

[†]These authors have contributed equally to this work

Specialty section:
This article was submitted to Paleoecology, a section of the journal Frontiers in Ecology and Evolution

Received: *02 July 2020*
Accepted: *19 November 2020*
Published: *15 December 2020*

Citation:
Britton K, Le Corre M, Willmes M, Moffat I, Grün R, Mannino MA, Woodward S and Jaouen K (2020) Sampling Plants and Malacofauna in $^{87}Sr/^{86}Sr$ Bioavailability Studies: Implications for Isoscape Mapping and Reconstructing of Past Mobility Patterns. Front. Ecol. Evol. 8:579473. doi: 10.3389/fevo.2020.579473

Establishing strontium isotope ($^{87}Sr/^{86}Sr$) geographical variability is a key component of any study that seeks to utilize strontium isotopes as tracers of provenance or mobility. Although lithological maps can provide a guideline, estimations of bioavailable $^{87}Sr/^{86}Sr$ are often necessary, both in qualitative estimates of local strontium isotope "catchments" and for informing/refining isoscape models. Local soils, plants and/or animal remains are commonly included in bioavailability studies, although consensus on what (and how extensively) to sample is lacking. In this study, 96 biological samples (plants and snails) were collected at 17 locations spanning 6 lithological units, within a region of south-west France and an area with a high concentration of Paleolithic archaeological sites. Sampling sites aligned with those from a previous study on soil bioavailable strontium, and comparison with these values, and the influence of environmental and anthropogenic variables, was explored. Data confirm a broad correspondence of plant and snail $^{87}Sr/^{86}Sr$ values with lithological unit/soil values, although the correlation between expected $^{87}Sr/^{86}Sr$ values from lithology and bioavailable $^{87}Sr/^{86}Sr$ ratios from biological samples was higher for plants than for snails. Grass, shrub and tree $^{87}Sr/^{86}Sr$ values were similar but grasses had a stronger relationship with topsoil values than trees, reflecting differences in root architecture. Variability in $^{87}Sr/^{86}Sr$ ratios from all plant samples was lower for sites located on homogeneous geological substrates than for those on heterogeneous substrates, such as granite. Among environmental and anthropogenic variables, only an effect of proximity to water was detected, with increased $^{87}Sr/^{86}Sr$ values in plants from sites close to rivers originating from radiogenic bedrock. The results highlight the importance of analyzing biological samples to complement, inform and refine strontium isoscape models. The sampling of plants rather than snails is

recommended, including plants of varying root depth, and (if sample size is a limitation) to collect a greater number of samples from areas with heterogeneous geological substrates to improve the characterizations of those regions. Finally, we call for new experimental studies on the mineralized tissues of grazers, browsers, frugivores and/or tree leaf feeders to explore the influence of $^{87}Sr/^{86}Sr$ variability with soil profile/root architecture on $^{87}Sr/^{86}Sr$ values of locally-feeding fauna.

Keywords: strontium, bioavailability, isoscape, provenance, mobility, snails, plants, archaeology

INTRODUCTION

Although the first strontium isotope studies on ancient skeletal materials took place almost forty years ago (Ericson, 1985), it has only been in the past two decades that the technique has emerged as a leading means of exploring past human and animal movements in archaeology and paleoecology. In archaeological studies, strontium isotope analysis is used to study the geographical origins of humans, animals and artifacts, and can thus help provide insights into diverse demographic, economic and socio-cultural aspects of past lives. This includes the identification of individual and population patterns of immigration and emigration (e.g., Knudson et al., 2004; Leach et al., 2009); the inference of social conventions such as matri- or patri-locality (e.g., Bentley et al., 2005); the reconstruction of trade and exchange networks (e.g., Thornton, 2011; Laffoon et al., 2015); and the exploration of animal husbandry and herding practices (Balasse et al., 2002; Bentley and Knipper, 2005).

In Paleolithic archaeology, given the otherwise sparse record, insights into the past movement habits of humans and animals can be particularly valuable. The strontium isotope analysis of zooarchaeological materials from Paleolithic sites has been used to explore prey-species movements and seasonality (Julien et al., 2012; Price et al., 2017), giving insights into hominin landscapes use and hunting strategies (Pellegrini et al., 2008; Britton et al., 2011). These methods have also been applied to the fossilized hominin teeth, largely through the application of minimally destructive laser ablation sampling and analyses. These approaches have, for example, been used to infer landscape use and home range size amongst early hominins in South Africa (Copeland et al., 2011; Balter et al., 2012; Joannes-Boyau et al., 2019). Strontium isotope studies have also illuminated the lifetime movement habits of Neanderthals (Richards et al., 2008; Willmes et al., 2016) and Upper Paleolithic humans in Europe (Lugli et al., 2019). Strontium isotope studies have also focused on raw materials to infer the movement of crafted objects. For example, strontium isotopes were used to infer the provenance of Late Upper Paleolithic beads from a child burial in southwest France, and whether their source was contemporary coastlines or local fossil assemblages from Miocene marine deposits (Vanhaeren et al., 2004). Other types of material culture have been studied using similar techniques: for example, $^{87}Sr/^{86}Sr$ ratios, along with other rare earth elements, were also used to identify a single, French source of colorful fluorites found at Upper Paleolithic sites in Belgium (Goemaere et al., 2013).

While showing great potential, the number of applications in Paleolithic archaeology remains small and—as in all other research areas using strontium isotopes in archaeology—is at least in part limited by the extent to which local strontium isoscapes are understood. Assessing the range of biologically available strontium isotope values around sites of interest and across the wider landscape, and establishing an isoscape, are key components for any mobility and provenance study—from the Middle Paleolithic to the post-medieval period. However, the strategies for the construction of isoscapes remain contentious, and methods used to characterize and describe spatial variation in strontium isotope ratios vary—along with the methods for gauging local values. Approaches used to generate isoscapes include GIS-based techniques, including *a priori* approaches (Bataille and Bowen, 2012; Bataille et al., 2014), often incorporating mixing models, machine learning (Bataille et al., 2018), or spatial aggregation (often based on underlying the lithology) to demark discrete strontium isotope units or packages (Evans et al., 2010, 2018; Snoeck et al., 2020). All these approaches rely on source strontium data. While lithological maps, or the direct measurement of strontium local rock samples, can provide a guide for local bioavailable strontium, samples are normally collected to assess bioavailability directly. These may include modern plants, soils, micro-fauna, local waters, archaeological fauna, or a mixture of analytes. However, only a few studies have been published comparing these sample types (see Maurer et al., 2012 for an example), and there is a lack of consensus concerning what (and how extensively) to sample for bioavailability when generating or refining isoscapes (see discussion in Snoeck et al., 2020).

In southwest France, the Dordogne is an area famed for its prehistoric archaeology, particularly the late Middle and Upper Paleolithic caves and rockshelters of the Vézère valley and its tributaries. In addition to large assemblages of archaeological artifacts (including lithics from a number of type sites) and, of course, world-renowned cave art, this region boasts one of the densest and most significant early paleoanthropological records of late Middle/early Upper Paleolithic human remains, along with abundant faunal assemblages. Situated between the coastal lowlands to the west, the Loire Valley to the north, the Pyrenees to the south, and the Massif Central to the east, the region is at the intersection of different ecological, geological and topographic zones. Indeed throughout the history of study in the region, researchers have sought to forge connections across this significant eco-cultural landscape: for example, sites in the Périgord and the Pyrenees have been described as representing

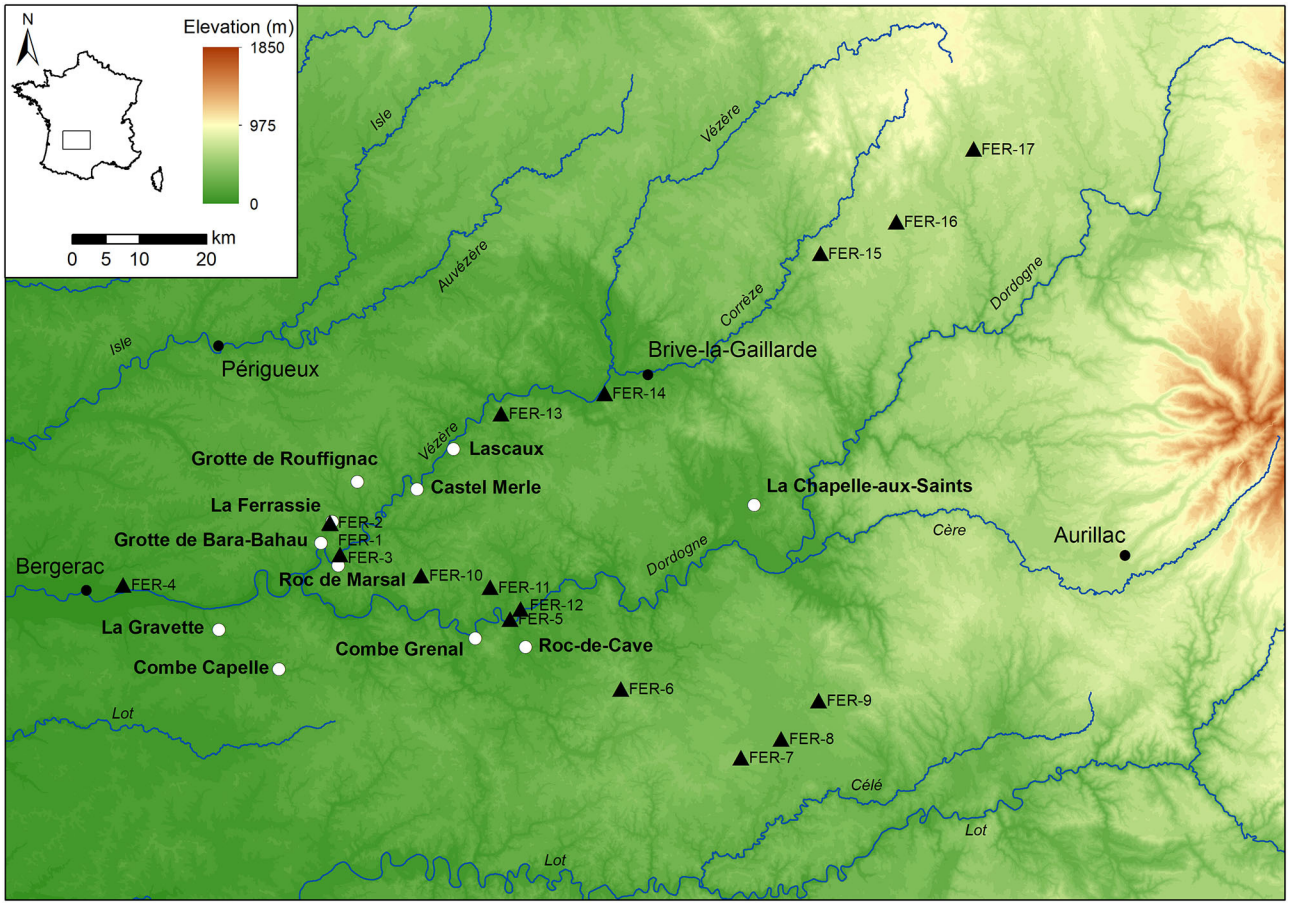

FIGURE 1 | Elevational map of the study area with the sampling locations (black triangles), and the location of selected Middle and Upper Paleolithic archaeological sites (white circles).

the different seasonal bases for the same groups of highly mobile Magdalenian "reindeer followers" (Bahn, 1977: 255; Gordon, 1988). The investigation of human movements in this region, and the landscape use of the prey-species they depended on, using strontium isotope analyses remains an important yet understudied research opportunity.

Here, we present a new strontium isotope bioavailability dataset for this region comprising almost 100 biological samples (plants, snails) collected at 17 different sampling locations and spanning 6 lithological units. Sampling locations were selected to align broadly with sampling locations of a previous study on soil strontium, including published and unpublished data (unpublished data from Moffat, 2013; published data from Willmes et al., 2014), allowing comparison of plant and snail measurements with soil values. The influence of a range of other variables was also explored including elevation, land-use/ forest cover, proximity to roads and rivers, and lithology. The aims of this research were three-fold: (1) to compare variability between substrate strontium values, and bioavailable values determined from the plants and malacofauna in this study; (2) to explore the influence of a range of landscape variables on those bioavailable strontium values in this region; and (3) to further refine the isoscape for this significant archaeological region.

MATERIALS AND METHODS

Field Sampling and Sample Identification

Field sampling for plants and snails was conducted in August 2013. Sampling locations (**Figure 1**) were based on the distribution of major geological units in the region of study, and then—specifically within each unit—selected to align as closely as possible with 24 locations included in a previous nationwide study of soil strontium isotope variability (Willmes et al., 2014) and from the doctoral thesis from one of the authors (Moffat, 2013) (see **Supplementary Table 1**). A handheld GPS was used to record the location of each plant and snail sampling locality (Garmin 2465, which is accurate to ± 15 m). Typical sites included areas of open unmanaged ground, areas of forest, and unmanaged areas at the edges of agricultural fields or track ways. At each location, samples were taken in close proximity to each other and included multiple samples of grass (i.e., shallow rooted plants), leaves from shrubs (i.e., medium root-depth plants) and tree leaves (i.e., deep rooted plants), along

with empty snail shells (where available). Plant samples were air dried in open polyethylene sample bags during the field season to avoid decomposition.

After initial assessment in the field, plant and snail samples were given taxonomic assignments by two of the authors (SW and MAM, respectively). Identifications of plant samples followed Stace (2010) and Rose (1989), and malacofauna were identified using reference materials, as well as Cossignani and Cossignani (1995) and Kerney (1999). Species consisted of common northern and western European species and are listed in **Supplementary Table 2** alongside all plant and snail strontium isotope data.

Laboratory Protocols and Data Generation

Plant and snail samples were prepared and analyzed at the Department of Human Evolution, Max Planck Institute for Evolutionary Anthropology, Leipzig, Germany. Air dried plant samples were sub-sampled and washed in ultra-pure MilliQ water to remove any adhering soils, dust or other materials, before being frozen and freeze dried. Snail shell samples were ultrasonicated for 15 min in ultra-pure MilliQ water for the same purpose, air dried overnight and crushed using a clean agate pestle and mortar. Dried plant samples were cut into smaller pieces and placed in porcelain crucibles with lids and then ashed in a muffle furnace overnight at 500°C.

Strontium was extracted from snails and plants using a modification of the method from Deniel and Pin (2001), described in detail in Copeland et al. (2008). Aliquots of ashed plant material and crushed snail shells (∼3 to 50 mg) were weighed into 3 ml Savillex vials (Minnetonka, MN, USA) and digested in 1 ml of 14.3 M HNO_3 (SupraPur grade, Sigma Aldrich) on a hotplate set at 80°C for 8 h. Samples were then dried down and re-dissolved in 1 ml 3 M HNO_3 before loading into pre-conditioned microcolumns containing Sr-specific resin (EiChrom, Darian, Il, USA). Strontium was eluted from the resin in ultrapure deionized water (18.2 MΩ), dried and then re-dissolved in 3% HNO_3 for analysis of $^{87}Sr/^{86}Sr$ ratios using a Thermo Fisher (Thermo Fisher Scientific, Bremen, Germany) Neptune multi-collector inductively coupled plasma mass spectrometer (MC-ICP-MS).

All $^{87}Sr/^{86}Sr$ measurements were corrected for interferences from krypton (Kr) and rubidium (Rb) and normalized for instrumental mass bias to $^{88}Sr/^{86}Sr = 8.375209$ (exponential law). Analysis of the international strontium isotope standard NIST SRM987 (National Institute of Standards and Technology, Gaithersburg, USA) during each analytical session was used for external normalization of data [long-term $^{87}Sr/^{86}Sr$ value $= 0.710273 \pm 0.000033$ (2 σ) ($n = 97$)]. All $^{87}Sr/^{86}Sr$ values reported here were adjusted so SRM987 = 0.710240 (Johnson and Fridrich, 1990), and this typically involved a data correction factor of −0.00002. Strontium concentrations of the enamel samples were determined using the method described in Copeland et al. (2008), which is accurate to within ±31 ppm. In addition, each batch of sample was prepared with the external standard SRM 1486 (bone meal). The nine samples analyzed gave an average value of 0.709297 ± 0.000030, to be compared to the long term in house value of 0.709298 ± 0.000026, $n = 139$ or the compiled value of GeoREM (0.70931, $n = 8$, http://georem.mpch-mainz.gwdg.de/).

Soil samples had been analyzed as part of a previous unrelated study and include published and unpublished data (Moffat, 2013; Willmes et al., 2014). Soil samples were prepared following the method described in Willmes et al. (2014). In brief, a ∼30 g subsample of each topsoil sample was dried overnight at 60°C, sieved through a 2 mm sieve, and a 1 g aliquot was subsampled and leached by adding 2.5 ml 1M ammonium nitrate (NH_4NO_3) following the protocol DIN ISO 19730 and shaking for 8 h. Samples were then centrifuged at 3,000 rpm for 15 min, the supernatant extracted (∼1–2 ml) and evaporated to dryness and then re-dissolved in 2 ml 2M nitric acid (HNO_3). Strontium concentration was determined using ICP-AES before the samples were processed by ion exchange chromatography to isolate strontium from other interfering elements using two sets of columns filled with Eichrom Sr-specific resin (pre-filter and Sr-spec resin). Strontium isotope ratios of soils were measured in the Environmental Geochemistry and Geochronology Laboratory at the Research School of Earth Sciences, ANU, also using a Neptune MC-ICP-MS. Data reduction includes Kr and ^{87}Rb isobar corrections, an exponential mass bias correction, and 3 sigma outlier rejection. Total procedural blanks varied between 50 and 250 pg strontium and measurements of the strontium carbonate standard SRM987 (National Institute of Standards and Technology) gave an average $^{87}Sr/^{86}Sr$ value of 0.71023 ± 0.00001 ($n = 167$, 2σ).

$^{87}Sr/^{86}Sr$ values of plant, snail and soil samples used in this study are shown in **Figure 2**, and in **Supplementary Table 1** (soils) and **Supplementary Table 2** (plants and snails) in the **Supplementary Material**.

DATA ANALYSIS

Environmental Data

For each of the 17 plant and snail sampling sites, data pertaining to the elevation, minimal distance to a road, minimal distance to water, and the local habitat, were extracted using ArcGIS v10.5. Elevation data came from the Digital Elevation Map of Europe (DEM 25m, Copernicus Land Monitoring Service, 2018© European Union, https://land.copernicus.eu/). Distance to road and distance to water were calculated using road and hydrographic network data[1]. Habitat was assessed from Corine Land Cover data (https://land.copernicus.eu/). Deciduous, coniferous and mixed forest habitats were grouped into a "forest" category, and pasture and complex cultivation pattern habitats into a "crop" category. Each plant and snail sampling site in the current study was associated with the closest soil sampling sites in the area (Moffat, 2013; Willmes et al., 2014). Finally, the underlying lithology of each site, as well as associated $^{87}Sr/^{86}Sr$ isotopes values, were extracted from the strontium isotope group of France map available at the IRHUM (Isotopic Reconstruction of Human Migration, www.irhumdatabase.com)

[1] *Institut National de l'Information Géographique et Forestière road: ROUTE 500 edition 191, Hydrography: DB TOPO v3*. Available online at: https://geoservices.ign.fr/.

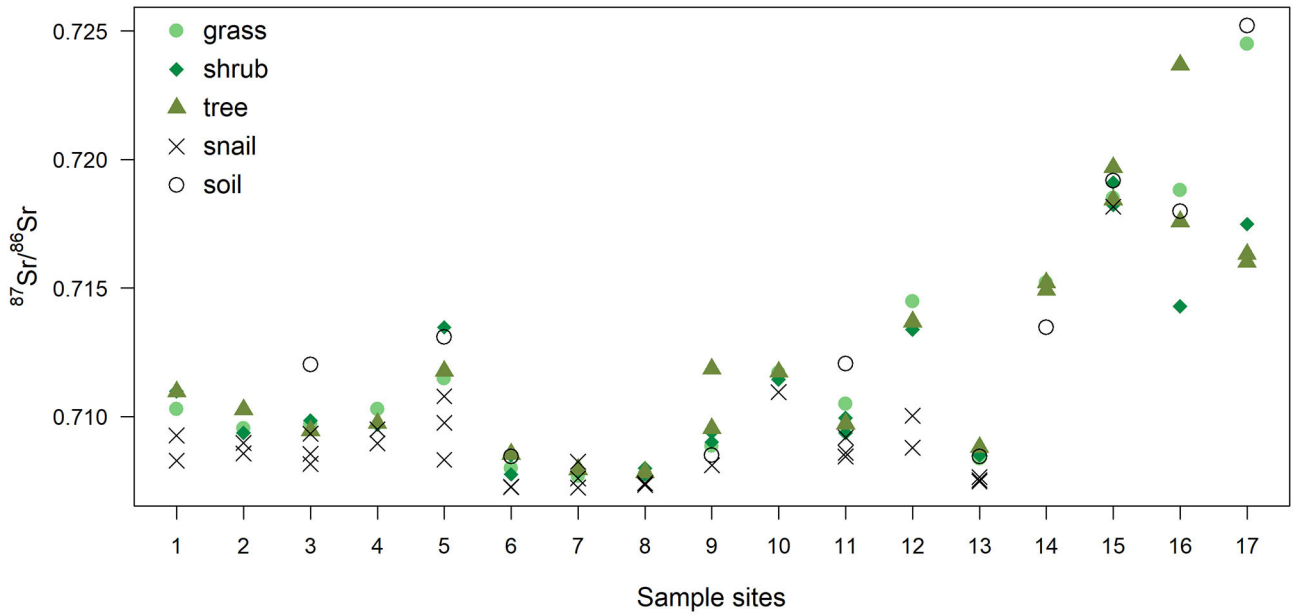

FIGURE 2 | $^{87}Sr/^{86}Sr$ values of plants (grass, shrub, tree), snails and soil for each site. Sites for biological and soil samples were different. Soil $^{87}Sr/^{86}Sr$ values presented are from the closest site sampled within 1 km from each plant sampling site, and include data from Willmes et al. (2014), and unpublished data from Moffat (2013) (see **Supplementary Table 1**).

website (Willmes et al., 2014, 2018). Willmes et al. (2018) grouped the lithological units observed in France into 5 isotope groups (**Table 1**). The western part of the study area is dominated by limestone and carbonaceous sediments (isotope group 2), ranging from middle-early Jurassic close to the Massif Central, to Eocene/Oligocene on the west, with Quaternary clastic sediments basins along rivers (**Figure 3**). The Massif Central area included on the eastern part of the study area is dominated by Cambrian paragneiss (isotope group 3) and orthogneiss (isotope group 5), and Carboniferous granite (isotope group 4). Oligocene to Pleistocene volcanic geological units (isotope group 1) are also present on the eastern edge of the study area. The lithological units observed at each sampling site were grouped within three of the five isotope groups: isotope group 2, limestone and other carbonaceous sediments; isotope group 3, sand and clay; and isotope group 4 sandstone and granite (**Table 1**, **Figure 3**).

TABLE 1 | Isotope groups with their corresponding lithologies and bioavailable $^{87}Sr/^{86}Sr$ range (adapted from Willmes et al., 2018).

Isotope group	Lithologies	Bioavailable $^{87}Sr/^{86}Sr$ range
Group 1	Volcanics	0.7033–0.7059
Group 2	Chalk, dolomite, limestone, impure carbonate sedimentary rocks	0.7072–0.7115
Group 3	Clay, sand, conglomerate, wacke, paragneiss, schist	0.7076–0.7170
Group 4	Gravel, sandstone, granite, migmatite, mica schist, rhyolitoid	0.7084–0.7252
Group 5	Orthogneiss	0.7155–0.7213
Other	Amphibols, mud, mafic/ultramafic igneous rocks, quartzites, minor lithological units	N/A

Statistical Analyses

A linear mixed-effects model was fitted to assess the effect of environmental variables on $^{87}Sr/^{86}Sr$ ratios within biological samples, with the sampling site as a random factor to control for inherent variability of each site (lme4 package in R software, Bates et al., 2015; R Core Team, 2019). In order to facilitate data analysis, strontium isotope ratios of biological and soil samples were presented in $\varepsilon^{87}Sr$ notation (Beard and Johnson, 2000), defined as:

$$\varepsilon^{87}Sr = ([^{87}Sr/^{86}Sr]_{sample} / [^{87}Sr/^{86}Sr]_{bulk\ earth} - 1) * 10000$$

where $[^{87}Sr/^{86}Sr]_{sample}$ is the $^{87}Sr/^{86}Sr$ values of the samples and $[^{87}Sr/^{86}Sr]_{bulkearth}$ is equal to 0.7045 (Beard and Johnson, 2000: 1050). To meet the assumptions of normality of the residuals and homogeneity of variance, the response variable was transformed from $\varepsilon^{87}Sr$ to $-(\varepsilon^{87}Sr)^{-1}$. Effects of the sample type (snail, grass, shrub, tree), the habitat (crop/forest), the distance to road, the distance to water and the elevation were tested separately. Variables were then regrouped into three categories: sample type, anthropogenic variables (habitat, distance to road), landscape structure (distance to water, elevation), and candidate models composed of various combinations of these categories were constructed. As the strontium isotope ratio of the underlying lithological units was expected to be the main driver of $\varepsilon^{87}Sr$ observed in both soils and biological samples (Bentley,

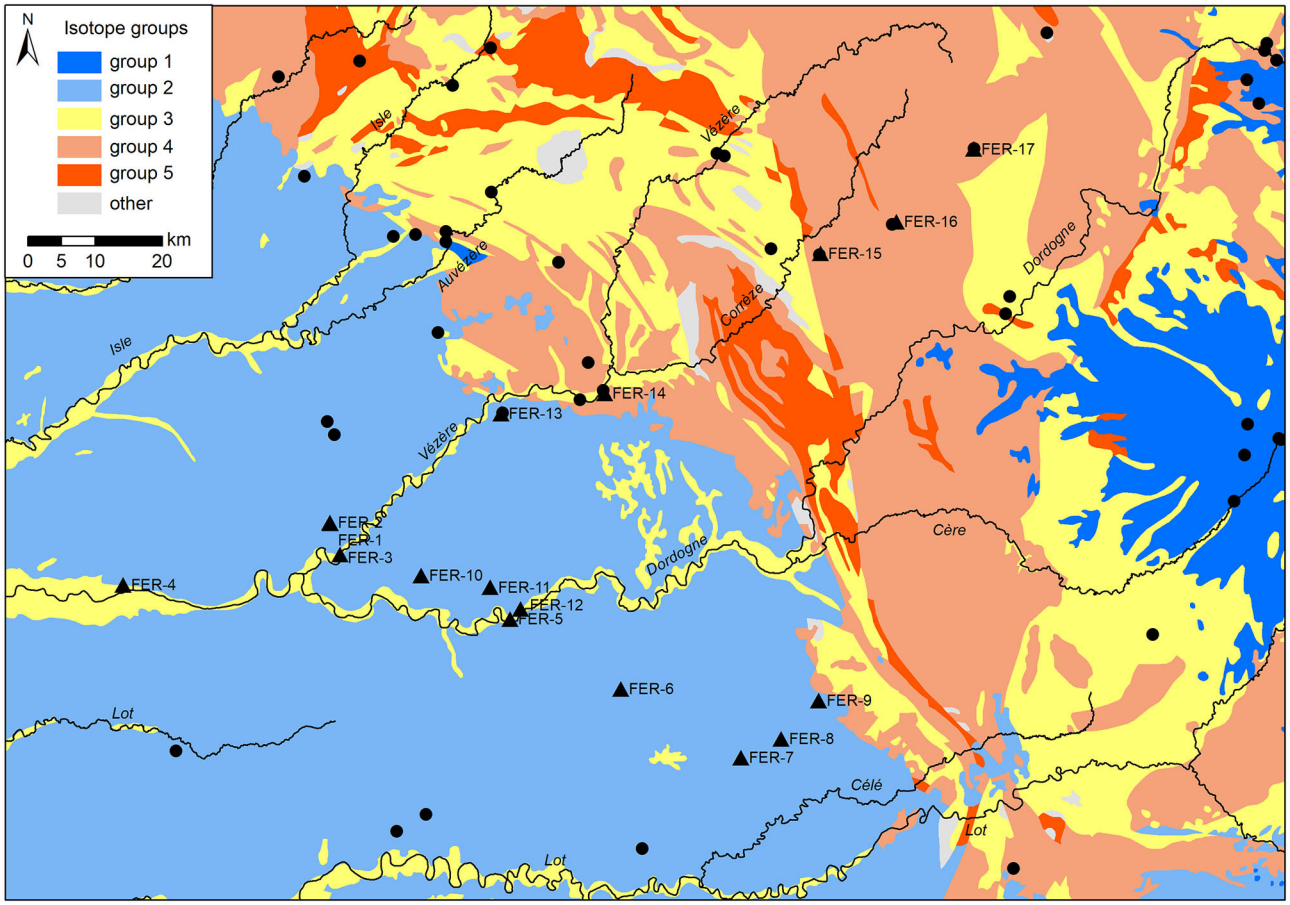

FIGURE 3 | Lithological units of the study area classified by isotopes groups (adapted from Willmes et al., 2018). Sampling locations of the study are indicated (black triangles) as well as IRHUM sampling sites (black circles).

2006; Bataille et al., 2018), the $\varepsilon^{87}Sr$ lithological values of each site were included in all models in order to control for its effect. The list of all models tested in this study is provided in **Supplementary Table 3**. Variance inflation factor (VIF; Zuur et al., 2010) did not reveal multicollinearity among explanatory variables, as all variables had a VIF < 3. All models were ranked using AICc (Akaike's information criterion) and models with $\Delta AICc \leq 2$ were considered as equivalent (see **Supplementary Table 3**). From these models, parameter estimates, *SE* and 95% *CI* were calculated using model averaging (Burnham and Anderson, 2002). Effects of explanatory variables were considered significant when the 95% *CI* did not include 0.

To investigate the relationship between bioavailable $\varepsilon^{87}Sr$ in soil and the $\varepsilon^{87}Sr$ observed in plant according the type of plant (grass, shrub, tree), a linear mixed-effect model was fitted with $-(\varepsilon^{87}Sr)^{-1}$ of plant as the response variable, the $\varepsilon^{87}Sr$ of soil in interaction with the plant type as explanatory variables, and the plant sample sites as a random factor. As plant and soil sampling sites originated from two unrelated studies, and were paired *post hoc*, only plant sampling sites <1000 m away from soil sampling sites were kept for this analysis (sites: $n = 10$, plant samples: $n = 39$). Parameter estimates were provided with their *SE* and 95% *CI*.

Heterogeneous lithological units such as granite are expected to have a higher variability in their $^{87}Sr/^{86}Sr$ ratio than more homogeneous units, which may also be reflected in more variable bioavailable strontium values (Sillen et al., 1998; Willmes et al., 2018). Variability in sample $^{87}Sr/^{86}Sr$ ratio between lithological groups was compared using robust Levene test because $^{87}Sr/^{86}Sr$ ratio values did not follow a normal distribution. A robust Levene test is equivalent to an ANOVA performed on the absolute difference between the $^{87}Sr/^{86}Sr$ values of the samples and the median $^{87}Sr/^{86}Sr$ value of the group to which they belong. Therefore, a *post-hoc* Tukey's HSD (honestly significant difference) test on this difference was performed in order to compare all possible pairs of groups and identify how variability differed between groups. Differences in variability were also tested between sample type (snail, shrub, grass, trees) and between habitats.

Generating a Local $^{87}Sr/^{86}Sr$ Isoscape

In order to produce a new local $^{87}Sr/^{86}Sr$ isoscape of the study area, newly sampled sites were incorporated to an existing $^{87}Sr/^{86}Sr$ isoscape map of France from Willmes et al. (2018). This isoscape was generated by geostatistical interpolation

TABLE 2 | Parameters estimates from the best mixed-effects models (random factor: sampling site) explaining variation in the $^{87}Sr/^{86}Sr$ ratio of biological samples expressed in $-(\varepsilon^{87}Sr)^{-1}$.

Variables	Beta	SE	CI95low	CI95up
(Intercept)	**−0.02118**	**0.00230**	**−0.02568**	**−0.01668**
ε^{87}Sr litho	**0.00010**	**0.00002**	**0.00006**	**0.00015**
samp.type (Snail)	**−0.00369**	**0.00047**	**−0.00461**	**−0.00276**
samp.type (Shrub)	0.00012	0.00054	−0.00094	0.00117
samp.type(Tree)	0.00064	0.00049	−0.00032	0.00161
Habitat	0.00216	0.00114	−0.00007	0.00440
d.road	0.00266	0.00309	−0.00339	0.00871
d.water	**−0.00072**	**0.00031**	**−0.00133**	**−0.00010**
elevation	−0.00250	0.00464	−0.01160	0.00659

Parameters were calculated by model averaging. Effects of variable for which 95% CI exclude 0 (indicated in bold) are considered statistically significant. $\varepsilon^{87}Sr$ litho: $^{87}Sr/^{86}Sr$ values of the lithological units presented in $\varepsilon^{87}Sr$ notation; samp.type: sample type with grass as reference category; d.road: distance to road; d.water: distance to water.

of the $^{87}Sr/^{86}Sr$ values observed at sites recorded in the IRHUM database (Willmes et al., 2014, http://dx.doi.org/10.1594/PANGAEA.819142), using kriging with external drift (Willmes et al., 2018). The IRHUM database provides $^{87}Sr/^{86}Sr$ ratios for plant and soil samples from >800 locations in France (see Willmes et al., 2014 for details of samples and isotope analyses) as well as information about the underlying lithology (type, age). Kriging relies on the spatial autocorrelation between the sampled locations to interpolate value and this spatial autocorrelation is quantified by fitting a variogram model. Values at a given location are predicted by averaging known neighboring values weighted according to the variogram model. Kriging with external drift allows the accounting of an additional spatial trend defined by an auxiliary variable, such as elevation or other environmental variables.

Following Willmes et al. (2018), sites from the IRHUM database with both soil and plant samples were selected, excluding sites that were not representative of the lithology of their geographic area (minor geologic outcrop, riverbanks, sites with a strong anthropogenic influence). Strontium isotope groups defined by Willmes et al. (2018) were used as the auxiliary variable for the kriging with external drift. Lithological units of the surface geology map of France available in the IRHUM (Willmes et al., 2018) were regrouped according the isotope group to which they belonged (**Table 1**). The isotope group of each site in the IRHUM database were then extracted. Kriging with external drift was first performed on 498 IRHUM sample sites to obtain a plant isoscape and a soil isoscape of France, using their corresponding $^{87}Sr/^{86}Sr$ values, and the average isoscape was computed (Willmes et al., 2018). Then, the plant and soil data from the current study were added to the IRHUM database. A single mean $^{87}Sr/^{86}Sr$ value per sampling site was used for the plant samples (as kriging analysis requires a unique value per site). Eight of the 24 soil sites were already recorded in the IRHUM database but without plant data, and, consequently, were not included in the IRHUM-only isoscape. Snails $^{87}Sr/^{86}Sr$ values were not included in the isoscape model for comparability (as these are not included in the IRHUM database). Kriging was performed with the new plant and soil data and the average isoscape was computed, also at the scale of France. For each isoscape, the kriging was done using an exponential variogram model and a search neighborhood set to min = 5 and max = 50 (Willmes et al., 2018). Analysis was carried out with the *gstat* package in R (krige function, Gräler et al., 2016).

RESULTS

Effects of Environmental Variables on $\varepsilon^{87}Sr$ of Biological Samples

The best models testing the effect of the environmental variables on $\varepsilon^{87}Sr$ within biological samples were the complete model that included $\varepsilon^{87}Sr$ lithological values, sample types, habitats, distance to road, distance to water and elevation, and the model with all variables but anthropogenic variables (**Supplementary Table 3**). Parameters estimates from the best mixed-effects models (random factor: sampling site) explaining variation in the $^{87}Sr/^{86}Sr$ ratio of biological samples, expressed in $-(\varepsilon^{87}Sr)^{-1}$, are shown in **Table 2**. As expected, $\varepsilon^{87}Sr$ observed in biological samples increased significantly with $\varepsilon^{87}Sr$ lithological values (**Table 2**).

As also shown in **Figure 4**, using $^{87}Sr/^{86}Sr$ ratios, $\varepsilon^{87}Sr$ values were lower in snails than in plants, but did not differ systematically between grasses, shrubs and trees (**Table 2**). Sample $\varepsilon^{87}Sr$ values decreased as the distance of sampling site from water increased (**Table 2**), with a mean $^{87}Sr/^{86}Sr$ value of 0.7126 ± 0.0043 (SD) for sites within 0.5 km of water, and 0.7088 $\pm$ 0.0014 for sites distant by more than 1 km. Anthropogenic variables, habitats and distance to road, did not have a significant effect on $\varepsilon^{87}Sr$ of biological samples (**Table 2**). Both $\varepsilon^{87}Sr$ observed in snails and plants correlated significantly with $\varepsilon^{87}Sr$ expected from lithological units but we observed the highest correlation with plants (plants: $n = 64$, $p < 0.001$, $R^2 = 0.79$, snails: $n = 32$, $p < 0.001$, $R^2 = 0.51$). Based on soil sampling sites within 5 km of plant sampling sites, $\varepsilon^{87}Sr$ in soil was not correlated with distance to water ($n = 19$, $p = 0.24$, $R^2 = 0.08$).

Variability of Biological Sample $^{87}Sr/^{86}Sr$ Values Between Lithological Groups

Table 3 details the results of the *post-hoc* Tukey's HSD test for variables for which robust Levene tests identified a significant difference in the variability of the sample $^{87}Sr/^{86}Sr$ values between the different lithological groups. Variability in sample $^{87}Sr/^{86}Sr$ differed between lithological isotope groups ($F = 4.86$, $p = 0.010$, **Figure 5**) with a higher variability observed in samples from isotope group 4 (granites, sandstone) than in samples from isotope group 2 (limestone, sediment, $p = 0.01$, **Table 3**). The samples from isotope group 3 (sand, clay) presented an intermediate variability in their $^{87}Sr/^{86}Sr$ values but not significantly different from group 2 ($p = 0.38$) and group 4 ($p = 0.25$). Variability in $^{87}Sr/^{86}Sr$ did not differ whether we compared samples from the forest and agricultural habitats ($F = 0.01$, $p = 0.907$) or, in more detail, from the five different class of habitats ($F = 1.28$, $p = 0.283$). Variability in $^{87}Sr/^{86}Sr$

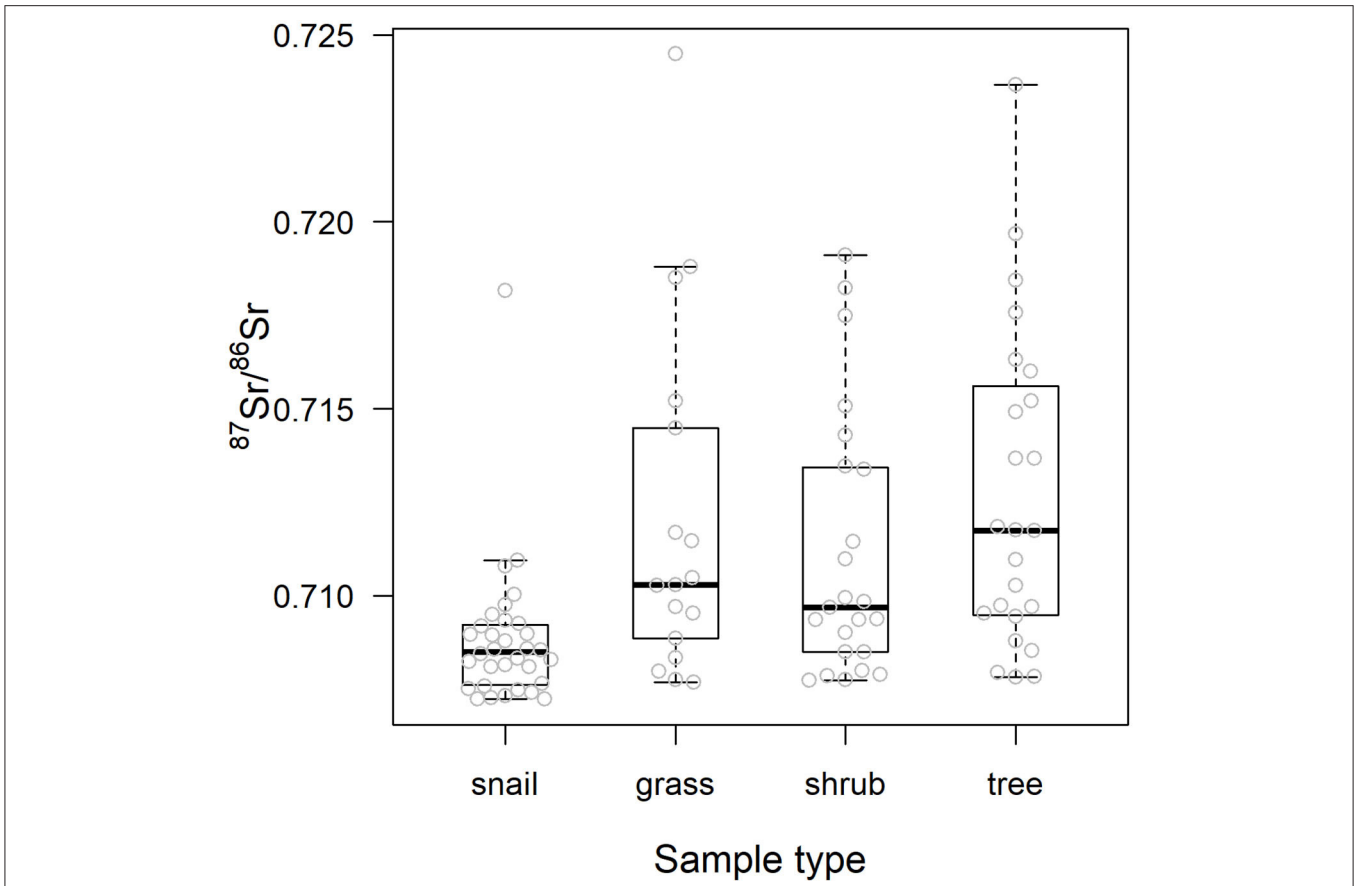

FIGURE 4 | $^{87}Sr/^{86}Sr$ values of the biological samples by sample type. Center line and box edges are, respectively the median and the 1st and 3rd quartiles, and whiskers represent data points within the range quartile ± 1.5*(interquartile range). Raw values are displayed with gray dots.

TABLE 3 | *Post-hoc* Tukey's HSD test for variables for which robust Levene tests identified a significant difference in the variability of the $^{87}Sr/^{86}Sr$ sample values between groups.

	Estimates	SE	*t*-value	*p*-value
Isotope groups				
group 3–group 2	0.0004	0.0003	1.34	0.376
group 4–group 2	**0.0011**	**0.0003**	**3.07**	**0.007**
group 4–group3	0.0006	0.0004	1.60	0.248
snail vs. plant				
plant–snail	**−0.0021**	**0.0006**	**3.50**	**0.001**
snail vs. plant detailed				
grass–snail	**0.0022**	**0.0008**	**2.71**	**0.039**
shrub–snail	0.0016	0.0007	2.23	0.123
tree–snail	**0.0024**	**0.0007**	**3.29**	**0.008**
shrub–grass	−0.0005	0.0009	−0.61	0.928
tree–grass	0.0002	0.0009	0.27	0.993
tree–shrub	0.0008	0.0008	0.95	0.778

Tukey's HSD tests were performed on the variability in $^{87}Sr/^{86}Sr$ sample values among isotope lithological groups and among sample types. The estimates correspond to the difference in the mean variability between the compared groups. Significant differences in mean variability between groups are indicated in bold. Isotope group 2: limestone, other carbonaceous sediments; group 3: sand, clay; group 4: sandstone, granite.

plant and snail samples was significantly different ($F = 12.25$, $p < 0.001$, **Figure 2**), with a lower variability in snails ($p < 0.001$, **Table 3**). Specifically, the variability in snail $^{87}Sr/^{86}Sr$ was lower than the variability observed in that of grasses and tree leaves but did not differ from variability observed in shrubs (**Table 3**). Grass, shrubs and trees presented the same variability in $^{87}Sr/^{86}Sr$ (**Table 3**). However, the relationship between soil and plant $^{87}Sr/^{86}Sr$, expressed in $\varepsilon^{87}Sr$, varied according the plant type, with the increase of $^{87}Sr/^{86}Sr$ of grasses as $^{87}Sr/^{86}Sr$ in soils increased being significantly stronger than in trees in particular (**Table 4**, **Figure 6**). According to the predictions of the model, an increase from 0.7100 to 0.7200 in soil $^{87}Sr/^{86}Sr$ would result in an increase from 0.7090 to 0.7206 and from 0.7094 to 0.7172, respectively for grass and tree $^{87}Sr/^{86}Sr$. Shrubs presented an intermediate increase (**Table 4**, **Figure 6**).

Modified Isoscape

Adding 17 plant sampling sites and 24 soil sampling sites to the 498 IRHUM sites did not improved the root-mean-square error (RMSE) of the kriging with external drift using the IRHUM sites for the whole of France (RMSE: $Plant_{IRHUM} = 0.0033$; $Plant_{IRHUM+studysites} = 0.0034$; $Soil_{IRHUM} = 0.0034$; $Soil_{IRHUM+studysites} = 0.0033$). However, at the local scale, the

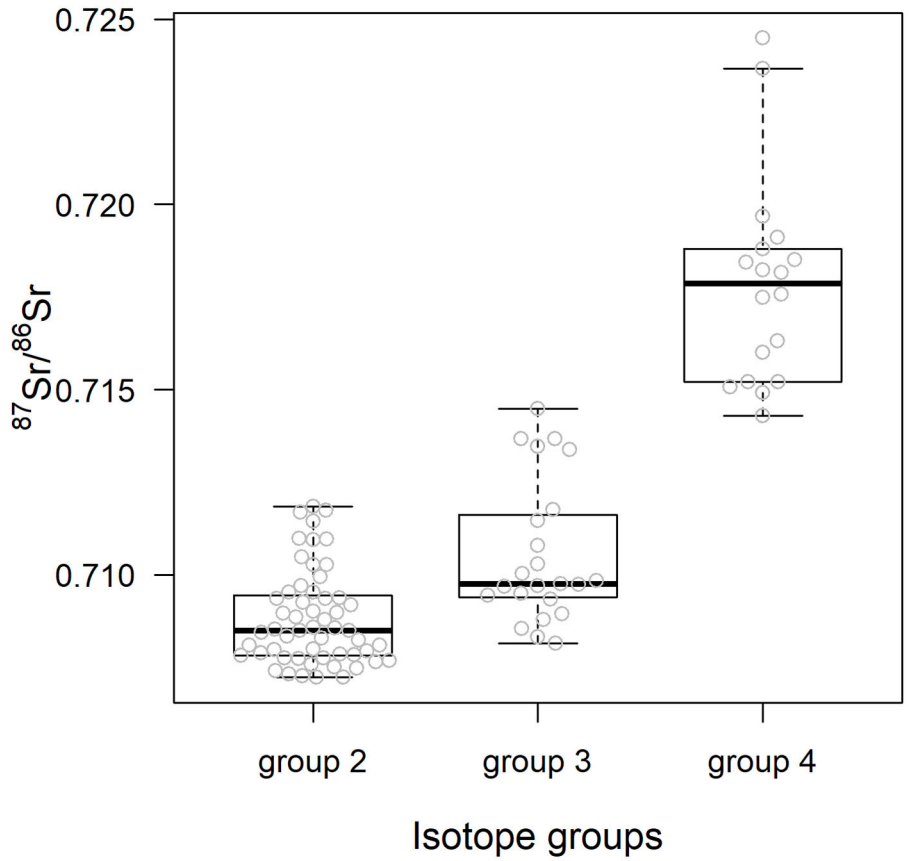

FIGURE 5 | $^{87}Sr/^{86}Sr$ values of the biological samples according the isotope group of the lithological unit underlying the sample sites. Center line and box edges are, respectively the median and the 1st and 3rd quartiles, and whiskers represent data points within the range quartile ± 1.5*(interquartile range). Raw values are displayed with gray dots.

kriging prediction error over the study area decreased with the new sites (**Figures 7c,d**). Moreover, including the new sites to the isoscape led to lower $^{87}Sr/^{86}Sr$ values in the lowland along the Vézère and the Dordogne rivers and slightly higher $^{87}Sr/^{86}Sr$ values at higher elevation (**Figures 7a,b**) than observed in the IRHUM database (Willmes et al., 2018). Plant and soil $^{87}Sr/^{86}Sr$ isoscapes used to compute the average isoscape were relatively similar, both presenting the decrease in kriging prediction error rate, as well as the changes in lowland and high elevation $^{87}Sr/^{86}Sr$ values (**Supplementary Figure 4**).

TABLE 4 | Parameters estimates from the mixed-effects model (random factor: sampling site) explaining variation in the $^{87}Sr/^{86}Sr$ ratio of biological samples, expressed in $-(\varepsilon^{87}Sr)^{-1}$, according $^{87}Sr/^{86}Sr$ ratio of soil samples, expressed in $\varepsilon^{87}Sr$, in interaction with the type of plant.

Variables	Beta	SE	CI95low	CI95sup
(Intercept)	−0.02013	0.00202	−0.02397	−0.01628
ε^{87}Sr soil	**0.00007**	**0.00001**	**0.00004**	**0.00009**
Plant type (Shrub)	0.00106	0.00112	−0.00106	0.00316e
Plant type (Tree)	**0.00324**	**0.00113**	**0.00113**	**0.00538**
ε^{87}Sr soil:Plant type (shrub)	−0.00001	0.00001	−0.00002	0.00000
ε^{87}Sr soil:Plant type (Tree)	**−0.00002**	**0.00001**	**−0.00003**	**−0.00001**

Effects of variable for which 95% CI exclude 0 (indicated in bold) are considered statistically significant. Reference category for plant type: grass.

DISCUSSION

The results explored above highlight several trends in the $^{87}Sr/^{86}Sr$ values of plants and malacofauna analyzed in this study, both inter- and intra- site, and in comparison to each other and to values expected based on underlying lithology. As expected, a positive relationship between the $^{87}Sr/^{86}Sr$ values of the lithological units and that of the biological samples analyzed (bioavailable $^{87}Sr/^{86}Sr$) was observed. This is in agreement with the findings of other bioavailability studies (e.g., Maurer et al., 2012; Willmes et al., 2018; Snoeck et al., 2020), which have shown that—despite there being multiple environmental factors known to influence bioavailable strontium—the type and age of the lithology are the main driver of the spatial distribution of bioavailable strontium (Bentley, 2006; Bataille et al., 2018).

Animals and plants acquire $^{87}Sr/^{86}Sr$ from different sources, and consequently some sample types may be more relevant to the

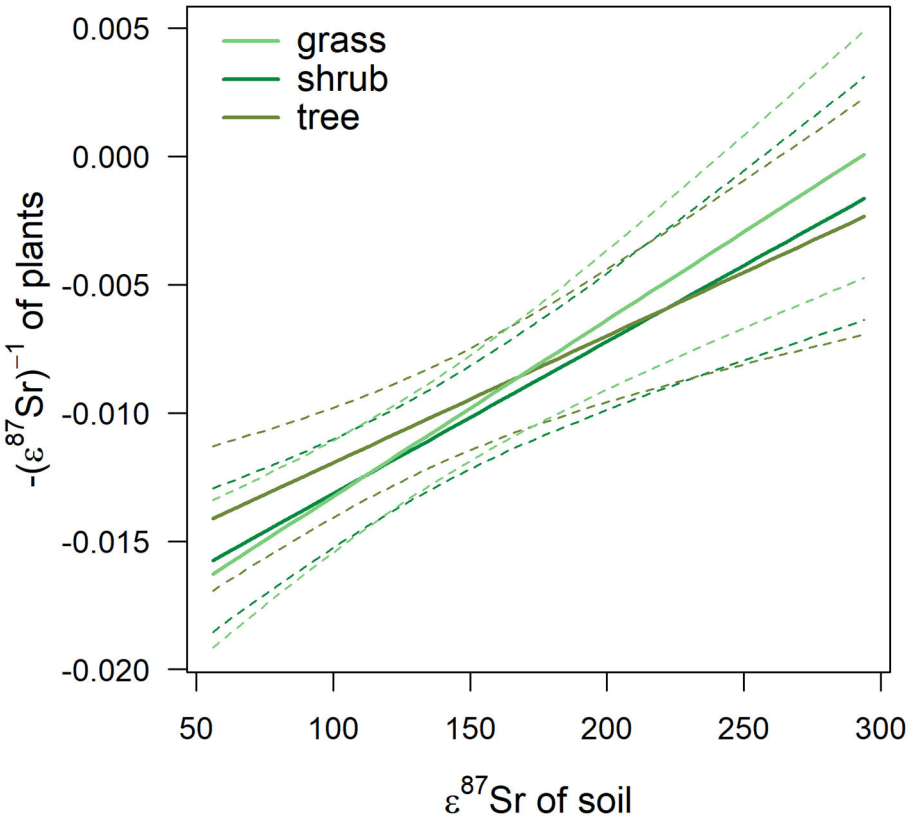

FIGURE 6 | Effect of $^{87}Sr/^{86}Sr$ values of soil, expressed in $\varepsilon^{87}Sr$, on the $^{87}Sr/^{86}Sr$ values of plant, expressed in $-(\varepsilon^{87}Sr)^{-1}$, according to plant type. Fitted trends are presented with 95% *CI* (dashed lines).

landscape mapping of bioavailable $^{87}Sr/^{86}Sr$ than others (Evans et al., 2010; Maurer et al., 2012). Here, $^{87}Sr/^{86}Sr$ in snail shells was lower than $^{87}Sr/^{86}Sr$ in plants across all sampling locations, and plants of all types generally had a better correlation with the $^{87}Sr/^{86}Sr$ values expected from the lithology and soils. The snail taxa included in this study feed primarily on living and dead plant material (e.g., leaf litter, see Williamson and Cameron, 1976). While the strontium isotope ratio of leaf litter should reflect the composition of exchangeable pools within soil, recent studies have shown $^{87}Sr/^{86}Sr$ (and thus Ca) sources in land snails can differ, and be obtained through sources other than major food sources (i.e., precipitation or stemflow) (Ohta and Saeki, 2020). Previous strontium bioavailability studies have also reported low $^{87}Sr/^{86}Sr$ values for snail shells, with a bias toward rainwater (Evans et al., 2010) and the $^{87}Sr/^{86}Sr$ values of soil carbonates (Maurer et al., 2012). The results of the current study agree with those of others and suggest malacofauna are a less suitable analyte than plants when mapping bioavailable strontium.

In the current study, differences in $^{87}Sr/^{86}Sr$ were also expected between plant types due to differences in root depth (Poszwa et al., 2004; Maurer et al., 2012) as water and nutrient uptake will occur in different soil horizons and soil $^{87}Sr/^{86}Sr$ can vary with depth. Mineral weathering is the main source of $^{87}Sr/^{86}Sr$ in deep soil horizons, but topsoil can be influenced by external sources such as atmospheric deposition or the application of fertilizers (Prohaska et al., 2005; Maurer et al., 2012). While in this study $^{87}Sr/^{86}Sr$ values in grasses, shrubs and trees were broadly similar, different rates of increase in plant $^{87}Sr/^{86}Sr$ as soil $^{87}Sr/^{86}Sr$ increased were observed between grasses and trees across different sites, with intermediate values for shrubs. Grasses thus appear to be more representative of bioavailable $^{87}Sr/^{86}Sr$ values of soil (**Figure 8**), which is in agreement with the findings of other studies (e.g., Maurer et al., 2012). Due to their deep and wide root systems, trees at the same location can display variable $^{87}Sr/^{86}Sr$ values in response to local variation in soil composition and mineral weathering rates as they can draw $^{87}Sr/^{86}Sr$ in different pools (Aguzzoni et al., 2019). On the other hand, water and nutrient uptake of grasses is mostly limited to topsoil horizons. External sources of $^{87}Sr/^{86}Sr$, such as rainfall (Evans et al., 2010), occurs at a large scale and—although rainwater values inland deviate from sea salts and can be similar to terrestrial underlying values due to the incorporation of atmospheric dust (e.g., Négrel et al., 2007; Raiber et al., 2009)—this could still serve to decrease the $^{87}Sr/^{86}Sr$ variability of the topsoil horizon between sites. Soil samples were taken from the topsoil horizon (Willmes et al., 2014) and the lower rate of increase in trees may be linked to their use of multiple and deeper $^{87}Sr/^{86}Sr$ sources.

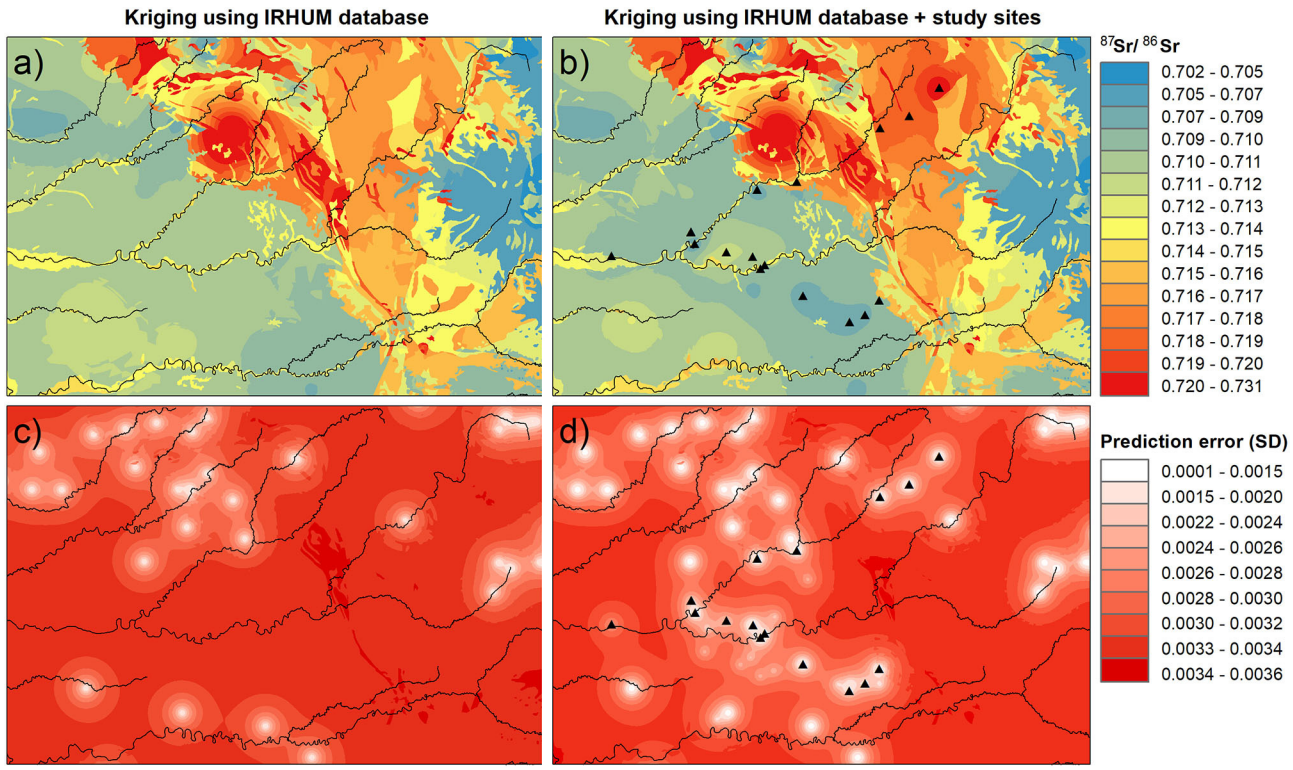

FIGURE 7 | Averaged $^{87}Sr/^{86}Sr$ isoscapes of plant and soil $^{87}Sr/^{86}Sr$ isoscapes generated by kriging with external drift using IRHUM sites **(a)** and IRHUM and sites in this study **(b)**, and their respective kriging prediction error maps **(c,d)**. Kriging prediction error is given as the standard deviation. Plant sampling sites are indicated by triangles.

Therefore, targeting a specific plant category in a sampling protocol would reflect the bioavailable $^{87}Sr/^{86}Sr$ values from a particular soil horizon. Sampling multiple species with different root systems/root depths at a same location should be more representative of the bulk soil bioavailable $^{87}Sr/^{86}Sr$. Beyond isoscape mapping, variations in plant $^{87}Sr/^{86}Sr$ with root depth could have implications for the reconstruction of human and animal mobility patterns in archaeology. Humans make choices about what they consume and when and where they source those foods, and are thus not passive recipients of environmental strontium (Johnson et al., 2019). Furthermore, while it has been long known that strontium inputs are normalized to dietary calcium budgets (e.g., Comar, 1963), the influence of dietary composition on $^{87}Sr/^{86}Sr$ in humans has received little attention. While it is currently accepted that the dominant contributor of metabolized strontium in both herbivores and omnivores originates from plant foods (as opposed to being derived from animal sources or water) (see review in Montgomery, 2010), little consideration has been given to the potential influence of different types of plant foods in the diet. Grazing animals, for example, would be expected to represent grass and therefore topsoil values, and perhaps be more directly relatable to isoscapes generated using such proxy data. The same may be true of human groups eating grain-based agricultural diets, and human tissues could reasonably be expected to show lower intra-group variability were those individuals subsisting on locally-grown grains. However, hunter-gatherer groups reliant on a wider range of plant food sources including berries, fruits or tubers, as well as greens (as well as animal foods, in varying quantities) could be incorporating strontium from a variety of different sources and catchments, even locally. Furthermore, these different plant foods may have different concentrations of strontium (Millour et al., 2012). Although any influence may not substantial enough to affect the inference of provenance, further studies are required to determine if a "soil profile" influence could be apparent in mammalian skeletal bioapatite. Experimental studies on browser and grazers, or even frugivorous and tree-leaf feeding species, with similar home range sizes from modern ecosystems would be an important first step in determining the extent of possible effects of different types of local plant foods on the $^{87}Sr/^{86}Sr$ of hard tissues. To date, however, experimental or controlled feeding studies incorporating $^{87}Sr/^{86}Sr$ have been rare (e.g., Lewis et al., 2017). Other experiments, for example concerning the extent to which the $^{87}Sr/^{86}Sr$ ratios of skeletal tissues are affected by marine resource consumption or by diets very low in plant foods would also be welcome in archaeology.

Beside differences in intra-site $^{87}Sr/^{86}Sr$ variability between sample type, samples from sites with different underlying lithology did not show the same $^{87}Sr/^{86}Sr$ variability. As a product of soil mineral weathering, variability in soil $^{87}Sr/^{86}Sr$ increases

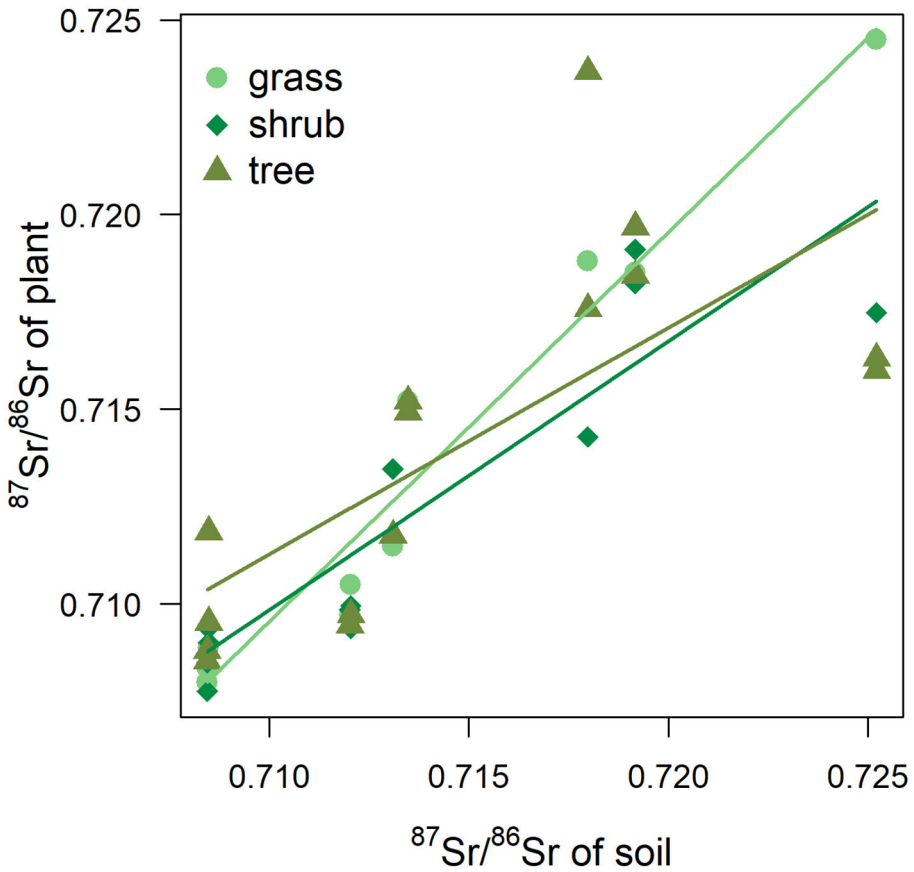

FIGURE 8 | $^{87}Sr/^{86}Sr$ values of plant according $^{87}Sr/^{86}Sr$ values of soil. Fitted trends correspond to simple linear regressions for each plant type (grass, shrub, tree).

with the heterogeneity of the geological substrates (Bataille et al., 2018; Willmes et al., 2018). It follows that such variability in soil $^{87}Sr/^{86}Sr$ should then be reflected in plants (e.g., Hartman and Richards, 2014; Aguzzoni et al., 2019). Indeed, in the current study, a positive correlation between sample variability and substrate variability (based on underlying lithology) was observed. Variability in bioavailable strontium values from different plants and snails at the same site was lower for sites located on homogeneous geologic substrates, such as limestones, than for sites located on heterogeneous geologic substrates, such as granites. These findings suggest that—when undertaking bioavailability studies—sampling efforts should focus on areas of expected greater heterogeneity to capture the whole range of bioavailable $^{87}Sr/^{86}Sr$. This heterogeneity can be broadly predicted from lithological maps, helping to guide sampling. The argument for more intensive and multi-proxy sampling (i.e., soils, water, plant leaves) in geologically complex areas has been made by others (e.g., Ladegaard-Pedersen et al., 2020); here we add that diverse sampling even within the same broad category of sample type as explained above (e.g., tree leaves, shrub leaves, grasses) may help to capture such variability.

Beyond lithology, the influence of other aspects of landscape structure, such as elevation and distance to water, was also explored in this study. While bioavailable $^{87}Sr/^{86}Sr$ values were generally increased in areas of higher elevation, when controlling for the $^{87}Sr/^{86}Sr$ values of the lithological units themselves, no effect of elevation on bioavailable $^{87}Sr/^{86}Sr$ values was observed. This is because, in this study area, the lithological units presenting high $^{87}Sr/^{86}Sr$ values, such as granite, also presented a higher elevation than lithological units with low $^{87}Sr/^{86}Sr$ values. On the other hand, distance to water seemed to affect the $^{87}Sr/^{86}Sr$ values of samples. A decrease in $^{87}Sr/^{86}Sr$ values was observed as distance to rivers increased, suggesting river water $^{87}Sr/^{86}Sr$ values in the region are higher than surrounding bedrock and/or that rivers are depositing sediments or other materials of higher $^{87}Sr/^{86}Sr$ values on areas close to rivers. Higher values in the rivers—of either water or suspended material—is consistent with the fact that the Vézère and the Dordogne rivers originate in the Massif Central, which is dominated by granite and metamorphic bedrocks that tend to have elevated $^{87}Sr/^{86}Sr$ ratios. Indeed, the radiogenic influence of the Massif Central bedrock was also observed in the Loire river in a previous study (Négrel et al., 2003). Mineral weathering is a major source of $^{87}Sr/^{86}Sr$ upstream (Pierson-Wickmann et al., 2009; Maurer et al., 2012). At lower elevations, the relationship between river content and local bedrock is blurred further, due to the carrying of

upstream rocks and solids (Bentley, 2006, 144). The absence of a relationship between distance to river and the $^{87}Sr/^{86}Sr$ ratio of soils suggests that the influence of rivers on the $^{87}Sr/^{86}Sr$ of plants was, however, not due to changes in soil/sediment composition, but due to the addition of strontium from river water itself. Indeed, other studies have observed variation in riverine $^{87}Sr/^{86}Sr$ values based on the size and lithological diversity of the watershed (Hegg et al., 2013).

Anthropogenic input of $^{87}Sr/^{86}Sr$ in the ecosystem is a major concern in bioavailability studies, and therefore for archaeological applications of strontium isotope analysis. For example, dust derived from road surfaces, such as that produced as a consequence of use by heavy vehicles, can modify topsoil composition (Prohaska et al., 2005, 246), and the use of mineral fertilizers or carbonate amendment (liming) has been demonstrated to lower soil $^{87}Sr/^{86}Sr$ (Pierson-Wickmann et al., 2009; Maurer et al., 2012). Lime has typically low $^{87}Sr/^{86}Sr$ values (∼0.7087), and analysis of deionized water-soluble strontium from three fertilizers in a French study determined strontium isotope ratios ranging from 0.70794 to 0.70830 (Négrel, 1999, 155). However, unlike some other bioavailability studies (e.g., Maurer et al., 2012; Thomsen and Andreasen, 2019), no differences were detected between plant samples collected in locations proximal to agricultural fields compared to those collected in forests in the current study. The landscape of the study area was a complex mosaic with small fields and forest patches, which may suggest the influence of fertilizers was either minimal due to a lack of significant local use or may have been homogenized across the landscape through runoff.

The addition of the new data to that in the IRHUM database did not improve the overall performance of the already existing France isoscape (Willmes et al., 2018), as south western France was already well covered by IRHUM with a low prediction error compared to areas with lower sampling density (Willmes et al., 2018). However, it has served to reduce the predicted error and refine the isoscape for the study area. Notably this addition has resulted in an increased difference in $^{87}Sr/^{86}Sr$ values between the areas of low and high elevation in this important archaeological region. Increased contrast between areas with lower uncertainty can help to achieve better isotopic discrimination between regions and thus in archaeological provenance studies using strontium isotopes (Bataille et al., 2018). This demonstrates that more extensive bioavailability mapping is essential, can increase resolution at the local scale in regional studies, and highlights the benefit of combining large scale mapping and modeling with focused sampling of specific areas of interest. More broadly, the current study in particular highlights the importance of focusing efforts on areas of heterogeneous geological substrate when undertaking bioavailability studies—in this case study, the granitic upland areas. Potential environmental and anthropogenic effects must also be considered. Despite no visible anthropogenic effects on the $^{87}Sr/^{86}Sr$ sample values in this study, modern and historic human activity should always be born in mind when seeking to apply modern datasets to the study of past landscape use (Maurer et al., 2012; Thomsen and Andreasen, 2019).

CONCLUSIONS

The results of this study confirm the consistency between plant and snail $^{87}Sr/^{86}Sr$ values with lithological unit and soil $^{87}Sr/^{86}Sr$ values observed in other studies. While no obvious impact of fertilizers or other modern contaminants on the samples included within this study could be discerned, we note these remain an ongoing concern for bioavailability studies. In the current study, plants appeared to be a more reliable analyte to describe $^{87}Sr/^{86}Sr$ bioavailability than snails. Results also highlight that sampling should ideally not only focus on one plant category but should integrate plants with different root systems/root depths in order to capture the bulk soil variability of any particular area. These data also serve to emphasize that dietary composition, even of type of plant consumed, could, theoretically, contribute to strontium isotope variability in the tissues of local humans or animals, and highlights the need for experimental studies.

In light of the data explored here, we also argue that sampling strategies in bioavailability studies should account for spatial heterogeneity in predicted bioavailable $^{87}Sr/^{86}Sr$ distribution, and sampling should ideally be more intensive in areas where high variability in bioavailable $^{87}Sr/^{86}Sr$ values is expected. This may, in many circumstances, be predictable based on lithological maps (e.g., areas with lithologies of more heterogeneous composition could be sampled more intensively than homogeneous deposits). Our results also demonstrate that the integration of new regional datasets into already existing datasets can improve overall isoscape accuracy and refine prediction at the local scale. Such datasets can in turn then be included in broader scale studies (e.g., Bataille et al., 2018), although we note that the integration of multiple data sources from different locations face disparity in sampling methods and analyses. While far from being a proposal for a unified framework of sampling, we suggest the sampling of plants of differing root depth at each sampling location (incorporating grasses, shrub and tree leaves, for example) can be a practical step in better representing variability in bioavailable $^{87}Sr/^{86}Sr$ on a local level.

DATA AVAILABILITY STATEMENT

The original contributions presented in the study are included in the article/**Supplementary Material**, further inquiries can be directed to the corresponding author/s.

AUTHOR CONTRIBUTIONS

KB designed the study, undertook field sampling, sample processing and laboratory analyses (plants), and wrote the initial draft of manuscript with ML. ML designed data treatment and undertook data analyses, including all statistics and produced all images. MW, IM, and RG undertook field sampling and laboratory analyses and isotope measurements (soils). MM and SW undertook identifications of malacofauna and plants respectively. KJ undertook isotope measurements (snails and plants). All the authors provided critical review of and contributions to subsequent versions of the manuscript.

FUNDING

This research was funded by the Max Planck Society and a Leverhulme Trust grant to KB (RPG-2017-410), with additional support from Australian Research Council Discovery grants DP0664144 and DP110101417 to RG. KJ thanks the ERC ARCHEIS 803676, and IM thanks Australian Research Council Discovery Early Career Award (DE160100703), for salary support during production of this manuscript.

ACKNOWLEDGMENTS

We thank Annabell Reiner and Sven Steinbrenner (MPI-EVA) for technical and practical support with preparation and analysis of samples. We thank the La Ferrassie Team for support during field sampling and project development, especially Harold Dibble, Shannon McPherron (MPI-EVA), Teresa Steele (UC Davies), Vera Aldeias (MPI-EVA, University of Algarve), Paul Goldberg (University of Wollongong, University Tübingen), Dennis Sandgathe (Simon Fraser University, University of Pennsylvania), Alain Turq (Musée national de Préhistoire, CNRS), and Jean-Jacques Hublin (MPI-EVA), as well as Mike Richards (SFU). Special thanks to Daphne Katranides and Aaron Katranides. We also thank the editor (TP) and two reviewers whose constructive comments greatly improved this manuscript.

SUPPLEMENTARY MATERIAL

The Supplementary Material for this article can be found online at: https://www.frontiersin.org/articles/10.3389/fevo.2020.579473/full#supplementary-material

REFERENCES

Aguzzoni, A., Bassi, M., Robatscher, P., Scandellari, F., Tirler, W., and Tagliavini, M. (2019). Intra- and intertree variability of the $^{87}Sr/^{86}Sr$ ratio in apple orchards and its correlation with the soil $^{87}Sr/^{86}Sr$ ratio. *J. Agricult. Food Chem.* 67, 5728–5735. doi: 10.1021/acs.jafc.9b01082

Bahn, P. (1977). Seasonal migration in South-west France during the late glacial period. *J. Arch. Sci.* 4, 245–257. doi: 10.1016/0305-4403(77)90092-9

Balasse, M., Ambrose, S. H., Smith, A. B., and Price, T. D. (2002). The seasonal mobility model for prehistoric herders in the South-western Cape of South Africa assessed by isotopic analysis of sheep tooth enamel. *J. Arch. Sci.* 29, 917–932. doi: 10.1006/jasc.2001.0787

Balter, V., Braga, J., Télouk, P., and Thackeray, J. F. (2012). Evidence for dietary change but not landscape use in South African early hominins. *Nature* 489, 558–560. doi: 10.1038/nature11349

Bataille, C. P., and Bowen, G. J. (2012). Mapping $^{87}Sr/^{86}Sr$ variations in bedrock and water for large scale provenance studies. *Chem. Geol.* 304–305, 39–52. doi: 10.1016/j.chemgeo.2012.01.028

Bataille, C. P., Brennan, S. R., Hartmann, J., Moosdorf, N., Wooller, M. J., and Bowen, G. J. (2014). A geostatistical framework for predicting variations in strontium concentrations and isotope ratios in Alaskan rivers. *Chem. Geol.* 389, 1–15. doi: 10.1016/j.chemgeo.2014.08.030

Bataille, C. P., von Holstein, I. C. C., Laffoon, J. E., Willmes, M., Liu, X.-M., and Davies, G. R. (2018). A bioavailable strontium isoscape for Western Europe: A machine learning approach. *PLoS ONE* 13:e0197386. doi: 10.1371/journal.pone.0197386

Bates, D., Mächler, M., Bolker, B., and Walker, S. (2015). Fitting linear mixed-effects models using lme4. *2015* 67, 48. doi: 10.18637/jss.v067.i01

Beard, B. L., and Johnson, C. M. (2000). Strontium isotope composition of skeletal material can determine the birth place and geographic mobility of humans and animals. *J. Foren. Sci.* 45, 1049–1061. doi: 10.1520/JFS14829J

Bentley, R. A. (2006). Strontium isotopes from the earth to the archaeological skeleton: a review. *J. Arch. Method Theor.* 13, 135–187. doi: 10.1007/s10816-006-9009-x

Bentley, R. A., and Knipper, C. (2005). *Transhumance at the Early Neolithic Settlement at Vaihingen (Germany)*. Antiquity 79, Online Project Gallery.

Bentley, R. A., Pietrusewsky, M., Douglas, M. T., and Atkinson, T. C. (2005). Matrilocality during the prehistoric transition to agriculture in Thailand? *Antiquity* 79, 865–881. doi: 10.1017/S0003598X00115005

Britton, K., Grimes, V., Niven, L., Steele, T., McPherron, S., Soressi, M., et al. (2011). Strontium isotope evidence for migration in late Pleistocene Rangifer: implications for Neanderthal hunting strategies at the Middle Palaeolithic site of Jonzac, France. *J. Hum. Evol.* 61, 176–185. doi: 10.1016/j.jhevol.2011.03.004

Burnham, K. P., and Anderson, D. R. (2002). *A Practical Information-Theoretic Approach. Model Selection and Multimodel Inference. 2nd ed.* New York, NY: Springer.

Comar, C. L. (1963). "Some over-all aspects of strontium-calcium discrimination," in *The Transfer of Calcium and Strontium Across Biological Membranes*, ed R. H. Wasserman (London: New York, NY: Academic Press), 405–417.

Copeland, S. R., Sponheimer, M., de Ruiter, D. J., Lee-Thorp, J. A., Codron, D., le Roux, P. J., et al. (2011). Strontium isotope evidence for landscape use by early hominins. *Nature* 474, 76–78. doi: 10.1038/nature10149

Copeland, S. R., Sponheimer, M., le Roux, P. J., Grimes, V., Lee-Thorp, J. A., de Ruiter, D. J., et al. (2008). Strontium isotope ratios ($^{87}Sr/^{86}Sr$) of tooth enamel: comparison of solution and laser ablation multicollector inductively coupled plasma mass spectrometry methods. *Rap. Commun. Mass Spectr.* 22, 3187–3194. doi: 10.1002/rcm.3717

Copernicus Land Monitoring Service. (2018). *Copernicus Land Monitoring Service*. European Environment Agency (EEA). Available online at: https://land.copernicus.eu/

Cossignani, T., and Cossignani, V. (1995). *Atlante delle Conchiglie Terrestri e Dulciacquicole Italiane*. Ancona: L'Informatore Piceno.

Deniel, C., and Pin, C. (2001). Single-stage method for the simultaneous isolation of lead and strontium from silicate samples for isotopic measurements. *Anal. Chim. Acta* 426, 95–103. doi: 10.1016/S0003-2670(00)01185-5

Ericson, J. E. (1985). Strontium isotope characterization in the study of prehistoric human ecology. *J. Hum. Evol.* 14, 503–514. doi: 10.1016/S0047-2484(85)80029-4

Evans, J. A., Mee, K., Chenery, C. A., Cartwright, C. E., Lee, K. A., and Marchant, A. P. (2018). *User Guide for the Biosphere Isotope Domains GB (Version 1) Dataset and Web Portal.* Nottingham: British Geological Survey, 21.

Evans, J. A., Montgomery, J., Wildman, G., and Boulton, N. (2010). Spatial variations in biosphere $^{87}Sr/^{86}Sr$ in Britain. *J. Geol. Soc.* 167, 1–4. doi: 10.1144/0016-76492009-090

Goemaere, E., Honings, J., Jungels, C., Golitko, M., Degryse, P., and Schneider, J. (2013). Discerning geological and geographical sources of Belgian Upper Paleolithic fluorites by rare earth elements and Sr-isotopic geochemistry. *J. Arch. Sci.* 40, 2892–2901. doi: 10.1016/j.jas.2013.02.029

Gordon, B. C. (1988). *Of Men and Reindeer Herds in French Magdalenian Prehistory*. Oxford: British Archaeological Reports (International Series 390). doi: 10.30861/9780860545040

Gräler, B., Pebesma, E., and Heuvelink, G. (2016). Spatio-Temporal Interpolation using gstat. *R J.* 8:204–18. doi: 10.32614/RJ-2016-014

Hartman, G., and Richards, M. (2014). Mapping and defining sources of variability in bioavailable strontium isotope ratios in the Eastern Mediterranean. *Geochim. Cosmochim. Acta* 126, 250–264. doi: 10.1016/j.gca.2013.11.015

Hegg, J. C., Kennedy, B. P., and Fremier, A. K. (2013). Predicting strontium isotope variation and fish location with bedrock geology: understanding the effects of geologic heterogeneity. *Chem. Geol.* 360–361, 89–98. doi: 10.1016/j.chemgeo.2013.10.010

Joannes-Boyau, R., Adams, J. W., Austin, C., Arora, M., Moffat, I., Herries, A. I. R., et al. (2019). Elemental signatures of *Australopithecus africanus* teeth reveal seasonal dietary stress. *Nature* 572, 112–115. doi: 10.1038/s41586-019-1370-5

Johnson, C. M., and Fridrich, C. J. (1990). Nonmonotonic Chemical and O, Sr, Nd, and Pb Isotope Zonations and Heterogeneity in the Mafic to Silicic-Composition Magma Chamber of the Grizzly Peak Tuff, Colorado. *Contrib. Mineral. Petrol.* 105, 677–690. doi: 10.1007/BF00306533

Johnson, L., Montgomery, J., Evans, J., and Hamilton, E. (2019). Contribution of strontium to the human diet from querns and millstones: an experiment in digestive strontium isotope uptake. *Archaeometry* 61, 1366–1381. doi: 10.1111/arcm.12485

Julien, M.-A., Bocherens, H., Burke, A., Drucker, D., Patou-Mathis, M., Krotova, O., et al. (2012). Were European steppe bison migratory? 18O, 13C and Sr intra-tooth isotopic variations applied to a palaeoethological reconstruction. *Q. Int.* 271:106–119. doi: 10.1016/j.quaint.2012.06.011

Kerney, M. P. (1999). *Atlas of Land and Freshwater Molluscs of Britain and Ireland*. Colchester: Harley Books.

Knudson, K. J., Price, T. D., Buikstra, J. E., and Blom, D. E. (2004). The use of strontium isotope analysis to investigate tiwanaku migration and mortuary ritual in Bolivia and Peru. *Archaeometry* 46, 5–18. doi: 10.1111/j.1475-4754.2004.00140.x

Ladegaard-Pedersen, P., Achilleos, M., Dörflinger, G., Frei, R., Kristiansen, K., and Frei, K. M. (2020). A strontium isotope baseline of Cyprus. Assessing the use of soil leachates, plants, groundwater and surface water as proxies for the local range of bioavailable strontium isotope composition. *Sci Total Environ.* 708, 134714. doi: 10.1016/j.scitotenv.2019.134714

Laffoon, J. E., Plomp, E., Davies, G. R., Hoogland, M. L. P., and Hofman, C. L. (2015). The movement and exchange of dogs in the prehistoric caribbean: an isotopic investigation. *Int. J. Osteoarchaeol.* 25, 454–465. doi: 10.1002/oa.2313

Leach, S., Lewis, M., Chenery, C., Müldner, G., and Eckardt, H. (2009). Migration and diversity in Roman Britain: a multidisciplinary approach to the identification of immigrants in Roman York, England. *Am. J. Phys. Anthropol.* 140, 546–561. doi: 10.1002/ajpa.21104

Lewis, J., Pike, A. W. G., Coath, C. D., and Evershed, R. P. (2017). Strontium concentration, radiogenic ($^{87}Sr/^{86}Sr$) and stable (δ88Sr) strontium isotope systematics in a controlled feeding study. *Sci. Technol. Archaeol. Res.* 3, 45–57. doi: 10.1080/20548923.2017.1303124

Lugli, F., Cipriani, A., Capecchi, G., Ricci, S., Boschin, F., Boscato, P., et al. (2019). Strontium and stable isotope evidence of human mobility strategies across the Last Glacial Maximum in southern Italy. *Nat. Ecol. Evol.* 3, 905–911. doi: 10.1038/s41559-019-0900-8

Maurer, A.-F., Galer, S. J. G., Knipper, C., Beierlein, L., Nunn, E. V., Peters, D., et al. (2012). Bioavailable $^{87}Sr/^{86}Sr$ in different environmental samples - effects of anthropogenic contamination and implications for isoscapes in past migration studies. *Sci. Total Environ.* 433, 216–229. doi: 10.1016/j.scitotenv.2012.06.046

Millour, S., Noël, L., Chekri, R., Vastel, C., Kadar, A., Sirot, V., et al. (2012). Strontium, silver, tin, iron, tellurium, gallium, germanium, barium and vanadium levels in foodstuffs from the Second French Total Diet Study. *J. Food Comp. Anal.* 25, 108–129. doi: 10.1016/j.jfca.2011.10.004

Moffat, I. (2013). *Spatially Resolved Strontium Isotope Micro-Analysis of Lower and Middle Palaeolithic Fauna from Archaeological Sites in Israel and Southern France*. Unpublished Ph.D. Thesis: The Australian National University.

Montgomery, J. (2010). Passports from the past: Investigating human dispersals using strontium isotope analysis of tooth enamel. *Ann. Hum. Biol.* 37, 325–346. doi: 10.3109/03014461003649297

Négrel, P. (1999). Geochemical study of a granitic area - the margeride mountains, france: chemical element behavior and $^{87}Sr/^{86}Sr$ constraints. *Aquat. Geochem.* 5, 125–165. doi: 10.1023/A:1009625412015

Négrel, P., Guerrot, C., and Millot, R. (2007). Chemical and strontium isotope characterization of rainwater in France: influence of sources and hydrogeochemical implications. *Isot. Environ. Health Stud.* 43, 179–196. doi: 10.1080/10256010701550773

Négrel, P., Petelet-Giraud, E., Barbier, J., and Gautier, E. (2003). Surface water-groundwater interactions in an alluvial plain: chemical and isotopic systematics. *J. Hydrol.* 277, 248–267. doi: 10.1016/S0022-1694(03)00125-2

Ohta, T., and Saeki, I. (2020). Comparisons of calcium sources between arboreal and ground-dwelling land snails: implication from strontium isotope analyses. *J. Zool.* 311, 137–144. doi: 10.1111/jzo.12767

Pellegrini, M., Donahue, R. E., Chenery, C., Evans, J., Lee-Thorp, J., Montgomery, J., et al. (2008). Faunal migration in late-glacial central Italy: implications for human resource exploitation. *Rapid Commun. Mass Spectr.* 22, 1714–1726. doi: 10.1002/rcm.3521

Pierson-Wickmann, A.-C., Aquilina, L., Weyer, C., Molénat, J., and Lischeid, G. (2009). Acidification processes and soil leaching influenced by agricultural practices revealed by strontium isotopic ratios. *Geochim. Cosmochim. Acta* 73, 4688–4704. doi: 10.1016/j.gca.2009.05.051

Poszwa, A., Ferry, B., Dambrine, E., Pollier, B., Wickman, T., Loubet, M., et al. (2004). Variations in bioavailable Sr concentration and $^{87}Sr/^{86}Sr$ ratio in boreal forest ecosystems: Role of biocycling, mineral weathering and depth of rooth uptake. *Biogeochemistry* 67, 1–20. doi: 10.1023/B:BIOG.0000015162.12857.3e

Price, T. D., Meiggs, D., Weber, M.-J., and Pike-Tay, A. (2017). The migration of Late Pleistocene reindeer: isotopic evidence from northern Europe. *Arch. Anthropol. Sci.* 9, 371–394. doi: 10.1007/s12520-015-0290-z

Prohaska, T., Wenzel, W. W., and Stingeder, G. (2005). ICP-MS-based tracing of metal sources and mobility in a soil depth profile via the isotopic variation of Sr and Pb. *Int. J. Mass Spectr.* 242, 243–250. doi: 10.1016/j.ijms.2004.11.028

R Core Team. (2019). *R: A Language and Environment for Statistical Computing*. Vienna: R Foundation for Statistical Computing. Available online at: http://www.R-project.org/.

Raiber, M., Webb, J. A., and Bennetts, D. A. (2009). Strontium isotopes as tracers to delineate aquifer interactions and the influence of rainfall in the basalt plains of southeastern Australia. *J. Hydrol.* 367, 188–199. doi: 10.1016/j.jhydrol.2008.12.020

Richards, M. P., Harvati, K., Grimes, V., Smith, C., Smith, T., Hublin, J. J., et al. (2008). Strontium isotope evidence of Neanderthal mobility at the site of Lakonis, Greece using laser-ablation PIMMS. *J. Arch. Sci.* 35, 1251–1256. doi: 10.1016/j.jas.2007.08.018

Rose, F. (1989). *Colour Identification Guide to the Grasses, Sedges, Rushes and Ferns of the British Isles and North Western Europe*. London: Viking (Penguin Group).

Sillen, A., Hall, G., Richardson, S., and Armstrong, R. (1998). $^{87}Sr/^{86}Sr$ ratios in modern and fossil food-webs of the Sterkfontein Valley: Implications for early hominid habitat preference. *Geochim. Cosmochim. Acta* 62, 2463–2478. doi: 10.1016/S0016-7037(98)00182-3

Snoeck, C., Ryan, S., Pouncett, J., Pellegrini, M., Claeys, P., Wainwright, A. N., et al. (2020). Towards a biologically available strontium isotope baseline for Ireland. *Sci. Total Environ.* 712:136248. doi: 10.1016/j.scitotenv.2019.136248

Stace, C. A. (2010). *New Flora of the British Isles (Third Edition)*. Cambridge: Cambridge University Press.

Thomsen, E., and Andreasen, R. (2019). Agricultural lime disturbs natural strontium isotope variations: implications for provenance and migration studies. *Sci. Adv.* 5:eaav8083. doi: 10.1126/sciadv.aav8083

Thornton, E. K. (2011). Reconstructing ancient Maya animal trade through strontium isotope ($^{87}Sr/^{86}Sr$) analysis. *J. Arch. Sci.* 38, 3254–3263. doi: 10.1016/j.jas.2011.06.035

Vanhaeren, M., d'Errico, F., Billy, I., and Grousset, F. (2004). Tracing the source of Upper Palaeolithic shell beads by strontium isotope dating. *J. Arch. Sci.* 31, 1481–1488. doi: 10.1016/j.jas.2004.03.011

Williamson, P., and Cameron, R. A. D. (1976). Natural diet of the landsnail cepaea nemoralis. *Oikos* 27, 493–500. doi: 10.2307/3543468

Willmes, M., Bataille, C. P., James, H. F., Moffat, I., McMorrow, L., Kinsley, L., et al. (2018). Mapping of bioavailable strontium isotope ratios in France for archaeological provenance studies. *Appl. Geochem.* 90, 75–86. doi: 10.1016/j.apgeochem.2017.12.025

Willmes, M., Kinsley, L., Moncel, M. H., Armstrong, R. A., Aubert, M., Eggins, S., et al. (2016). Improvement of laser ablation *in situ* micro-analysis to identify diagenetic alteration and measure strontium isotope ratios in fossil human teeth. *J. Arch. Sci.* 70, 102–116. doi: 10.1016/j.jas.2016.04.017

Willmes, M., McMorrow, L., Kinsley, L., Armstrong, R., Aubert, M., Eggins, S., et al. (2014). The IRHUM (Isotopic Reconstruction of Human Migration) database - bioavailable strontium isotope ratios for geochemical fingerprinting in France. *Earth Syst. Sci. Data* 6, 117–122. doi: 10.5194/essd-6-117-2014

Zuur, A. F., Ieno, E. N., and Elphick, C. S. (2010). A protocol for data exploration to avoid common statistical problems. *Methods Ecol. Evol.* 1, 3–14. doi: 10.1111/j.2041-210X.2009.00001.x

Conflict of Interest: The authors declare that the research was conducted in the absence of any commercial or financial relationships that could be construed as a potential conflict of interest.

frontiers in Ecology and Evolution

ORIGINAL RESEARCH
published: 17 December 2020
doi: 10.3389/fevo.2020.570032

Strontium and Oxygen Isotope Analyses Reveal Late Cretaceous Shark Teeth in Iron Age Strata in the Southern Levant

Thomas Tütken[1], Michael Weber[1], Irit Zohar[2,3], Hassan Helmy[4], Nicolas Bourgon[5], Omri Lernau[3], Klaus Peter Jochum[6] and Guy Sisma-Ventura[7]**

[1] *Institute of Geosciences, Johannes Gutenberg University of Mainz, Mainz, Germany,* [2] *Beit Margolin, Oranim Academic College, Kiryat Tivon, Israel,* [3] *Zinman Institute of Archaeology, University of Haifa, Haifa, Israel,* [4] *Department of Geology, Minia University, Minia, Egypt,* [5] *Max Planck Institute for Evolutionary Anthropology, Leipzig, Germany,* [6] *Department of Climate Geochemistry, Max Planck Institute for Chemistry, Mainz, Germany,* [7] *Oceanographic and Limnological Research, Haifa, Israel*

Skeletal remains in archaeological strata are often assumed to be of similar ages. Here we show that combined Sr and O isotope analyses can serve as a powerful tool for assessing fish provenance and even for identifying fossil fish teeth in archaeological contexts. For this purpose, we established a reference Sr and O isotope dataset of extant fish teeth from major water bodies in the Southern Levant. Fossil shark teeth were identified within Iron Age cultural layers dating to 8–9th century BCE in the City of David, Jerusalem, although the reason for their presence remains unclear. Their enameloid $^{87}Sr/^{86}Sr$ and $\delta^{18}O_{PO4}$ values [0.7075 ± 0.0001 (1 SD, n = 7) and 19.6 ± 0.9‰ (1 SD, n = 6), respectively], are both much lower than values typical for modern marine sharks from the Mediterranean Sea [0.7092 and 22.5–24.6‰ (n = 2), respectively]. The sharks' $^{87}Sr/^{86}Sr$ are also lower than those of rain- and groundwater as well as the main soil types in central Israel (≥0.7079). This indicates that these fossil sharks incorporated Sr ($^{87}Sr/^{86}Sr \approx 0.7075$) from a marine habitat with values typical for Late Cretaceous seawater. This scenario is in line with the low shark enameloid $\delta^{18}O_{PO4}$ values reflecting tooth formation in the warm tropical seawater of the Tethys Ocean. Age estimates using $^{87}Sr/^{86}Sr$ stratigraphy place these fossil shark teeth at around 80-million-years-old. This was further supported by their taxonomy and the high dentine apatite crystallinity, low organic carbon, high U and Nd contents, characteristics that are typical for fossil specimens, and different from those of archaeological Gilthead seabream (*Sparus aurata*) teeth from the same cultural layers and another Chalcolithic site (Gilat). Chalcolithic and Iron Age seabream enameloid has seawater-like $^{87}Sr/^{86}Sr$ of 0.7091 ± 0.0001 (1 SD, n = 6), as expected for modern marine fish. Fossil shark and archaeological Gilthead seabream teeth both preserve original, distinct enameloid $^{87}Sr/^{86}Sr$ and $\delta^{18}O_{PO4}$ signatures reflecting their different aquatic habitats. Fifty percent of the analysed Gilthead seabream teeth derive from hypersaline seawater, indicating that these seabreams were exported from the hypersaline Bardawil Lagoon in Sinai (Egypt) to the Southern Levant since the Iron Age period and possibly even earlier.

Keywords: strontium isotopes, oxygen isotopes, Nile, Selachii, Teleostei, fish provenance, fossil shark teeth, enameloid

OPEN ACCESS

Edited by:
Brooke Crowley, University of Cincinnati, United States

Reviewed by:
Laszlo Kocsis, Universiti Brunei Darussalam, Brunei
Malte Willmes, University of California, Santa Cruz, United States

****Correspondence:***
Thomas Tütken
tuetken@uni-mainz.de
Guy Sisma-Ventura
guy.siv@ocean.org.il;
guysis132@gmail.com

Specialty section:
This article was submitted to Paleoecology, a section of the journal Frontiers in Ecology and Evolution

Received: *05 June 2020*
Accepted: *10 November 2020*
Published: *17 December 2020*

Citation:
Tütken T, Weber M, Zohar I, Helmy H, Bourgon N, Lernau O, Jochum KP and Sisma-Ventura G (2020) Strontium and Oxygen Isotope Analyses Reveal Late Cretaceous Shark Teeth in Iron Age Strata in the Southern Levant. Front. Ecol. Evol. 8:570032. doi: 10.3389/fevo.2020.570032

HIGHLIGHTS

- Sr and O isotope reference dataset established for modern fish from the Levant.
- Fish origin inferred from coupled $^{87}Sr/^{86}Sr$ and $\delta^{18}O_{PO4}$ analysis.
- Iron Age fish assemblage from the City of David, Jerusalem, bears fossil shark teeth.
- Late Cretaceous shark teeth identified in Iron age strata by Sr and O isotopes.

INTRODUCTION

Past fish habitats have traditionally been reconstructed based on taxonomic identification of fish remains recovered in archaeological sites (e.g., Wheeler and Jones, 1989; Zohar and Biton, 2011; Zohar, 2017). Recently, stable isotope analyses of fish bioapatite have also been used as palaeoenvironmental proxies for fish habitat and provenance (e.g., Dufour et al., 2007; Otero et al., 2011; Leuzinger et al., 2015; Sisma-Ventura et al., 2015, 2018, 2019; Fetner and Iwaszczuk, 2020). In this study, we analyse the Sr and O isotope composition of teeth from modern fish derived from different marine and freshwater bodies in the Levant to provide a reference dataset for assessing the provenance of ancient fish teeth from Chalcolithic and Iron Age cultural layers in Israel.

The Use of Strontium and Oxygen Isotopes as Provenance Proxies for Fish

The strontium isotope composition ($^{87}Sr/^{86}Sr$) of the well-preserved bioapatite of fish tooth enameloid has been widely used as a chemostratigraphic dating method for marine sediments (e.g., Ingram, 1995; Kocsis et al., 2009; Harrell et al., 2016) as a proxy to infer the palaeosalinity levels of oceanic basins and brackish water bodies (e.g., Schmitz et al., 1991, 1997; Bryant et al., 1995; Reinhardt et al., 1998; Kocsis et al., 2009), as well as for tracing past freshwater habitat use in sharks (e.g., Fischer et al., 2013) and to track their migration from the marine realm into fresh water systems (Kocsis et al., 2007, 2015). This is possible because the $^{87}Sr/^{86}Sr$ of ambient (sea)water is incorporated into the bioapatite of the teeth of Elasmobranchii (subclass of cartilaginous fish) and Teleostei (bony fish) *in vivo*, without any apparent measurable isotope fractionation (Vennemann et al., 2001). Marine fish tooth enameloid thus has a Sr isotope composition that reflects seawater $^{87}Sr/^{86}Sr$, which today is a globally constant value of 0.70918 (Hodell et al., 1990; Mokadem et al., 2015; McArthur et al., 2020), but has varied over geological time (i.e., Phanerozoic) between values of around 0.7072–0.7092 (McArthur et al., 2020). Across the last glacial-interglacial cycle the seawater $^{87}Sr/^{86}Sr$ did not deviate measurably from the modern-day value ($^{87}Sr/^{86}Sr$ = 0.7091792 ± 0.00000212 SE, n = 17; Mokadem et al., 2015). In contrast, the $^{87}Sr/^{86}Sr$ of Sr dissolved in surface freshwater bodies (rivers and lakes) depends both on the Sr isotope composition of the local bedrock (age and lithology; e.g., Goldstein and Jacobsen, 1987) and groundwater and precipitation (Herut et al., 1993; Chadwick et al., 1999; Vengosh et al., 1999) in the drainage area of rivers and lakes. Freshwater will thus have $^{87}Sr/^{86}Sr$ below or above the contemporaneous global seawater value (Dufour et al., 2007). The $^{87}Sr/^{86}Sr$ in fish teeth can be used as a proxy to distinguish between freshwater and marine habitats (**Figure 1A**; e.g., Schmitz et al., 1997; Kocsis et al., 2007, 2014; Tütken et al., 2011; Fischer et al., 2013), whereas for brackish water bodies the $^{87}Sr/^{86}Sr$ depends on the sea-to-freshwater mixing ratio (Bryant et al., 1995; Reinhardt et al., 1998).

The phosphate oxygen isotope composition ($^{18}O/^{16}O$ expressed as $\delta^{18}O_{PO4}$ value) of bony fish and shark (we refer to these collectively as 'fish' elsewhere in the paper) tooth enameloid has been used to reconstruct past seawater temperatures (e.g., Kolodny and Raab, 1988; Kolodny and Luz, 1991; Pucéat et al., 2003), seawater salinity changes (Zacke et al., 2009; Leuzinger et al., 2015) and past aquatic fish habitats such as rivers, lakes, and lagoons (Kolodny et al., 1983; Dufour et al., 2007; Klug et al., 2010; Otero et al., 2011; Kocsis et al., 2015; Leuzinger et al., 2015; Sisma-Ventura et al., 2015, 2018, 2019). Fish bones and teeth are mineralised in oxygen isotope equilibrium with their body fluids. The body fluids of fish have the same oxygen isotope composition as the ambient water ($\delta^{18}O_{Water}$) in which they reside and the body (i.e., tooth formation) temperature of fish is identical to the ambient water temperature (**Figure 1A**). Thus, the bioapatite $\delta^{18}O_{PO4}$ values of fish bones and teeth are controlled by the local $\delta^{18}O_{Water}$ value and water temperature according to the temperature-dependent water-phosphate oxygen isotope fractionation (Longinelli and Nuti, 1973; Kolodny et al., 1983; Pucéat et al., 2010; Lécuyer et al., 2013). The $\delta^{18}O_{Water}$ values of the modern oceans are ≈ 0.0‰ in tropical and subtropical regions and are more positive in evaporative basins such as the Mediterranean Sea (≈ 1.5‰), while fresh- and meltwater influx at high latitudes results in negative surface water values (between −2.0 and −4.0‰; Rohling, 2007).

The $^{87}Sr/^{86}Sr$ of rivers and lakes is controlled by dissolved Sr released from the weathering of bedrock in catchment areas (Goldstein and Jacobsen, 1987; Woodward et al., 2015). This enables us to distinguish fish from bodies of freshwater draining bedrocks of different ages and lithologies, which have distinct $^{87}Sr/^{86}Sr$ (**Figure 1A**). Brackish water, which is a mixture of seawater and freshwater, will have variable $^{87}Sr/^{86}Sr$, depending on the mixing ratio of the waters, Sr content, and the $^{87}Sr/^{86}Sr$ of the freshwater input (e.g., Bryant et al., 1995; Reinhardt et al., 1998; Hobbs et al., 2019). Brackish water is typical in estuaries of rivers and coastal wetlands.

Combined Sr and O isotope analysis of fish remains therefore represents a promising geochemical approach for assessing fish provenance in archaeological and palaeontological contexts. In this study we establish a reference dataset of Sr and O isotope values by analysing the teeth of modern fish from different water bodies in Egypt and Israel. We then use this reference dataset to reconstruct past fish habitats by analysing fish remains from Chalcolithic (Gilat) and Iron Age (City of David, Jerusalem) archaeological sites in the Southern Levant.

Fish as a Commodity

Identification of fish trade in antiquity is traditionally based on the presence of "exotic" fish remains in archaeological sites, which are distantly located from the original habitat of the fish (Davis,

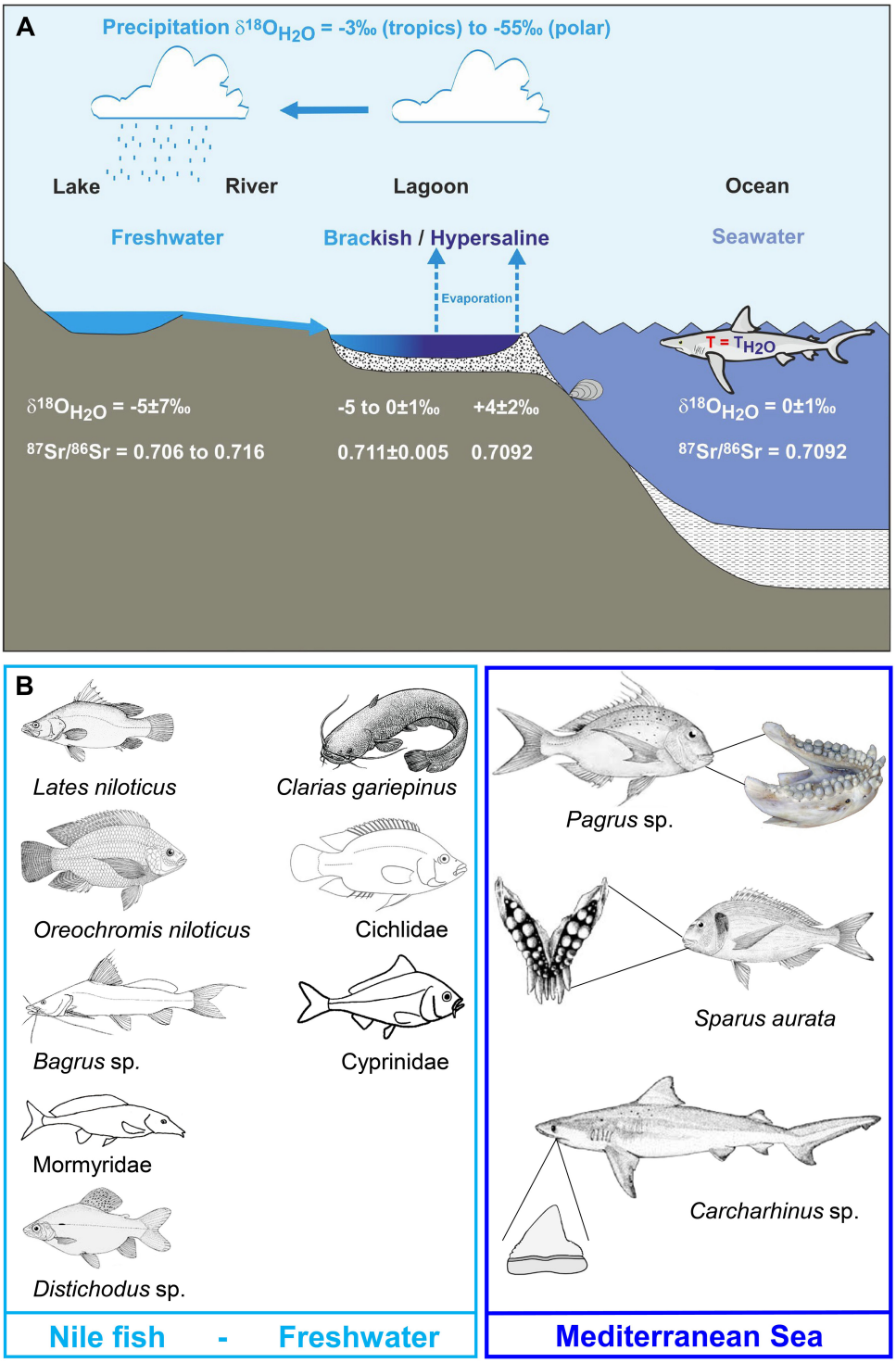

FIGURE 1 | Illustration of the environmental effects on the isotope signatures of water bodies and the fish species living in these aquatic habitats in the Southern Levant. **(A)** Schematic overview of the hydrological cycle affecting the $^{87}Sr/^{86}Sr$ and the $\delta^{18}O_{Water}$ of marine to freshwater bodies that represent typical fish habitats. The $^{87}Sr/^{86}Sr$ and $\delta^{18}O_{Water}$ values for assigning the major water bodies in Egypt and the Southern Levant to such habitat types are provided at the bottom of the figure. Note that Mediterranean seawater has a value of 1.6 ± 0.3‰ (Sisma-Ventura et al., 2016) but the same $^{87}Sr/^{86}Sr$ as global seawater. The Sr and O isotope composition of these aquatic fish habitats is controlled by the mixing of marine and freshwater which both have distinct $^{87}Sr/^{86}Sr$ and $\delta^{18}O_{Water}$ as well as by additional effects of evaporation (i.e., ^{18}O-enrichment) which only affect $\delta^{18}O_{Water}$ values. **(B)** Key freshwater and marine staple food fish (by family and species) frequently used as indicators of their habitats: Nilotic fish, Southern Levant fresh water fish, and southeast Mediterranean area (Fish belonging to Claridae, Cichlidae and Cyprinidae may represent Nilotic habitat or other freshwater habitats in the Southern Levant).

1985; Van Neer et al., 2005). In the Eastern Mediterranean region, several key species have been identified as indicators of fish trade as they occur only in one of three main aquatic habitats: the Nile (Egypt), Eastern Mediterranean and the Red Sea (**Figure 1B**). For example, Nilotic species such as *Lates niloticus* (Latidae, Nile perch), *Oreochromis niloticus* (Cichlidae; Nile tilapia), *Bagrus* sp. (Bagridae, bagrid catfish) (Van Neer et al., 1997, 2004, 2005, 2015; Van Neer and Depraetere, 2005) are considered typical indicators of fish trade from Egypt to the Southern Levant. Recently, stable isotope studies of archaeological fish teeth demonstrated that Gilthead seabream (Sparidae; *Sparus aurata*) were also exported from Egypt to this area of modern-day Israel as they derive from the hypersaline Bardawil Lagoon in northern Sinai (**Figure 2A**) and not from local fishing activity (Sisma-Ventura et al., 2015, 2018, 2019). The occurrence of imported fish in archaeological layers demonstrates that Nilotic and lagoonal fish were common trade goods from the Bronze Age onwards (Van Neer and Ervynck, 2004; Van Neer et al., 2004, 2005, 2015; Raban-Gerstel et al., 2008; Sisma-Ventura et al., 2015, 2018, 2019; Zohar and Artzy, 2019).

However, most of these studies have concentrated on bony fish, while shark (Elasmobranchii) exploitation and trade routes have received little attention. In general, Elasmobranchii (Chondrichthyes) do not preserve well because, with the exception of their teeth, dermal denticles, spines and vertebrae centra, the rest of their skeleton is composed of cartilage (Wheeler and Jones, 1989; Rick et al., 2002). Teeth and vertebrae centra are typically the main shark remains found in archaeological contexts. While shark vertebrae centra are commonly found and usually well preserved, shark teeth are rarely recovered, even when the soil is carefully sieved (**Table 1** and references therein). Interestingly, previous studies (Cione and Bonomo, 2003; Betts et al., 2012; Charpentier et al., 2020) determined that fossil shark teeth recovered from archaeological contexts have been employed as ornaments and tools, while shark vertebrae centra are only rarely identified as jewelry (Boulanger et al., 2020) and are usually interpreted as food remnants.

A review of published data on *ca.* 30,000 fish remains recovered in Holocene archaeological sites in the Southern Levant (**Table 1**) shows that 511 elasmobranch remains (sharks or rays), were recovered from 37 sites dated from the Pre-Pottery Neolithic A (*ca.* 10,000 BC) until the Crusader period (*ca.* 1099 AD). Most of the remains are vertebrae centra, and the earliest appearance of elasmobranchs occur in the Pre-Pottery Neolithic A (Sultanian) level of the inland site of Hatoula (Lernau and Lernau, 1994), and in the Pre-Pottery Neolithic C (PPNC) coastal sites of Ashkelon (Garfinkel et al., 2005; Lernau, 2008) and Atlit-Yam (Galili et al., 2004). Shark remains from the Late Chalcolithic are reported only from Namir road (Van den Brink et al., 2016) and from the Early Bronze Age layer of coastal Ashkelon Afridar (Lernau, 2004). Elasmobranch remains occur in most sites dating to the Late Bronze Age until the Crusader period, regardless of the sieving method applied. However, in all cases shark teeth are rarely recovered (8.4% of all shark remains), and out of 43 identified shark teeth, 38 (88%) were excavated in the City of David, Jerusalem (**Table 1**).

From an economic and dietary perspective, elasmobranchs (sharks and rays) are regarded as attractive food source since they are rich in protein, vitamin A, and oil. Additionally, their skin may be used as sandpaper and their spines and teeth (including

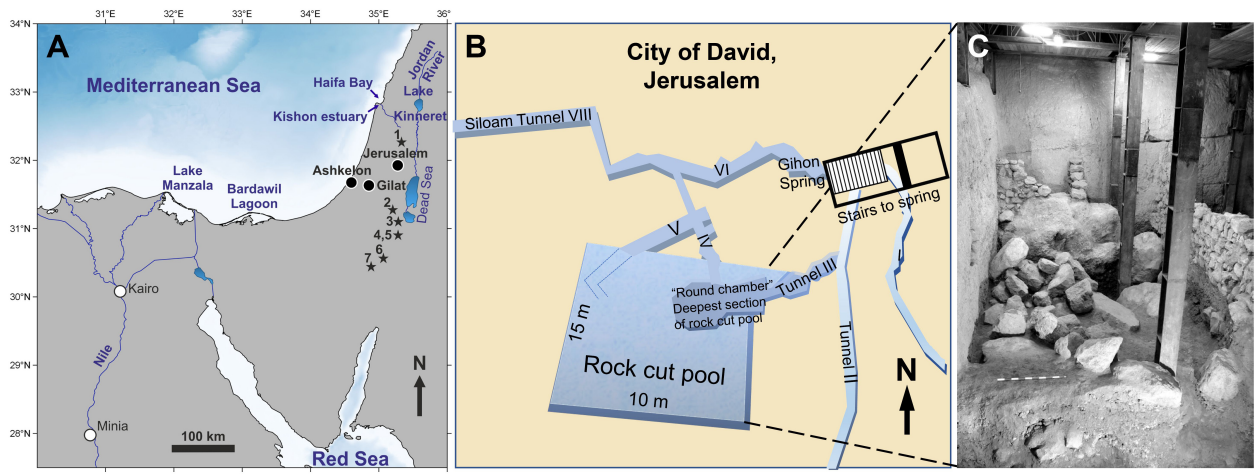

FIGURE 2 | (A) Map of the main water bodies and potential fish habitats of Egypt and the Southern Levant: Mediterranean Sea, Red Sea, upper Nile River, the brackish Lake Manzala on the Nile delta, the hypersaline Bardawil Lagoon in northern Sinai, and the freshwater Lake Kinneret and Jordan River, its main tributary, in northern Israel. These represent the key modern and past fish habitats from which we analysed modern fish samples to establish a Sr and O isotope reference dataset with which to assess the provenance of archaeological fish specimens. The ancient (i.e., fossil and historic) fish teeth were analysed from three different archaeological sites (black circles): Gilat (Chalcolithic), Ashkelon (Iron Age I), and Jerusalem/City of David (Iron Age I-II). Localities where fossil Cretaceous shark teeth were found in Israel (stars) after Kolodny and Raab (1988) and Retzler et al. (2013): **1** Ein Yabrud, **2** Letaot Mt., **3** Mishor Rotem, **4** HaMakhtesh HaKatan, **5** Ein Aqrabbim, **6** Hor Hahar, **7** Makhtesh Ramon. **(B)** Location map of the "Rock Cut Pool" adjacent to the Gihon spring, City of David, Jerusalem, and the nearby Siloam stream. **(C)** Photograph of the eastern wall of the "Rock Cut Pool" with the limestone boulders of the infill. Both **(B,C)** modified after Reich et al. (2007, 2008) and Sneh et al. (2010).

TABLE 1 | Elasmobranchii (sharks and rays) remains recovered from coastal and inland archaeological sites, by period, total number of fish remains recovered (NISP), number of cartilaginous fish, number of shark teeth and published reference.

Site	Period	Site location	Total NISP	Elasmobranchii		References
				NISP	Teeth	
Hatoula	Sultanian	Inland	110	1	0	Lernau and Lernau, 1994
Ashkelon	PPNC	Coastal	1753	19	0	Garfinkel et al., 2005
Atlit–Yam	PPNC	Coastal	3842	1	0	Zohar et al., 1994; Galili et al., 2004
Namir Road	Late Chalcolithic	Coastal	358	3	0	Van den Brink et al., 2016
Qatif	Chalcolithic	Coastal	129	14	0	Van den Brink et al., 2016
Gilat	Chalcolithic	Inland	36	3	0	Van den Brink et al., 2016
Ashkelon Afridar	EB	Coastal	54	1	0	Lernau, 2004
Tel Yoqneam	PN–IA II	Inland	192	4	1	Horwitz et al., 2005
Tel Kabri	MB IIb	Inland	2	1	0	Lernau, 2002a
Haruvit	LB	Inland	564	89	0	Van Neer et al., 2005
Tel Dor G 11–12	LB II	Coastal	356	6	0	Bartosiewicz et al., 2018
Tel Abu Hawam	LB II	Coastal	86	1	0	Zohar and Artzy, 2019
Tel Aphek	LB IIb	Coastal	4		0	Lernau, 2009
Lachish	LB III	Inland	752	70	0	Lernau and Golani, 2004
Timna	LB–IA	Inland	95	1	0	Lernau, 1988
Tel Dor D	IA–I	Coastal	755	29	0	Raban-Gerstel et al., 2008
el Ahwat	IA	Inland	88	0	0	Lernau, 2011a
Jerusalem Rock cut Pool	IA	Inland	10600	39	29	Reich et al., 2007, 2008
Tel Dor-G10	IA	Coastal	737	13	0	Bartosiewicz et al., 2018
Megido	IA	Inland	157	1	0	Lernau, 2000
Tel Dor-D	IA I–II	Coastal	209	19	0	Raban-Gerstel et al., 2008
Megido	IA	Inland	70	1	0	Lernau, 2000
Tel Dor-D	IA II	Coastal	80	5	0	Raban-Gerstel et al., 2008
Tel Harasim	IA II	Inland	18	2	0	Lernau, 2002b
Ashkelon Grid 38 and 50*	IA II–604 BC	Coastal	3890	154	4	Lernau, 2011b
Jerusalem Haophel	IA IIb	Inland	291	1	0	Horwitz and Lernau, 2018
Jerusalem Area G	586 BCE	Inland	3062	10	9	Lernau, 2015
Tel Harrasim	Persian	Inland	13	3	0	Lernau, 2002b
Tel Dor D	Persian	Coastal	179	8	0	Raban-Gerstel et al., 2008
Tel Dor D	Hellenistic	Coastal	119	2	0	Raban-Gerstel et al., 2008
City of David	Hellenistic–Byzantine	Inland	19	1	0	Reich et al., 2007; Lernau, 2015
Upper Zohar	Early Byzantine	Inland	727	1	0	Lernau, 1995
Tel Harrasim	Inland	Inland	2	1	0	Lernau, 2002b
Ceasarea Area LL	Byzantine	Coastal	137	1	0	Fradkin and Lernau, 2008
Ceasarea Area TP	Crusader	Coastal	118	2	0	Fradkin and Lernau, 2008
Ceasarea Area TP	Islamic	Coastal	166	1	0	Fradkin and Lernau, 2008
Tel Tanninim Area A2	Crusader	Coastal	648	3	0	Fradkin and Lernau, 2006

fossil teeth) can be used as raw material for tools (Borhegyi, 1961; Noe-Nygaard, 1971; Luomala, 1984; Rick et al., 2002). Therefore, despite rare preservation in archaeological sites, when recovered in cultural contexts shark teeth have been interpreted to reflect exploitation of coastal water bodies, lagoons and estuaries and shed new light on the habitat the sharks exploited and fishing practices in the past (Serena, 2005).

The Archaeological Assemblage

Large numbers of fish remains (>10,000) were recovered in the City of David, located outside and south of the southern walls of Jerusalem Old City (present day Silwan village) (Mazar, 2015). These remains were recovered from a structure located adjacent to the Gihon spring named "The Rock Cut Pool" and dated to the Iron Age II period, 8–7th century BCE (**Figure 2B**; Reich et al., 2007, 2008; De Groot and Fadida, 2011; Reich and Shukron, 2011). This large rectangular structure (15 × 10 m) cut into the limestone bedrock has straight, almost vertical rock walls, and during the Bronze Age period, prior to the operation of Siloam water Tunnel, was probably part of a complex underground water system allowing access to water during times of siege. During the end of the 9th century BCE/beginning of the 8th century BCE, it was converted to a private house. For this purpose, the pool was filled with large limestone boulders and soil (**Figure 2C**) in order to raise the floor-level by 3 m, and then sealed by the floor of the building above it. During excavation, the sediments beneath the

floor were dry and wet sieved through a 5 mm mesh. More than 10,000 fish remains, together with 6.5 tons of pottery and several hundred broken clay seals, known as "bullae" were recovered and dated to Iron Age IIB. The "bullae" were used to seal letters or packages and thus would have been broken and thrown away when the packages and letters were opened. Fish taxonomic composition included 14 families of fish, most of them (*ca.* 90%) originating from the Mediterranean Sea (mainly Sparidae and Mugilidae) as well as some from freshwater habitats (*ca.* 8.5%) including the Nile (Reich et al., 2007, 2008). Of these fish, 39 teeth and vertebrae centra belonged to Chondrichthyes fish (sharks and rays; **Table 1**). Several of these shark teeth were analysed for this study alongside *Sparus aurata* (Gilthead seabream) teeth from this site and from the Chalcolithic site of Gilat (5800–5500 BP; Rowan and Golden, 2009).

Shark Tooth Formation

Extant elasmobranchs (a subclass of cartilaginous fish that includes sharks, skates and rays) exhibit huge diversity in tooth shape. Their dentition is comprised of a large number of highly specialised single teeth that are organised in rows, and undergo continuous replacement throughout the life of the shark (**Figure 3A**; Debiais-Thibaud et al., 2007, 2015; Jernvall and Thesleff, 2012; Rasch et al., 2016; Meredith Smith et al., 2018). Tooth replacement and dentition patterns are distinctive for sharks and rays (Underwood et al., 2016; Meredith Smith et al., 2018). In sharks, only teeth in the outer row are fully upright and functional while replacement teeth lie posteriorly with their tips angled toward the rear. Tooth development and regeneration in Chondrichthyes is still poorly understood and characterised from a developmental and genetic perspective (Rasch et al., 2016). In different modern shark species, tooth replacement cycles vary and can be as rapid as 8–10 days, as in Lemon sharks (*Negaprion brevirostris*), 28 days as in Nurse sharks (*Ginglymostoma cirratum*), 38 days as in Leopard sharks (*Triakis semifasciata*) or as long as 150 days as in Sandy dogfish (*Scyliorhinus canicular*) (Moss, 1967; Reif et al., 1978; Luer et al., 1990; Botella et al., 2009 and references therein). Thus, while all sharks replace their teeth continuously, the timing of tooth formation and replacement varies depending on the species and age of the individual (younger sharks replace their teeth faster and thus more frequently).

The teeth of sharks and bony fish consist of a compact outer layer of hard, highly mineralised enameloid and an interior core of softer, less mineralised dentine (**Figure 3A**; Enault et al., 2015; Jambura et al., 2018, 2020). The tooth root is made up of porous osteodentine, a specific kind of dentine, which contains dentinal osteons and inter-osteonal tissue, and superficially resembles osteonal bone (Enault et al., 2015; Jambura et al., 2018, 2020). Enameloid is harder and has a lower solubility than hydroxylapatite characteristic of enamel, because the bioapatite often has a high fluorine content (i.e., fluorapatite; Miake et al., 1991; Suga et al., 1993; Enax et al., 2014). Thus, enameloid is highly resistant to diagenetic alteration following *post mortem* burial, even over geological time periods (Sharp et al., 2000). In Chondrichthyes, enameloid is composed of two units: a dense tissue of single crystallite enameloid (SCE), and an inner tissue of bundled crystallite enameloid (BCE) (**Figure 3A**; Enault et al., 2015). In this study, we sampled material from SCE, wherever possible, but in some cases sampled a mixture of both of these layers.

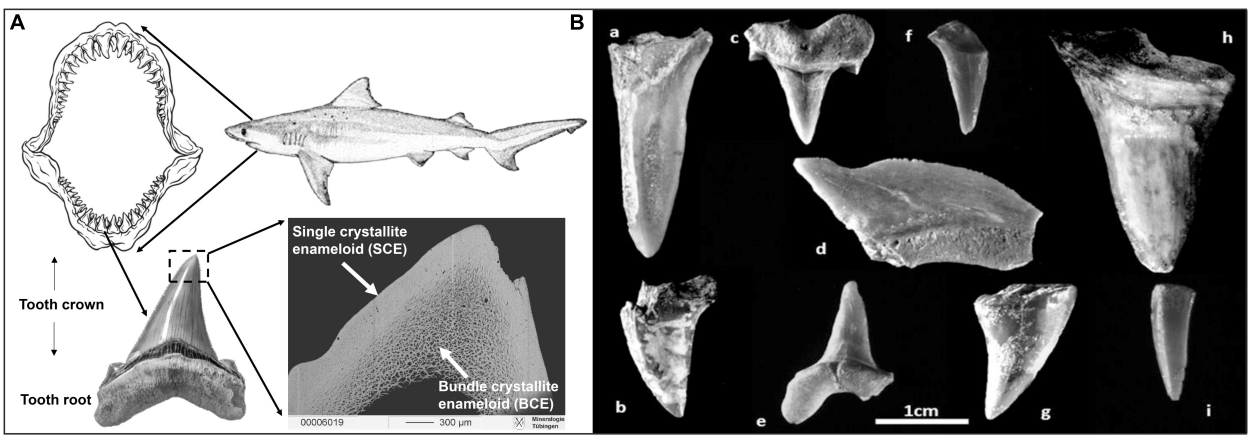

FIGURE 3 | Shark teeth illustrations. **(A)** Schematic drawing of a shark dentition with multiple rows of teeth that are continuously replaced. A photograph of a *Carcharhinus* sp. tooth is shown with the crown part covered by enameloid (consisting of fluorapatite; Enax et al., 2014) and the root part comprised of dentine (which consists of fluor-bearing hydroxylapatite). The backscattered electron image illustrates the internal enameloid microstructure of the tip of a modern Great white shark tooth showing the outer enameloid layer of single crystallites (SCE) and the inner layer of bundle crystallites (BCE). **(B)** Photographs of fossil shark teeth from the Iron Age cultural layers of the City of David from the "Rock Cut Pool" dating to the 8–9th century BCE in Jerusalem: **(a)** lamniform shark, Odontaspididae; **(b)** SK-86: shark, no taxonomic identification (NTI); **(c)** SK-79: lamniform shark, Odontaspididae, Cretaceous; **(d)** SK-85: *Squalicorax,* Late Cretaceous; **(e)** SK-84, **(f)** NTI, **(g)** SK-82, **(h)** SK-83, **(i)** SK-77: shark, NTI. Except for specimens **(a,f)**, seven of these fossil shark teeth were analysed for their Sr and O isotope composition (the unidenfied lamniform shark **(a)** and specimen **(f)** did not contain enough enameloid to sample). All of these teeth are presumably from the Late Cretaceous (**Table 2**). Note that enameloid $^{87}Sr/^{86}Sr$ of these shark teeth are fully in line with an early Campanian Sr stratigraphic age (80.29 Ma +3.24, –2.64 Ma) using the McArthur et al. (2020) dataset; **Table 2**.

MATERIALS AND METHODS

The provenance of archaeological fish remains (sharks and bony fish) recovered in the Southern Levant both from inland and coastal sites (**Figure 2**) was examined by analysing $^{87}Sr/^{86}Sr$ and $\delta^{18}O_{PO4}$ of the bioapatite of their teeth (i.e., enameloid). To assess past fish habitats and provenance we first establish a reference database of $^{87}Sr/^{86}Sr$ and $\delta^{18}O_{PO4}$ values for modern sharks as well as marine and freshwater bony fish from the major water bodies in Egypt and in the Southern Levant (Nile, Lake Kinneret, Jordan River, Bardawil Lagoon, **Figure 2A** and **Table 2**). The isotope data from archaeological fish teeth are then compared with those of modern fish to assess their origin. Additional $\delta^{18}O$ values and $^{87}Sr/^{86}Sr$ of rainwater and bedrock for each archaeological site are considered in order to infer the soil water Sr and O isotope composition and identify possible effects of *post mortem* diagenetic alteration. Additionally, the dentine apatite crystallinity, organic carbon content and trace element composition were analysed to further characterise the degree of diagenesis.

Material for Isotope Analysis

Modern Fish Tooth Samples

For O and Sr isotope analysis, we sampled teeth from bony and cartilaginous fish from different aquatic habitats in Egypt and the Southern Levant: the South-eastern Mediterranean Sea, the Nile (Minia, central Egypt), the Nile delta (Lake Manzala), the hypersaline Bardawil Lagoon (Sinai, northern Egypt), Lake Kinneret (Israel), and the Jordan River (Israel) (**Figure 2A**). Cartilaginous fish included an Eastern Mediterranean deep-sea shark (*Centrophorus granulosus;* ≈1400 m) and a Red Sea shark (*Carcharhinus plumbeus*; surface water). Bony fish included two different species of Mediterranean fish: *Conger conger* (Congridae, European Conger; deep water ≈ 1000 m) and *Sparus aurata* (Sparidae, Gilthead seabream; coastal water, Haifa Bay). From an estuarine habitat, we sampled the teeth of *Pomatomus salatrix* (Pomatomidae, blue fish; Kishon estuary, Haifa Bay). Freshwater habitats included three species of cyprinids sampled from Lake Kinneret: *Carasobarbus canis*, *Luciobarbus longiceps*, and *Capoeta damascina* (Cyprinidae). From the Nile (Egypt) we sampled four species of fish: *Lates niloticus* (Latidae; Nile perch), *Oreochromis niloticus* (Cichlidae; Nile tilapia), *Synodontis schall* (Mochokidae; upside-down catfish), and *Bagrus bajad* (Bagridae; bagrid catfish) (**Table 2**).

Archaeological Assemblage

Analysed archaeological material included six *Sparus aurata* teeth recovered from the Chalcolithic site of Gilat (Rowan and Golden, 2009; Van den Brink et al., 2016) and from the Iron Age period of the City of David (Jerusalem), as well as 10 shark teeth from the Iron Age period of the City of David, Jerusalem (Reich et al., 2007, 2008) (**Table 3** and **Figure 3B**).

Taxonomic Identification

Identification of *S. aurata* was performed using the first molariform tooth (Sisma-Ventura et al., 2019). Photos of these teeth are provided in the supplements (**Supplementary Figure S1**). Shark teeth were identified by Jürgen Kriwet from the University of Vienna. Two of these teeth were identified to the order of Lamniformes (tooth a and c in **Figure 3B**), the latter probably from the family Odontaspididae (SK-79, tooth c in **Figure 3B**), and two teeth (SK-85, tooth d in **Figure 3B** and S07815 **Supplementary Figure S1B**) were identified as *Squalicorax* an extinct taxon only occurring in the Late Cretaceous (Shimada and Cicimurri, 2005, 2006; Cappetta, 2012; Siversson et al., 2018). All identified taxa represent extinct fossil sharks belonging to the Late Cretaceous. The other shark teeth could not be identified due to poor preservation but displayed the same macroscopic appearance and preservation as the other fossil teeth (**Supplementary Figure S1**).

Isotope Analysis of Dental Tissue

Enameloid was carefully separated from the dentine by manual drilling. For *S. aurata* the cleaned tooth crown was crushed in an agate mortar after dentine removal to obtain a homogenous enameloid powder that was used for O and solution mode Sr isotope analysis. *In situ* LA-MC-ICP-MS Sr isotope analyses were performed directly on the tooth surface (in the SCE layer) of the shark teeth (**Figure 3A**). The teeth of modern Conger eel, Tilapia, Nile Perch and Gulper shark were crushed whole (due to their very small size) and analysed for Sr and O isotopes.

Screening for Diagenetic Alteration

The preservation of fish teeth excavated from the Chalcolithic and Iron Age cultural layers was determined using various analytical methods including X-ray diffraction analysis (XRD), total organic carbon (TOC) content determination, and laser ablation inductively coupled plasma mass spectrometry (LA-ICP-MS) analysis of trace elements. These analyses were performed on the dentine of the shark and Gilthead seabream teeth, as dentine is much more sensitive to diagenetic alteration than enamel(oid) (Ayliffe et al., 1994; Kohn et al., 1999; Tütken et al., 2008). Diagenesis leads to recrystallization of the bioapatite, loss of collagen (i.e., organic matter), and *post mortem* uptake of fluorine, uranium and rare earth elements (REE) (Staudigel et al., 1985; Toyoda and Tokonami, 1990; Kohn et al., 1999). Therefore, million-year-old fossil fish teeth are expected to have a much higher apatite crystallinity (i.e., larger apatite crystallite size), lower TOC and up to several orders of magnitude higher REE and U content in the dentine relative to the archaeological fish teeth (which are only a few thousand years old). In modern fish teeth, REE and U occur in very low ng/g-level concentrations (Vennemann et al., 2001; Kocsis et al., 2015; this study) - often below the detection limit of LA-ICP-MS - and are only strongly enriched in cases of *post mortem* alteration. Such mineralogical and geochemical changes enable us to clearly distinguish whether fish teeth are contemporaneous to the cultural layer being excavated, or are fossil fish teeth. For comparison, dentine from a modern Great white shark and Gilthead seabream were analysed with the same methods as unaltered reference points.

TABLE 2 | Strontium and oxygen isotope composition of modern fish teeth.

Sample ID	Family	Species	Location/Habitat	Hard tissue	$^{87}Sr/^{86}Sr$	2 SE	Type of $^{87}Sr/^{86}Sr$ Analysis	$\delta^{18}O_{PO4}$ (‰) VSMOW
Z Hai IS 1	Centrophoridae	*Centrophorus granulosus*	Mediterranean deep water	Enamel	0.70914	0.00001	S	24.6
Z Aal IS 1	Congridae	*Conger conger*	Mediterranean deep water	Enamel	0.70912	0.00001	S	24.0
K Car IS 1	Carcharhinidae	not identified	Pelagic – Mediterranean	Bone (vertebra)	0.70920	0.00005	LA	22.5
Z SP IS 1	Sparidae	*Sparus aurata*	Haifa Bay, Israel	Enamel	0.70917	0.00005	LA	23.2
				Enamel	0.70918	0.00005	LA	23.3
				Enamel	0.70921	0.00005	LA	22.5
Z Hai IS 2	Carcharhinidae	*Carcharhinus plumbeus*	Red Sea surface water	Enamel	0.70920	0.00004	LA	22.7
				Enamel	0.70918	0.00004	LA	
				Dentin	0.70919	0.00004	LA	
				Dentin	0.70917	0.00003	LA	
				Dentin	0.70915	0.00003	LA	
Z PO IS 1	Pomatomidae	*Pomatomus salatrix*	Kishon estuary, Israel	Tooth	0.70909	0.00004	LA	19.0
				Tooth	0.70908	0.00004	LA	
				Tooth	0.70893	0.00005	LA	
				Bone (jaw)	0.70895	0.00003	LA	
				Bone (jaw)	0.70901	0.00004	LA	
				Bone (jaw)	0.70898	0.00003	LA	
K BAG ÄGY 2	Bagridae	*Bagrus bajad*	Nile River, Egypt	Bone (rib)	0.70737	0.00004	LA	
				Bone (rib)	0.70729	0.00004	LA	
				Bone (rib)	0.70720	0.00005	LA	
K NI ÄGY 2	Latidae	*Lates niloticus*	Nile, from Cairo market	Bone (jaw)	0.70716	0.00005	LA	23.4
				Bone (jaw)	0.70728	0.00004	LA	
				Bone (jaw)	0.70726	0.00004	LA	
K NI ÄGY 1	Mochokidae	*Synodontis schall*	Nile River, Egypt	Bone (pectoral spine)	0.70709	0.00005	LA	24.5
				Bone (pectoral spine)	0.70698	0.00005	LA	
				Bone (pectoral spine)	0.70704	0.00005	LA	
				Bone (pectoral spine)	0.70691	0.00004	LA	
				Bone (pectoral spine)	0.70682	0.00004	LA	
				Bone (pectoral spine)	0.70683	0.00005	LA	
K NI ÄGY 3	Latidae	*Lates niloticus*	Nile River, Egypt	Bone (jaw)	0.70681	0.00002	S	20.1
Manzala 1-Z	Cichlidae	*Oreochromis niloticus*	Lake Manzala, Port Said, Egypt	Enamel	0.70828	0.00002	S	24.4
Manzala 2-Z	Cichlidae	*Oreochromis niloticus*	Lake Manzala, Port Said, Egypt	Enamel				24.2
Manzala 2-B				Bone (jaw)				22.7
Manzala 3-Z	Cichlidae	*Oreochromis niloticus*	Lake Manzala, Port Said, Egypt	Enamel				23.8
Manzala 4-Z	Cichlidae	*Oreochromis niloticus*	Lake Manzala, Port Said, Egypt	Enamel	0.70821	0.00002	S	24.0
Manzala 4-B				Bone (jaw)	0.70821	0.00001	S	22.5
Nile 1-Z	Cichlidae	*Oreochromis niloticus*	Nile, Minia, Egypt	Enamel	0.70704	0.00002	S	23.9
Nile 2-Z	Cichlidae	*Oreochromis niloticus*	Nile, Minia, Egypt	Enamel	0.70703	0.00002	S	23.3
Nile 2-B				Bone (jaw)	0.70704	0.00002	S	21.3
Nile 3-Z	Cichlidae	*Oreochromis niloticus*	Nile, Minia, Egypt	Enamel				23.2
Nile 3-B				Bone (jaw)				22.3
Nile 4-Z	Cichlidae	*Oreochromis niloticus*	Nile, Minia, Egypt	Enamel				21.7

(Continued)

TABLE 2 | Continued

Sample ID	Family	Species	Location/Habitat	Hard tissue	$^{87}Sr/^{86}Sr$	2 SE	Type of $^{87}Sr/^{86}Sr$ Analysis	$\delta^{18}O_{PO4}$ (‰) VSMOW
Nile 4-B				Bone (jaw)				23.4
Nile 5-Z	Cichlidae	*Oreochromis niloticus*	Nile, Minia, Egypt	Enamel				24.1
Z BA IS 2	Cyprinidae	*Carasobarbus canis*	Lake Kinneret/Jordan River, Israel	Enamel	0.70757	0.00008	LA	15.5
				Enamel	0.70752	0.00006	LA	
				Enamel	0.70745	0.00006	LA	
Z BA IS 1	Cyprinidae	*Luciobarbus longiceps*		Enamel	0.70731	0.00006	LA	20.1
				Enamel	0.70750	0.00006	LA	
				Enamel	0.70741	0.00006	LA	
Z CA IS 1	Cyprinidae	*Capoeta damascina*		Enamel	0.70681	0.00005	LA	13.8
				Enamel	0.70690	0.00005	LA	
				Enamel	0.70729	0.00005	LA	
K CA IS 1	Mochokidae	Not identified	Lake Kinneret/Jordan River, Israel	Bone (spine)	0.70715	0.00005	LA	17.3
				Bone (spine)	0.70696	0.00007	LA	
				Bone (spine)	0.70731	0.00004	LA	

S: solution mode $^{87}Sr/^{86}Sr$ analysis; LA: in situ MC-LA-ICP-MS $^{87}Sr/^{86}Sr$ analysis; Note if the sample ID number is the same but a different letter at the end then B: bone and Z: enameloid are from the same fish.

TABLE 3 | Strontium and oxygen isotope composition of archaeological and fossil fish teeth.

Sample	Hard tissue	Species	Archaeological site	Age	$^{87}Sr/^{86}Sr$	2 SE	Age (Ma)[a]	$\delta^{18}O_{PO4}$ (‰) VSMOW
SP-13	Enameloid	*Sparus aurata*	City of David	Iron Age II	0.70925	0.00005		24.5*
	Bone	*Sparus aurata*			0.70875	0.00004		22.9*
SP-11	Enameloid	*Sparus aurata*	City of David	Iron Age II	0.70906	0.00006		24.2*
EB-1	Enameloid	*Sparus aurata*	Gilat	Chalcolithic	0.70916	0.00005		23.4*
EB-3	Enameloid	*Sparus aurata*	Gilat	Chalcolithic	0.70914	0.00006		23.7*
	Dentine	*Sparus aurata*			0.70902	0.00006		
EB-2	Enameloid	*Sparus aurata*	Gilat	Chalcolithic	0.70909	0.00006		22.4*
	Dentine	*Sparus aurata*			0.70867	0.00013		
EB-5	Enameloid	*Sparus aurata*	Gilat	Chalcolithic	0.70910	0.00005		24.6*
	Dentine	*Sparus aurata*			0.70918	0.00005		
SK-85	Enameloid	*Squalicorax* sp.	Jerusalem G	Late Cretaceous	0.70755	0.00006	78.23	20.0
SK-32	Enameloid	Shark NTI						20.7
SK-82	Enameloid	Shark NTI		Late Cretaceous	0.70750	0.00005	80.66	20.0
	Dentine	Shark NTI		Late Cretaceous	0.70761	0.00005		
SK-77	Enameloid	Shark NTI	Jerusalem P	Late Cretaceous	0.70760	0.00004	76.29	20.4
SK-86	Enameloid	Shark NTI		Late Cretaceous	0.70740	0.00005	86.47	20.3
SK-80	Enameloid	Shark NTI						20.2
SK-83	Enameloid	Shark NTI		Late Cretaceous	0.70750	0.00003	80.66	18.3
SK-84	Enameloid	Shark NTI		Late Cretaceous	0.70751	0.00002	80.15	
SK-79	Enameloid	Lamniform shark		Late Cretaceous	0.70752	0.00005	79.61	18.8
	Dentine			Late Cretaceous	0.70772	0.00004		
SK-76	Enameloid	Shark NTI						20.4
LN-36	Bone	*Lates niloticus*	Ashkelon	Iron Age I	0.70892	0.00006		21.0

**$\delta^{18}O_{PO4}$ data from Sisma-Ventura et al. (2018). NTI: No taxonomic identification.*
[a]*Strontium stratigraphic age in millions of years (Ma) based on the seawater $^{87}Sr/^{86}Sr$ data of McArthur et al. (2020).*

X-Ray Diffraction (XRD) Analysis

Dentine powder samples were placed on a monocrystalline, background-free silicon sample holder and X-ray diffraction patterns were analysed using a Seifert XRD 3000 TT diffractometer using a Cu cathode at 40 kV and 30 mA and Cu K_α radiation of 0.15406 nm with 0.03° (2Θ) steps in 2 s over the range from 5° to 70° 2Θ at the Institute of Geosciences, University of Mainz.

Total Organic Carbon (TOC) Analysis

The TOC content was determined in two steps. First, by analysing the dentine powders (about 10–15 mg/per sample) for total carbon (TC) content using a CN-analyser (Vario EL Cube, Elementar GmbH, Hanau, Germany) at the Institute for Geography, University of Mainz. Then, the structurally bound carbonate total inorganic carbon content (TIC) of dentine was measured using a Gasbench II coupled to a Delta V continuous flow isotope ratio gas mass spectrometer at the Max Planck Institute for Chemistry, Mainz. An internal modern elephant (*Loxodonta africana*) enamel standard (AG-Lox) of known TIC content (7.5 wt.%; Wacker et al., 2016) was analysed in different amounts to establish a regression between TIC and peak area of the mass-44 CO_2 peak. The dentine TOC content was then calculated as the difference between the TC and TIC content.

LA-ICP-MS Analysis of Trace Elements

Shark and Gilthead seabream teeth were embedded in epoxy resin to produce polished one-inch mounts. To determine the trace element compositions of enameloid and dentine, line scans were measured across the teeth (including both enameloid and dentine) by laser ablation (**Supplementary Figure S2**). The trace element measurements were performed using an ArF Excimer laser system (193 nm wavelength, NWR193 by ESI/NewWave) equipped with a TwoVol2 ablation cell and coupled to an Agilent 7500ce quadrupole ICP-MS at the Institute of Geoscience, Mainz. Laser repetition rate was set to 10 Hz with a transition speed of 10 μm/s, using a fluence of 3.5 J/cm^2. Line scans were carried out with a rectangular spot size of 130 μm × 30 μm. Pre-ablation was performed prior to each analysis to clean the surface. Background signals were acquired for 15 s during laser warm-up prior to each scan. ^{43}Ca was used as internal standard and NIST SRM 612 was used for calibration, using the preferred values from the GeoReM Database (Jochum et al., 2005). NIST SRM 610, NIST SRM 1400 and NIST SRM 1486 were used as quality control materials to test accuracy and reproducibility of the measurements (**Supplementary Table S1**). All reference materials were measured prior to and after each sample block.

Strontium Isotope (^{87}Sr/^{86}Sr) Analysis of Fish Teeth

Sr isotope analyses of all teeth were performed either by solution-based or LA-MC-ICP-MS (laser ablation inductively coupled plasma mass spectrometry) using a Nu Plasma MC-ICP-MS (Nu Instruments^{TM}) at the Max Planck Institute for Chemistry, Mainz, following the methods described by Weber et al. (2017). For solution-based analysis, the MC-ICP-MS was coupled to a CETAC Aridus 2 desolvator nebulizer system and samples were diluted to ≈ 100 ng/g Sr. A standard-sample bracketing approach was applied, using a static multi-collection mode with 100 cycles and 5 s integration time. All measurements were corrected using NIST SRM 987 (^{87}Sr/^{86}Sr of 0.710248; McArthur et al., 2020). Prior to analysis, Sr was separated by ion-exchange chromatography using Sr spec resin, following the protocol presented in Weber et al. (2018). For *in situ* laser ablation analysis, the MC-ICP-MS was coupled to a 213 nm Nd:YAG laser ablation system (New Wave Research^{TM} UP-213). Signals of the following masses were monitored during the analysis: ^{82}Kr, ^{83}Kr, ^{84}Sr, ^{85}Rb, ^{86}Sr, ^{87}Sr, ^{88}Sr and half masses 85.5 and 86.5 (half masses were only monitored during LA-MC-ICP-MS). Mass bias correction was performed using the exponential law (Ingle et al., 2003) and assuming a constant ^{86}Sr/^{88}Sr of 0.1194. Laser ablation analysis was performed by linescan analysis, each linescan with a length of 1000 μm, a circular spot size of 65–100 μm (depending on the sample and daily tuning parameter), a transition rate of 5 μm/s and a laser repetition rate of 10 Hz. The resulting fluence varied between 10–30 J/cm^2, depending on the chosen energy output (70–100%). Prior to each analysis, a pre-ablation was performed to prevent surface contamination.

To correct for Kr in the plasma, we used the "on peak zero" method by measuring a 45 s gas background prior to each analysis without the laser firing. After background subtraction, the remaining signal on mass 82 was used to check for Ca argide and dimer formation (<0.1 mV). Half masses were checked for doubly charged rare earth elements (Yb and Er) and the signals were corrected using constant isotope ratios (Berglund and Wieser, 2011). To correct for the occurrence of ^{87}Rb on mass 87, we used a ^{87}Rb/^{85}Rb of 0.3857 (Berglund and Wieser, 2011).

Samples for LA-MC-ICP-MS were measured in a standard-bracketing approach, as has been recommended as the calibration strategy for *in situ* Sr isotope analysis (Irrgeher et al., 2016; Weber et al., 2017), using the same laser parameters for both the reference material and the samples. An in-house marine shark tooth was used as reference material, assuming a modern-day ocean seawater ^{87}Sr/^{86}Sr of 0.70918 ± 0.00001. This is in the range of the modern day sea water value (Hodell et al., 1990; Mokadem et al., 2015; McArthur et al., 2020) and modern-day marine organisms (e.g., marine carbonate reference materials JCt-1 (giant clam, *Tridacna gigas*) and JCp-1 (coral, *Porites* sp.), yielding ^{87}Sr/^{86}Sr of 0.709169 ± 0.000009 (2 SE, n = 3) and 0.709170 ± 0.000006 (2 SE, n = 3, Weber et al., 2018), respectively, and modern shark samples averaging ^{87}Sr/^{86}Sr of 0.709167 ± 0.000009 (2 SE, n = 10, Vennemann et al., 2001).

Phosphate Oxygen Isotope ($\delta^{18}O_{PO4}$) Analysis of Fish Tooth Enameloid

The phosphate fraction of the fish tooth enameloid was separated using a method modified after Dettmann et al. (2001) and described in detail by Tütken et al. (2006). In summary, approximately 5 mg of pretreated sample powder was digested in 0.8 ml HF (2 M) on a vibrating table for *ca.* 12 h. After centrifugation (3 min at 10,000 rpm), the supernatant sample solution was separated from the CaF precipitates into a new

vial. After neutralising the HF solution with NH_4OH (25%) in the presence of bromothymol blue as pH indicator, Ag_3PO_4 was precipitated by adding 0.8 ml of 2 M $AgNO_3$. After settling of the Ag_3PO_4 crystals, the samples were centrifuged and the supernatant solution containing excess $AgNO_3$ was removed by pipette. The Ag_3PO_4 precipitate was then rinsed five times with Milli-Q water and dried overnight in an oven at 50°C.

Ag_3PO_4 aliquots of 0.5 mg were placed into silver capsules and analysed in triplicate by means of high temperature reduction using a Finnigan TC-EA coupled via a Conflo III to a Micromass 100 GC-IRMS at the University of Mainz, or to a Finnigan Delta Plus XL GC-IRMS at the Universities of Tübingen and Lausanne, according to the method of Vennemann et al. (2002). The raw $\delta^{18}O_{PO4}$ values were normalised to an Ag_3PO_4 reference material produced by Elemental Microanalysis with a certified value of 21.7‰ (silver phosphate P/N IVA33802207, batch no. 180097, distributed by IVA Analysentechnik, Germany). The analytical precision for this reference material was better than ± 0.3‰ (1 SD). For untreated NIST SRM 120c Florida phosphate rock, we obtained a $\delta^{18}O_{PO4}$ value of 21.9 ± 0.3‰ (1 SD, n = 15). This value compares well with the values from most other laboratories as compiled in Chenery et al. (2010).

Bioapatite $\delta^{18}O_{PO4}$ Value Reconstruction for Fish From Levantine Water Bodies

The expected isotope equilibrium range of $\delta^{18}O_{PO4}$ values for fish tooth bioapatite was calculated for each of the water bodies in Egypt and Israel from which fish were sampled using published and a few measured $\delta^{18}O_{H2O}$ values (**Table 4**). The calculations are based on the temperature-dependent isotope fractionation during biomineralisation of apatite by Lécuyer et al. (2013): T°C = 117.4 – 4.5 ($\delta^{18}O_{PO4}$ - $\delta^{18}O_{Water}$), where $\delta^{18}O_{PO4}$ and $\delta^{18}O_{Water}$ correspond to the isotope compositions of bioapatite and ambient water relative to VSMOW, respectively. This relationship is valid for the temperature range of 8°C < T < 32°C thus covering water temperatures typically encountered in the Mediterranean region. For Mediterranean surface water, we used a $\delta^{18}O_{Water}$ of 1.6 ± 0.3‰ and an annual temperature range of 17–30°C (Sisma-Ventura et al., 2014). The estimated $\delta^{18}O_{PO4}$ of Mediterranean deep water was calculated for a temperature range of 13–15°C and a $\delta^{18}O_{Water}$ value of 1.5 ± 0.2‰ (Sisma-Ventura et al., 2016). For the Nile delta water bodies, we used the post-Aswan dam $\delta^{18}O_{Water}$ range between 0.0 and 3.0‰ (Nile near Minia) and between 2.0 and 5.0‰ (Lake Manzala) and a water temperature range between 18 to 30°C (Kolodny et al., 1983; Aly et al., 2004). For Lake Kinneret and its main tributary, the Jordan River, we used a $\delta^{18}O_{Water}$ range between −6.0 and 2.0‰ and between −8.0 and −5.0‰ and a temperature range between 16–28°C and 10–22°C, respectively (Stiller and Magaritz, 1974; Talbot, 1990; Zohary et al., 1994). We also estimated the $\delta^{18}O_{PO4}$ equilibrium range of fish from past Nile delta water bodies during the Iron Age, the New Kingdom period, by using the Nile $\delta^{18}O_{Water}$ range of −2.0 to −1.0‰, reconstructed from the $\delta^{18}O_{PO4}$ values of tooth enamel from human mummies (Touzeau et al., 2013) and assuming a temperature range similar to today.

The $^{87}Sr/^{86}Sr$ and $\delta^{18}O_{PO4}$ Expectation Fields for Levantine Fish Habitats

For each of the major water bodies in Egypt and the Southern Levant we also compiled a range of expected $^{87}Sr/^{86}Sr$ water

TABLE 4 | Strontium and oxygen isotope composition of different water bodies and Sr sources in the SE Mediterranean area.

Water body/Substrate	$^{87}Sr/^{86}Sr$ range	$^{87}Sr/^{86}Sr$ mean (±1 SD)	References	$\delta^{18}O$ (‰) VSMOW range	$\delta^{18}O$ (‰) VSMOW mean (±1 SD)	References
Mediterranean seawater		0.70918	4, 6	1.3 – 1.9	1.6 (±0.3)	10
Bardawil Lagoon		0.70916	This study	1.8 – 7.2	3.7 (±2.0)	9, 14, this study
Nile (Minia, Egypt, 2019)		0.70718	This study		3.3	this study
Nile (Minia, Egypt, 1996)		0.70690	13		2.4	8
Nile (modern)	0.7060 – 0.7072		7, 13	1.0 – 2.0	1.5 (±0.5)	8, 15
Nile (New Kingdom)	0.7052 – 0.7061		5	−3.0 – 0.0	−1.4 (±1.0)	8
Lake Manzala	0.7068 – 0.7088		5, 6	3.0 – 7.0	3.5 (±1.5)	6, 14
Lake Manzala (2019)		0.70843	This study		5.0	This study
Lake Kinneret		0.70750 (±0.00005)	2	−2.5 – 0.0		12
Jordan River		0.70678 (±0.00006)	2	−6.0 to −7.0	−6.5 (±0.5)	12
Rainfall in Israel	0.7079 – 0.7092	0.7087 (±0.0004)	1	−2.0 to −8.0	−5.0 (±3.0)	11
Saharan dust		0.7078	1			
Seashore sand	0.7090 – 0.7092		3			
Calcareous sandstone		0.7090 (±0.0002)	3			
Terra rossa soils		0.70857 (±0.00026)	3			
Rendzina soils	0.7079 – 0.7084		3			

Strontium isotope data from 1: Herut et al. (1993); 2: Fruchter et al. (2017); 3: Hartman and Richards (2014); 4: McArthur et al. (2020); 5: Woodward et al. (2015); 6: Reinhardt et al. (2001); 7: Brass (1976); 8: Touzeau et al. (2013); 9: Kolodny et al. (1983); 10: Sisma-Ventura et al. (2016); 11: Gat and Dansgaard (1972); 12: Gat (1970); 13: Gerstenberger et al. (1997); 14: Aly et al. (2004); 15: Schilman et al. (2001); water samples in this study were taken in January 2019 at the following geographic coordinates: Nile (28 06 22 03 N; 30 45 17 58 E); Lake Manzala (31 16 12 82 N; 31 12 39 28 E); Bardawil Lagoon (31 03 14 32 N; 33 09 28 01 E).

values based on literature values (**Table 4**). For this purpose, we used the $^{87}Sr/^{86}Sr$ value of modern seawater of 0.70918 (Mokadem et al., 2015; McArthur et al., 2020) for the Mediterranean (including the Bardawil Lagoon) and the Red Sea. For the Nile a $^{87}Sr/^{86}Sr$ range of 0.70680–0.70718 (Minia, central Egypt, Gerstenberger et al., 1997 and this study) and for the Nile delta and Lake Manzala a range of 0.70680–0.70880 (Reinhardt et al., 2001; Woodward et al., 2015) were used. For Lake Kinneret and the Jordan River, we used a $^{87}Sr/^{86}Sr$ range of 0.70684–0.70755 (Fruchter et al., 2017). For Late Cretaceous seawater we used the $^{87}Sr/^{86}Sr$ range of 0.70728–0.70783 (for the Campanian: 0.70746–0.70774) from the $^{87}Sr/^{86}Sr$ seawater curve LOWESS 6 Fit of McArthur et al. (2020) (**Figure 4**). These $^{87}Sr/^{86}Sr$ ranges were then combined with the calculated $\delta^{18}O_{PO4}$ equilibrium ranges based on published $\delta^{18}O_{Water}$ and water temperature values to characterise each water body isotopically, and to define expected $^{87}Sr/^{86}Sr$ versus $\delta^{18}O_{PO4}$ fields for the different potential past and present main fish habitats. For fish that formed their bioapatite in Late Cretaceous seawater, we used $\delta^{18}O_{PO4}$ values ranging between 17.2 and 20.3‰ (Campanian: 18.3–20.0‰) measured in fossil shark teeth in the Southern Levant by Kolodny and Raab (1988). This reference dataset was then used as an interpretive framework to assess the provenance of the archaeological *S. aurata* and sharks based on their enameloid Sr and O isotope composition using Linear Discriminant Analysis (LDA).

Linear Discriminant Analysis (LDA)

For assessing the fish provenance from different waterbodies, we applied a LDA, a commonly used supervised pattern data-reduction and recognition method that assigns new observations to certain classes. This is achieved through a linear discriminant function (LDF) that maximises ratios of between-group variance and within-group variance. We used LDA (R package MASS version 7.3-51.6, Ripley, 2002) in order to assign provenance to archaeological fish tooth samples based on their enameloid Sr and O isotope composition. The $^{87}Sr/^{86}Sr$ ratios and $\delta^{18}O_{PO4}$ values from published and measured water samples of known provenance and associated modern fish bioapatite (bone, dentine, enameloid) samples were used as predictors. Note that the expected fish bioapatite $\delta^{18}O_{PO4}$ values for each waterbody were calculated from the $\delta^{18}O_{H2O}$ values and water temperatures using the phosphate-water oxygen isotope fractionation equation of Lécuyer et al. (2013).

In order to compute the LDF, a total of 82 observations from six different water bodies in the Southern Levant (Bardawil Lagoon, Lake Manzala, Nile River, Lake Kinneret/Jordan River, and modern Mediterranean seawater) were used. These comprise 44 observations from water samples (using min, max and mean

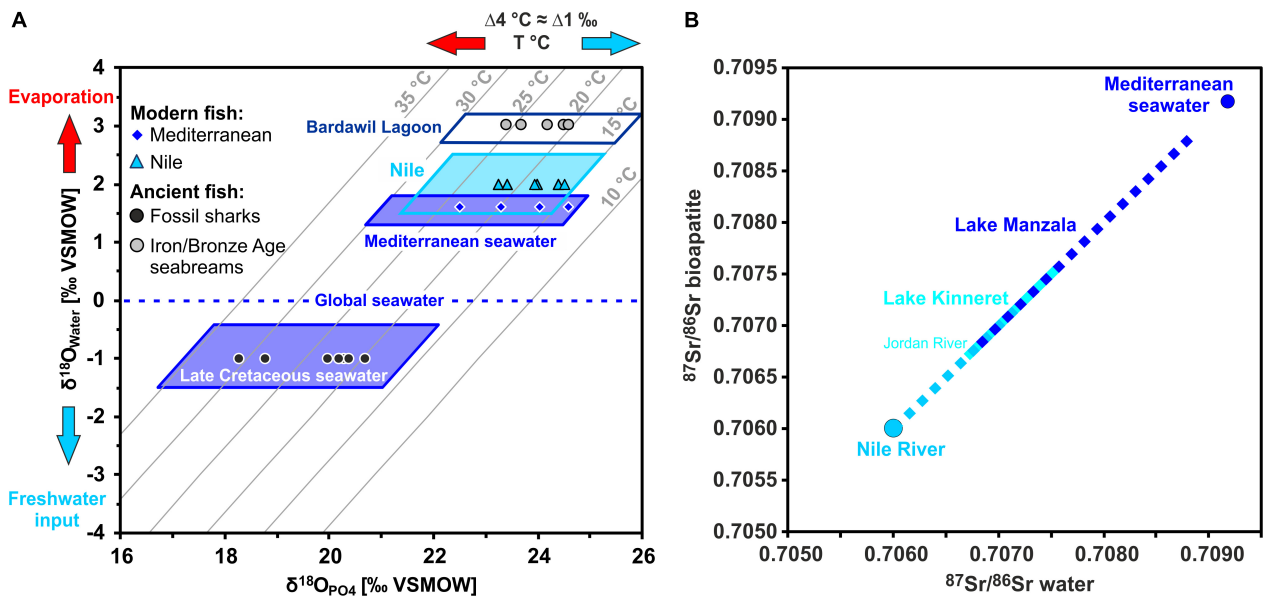

FIGURE 4 | Strontium and oxygen isotope compositions of fish teeth and their expected isotopic ranges for different waterbodies in the Southern Levant. **(A)** Enameloid phosphate oxygen isotope compositions ($\delta^{18}O_{PO4}$) of modern Mediterranean and Nile fish vs. the predicted $\delta^{18}O_{PO4}$ range expected for fish from these water bodies presented on a cross plot of $\delta^{18}O_{PO4}$ versus $\delta^{18}O_{Water}$ for seawater and Nile water, with isotherms of bioapatite formation calculated after Lécuyer et al. (2013). Note that modern Nile water is ^{18}O-enriched due to evaporation after building of the Aswan High Dam (Bialik and Sisma-Ventura, 2016) and thus has even slightly higher $\delta^{18}O_{Water}$ than the Mediterranean seawater. Therefore, calculated bioapatite $\delta^{18}O_{PO4}$ values for fish from Nile and Mediterranean seawater overlap. However, Sr isotopes are clearly distinct for both settings. The enameloid $\delta^{18}O_{PO4}$ values of fossil shark teeth from the City of David fall well into the expectation field for Late Cretaceous seawater based on Late Cretaceous shark teeth $\delta^{18}O_{PO4}$ values of Kolodny and Raab (1988) and Pucéat et al. (2003). **(B)** The $^{87}Sr/^{86}Sr$ from the Nile and Mediterranean represent two, clearly distinct endmembers of the water values encountered in the main fish-bearing water bodies in Egypt and the Southern Levant that are incorporated into fish teeth from the respective rivers, lakes and lagoons. Note that Lake Kinneret and Lake Manzala overlap in their $^{87}Sr/^{86}Sr$ as both have volcanically influenced fresh water sources. Late Cretaceous seawater values (range: 0.70729–0.70773; McArthur et al., 2020) also overlap with both waterbodies.

values taken from literature data and few measurements) and 38 observations from 14 modern fish specimens of known provenance (**Table 1** and **Supplementary Tables S4–S6**). In order to increase the sample size of data used to compute the LDF, specimens that underwent several Sr isotope analyses per tooth but only a single O isotope analysis were used. Thus a single $\delta^{18}O_{PO4}$ value was used for each $^{87}Sr/^{86}Sr$ measured in the same individual. Seven Bronze and Iron Age archaeological Gilthead seabream teeth were subsequently assigned a provenance to one of the six different water bodies using LDA. Provenance of the fossil, presumably Late Cretaceous sharks (n = 7; **Table 3**) was tested in a separate analysis (**Supplementary Table S7–S9**). For this purpose, Late Cretaceous seawater $^{87}Sr/^{86}Sr$ values taken from the LOWESS 6 Fit of McArthur et al. (2020) and $\delta^{18}O_{PO4}$ from Late Cretaceous shark teeth from Israel (Kolodny and Raab, 1988; Kolodny and Luz, 1991) were added to the reference dataset used to compute the LDF to assess the robusticity of the model (**Supplementary Tables S7–S9**). All values were transformed by subtracting the mean of the predictor's data from the observation's value and then by dividing by the standard deviation.

Accuracy of the groups assigned by the LDF were assessed with a confusion matrix using a "leave-one-out" cross-validation method, where an observation is omitted and then assigned by the LDF. The procedure is then repeated for each observation and allows for the success-rate of classification to be calculated (Friedman et al., 2001). All statistical analyses were performed using the statistical program R (version 4.0.2; R Core Team, 2018).

RESULTS

Shark Taxonomy and Biostratigraphic Age

All of the shark teeth displayed a grey-beige colouration and macroscopic preservation typical for Cretaceous fossil shark teeth from the Near East (**Supplementary Figure S1**). Several shark teeth were identified to the order of Lamniformes and some were assigned to *Squalicorax* sp. (Anacoracidae; n = 2), a taxon that only occurred during the Late Cretaceous (Shimada and Cicimurri, 2005, 2006). Another tooth was assigned to the family Odontaspididae (Sand shark; n = 1), also from the Cretaceous (**Figure 3B** and **Table 3**). The fossil nature of the shark teeth was further tested by analysing different mineralogical and geochemical proxies for diagenesis.

X-Ray Diffraction Analysis

The differences in crystallinity of the analysed fish tooth dentine samples are quite significant, and any peak broadening contribution from the instrument and sample preparation are considered to be negligible. The X-ray diffraction pattern of the dentine from four shark teeth exhibited three well-separated diffraction peaks (211, 112, 300) typical of recrystallised bioapatite in fossil dentine or bone (**Supplementary Figure S3**). In contrast, the dentine of the Chalcolithic Gilthead seabream teeth still had one broad diffraction peak, similar to the unaltered dentine of a modern Great white shark (**Supplementary Figure S3**). Therefore, the Gilthead seabream have a lower apatite crystallinity than the shark tooth samples. Fluorapatite was identified as the primary mineral phase, indicating diagenetic fluorine uptake into the dentine that would have originally consisted of a fluor-bearing hydroxylapatite in teleost fishes (<0.3 wt.% F; Suga et al., 1993). Modern shark dentine can contain high fluorine content (0.6–1.5 wt.%; Enax et al., 2012) in its carbonated bioapatite but this content is still much lower than in enameloid that consists of fluorapatite (3.1 wt.%; Enax et al., 2012; Kocsis et al., 2015). Some dentine samples (e.g., SK-84) also contained small amounts of calcite as a secondary diagenetic mineral infilling.

Total Organic Carbon (TOC) Analysis

The dentine of the four shark teeth had low TOC contents of 0.23 ± 0.26 wt.% (n = 4) which is more than 40 times lower than the TOC content of dentine in the modern Great white shark (9.54 wt.%) and more than eight times lower than in the dentine of Chalcolithic *Sparus aurata* teeth (1.99 ± 0.47 wt.%; n = 3) (**Supplementary Table S2** and **Supplementary Figure S4**).

Trace Element *in situ* LA-ICP-MS Analysis

Profiles of trace element content were measured across both dental tissues (enameloid and dentine) of all *S. aurata* (n = 5) and shark teeth (n = 7) from Chalcolithic and Iron Age cultural layers as well as one modern Great white shark and two *S. aurata* teeth as comparison to obtain unaltered dental tissue compositions (**Supplementary Figure S5** and **Supplementary Table S3**). Here we focus on two trace elements that are highly sensitive to diagenetic alteration – uranium and neodymium – to identify fossil specimens. Uranium and Nd are both typically only present in very low, ng/g-level concentrations in modern mammalian tooth bioapatite (Kohn et al., 1999) and also in modern fish teeth (Shaw and Wasserburg, 1985; Vennemann et al., 2001; Kocsis et al., 2015). The analysed modern Gilthead seabream and Great white shark dentine yield low Nd and U contents of 0.001–0.006 μg/g and 0.05–0.09 μg/g, respectively (**Figure 5**). This is in good agreement with the Nd content of 0.011 ± 0.011 μg/g in modern shark teeth (Shaw and Wasserburg, 1985; Vennemann et al., 2001). In contrast, the dentine of the shark teeth excavated from the City of David site had ≈ 100–1000 times higher U and Nd concentrations of ≈ 10–100 μg/g, typical for fossil dentine of shark teeth (Vennemann and Hegner, 1998; Kocsis et al., 2009). The dentine of the seabream teeth had intermediate Nd and U concentrations of ≈ 1–10 μg/g, and thus are ≈ 10–100 times enriched in U but less enriched in Nd as compared to the shark teeth (**Figure 5**). Enameloid is much less enriched (i.e., altered) in Nd and U compared to the dentine of the same tooth, both for Gilthead seabream and shark teeth.

Sr and O Isotope Data for Modern Fish Teeth and Bones

The $^{87}Sr/^{86}Sr$ and $\delta^{18}O_{PO4}$ data for modern sharks and bony fish from different water bodies in Egypt and the

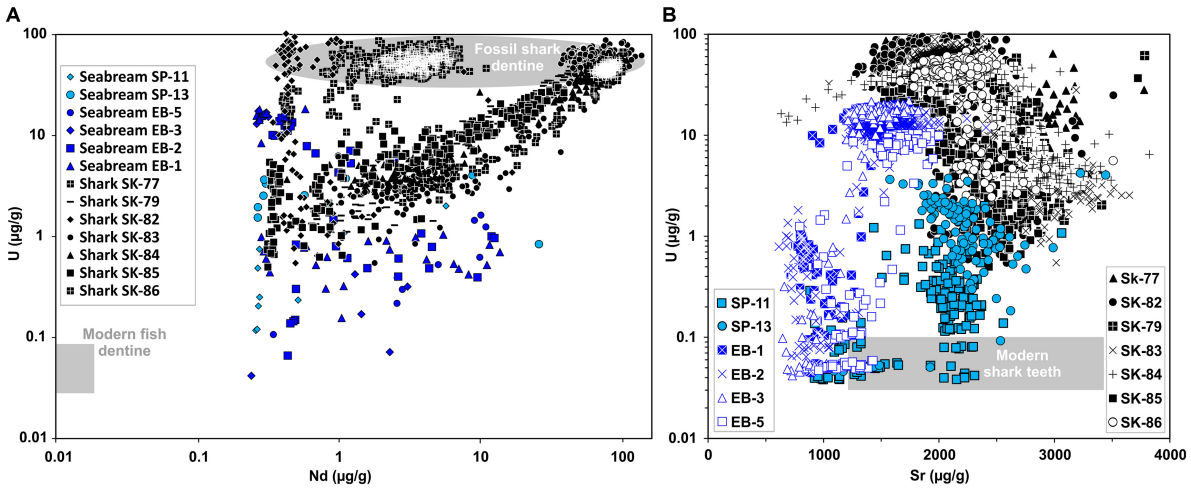

FIGURE 5 | Trace element compositions (U, Nd, Sr) of enameloid and dentine in ancient and modern Gilthead seabream and shark teeth measured by LA-ICP-MS line scans (**Supplementary Table S3**). Archaeological Gilthead seabream teeth are from the Chalcolithic and Iron Age periods and the Late Cretaceous fossil shark teeth are from the Iron Age cultural layers of the City of David, Jerusalem. **(A)** Cross plot of U and Nd concentrations. Note the logarithmic scale of both axes. Modern fish tooth dentine Nd and U field drawn after data from Vennemann et al. (2001) and this study. Fossil shark teeth have much higher dentine U and Nd contents than archaeological Gilthead seabream teeth. **(B)** Uranium (U) and strontium (Sr) concentration in fish teeth. Note the logarithmic scale of the *y*-axis. The grey Sr and U field for modern shark teeth is based on Sr concentrations from Vennemann et al. (2001) and Kocsis et al. (2015), U concentrations from this study. Note, despite U enrichment enameloid Sr concentrations of both archaeological Gilthead seabream and fossil shark teeth are still in the range of modern sharks.

Southern Levant are summarised in **Table 2** and are presented with respect to the expected values for each water body (**Figure 6**). A typical modern marine $^{87}Sr/^{86}Sr$ of ≈ 0.7092 was measured in tooth enameloid of extant deep-sea Gulper shark (*Centrophorus granulosus*) from the east Mediterranean, in European conger eels (Congridae; *Conger conger*), in native Eastern Mediterranean (Haifa Bay, Israel) Gilthead seabream (Sparidae; *Sparus aurata*) and also in Red Sea Sandbar shark (*Carcharinus plumbeus*). The high $\delta^{18}O_{PO4}$ values of both *C. granulosus* and *C. conger*, between 24.0 and 24.6‰ (**Table 2**), is a function of the low Mediterranean deep-water temperature range of 13–15°C and the deep-water $\delta^{18}O_{Water}$ value of 1.5 ± 0.2‰ (1 SD) (Sisma-Ventura et al., 2016). *S. aurata* $\delta^{18}O_{PO4}$ values of 22.5–23.5‰ (Sisma-Ventura et al., 2015, 2018) reflect the southeast Mediterranean coastal water temperature range of 17–30°C and the $\delta^{18}O_{Water}$ range between 1.4 and 1.9‰ (Sisma-Ventura et al., 2014, 2015). All extant Mediterranean fish fall within the range of seawater $^{87}Sr/^{86}Sr$ and $\delta^{18}O_{PO4}$ expected for marine fish (**Figure 6**) as well as the $^{87}Sr/^{86}Sr$ and the $\delta^{18}O_{PO4}$ values of the Red Sea Sandbar shark (**Table 2**).

Teeth of Blue fish (Pomatomidae; *Pomatomus salatrix*) from the Kishon River estuary yielded $^{87}Sr/^{86}Sr$ of 0.70901 ± 0.00006 (2 SE) and $\delta^{18}O_{PO4}$ value of 19.0 ± 0.3‰ (1 SD), which are lower than values for marine fish. Nevertheless, the Blue fish values agrees well with the expected $^{87}Sr/^{86}Sr$ and $\delta^{18}O_{PO4}$ values of the Kishon estuary, which is controlled by mixing of Israeli coastal groundwater and Mediterranean seawater (**Figure 6** and **Table 4**). The $^{87}Sr/^{86}Sr$ of extant freshwater fish from the Nile (Egypt) and Lake Kinneret (Israel), exhibited lower values between 0.707 and 0.708. The $^{87}Sr/^{86}Sr$ of extant Nilotic fish: Nile tilapia (Cichlidae; *Oreochromis niloticus*), upside-down catfish (Mochokidae: *Synodontis schall*) and bagrid catfish (Bagridae; *Bagrus bajad*) caught at different places in the Nile are very similar, yielding an average of 0.7071 ± 0.0002 (1 SD) and likewise for extant freshwater fish from Lake Kinneret (0.7073 ± 0.0003, 1 SD; **Figure 6** and **Table 4**). This similarity results from the fact that the drainage area of both freshwater bodies is comprised of extended volcanic bedrocks with low $^{87}Sr/^{86}Sr$ (Krom et al., 1999; Hartman and Richards, 2014).

Relatively high $\delta^{18}O_{PO4}$ values were observed in extant Nilotic fish, ranging between 20.1 and 24.5‰, reflecting the Nile's source water which derives from monsoonal rains ($\delta^{18}O_{Water}$ range of −3.0 to 0.0‰; Schilman et al., 2001) with additional ^{18}O-enrichment due to evaporation effects along the Nile trajectory through the desert and in the Aswan High Dam (Bialik and Sisma-Ventura, 2016).

Three species of extant freshwater cyprinids were analysed for their $^{87}Sr/^{86}Sr$: *Luciobarbus longiceps*, *Carasobarbus canis*, and *Capoeta damascina*. The first two species have $^{87}Sr/^{86}Sr$ that vary between 0.70731 and 0.70757, agreeing well with water from different depths of Lake Kinneret which have an average $^{87}Sr/^{86}Sr$ of 0.70750 ± 0.00005 (2 SE) (Fruchter et al., 2017). Even lower values, between 0.70681 ± 0.00008 and 0.70729 ± 0.00006 (2 SE) were obtained for the *C. damascina* samples. Modern Lake Kinneret fish display a large $\delta^{18}O_{PO4}$ range between 13.8 and 20.1‰, reflecting the local hydrological conditions with an average rainwater $\delta^{18}O_{Water}$ value around −7.0 to −6.0‰ (Gat and Dansgaard, 1972) and the strong evaporation effects in the Kinneret basin that lead to an ^{18}O-enrichment in the

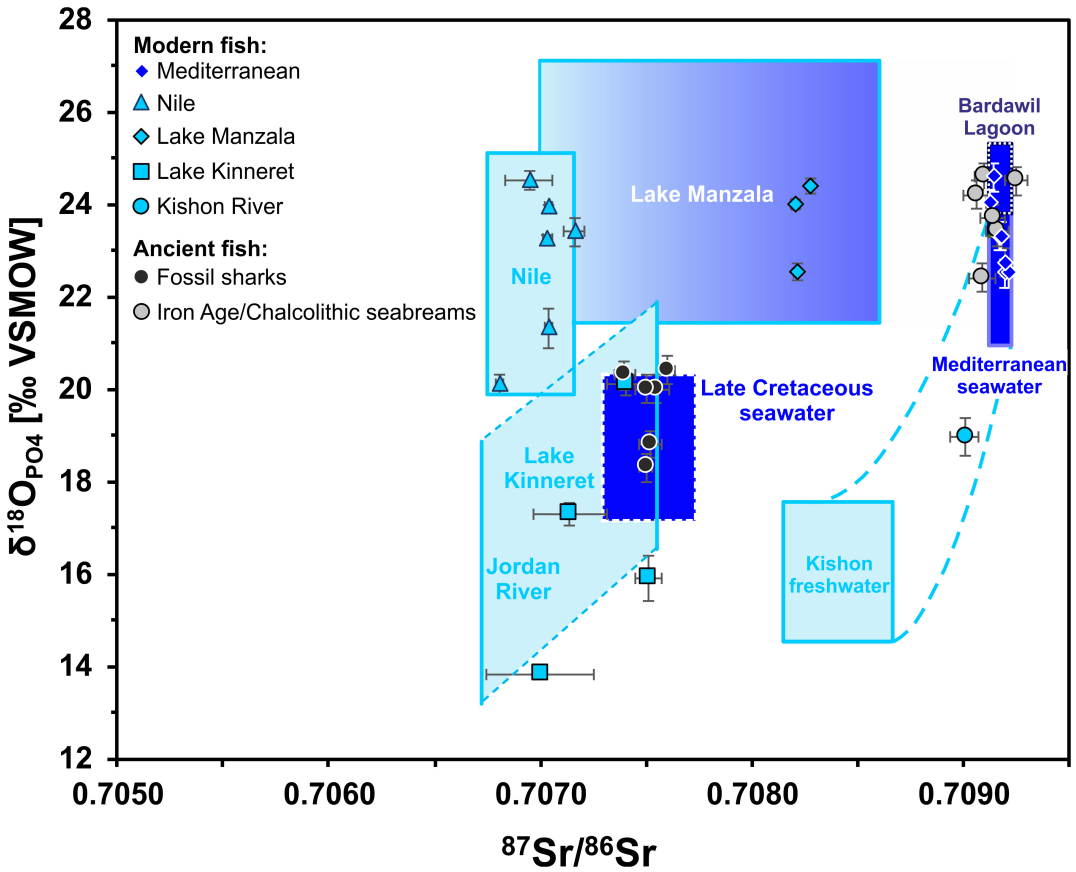

FIGURE 6 | Cross plot of $^{87}Sr/^{86}Sr$ versus $\delta^{18}O_{PO4}$ isotope data for modern fish teeth from Egypt and Israel as well as archaeological (Chalcolithic and Iron Age) Gilthead seabream and fossil shark teeth from the Southern Levant. Fish tooth $^{87}Sr/^{86}Sr$ and $\delta^{18}O_{PO4}$ data are plotted in comparison to the expected ranges of the fish habitats, calculated based on published water data (see text for details and **Table 4**). Note that all modern fish teeth fall within the according expected isotopic ranges of the water bodies in which they were captured. The modern blue fish from the brackish Kishon River estuary falls within the calculated range of mixed Mediterranean seawater and Israeli groundwater (blue stippled lines), with Kishon River as the primary freshwater source. Note the fossil marine sharks fall within the expectation field for Late Cretaceous seawater and do not overlap with any modern marine influenced water body.

lake water resulting in $\delta^{18}O_{Water}$ values between −2.5 and 0.0‰ (**Figure 6**; Gat, 1970).

Linear discriminant analysis was performed on water samples of known provenance and associated modern fish tooth samples for cross-validation, producing an error rate of 18%. This is due to the multiple partial overlaps in $^{87}Sr/^{86}Sr$ and $\delta^{18}O_{PO4}$ values from the different bodies of water: Bardawil Lagoon with the Mediterranean Sea, and the Nile River with both Lake Manzala as well as Lake Kinneret/Jordan River (**Figures 4, 6** and **Table 4**). Nevertheless, more than 80% of the modern fish of known provenance were correctly assigned to their respective water bodies using LDA (**Supplementary Table S4**).

Sr and O Isotope Data of Archaeological and Fossil Fish Teeth

The $^{87}Sr/^{86}Sr$ and $\delta^{18}O_{PO4}$ data of sharks and *S. aurata* from Chalcolithic and Iron Age archaeological layers of Israel are summarised in **Table 3** and shown in **Figure 6**. The shark teeth obtained from the Iron Age I-II periods of Jerusalem, all yielded unexpectedly low enameloid $^{87}Sr/^{86}Sr$ and $\delta^{18}O_{PO4}$ values for contemporaneous sharks, ranging between 0.7074 and 0.7076, and between 18.3 and 20.7‰, respectively. Placing the $^{87}Sr/^{86}Sr$ of the seven shark teeth on the Sr seawater curve (McArthur et al., 2020) yields Late Cretaceous Sr stratigraphic ages ranging from 86.5 to 76.3 Ma (**Table 3**) with an average late Santonian/early Campanian age of around 80.29 Ma +3.24, −2.64 Ma. The age uncertainties include analytical uncertainties, the 95% confidence interval of the Sr seawater curve, as well as the standard deviation of the calculated Sr stratigraphic ages. Six shark teeth cluster between 76.3 to 80.7 Ma (early Campanian). Only specimen SK-86 yields an older age of 86.5 Ma (latest Cenomanian/early Santonian) (**Table 3**). Their $\delta^{18}O_{PO4}$ are in good agreement with those of Campanian fossil fish teeth (teleosts and sharks) from Israel and Jordan ranging from 18.3 to 20.0‰ (Kolodny and Raab, 1988). In contrast, *S. aurata* teeth from similar archaeological contexts exhibited marine $^{87}Sr/^{86}Sr$ of around 0.7092, typical for modern seawater, and $\delta^{18}O_{PO4}$ values that agree well with the range expected for fish from

Mediterranean surface water or the hypersaline water of the Bardawil Lagoon (**Figures 4A, 6**), which formed as the result of seawater evaporation at the north Sinai coast.

To assign a provenance to archaeological fish samples, LDA was performed using the modern water and fish tooth reference dataset. All Chalcolithic/Iron Age seabream specimens were assigned to either the Bardawil Lagoon (50%, n = 3) or to the Mediterranean Sea (50%, n = 3) (**Supplementary Tables S4–S6**). Both Iron Age seabream teeth SP-11 and SP-13 from the City of David as well as one Chalcolithic specimen (EB-5) from Gilat (also with a high, Bardawil-like, $\delta^{18}O_{PO4}$ value) derive from the hypersaline Bardawil Lagoon. The other three seabream specimens from Gilat were all assigned a Mediterranean provenance (**Supplementary Table S5**). For the fossil shark teeth, all specimens were assigned to the Late Cretaceous seawater field, except for sample SK-83 (**Supplementary Tables S7–S9**). The LDA gave the same result when Late Cretaceous seawater values were restricted to those of the Campanian period. In both scenarios the sample SK-83 was assigned to Lake Kinneret/Jordan River, which is obviously incorrect for an 80 million-year-old fossil shark, and thus is best explained by the overlap of the two water bodies in Sr and O isotope space. Note also the incorrect assignment of the Nile perch (*Lates niloticus*) to the Mediterranean (**Supplementary Table S5**), resulting from diagenetic alteration of its bone Sr isotope composition (**Figure 7**).

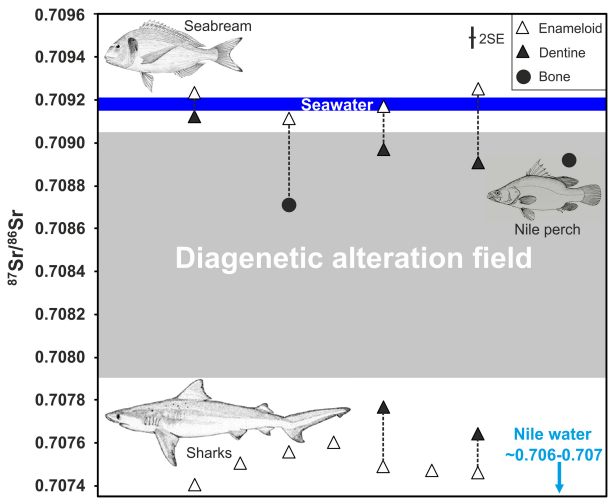

FIGURE 7 | Strontium isotope ratios of pairs of enameloid and dentine of fossil shark and archaeological Gilthead seabream (*Sparus aurata*) teeth from Iron Age (Jerusalem, City of David) and Chalcolithic (Gilat) archaeological sites (**Table 3**). A Nile perch vertebra bone from the Iron Age site of Ashkelon and one jawbone from *S. aurata* from the City of David are also plotted. Both are clearly diagenetically altered and fall within the range of values expected due to diagenetic alteration (grey field) defined by the range of $^{87}Sr/^{86}Sr$ for soil and rainwater compositions from Israel (**Table 4**). In contrast, none of the enameloid samples seem to be affected by diagenesis and instead preserve the original water $^{87}Sr/^{86}Sr$ of the Gilthead seabream and shark habitats. Note that all seven shark enameloid samples from different taxa have low $^{87}Sr/^{86}Sr$ between 0.7074 and 0.7076 reflecting Late Cretaceous (mostly Campanian) seawater values (McArthur et al., 2020).

DISCUSSION

Using fish tooth enameloid $^{87}Sr/^{86}Sr$ and $\delta^{18}O_{PO4}$ values collected from extant fish from different water bodies in Egypt and the Southern Levant enabled us to establish an isotopic reference dataset, which we then used as an interpretive framework for inferring the provenance of ancient *S. aurata* and different shark species recovered in coastal and inland archaeological layers from the Chalcolithic and Iron Age I-II periods (**Figure 2A**). *Post mortem* diagenetic alteration was carefully assessed to ensure that the original Sr and O isotope compositions are well preserved and still reflect the isotope values of the ambient water of the fish habitat. Fish taxonomic identification, combined with XRD, TOC and trace element (i.e., REE, U) analysis of dentine clearly demonstrated that the *S. aurata* teeth are sub-fossil archaeological fish teeth while the shark teeth from the same Iron Age cultural layers are all fossil teeth, most likely from the Late Cretaceous.

Variation of $^{87}Sr/^{86}Sr$ in Extant Shark and Bony Fish as Marker of Their Habitat

Marine shark and bony fish tooth enameloid both record the $^{87}Sr/^{86}Sr$ of ambient seawater. Hence, extant sharks from different oceanic basins and water depths with different hydrological conditions in temperature and salinity have rather uniform, seawater-like tooth $^{87}Sr/^{86}Sr$ values, averaging 0.709167 (range: 0.709160–0.709172, n = 8; Vennemann et al., 2001). In this study we obtained a similar value of 0.70919 ± 0.00005 (2 SE, n = 2; **Table 2**) for extant sharks from the Mediterranean (*Centrophorus granulosus*) and from the Red Sea (*Carcharinus plumbeus*), which matches the modern-day global seawater value of 0.70918 (McArthur et al., 2020). Similarly, tooth enameloid of modern *S. aurata* from the Eastern Mediterranean Sea also yields a typical marine values (**Table 2**). Much lower $^{87}Sr/^{86}Sr$, between 0.70681 ± 0.00008 and 0.70757 ± 0.00005 (2 SE), were measured in the teeth of three species of modern Cyprinidae from Lake Kinneret, which receives its water from the Golan Heights drainage area that is mainly underlain by basaltic bedrocks (Hartman and Richards, 2014). The two freshwater cyprinids *Luciobarbus longiceps* and *Carasobarbus canis* have $^{87}Sr/^{86}Sr$ that vary between 0.70731 and 0.70757, agreeing well with Lake Kinneret water with an average $^{87}Sr/^{86}Sr$ of 0.70750 ± 0.00005 (2 SE) (Fruchter et al., 2017). Even lower values, between 0.70681 ± 0.00008 and 0.70729 ± 0.00006 (2 SE), were obtained for the *C. damascina* samples that are in good agreement with the Sr isotope composition of the main fresh water source of Lake Kinneret and the Jordan River, which has an average $^{87}Sr/^{86}Sr$ of 0.70678 ± 0.00006 (1 SD) (Fruchter et al., 2017). This is well in line with the known migration behavior of some Cyprinidae species, including *C. damascina*, between Lake Kinneret and the Jordan River (Fishelson et al., 1996). All of these results further support the argument that fish, including sharks, record the $^{87}Sr/^{86}Sr$ of their ambient water. All extant marine and freshwater fish fall well within their respective expected isotopic ranges for the aquatic habitats in which they were caught (**Figure 6**). This

was supported by Linear Discriminant (LDA) analysis, which correctly assigned more than 80% of the modern fish to the correct water bodies based on their tooth Sr and O isotope composition (**Supplementary Table S4**).

Nilotic fish teeth and bones have $^{87}Sr/^{86}Sr$ between 0.70681 and 0.70737 (**Table 2** and **Figure 6**), which are in good agreement with modern Nile water values ranging from 0.70600 to 0.70718 (Brass, 1976; Gerstenberger et al., 1997; this study; **Table 4**). Similar values occur in freshwater fish from Lake Kinneret and the Jordan River. This similarity results from the fact that the drainage area for each of these water bodies is underlain by volcanic bedrocks. In this case, the coupling of $^{87}Sr/^{86}Sr$ and $\delta^{18}O_{PO4}$ data from the same teeth can be used to further differentiate fish from different aquatic habitats with similar bedrock types (and hence dissolved Sr of similar $^{87}Sr/^{86}Sr$) in their drainage area, but different hydrological regimes (i.e., water sources, salinities and/or degree of evaporation).

Assessing *Post Mortem* Diagenetic Alteration and Fish Provenance

Post mortem diagenetic alteration in the burial environment may have overprinted and shifted the original marine Sr isotope signature of fish teeth toward lower $^{87}Sr/^{86}Sr$. We assess diagenetic alteration by comparing the $^{87}Sr/^{86}Sr$ of dentine, which is much more prone to alteration than enamel (oid) (Ayliffe et al., 1994; Hoppe et al., 2003; Tütken et al., 2008), to that of enameloid from the same tooth (**Figure 7**). Both dental tissues record *in vivo* the same $^{87}Sr/^{86}Sr$ of the ambient water (**Table 2**; Vennemann et al., 2001; Tütken et al., 2011) but *post mortem* dentine is more prone to exchange of Sr with water in the soil (Tuross et al., 1989; Becker et al., 2008), similar to bone (Nelson et al., 1986; Hoppe et al., 2003). Thus, $^{87}Sr/^{86}Sr$ of dentine and bone are both expected to shift toward diagenetic soil water values more easily than enameloid. To infer Sr isotopic compositions of potential diagenetic fluids, rain and bedrock $^{87}Sr/^{86}Sr$ in Israel are considered (**Figure 7** and **Table 4**).

The main soil types in the area where the fish teeth were excavated are Rendzina, which typically has $^{87}Sr/^{86}Sr$ between 0.7079 and 0.7084 and Terra rossa, with a mean value of 0.70857 ± 0.00026 (1 SD) (Hartman and Richards, 2014). Both soils developed by weathering over Cretaceous-Eocene marine sedimentary rocks, thus soil pore water values are expected to have similar $^{87}Sr/^{86}Sr$ (**Table 4**). Several studies have demonstrated that Sr from pore water in soils can exchange with bioapatite (Nelson et al., 1986; Hoppe et al., 2003). Thus, diagenetic alteration would be expected to shift $^{87}Sr/^{86}Sr$ toward soil water values. Indeed, the dentine of the Chalcolithic *S. aurata* teeth shows slight modification toward the soil water field, as do the fossil shark teeth from Jerusalem.

Furthermore, the $^{87}Sr/^{86}Sr$ measured in modern rainwater samples from Israel range between 0.7079 and 0.7092 (mean 0.7087 ± 0.0004, 1 SD; n = 18; Herut et al., 1993; Frumkin and Stein, 2004). The major sources contributing to the $^{87}Sr/^{86}Sr$ in rainfall are Cretaceous-Eocene marine sedimentary rocks, dissolved Mid-Cretaceous-Eocene chalk dust from the Sahara (0.7078) and small quantities of sea spray (0.7092) (Herut et al., 1993). However, none of these Sr sources has low enough $^{87}Sr/^{86}Sr$ to explain the values we obtained from the fossil shark teeth from the Iron Age cultural layers. Groundwater from Late Cretaceous aquifers of Israel have low $^{87}Sr/^{86}Sr$ of around 0.7075 but these deep aquifers are located further inland in the Judean and Samarian arches (Starinsky et al., 1980) and thus cannot have contributed Sr to cause diagenetic alteration in the archaeological sites investigated.

Thus, the low enameloid $^{87}Sr/^{86}Sr$ of the shark teeth cannot be explained by diagenesis as no potential Sr source with such low values is present in the burial setting. In contrast, diagenesis should increase the $^{87}Sr/^{86}Sr$ of the shark teeth, as occurs in the dentine of the same teeth, which are clearly altered (**Figure 5**) and shifted to higher $^{87}Sr/^{86}Sr$ (**Figure 7**). Even if some degree of diagenesis is invoked, the original shark enameloid $^{87}Sr/^{86}Sr$ are even lower, suggesting that measured data should be considered as maximum values. Regardless, any significant alteration is rather unlikely as enameloid of marine *S. aurata* still reflects expected seawater $^{87}Sr/^{86}Sr$ within an uncertainty of 0.00002 (2 SE) and is not shifted toward lower values of the diagenetic soil water endmember, as is the case for the dentine/bone of the same teeth/fish (**Figure 7**). Therefore, their original enameloid $^{87}Sr/^{86}Sr$ is very likely preserved.

Moreover, the dentine in the shark teeth has higher $^{87}Sr/^{86}Sr$ than the enameloid, approaching $^{87}Sr/^{86}Sr$ of bedrocks and rainfall in the study area (**Figure 7**). In contrast, dentine $^{87}Sr/^{86}Sr$ of *S. aurata* are shifted to lower values compared to the seawater-like enameloid values. Thus, dentine $^{87}Sr/^{86}Sr$ of both sharks and *S. aurata* converge on the diagenetic fluid values, which are controlled by the local bedrock substrate (**Figure 7**). The opposing directions of the isotopic shifts in $^{87}Sr/^{86}Sr$ between the enameloid-dentine/jawbone pairs of shark and *S. aurata* teeth further support preservation of original enameloid $^{87}Sr/^{86}Sr$ in fish teeth. Therefore, we can conclude that original, low enameloid $^{87}Sr/^{86}Sr \approx 0.7075$ values in the shark teeth and high, modern seawater-like enameloid $^{87}Sr/^{86}Sr \approx 0.7092$ in *S. aurata* teeth from the same layers are still preserved. The shark enameloid $^{87}Sr/^{86}Sr$ fall well into the Late Cretaceous seawater field (**Figure 6**), as expected based on the taxonomic identification of some of the shark teeth (i.e., *Squalicorax* sp.) to Late Cretaceous taxa. Thus, these shark teeth are clearly fossils although they were found together with thousands of other archaeological fish remains in Iron Age cultural deposits (**Table 1**).

Sparus aurata is a marine fish with a unique life cycle that includes exploitation of hypersaline lagoons (Tancioni et al., 2003). We observed elevated $\delta^{18}O_{PO4}$ values in the teeth of *S. aurata*, implying that these fish originated from closed or semi-closed water bodies with a high degree of evaporation, such as the hypersaline Bardawil Lagoon situated on the Northern Sinai coast in Egypt (Kolodny et al., 1983; Sisma-Ventura et al., 2015, 2018, 2019). A high rate of evaporation increases the $\delta^{18}O_{Water}$ of the Mediterranean seawater from which the shallow, nearshore Bardawil Lagoon forms. It does not, however, change its water $^{87}Sr/^{86}Sr$. This was confirmed by strontium isotope

analysis of a water sample taken from the Bardawil Lagoon in January 2019 yielding a $^{87}Sr/^{86}Sr$ of 0.70916 ± 0.00002 (2 SE) which is the same (within error) as the value for hypersaline eastern Mediterranean seawater (0.709172; Reinhardt et al., 2001 and references therein; **Table 4**). One *S. aurata* tooth from Gilat (EB-5) and two from the City of David (SP-11, SP-13) are characterised by hypersaline $\delta^{18}O_{PO4}$ (**Figure 4A**) and seawater-like $^{87}Sr/^{86}Sr$ (**Figure 4** and **Table 3**). Based on their Sr and O isotope signature, the LDA assigned 50% (three out of six) of the archaeological *S. aurata* teeth to a hypersaline water origin, most likely the Bardawil Lagoon, and the remainder to the Mediterranean (**Supplementary Table S5**). This agrees well with previous $\delta^{18}O_{PO4}$ results for *S. aurata* teeth from other Late Bronze Age to Iron Age sites in Israel and indicates a Bardawil Lagoon origin for these fish (Sisma-Ventura et al., 2018). Thus, seabreams were presumably exported from Northern Egypt (Bardawil Lagoon) to the Southern Levant (specifically to the City of David, Jerusalem) during the Iron Age, and perhaps even as early as the Chalcolithic. Since there are no indications for hypersaline lagoons (only for some brackish lagoons) along the Israeli coast during the Holocene (Sivan et al., 2011, 2016), the Bardawil and/or other hypersaline lagoons must have existed elsewhere in the Southern Levant.

Finally, while the $^{87}Sr/^{86}Sr$ of the dentine of *S. aurata* is only somewhat altered by diagenesis, the $^{87}Sr/^{86}Sr$ (0.70892 ± 0.00006, 2 SE) of the Iron Age Nile perch vertebra from the coastal site of Ashkelon (**Figure 7**) is strongly altered and clearly shifted by >0.002 from expected Nilotic values ≈ 0.706 to 0.707 (Brass, 1976; Gerstenberger et al., 1997; **Table 4**) toward a much higher $^{87}Sr/^{86}Sr$ within in the soil water alteration field (**Figure 7**). This indicates that fish vertebrae, although abundant in archaeological sites, are prone to diagenetic alteration and thus not suitable to assess fish provenance.

Assessing the Origin and Age of Fossil Shark Teeth From Jerusalem

Some of the shark teeth recovered from strata dated to the 8–9th century BCE (Iron Age I-II) (Reich et al., 2007, 2008) in the City of David, Jerusalem, were identified (based on morphology) as extinct species from the Upper Cretaceous (e.g., *Squalicorax*). All shark teeth (including those which were not taxonomically identifiable), display trace element signatures of high U and Nd contents (**Figure 5A**), typical for fossilised fish teeth (Staudigel et al., 1985; Pucéat et al., 2003; Kocsis et al., 2009). This was further supported by the high apatite crystallinity (**Supplementary Figure S3**) and low organic carbon content of the dentine (**Supplementary Figure S4**) typical for fossil specimens but different from archaeological *S. aurata* teeth from the same cultural layers (thus, providing a special case for which the $^{87}Sr/^{86}Sr$ can be used as a tool to date marine fossils deposited in much younger archaeological contexts). This could improve our understanding regarding the extent and the meaning of this phenomenon in archaeological sites.

The $^{87}Sr/^{86}Sr$ values of these fossil shark teeth do not fit the modern reference dataset compiled for contemporaneous fish in the southern Levant. The mean enameloid $^{87}Sr/^{86}Sr$ value of 0.70751 ± 0.00006 (1 SD; n = 7) of the fossil shark teeth from Jerusalem is much lower than the $^{87}Sr/^{86}Sr$ measured in modern sharks (≈ 0.70917, **Table 2** and **Figure 6**), but agrees well with Late Cretaceous seawater $^{87}Sr/^{86}Sr$ values. These sharks likely incorporated Sr ($^{87}Sr/^{86}Sr$ ≈ 0.7075) from a Late Cretaceous marine habitat as they fall into the Late Cretaceous seawater field according to the LDA (**Supplementary Table S8**). Indeed, age estimates using the $^{87}Sr/^{86}Sr$ seawater curve of McArthur et al. (2020) place these teeth at late Santonian/early Campanian age of around 80.29 Ma +3.24, −2.64 Ma (range: 76.3–86.5 Ma; **Table 3**). This age was further supported by the $\delta^{18}O_{PO4}$ values of fossil shark teeth from Jerusalem, agreeing well with the range of $\delta^{18}O_{PO4}$ between 18.3 and 20.0‰ of late Santonian to late Campanian shark teeth from the Southern Levant, i.e., Negev Desert (Kolodny and Raab, 1988). Assuming a seawater $\delta^{18}O$ of −1‰ for a continental ice-free Earth, marine temperatures in the subtropical zone (i.e., 30–35° N) were estimated to around 28–29°C in the Cenomanian-Turonian period (Pucéat et al., 2003). The low shark enameloid $\delta^{18}O_{PO4}$ values thus reflect tooth formation in the warm shallow, tropical seawater of the Tethys Ocean shelf (Kolodny and Raab, 1988).

The recovery of a relatively large number of shark teeth in the Iron Age assemblage of the City of David together with diverse fish remains is puzzling for two main reasons: (1) shark teeth are rare in archaeological sites in the Southern Levant (**Table 1**); (2) this study clearly demonstrates that these shark teeth are fossils and hence do not represent shark consumption. Instead the presence of these teeth may reflect collection for other cultural purposes (tools, pendants, etc.), as has been observed in different contexts worldwide (Cione and Bonomo, 2003; Betts et al., 2012; Charpentier et al., 2020). Alternatively, the fossils were simply a component of the local soil substrate and derive from weathering processes of the Late Cretaceous limestone substrate. However, this is not very likely as the Late Cretaceous marine sedimentary strata beneath the City of David are stratigraphically older (Turonian; **Figure 8**) than the Sr-stratigraphic age of the fossil shark teeth (late Santonian/early Campanian). However, fossil shark teeth from the Late Cretaceous are abundant in the marine sediments of the Mount Scopus group in Israel and in the Menuha Formation of the Southern Negev (**Figure 2A**; Gvirtzman, 2004; Gvirtzman et al., 2008; Wilson et al., 2012; Retzler et al., 2013).

Shark teeth recovered in the City of David were mainly from the "Rock Cut Pool" (**Figure 2B**; note that the complete area of this structure was fully excavated and sieved, Reich et al., 2007, 2008), and from area G, a mixed dump deposition, dated to *ca.* 586 BCE (Lernau, 2015). In area G, nine shark teeth were recovered, but these were not used in this study. However, except for these two locations, no fossil shark teeth have been reported from geological strata in the city of David or anywhere else in Jerusalem. Thus, the fossil shark teeth found in the City of David are probably not derived from the underlying marine limestone and dolomite of the Shivta Formation, which is of Turonian age (Rosenfeld and Hirsch, 2005; **Figure 8**), and is thus older than the Santonian/Campanian age inferred by Sr stratigraphy for the

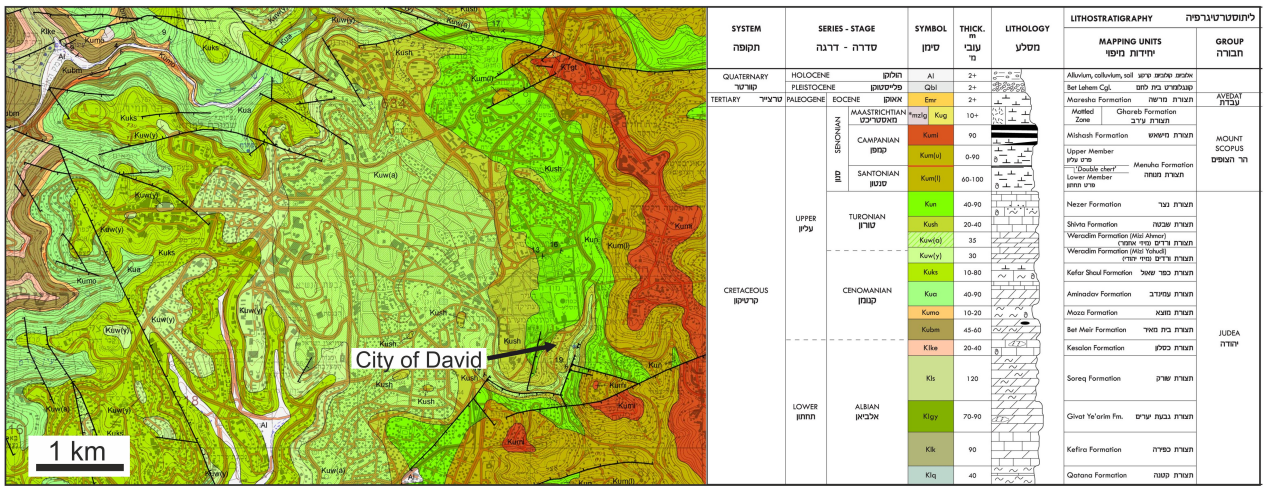

FIGURE 8 | Geological map of Jerusalem with the City of David modified from Rosensaft and Sneh (2011). Therefore, rock formation names are provided in both English and Hebrew (as provided in the official geological map of Jerusalem). The City of David is situated on marine sedimentary strata of the Shivta Formation being Turonian in age. Note that the fossil shark teeth found in the Iron Age strata yielded younger late Santonian/early Campanian Sr stratigraphic ages. Such fossil shark teeth are only known from the Menuha Formation of the Mount Scopus group in the Negev Desert (Kolodny and Raab, 1988; Retzler et al., 2013). These shark teeth bearing outcrops are 90 km up to 180 km south of Jerusalem in the Negev Desert (**Figure 2A**). Note that sediments of the Menuha Formation also crop out at the hillslopes a few hundred meters east/southeast of the City of David, however, no fossil shark teeth were reported from these strata.

fossil shark teeth. However, Turonian (0.70732 ± 0.00002 1 SD) and Campanian (0.70758 ± 0.00008 1 SD) seawater $^{87}Sr/^{86}Sr$ differ on average by only 0.00026 (McArthur et al., 2020). Therefore, only a slight diagenetic alteration of the enameloid $^{87}Sr/^{86}Sr$ by +0.00016 would be sufficient to shift the value of Turonian shark teeth to the observed value 0.70751 and hence a late Santonian/early Campanian age. The dentine of two of the shark teeth was diagentically shifted by 0.0001–0.0002, yielding higher $^{87}Sr/^{86}Sr$ values compared to enameloid. Strontium isotopes in sub-mm sized Cenozoic fossil fish teeth from marine sediment drill cores are prone to diagenetic alteration (Martin and Scher, 2004). However, the fluorapatite of the enameloid of larger cm-sized shark teeth is less prone to diagenesis and still has low U and Nd contents (about 10 times lower compared to the dentine; **Figure 5A**) and no correlation was observed between Sr and U contents (**Figure 5B**), which could be taken as an indication against significant diagenetic alteration of the Sr isotope composition. The Sr stratigraphic age of the fossil shark teeth from the City of David fits perfectly to the Santonian to early Campanian age of the fossil shark teeth-bearing Menuha Formation in the southern Negev (Retzler et al., 2013). Therefore, we can conclude that these fossil shark teeth may have been collected in the Negev Desert up to 90 km south of Jerusalem (**Figure 2A**). For instance from the Letaot Mountain fossil shark teeth of late Santonian/early Campanian age are known (Kolodny and Raab, 1988). The Menuha Formation also crops out in hill slopes a few hundred meters to the east/southeast of the City of David (**Figure 8**), however, no finds of fossil shark teeth are reported from this or other areas in Jerusalem thus far. Therefore, it is entirely feasible that the fossil teeth were transported to the City of David although the reason for bringing these teeth to the city and their function remains elusive.

CONCLUSION

We establish a Sr and O isotope reference dataset for bioapatite of modern marine and freshwater fish from the Mediterranean, Bardawil Lagoon, Lake Kinneret, Jordan River and Nile River. Fish from these different water bodies in Egypt and the Southern Levant have distinct Sr and O isotope signatures that enable us to distinguish their provenance from Nilotic, hypersaline, marine and fresh water bodies using LDA. This will be an important asset for future provenance studies of archaeological fish remains in the Levant and will shed new light on the Levantine fish provenance and trade. Unexpectedly, multiple Late Cretaceous (80.3 ± 3.2 Ma) fossil shark teeth were encountered in the same Iron Age cultural layers of the City of David, Jerusalem together with a wide diversity of archaeological fish originating from the Mediterranean Sea and the Nile. These fossil shark teeth clearly do not represent food remnants although their use remains elusive. It may be they were brought to the city intentionally as the nearest fossil shark teeth bearing outcrops of Campanian age are situated in the Negev Desert (≈ 90 km south of Jerusalem), although similar aged strata also crop out near the City of David. Thus, in archaeological fish assemblages, fossil fish teeth can also be encountered. This should be carefully evaluated, and we here provide a toolset comprised of combined dentine XRD, TOC and trace element (i.e., U, REE) analysis to distinguish fossil from archaeological teeth based on degree of diagenetic alteration. In contrast, the enameloid of the fossil shark and the archaeological Gilthead seabream (*S. aurata*) teeth still preserves its original $^{87}Sr/^{86}Sr$ and $\delta^{18}O_{PO4}$ values. The Sr and O isotope signatures indicate that some of the Gilthead seabreams were not caught locally in the Mediterranean, but instead in the hypersaline water of the Bardawil Lagoon and were

imported from Egypt to coastal and inland sites in Israel during the Iron Age and probably already since the Chalcolithic. We demonstrate that this dual-isotope approach, frequently used to assess provenance of terrestrial vertebrates, is also a powerful toolset for tracing the provenance of fish and provides new insights into past human fish exploitation (even of fossil fish teeth) and trade patterns.

DATA AVAILABILITY STATEMENT

The original contributions presented in the study are included in the article/**Supplementary Material**, further inquiries can be directed to the corresponding author/s.

ETHICS STATEMENT

Ethical review and approval was not required for the animal study because we analysed modern staple food fish obtained from fishermen as well as archaeological and fossil fish teeth.

AUTHOR CONTRIBUTIONS

TT and GS-V designed the research. TT, GS-V, IZ, and MW wrote the manuscript. GS-V and TT interpreted the isotope data. HH, IZ, and OL provided and prepared the fish samples. IZ determined the fish species and provided the all fish related information. MW performed the Sr isotope and LA-ICP-MS analysis and evaluated the Sr isotope data. TT evaluated TOC, XRD and trace element data. NB performed the statistics using Linear Discriminant Analysis (LDA). GS-V prepared the tooth samples for oxygen isotope analysis. KJ provided the analytical facilities for Sr isotope analysis. All authors contributed to the article and approved the submitted version.

FUNDING

This project received funding from the European Research Council (ERC) under the European Union's Horizon 2020 Research and Innovation Programme (grant agreement no. 681450). MW is thankful to the Max Planck Graduate Center for funding.

ACKNOWLEDGMENTS

We thank Torsten Vennemann and Michael Maus for performing phosphate oxygen isotope measurements and Hubert Vonhof for running water samples for oxygen isotope analyses and the dentine for carbonate content. We thank B. Stoll and U. Weis for assistance in the LA-MC-ICP-MS laboratory. Modern Mediterranean fish were collected as part of the Israel Oceanographic and Limnological Research deep-sea national monitoring program. We thank Sabine Fiedler and Björn Glasner for total carbon analysis, Sven Brömme for TIC analysis, and Ralf Meffert for the XRD analysis of the dentine samples. Special thanks to Jürgen Kriwet for taxonomic shark tooth identification. Or Bilak is kindly acknowledged for discussing Cretaceous geology of Israel and fossil shark tooth occurrence. Menachem Goren, from the Steinhardt Museum, Tel Aviv University, provided us information regarding the biogeographic distribution of *Oreochromis niloticus*. We also thank especially Jennifer Leichliter for meticulously proofreading the English. Finally, yet importantly, we want to thank the two reviewers who helped with their constructive comments to significantly improve the manuscript. Especially the reviewer who pointed us to the possibility that the shark teeth from the archaeological layers could be fossil teeth, which was a game changer. It led us to perform additional analysis and, ultimately, to rework the narrative of the manuscript, changing the story from shark exportation from the Nile delta to fossil shark finds in cultural layers. This was a textbook example how a good review should work and we are very appreciative.

SUPPLEMENTARY MATERIAL

The Supplementary Material for this article can be found online at: https://www.frontiersin.org/articles/10.3389/fevo.2020.570032/full#supplementary-material

REFERENCES

Aly, A. I. M., Hamed, M. A., Abd El-Samie, S. G., and Eweida, E. A. (2004). Environmental isotopes and hydrochemistry approach to evaluate the source of recharge and pollution load in Manzala and Bardawil Lakes, Egypt (IAEA-CN-118/85). Isotopes in Environmental Studies Aquatic Forum Conference and Symposium Papers 26, 172–173.

Ayliffe, L. K., Chivas, A. R., and Leakey, M. G. (1994). The retention of primary oxygen isotope compositions of fossil elephant skeletal phosphate. *Geochim. Cosmochim. Acta* 58, 5291–5298. doi: 10.1016/0016-7037(94)90312-3

Bartosiewicz, L., Lisk, E., and Zohar, I. (2018). "Non-mammalian vertebrate remains," in *Excavations at Dor, Final Report. Volume IIB, Area G, The Late Bronze and Iron Ages: Pottery, Artifacts, Ecofacts and other studies, Qedem Reports*, eds A. Gilboa, I. Sharon, J. R. Zorn, S. Matskevich (Jerusalem: The Hebrew University of Jerusalem), 313–322.

Becker, M. A., Seidemann, D. E., Chamberlain, J. A., Buhl, D., and Slattery, W. (2008), Strontium isotopic signatures in the enameloid and dentine of upper Cretaceous shark teeth from western Alabama: paleoecologic and geochronologic implications. *Palaeogeogr. Palaeoclimatol. Palaeoecol.* 264, 188–194. doi: 10.1016/j.palaeo.2008.04.006

Berglund, M., and Wieser, M. E. (2011). Isotopic compositions of the elements 2009 (IUPAC Technical Report). *Pure Appl. Chem.* 83, 397–410. doi: 10.1351/pac-rep-10-06-02

Betts, M., Blair, S., and Black, D. (2012). Perspectivism, mortuary symbolism, and human-shark relationships on the Maritime Peninsula. *Am. Antiq.* 77, 621–645. doi: 10.7183/0002-7316.77.4.621

Bialik, O. M., and Sisma-Ventura, G. (2016). Proxy-based reconstruction of surface water acidification and carbonate saturation of the Levant Sea during the Anthropocene. *Anthropocene* 16, 42–53. doi: 10.1016/j.ancene.2016.08.001

Borhegyi, S. F. (1961). Shark teeth, stingray spines, and shark fishing in ancient Mexico and Central America. *Southwest. J. Anthropol.* 17, 273–296. doi: 10.1086/soutjanth.17.3.3629046

Botella, H., and Valenzuela-Ríos, J. I., and Martínez-Perez, C. (2009). Tooth replacement rates in early chondrichthyans: a qualitative approach. *Lethaia* 42, 365–376. doi: 10.1111/j.1502-3931.2009.00152.x

Boulanger, C., Puaud, S., Ly, V., Glémarec, L., Heng, S., and Forestier, H. (2020). Fishbone artefacts from the Samrong Sen site, Cambodia, cast new light on Bronze Age networking between inland and coastal communities. *Int. J. Osteoarchaeol.* doi: 10.1002/oa.2922

Brass, G. W. (1976). The variation of the marine $^{87}Sr/^{86}Sr$ ratio during Phanerozoic time: interpretation using a flux model. *Geochim. Cosmochim. Acta* 40, 721–730. doi: 10.1016/0016-7037(76)90025-9

Bryant, J. D., Jones, D. S., and Mueller, P. A. (1995). Influence of freshwater flux on 87Sr/86Sr chronostratigraphy in marginal marine environments and dating of vertebrate and invertebrate faunas. *J. Paleontol.* 69, 1–6. doi: 10.1017/s002233600002686x

Cappetta, H. (2012). "Mesozoic and Cenozoic Elasmobranchii: teeth. Chondrichthyes," in *Handbook of Palaeoichthyology, 3E*, ed. H. P. Schulze (München: Dr. Friedrich Pfeil), 512.

Chadwick, O. A., Derry, L. A., Vitousek, P. M., Huebert, B. J., and Hedin, L. (1999). Changing sources of nutrients during four million years of ecosystem development. *Nature* 397, 491–497. doi: 10.1038/17276

Charpentier, V., Adnet, S., and Cappetta, H. (2020). The tooth of a giant sea creature *Otodus* (*Megaselachus*) in the material culture of Neolithic maritime hunter-gatherers at Sharbithat (Sultanate of Oman). *Int. J. Osteoarchaeol.* doi: 10.1002/oa.2914

Chenery, C., Müldner, G., Evans, J., Eckardt, H., and Lewis, M. (2010). Strontium and stable isotope evidence for diet and mobility in Roman Gloucester, UK. *J. Archaeol. Sci.* 37, 150–163. doi: 10.1016/j.jas.2009.09.025

Cione, A., and Bonomo, M. (2003). Great white shark teeth used as pendants and possible tools by Early-Middle Holocene terrestrial mammal hunter-gatherers in the Eastern Pampas (Southern South America). *Int. J. Osteoarchaeol.* 13, 222–231. doi: 10.1002/oa.678

Davis, S. J. M. (1985). "A preliminary report of fauna from Hatula: a Natufian-Khiamian (PPNA) site near Latroun, Israel," in *Le site Natufian-Khiamien de Hatoula, pres de Latroun, Israel*, eds M. Lechevallier and A. Ronen (Jerusalem: Centre de Recherche Français de Jérusalem), 71–118.

De Groot, A., and Fadida, A. (2011). The Pottery Assemblage from the Rock Cut Pool near the Gihon Spring. *Tel Aviv* 38, 158–166. doi: 10.1179/033443511x13099584885501

Debiais-Thibaud, M., Borday-Birraux, V., Germon, I., Bourrat, F., Metcalfe, C., Casane, D., et al. (2007). Development of oral and pharyngeal teeth in the Medaka (*Oryzias latipes*): comparison of morphology and expression of eve1 Gene. *J. Exp. Zool. B Mol. Dev. Evol.* 308, 693–708. doi: 10.1002/jez.b.21183

Debiais-Thibaud, M., Chiori, R., Enault, S., Oulion, S., Germon, I., Martinand-Mari, C., et al. (2015). Tooth and scale morphogenesis in shark: an alternative process to the mammalian enamel knot system. *BMC Evol. Biol.* 15:292. doi: 10.1186/s12862-015-0557-0

Dettmann, I., Kohn, M., Quade, J., Reyerson, F. J., Ojah, T. P., and Hamidullah, S. (2001). Seasonal stable isotope evidence for a strong Asian monsoon throughout the past 10.7 Ma. *Geology* 29, 31–34. doi: 10.1130/0091-7613(2001)029<0031:ssiefa>2.0.co;2

Dufour, E., Holmden, C., Van Neer, W., Zazzo, A., Patterson, W. P., Degryse, P., et al. (2007). Oxygen and strontium isotopes as provenance indicators of fish at archaeological sites: the case study of Sagalassos, SW Turkey. *J. Archaeol. Sci.* 34, 1226–1239. doi: 10.1016/j.jas.2006.10.014

Enault, S., Guinot, G., Koot, M., and Cuny, G. (2015). Chondrichthyan tooth enameloid: past, present, and future. *Zool. J. Linn. Soc.* 174, 549–570. doi: 10.1111/zoj.12244

Enax, J., Janus, A. M., Raabe, D., Epple, M., and Fabritius, H.-O. (2014). Ultrastructural organization and micromechanical properties of shark tooth enameloid. *Acta Biomater.* 10, 3959–3968. doi: 10.1016/j.actbio.2014.04.028

Enax, J., Prymak, O., Raabe, D., and Epple, M. (2012). Structure, composition and mechanical properties of shark teeth. *J. Struct. Biol.* 118, 290–299. doi: 10.1016/j.jsb.2012.03.012

Fetner, R. A., and Iwaszczuk, U. (2020). Isotopic evidence of possible long-distance freshwater fish trade in the 13th to 14th century Chełm, modern Poland. *Int. J. Osteoarchaeol.* doi: 10.1002/oa.2931

Fischer, J., Schneider, J., Voigt, S., Joachimski, M., Tichomirowa, M., Tütken, T., et al. (2013). Oxygen and strontium isotopes from fossil shark teeth: environmental and ecological implications for Late Palaeozoic European basins. *Chem. Geol.* 342, 44–62. doi: 10.1016/j.chemgeo.2013.01.022

Fishelson, L., Goren, M., Van Vuren, J., and Manelis, R. (1996). Some aspects of the reproductive biology of *Barbus* spp., *Capoeta damascina* and their hybrids (Cyprinidae, Teleostei) in Israel. *Hydrobiologia* 317, 79–88. doi: 10.1007/bf00013728

Fradkin, A., and Lernau, O. (2006). "The fish bone remains," in *Tel Tanninim: Excavations at Krokodeilon Polis, 1996-1999*, ed. R. R. Stieglitz (Boston, MA: The American Schools of Oriental Research), 211–222.

Fradkin, A., and Lernau, O. (2008). "The fishing economy at Caesarea," in *Caesarea Reports and Studies: Excavations 1995-2007 within the Old City and the Ancient Harbor, BAR International Series 1784*, eds K. G. Holum, J. A. Stabler, and E. G. Reinhardt (Oxford: Archaeopress), 189–200.

Friedman, J., Hastie, T., and Tibshirani, R. (2001). *The Elements of Statistical Learning* (Vol. 1). (New York, NY: Springer).

Fruchter, N., Lazar, B., Nishri, A., Almogi-Labin, A., Eisenhauer, A., Be'eri Shlevin, Y., and Stein, M. (2017). $^{88}Sr/^{86}Sr$ fractionation and calcite accumulation rate in the Sea of Galilee. *Geochim. Cosmochim. Acta* 215, 17–32. doi: 10.1016/j.gca.2017.07.026

Frumkin, A., and Stein, M. (2004). The Sahara–East Mediterranean dust and climate connection revealed by strontium and uranium isotopes in a Jerusalem speleothem. *Earth Planet. Sci. Lett.* 217, 451–464. doi: 10.1016/s0012-821x(03)00589-2

Galili, E., Lernau, O., and Zohar, I. (2004). Fishing and coastal adaptations at 'Atlit-Yam- A submerged PPNC fishing village off the Carmel Coast, Israel. *Atiqot* 48, 1–34.

Garfinkel, Y., Dag, D., Hesse, B., Wapnish, P., Rookis, D., Hartman, G., Bar-Yosef Mayer, D. E., and Lernau, O. (2005). Neolithic Ashkelon: meat processing and early pastoralism on the Mediterranean coast. *Eurasian Prehist.* 3, 43–72.

Gat, J. R., and Dansgaard, W. (1972). Stable isotope survey of the fresh water occurrences in Israel and the northern Jordan rift valley. *J. Hydrol.* 16, 177–212. doi: 10.1016/0022-1694(72)90052-2

Gat, J. R. (1970). "Environmental isotope balance of Lake Tiberias," in *Proceedings of IAEA Symposium on Isotope Hydrology*, Vienna 109–127.

Gerstenberger, H., Haase, G., and Abou El Nour, F. (1997). The origin of strontium and the strontium isotope budget of the River Nile. *Isotopes Environ. Health Stud.* 33, 349–356. doi: 10.1080/10256019708234047

Goldstein, S. J., and Jacobsen, S. B. (1987). The Nd and Sr isotopic systematics of river-water dissolved material: implications for the sources of Nd and Sr in seawater. *Chem. Geol.* 66, 245–272. doi: 10.1016/0168-9622(87)90045-5

Gvirtzman, Z. (2004). Chronostratigraphic table and subsidence curves of southern Israel. *Isr. J. Earth Sci.* 53, 48–61. doi: 10.1560/krh0-1q21-u1yg-yh4h

Gvirtzman, Z., Zilberman, E., and Folkman, Y. (2008). Reactivation of the Levant passive margin during the late Tertiary and formation of the Jaffa Basin offshore central Israel. *J. Geol. Soc.* 165, 563–578. doi: 10.1144/0016-76492006-200

Harrell, T. L., Pérez-Huerta, A., and Phillips, G. (2016). Strontium isotope age-dating of fossil shark tooth enameloid from the Upper Cretaceous Strata of Alabama and Mississippi, USA. *Cretac. Res.* 62, 1–12. doi: 10.1016/j.cretres.2016.01.011

Hartman, G., and Richards, M. (2014). Mapping and defining sources of variability in bioavailable strontium isotope ratios in the Eastern Mediterranean. *Geochim. Cosmochim. Acta* 126, 250–264. doi: 10.1016/j.gca.2013.11.015

Herut, B., Starinsky, A., and Katz, A. (1993). Strontium in rainwater from Israel – sources, isotopes and chemistry. *Earth Planet. Sci. Lett.* 120, 77–84. doi: 10.1016/0012-821x(93)90024-4

Hobbs, J. A., Lewis, L. S., Willmes, M., Denney, C., and Bush, E. (2019). Complex life histories discovered in a critically endangered fish. *Sci. Rep.* 9:16772.

Hodell, D. A., Mead, G. A., and Mueller, P. A. (1990). Variation in the strontium isotope composition of seawater (8 Ma to present): implications for chemical weathering rates and dissolved fluxes to the oceans. *Chem. Geol.* 80, 291–307. doi: 10.1016/0168-9622(90)90011-z

Hoppe, K. A., Koch, P. L., and Furutani, T. T. (2003). Assessing the preservation of biogenic strontium in fossil bones and tooth enamel. *Int. J. Osteoarchaeol.* 13, 20–28. doi: 10.1002/oa.663

Horwitz, L. K., Bar Giora, N., Mienis, H. K., and Lernau, O. (2005). "Faunal and malacological remains from the Middle Bronze, Late Bronze, and Iron Age levels at Tel Yoqne'am," in *Yone'am II: The Middle and Late Bronze Ages. Final Report of the Archaeological Excavations (1977-1988), Qedem Reports*, eds A. Ben-Tor, D. Ben-Ami, and A. Livneh (Jerusalem: Qedem), 395–431.

Horwitz, L.K., and Lernau, O. (2018). "Iron Age IIb faunal remains from the Ophel, Area A2009," in *The Ophel Excavations to the South of the Temple Mount 2009-2013*, ed. E. Mazar (Shoam: Shoam Academic Research Publication), 289–309.

Ingle, C. P., Sharp, B. L., Horstwood, M. S. A., Parrish, R. R., and Lewis, D. J. (2003). Instrument response functions, mass bias and matrix effects in isotope ratio measurements and semi-quantitative analysis by single and multi-collector ICP-MS. *J. Anal. At. Spectrom.* 18, 219–229. doi: 10.1039/b211527a

Ingram, B. L. (1995). High-resolution dating of deep-sea clays using Sr isotopes in fossil fish teeth. *Earth Planet. Sci. Lett.* 134, 545–555. doi: 10.1016/0012-821x(95)00151-2

Irrgeher, J., Galler, P., and Prohaska, T. (2016). $^{87}Sr/^{86}Sr$ isotope ratio measurements by laser ablation multicollector inductively coupled plasma mass spectrometry: reconsidering matrix interferences in bioapatites and biogenic carbonates. *Spectrochim. Acta Part B At. Spectrosc.* 125, 31–42. doi: 10.1016/j.sab.2016.09.008

Jambura, P. L., Pfaff, C., Underwood, C. J., Ward, D. J., and Kriwet, J. (2018). Tooth mineralization and histology patterns in extinct and extant snaggletooth sharks, *Hemipristis* (Carcharhiniformes, Hemigaleidae)—Evolutionary significance or ecological adaptation? *PloS ONE* 13:e0200951. doi: 10.1371/journal.pone.0200951

Jambura, P. L., Türtscher, J., Kindlimann, R., Metscher, B., Pfaff, C., Stumpf, S., et al. (2020). Evolutionary trajectories of tooth histology patterns in modern sharks (Chondrichthyes, Elasmobranchii). *J. Anat.* 236, 753–771. doi: 10.1111/joa.13145

Jernvall, J., and Thesleff, I. (2012). Tooth shape formation and tooth renewal: evolving with the same signals. *Development* 139, 3487–3497. doi: 10.1242/dev.085084

Jochum, K. P., Pfänder, J., Woodhead, J. D., Willbold, M., Stoll, B., Herwig, K., et al. (2005). MPI-DING glasses: New geological reference materials for in situ Pb isotope analysis. *Geochem. Geophys. Geosys.* 6:Q10008. doi: 10.1029/2005GC000995

Klug, S., Tütken, T., Wings, O., Pfretzschner, H., and Martin, T. (2010). A Late Jurassic freshwater shark assemblage (Chondrichthyes, Hybodontiformes) from the southern Junggar Basin, Xinjiang, Northwest China. *Palaeobiodiv. Palaeoenviron.* 90, 241–257. doi: 10.1007/s12549-010-0032-2

Kocsis, L., Gheerbrant, E., Mouflih, M., Cappetta, H., Yans, J., and Amaghzaz, M. (2014). Comprehensive stable isotope investigation of marine biogenic apatite from the late Cretaceous-early Eocene phosphate series of Morocco. *Palaeogeogr. Palaeoclimatol. Palaeoecol.* 394, 74–88. doi: 10.1016/j.palaeo.2013.11.002

Kocsis, L., Vennemann, T. W., and Fontignie, D. (2007). Migration of sharks into freshwater systems during the Miocene and implications for Alpine paleoelevation. *Geology* 35, 451–454. doi: 10.1130/g23404a.1

Kocsis, L., Vennemann, T. W., Hegner, E., Fontignie, D., and Tütken, T. (2009). Constraints on the paleoceanography and paleoclimate of the Miocene north Alpine Molasse, Vienna and Pannonian Basins: records of the O-, Sr-, and Nd-isotope composition of marine fish and mammal remains. *Palaeogeogr. Palaeoclimatol. Palaeoecol.* 271, 117–129. doi: 10.1016/j.palaeo.2008.10.003

Kocsis, L., Vennemann, T. W., Ulianov, A., and Brunnschweiler, J. M. (2015). Characterizing the bull shark *Carcharhinus leucas* habitat in Fiji by the chemical and isotopic compositions of their teeth. *Environ. Biol. Fish.* 98, 1609–1622. doi: 10.1007/s10641-015-0386-4

Kohn, M. J., Schoeninger, M. J., and Barker, W. B. (1999). Altered states: effects of diagenesis on fossil tooth chemistry. *Geochim. Cosmochim. Acta* 63, 2737–2747. doi: 10.1016/s0016-7037(99)00208-2

Kolodny, Y., and Luz, B. (1991). *Oxygen Isotopes in Phosphates of Fossil Fish-Devonian to Recent. Stable Isotope Geochemistry: A Tribute to Samuel Epstein. The Geochemical Society, Special Publication No. 3.* (Washington, DC: Geochemical Society), 105–119.

Kolodny, Y., Luz, B., and Navon, O. (1983). Oxygen isotope variations in phosphate of biogenic apatites, I. Fish bone apatite – rechecking the rules of the game. *Earth Planet. Sci. Lett.* 64, 398–404. doi: 10.1016/0012-821x(83)90100-0

Kolodny, Y., and Raab, M. (1988). Oxygen isotopes in phosphatic fish remains from Israel: paleothermometry of tropical Cretaceous and Tertiary shelf waters. *Palaeogeogr. Palaeoclimatol. Palaeoecol.* 64, 59–67. doi: 10.1016/0031-0182(88)90142-3

Krom, M. D., Michard, A., Cliff, R. A., and Strohle, K. (1999). Sources of sediment to the Ionian Sea and western Levantine basin of the Eastern Mediterranean during S-1 sapropel times. *Mar. Geol.* 160, 45–61. doi: 10.1016/s0025-3227(99)00015-8

Lécuyer, C., Amiot, R., Touzeau, A., and Trotter, J. (2013). Calibration of the phosphate $\delta^{18}O$ thermometer with carbonate–water oxygen isotope fractionation equations. *Chem. Geol.* 347, 217–226. doi: 10.1016/j.chemgeo.2013.03.008

Lernau, O. (2004). Fish remains from Early Bronze Age Ashqelon, Afridar. *Atiqot* 45, 299–303.

Lernau, H. (1988). "Fish remains from two smelting camps and the Timna temple," in *The Egyptian Mining temple at Timna. Institute for Archaeo-Metallurgical Studies [and] Institute of Archaeology*, ed. B. Rothenberg (London: University College London), 241–246.

Lernau, H., and Lernau, O. (1994). "The Fish Remains," in *Le Gisement de Hatoula en Judee occidentale, Israel. Association Paléorient*, eds M. Lechevallier and A. Ronen (Paris: Mémoires et Travaux du Centre de Recherche Français de Jerusalem), 111–121.

Lernau, O. (1995). "The fish remains of Upper Zohar," in *Upper Zohar. An Early Byzantine Fort in Palestina Tertia. Final Report of Excavations in 1985-1986*, ed. R. P. Harper (Oxford: Oxford University Press), 99–161.

Lernau, O. (2000). "Fish bones," in *Megido III-the 1992-1996 Seasons, Institute of Archeology, Emery and Claire Yass Publication in Archaeology*, eds I. Finkelstein, D. Ussishkin, and B. Halpern (Tel Aviv: Tel-Aviv University), 463–477.

Lernau, O. (2002a). "Fish bones," in *Tel Kabri. The 1986-1993 Excavation Seasons, Institute of Archaeology, Emery and Claire Yass Publications in Archaeology*, ed. A. Kempinski (Tel Aviv: Tel-Aviv University), 409–427.

Lernau, O. (2002b). "Fish remains at Tel Harassim," in *The Sixth Season of Excavation at Tel Harassim (Nahel Barkai) 2000*, ed. S. Givon (Tel Aviv: Tel-Aviv University), 4–13.

Lernau, O. (2008). "The fish bones," in *Neolithic Ashkelon, Qedem Monographs of the Institute of Archaeology*, eds Y. Garfinkel, and D. Dag (Jerusalem: The Hebrew University), 263–268.

Lernau, O. (2009). "Fish Remains," in *Aphek-Anthipatris II, Monograph Series of The Sonia and Marco Nadler Institute of Archaeology*, eds Y. Gadot and E. Yadin (Tel Aviv: Tel-Aviv University), 569–574.

Lernau, O. (2011a). "Fish remains from el-Ahwat," in *El-Ahwat: A Fortified Site from the Early Iron Age Near Nahal 'Iron, Israel. Excavations 1993-2000*, ed. A. Zertal (Leiden: Brill), 362–368. doi: 10.1163/ej.9789004176454.i-488.101

Lernau, O. (2011b). "Fish remains," in *Ashkelon 3: The Seventh Century B.C. (Final Reports of the Leon Levy Expedition to Ashkelon),* eds L. E. Stager, D. M. Master, and J. D. Schloen (Winona Lake, IN: Eisenbrauns).

Lernau, O. (2015). "Fish Bones," in *The Summit of The City of David Excavations 2005-2008. Final Reports Volume I. Area G*, ed. E. Mazar (Jerusalem: Old City Press), 525–538.

Lernau, O., and Golani, D. (2004). "Section B: the osteological remains (aquatic)," in *The Renewed Archaeological excavations at Lachish (1973-1994), Emery and Claire Yass Publications in Archaeology*, ed. D. Ussishkin (Tel Aviv: Tel-Aviv University), 2456–2489.

Leuzinger, L., Kocsis, L., Billon-Bruyat, J.-P., Spezzaferri, S., and Vennemann, T. (2015). Stable isotope study of a new chondrichthyan fauna (Kimmeridgian, Porrentruy, Swiss Jura): an unusual freshwater-influenced isotopic composition for the hybodont shark *Asteracanthus*. *Biogeosciences* 12, 6945–6954. doi: 10.5194/bg-12-6945-2015

Longinelli, A., and Nuti, S. (1973). Revised phosphate–water isotopic temperature scale. *Earth Planet. Sci. Lett.* 19, 373–376. doi: 10.1016/0012-821x(73)90088-5

Luer, C. A., Blum, P. C., and Gilbert, P. W. (1990). Rate of Tooth Replacement in the Nurse Shark, *Ginglymostoma cirratum*. *Copeia* 1990, 182–191. doi: 10.2307/1445834

Luomala, K. (1984). "Sharks and shark fishing in the culture of Gilbert Islands, Micronesia," in *The Fishing Culture of the World: Studies in Ethnology, Cultural Ecology and Folklore,* ed. B. Gunda (Budapest: Akademiai Kiado), 1203–1252.

Martin, E. E., and Scher, H. D. (2004). Preservation of seawater Sr and Nd isotopes in fossil fish teeth: bad news and good news. *Earth Planet. Sci. Lett.* 220, 25–39. doi: 10.1016/s0012-821x(04)00030-5

Mazar, E. (2015). *The Summit of the City of David Excavations 2005-2008. Final Reports Volume I. Area G.* (Jerusalem: Old City Press).

McArthur, J. M., Howarth, R. J., Shields, G. A., and Zhou, Y. (2020). "Chapter 7: Strontium isotope stratigraphy," in *Geologic Time Scale 2020*, Vol. 1, 2, eds F. M. Gradstein, J. G. Ogg, M. D. Schmitz, and G. M. Ogg (Amsterdam: Elsevier), 211–238.

Meredith Smith, M., Underwood, C., Clark, B., Kriwet, J., and Johanson, Z. (2018). Development and evolution of tooth renewal in neoselachian sharks as a model for transformation in chondrichthyan dentitions. *J. Anat.* 232, 891–907. doi: 10.1111/joa.12796

Miake, Y., Aoba, T., Moreno, E. C., Shimoda, S., Prostak, K., and Suga, S. (1991). Ultrastructural studies on crystal growth of enameloid minerals in elasmobranch and teleost fish. *Calcif. Tissue Int.* 48, 204–217. doi: 10.1007/bf02570556

Mokadem, F., Parkinson, I. J., Hathorne, E. C., Anand, P., Allen, J. T., and Burton, K. W. (2015). High precision radiogenic strontium isotope measurements of the modern and glacial ocean: limits on glacial-interglacial variations in continental weathering. *Earth Planet. Sci. Lett.* 415, 111–120. doi: 10.1016/j.epsl.2015.01.036

Moss, S. A. (1967). "Tooth replacement in the lemon shark, *Negaprion brevirostris*," in *Sharks, Skates and Rays*, eds P. W. Gilbert, R. F. Mathewson, and D. P. Rall (Baltimore, MD: Johns Hopkins Press), 319–329.

Nelson, B. K., DeNiro, M. J., Schoeninger, M. J., and De Paolo, D. J. (1986). Effects of diagenesis on strontium, carbon, nitrogen and oxygen concentration and isotopic composition of bone. *Geochim. Cosmochim. Acta* 50, 1941–1949. doi: 10.1016/0016-7037(86)90250-4

Noe-Nygaard, N. (1971). Spur Dog spines from Prehistoric and Early Historic Denmark. *Bull. Geol. Soc. Denmark* 21, 18–33.

Otero, O., Lécuyer, C., Fourel, F., Martineau, H., Mackaye, T., Vignaud, P., et al. (2011). Freshwater fish $\delta^{18}O$ indicates a Messinian change of the precipitation regime in Central Africa. *Geology* 39, 435–438. doi: 10.1130/g31212.1

Pucéat, E., Joachimski, M. M., Bouilloux, A., Monna, F., Bonin, A., Motreuil, S., et al. (2010). Revised phosphate-water fractionation equation reassessing paleotemperatures derived from biogenic apatite. *Earth Planet. Sci. Lett.* 298, 135–142. doi: 10.1016/j.epsl.2010.07.034

Pucéat, E., Lécuyer, C., Sheppard, S. M. F., Dromart, G., Reboulet, S., and Grandjean, P. (2003). Thermal evolution of Cretaceous Tethyan marine waters inferred from oxygen isotope composition of fish tooth enamels. *Paleoceanography* 18:1029

R Core Team (2018). *R: A Language, and Environment for Statistical Computing* Vienna: R Foundation for Statistical Computing.

Raban-Gerstel, N., Bar-Oz, G., Zohar, I., Sharon, I., and Gilboa, A. (2008). Early Iron Age Dor (Israel): a faunal perspective. *Bull. Am. School Orient. Res.* 349, 25–59. doi: 10.1086/basor25067055

Rasch, L., Martin, K., Cooper, R., Metscher, B., Underwood, C., and Fraser, G. (2016). An ancient dental gene set governs development and continuous regeneration of teeth in sharks. *Dev. Biol.* 415, 347–370. doi: 10.1016/j.ydbio.2016.01.038

Reich, R., Shukron, E., and Lernau, O. (2007). Recent discoveries in the City of David, Jerusalem. *Isr. Explor. J.* 57, 153–169.

Reich, R., and Shukron, E. (2011). The date of the Siloam Tunnel reconsidered. *Tel Aviv* 38, 147–157. doi: 10.1179/033443511x13099584885268

Reich, R., Shukron, E., and Lernau, O. (2008). "The Iron Age II Finds from the Rock-Cut 'Pool' near the spring in Jerusalem: A preliminary report," in *Israel in Transition: From Late Bronze II to Iron IIa (c.1250-850 BCE)*, ed. L. L. Grabbe (New York, NY: T&T Clark), 138–143.

Reif, W. E., McGill, D., and Motta, P. (1978). Tooth replacement rates of the sharks *Triakis semifasciata* and *Ginglymostoma cirratum*. *Zool. Jahrb. Abt. Anat. Ontogenie* 99, 151–156.

Reinhardt, E. G., Stanley, D. J., and Patterson, R. T. (1998). Strontium isotopic-paleontological method as a high-resolution paleosalinity tool for lagoonal environments. *Geology* 26, 1003–1006. doi: 10.1130/0091-7613(1998)026<1003:sipmaa>2.3.co;2

Reinhardt, E. G., Stanley, D. J., and Schwarcz, H. P. (2001). Human-induced desalination of Manzala Lagoon, Nile delta, Egypt: evidence from isotopic analysis of benthic invertebrates. *J. Coast. Res.* 17, 431–442.

Retzler, A., Wilson, M. A., and Avni, Y. (2013). Chondrichthyans from the Menuha Formation (Late Cretaceous: Santonian–Early Campanian) of the Makhtesh Ramon region, southern Israel. *Cretac. Res.* 40, 81–89. doi: 10.1016/j.cretres.2012.05.009

Rick, T. C., Erlandson, J. M., Glassow, M. A., and Moss, M. L. (2002). Evaluating the economic significance of sharks, skates, and rays (Elasmobranchs) in prehistoric economies. *J. Archaeol. Sci.* 29, 111–122. doi: 10.1006/jasc.2000.0637

Ripley, B. D. (2002). *Modern Applied Statistics with S*, 4th Edn. (New York, NY: Springer).

Rohling, E. J. (2007). "Oxygen isotope composition of seawater," in *Encyclopedia of Quaternary Science*, Vol. 3, ed. S. A. Elias (Amsterdam: Elsevier), 1748–1756. doi: 10.1016/b0-444-52747-8/00304-5

Rosenfeld, A., and Hirsch, F. (2005). "The Cretaceous of Israel," in *Geological Framework of the Levant: The Levantine Basin and Israel*, Vol. II, eds J. K. Hall, V. A. Krasheninnikov, F. Hirsch, C. Benjamini, A. Flexer (Jerusalem: Historical Productions-Hall), 393–436.

Rosensaft, M., and Sneh, A. (2011). *Geological Map of Israel 1:50,000, Jerusalem Sheet 11-II, State of Israel, Ministry of National Infrastructures, Earth and Marine Research Administration*. Jerusalem: Geological Survey of Israel.

Rowan, Y. M., and Golden, J. (2009). The chalcolithic period of the Southern Levant: a synthetic review. *J. World. Prehist.* 22, 1–92. doi: 10.1007/s10963-009-9016-4

Schilman, B., Bar-Matthews, M., Almogi-Labin, A., and Luz B. (2001). Global climate instability reflected by eastern Mediterranean marine records during the late Holocene. *Palaeogeogr. Palaeoclimatol. Palaeoecol.* 176, 157–176. doi: 10.1016/s0031-0182(01)00336-4

Schmitz, B., Aberg, G., Werdelin, L., Forey, P., and Bendix-Almgreen, S. E. (1991). Sr-87/Sr-86, Na, F, Sr, and La in skeletal fish debris as a measure of the paleosalinity of fossil-fish habitats. *Geol. Soc. Am. Bull.* 103, 786–794. doi: 10.1130/0016-7606(1991)103<0786:ssnfsa>2.3.co;2

Schmitz, B., Ingram, S. L., Dockery, D. T., and Aberg, G. (1997). Testing $^{87}Sr/^{86}Sr$ as a paleosalinity indicator on mixed marine, brackish-water and terrestrial vertebrate skeletal apatite in late Paleocene–early Eocene near-coastal sediments, Mississippi. *Chem. Geol.* 140, 275–287. doi: 10.1016/s0009-2541(97)00023-5

Serena, F. (2005). *Field Identification Guide to the Sharks and Rays of the Mediterranean and Black Sea. FAO Species Identification Guide for Fishery Purposes*. (Rome: FAO), 97.

Sharp, Z. D., Atudorei, V., and Furrer, H. (2000). The effect of diagenesis on oxygen isotope ratios of biogenic phosphates. *Am. J. Sci.* 300, 222–237. doi: 10.2475/ajs.300.3.222

Shaw, H. F., and Wasserburg, G. J. (1985). Sm-Nd in marine carbonates and phosphates: implications for Nd isotopes in seawater and crustal age. *Geochim. Cosmochim. Acta* 49, 503–518. doi: 10.1016/0016-7037(85)90042-0

Shimada, K., and Cicimurri, D. J. (2005). Skeletal anatomy of the Late Cretaceous shark, *Squalicorax* (Neoselachii: Anacoracidae). *PalZ* 79, 241–261. doi: 10.1007/bf02990187

Shimada, K., and Cicimurri, D. J. (2006). "The oldest record of the Late Cretaceous anacoracid shark *Squalicorax pristodontus* (Agassiz), from the Western Interior, with comments on *Squalicorax* phylogeny," in *Late Cretaceous vertebrates from the Western Interior*, eds S. G. Lucas, and R. M. Sullivan (Albuquerque: New Mexico Museum of Natural History and Science), 177–184.

Sisma-Ventura, G., Tütken, T., Peters, S. T. M., Bialik, O. M., Zohar, I., and Pack, A. (2019). Past aquatic environments in the Levant inferred from stable isotope compositions of carbonate and phosphate in fish teeth. *PloS ONE* 14:e0220390. doi: 10.1371/journal.pone.0220390

Sisma-Ventura, G., Tütken, T., Zohar, I., Pack, A., Sivan, D., Lernau, O., et al. (2018). Tooth oxygen isotopes reveal Late Bronze Age origin of Mediterranean fish aquaculture and trade. *Sci. Rep.* 8:14086

Sisma-Ventura, G., Yam, R., Kress, N., and Shemesh, A. (2016). Water column distribution of oxygen and carbon isotopes in the Levantine basin: temporal and vertical change. *J. Mar. Syst.* 158, 13–25. doi: 10.1016/j.jmarsys.2016.01.012

Sisma-Ventura, G., Yam, R., and Shemesh, A. (2014). Recent unprecedented warming and oligothrophy of the Eastern Mediterranean Sea within the last millennium. *Geophys. Res. Lett.* 41, 5158–5166. doi: 10.1002/2014gl060393

Sisma-Ventura, G., Zohar, I., Sarkar, A., Bhattacharyya, K., Zidane, A., Gilboa, A., et al. (2015). Oxygen isotope composition of Sparidae (sea bream) tooth enamel from well-dated archaeological sites as an environmental proxy in the East Mediterranean: a case study from Tel Dor, Israel. *J. Archaeol. Sci.* 64, 46–53. doi: 10.1016/j.jas.2015.10.004

Sivan, D., Greenbaum, N., Cohen-Seffer, R., Sisma-Ventura, G., and Almogi-Labin, A. (2011). The origin and disappearance of the Late Pleistocene – Early Holocene short-lived coastal wetlands along the Carmel coast, Israel. *Quat. Res.* 76, 83–92. doi: 10.1016/j.yqres.2011.04.006

Sivan, D., Sisma-Ventura, G., Greenbaum, N., Bialik, O., Williams, F., Tamisiea, M. E., et al. (2016). Eastern Mediterranean sea levels through the last interglacial from a coastal-marine sequence in northern Israel. *Quat. Sci. Rev.* 141, 204–225. doi: 10.1016/j.quascirev.2016.06.001

Siversson, M., Cook, T. D., Ryan, H. E., Watkins, D. K., Tatarnic, N. J., Downes, P. J., et al. (2018). Anacoracid sharks and calcareous nannofossil stratigraphy of the mid-Cretaceous Gearle Siltstone and Haycock Marl in the lower Murchison River area, Western Australia. *Alcheringa* 43, 85–113. doi: 10.1080/03115518.2018.1462401

Sneh, A., Ram, W., and Eyal, S. (2010). The why, how, and when of the Siloam Tunnel reevaluated. *Bull. Am. Sch. Orient. Res.* 359, 57–65. doi: 10.1086/basor25741828

Starinsky, A., Bielsky, M., Lazar, B., Wakshal, E., and Steinitz, G. (1980). Marine $^{87}Sr/^{86}Sr$ ratios from the Jurassic to Pleistocene: evidence from groundwaters in Israel. *Earth Plant. Sci. Lett.* 47, 75–80. doi: 10.1016/0012-821x(80)90105-3

Staudigel, H., Doyle, P., and Zindler, A. (1985). Sr and Nd isotope systematics in fish teeth. *Earth Planet. Sci. Lett.* 76, 45–56. doi: 10.1016/0012-821x(85)90147-5

Stiller, M., and Magaritz, M. (1974). Carbon-13 enriched carbonate in interstitial waters of Lake Kinneret sediments. *Limnol. Oceanogr.* 19, 849–853. doi: 10.4319/lo.1974.19.5.0849

Suga, S., Taki, Y., and Ogawa, M. (1993). Fluoride and iron concentrations in the enameloid of lower teleostean fish. *J. Dent. Res.* 72, 912–922. doi: 10.1177/00220345930720051301

Talbot, M. R. (1990). A review of the palaeohydrological interpretation of carbon and oxygen isotopic ratios in primary lacustrine carbonates. *Chem. Geol.* 80, 261–279. doi: 10.1016/0168-9622(90)90009-2

Tancioni, L., Mariani, S., Maccaroni, A., Mariani, A., Massa, F., Scardi, M. et al. (2003). Locality-specific variation in the feeding of *Sparus aurata* L.: evidence from two Mediterranean lagoon systems. *Estuar. Coast. Shelf Sci.* 57, 469–474. doi: 10.1016/s0272-7714(02)00376-1

Touzeau, A., Blichert-Toft, J., Amiot, R., Fourel, F., Martineau, F., Cockitt, J., et al. (2013). Egyptian mummies record increasing aridity in the Nile valley from 5500 to 1500 yr before present. *Earth Plant. Sci. Lett.* 375, 92–100. doi: 10.1016/j.epsl.2013.05.014

Toyoda, K., and Tokonami, M. (1990). Diffusion of rare-earth elements in fish teeth from deep-sea sediments. *Nature* 345, 607–609. doi: 10.1038/345607a0

Tuross, N., Behrensmeyer, A. K., and Eanes, D. (1989). Strontium increases and crystallinity changes in taphonomic and archaeological bone. *J. Archaeol. Sci.* 16, 661–672. doi: 10.1016/0305-4403(89)90030-7

Tütken, T., Vennemann, T. W., Janz, H., and Heizmann, H. E. P. (2006). Palaeoenvironment and palaeoclimate of the Middle Miocene lake in the Steinheim basin, SW Germany: A reconstruction from C, O, and Sr isotopes of fossil remains. *Palaeogeogr. Palaeoclimatol. Palaeoecol.* 241, 457–491. doi: 10.1016/j.palaeo.2006.04.007

Tütken, T., Vennemann, T. W., and Pfretzschner, H.-U. (2008). Early diagenesis of bone and tooth apatite in fluvial and marine settings: constraints from combined oxygen isotope, nitrogen and REE analysis. *Palaeogeogr. Palaeoclimatol. Palaeoecol.* 266, 254–268. doi: 10.1016/j.palaeo.2008.03.037

Tütken, T., Vennemann, T. W., and Pfretzschner, H.-U. (2011). Nd and Sr isotope compositions in modern and fossil bones - proxies for vertebrate provenance and taphonomy. *Geochim. Cosmochim. Acta* 75, 5951–5970. doi: 10.1016/j.gca.2011.07.024

Underwood, C., Johanson, Z., and Smith, M. M. (2016). Cutting blade dentitions in squaliform sharks form by modification of inherited alternate tooth ordering patterns. *R. Soc. Open Sci.* 3:160385. doi: 10.1098/rsos.160385

Van den Brink, E. C. M., Barzilai, O., Vardi, J., Cohen Weinberger, A., Lernau, O., Liphschitz, N., et al. (2016). Late Chalcolithic settlement remains East of Namir Road, Tel Aviv. *J. Isr. Prehist. Soc.* 46, 20–121.

Van Neer, W., Ervynck, A., and Monsieur, P. (2015). Fish bones and amphorae: evidence for the production and consumption of salted fish products outside the Mediterranean region. *J. Rom. Archaeol.* 23, 161–195. doi: 10.1017/s104775940000235x

Van Neer, W., Lernau, O., Friedman, R., Mumford, G., Poblome, J., and Waelkens, M. (2004). Fish remains from archaeological sites as indicators of former trade connections in the Eastern Mediterranean. *Paléorient* 30, 101–148. doi: 10.3406/paleo.2004.4775

Van Neer, W., Zohar, I., and Lernau, O. (2005). The emergence of fishing communities in the eastern Mediterranean region: a survey of evidence from pre- and protohistoric periods. *Paléorient* 31, 131–157. doi: 10.3406/paleo.2005.4793

Van Neer, W., De Cupere, B., and Waelkens, M. (1997). "Remains of local and imported fish at the ancient site of Sagalassos (Burder Prov. Turkey)," in *Sagalassos IV: Report on the Survey and Excavation Campaigns of 1994 and 1995*, eds M. Waelkens, and J. Poblome (Leuven: Leuven University Press), 571–586.

Van Neer, W., and Depraetere, D. (2005). Pickled fish from the Egyptian Nile: osteological evidence from a Byzantine (Coptic) context at Shanhûr. *Rev. Paléobiol.* 25, 159–170.

Van Neer, W., and Ervynck, A. (2004). "Remains of traded fish in archaeological sites: indicators of status, or bulk food?" in *Behaviour Behind Bones: The Zooarchaeology of Ritual, Religion, Status and Identity*, eds S. J. O'Day, W. Van Neer, and A. Ervynck (Oxford: Oxbow Books), 203–214.

Vengosh, A., Sprivack, A. J., Artzi, Y., and Ayalón, A. (1999). Geochemical and boron, strontium, and oxygen isotopic constraints on the origin of the salinity in groundwater from the Mediterranean coast of Israel. *Water Resour. Res.* 35, 1877–1894. doi: 10.1029/1999wr900024

Vennemann, T. W., Fricke, H. C., Blake, R. E., O'Neil, J. R., and Colman, A. (2002). Oxygen isotope analysis of phosphates: a comparison of techniques for analysis of Ag_3PO_4. *Chem. Geol.* 185, 321–336. doi: 10.1016/S0009-2541(01)00413-2

Vennemann, T. W., and Hegner, E. (1998). Oxygen, strontium, and neodymium isotope composition of fossil shark teeth as a proxy for the palaeoceanography and palaeoclimatology of the Miocene northern Alpine Paratethys. *Palaeogeogr. Palaeoclimatol. Palaeoecol.* 142, 107–121. doi: 10.1016/s0031-0182(98)00062-5

Vennemann, T. W., Hegner, E., Cliff, G., and Benz, G. W. (2001). Isotopic composition of recent shark teeth as a proxy for environmental conditions. *Geochim. Cosmochim. Acta* 65, 1583–1599. doi: 10.1016/s0016-7037(00)00629-3

Wacker, U., Rutz, T., Löffler, N., Conrad, A. C., Tütken, T., Böttcher, M. E., et al. (2016). Clumped isotope thermometry of carbonate-bearing apatite: revised sample pre-treatment, acid digestion, and temperature calibration. *Chem. Geol.* 443, 97–110. doi: 10.1016/j.chemgeo.2016.09.009

Weber, M., Lugli, F., Jochum, K. P., Cipriani, A., and Scholz, D. (2018). Calcium Carbonate and Phosphate Reference Materials for Monitoring Bulk and Microanalytical Determination of Sr Isotopes. *Geostand. Geoanal. Res.* 42, 77–89. doi: 10.1111/ggr.12191

Weber, M., Wassenburg, J. A., Jochum, K. P., Breitenbach, S. F. M., Oster, J., and Scholz, D. (2017). Sr-isotope analysis of speleothems by LA-MC-ICP-MS: high temporal resolution and fast data acquisition. *Chem. Geol.* 468, 63–74. doi: 10.1016/j.chemgeo.2017.08.012

Wheeler, A., and Jones, A. K. G. (1989). *Fishes*. (Cambridge: Cambridge University Press).

Wilson, M. A., Zatoń, M., and Avni, Y. (2012). Origin, palaeoecology and stratigraphic significance of bored and encrusted concretions from the Upper Cretaceous (Santonian) of southern Israel. *Palaeobiodiv. Palaeoenviron.* 92, 343–352. doi: 10.1007/s12549-012-0082-8

Woodward, J. C., Macklin, M. G., Fielding, L., Millar, I., Spencer, N., Welsby, D., et al. (2015). Shifting sediment sources in the world's longest river: a strontium isotope record for the Holocene Nile. *Quat. Sci. Rev.* 130, 124–140. doi: 10.1016/j.quascirev.2015.10.040

Zacke, A., Voigt, S., Joachimski, M., Gale, A., Ward, D., and Tütken, T. (2009). Surface-water freshening and high-latitude river discharge in the Eocene North Sea. *J. Geol. Soc.* 166, 969–980. doi: 10.1144/0016-76492008-068

Zohar, I. (2017). "Fish exploitation during the Quaternary: recent knowledge," in *Quaternary of the Levant: Environments, Climate Change, and Humans*, eds Y. Enzel and O. Bar-Yosef (Cambridge: Cambridge University Press), 369–376. doi: 10.1017/9781316106754.043

Zohar, I., and Artzy, M. (2019). The role of preserved fish: evidence of fish exploitation, processing, and long-term preservation at the Eastern Mediterranean, during the Late Bronze Age (14th-13th centuries BCE). *J. Archaeol. Sci. Rep.* 23, 900–909. doi: 10.1016/j.jasrep.2018.12.008

Zohar, I., and Biton, R. (2011). Land, lake, and fish: investigation of fish remains from Gesher Benot Ya'aqov (paleo-Lake Hula). *J. Hum. Evol.* 60, 343–356. doi: 10.1016/j.jhevol.2010.10.007

Zohar, I., Dayan, T., Spanier, E., Galili, E., and Lernau, O. (1994). Exploitation of gray triggerfish (*Balistes carolinensis*) by the prehistoric inhabitants of Atlit-Yam, Israel: a preliminary report, in *Fish Exploitation in The Past: Proceedings of the 7th meeting of the ICAZ Fish Remains Working Group*, ed. W. Van Neer (Tervuren: Musée Royal de l'Afrique Centrale), 231–237.

Zohary, T., Erez, J., Gophen, M., Berman-Frank, I., and Stiller, M. (1994). Seasonality of stable carbon isotopes within the pelagic food web of Lake Kinneret. *Limnol. Oceanogr.* 39, 1030–1043. doi: 10.4319/lo.1994.39.5.1030

Conflict of Interest: The authors declare that the research was conducted in the absence of any commercial or financial relationships that could be construed as a potential conflict of interest.

frontiers in Ecology and Evolution

ORIGINAL RESEARCH
published: 12 January 2021
doi: 10.3389/fevo.2020.589154

Testing Various Pre-treatments on Artificially Waterlogged and Pitch-Contaminated Wood for Strontium Isotope Analyses

Christophe Snoeck[1,2,3], Rick J. Schulting[4], Fiona Brock[5], Alexandra S. Rodler[1], Alicia Van Ham-Meert[6,7], Nadine Mattielli[2] and Joanna Ostapkowicz[4]*

[1] Research Unit Analytical, Environmental and Geo-Chemistry, Department of Chemistry, Vrije Universiteit Brussel, AMGC-WE-VUB, Brussels, Belgium, [2] Laboratoire G-Time, Université Libre de Bruxelles, Brussels, Belgium, [3] Department of Art Sciences & Archaeology, Maritime Cultures Research Institute, Vrije Universiteit Brussel, MARI-LW-VUB, Brussels, Belgium, [4] School of Archeology, University of Oxford, Oxford, United Kingdom, [5] Defense Academy of the United Kingdom, Cranfield Forensic Institute, Cranfield University, Shrivenham, United Kingdom, [6] The Saxo Institute, University of Copenhagen, Copenhagen, Denmark, [7] Department of Geosciences and Natural Resource Management (Geology Section), University of Copenhagen, Copenhagen, Denmark

OPEN ACCESS

Edited by:
Kate Britton, University of Aberdeen, United Kingdom

Reviewed by:
Michael Weber, Johannes Gutenberg University Mainz, Germany
Andrew Millard, Durham University, United Kingdom

***Correspondence:**
Christophe Snoeck
christophe.snoeck@vub.be

Specialty section:
This article was submitted to Paleoecology, a section of the journal Frontiers in Ecology and Evolution

Received: *30 July 2020*
Accepted: *11 December 2020*
Published: *12 January 2021*

Citation:
Snoeck C, Schulting RJ, Brock F, Rodler AS, Van Ham-Meert A, Mattielli N and Ostapkowicz J (2021) Testing Various Pre-treatments on Artificially Waterlogged and Pitch-Contaminated Wood for Strontium Isotope Analyses. Front. Ecol. Evol. 8:589154. doi: 10.3389/fevo.2020.589154

Strontium isotope ratios ($^{87}Sr/^{86}Sr$) are commonly used in archeological and forensic studies to assess if humans and fauna are local to the place they were found or not. This approach is largely unexplored for wooden artifacts recovered in archeological contexts, as wood – in the rare instances it does survive – is often poorly preserved. One of the most common ways wood is preserved is through the anoxic conditions found in waterlogged contexts. A more unusual form of preservation is through submergence in natural pitch. These depositional media contribute their own strontium values to the *in vivo* $^{87}Sr/^{86}Sr$ wood values, which needs to be removed prior to analysis. Here we test several pre-treatment methods to remove potential strontium contamination from wood samples that were artificially immersed in seawater and pitch from Trinidad's Pitch Lake. Water rinses and acid-leaching tests were carried out with hydrochloric acid and acetic acid to remove exogenous strontium from experimentally waterlogged wood. These tests removed large amounts of strontium from the samples and did not enable the recovery of the endogenous $^{87}Sr/^{86}Sr$ signal. For samples artificially immersed in pitch, the pre-treatments tested were based on radiocarbon dating procedures and carried out with and without the aqueous-based acid-base-acid (ABA) step. The use of organic solvents alone (methanol and toluene) removed exogenous strontium originating from the pitch. However, the ABA step eliminates large amounts of *in vivo* strontium from the samples. These tests show that $^{87}Sr/^{86}Sr$ values of wood are altered by the presence of pitch and water. With adequate pre-treatment using exclusively organic solvents, it may be possible to remove this contamination for samples immersed in pitch. However, the aqueous-based ABA pre-treatment should be avoided. The removal of contamination from waterlogged samples was unsuccessful with the current pre-treatment protocols and more research is needed. More importantly, and unexpectedly, $^{87}Sr/^{86}Sr$ values may

extend outside of the mixing line between the wood's endogenous strontium and the water. These results indicate the need for extreme caution when attempting to determine the provenance of waterlogged wood.

Keywords: strontium isotope ($^{87}Sr/^{86}Sr$), waterlogged wood, provenance, pitch, pre-treatment

INTRODUCTION

Wood artifacts are rarely encountered in the archeological record, as their permeable, organic nature quickly deteriorates in typical depositional contexts. However, wood does survive when charred, desiccated or waterlogged. An additional, though very rare, means of preservation occurs in the anoxic conditions of natural asphalt or pitch deposits. Such artifacts, and particularly the materials from which they were carved, offer valuable insights on a variety of issues – from resource and landscape utilization to potential exchange links. It is vital to access as much of this information as possible, including radiocarbon dating of variously preserved objects (Ostapkowicz et al., 2012, 2013; Brock et al., 2017) and exploring possibilities for carrying out strontium (Sr) isotope analyses to assess the geographical origin of these artifacts.

Strontium-87 is the product of the radioactive decay of Rubidium-87 (^{87}Rb), so Sr isotope ratios ($^{87}Sr/^{86}Sr$) vary between different types of bedrock, depending on the initial Rb-Sr ratio and time since deposition: the amount of ^{87}Sr in relation to ^{86}Sr increases with bedrock age as ^{87}Rb decays to ^{87}Sr (Faure and Powell, 1972). $^{87}Sr/^{86}Sr$ values as high as 0.9000 may be observed in some granites, for instance in the Mourne Mountains in Northern Ireland (Meighan et al., 1988) and in South Africa (Sillen et al., 1998). Younger geological formations often have values below 0.7060, and those with very low initial Rb/Sr ratios, such as basalt, typically have values of 0.7027–0.7040 (GEOROC, 2014). Modern ocean water has a $^{87}Sr/^{86}Sr$ ratio of 0.7092 (Hess et al., 1986), an important value as it contributes to world-wide precipitation and to geologically recent calcareous marine deposits. These general trends provide a first idea of the type and age of a deposit based on the Sr isotopic composition, however, to be confident in the interpretation appropriate baselines are needed.

Previous research has shown that, in plants, Sr follows similar pathways to calcium (Rediske and Selders, 1953; Storey and Leigh, 2004). Soluble Sr is taken up by plants from the soil and hence reflects the geology on which the plants are growing. While a large number of studies have focussed on measuring Sr isotopes in archeological human and animal remains (e.g., Price et al., 2006; Bentley, 2013; Laffoon et al., 2014) or charred/carbonized grains (e.g., Benson et al., 2010; though not always successfully – see Styring et al., 2019), as well as on modern plants to establish a biologically available Sr baseline (e.g., Evans et al., 2010; Snoeck et al., 2016, 2020), less has been done with archeological wood remains. Exceptions include a study of the well-preserved desiccated structural timbers at Chaco Canyon (English et al., 2001), and of desiccated prehistoric willow and tule textiles in the Great Basin (Benson et al., 2006), as well as some more recent work on pre-Columbian wood sculptures from Florida (Ostapkowicz et al., 2017a) and Trinidad (Ostapkowicz et al., 2017b), waterlogged shipwrecks (Rich et al., 2016; Hajj et al., 2017; Van Ham-Meert et al., 2020), and South American/Lesser Antillean wooden clubs from museum collections (Ostapkowicz et al., 2018). Little targeted research has focused on pre-treatments for archeological wood. Desiccated remains should not present a problem, as long as dust particles are removed prior to analysis, as they have not been exposed to Sr in solution. For all other cases, however, pre-treatments are required, as it is clear from studies carried out on human and animal remains as well as charred grains that pre-treatment is required to remove depositional Sr contamination (Sillen and LeGeros, 1991; Budd et al., 2000; Benson et al., 2010; Snoeck et al., 2015; Styring et al., 2019).

In trees Sr does not play a physiological role, but it is taken-up through the root system via the same pathways as calcium. Since it does not have a physiological role, there is no metabolic regulation of its concentration in (different parts of) the trees (Blum et al., 2012). Calcium is present as whewellite in oaks (Ca-oxalate monohydrate: $CaC_2O_4.H_2O$). A Sr isomorph of this crystal exists, and it is probable Sr is present in those (water-soluble crystals) mostly in cell walls, particularly in pectin, cellulose, and lignin (Serdar and Demiray, 2012; Hajj et al., 2017). Strontium can also be present adsorbed on active groups in cell-walls, but probably not cellulose, while results on lignin as a candidate are mixed (Chen, 1997; Schmitt et al., 2017; Boyer et al., 2018). A spatially resolved chemical analysis (e.g., FTIR, Raman or XRD) of wood would help understand where Sr is present, and which type of chemical bonds are involved.

In waterlogged contexts and waterlogging experiments, $^{87}Sr/^{86}Sr$ measured on shipwrecks showed the impact of water on the Sr isotopic composition of the wood (Rich et al., 2016; Hajj et al., 2017; Van Ham-Meert et al., 2020). Two Mediterranean shipwrecks were investigated by Rich et al. (2016): the Bronze Age Uluburun shipwreck and the Athlit Ram galley from the Hellenistic period. Samples were washed to remove precipitates such as NaCl because biostratinomic and diagenetic Sr sources were a concern in waterlogged wood, but no other pre-treatment seems to have been undertaken. Similarly, no pre-treatment was carried out by Hajj et al. (2017) prior to analysis of the Ribadeo, a sixteenth century Spanish shipwreck. The few studies that have so far investigated pre-treatments for Sr isotope analysis of wood recovered from natural pitch (Ostapkowicz et al., 2017b) or on which consolidants have been applied (Ostapkowicz et al., 2017a, 2018) have used the pre-treatments commonly used in radiocarbon dating to remove carbon contamination (Brock et al., 2010, 2017, 2018). These pre-treatments showed that such carbon contamination can be successfully removed adequately using different organic solvents and acid-base-acid (ABA) steps (Brock et al., 2010, 2017,

2018; Dee et al., 2011; Ostapkowicz et al., 2012, 2013). Recent stable carbon and nitrogen isotope analyses of charred grain, however, highlighted possible issues with the use of ABA as it removed large amounts of material (Vaiglova et al., 2014), which is problematic when only small samples are available, as is often the case with archeological materials. Further work using HCl (6 M at room temperature) to remove exogenous soil Sr from charred grain was only partially successful (Styring et al., 2019). Recently, various pre-treatments including successive MilliQ^{TM} washes, a combination of HF and MilliQ^{TM} and alpha-cellulose extraction (which is used in oxygen isotope studies) were tested as means to remove exogeneous Sr from experimentally waterlogged oaks (Van Ham-Meert et al., 2020). However, none of these methods were successful, the different procedures removed both endogenous and exogeneous Sr and did not succeed in retrieving the original Sr isotopic composition. A sample from a shipwreck was also included in this study and behaved similarly (Van Ham-Meert et al., 2020).

In this paper, several artificially waterlogged wood and pitch-contaminated samples are studied using $^{87}Sr/^{86}Sr$ analyses. The effect of various pre-treatments on the Sr isotope ratio of these samples is investigated to (1) assess to what extent water and/or pitch have an impact on the original Sr isotope ratio of wood and wood artifacts; (2) determine which, if any, pre-treatment is the most effective in removing these sources of exogenous Sr prior to analyses.

MATERIALS AND METHODS

Samples

The waterlogging experiments were carried out on (1) two modern wood samples from Trinidad (T69 and T88 – Ostapkowicz et al., 2017b; **Table 1**) and (2) six modern pine and cypress samples from Florida (FR2, FS3, GOE3, RC1, SW1, and TR4 – Schulting and Snoeck, unpublished data; **Table 1**). The samples weighing approximately 5 *g* were placed in individual 50 mL metal-free, sterile polypropylene (PP) tubes and immersed for 1 month in unfiltered seawater obtained from the North Sea in Knokke (Belgium) that has a $^{87}Sr/^{86}Sr$ isotope ratio of 0.7092 and a Sr concentration of 7.1 mg/L (similar to the range of 7.2 to 7.8 mg/L reported by Angino et al., 1966). Two fractions of samples FR2 and GOE3 were placed in separate tubes to assess the reproducibility of the pre-treatments. Samples T69 and T88 were also placed for 1 month in a Sr-87 enriched solution (11 mg/L of $SrCO_3$ – MSR87C from Euriso-top, Saint-Aubin, France – of which 89.7% is composed of ^{87}Sr) with a $^{87}Sr/^{86}Sr$ of 91.5306 (see Snoeck et al., 2015). All samples sank to the bottom of the tubes before the end of the month. The samples were then removed from the tubes and left to airdry at room temperature for a few days.

To test the impact of pitch on the $^{87}Sr/^{86}Sr$ isotope composition of wood samples, three modern wood samples from Trinidad (T34, T71, and T81 – Ostapkowicz et al., 2017b) were selected and about 5 *g* of each were placed in 50 mL pitch obtained from southwest Trinidad's Pitch Lake for 3 months (**Table 1**). Two aliquots of the pitch (ca. 50 mg) were also analyzed to assess its Sr isotope ratio.

TABLE 1 | Wood samples used in the waterlogging and pitch-contamination experiments.

Samples ID	Common name	Species	Origin
T34*	Angelin	*Andira* sp.	Between Blanchisseuse and La Filette, along Yarra River, Trinidad
T69*	Olivier	*Terminalia dichotoma*	Irois Forest, Trinidad
T71*	Angelin	*Andira* sp.	Icacos beach, Trinidad
T81*	Angelin	*Andira* sp.	Trinidad Sobo Village, La Brea, Trinidad
T88*	Carap	*Carapa* sp.	Navet Dam, Trinidad
FR2	Cypress	*Taxodium* sp.	Flatwood Reserve, Tampa, Florida
FS3	Pine	*Pinus* sp.	Fanning Springs State Park, Florida
GOE3	Cypress	*Taxodium* sp.	Goethe State Park, Florida
RC1	Cypress	*Taxodium* sp.	Rice Creek, Florida
SW1	Pine	*Pinus* sp.	Suwannee River, Falmouth, Florida
TR4	Pine	*Pinus* sp.	Twin Rivers State Forest, Florida

Samples from Ostapkowicz et al. (2017b).

Pre-treatments

After drying, the waterlogged samples of the first experiment (T69 and T88) were ultrasonicated for 10 min in ultrapure MilliQ^{TM} and before being split into four fractions: (1) no further pre-treatment; (2) ultrasonication for 10 min in 1 M acetic acid and; (3) ultrasonication for 10 min in 1 M acetic acid, crushed to <5 mm using a coffee grinder and ultrasonicated again for 10 min in 1 M acetic acid; and (4) ultrasonication for 10 min in 1 M HCl. After pre-treatments 2, 3, and 4, the samples were ultrasonicated for 10 min again in MilliQ^{TM}. All experiments were at room temperature.

In the second waterlogging contamination experiment, several modern pine and cypress samples (FR2, FS3, GOE3, RC1, SW1, and TR4 – **Table 1**) were immersed in seawater from the Belgian coast (Knokke) until they sank. They were then crushed using a coffee grinder and separated into two fractions by sieving: between 2 and 5 mm (G – gross) and less than 2 mm (F – fine). All fractions were ultrasonicated in MilliQ^{TM} for 10 min. All fractions were then split in two: (1) no further pre-treatment; (2) ultrasonication for 10 min in 1 M acetic acid. For FS3 and SW1, large amount of materials were available from the less than 2 mm fraction and were separated in two aliquots that were pre-treated separately (allowing assessment of repeatability).

For samples contaminated with pitch from Trinidad's Pitch Lake (T34, T71, and T81), even though Sr and carbon are different elements, present in different parts of the plant, the contamination source in both cases is the pitch in which they are immersed. Hence, radiocarbon pre-treatments were used as a first approach, using methanol and toluene (**Table 2**; Brock et al., 2017). Prior observations

TABLE 2 | Details of the pre-treatments used for pitch removal prior to Sr isotope analyses.

Steps	Protocol			
	Solvent	Temperature (°C)	Time (h)	Repeats
1	Toluene:Methanol 2:1	Room temperature and ultrasonication	0.5	4
2	Toluene:Methanol 2:1		Overnight	1
3	Toluene:Methanol 2:1		0.5	1
4	Methanol		0.5	2
5	MilliQ water		0.5	2
6	ABA (see WW in Brock et al., 2010)			

on charred grains showed that ABA pre-treatments can, in some cases, remove large amounts of sample, mostly in the form of humic acids (Vaiglova et al., 2014). Therefore, the pre-treatments were tested with (pre-treatment 5) and without ABA (pre-treatment 6) at the end of the sequence. Some samples were also pre-treated only with the ABA procedure (pre-treatment 7) to assess its impact on the $^{87}Sr/^{86}Sr$ of wood. All ABA procedures followed the protocol outlined for non-woody plant remains (WW) in Brock et al. (2010) rather than the one outlined for wood (UW) as the bleach step was not carried out. Each pre-treatment started with ca. 50 mg of sample – the standard amount usually available for $^{87}Sr/^{86}Sr$ analyses. The pre-treatment of the wood samples was carried out directly on uncontaminated wood as well as wood samples that had been contaminated with pitch to assess whether the observed $^{87}Sr/^{86}Sr$ variations are linked to the presence of pitch or to the pre-treatment method used. For both the waterlogging and pitch contamination experiments, $^{87}Sr/^{86}Sr$ were measured before and after pre-treatment directly on the wood material (not on the leachates).

Strontium Isotope and Concentration Analyses

The entire acid digestion process and subsequent Sr purification were achieved under a class 100 laminar flow hood in a class 1000 clean room (Université Libre de Bruxelles, Belgium, hereafter ULB). One gram from each of the untreated wood samples (**Table 1**) was ashed in porcelain crucibles and a muffle furnace by step heating to 650°C prior to digestion. For these samples, about 50 mg of ashed sample was dissolved in closed ® Savillex containers (LabAS, Brussels, Belgium) overnight using 14 M HNO_3 on a heating plate at 110°C. For all the waterlogged and pitch-contaminated samples, about 50 mg of non-ashed sample was dissolved in closed ® Savillex containers overnight using 14 M HNO_3 and 23 M HF (2:1) on a heating plate at 110°C. The samples were then dried and dissolved in a mixture of 14 M HNO_3 and 6 M HCl (1:1) and left overnight on a heating plate at 110°C. If the solution was completely clear, the samples were dried awaiting column separation. If not, the dried samples were repeatedly dissolved in 8 M HCl until a clear solution was obtained.

The dried samples were re-dissolved in 2.5 mL of 2 M sub-boiled HNO_3. 0.5 mL were extracted for Sr concentration measurements (see below). The Sr of the remaining 2 mL was then extracted, and purified following the protocol described in Snoeck et al. (2015), and measured on a Nu Plasma MC-ICP Mass Spectrometer (Nu015 from Nu Instruments, Wrexham, United Kingdom) at a Sr concentration ULB using a spray chamber and at a Sr concentration of ca. 300 ng/g. NIST SRM987 ($^{87}Sr/^{86}Sr$ = 0.710248 – Weis et al., 2006) was used as reference material and measured following the samples-standard bracketing method, every two samples being bracketed by the NIST SRM987 standard solution. Nine additional NIST SRM987 measurements were carried out and returned an average $^{87}Sr/^{86}Sr$ value of 0.710253 ± 0.000042 (2 SD) consistent with measurements carried out on TIMS (Weis et al., 2006). Procedural blanks were considered negligible [total Sr (V) of max 0.02 V versus 7–8 V for sample analyses; i.e., ≈0.3%]. For each sample, the $^{87}Sr/^{86}Sr$ value is reported with ±2 SE representing the analytical uncertainty on each individual sample calculated from the 60 measurements within each run. To ensure that the various chemicals used in the pre-treatment do not contribute any Sr to the system, several blanks were measured. These showed that the various chemicals did not contain enough Sr to affect the results (i.e., the Sr beam intensity was at least 100x smaller than any of the analyzed samples).

Strontium concentrations in a fraction of the sample digests (see above) were determined using a Thermo Scientific Element 2 sector field ICP mass spectrometer at the Vrije Universiteit Brussel (VUB), Belgium, in low (^{88}Sr) resolution using Indium (In) as an internal standard and external calibration versus various reference materials (SRM1400, CCB01). Accuracy was evaluated by the simultaneous analysis of two internal bioapatite standards (ENF and CBA). Based on repeated digestion and measurement of these reference materials, the analytical precision of the procedure outlined above is estimated to be better than 5% (1 SD, n = 33 for CBA and n = 5 for ENF).

RESULTS

Waterlogging Experiment 1

The results of the first contamination experiment (**Table 3**) show that uncontaminated (i.e., untreated) samples (T69 and T88) are not affected by rinsing with MilliQ water and ultrasonication. The $^{87}Sr/^{86}Sr$ results of wood samples immersed in both seawater (Sea) and the Sr-87 enriched solution (Sr) are heavily affected in the direction of the solution in which they were immersed. Furthermore, there is a small decrease in Sr concentration in the samples immersed in seawater. The Sr concentrations in the samples immersed in the Sr-87 enriched solution, however, are much higher compared to the uncontaminated sample rinsed with MilliQ.

The use of acid on uncontaminated samples can have an effect on the measured $^{87}Sr/^{86}Sr$. Acetic acid has a minor effect ($\Delta^{87}Sr/^{86}Sr$ of 0.0004; $\Delta^{87}Sr/^{86}Sr$ represents the difference between two $^{87}Sr/^{86}Sr$ measurements) on one of the uncrushed samples but no effect at all on the other untreated samples.

TABLE 3 | Strontium isotope and concentration results for the first waterlogging experiment (full data available in **Supplementary Table 1**); Sea = immersed in seawater; and Sr = immersed in a Sr-87 enriched solution.

Sample	Before immersion	After						
		(1) MilliQ		(2) 1 M AcAc		(3) AcAc crushed*	(4) 1 M HCl	
	$^{87}Sr/^{86}Sr$	$^{87}Sr/^{86}Sr$	[Sr] (μg/g)	$^{87}Sr/^{86}Sr$	[Sr] (μg/g)	$^{87}Sr/^{86}Sr$	$^{87}Sr/^{86}Sr$	[Sr] (μg/g)
T69	0.7154	0.7154	10.5	0.7160	4.0	0.7154	0.7172	0.3
T69Sea		0.7124	10.0	0.7132	0.1	0.7154	0.7227	1.2
T69Sr		8.7132	108.5	1.7502	7.8	1.0497	2.3887	0.4
T88	0.7136	0.7136	3.8	0.7136	4.0	0.7136	0.7204	1.1
T88Sea		0.7120	2.7	0.7129	7.1	0.7126	0.7229	1.0
T88Sr		4.8703	35.8	1.2996	5.9	2.2222	1.1273	1.1

**Insufficient material left to measure [Sr] after pre-treatment (3).*

Hydrochloric acid, however, has a large impact on the Sr isotope ratios of uncontaminated samples with $\Delta^{87}Sr/^{86}Sr$ up to 0.0068. In the samples immersed in seawater and the Sr-87 enriched solution, some of the contamination is removed after pre-treatment with acetic acid, and all of it in the case of T69Sea after crushing and pre-treatment with acetic acid (3). Pre-treatment with 1 M HCl, however, causes dramatic shifts in the Sr isotope ratios, probably due to the fact that it is too strong and removes endogenous Sr as also suggested by the very low Sr concentrations ([Sr] < 1.5 μg/g).

Waterlogging Experiment 2

Following the results from the first contamination experiments, several modern pine and cypress wood samples from Florida with known (i.e., previously measured) $^{87}Sr^{86}Sr$ values were immersed in seawater until they sank, and were subsequently dried, crushed and rinsed with MilliQ. Some were then also pre-treated with acetic acid and ultrasonication. Two pieces (labeled "A" or "B") of both FR2 and GOE3 were immersed separately to assess the variability in contamination. For FS3 and SW1, the fine fraction was split in two (labeled "1" or "2") to test the reproducibility of the pre-treatment method (**Table 4**). The results show that all samples were heavily contaminated with seawater Sr and that rinsing with MilliQ water is ineffective in removing that contamination. Indeed, the samples have a mean $^{87}Sr/^{86}Sr$ value of 0.7092 ± 0.0001 (1 SD) after immersion in seawater and rinsing with MilliQ (**Figure 1**), equivalent at four decimals to the value of seawater (0.7092 – Hess et al., 1986). The Sr concentrations in 15 out of 18 cases are lower after immersion in seawater and rinsing. After pre-treatment with acetic acid, the Sr concentrations are even lower with values ranging from 0.1 to 4.9 μg/g (**Figure 1**). Additionally, none of the samples show a complete removal of contamination based on their $^{87}Sr/^{86}Sr$. On the contrary, after pre-treatment some samples have ratios further away from their original value than before pre-treatment (e.g., RC1SeaG) while others retain the seawater value (e.g., FR2SeaAF). Comparing the results obtained for the fractions of different size, the $^{87}Sr/^{86}Sr$ values of the larger fraction (G; between 2 and 5 mm) after pre-treatment with acetic acid are generally further away from the original value than the smaller fraction (F; <2 mm). Most strikingly, and contrary to mass balance expectations, many of the acetic acid pre-treatments resulted in $^{87}Sr/^{86}Sr$ well above both the original wood value and the value of the contaminant seawater (**Figure 1**).

Pitch Contamination Experiment

Two fraction of pitch from Trinidad's Pitch Lake used in this experiments returned $^{87}Sr/^{86}Sr$ (±2 SE) values of 0.712275 ± 0.000039 and 0.712251 ± 0.000039 which is distinct from the values of the modern trees sampled from around the lake [0.7107 ± 0.0013 (1 SD; n = 13); Ostapkowicz et al., 2017b]. The pitch $^{87}Sr/^{86}Sr$ value is identical to that of T34 and close to that of T81 (0.7130) but very distinct from the $^{87}Sr/^{86}Sr$ of T71 (0.7093). The first part of the experiment was to evaluate the impact of the pre-treatment [with (5) and without (6) ABA] on the $^{87}Sr/^{86}Sr$ of uncontaminated wood samples (**Table 5**). Several procedural blanks were measured and confirmed that the various chemicals used in these pre-treatments did not significantly add Sr to the system. Still, the results clearly show that the complete pre-treatment highly affects the uncontaminated samples leading to variation in Sr isotope ratios ($\Delta^{87}Sr/^{86}Sr$ between 0.0009 and 0.0023 – **Figure 2**). ABA alone (7) also impacts the Sr isotope ratios of the wood samples but to a lesser extent ($\Delta^{87}Sr/^{86}Sr$ up to 0.0004). Visually, it was clear during the pre-treatments that large amounts of material were removed from the wood samples (whether it had been immersed in pitch or not) during the ABA steps (mainly the base step), with the solutions turning light to dark brown (especially for sample T81). However, when this pre-treatment is used without the ABA step (pre-treatment 6, i.e., just using organic solvents), the wood samples are unaffected by the pre-treatment ($\Delta^{87}Sr/^{86}Sr \leq 0.0001$). The $^{87}Sr/^{86}Sr$ results for the pitch-contamination experiments (**Table 5**) show some variations between uncontaminated and pitch-contaminated samples as well as a variable effect of the different pre-treatments applied. However, when only organic solvents are used (6), the original uncontaminated value is reached, ±0.0002, which for the purpose of interpretation may be adequate (**Figure 2**).

TABLE 4 | Strontium concentration and isotope results from the second waterlogging experiment using seawater (full data available in **Supplementary Table 2**); F = fine fraction < 2 mm; G = gross fraction between 2 and 5 mm; A/B = two different immersions; and 1/2 = two aliquots of the same immersion pre-treated separately.

Sample	Before immersion		After			
			(1) MilliQ only		(2) 1 M AcAc	
	$^{87}Sr/^{86}Sr$	[Sr] (μg/g)	$^{87}Sr/^{86}Sr$	[Sr] (μg/g)	$^{87}Sr/^{86}Sr$	[Sr] (μg/g)
FR2-AF	0.7080	23.4	0.7092	8.5	0.7092	2.1
FR2-AG			0.7092	7.1	0.7102	0.1
FR2-BF			0.7092	9.3	0.7106	1.9
FR2-BG			0.7092	9.3	0.7125	1.3
FS3-1F	0.7082	14.9	0.7092	7.8	0.7091	1.9
FS3-2F			0.7092	6.9	0.7111	2.1
FS3-G			0.7091	10.9	0.7132	1.9
GOE3-AF	0.7108	31.5	0.7091	12.6	0.7097	1.0
GOE3-AG			0.7092	12.3	0.7119	0.5
GOE3-BF			0.7092	13.3	0.7092	0.4
GOE3-BG			0.7092	10.0	0.7118	2.1
RC1-F	0.7080	18.5	0.7095	27.7	0.7092	4.9
RC1-G			0.7089	18.8	0.7126	2.3
SW1-1F	0.7108	16.2	0.7094	11.6	0.7093	1.9
SW1-2F			0.7094	17.5	0.7097	3.6
SW1-G			0.7093	6.3	0.7156	1.1
TR4-F	0.7098	26.4	0.7091	23.1	0.7092	3.4
TR4-G			0.7093	6.9	0.7104	2.6

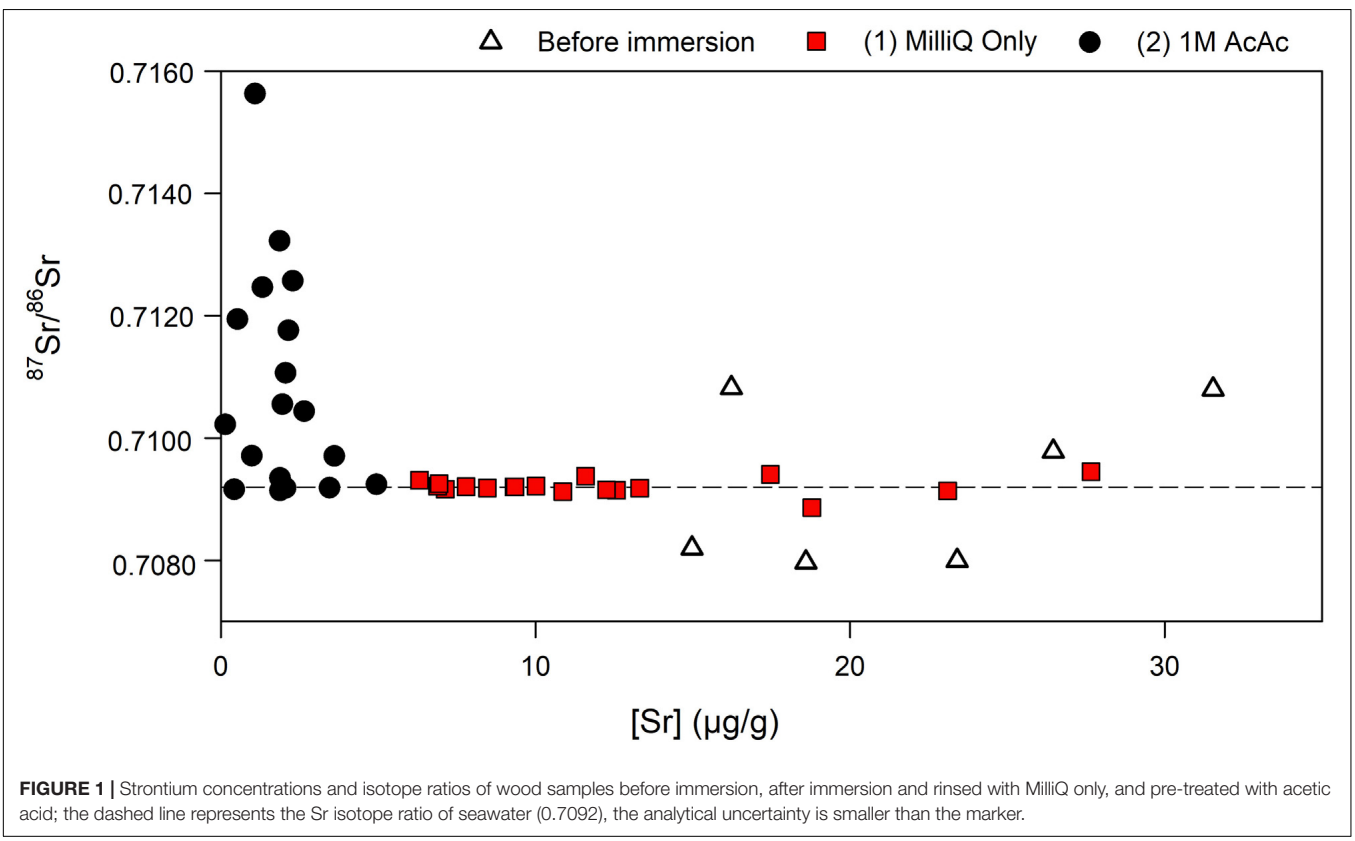

FIGURE 1 | Strontium concentrations and isotope ratios of wood samples before immersion, after immersion and rinsed with MilliQ only, and pre-treated with acetic acid; the dashed line represents the Sr isotope ratio of seawater (0.7092), the analytical uncertainty is smaller than the marker.

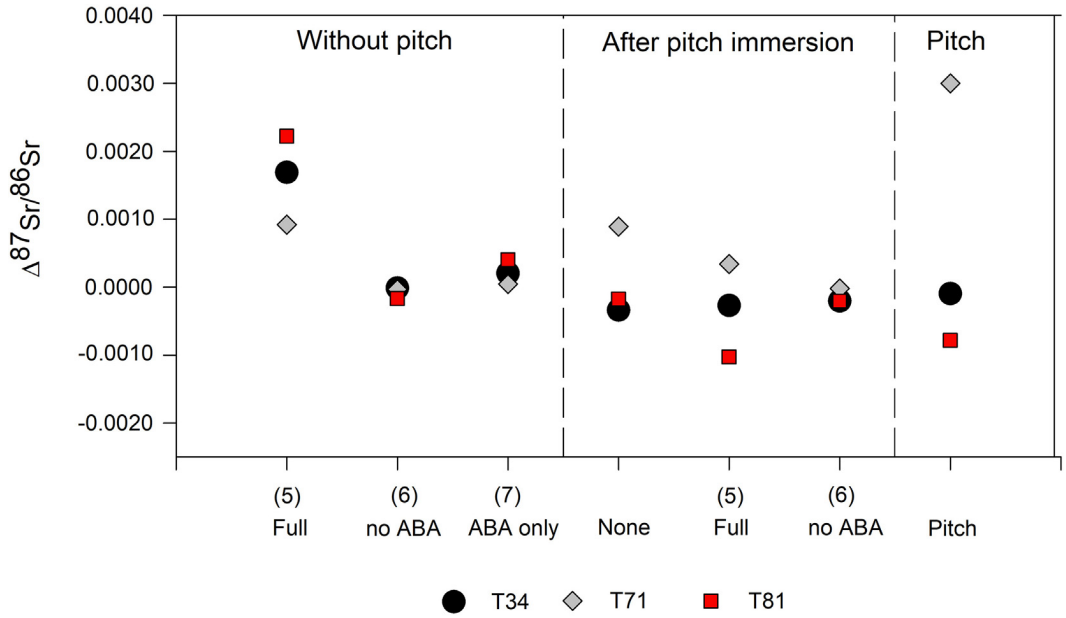

FIGURE 2 | Strontium isotope ratios of the contaminated and/or pre-treated wood samples compared to the $^{87}Sr/^{86}Sr$ values of the respective untreated and uncontaminated sample ($\Delta^{87}Sr/^{86}Sr$ represents the difference between two $^{87}Sr/^{86}Sr$ measurements).

TABLE 5 | Strontium isotope ratios (±2 SE) for the pitch-contamination experiments; see **Table 2** for details about the pre-treatments; bold values show measurements with particularly large uncertainties resulting from low amounts of Sr still present after pre-treatment.

		Pre-treatment							
		None		**(5) Full**		**(6) no ABA**		**(7) ABA only**	
	Samples	**$^{87}Sr/^{86}Sr$**	**2 SE**	**$^{87}Sr/^{86}Sr$**	**2 SE**	**$^{87}Sr/^{86}Sr$**	**2SE**	**$^{87}Sr/^{86}Sr$**	**2 SE**
Without pitch	T34	0.712358	0.000013	0.714048	**0.000758**	0.712345	0.000015	0.712563	**0.000053**
	T71	0.709263	0.000016	0.710183	**0.000096**	0.709232	0.000013	0.709308	**0.000034**
	T81	0.713043	0.000013	0.715267	**0.000508**	0.712877	0.000025	0.713448	**0.000224**
After pitch immersion	T34	0.712019	0.000021	0.712087	**0.000035**	0.712154	0.000024		
	T71	0.710155	0.000014	0.709604	**0.000104**	0.709245	0.000023		
	T81	0.712870	**0.000041**	0.712019	0.000029	0.712840	0.000017		

DISCUSSION

Waterlogged Samples

The $^{87}Sr/^{86}Sr$ values of wood placed in water are heavily impacted by the Sr present in that water, confirming the observations of Hajj et al. (2017). Indeed, the samples immersed in seawater (even after only 1 month) have $^{87}Sr/^{86}Sr$ values closer to that of seawater (0.7092 – Hess et al., 1986) with all samples from the second water contamination experiment having values between 0.7089 and 0.7095, with a mean of 0.7092 ± 0.0001 (1 SD). While this could be due to the absorption/incorporation of exogenous Sr from water, the Sr concentrations are in all but three cases lower after immersion and rinsing with MilliQ than before. This strongly suggests that large amounts of endogenous Sr are actually leached during the waterlogging experiments and replaced by Sr from the water and/or removed during rinsing with MilliQ as Sr is highly water-soluble. It is likely that this results from an equilibrium exchange between the wood and water, especially since Sr is likely present as Sr^{2+} in water-soluble chemical compounds such as Sr oxalate (Serdar and Demiray, 2012). In both cases, the Sr that remains in waterlogged wood samples after rinsing seems to originate mainly from the water in which it was immersed. The question then remains whether or not there is any endogenous Sr left and, if so, whether it is possible to retain this for provenance studies while selectively removing exogenous Sr (cf., Van Ham-Meert et al., 2020).

The results obtained after the various pre-treatments show that returning to the original value of wood was possible in only one case. This sample (T69Sea) was crushed and pre-treated with acetic acid. Why this particular specimen should have been successfully cleaned is not clear, since both this and T88 were moderately dense tropical hardwoods, though of different genera. Thus, it may in fact be coincidental. The samples pre-treated with acetic acid without prior crushing or with HCl provide

unsatisfactory results. The alpha-cellulose extraction method applied to experimentally water-logged oak samples by Van Ham-Meert et al. (2020), modified from Andreu-Hayles et al. (2019) to avoid equilibration between wood samples, also involves treatment with acetic acid. This method led to what the authors termed "enigmatic results," proposing a possible explanation the presence of various Sr reservoirs within the wood (in alpha-cellulose, lignin, and beta-cellulose, etc.) with distinct isotopic compositions. The present study returned a number of results departing even more strongly from mass balance expectations, but in the opposite direction to that seen in Van Ham-Meert et al. (2020), i.e., higher rather than lower, making the situation even more puzzling. This might reflect Sr present in oxalate crystals as opposed to adsorbed Sr and/or different parts of the tree being fed through different root systems (shallow versus deep) tapping into different Sr reservoirs (Schmitt et al., 2017). All of this remains speculative and leaves room for new research venues to be explored where combining radiogenic ($^{87}Sr/^{86}Sr$) with stable Sr isotope ratios ($\delta^{88}Sr$) might provide new insights in the biogeochemistry of Sr in wood (e.g., Andrews et al., 2016). Overall, these experiments, along with the work of Hajj et al. (2017), show that wood becomes contaminated with exogenous Sr within a few weeks when immersed in water and that the various pre-treatments tested here are inadequate for its removal. There is also a possibility that most of the endogenous Sr is removed during immersion in water.

HCl should be avoided as after pre-treatment almost no Sr remains in the samples thus removing both endogenous and exogenous Sr. The results also suggest that pre-treatment of waterlogged wood with acetic acid on bulk material (crushed or not) led to variable results even on the same samples (e.g., the four fractions of FR2 give very different results after pre-treatment with acetic acid with $^{87}Sr/^{86}Sr$ values ranging from 0.7092 to 0.7125) and is not a viable method. Future research should investigate other alternatives. Moreover, the fact that $^{87}Sr/^{86}Sr$ values may be altered beyond any mixing line between the original, endogenous bulk value *and* that of the source of exogenous contamination means that it is not possible to rely on values that appear to differ significantly from those expected even assuming full contamination with a known source (i.e., seawater). This in turn calls into question published results for waterlogged wood samples such as Mediterranean shipwrecks (Rich et al., 2016) and the pre-Columbian wood carvings from Thursby Island, Florida (Ostapkowicz et al., 2017a). This matter needs to be resolved in future work.

Pitch Contaminated Samples

From the results of the pitch contamination experiment, it appears that when comparing uncontaminated wood with pitch-contaminated wood, some but not all samples show a shift in their $^{87}Sr/^{86}Sr$. Those that show no difference (T34 and T81) had original values close to that of the pitch with which they were contaminated. After immersion, the $^{87}Sr/^{86}Sr$ value of T71 shifts closer to that of the pitch compared to its original, less radiogenic value, suggesting that samples recovered from pitch should be pre-treated to remove potential contamination. Nevertheless, the tests carried out here used Angelin (*Andira sp.*) and pitch from Trinidad's Pitch Lake; different wood species (i.e., with different levels of resin) as well as different asphalt deposits (i.e., with different compositions) should be further tested.

The pre-treatment tests on uncontaminated wood show the large impact of the combination of organic solvents and aqueous-based pre-treatment (i.e., ABA) on their $^{87}Sr/^{86}Sr$ values. Using only organic solvents (i.e., without ABA), however, has little to no effect on the $^{87}Sr/^{86}Sr$ of uncontaminated wood. Together with the visual observation that large amounts of material are lost, this suggests that ABA is not only removing exogenous but also endogenous Sr and as such should be avoided. This is confirmed by the results obtained for the pitch-contaminated samples. Indeed, only when organic solvents are used without ABA are the original $^{87}Sr/^{86}Sr$ values of the pitch-contaminated samples regained. This pre-treatment, consisting of several washes with a mixture of methanol and toluene (**Table 2**), seems, therefore, efficient at removing pitch contamination. Radiocarbon dating results, however, have shown that pitch from different locations (e.g., Rancho La Brea, CA, United States) can have different chemical compositions and require different protocols (Brock et al., 2017) and specific protocols should be tested for each pitch/asphalt. These results also suggest that in contrast to waterlogged samples where endogenous Sr is replaced by Sr from the water, due to its higher viscosity and the apparently lower solubility of Sr in pitch, pitch from Trinidad's Pitch Lake does not exchange Sr with the wood, but instead, protects it from external contamination.

These experiments show that, depending on the conditions under which wood materials and artifacts survive through time, they may or may not preserve their initial $^{87}Sr/^{86}Sr$ values. Due to its high solubility in aqueous solution, it is not altogether surprising that waterlogged wood samples are more affected than those immersed in pitch. Conversely, archeological wood preserved in dry desiccated environments and/or ethnographic wooden artifacts collected directly at the source and stored in museum collections (e.g., Ostapkowicz et al., 2018) face a different set of issues, relating to their post-collection histories such as the application of surface treatments and consolidants. Their removal must be dealt with on a case-by-case basis, as different materials will be involved, and penetrating to different depths on different woods, etc. A discussion of this issue is well beyond the scope of this paper. Nevertheless, such objects represent a valuable source of information for provenance studies, though it is critical to first assess and discount any conservation interventions that might have impacted on their Sr isotope ratios.

CONCLUSION

Our results identify potential issues linked to (sea)water and pitch contamination on wood and wooden artifacts when investigating their origin using Sr isotope analyses. The various aqueous-based pre-treatments were not successful at removing Sr contamination from waterlogged wood and more research is needed before $^{87}Sr/^{86}Sr$ from such materials can be used for

provenance studies. Furthermore, these results show that even when a $^{87}Sr/^{86}Sr$ value deviates from the value of water in which the sample was immersed (before or after pre-treatment) it cannot be assumed the sample preserves an endogenous signal and thus that is it "non-local." In the case of pitch, it is difficult to predict if the $^{87}Sr/^{86}Sr$ ratios will be affected by contamination. Therefore, all wood and wood artifacts believed to be contaminated with pitch should be pre-treated adequately by using, for example, organic solvents pre-treatments developed for radiocarbon dating. However, it is observed that, as for the waterlogging experiments, aqueous-based pre-treatments (in this case ABA) lead to inaccurate and/or imprecise results as it probably removes large amounts of endogenous Sr, and should, therefore, be avoided.

DATA AVAILABILITY STATEMENT

The original contributions presented in the study are included in the article/**Supplementary Material**, further inquiries can be directed to the corresponding author/s.

AUTHOR CONTRIBUTIONS

CS, RS, FB, and JO: conceptualization. CS: formal analysis. JO, CS, and NM: funding acquisition. CS, RS, FB, AR, AV, and NM: methodology. CS, RS, FB, and JO: writing – original draft. CS, RS, FB, AR, AV, NM, and JO: writing – review and editing. All authors contributed to the article and approved the submitted version.

FUNDING

The work undertaken on Trinidad's Pitch Lake material was supported by the United Kingdom's Arts and Humanities Research Council (AHRC) as part of the *Black Pitch, Carved Histories* project (AH/L00268X/1). The Trinidad herbarium collections that were part of the pitch contamination experiments were collected in partnership with colleagues from the National Herbarium of Trinidad and Tobago and Trinidad's Forestry Division, including Yasmin Baksh-Comeu, Harris Sooklal, Jason Mungalsingh, K. Manaure, and N. Falby-Peters. Cyril Billy assisted in acquiring the samples of pitch from Pitch Lake. The collection of the Florida wood samples was supported by a grant from the Wenner-Gren Foundation to RS, with the permission from Florida State Parks and the Florida Forest Service.

ACKNOWLEDGMENTS

The VUB and VUB Strategic Research fund are thanked for their financial support for analyses; the Research Foundation–Flanders (FWO) is thanked for CS's postdoctoral fellowship. Wendy Debouge and Jeroen de Jong from the Laboratoire G-Time (Geochemistry: Tracing by Isotope, Mineral, and Element), Université Libre de Bruxelles (Belgium) are acknowledged for their help with the strontium isotope analyses by MC-ICP-MS. Philippe Claeys, Steven Goderis and Martine Leermakers from the Vrije Universiteit Brussel (VUB – Belgium) are thanked for their help with the strontium concentrations measurements by ICP-MS.

SUPPLEMENTARY MATERIAL

The Supplementary Material for this article can be found online at: https://www.frontiersin.org/articles/10.3389/fevo.2020.589154/full#supplementary-material

REFERENCES

Andreu-Hayles, L., Levesque, M., Martin-Benito, D., Huang, W., Harris, R., Oelkers, R., et al. (2019). A high yield cellulose extraction system for small whole wood samples and dual measurement of carbon and oxygen stable isotopes. *Chem. Geol.* 504, 53–65. doi: 10.1016/j.chemgeo.2018.09.007

Andrews, M. G., Jacobson, A. D., Lehn, G. O., Horton, T. W., and Craw, D. (2016). Radiogenic and stable Sr isotope ratios (87Sr/86Sr, δ88/86Sr) as tracers of riverine cation sources and biogeochemical cycling in the Milford Sound region of Fiordland, New Zealand. *Geochim. Cosmochim. Acta* 173, 284–303. doi: 10.1016/j.gca.2015.10.005

Angino, E. E., Billings, G. K., and Andersen, N. (1966). Observed variations in the strontium concentration of seawater. *Chem. Geol.* 1, 145–153. doi: 10.1016/0009-2541(66)90013-1

Benson, L. V., Hattori, E. M., Taylor, H. E., Poulson, S. R., and Jolie, E. A. (2006). Isotope sourcing of prehistoric willow and tule textiles recovered from western Great Basin rock shelters and caves - proof of concept. *J. Arch. Sci.* 33, 1588–1599. doi: 10.1016/j.jas.2006.02.012

Benson, L. V., Taylor, H. E., Plowman, T. I., Roth, D. A., and Antweiler, R. C. (2010). The cleaning of burned and contaminated archaeological maize prior to $^{87}Sr/^{86}Sr$ analysis. *J. Arch. Sci.* 37, 84–91. doi: 10.1016/j.jas.2009.09.005

Bentley, R. A. (2013). Mobility and the diversity of early Neolithic lives: isotopic evidence from skeletons. *J. Anthropol. Archaeol.* 32, 303–312. doi: 10.1016/j.jaa.2012.01.009

Blum, J. D., Hamburg, S. P., Yanai, R. D., and Artur, M. A. (2012). Determination of foliar Ca/Sr discrimination factors for six tree species and implications for Ca sources in northern hardwood forests. *Plant Soil* 356, 303–314. doi: 10.1007/s11104-011-1122-2

Boyer, A., Ning, P., Killey, D., Klukas, M., Rowan, D., Simpson, A. J., et al. (2018). Strontium adsorption and desorption in wetlands: role of organic matter functional groups and environmental implications. *Water Res.* 133, 27–36. doi: 10.1016/j.watres.2018.01.026

Brock, F., Dee, M., Hughes, A., Snoeck, C., Staff, R., and Bronk Ramsey, C. (2018). Testing the effectiveness of protocols for removal of common conservation treatments for radiocarbon dating. *Radiocarbon* 60, 35–50. doi: 10.1017/rdc.2017.68

Brock, F., Higham, T., Ditchfield, P., and Bronk Ramsey, C. (2010). Current pretreatment methods for AMS radiocarbon dating at the Oxford Radiocarbon Accelerator Unit (ORAU). *Radiocarbon* 52, 103–112. doi: 10.1017/s0033822200045069

Brock, F., Ostapkowicz, J., Wiedenhoeft, A. C., and Bull, I. D. (2017). Radiocarbon dating wooden carvings and skeletal remains from Pitch Lake, Trinidad. *Radiocarbon* 59, 1447–1461. doi: 10.1017/rdc.2017.78

Budd, P., Montgomery, J., Barreiro, B., and Thomas, R. G. (2000). Differential diagenesis of strontium in archaeological human dental tissues. *Appl. Geochem.* 15, 687–694. doi: 10.1016/s0883-2927(99)00069-4

Chen, J.-P. (1997). Batch and continuous adsorption of strontium by plant root tissues. *Bioresour. Technol.* 60, 185–189. doi: 10.1016/s0960-8524(97)00021-7

Dee, M. W., Brock, F., Bowles, A., and Bronk Ramsey, C. (2011). Using a silica substrate to monitor the effectiveness of radiocarbon pretreatment. *Radiocarbon* 53, 705–711. doi: 10.1017/s0033822200039151

English, N., Betancourt, J., Dean, J., and Quade, J. (2001). Strontium isotopes reveal distant sources of architectural timber in Chaco Canyon, New Mexico. *Proc. Natl. Acad. Sci. U.S.A.* 98, 11891–11896. doi: 10.1073/pnas.211305498

Evans, J. A., Montgomery, J., Wildman, G., and Boulton, N. (2010). Spatial variations in biosphere $^{87}Sr/^{86}Sr$ in Britain. *J. Geol. Soc. Lond.* 167, 1–4.

Faure, G., and Powell, T. (1972). *Strontium Isotope Geology*. New York, NY: Springer.

GEOROC (2014). *Geochemistry of Rocks of the Oceans and Continents*. Available online at: http://georoc.mpch-mainz.gwdg.de/georoc/ (accessed July 8, 2014).

Hajj, F., Poszwa, A., Bouchez, J., and Guérold, F. (2017). Radiogenic and "stable" strontium isotopes in provenance studies: a review and first results on archaeological wood from shipwrecks. *J. Archaeol. Sci.* 86, 24–49. doi: 10.1016/j.jas.2017.09.005

Hess, J., Bender, M. L., and Schilling, J. G. (1986). Evolution of the ratio of strontium-87 to strontium-86 in -water from Cretaceous to present. *Science* 231, 979–984. doi: 10.1126/science.231.4741.979

Laffoon, J. E., Rodríguez Ramos, R., Chanlatte Baik, L., Storde, Y. N., Rodríguez Lopez, M., Davies, G. R., et al. (2014). Long-distance exchange in the precolonial Circum-Caribbean: a multi-isotope study of animal tooth pendants from Puerto Rico. *J. Anthropol. Archaeol.* 35, 220–233. doi: 10.1016/j.jaa.2014.06.004

Meighan, I. G., McCormick, A. G., Gibson, D., Gamble, J. A., and Graham, I. J. (1988). Rb-Sr isotopic determinations and the timing of Tertiary central complex magmatism in NE Ireland. *Geol. Soc. Lond. Special Publ.* 39, 349–360. doi: 10.1144/gsl.sp.1988.039.01.30

Ostapkowicz, J., Brock, F., Wiedenhoeft, A. C., Snoeck, C., Pouncett, J., Baksh-Comeau, Y., et al. (2017a). Black pitch, carved histories: radiocarbon dating, wood species identification and strontium isotope analysis of prehistoric wood carvings from Trinidad's Pitch Lake. *J. Archaeol. Sci. Reports* 16, 341–358. doi: 10.1016/j.jasrep.2017.08.018

Ostapkowicz, J., Ramsey, C. B., Brock, F., Cartwright, C., Stacey, R., and Richards, M. (2013). Birdmen, *cemís* and *duhos*: material studies and AMS ^{14}C dating of Pre-Hispanic Caribbean wood sculptures in the British Museum. *J. Archaeol. Sci.* 40, 4675–4687. doi: 10.1016/j.jas.2013.07.015

Ostapkowicz, J., Ramsey, C. B., Brock, F., Higham, T., Wiedenhoeft, A. C., Ribechini, E., et al. (2012). Chronologies in wood and resin: AMS 14C dating of pre-Hispanic Caribbean wood sculpture. *J. Archaeol. Sci.* 39, 2238–2251. doi: 10.1016/j.jas.2012.01.035

Ostapkowicz, J., Roberts, A., Thistlewood, J., Brock, F., Wiedenhoeft, A. C., Snoeck, C., et al. (2018). The origins of Tradescant's 'India occidentali' wooden clubs: 14C dating, material identification and strontium isotope studies. *Antiquaries J.* 98, 1–32.

Ostapkowicz, J., Schulting, R. J., Wheeler, R., Newsom, L., Brock, F., Bull, I., et al. (2017b). East-central Florida Pre-Columbian wood sculpture: radiocarbon dating, wood identification and strontium isotope studies. *J. Archaeol. Sci. Reports* 13, 595–608. doi: 10.1016/j.jasrep.2017.03.035

Price, T. D., Tiesler, V., and Burton, J. H. (2006). Early African diaspora in colonial Campeche, Mexico: strontium isotopic evidence. *Am. J. Phys. Anthropol.* 130, 485–490. doi: 10.1002/ajpa.20390

Rediske, J. H., and Selders, A. A. (1953). The absorption and translocation of strontium by plants. *Plant Physiol.* 28, 594–605. doi: 10.1104/pp.28.4.594

Rich, S., Manning, S. W., Degryse, P., Vanhaecke, F., Latruwe, K., and Van Lerberghe, K. (2016). To put a cedar ship in a bottle: dendroprovenancing three ancient East Mediterranean watercraft with the $^{87}Sr/^{86}Sr$ isotope ratio. *J. Archaeol. Sci. Reports* 9, 514–521. doi: 10.1016/j.jasrep.2016.08.034

Schmitt, A.-D., Gangloff, S., Labolle, F., Chabaux, F., and Stille, P. (2017). Calcium biogeochemical cycle at the beech tree-soil solution interface from the Strengbach CZO (NE France): insights from stable Ca and radiogenic Sr isotopes. *Geochim. Cosmochim. Acta* 213, 91–109. doi: 10.1016/j.gca.2017.06.039

Serdar, B., and Demiray, H. (2012). Calcium oxalate crystal types in three oak species (Quercus L.) in Turkey. *Turkish J. Biol.* 36, 386–393.

Sillen, A., Hall, G., Richardson, S., and Armstrong, R. (1998). $^{87}Sr/^{86}Sr$ ratios in modern and fossil food-webs of the Sterkfontein Valley: implications for early hominid habitat preferences. *Geochim. Cosmochim. Acta* 62:2463. doi: 10.1016/s0016-7037(98)00182-3

Sillen, A., and LeGeros, R. (1991). Solubility profiles of synthetic apatites and of modern and fossil bones. *J. Archaeol. Sci.* 18, 385–397. doi: 10.1016/0305-4403(91)90073-x

Snoeck, C., Pouncett, J., Ramsey, G., Meighan, I., Mattielli, N., Goderis, S., et al. (2016). Mobility during the Neolithic and Bronze Age in Northern Ireland explored using strontium isotope analysis of cremated human bone. *Am. J. Phys. Anthropol.* 160, 397–413. doi: 10.1002/ajpa.22977

Snoeck, C., Ryan, S., Pouncett, J., Pellegrini, M., Claeys, Ph, Wainwright, A. N., et al. (2020). Towards a biologically available strontium isotope baseline for Ireland. *Sci. Total Environ.* 712:136248. doi: 10.1016/j.scitotenv.2019.136248

Snoeck, C., Schulting, R. J., Lee-Thorp, J. A., de Jong, J., Debouge, W., and Mattielli, N. (2015). Calcined bone provides a reliable substrate for strontium isotope ratios as shown by an enrichment experiment. *Rapid Commun. Mass Spectr.* 29, 107–114. doi: 10.1002/rcm.7078

Storey, R., and Leigh, R. A. (2004). Processes modulating calcium distribution in citrus leaves. An investigation using X-Ray microanalysis with strontium as a tracer. *Plant Physiol.* 136, 3838–3848. doi: 10.1104/pp.104.045674

Styring, A. K., Evans, J. A., Nitsch, E. K., Lee—Thorp, J. A., and Bogaard, A. (2019). Revisiting the potential of carbonized grain to preserve biogenic $^{87}Sr/^{86}Sr$ signatures within the burial environment. *Archaeometry* 61, 179–193. doi: 10.1111/arcm.12398

Vaiglova, P., Snoeck, C., Nitsch, E., Bogaard, A., and Lee-Thorp, J. A. (2014). Impact of contamination and pre-treatment on stable carbon and nitrogen isotopic composition of charred plant remains. *Rapid Commun. Mass Spectr.* 28, 2497–2510. doi: 10.1002/rcm.7044

Van Ham-Meert, A., Rodler, A. S., Waight, T. E., and Daly, A. (2020). Determining the Sr isotopic composition of waterlogged wood – cleaning more is not always better. *J. Archaeol. Sci.* 124:105261. doi: 10.1016/j.jas.2020.105261

Weis, D., Kieffer, D., Maerschalk, C., Barling, J., de Jong, J., Williams, G. A., et al. (2006). High-precision isotopic characterization of USGS reference materials by TIMS and MC-ICP-MS. *Geochem. Geophys. Geosyst.* 7:Q08006.

Conflict of Interest: The authors declare that the research was conducted in the absence of any commercial or financial relationships that could be construed as a potential conflict of interest.

frontiers in Ecology and Evolution

ORIGINAL RESEARCH
published: 15 January 2021
doi: 10.3389/fevo.2020.588318

Homogeneous Glacial Landscapes Can Have High Local Variability of Strontium Isotope Signatures: Implications for Prehistoric Migration Studies

Erik Thomsen[1]*, *Rasmus Andreasen*[1] and *Tine L. Rasmussen*[2]

[1] Department of Geoscience, Faculty of Natural Sciences, Aarhus University, Aarhus, Denmark, [2] Department of Geology, UiT, CAGE-Center for Arctic Gas Hydrate, Environment and Climate, Arctic University of Norway, Tromsø, Norway

Increasingly, strontium (Sr) isotopes are used to distinguish locals and migrants in prehistoric studies, by measuring $^{87}Sr/^{86}Sr$ in human remains and comparing these values to the distribution of the bioavailable $^{87}Sr/^{86}Sr$ in the study area, often in surface water. However, it has recently been shown that agricultural lime can have a substantial impact on the $^{87}Sr/^{86}Sr$ ratio and strontium concentration in surface water in areas where soils are low- to non-calcareous. Agricultural lime is rich in strontium with low $^{87}Sr/^{86}Sr$ ratios, such that interpretations of prehistoric migration based on surface waters affected by agricultural lime often overestimate the number of migrants in a given area. However, the impact of agricultural lime was questioned in a new study, which argues that strontium derived from agricultural lime is retained in the topsoil of the fields and therefore do not contaminate the surface water. In the present study and in a companion study in this volume, we show that strontium derived from agricultural lime is highly mobile in soils, and so contaminate surface waters extensively. We also show that the $^{87}Sr/^{86}Sr$ ratios are consistently higher in waters from "pristine areas" (where no agricultural lime has been applied within a distance of 150 m from the sample locality) than in water from farmland, thus confirming that it is of vital importance for accurate mapping of isoscapes to avoid sampling waters contaminated by agricultural lime. Our new measurements of $^{87}Sr/^{86}Sr$ ratios in central Jutland, Denmark, raise the highest measured values to 0.7186. High values between 0.7140 and 0.7156 occur repeatedly and it is apparent that nearly all prehistoric human finds in Jutland, previously believed to have journeyed from afar are more likely of local origin. Furthermore, we show that carbonate-rich areas along the coast of southwest Zealand carry high $^{87}Sr/^{86}Sr$ values (0.7112–0.7132), where we would expect low values. This surprising result indicates that nearly all humans buried at the Viking Age site, Trelleborg could well have originated locally, in contrast to past studies, which have suggested that about 50% of the burials were of individuals who came from afar.

Keywords: $^{87}Sr/^{86}Sr$, agricultural lime, prehistoric human migration, Bronze Age, Viking Age, glacial deposit, surface water chemistry

OPEN ACCESS

Edited by:
Joshua H. Miller,
University of Cincinnati, United States

Reviewed by:
Jason Laffoon,
Leiden University, Netherlands
Ian Moffat,
Flinders University, Australia

***Correspondence:**
Erik Thomsen
erik.thomsen@geo.au.dk

Specialty section:
This article was submitted to Paleoecology, a section of the journal Frontiers in Ecology and Evolution

Received: *28 July 2020*
Accepted: *18 December 2020*
Published: *15 January 2021*

Citation:
Thomsen E, Andreasen R and Rasmussen TL (2021) Homogeneous Glacial Landscapes Can Have High Local Variability of Strontium Isotope Signatures: Implications for Prehistoric Migration Studies. Front. Ecol. Evol. 8:588318. doi: 10.3389/fevo.2020.588318

INTRODUCTION

The strontium isotopic signature $^{87}Sr/^{86}Sr$ has been used to evaluate origin and mobility in prehistoric humans with considerable success (e.g., Ericson, 1985; Bentley, 2006; Montgomery, 2010; Guede et al., 2017; Knipper et al., 2017; Blank et al., 2018; Madgwick et al., 2019). Strontium signatures measured in human remains are compared to isotope maps (i.e., isoscapes or baselines) of the natural distribution of the biologically available $^{87}Sr/^{86}Sr$ in the study area. In many investigations, these maps are constructed from $^{87}Sr/^{86}Sr$ measured in present-day surface waters, but other proxies such as surface soils, plants, and fossilized- and living animals are also used (Capo et al., 1998; Evans et al., 2010; Price et al., 2011, 2012; Frei and Price, 2012; Maurer et al., 2012; Grimstead et al., 2017).

The accuracy of the isoscape is critical to the success of the method, and thus, new isoscapes are constantly published and older isoscapes improved, either by increasing the number of sample sites or by omitting sites deemed to have been contaminated, just as new mathematical methods for analyzing the strontium isotopic distribution in an area are regularly introduced (Bataille and Bowen, 2012; Bataille et al., 2018).

Today, the most wide-ranging isoscapes examine the distribution of strontium isotopes on continental scales (Widga et al., 2017; Bataille et al., 2018, 2020; Hoogewerff et al., 2019). The purpose of these isoscapes is primarily to create overviews, and they are generally not sufficiently detailed to allow for the evaluation of prehistoric mobility of individuals. The isoscapes published for Great Britain (Evans et al., 2010, 2018), France (Willmes et al., 2018), the Netherlands (Kootker et al., 2016), and Denmark (Frei and Frei, 2011; Frei and Price, 2012) were constructed from a much higher density of samples. For example, the Danish isoscape of Frei and Frei (2011) is based on close to 200 water samples covering an area of 43,000 km^2, and in 2013, Frei and Frei published a baseline for the Danish island of Bornholm (588 km^2) based on 51 samples. The isoscape for mainland Denmark has subsequently served as a reference map in several studies of prehistoric provenance and mobility ranging in time from the Neolithic to the early Middle age (e.g., Frei et al., 2015, 2017a,b; Felding et al., 2020; Van der Sluis et al., 2020). In practice, these large-scale isoscapes are typically combined with- or replaced by local isoscapes developed for specific mobility studies in the areas surrounding the archaeological sites under study (Price et al., 2002; Bentley, 2006; Slovak and Paytan, 2011; Maurer et al., 2012). The density of sample localities may be quite high in these studies. For example, Maurer et al. (2012) collected water samples from eighteen localities within a radius of 4 km from their archaeological targets.

The $^{87}Sr/^{86}Sr$ signature of a particular lake or stream is influenced by numerous factors, of which the underlying geology typically is the most important (Willmes et al., 2018). This means that a higher number of sample localities are needed in geologically heterogeneous areas than in more homogeneous ones (Grimstead et al., 2017: Bataille et al., 2020). The surface deposits across Denmark consist largely of glaciogenic weathering products from the Scandinavian shield carried to Denmark by ice during the last two major glaciations. The siliciclastic deposits are mixed with Cretaceous chalk and Early Paleocene limestones eroded in the Kattegat and Baltic Sea areas, where these carbonates are exposed (**Figure 1**). According to Frei and Price (2012), the content of strontium in the Danish soils is strongly dominated by contributions from these carbonates, which are rich in strontium with a low isotopic signature.

Frei and Frei (2011) published $^{87}Sr/^{86}Sr$ values for 192 samples of surface water from Danish streams and lakes ranging from 0.70787 to 0.71282. From these values they calculated an isoscape for Denmark spanning from 0.708 to 0.711 (mean = 0.7096 ± 0.0015; 2σ). According to Price et al. (2011) and Frei and Price (2012), this relatively narrow range is the result of a rather simple and homogenous glacial geology. Nevertheless, in a recent study, Thomsen and Andreasen (2019) found a much higher variability within three areas of central and western Jutland. Within an area of a few square kilometers, these authors measured values ranging from 0.70847 to 0.71495, which greatly exceeded the total range in the isoscape for Denmark published by Frei and Frei (2011). The high values were encountered in water bodies from pristine areas, that is areas that have been sheltered from the influence of agricultural activity, and, in particular, from the effect of agricultural lime. Thomsen and Andreasen (2019) concluded that the narrow range observed by Frei and Frei (2011) was due to the fact that most of their samples came from areas that were affected by farming, here, in particular, by an extensive use of agricultural lime. The significance of the results of Thomsen and Andreasen (2019) has since been questioned (Frei et al., 2020), but in this paper and in an accompanying paper by Andreasen and Thomsen, 2021 in this volume, we present results that confirm and expand upon the central findings of Thomsen and Andreasen (2019) and that do not support the interpretations of Frei et al. (2020).

The main goal of the present study is to further investigate the high variability in the strontium signature and strontium concentration in water samples from pristine areas observed by Thomsen and Andreasen (2019). The high variability seems surprising since the surficial geological deposits of Denmark appear relative homogeneous consisting predominantly of siliciclastic glaciogenic sediments transported by ice from central Scandinavia during the Saalian and Weichselian glaciations and mixed with various amount of calcium carbonate mainly from chalk.

For the investigation, we selected three areas representing contrasting geological environments. Study area 1 (70 km^2) comprises mainly non-calcareous water- or aeolian-sorted sandy deposits. The deposits of study area 2 (300 km^2) are very different composed of strongly calcareous clayey tills. Study areas 1 and 2 are geologically relatively homogeneous. Study area 3 (200 km^2) is much more heterogeneous as it can be subdivided into several geological zones ranging from pure non-calcareous sand in the west to calcareous clay in the east. The goal of the sampling strategy was to capture the lithological variability within each area as closely as possible, and to correlate the strontium results with the changing geology. The new elevated $^{87}Sr/^{86}Sr$ values for central Jutland and western Zealand has significant consequences for previous interpretations of prehistoric migrations in Denmark. This is exemplified by four case studies.

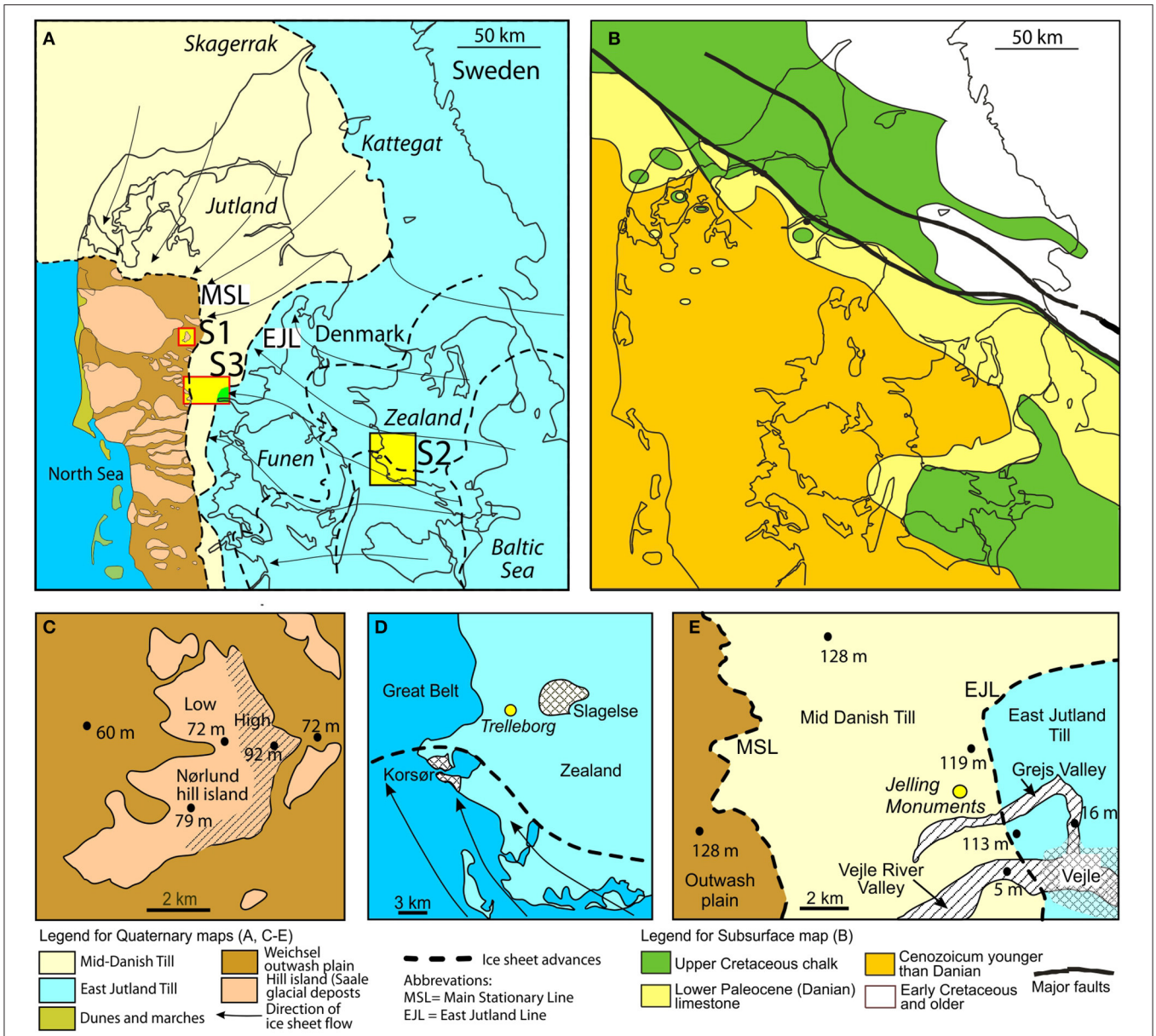

FIGURE 1 | Simplified geological maps of Denmark with study areas depicted. **(A)** Map showing main features of the Quaternary glacial deposits. The Main Stationary Line (MSL) and the East Jutland Line (EJL) indicate the maximum extent of the Weichselian ice sheet in Denmark and the maximum extent of the East Jutland Advance, respectively. The two lines subdivide Jutland into three glaciogenic provinces: West Jutland, Central Jutland, and East Jutland. The distribution in West Jutland of hill islands (Saale glacial deposits) and Weichselian outwash plains is indicated. Arrows indicate direction of ice movement during advances to the Main Stationary Line and East Jutland Line. Locations of study areas S1–S3 are shown. Map is based on Krüger (1983); Madsen et al. (1992), Kjær et al. (2003), and Smed (2013). **(B)** Map showing the distribution of pre-Quaternary deposits in Denmark. Note distribution of Cretaceous chalk and Lower Paleocene limestone. Map is based on Håkansson and Pedersen (1992). **(C)** Map showing main features of study area S1, Nørlund hill island. **(D)** Map showing main features of study area S2, SWZealand. **(E)** Map showing main features of study area S3, Jelling.

DISTRIBUTION OF GLACIOGENIC DEPOSITS IN DENMARK

The landscapes and surface deposits of Denmark are almost ubiquitously formed by glacial activity during the Saalian and Weichselian glaciations. The Main Stationary Line marks the maximum extent of the Weichselian glaciation in Denmark, and dates to ca. 22.000 years (**Figure 1A**). It subdivides the country into two distinctly different geological provinces (Krüger, 1983; Houmark-Nielsen, 1987, 2003; Larsen and Kronborg, 1994; Kjær et al., 2003; Houmark-Nielsen et al., 2005) (**Figure 1A**). The landscapes west of the Main Stationary Line are dominated by flat outwash plains composed of sandy, often cross-bedded, meltwater deposits. Protruding through the outwash plains are

numerous older, higher-lying landscape features, termed "hill islands" in the Danish geologic literature. They are generally remnants of the Saale glaciation. The hill islands consist of tills and meltwater deposits, with occasional outcrops of Quaternary marl and of Miocene sand, but their geology is not always well-understood (Krüger, 1983; Houmark-Nielsen et al., 2005). Apart from local marl deposits, the upper 10 m or more of both the outwash plains and hill island deposits are generally non-calcareous.

The landscapes east of the Main Stationary Line are referred to the Mid Danish Till. This unit consists of rather sandy tills mixed with local meltwater deposits. The upper 2–10 m is often non-calcareous (Madsen et al., 1992). After a major ice retreat, a new advance started about 19,000–18,000 years ago. This event is termed the East Jutland Advance (Houmark-Nielsen, 2003; Smed, 2013) (**Figure 1A**). The maximum extent of this new advance is marked by a number of terminal moraines forming the East Jutland Line. The East Jutland advance came from the southeast through the Baltic Sea depression and the deposits are both more clayey and more calcareous than the Mid Danish Till, which came from a more northeasterly direction (Houmark-Nielsen, 1987; Kjær et al., 2003) (**Figure 1A**).

After 18,000 years BP, the ice retreated rapidly from the East Jutland Line. Around 17,000 years, the general retreat was interrupted by several small advances, which, on the islands of Funen and Zealand, are marked by distinct terminal and lateral moraines (Houmark-Nielsen et al., 2005; Smed, 2013) (**Figure 1A**).

Distribution and Origin of the Natural Calcium Carbonate Component

The glacial deposits of western and central Jutland are low- to non-calcareous, while the deposits of eastern Jutland and the islands of Funen and Zealand are strongly calcareous. The reason for this change is primarily due to differences in the amount of lime, picked up by the various ice advances. The natural calcareous part of the glaciogenic sediments of Denmark consists predominantly of Cretaceous chalk and early Paleocene (Danian) limestone eroded by the advancing glaciers as they passed Skagerrak, Kattegat, the western Baltic Sea and eastern Denmark, where these deposits are exposed immediately below the glacial sediments (Kjær et al., 2003) (**Figure 1B**). The relatively soft Cretaceous and Paleocene carbonates consist mainly of well-preserved calcareous nannofossils (coccoliths) mixed with a diverse fauna of calcareous invertebrates. The chalk and limestone deposits disintegrate easily when subjected to normal weathering and are smeared into the siliciclastic sediments. These soft carbonates are mixed with smaller amounts of hard fragments of Ordovician and Silurian limestone transported primarily from central Scandinavia (Kjær et al., 2003).

Natural Strontium Sources

The natural strontium content of surface waters in Denmark are almost exclusively the result of a mixing of strontium from two major sources. The first source is the siliciclastic weathering products brought to Denmark during the Quaternary (Frei and Frei, 2011; Price et al., 2011). The origin of these deposits is the granitic and gneissic bedrocks of central Scandinavia. The $^{87}Sr/^{86}Sr$ signature in surface waters from pure siliciclastic deposits sampled in pristine areas is relatively high, ranging between 0.7108 and 0.7186, whereas the concentration is low, ranging from 0.002 to 0.064 (Thomsen and Andreasen, 2019; this study). The second source is the upper Cretaceous chalk and Lower Paleocene limestone, with minor contributions of Palaeozoic limestone (see above). Cretaceous and Paleocene carbonates are rich in strontium (∼800–1,000 ppm) with a low $^{87}Sr/^{86}Sr$ ratio (∼0.70785; Frei and Frei, 2011; Thomsen and Andreasen, 2019).

AGRICULTURAL LIME

About 57% of the total Danish area is farmland under plow, and nearly all of this land is regularly treated with agricultural lime, typically about 500 kg/ha/year (Thomsen and Andreasen, 2019). Agricultural lime is used to ameliorate the acidity of the soils and improve crop yield. It is most intensively applied in central and western Jutland, where the soil is naturally low- to non-calcareous.

In Denmark, agricultural lime and natural lime are basically the same product, namely chalk and limestone from the Upper Cretaceous and Lower Paleocene. The natural lime was eroded into the soil during the glaciations (**Figures 1A,B**). The agricultural lime is quarried from the same deposits in northeastern Jutland and eastern Zealand. The strontium content of agricultural lime and natural lime is therefore basically the same. We here disregard the Palaeozoic limestone fragments that contributes to the carbonate content in the glacial deposits, but are absent in the agricultural lime.

Thomsen and Andreasen (2019) showed that in western Jutland the $^{87}Sr/^{86}Sr$ ratio was distinctly higher in pristine surface water (0.7108–0.7150, $N = 37$), than in surface water from farmland (0.7091–0.7110, $N = 16$). The study also indicated that the majority of ponds, lakes, and streams in Denmark are contaminated by agricultural lime, such that their waters cannot be used in the construction of strontium isoscapes. The effect of agricultural lime was particularly strong in central and western Jutland, where the soil is naturally low- to non-calcareous. In eastern Jutland and on the islands of Funen and Zealand, where the natural content of lime is high, the effect was small and difficult to trace.

MATERIALS AND METHODS

Sampling of Individual Samples

Nearly all samples were collected from ponds and small lakes. Only a few samples were taken in streams and larger lakes, as these water bodies in Denmark nearly always have been in contact with farmland and therefore are contaminated. The distinction between pristine (water bodies from non-agricultural areas) and non-pristine surface waters (water bodies from agricultural areas) was made during the planning of the field trips. For a pond to qualify as a pristine there must be a distance of at least 150 m between the pond and the nearest farmland (Thomsen and Andreasen, 2019 and references therein).

Sample sites were selected from studies of new and old topographical maps and aerial photographs in combination with the geological maps of Smed (1978). In principle, all selected water bodies were sampled. However, a few samples were not analyzed as the water bodies turned out to be contaminated (e.g., by bird feed, building waste).

Water samples were collected in acid-cleaned 250 ml polyethylene bottles. During field sampling, bottles were filled twice with sample water before final sampling. Most samples were taken 15–20 cm below the surface. However, a few samples were taken at a depth of 40–50 cm. Samples were stored in a cool room at 4 °C. The data for all analyzed samples are given in **Table 1**.

Strontium Isotope Analyses

Twenty ml of water were dried down and digested overnight in 2 ml of aqua regia, dried down again, and dissolved in nitric acid for strontium separation chemistry. Strontium was separated from the sample matrix using Eichrom (TrisKem International) Sr spec resin and analyzed for isotopic composition using a Nu Plasma II multicollector ICP-MS (inductively coupled plasma mass spectrometry) at the Department of Geoscience, Aarhus University. The four stable isotopes of strontium (^{84}Sr, ^{86}Sr, ^{87}Sr, and ^{88}Sr) were measured simultaneously, as were isotopes of Kr, Rb, Y, and doubly charged REE, to monitor and correct for interferences. Masses 82, 83, 84, 85, 86, 87, 88, and 89 were measured simultaneously, as were half-masses 83.5, 84.5, 85.5, 86.5, and 87.5. Baselines were determined by on-peak zero, and each sample run consisted of 400 s of peak time. Data were fractionation-corrected using the exponential law and normalized to NBS SRM 987 (^{87}Sr/^{86}Sr = 0.71025); and samples of Holocene foraminifera (*Baculogypsina sphaerulata*) expected to give a modern-day seawater Sr isotope value (^{87}Sr/^{86}Sr = 0.70917, Dia et al., 1992) were processed along with the samples as a secondary standard. Three samples of foraminifera analyzed throughout the analytical campaign gave ^{87}Sr/^{86}Sr = 0.709173 ± 0.000005 (2σ). Reproducibility of individual measurement of samples is estimated to be 0.0025% (0.000018, 2σ) based on repeat analyses of standards and samples. The Sr isotopic compositions of the analyzed samples are given in **Table 1**.

Selection of Study Areas

The main purpose of the present study is to investigate local variability in the strontium signature and strontium concentration in surface water from a region with a relatively simple glacial geology. We selected three study areas representing some of the most characteristic glacial landscape types in Denmark (**Figure 1A**). Sampling density was generally limited by the number of pristine water bodies making it impossible to capture the full geological variability. However, it was possible to sample all geological facies types and often with several samples.

Study Area S1. Nørlund Hill Island

The Nørlund hill island was selected to represent the Saalian hill island terrains, which, to our knowledge, have never been investigated for strontium. The Nørlund hill island was chosen because of its manageable size (30 km^2; 70 km^2 including surrounding outwash plains), because it has never been cultivated for farming, and because it contains several water bodies (ponds to small lakes) available for sampling (**Figures 1A,C**). Some of the larger water bodies in the central part of the island had to be omitted, because they are contaminated by feces from thousands of whooper swans, who uses them as a refuge, after feeding on nearby farmland (according to information from local forester). To the east, the hill island rises 20–25 m above the outwash plain (**Figure 1C**). The terrain falls gradually toward the west and the western delimitation is difficult to establish with certainty. This difficulty is enhanced by the fact that the sediments of the hill island and the outwash plain are very similar, composed of medium to coarse sand with some gravel. We also sampled three small isolated marl pits that were in use during the early part of the nineteenth century.

The hill island has periodically been subject to intense sand drift, and substantial areas are covered by sand dunes. The age of the sand dunes is poorly known, but most of them are probably of late glacial age. Today, about 1/3 of the Nørlund hill island is heathland, while 2/3 is coniferous forests. This is in contrast to the surrounding outwash plains, which for the most part are intensively farmed.

Study Area S2, SW Zealand

The costal terrain of southwest Zealand seems typical for the highly calcareous clayey tills that dominate eastern Jutland, and the islands of Funen and Zealand (Madsen et al., 1992; Kjær et al., 2003; Balstrøm et al., 2013) (**Figures 1A,D**). The main reason for selecting this particular region is that it is home for the Trelleborg Viking Fortress, where numerous human remains have been excavated and analyzed for their strontium content (Price et al., 2011) (**Figure 1D**).

This study area (∼300 km^2) is the largest of the three areas selected for this investigation, but, geologically, it is also the simplest, as it contains only a single landscape type, namely hilly moraines dominated by calcareous tills (Houmark-Nielsen et al., 2005; Smed, 2013). Nevertheless, it is not completely homogeneous. Parallel to the coastline at a distance of 4–10 km runs a series of low ridges marking a lateral moraine (Milthers, 1931; Smed, 1978, 2013) (see dashed line in **Figures 1A,D**). The ridges are the result of a late Weichselian glacier advance from the southeast dated to about 17,000 years (Houmark-Nielsen et al., 2005).

SW Zealand is densely farmed limiting the number of available pristine water bodies. This investigation of study area 2 should, therefore, be considered as only preliminary.

Study Area S3, Jelling and the North Side of the Vejle River Valley

The Jelling area was selected as a study area, because it constitutes one of the most complex glaciogenic landscapes in Denmark (**Figures 1A,E**). Although the selected area is only about 220 km^2, it is intersected by two important glaciogenic boundaries in the country, namely the Main Stationary Line, which marks the maximum extent of the Fennoscandian ice sheet during the last glaciation, and the East Jutland Line, which marks the maximum extent of the East Jutland Advance (**Figures 1A,E**). The outwash

TABLE 1 | Strontium isotopic composition and concentration of surface water of investigated samples.

Locality	Sample	Date	Longitude	Lattitude	$^{87}Sr/^{86}Sr$	2 sd	ng Sr/ml	Sr (mg/l)	1/Sr	Size (m)*	Prist/Ag	Hill/Out#
S1	NP-1	31-08-17	56.053104	9.197114	0.71097	0.00002	10.75	0.011	93.0	Swamp	Pristine	O
Nørlund	NP-2	31-08-17	56.052616	9.193974	0.71195	0.00002	5.66	0.006	176.8	14 × 7	Pristine	O
	NP-3	01-08-17	56.05027+	9.189274	0.71142	0.00002	36.87	0.037	27.1	100 × 15	Pristine	O
	NP-4	31-08-17	56.055471	9.139040	0.71011	0.00002	94.98	0.095	10.5	Stream	Ag	O
	NP-5	03-10-17	56.059590	9.111094	0.70980	0.00002	65.17	0.065	15.3	Stream	Ag	O
	HAR-1	19-09-17	56.014125	9.183813	0.71338	0.00002	5.07	0.005	197.4	50 × 9	Pristine	O
	NL-1	23-01-20	56.045517	9.179881	0.71354	0.00003	13.26	0.013	75.4	52 × 16	Pristine	H
	NL-2	23-01-20	56.043241	9.163575	0.71381	0.00002	7.23	0.007	138.3	27 × 14	Pristine	H
	NL-3	23-01-20	56.025971	9.194020	0.71103	0.00003	4.94	0.005	202.5	120 × 15	Pristine	H
	NL-4	23-01-20	56.032175	9.209864	0.71142	0.00003	6.29	0.006	159.0	53 × 25	Pristine	H
	NL-5	23-01-20	56.022300	9.206318	0.71225	0.00002	30.89	0.031	32.4	75 × 30	Pristine	O
	NL-6	23-01-20	56.020302	9.173211	0.71248	0.00002	3.71	0.004	269.4	150 × 20	Pristine	H
	NL-7	23-01-20	56.007275	9.158151	0.71222	0.00003	3.56	0.004	280.7	40 × 9	Pristine	O
	NL-8	23-01-20	56.060116	9.193487	0.71144	0.00003	2.06	0.002	486.4	5 × 5	Pristine	H
	NL-9	23-01-20	56.060880	9.200380	0.71272	0.00002	8.85	0.009	112.9	80 × 15	Pristine	H
	NL-10	23-01-20	56.061880	9.185256	0.71271	0.00002	4.63	0.005	215.9	56 × 36	Pristine	H
	NL-11	23-01-20	56.053509	9.204958	0.71211	0.00003	5.04	0.005	198.6	40 × 14	Pristine	H
	NL-12	23-01-20	56.009467	9.190742	0.71191	0.00002	2.04	0.002	489.6	48 × 44	Pristine	O
	NL-13	17-05-20	56.065753	9.219766	0.70892	0.00003	151.47	0.151	6.6	70 × 5	Pristine	H-MP
	NL-14	17-05-20	56.034103	9.234875	0.71174	0.00003	7.67	0.008	130.4	75 × 53	Pristine	O
	NL-15	17-05-20	56.048448	9.223591	0.7098	0.00003	66.07	0.066	15.1	15 × 15	Pristine	H-MP
	NL-16	20-05-10	56.078136	9.218931	0.71009	0.00003	90.75	0.091	11.0	Stream	Ag	O
	NL-17	20-05-10	56.078870	9.224005	0.70829	0.00003	77.29	0.077	12.9	46 × 7	Ag	O
	NL-18	20-05-10	56.078901	9.231485	0.70954	0.00003	58.99	0.059	17.0	70 × 16	Ag	O
	Nl-19	20-05-20	56.057669	9.254785	0.70873	0.00003	88.01	0.088	11.4	40 × 40	Ag	O
	NL-20	20-05-20	56.035484	9.297641	0.71004	0.00003	190.64	0.191	5.2	Ditch	Ag	O
	NL-21	20-05-20	56.031944	9.258563	0.70909	0.00003	137.66	0.138	7.3	30 × 18	Ag	O
	NL-22	20-05-20	56.039013	9.1546575	0.70937	0.00003	35.94	0.036	27.8	40 × 30	Pristine	H-MP
	NL:24	20-05-20	56.073063	9.141906	0.70917	0.00002	58.94	0.059	17.0	40 × 17	Ag	H
	NL-25	20-05-20	56.074506	9.135277	0.71152	0.00002	35.75	0.036	28.0	25 × 20	Pristine	O
	NL-29	14-05-20	56.040435	9.165696	0.71324	0.00002	4.44	0.004	225.3	125 × 50	Pristine	H
	NL-30	14-05-20	56.041700	9.165873	0.71855	0.00002	5.67	0.006	176.3	80 × 35	Pristine	H
	VL-N GW	14-05-20	56.038693	9.170635	0.71629	0.00003	5.19	0.005	192.8	Soil Pit	Pristine	H
S2 SW	TR-1	28-09-19	55.393295	11.264667	0.70976	0.00002	668.8	0.669	1.5	10 × 4	Pristine	
Zealand	TR-3	28-09-19	55.403629	11.288475	0.70987	0.00002	556.7	0.557	1.8	26 × 14	Pristine	
	TR-4	28-09-19	55.389269	11.231064	0.70937	0.00002	1537.1	1.537	0.7	40 × 8	Pristine	
	TR-6	28-09-19	55.488005	11.230908	0.70816	0.00002	5781.6	5.782	0.2	95 × 29	Pristine	
	TR-7	28-09-19	55.421516	11.258694	0.70938	0.00002	869.3	0.869	1.2	27 × 33	Pristine	
	TR-8	28-09-19	55.420978	11.259229	0.70871	0.00002	1287.0	1.287	0.8	25 × 16	Pristine	
	TR-11	28-09-19	55.320527	11.180471	0.71271	0.00002	24.0	0.024	41.6	15 × 15	Pristine	
	KS-1	10-06-20	55.320934	11.178259	0.71140	0.00002	95.2	0.095	10.5	30 × 16	Pristine	
	KS-2	10-06-20	55.306724	11.176287	0.71117	0.00002	66.7	0.067	15.0	45 × 22	Pristine	
	KLA-1	10-06-20	55.304217	11.195018	0.71160	0.00002	220.3	0.220	4.5	37 × 21	Pristine	
	AP-1	10-06-20	55.286459	11.256995	0.71318	0.00002	175.2	0.175	5.7	100 × 1	Pristine	
	STIG-1	10-06-20	55.219445	11.246570	0.71014	0.00002	1041.3	1.04	1.0	35 × 24	Pristine	
	GLA-1	10-06-20	55.202282	11.439634	0.70969	0.00002	591.5	0.592	1.7	90 × 50	Pristine	
	RUDE-1	10-06-20	55.222581	11.487030	0.71232	0.00002	226.0	0.226	4.4	130 × 75	Pristine	
	CHA-1	10-06-20	55.385198	11.414902	0.71011	0.00002	263.8	0.2638	3.8	90 × 45	Pristine	
S3	BRAN-1	13-04-19	55.774467	9.481886	0.70934	0.00003	204.69	0.205	4.9	35 × 35	Pristine	
Jelling	BRAN-2	13-04-19	55.773379	9.478093	0.70937	0.00003	261.13	0.261	3.8	spring	Pristine	
	STAG-2	13-04-19	55.711176	9.167390	0.71254	0.00002	7.11	0.007	140.6	10 × 6	Pristine	

(Continued)

TABLE 1 | Continued

Locality	Sample	Date	Longitude	Lattitude	$^{87}Sr/^{86}Sr$	2 sd	ng Sr/ml	Sr (mg/l)	1/Sr	Size (m)*	Prist/Ag	Hill/Out#
	GOD-1	13-04-19	55.710359	9.288341	0.71360	0.00002	17.85	0.018	56.0	70 × 40	Pristine	
	RIIS-1	13-04-19	55.848059	9.325621	0.71234	0.00002	2.53	0.003	395.2	45 × 13	Pristine	
	RIIS-2	13-04-19	55.847067	9.328636	0.71556	0.00002	14.57	0.015	68.6	4 × 4	Pristine	
	Giv-1	01-06-20	55.845244	9.310155	0.71007	0.00002	50.49	0.050	19.8	60 × 50	Pristine	
	Giv-2	01-06-20	55.840487	9.294729	0.71009	0.00002	2.43	0.002	411.4	90 × 75	Pristine	
	BH-1	01-06-20	55.820398	9.393342	0.71416	0.00002	11.54	0.012	86.7	40 × 7	Pristine	
	SMI-1	01-06-20	55.770755	9.305679	0.71034	0.00002	93.74	0.094	10.7	30 × 25	Pristine	
	BILL-1	27-04-19	55.749575	9.149687	0.71102	0.00002	26.00	0.026	38.5	20 × 7	Pristine	
	AST-1	13-04-19	55.745128	9.220665	0.71143	0.00002	46.35	0.046	21.6	stteam	Pristine	
	ASTV-1	27-04-19	55.750885	9.209216	0.7085	0.00002	115.13	0.115	8.7	95 × 15	Pristine	
	ASTV-2	27-04-19	55.750588	9.213274	0.71341	0.00002	10.79	0.011	92.7	15 × 15	Pristine	
	ASTV-6	11-04-20	55.749394	9.213206	0.71358	0.00002	3.19	0.003	313	18 × 10	Pristine	
	GRE-1	11-04-20	55.759253	9.535392	0.70943	0.00002	95.19	0.095	10.5	stream	Pristine	
	GRE-2	11-04-20	55.754246	9.530884	0.70942	0.00002	179.33	0.179	5.6	stream	Pristine	
	GRE-3	11-04-20	55.751665	9.488106	0.70890	0.00002	270.96	0.271	3.7	30 × 12	Pristine	
	BA-1	11-04-20	55.743355	9.339462	0.71007	0.00002	102.20	0.102	9.8	40 × 20	Pristine	
	JEL-1	13-04-19	55.745023	9.443107	0.71232	0.00002	15.2	0.015	65.8	30 × 10	Pristine	
	JEL-2	13-04-19	55.745136	9.441398	0.71284	0.00002	14.55	0.015	68.7	40 × 28	Pristine	
Vejle	EGS-1	22-07-18	55.619683	9.283325	0.71145	0.00002	9.07	0.009	111.1	spring	Pristine	
River	VVS-1	22-07-18	55.653713	9.315806	0.70949	0.00002	183.46	0.183	5.5	spring	Pristine	
Valley	RS-1	22-07-18	55.676078	9.354599	0.70849	0.00002	305.51	0.306	3.3	spring	Pristine	

For each water sample, we show sample locality, sample number, sampling date, geographic coordinates (Decimal Grade System), $^{87}Sr/^{86}Sr$ ratio, strontium concentration, 1/Sr concentration and size of sampled water body. External reproducibility is determined from repeated analyses of Holocene Okinawa foraminiferal standards.

**Size of water body [length × width (meter)].*

#Hill, Hill island; Out, Outwash plain; MP, Marl Pit.

plain in front of the Main Stationary Line and the Mid Danish Till behind the line date to about 22,000 years (Kjær et al., 2003). The East Jutland Line dates to about 19,000–18,000 years (see Geological Setting). The landscape west of the Main Stationary Line is dominated by flat, sandy, non-calcareous outwash plains. The Mid Danish Till between the Main Stationary Line and the East Jutland Line is rather sandy, and in the upper layers often low- to non-calcareous. This is in contrast to the tills of the East Jutland Advance, which are clayey and calcareous (Kjær et al., 2003). The area is intersected by several late Glacial and Holocene erosional valleys of which the Vejle River Valley and the Grejs Valley are the largest (**Figure 1E**).

RESULTS AND INTERPRETATIONS

In presenting the data, we informally use the terms "high" and "low" $^{87}Sr/^{86}Sr$ values." "High" values are used for signatures above the maximum $^{87}Sr/^{86}Sr$ ratio of 0.711 in the baseline for Denmark of Frei and Frei (2011), while "low" values are used for signatures below 0.711.

Study Area S1. Nørlund Hill Island and Surrounding Outwash Plains

A total of 33 ponds and lakes have been sampled and analyzed from Study Area S1 (**Figure 2** and **Table 1**). Sixteen of these are from the hill island, while seventeen are from the surrounding outwash plains (**Figure 2**). Nine of the samples from the outwash plain are pristine; eight are from farmland. All sixteen samples from the hill island are pristine (**Figure 2** and **Table 1**). The $^{87}Sr/^{86}Sr$ signature in the samples from the hill island varies from 0.70892 to 0.71855, while the concentration varies from 0.002 to 0.151 (**Figures 3**, **4A**). The $^{87}Sr/^{86}Sr$ signatures from the central part of the hill island show relatively low variability ranging from 0.71103 to 0.71271. The lowest $^{87}Sr/^{86}Sr$ signatures (0.70892, 0.70980, and 0.70937) and highest Sr concentrations (0.036–0.151 mg/l), are found in the water from the three abandoned marl pits (**Figures 3**, **4A**). The highest values (0.71324–0.71855) are from a relatively small area, which forms a peninsula on the western side of the hill island (**Figure 3**). The pristine $^{87}Sr/^{86}Sr$ values from the outwash plains vary from 0.71097 to 0.71338. The values from the farmland are distinctly lower, ranging from 0.70829 to 0.71011 (**Figure 4A**).

One surprising discovery from the Nørlund hill island study is the very high maximum $^{87}Sr/^{86}Sr$ values of 0.71629 and 0.71855. The large span between the lowest ratio (0.70829) and highest (0.71855) was also unexpected, particularly as the total area of the hill island is only about 30 km^2. Twelve out of fifteen samples from the hill island exhibit higher $^{87}Sr/^{86}Sr$ values than the maximum value in the isoscape for the whole of Denmark, created by Frei and Frei (2011). As they also exhibit low Sr concentrations (0.002–0.031 mg/l), there can be

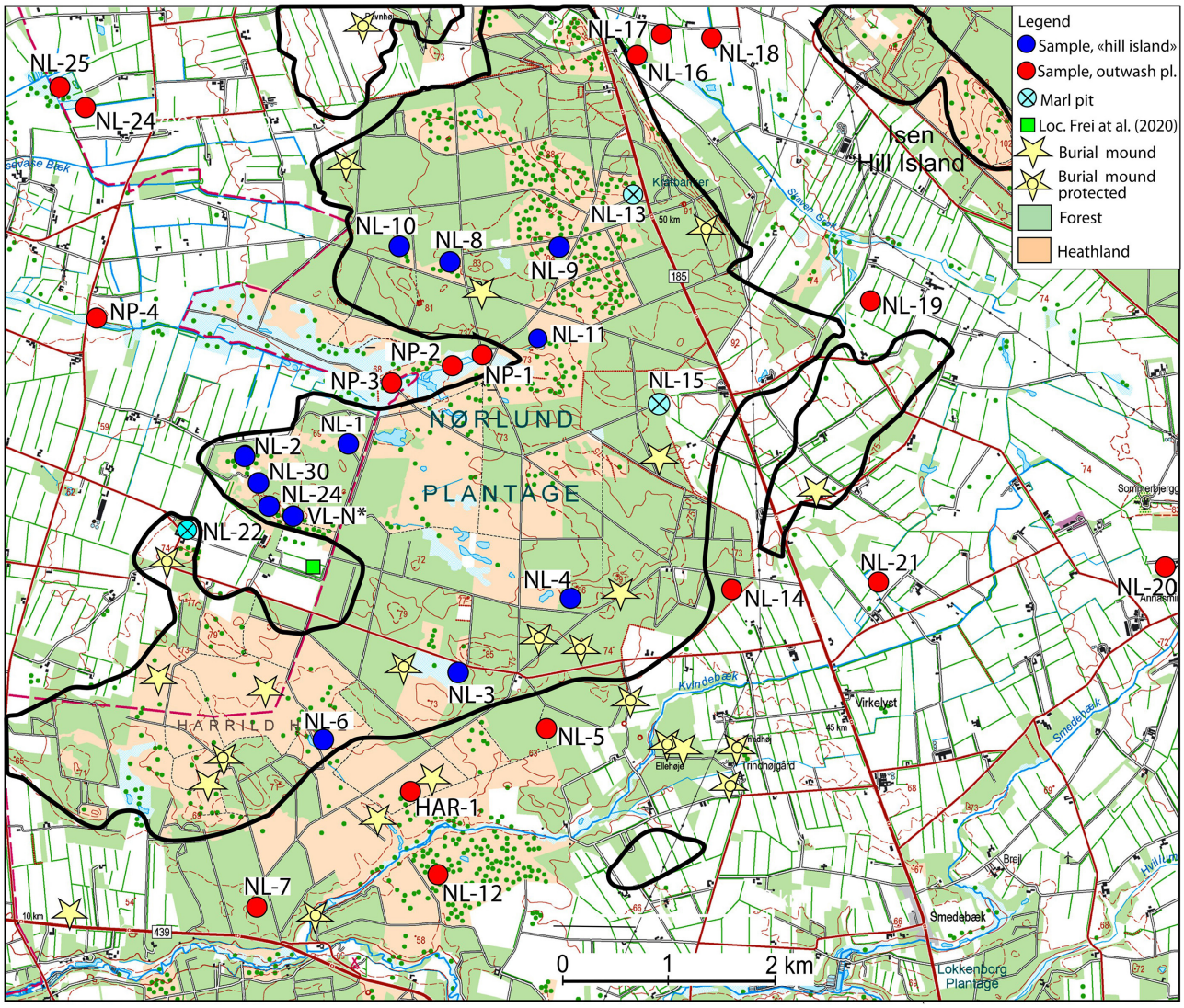

FIGURE 2 | Modern topographical map of study area S1, the Nørlund hill island and surrounding outwash plains. The outline of the "hill island" is transferred from **Figure 3** and indicated with a black line. Sample locations are indicated by colored dots. Sample number and detailed information on location and laboratory data is given in **Table 1**. Yellow stars mark location of preserved prehistoric burial mounds. See **Figure 1A** for location of study area. Location of the site investigated by Frei et al. (2020) is marked by a green square. Map is based on free data from "Styrelsen for Dataforsyning og Effektivisering, topografisk kort, WMS-tjeneste".

no doubt that these samples are from non-calcareous surface waters, and that the surface deposits of most of the hill island are non-calcareous.

The only pristine samples with $^{87}Sr/^{86}Sr$ values within the baseline of Frei and Frei (2011) are from the marl pits (**Figure 4A**). These small pits (diameter 30–<60 m) are surrounded by non-calcareous sandy deposits and appear isolated. The marl has previously been dug for soil improvement by nearby farms, but the pits have been abandoned for many decades. The marl is regarded to be of Saalian age. The Sr concentration in the marl-pit water is relatively high (0.036–0.151 mg/l), in accordance with the high content of calcium carbonate in these deposits (**Figure 3**).

According to historic maps (Høje Målebordsblade, 1842–99), the Nørlund hill island has not been under plow in historic times. The same is true for the outwash plain south of the hill island (**Figure 2**), which despite having a different origin and a different age, exhibits the same $^{87}Sr/^{86}Sr$ values and the same Sr concentrations as the samples from the hill island (**Figure 3**). The situation is different for the outwash plains to the east, north, and west. During the last 150 years, these plains have been increasingly cultivated, and today only small remnants of pristine land remain (**Figure 2**). From the outwash plains, we collected nine water samples from farmland and five from pristine land. The $^{87}Sr/^{86}Sr$ values of the pristine samples resemble the majority of samples from the hill island, with high $^{87}Sr/^{86}Sr$ values and

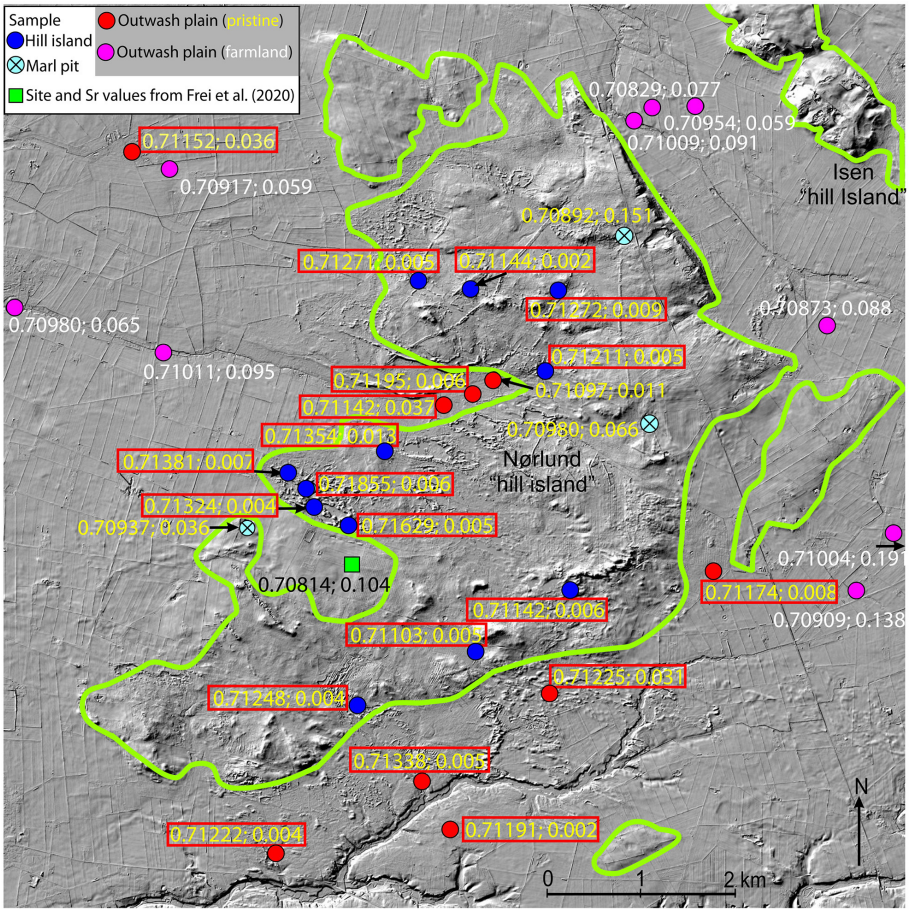

FIGURE 3 | Hillshade map of study area S1, the Nørlund hill island, and surrounding outwash plains. The outline of the "hill island" is indicated by a green line. Sample locations are indicated by colored dots (for color code see legend and **Figure 4**). For numbering of sample stations see **Figure 2**. $^{87}Sr/^{86}Sr$ ratio and strontium concentration are shown for each sample. Sample stations with $^{87}Sr/^{86}Sr$ ratios exceeding the maximum value of 0.711 in the baseline for Denmark (Frei and Frei, 2011) are highlighted with a red box. Location of the site investigated by Frei et al. (2020) is marked by a green square. Map is based on free data from "Styrelsen for Dataforsyning og Effektivisering, skyggekort, WMS-tjeneste".

low Sr concentrations whereas the values from the farmland samples show the opposite pattern and resemble the samples from the three marl pits (**Figures 3**, **4A** and **Table 1**). This indicate that the farmland samples like the marl pit samples are affected by calcium carbonate. The only difference between them is that in the marl accumulations, the calcium carbonate is natural, whereas it is anthropogenically added agricultural lime in the farmland.

The results from the Nørlund hill island underline the main conclusion of Thomsen and Andreasen (2019) that agricultural lime in areas with low- to non-calcareous soils can significantly alter the isotopic composition and concentrations of the strontium in the surface waters (**Figure 4A**).

The highest $^{87}Sr/^{86}Sr$ values (0.71324–0.71855) on the Nørlund hill island are found in a series of shallow lakes and ponds located on the low peninsula on the western side of the hill island (**Figures 2**, **3**). During the spring and summer of the year 2020, we dug a number of small pits a few hundred meters from the lakes and met groundwater at increasing depth of 70–100 cm over time (63.3–63.0 m above sea level). The groundwater table in the excavations coincides with and fluctuates simultaneously with the water level in the lakes, which is consistent with a groundwater source for the lake waters. The $^{86}Sr/^{87}Sr$ ratio of the groundwater from the excavations is high (0.71629) and close to the average signature value of the surrounding lakes. A groundwater control of the lakes on the peninsula is in accordance with several investigations, which have found that the water in many lakes and ponds on the sandy soils of central and western Jutland is dominated by groundwater or is a mixture of groundwater and surface water (Refsgaard et al., 2002). If and to what extent groundwater is infiltrating the ponds and lakes on the low-lying central part of the hill island is uncertain, just as it is uncertain what causes the difference between the relative low signatures values here and the high values on the peninsula.

Study Area S2. Southwest Zealand

Southwest Zealand is densely farmed and has a relatively low percentage of pristine areas (**Figure 5**). In the northern part of

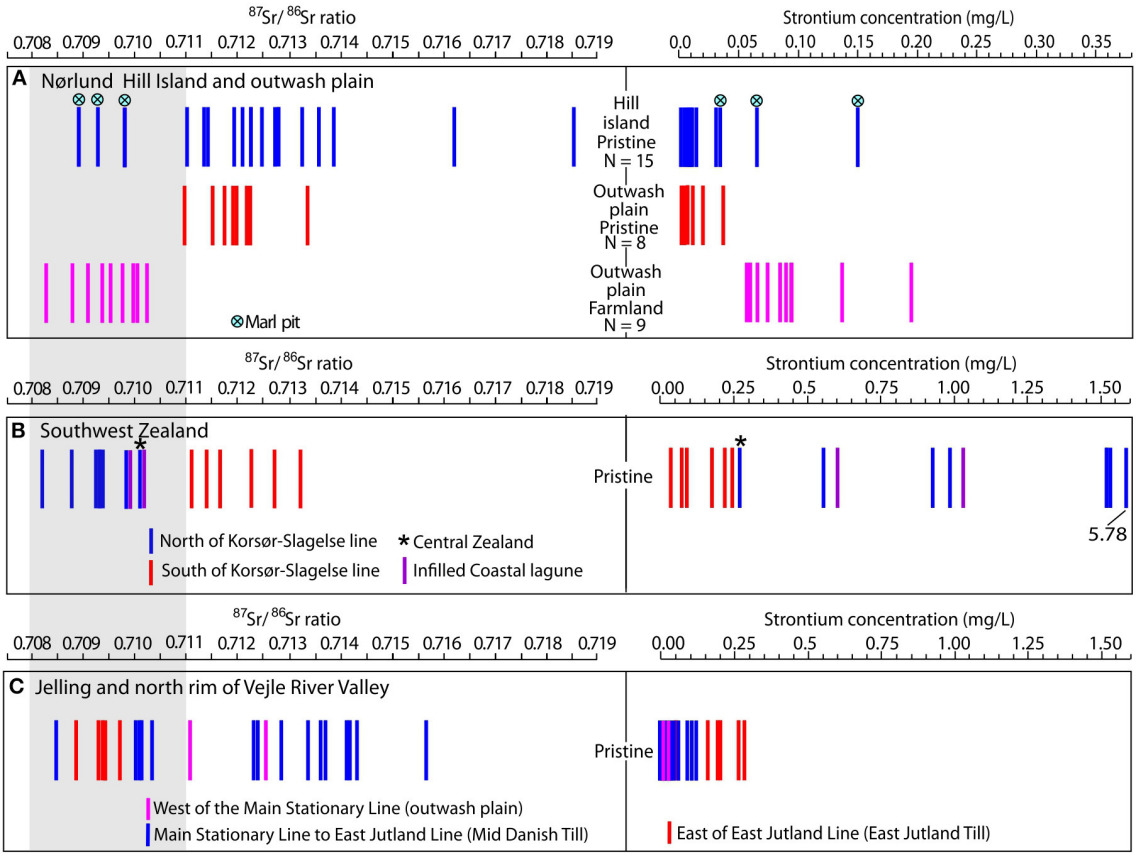

FIGURE 4 | $^{87}Sr/^{86}Sr$ ratios and strontium concentrations for all surface water samples in each of the three study areas: **(A)** S1; Nørlund hill island, **(B)** S2; Southwest Zealand and **(C)** S3; Jelling and Vejle River Valley. Each sample is represented by two vertical bars; one for the $^{87}Sr/^{86}Sr$ ratio and one for the strontium concentration. The samples of study area S1 in **(A)** are subdivided into two main groups: Samples from the hill island and samples from the outwash plain. The samples from the outwash plain are further subdivided into pristine sample and samples from farmland. For study area S2 **(B)** and S3 **(C)** we have analyzed only pristine samples. In study area S2, we distinguish between samples from within the glacial advance at 17,000 years (see **Figure 5**, red and purple arrows) and samples from outside of this advance) (**Figure 5**, blue arrows). In study area S3, we mark the samples according to their geographical location (see **Figure 7**). Gray box to the left marks the $^{87}Sr/^{86}Sr$ isoscape for Denmark of Frei and Frei (2011). *N* = number of samples in each category.

the study area, north of the main road between the cities of Korsør and Slagelse, the samples are from large low-lying bogs (**Figure 5**). In the southern part, the samples are from deciduous forests. All water bodies investigated from southwest Zealand are classified as pristine.

The $^{87}Sr/^{86}Sr$ signature of the bogs north of Korsør ranges from 0.70816 to 0.70938, while Sr concentrations vary from 0.557 to 5.738 (**Figure 5,** blue arrows). The low $^{87}Sr/^{86}Sr$ signature values, the high Sr concentrations and the overall low variability of the data indicate a strong influence of calcium carbonate on strontium, which is in good agreement with the typical high percentages of calcium carbonate in the tills of eastern Zealand (Madsen et al., 1992; Kjær et al., 2003, Smed, 2013). However, the eight samples obtained south of Korsør show a very different pattern. Geographically and isotopically, these samples fall into two groups. The first group consists of the six samples (TR-11, KS-1, KS-2, KLA-1, AP-1 and RUDE-1) taken in the hilly moraine landscape behind the coastline (**Figure 5**, red arrows, **Table 1**). Their $^{87}Sr/^{86}Sr$ values range from 0.71117 to 0.71318, while their Sr concentrations range from 0.024 to 0.226 (**Figure 4B**). The second group consists of the two samples taken in forests growing on infilled low-lying lagoons (elevation ∼1 m) (**Figure 5**, purple arrows). They exhibit relatively low $^{87}Sr/^{86}Sr$ values (STIG-1=0.71014 and GLA-1=0.70969) (**Figure 4B**). The six samples from the moraine landscape show an unusual combination of both high $^{87}Sr/^{86}Sr$ values and relatively high Sr concentrations. Due to the influence of lime in the soil, high $^{87}Sr/^{86}Sr$ values are generally correlated with low Sr concentration and *vice versa*. However, a similar combination occurs on the Danish island of Bornholm (Frei and Frei, 2013), where the content of lime in the soil is low. The high Sr concentrations here are apparently caused by a higher content of radiogenic Sr-rich minerals in the soil. A similar explanation may be suggested for the tills along the western coast of Zealand. The area was affected by one of the last re-advances during the deglaciation (see **Figure 1A**). This advance could have brought material from the central part of the Baltic depression, where Bornholm is located, to the southwest coast of Zealand.

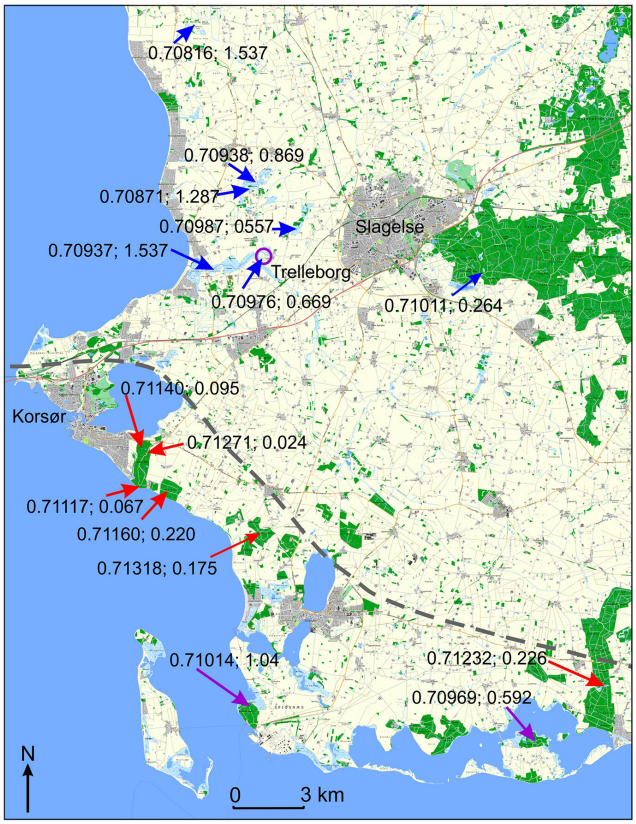

FIGURE 5 | Map of study area S2, southwestern Zealand, showing location of sample stations. $^{87}Sr/^{86}Sr$ ratio and strontium concentration are shown for each sample. Sample number and detailed information on sample location and laboratory data are given in **Table 1**. The dashed line indicates the position of a lateral moraine associated with a glacial advance from the southeast dated to about 17,000 years (Houmark-Nielsen et al., 2005). Samples taken within the tills of the glacial advance are marked with red arrows. Samples taken in low-lying lagoonal deposits are marked with purple arrows. Samples taken outside of the advance are marked with blue arrows. For location of study area and full extent of the glacial advance see **Figure 1A**. Map is based on free data from "Styrelsen for Dataforsyning og Effektivisering, GeoDanmark natur og friluftskort, WMS-tjeneste".

The low $^{87}Sr/^{86}Sr$ values in the two samples from the low-lying coastal areas are consistent with a marine influence as also indicated by unusually high concentrations of Na. In STIG-1, the Na concentration is nearly 30 times the average of the investigated surface water from Zealand; in GLA-1 it is a little lower. High concentrations of Na are a good indicator of an influence by seawater, which has a high concentration of Sr around 8 mg/L and a $^{87}Sr/^{86}Sr$ signature of 0.70917 (Dia et al., 1992).

The number of samples obtained south of Korsør is relatively low due to a scarcity of pristine areas. Nevertheless, the $^{87}Sr/^{86}Sr$ values of the analyzed water bodies are consistently high, indicating that the moraine landscape along the southwest coast of Zealand was dominated by high $^{87}Sr/^{86}Sr$ ratios. How far inland these high values continue has not been investigated, but a sample taken in the forests south of the town of Slagelse, ca. 17 km from the Great Belt show a low $^{87}Sr/^{86}Sr$ signature resembling the values from the northern part of the study area (**Figures 4B**, **5**).

In conclusion, a substantial part of the moraine landscapes along the southwest coast of Zealand carries $^{87}Sr/^{86}Sr$ ratios above the maximum value in the isoscape for Denmark of Frei and Frei (2011) (**Figure 4B**). The archaeological implications of these findings are significant as discussed in the last chapter.

Study Area S3. Jelling and the North Side of the Vejle River Tunnel Valley

A total of 26 samples were analyzed from the Jelling area and the Vejle River Valley (**Figure 6**). Spatially, the samples are distributed irregularly, and they cannot be expected to show the full range of $^{87}Sr/^{86}Sr$ values and Sr concentrations in the area. The limiting factor is primarily the number and distribution of ponds and lakes with pristine surface waters, as the central area around Jelling is densely farmed (**Figure 6**). To supplement the data from this study, we include data from a neighboring area to the south investigated by Thomsen and Andreasen (2019).

The two $^{87}Sr/^{86}Sr$ values from the sandy plains west of the Main Stationary Line (**Figure 7**) (0.71102 and 0.71254) are typical for the outwash plains of Jutland. This is evidenced by a comparison with the results from Study area S1 and with 24 analyses of pristine waters from outwash plains at Egtved southwest of the study area, which show a range from 0.70929 to 0.71495 (**Figure 8**) (Thomsen and Andreasen, 2019).

The central part of the study area is occupied by the Mid Danish Till. This till became exposed shortly after 22,000 years, when the ice-sheet rapidly withdrew from the Main Stationary Line (MSL) (**Figure 1A**). The till is complex and sometimes clayey and calcareous, but is mostly sandy and non-calcareous, especially in the upper few meters, possibly due to leaching (Smed, 1978; Madsen et al., 1992). Low-lying areas are often covered by small local outwash plains developed, as the ice sheet returned to the East Jutland Line about 18,000 years ago.

The $^{87}Sr/^{86}Sr$ values for the eighteen samples from the Mid Danish Till are highly variable, ranging from 0.70850 to 0.71556, with a mean $^{87}Sr/^{86}Sr$ value of 0.71170 (**Figures 4C**, **7**). The geological complexity of the area is reflected in the $^{87}Sr/^{86}Sr$ data, where nearby ponds may have highly different $^{87}Sr/^{86}Sr$ values. This is exemplified in four ponds and lakes near Give, which have values ranging from 0.71007 to 0.71556, though they are located just 1 km apart (**Figures 6**, **7**). The reason for these large differences is likely geological. According to landscape studies by Smed (1978), the ponds showing low values are located on a clayey till, whereas the ponds producing high values are located on a local outwash plain.

Similar contrasts are characteristic for the area around Kulkær Creek, in the western part of the study area (**Figures 6**, **7**). This creek runs in a relatively steep gully cut into a higher-lying glacial landscape during the Holocene. Two ponds from the surrounding hills produce high values of 0.71358 and 0.71341, respectively, as compared to the low values found in ponds and spring near the bottom of the gully (around 0.70850) (**Figure 7**). The distribution of high and low $^{87}Sr/^{86}Sr$ values here may be

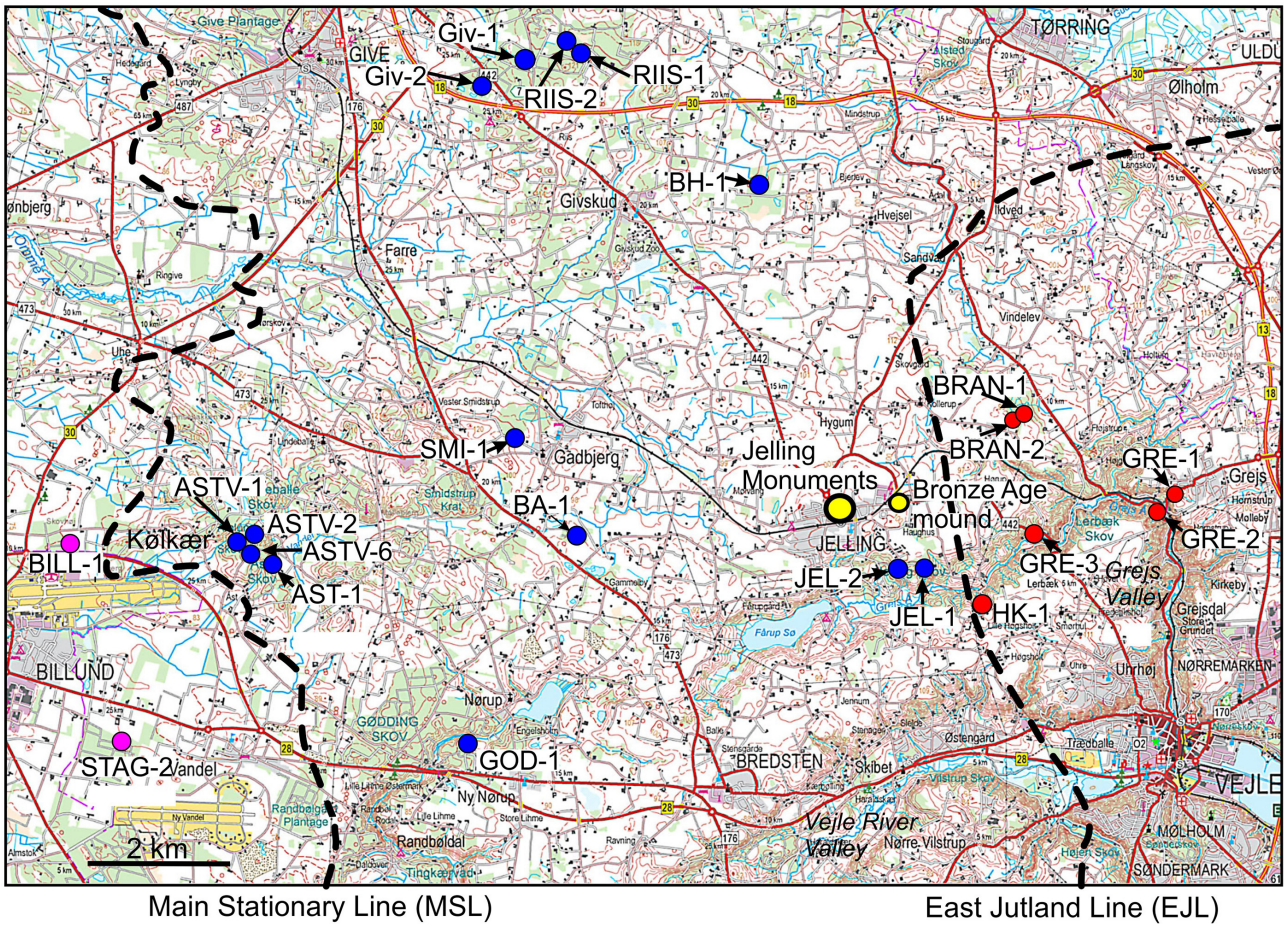

FIGURE 6 | Modern topographical map of study area S3, Jelling. Sample location and sample number are indicated. Detailed information on location of samples and laboratory data are given in **Table 1**. For location of study area see **Figure 1A**. Location of the Jelling Viking Monuments and a recently analyzed Bronze Age burial (Felding et al., 2020) are indicated. Map is based on free data from "Styrelsen for Dataforsyning og Effektivisering, topografisk kort, WMS-tjeneste".

due to leaching that dissolved the calcium carbonate from the top few meters of the soils atop the plateau. Great contrasts are also found in the Jelling area. Ponds from the upland along the edge of the Grejs Valley about 1 km south of the Jelling Monuments show high values (0.71284 and 0.71232). About 1 km east of these two ponds, we enter the calcareous East Jutland Till (**Figures 6**, **7**). We have analyzed samples from six water bodies (streams and ponds) from this till and they all produce low $^{87}Sr/^{86}Sr$ values (0.70890–0.70967) and high concentrations (0.095–0.271) in accordance with the overall high content of calcareous material in this unit (Madsen et al., 1992; Balstrøm et al., 2013). The homogeneity of this till is underlined by the fact that we in the Grejs Valley area find the same values in ponds and springs from the upper rim to the bottom of the valley (**Figure 7**).

In summary, the $^{87}Sr/^{86}Sr$ distribution in the Mid Danish Till is characterized by great variability and contrasts. Water bodies with $^{87}Sr/^{86}Sr$ values ranging from 0.708 to 0.710 can be found just a few hundred meters from water bodies ranging from 0.713 to 0.716 (**Figure 7**). This is in accordance with the geology of The Danish Till, which also is rich in contrasts, both in terms of the calcium carbonate content, but also in the composition of the non-calcareous siliciclastic component, which may vary from coarse-grained sandy gravel to fine grained clays with scattered stones (Smed, 1978; Thomsen and Andreasen, 2019).

DISCUSSION

Sampling Media

Numerous methods have been used to estimate the local bioavailable $^{87}Sr/^{86}Sr$ range comprising both geological and biological materials (Bentley, 2006; Montgomery et al., 2007; Evans et al., 2010, 2018; Maurer et al., 2012). Based on a location in central Germany, Maurer et al. (2012) compared a large number of materials (ground vegetation, tree leaves, rock leachates, water, soil extracts, as well as modern and fossil animals) for best estimation of local bioavailable ratios when dealing with origin and movements of past populations. Of the many proxies investigated by Maurer et al. (2012), water and plant samples appear to provide the most accurate $^{87}Sr/^{86}Sr$ isoscapes. Principally, however, archaeological teeth

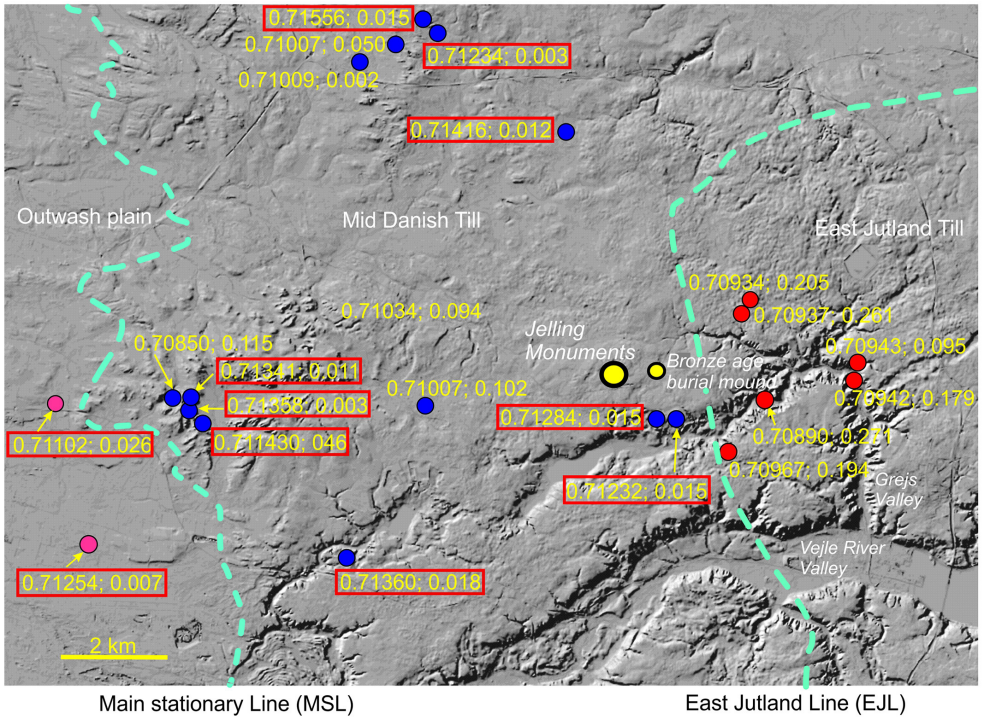

FIGURE 7 | Hillshade map of the study area S3 (Jelling). Location of sample stations is indicated by colored dots. For numbering of sample stations see **Figure 6**. $^{87}Sr/^{86}Sr$ ratio and strontium concentration are shown for each sample. Sample stations with $^{87}Sr/^{86}Sr$ ratios exceeding the maximum value of 0.711 in the baseline for Denmark (Frei and Frei, 2011) are highlighted with a red box. Map is based on free data from "Styrelsen for Dataforsyning og Effektivisering, skyggekort, WMS-tjeneste".

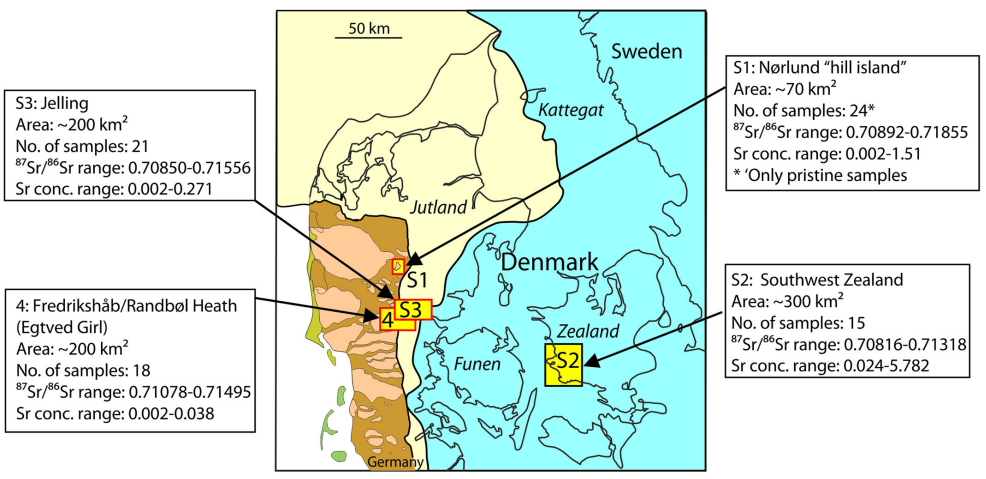

FIGURE 8 | Statistical summary of $^{87}Sr/^{86}Sr$ ratios and strontium concentration for each of the three study areas. Location of study areas is indicated on Quaternary geological map. Site 4 is based on data from Thomsen and Andreasen (2019).

enamel of rodents and selected mammals may provide an even better proxy Kootker et al. (2016). Unfortunately, they are rarely preserved in acidic environments (Kootker et al., 2016), and they are also absent or poorly preserved in acidic soils in central Jutland (Tjelldén et al., 2016), where two of our three study areas are located. Frei and Price (2012) published an isoscape for Denmark based on modern bones picked from owl pellets (mostly from rodents) mixed with a few archeological animal remains. The $^{87}Sr/^{86}Sr$ values show a narrow range (0.709–0.7108) and a homogeneous distribution pattern very similar to the isoscape of Frei and Frei (2011). The similarity of the two isoscapes suggests that strontium

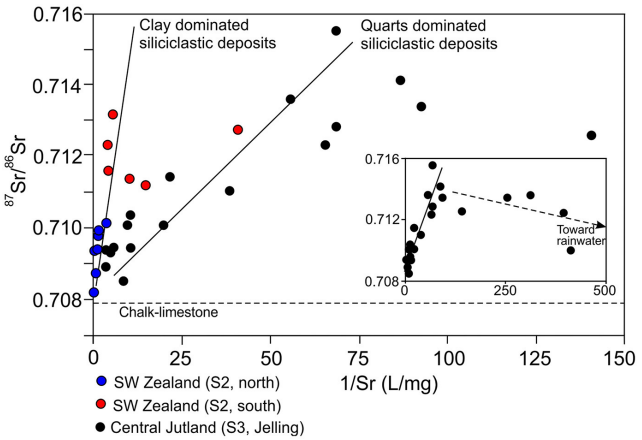

FIGURE 9 | Strontium isotope ratio vs. inverse strontium concentration for pristine samples from SW Zealand (study area S2, blue and red dots) and central Jutland (study area S3, black dots). Samples from SW Zealand define a mixing line with steep slope (high Sr concentration) between a calcareous end-member dominant in the northern samples and a siliciclastic end-member dominant in the southern samples. Samples from central Jutland define a mixing line with a shallower slope (lower Sr concentration) indicating different compositions of the siliciclastic end-members in the two study areas. A few samples, particularly in Jutland (insert), fall off the mixing line and trend toward dilution with rainwater [$^{87}Sr/^{86}Sr = 0.7092$ and $1/Sr = 1{,}000$–$10{,}000$ (Frei and Frei, 2011; Thomsen and Andreasen, 2019)].

derived from modern animals may also be affected by agricultural liming.

In the present study, we prefer water for two reasons. Firstly, it allows us to directly compare our $^{87}Sr/^{86}Sr$ values with existing values. Secondly, water permits us to obtain Sr concentration data to use in modeling, which is difficult in plants, where the concentration may vary within a single plant and also between species (Poszwa et al., 2004). Strontium concentration data are often essential in order to understand the geological background for the spatial variations in $^{87}Sr/^{86}Sr$ values. This is exemplified in **Figure 9**, where we plot strontium concentration vs. $^{87}Sr/^{86}Sr$ ratios in water samples from Zealand (Study area S2) and Jutland (Study area S3), respectively. The plot indicates that the strontium in the two areas have a chalk/limestone source in common whereas the siliciclastic sources are different (see Results and interpretation, Study area S2).

Agricultural Lime Affects Natural $^{87}Sr/^{86}Sr$ Ratios

The reliability of the $^{87}Sr/^{86}Sr$ method to discriminate between prehistoric local and non-local individuals depends very much on the accuracy of the isoscapes used in the interpretation (Price et al., 2002; Frei and Frei, 2011; Maurer et al., 2012). These maps are intended to reflect the distribution of $^{87}Sr/^{86}Sr$ ratios in the past, but most are based on modern proxies such as surface waters and plants, which may be subjected to contamination by modern-day humans. Frei and Frei (2011) published a baseline for Denmark promoting a rather homogeneous $^{87}Sr/^{86}Sr$ range of 0.708–0.711, excepting the island of Bornholm. This range has since been adopted as a reference in numerous studies of prehistoric human mobility in Denmark (see below). However, the range of the baseline of Frei and Frei (2011) was extended when Thomsen and Andreasen (2019) obtained ratios of up to 0.71495 within areas of central and western Jutland. Moreover, Thomsen and Andreasen (2019) demonstrated that the main reason for the homogeneous baseline of Frei and Frei (2011) is that most of their samples were obtained from lakes and streams that were affected by additions of agricultural lime.

Frei et al. (2020) argued against Thomsen and Andreasen (2019), suggesting that strontium derived from agricultural lime is permanently retained in the organic-rich topsoil and therefore have no effect on the strontium content in the pore- and groundwater below or in groundwater-supported surface water. This conclusion is based on a single borehole bored in 2014 and located on the outwash plain immediately west of the Nørlund hill island (see **Figures 1**, **2**). The site is regularly treated with agricultural lime and according to Frei et al. (2020), the content of strontium in the topsoil corresponds to about 50 years of normal liming (= 500 kg/ha/year). Frei et al. (2020) consider the site as representative for farm fields on the outwash plains of western Jutland. However, the groundwater (groundwater level 61.5 m above sea level) at the site is actually rich in strontium with a clear carbonate affinity ($^{87}Sr/^{86}Sr$ ratio = 0.708135, Sr concentration = 0.104 ppm). According to Frei et al. (2020), the source of the strontium in the groundwater is not agricultural lime, but fragments of undissolved natural carbonate "relicts." These should be present almost everywhere in the subsurface Quaternary deposits of western Jutland (Frei et al., 2020). The groundwater and groundwater-supported water bodies investigated by us, several of which are located only a few hundred meters from the site of Frei et al. (2020), should therefore also exhibit low strontium signatures and high concentrations. However, values comparable to those of Frei et al. (2020) were only found in water bodies in close contact with farmland and affected by agricultural lime plus at the three small, localized natural occurrences of marl (**Figures 2**, **3**). All our samples from areas unaffected by agricultural lime show high $^{87}Sr/^{86}Sr$ values (up to 0.71855) and low Sr concentrations (down to 0.002 mg/l), indicative of absence of an input from lime (**Figure 3**). Thus, it seems unlikely that the source of the low $^{87}Sr/^{86}Sr$ ratios in the pore- and groundwater at the site of Frei et al. (2020) are subsurface carbonate relicts. The most plausible strontium source is agricultural lime. It is here important to convey that the investigated site in 2014 was not an ordinary farm field, as indicated by the authors, but a test field to investigate CO_2 storage in soil (Jessen et al., 2014a,b). In the course of testing, no <48 t/ha of agricultural lime was spread across the test site in 2012–2013, before the samples used in Frei et al. (2020) were collected in 2014. We suggest that this lime, which incidentally corresponds to ∼96 years of standard liming, is the main source for the high strontium content in the topsoil and in the pore- and groundwater at the site of Frei et al. (2020). This conclusion is in agreement with new studies, which indicate that strontium is not retained in the topsoil of the outwash plains of western Jutland, but rapidly transported into the pore and groundwater below (Andreasen and Thomsen, this volume).

Agricultural Lime Outside of Denmark

Agricultural lime is applied to farmland to reduce acidity in the soil and improve growth conditions for plants (Goulding, 2016). Agricultural lime is essential in non- to low-calcareous regions. It is also used in regions with calcareous soil to counteract the effect of leaching. Soils comparable to the Danish deposits described here occur widespread on most continents. In Europe, they are especially common along the rim of the Weichselian and Saalian ice sheets from Ukraine in the east to Ireland in the west (Böse et al., 2012; Ballabio et al., 2016; Price et al., 2017). In Europe and North America, the application of lime generally varies from 200 to 1,000 kg/ha/year (Adams, 1984; Goulding, 2016). These levels are comparable to the rates of agricultural liming in Jutland, suggesting that the use of lime in these countries would have a similar effect on the strontium content in the environment.

That agricultural lime can have a significant effect on even large river systems is exemplified in a study from the Ohio River system, eastern USA (Oh and Raymond, 2006). In two of the most intensively farmed watersheds from this system (∼85% farmland), 29% of the riverine bicarbonate export in the years 1971–1987 could be attributed to agricultural lime. Furthermore, 30% of the observed difference in bicarbonate export between an agricultural and a forested watershed could be directly related to liming. Average yearly supply of lime in the investigated area is estimated to have been about 200–280 kg/ha (Oh and Raymond, 2006).

Archaeological Implications

Together, the three study areas analyzed in this paper plus the similarly sized area analyzed in Thomsen and Andreasen (2019) make up <1.8% of Denmark (**Figure 8**). This is clearly insufficient for proposing a new isoscape for Denmark. However, the data give $^{87}Sr/^{86}Sr$ ranges for three areas from the central part Jutland and one from western Zealand that cautiously may be used in prehistoric provenance studies from these regions. Here we are only concerned with the maximum isotopic values; the minimum value in Denmark will nearly always be close the value of chalk (0.7078) and it is rarely critical for Danish interpretations. The maximum $^{87}Sr/^{86}Sr$ values in surface water from the three study areas from Jutland are 0.71629 and 0.71855 for Study area S1, 0.71556 for Study area S2, and 0.71495 for the Egtved area (area 4 in **Figure 8**). Based on these values, we tentatively suggest that archaeological objects from the central part of Jutland with $^{87}Sr/^{86}Sr$ values up to 0.716 (or 0.715 for a more conservative estimate) most likely are of local origin. For SW Zealand, we propose a value 0.71318 corresponding to the maximum value found so far in Study area S2.

Accepting that $^{87}Sr/^{86}Sr$ values up to 0.716 (or more conservative 0.715) are obtainable in central Jutland and that values up 0.71328 are obtainable in western Zealand, it appears that many provenance and migration interpretations of prehistoric artifacts and individuals from Denmark warrant revision (e.g., Frei et al., 2017b, 2019; Nielsen et al., 2020; Van der Sluis et al., 2020). Below we will comment in more detail on four investigations, which are within the realm of our study areas.

Egtved and Skrydstrup Females

The iconic Bronze Age females from Egtved and Skrydstrup were re-interpreted in 2019 on the basis of new $^{87}Sr/^{86}Sr$ data from the vicinity of the burial mounds (Thomsen and Andreasen, 2019). Frei et al. (2015) and Frei et al. (2017b) obtained $^{87}Sr/^{86}Sr$ ranges for the Egtved Girl of 0.71028–0.71255 and for the Skrydstrup Woman of 0.7086–0.7138, based on samples from hair, nail and teeth. Frei et al. (2015) and (Frei et al., 2017b) compared these $^{87}Sr/^{86}Sr$ values to the isoscapes of Frei and Frei (2011) (max $^{87}Sr/^{86}Sr$ - 0.708–711) and concluded that both females were born and raised outside of Denmark, probably in central Europe, and that they first came to Denmark as teenagers. In 2019, Thomsen and Andreasen found high values in several pristine water bodies in the vicinity of the two burial sites indicating that the high values measured in their remains could have been obtained locally, thus challenging the interpretation that they originated from elsewhere.

Jelling Male

Felding et al. (2020) analyzed the $^{87}Sr/^{86}Sr$ ratios in six teeth from two Bronze age males buried in eastern Jutland, Denmark. The $^{87}Sr/^{86}Sr$ values of the three teeth from the eastern-most skeleton were all within the baseline range of Frei and Frei (2011) and the individual was determined to be of local origin. The inhabitant of the western-most grave (VKH 3418) near Jelling, (see Study area S3 in **Figures 1**, **6**, **7**) was determined to be different, as two of the three molars yielded values (0.71151 and 0.71128) above the isoscape of Frei and Frei (2011), indicating that this male may be of non-local origin and may have moved from a place outside present-day Denmark to the region of Jelling during his youth (Felding et al., 2020). However, these ratios are well below the values we have obtained from pristine waters in the Jelling area, which have $^{87}Sr/^{86}Sr$ ratios up to 0.71556 (**Figures 6**, **7**). In fact, we have measured $^{87}Sr/^{86}Sr$ ratios of 0.71232 and 0.71284 in two ponds located <1 km from the investigated grave (**Figure 7**). The $^{87}Sr/^{86}Sr$ ratios obtained in the remains of the Jelling male could therefore have been obtained locally, challenging the interpretation that he originated elsewhere outside of present-day Denmark.

Origin of Bronze Age Wool Textiles

The results of a strontium isotope analysis of 42 pieces of wool textiles from the Danish Bronze Age suggests that at least 75% of the tested textiles were produced outside of present-day Denmark (Frei et al., 2017a) when compared to the isoscape of Frei and Frei (2011). In the present study, we propose a maximum $^{87}Sr/^{86}Sr$ value for central Jutland of 0.716 (or more conservative 0.715). Applying these figures, we calculated that only about 12% (or 21% using 0.715) of the wool textiles are of non-local origin.

Trelleborg Graveyard

Finally, we propose a re-interpretation of the Viking Age individuals buried at the Trelleborg fortress (**Figure 5**) located in western Zealand within Study Area S2. Price et al. (2011) analyzed remains of 48 individuals from a graveyard near the fortress for their $^{87}Sr/^{86}Sr$ compositions. Based on a maximum isoscape value for Denmark of 0.7108 (Price et al., 2011), the

conclusion of the study was that just 16 out of 48 individuals were of local origin, while 32 individuals came from afar, possibly Norway and Poland. However, as all sites from coastal southwest Zealand investigated in this study show values above the maximum value of Price et al. (2011) with 0.71318 as the highest, it appears that all but four individuals could well be of local, southwest Zealandic origin. Of the remaining four, a young female with a $^{87}Sr/^{86}Sr$ value of 0.71542 and buried with a silver chest (Price et al., 2011) may possibly be from the Jelling region, as we have a $^{87}Sr/^{86}Sr$ value of 0.71556 just 10 km north of the Jelling Monuments (**Figure 7**). During this period, Jelling served as the royal seat for King Harold Bluetooth, and a connection between Jelling and the prominent contemporaneous fortress at Trelleborg is to be expected.

CONCLUDING REMARKS

Our expanded study of the high local variability seen in some of the most characteristic glaciogenic environments in Denmark confirms the central conclusions of Thomsen and Andreasen (2019) that isoscapes of $^{87}Sr/^{86}Sr$ ratios based on surface waters should be constructed exclusively from data from pristine areas. This implies that all data from water that are or have been exposed to agricultural lime should be avoided, especially in areas having low- to non-calcareous soils. Streams should be avoided once they have been in contact with farmland. Yet, even though the distinction between pristine and farmland samples may be of less significance in areas with highly calcareous soils, it is still advisable in such areas to collect pristine samples. This is exemplified by the high $^{87}Sr/^{86}Sr$ values observed along the southwest coast of Zealand (Study Area S2) where the tills are classified as calcareous (Madsen et al., 1992). Had we used an approach in which sampling was concentrated on major lakes and streams, we would probably have missed these high values, with significant consequences for the interpretation of the Viking Age individuals buried at Trelleborg. For this reason, a lower number of pristine samples should always take precedence over a higher number of randomly collected samples, in spite of the fact that a high sampling density normally would increase the accuracy of the resulting isoscape.

In Denmark, agricultural lime generally lowers the natural $^{87}Sr/^{86}Sr$ values of streams in water bodies in contact with farmland. The range of $^{87}Sr/^{86}Sr$ isoscapes becomes narrower with lower maximum values. Interpretation of prehistoric migration based on modern surface waters affected by agricultural lime therefore tends to overestimate the number of migrants in a given area. In areas, where the natural $^{87}Sr/^{86}Sr$ ratio mostly is below that of the applied agricultural lime, the situation may be reverse.

DATA AVAILABILITY STATEMENT

The original contributions presented in the study are included in the article, further inquiries can be directed to the corresponding author/s.

AUTHOR CONTRIBUTIONS

The study was devised by ET and RA. Sampling was planned and carried out by ET and TR. Sample processing and analyses as well as the initial geochemical interpretation was done by RA. ET planned and wrote the first draft of the manuscript and was responsible for the overall interpretation, continuously assisted by RA and TR. All authors contributed to the final version of the manuscript and approved the submitted version.

ACKNOWLEDGMENTS

We are grateful to C. Heilmann-Clausen, S. B. Andersen, C. Kronborg, A. Clemmensen, J. Thomsen, and S. Thomsen for enthusiastic assistance during fieldwork. We are grateful to L. Rasmussen, and forester H. Jensen, and several farmers and landowners from the three study areas, in particular J. Mølby and H. Pedersen for support and advice. We are grateful to E. J. Rosenberg, who improved the manuscript. Part of the research was supported by the Research Council of Norway through its Centers of Excellence funding scheme, grant number 223259 and Aarhus University Research Foundation (AUFF) NOVA grant E-2019-9-27.

REFERENCES

Adams, F. (ed.) (1984). *Soil Acidity and Liming, 2nd Edn, Agronomy 12*. American Society of Agronomy/Crop Science Society of America/Soil Science Society of America, Madison, Wisconsin.

Andreasen, R., and Thomsen, E. (2021). Strontium is released rapidly from agricultural lime implications for provenance and migration studies. *Front. Ecol. Evolut.* 8:588422.

Ballabio, C., Panagos, P., and Monatanarella, L. (2016). Mapping topsoil physical properties at European scale using the LUCAS database. *Geoderma* 26, 110–123. doi: 10.1016/j.geoderma.2015.07.006

Balstrøm, T., Breuning-Madsen, H., Krüger, J., Jensen, N. H., and Greve, M. H. (2013). A statistically based mapping of the influence of geology and land use on soil pH. A case study from Denmark. *Geoderma* 192, 453–462. doi: 10.1016/j.geoderma.2012.08.024

Bataille, C. P., and Bowen, G. J. (2012). Mapping $^{87}Sr/^{86}Sr$ variations in bedrock and water for large scale provenance studies. *Chem. Geol.* 304–305, 39–52. doi: 10.1016/j.chemgeo.2012.01.028

Bataille, C. P., Crowley, B. E., Wooller, M. J., and Bowen, G. J. (2020). Advances in global bioavailable strontium isoscapes. *Palaeogeogr. Palaeoclimatol. Palaeoecol.* 555:109849. doi: 10.1016/j.palaeo.2020.109849

Bataille, C. P., von Holstein, I. C. C., Laffoon, J. E., Willmes, M., Liu, X. -M., and Davies, G. R. (2018). A bioavailable strontium isoscape for Western Europe: a machine learning approach. *PLoS ONE* 13:e019738. doi: 10.1371/journal.pone.0197386

Bentley, R. A. (2006). Strontium isotopes from the earth to the archaeological skeleton: a review. *J. Archaeol. Meth. Theor.* 13, 135–187. doi: 10.1007/s10816-006-9009-x

Blank, M., Sjögren, K. -G., Knipper, C., Frei, K. M., and Storå, J. (2018). Isotope values of the bioavailable strontium in inland southwestern

Sweden - A baseline for mobility studies. *PLoS ONE* 13:e0204649. doi: 10.1371/journal.pone.0204649

Böse, M., Lüthgens, C., Lee, J. R., and Rose, J. (2012). Quaternary glaciations of northern Europe. *Quat. Sci. Rev.* 44, 1–25. doi: 10.1016/j.quascirev.2012.04.017

Capo, R. C., Stewart, B. W., and Chadwick, O. A. (1998). Strontium isotopes as tracers of ecosystem processes: theory and methods. *Geoderma* 82, 197–225. doi: 10.1016/S0016-7061(97)00102-X

Dia, A. N., Cohen, A. S., O'Nions, R. K., and Shackleton, N. J. (1992). Seawater Sr isotope variation over the past 300 kyr and influence of global climate cycles. *Nature* 356, 786–788. doi: 10.1038/356786a0

Ericson, J. E. (1985). Strontium isotope characterisation in the study of prehistoric human ecology. *J. Hum. Evol.* 14, 503–504. doi: 10.1016/S0047-2484(85)80029-4

Evans, J. A., Chenery, C. A., Mee, K., Cartwright, C. E., Lee, K. A., Marchant, A. P., et al. (2018). *Biosphere Isotope Domains GB (V1): Interactive Website*. British Geological Survey. (Interactive Resource).

Evans, J. A., Montgomery, J., Wildman, G., and Bouton, G. (2010). Spatial variations in biosphere $^{87}Sr/^{86}Sr$ in Britain. *J. Geol. Soc.* 167, 1–4. doi: 10.1144/0016-76492009-090

Felding, L., Reiter, S. S., Frei, K. M., and Vandkilde, H. (2020). Male social roles and mobility in the early nordic bronze age. A Perspective from SE Jutland. *Danish J. Archaeol.* 9, 1–167. doi: 10.7146/dja.v9i0.117955

Frei, K. M., Bergerbrant, S., Sjögren, K. -G., Jørkov, M. L., and Lynnerup, N., Harvig, L. et al. (2019). Mapping human mobility during the third and second millennia BC in present-day Denmark. *PLoS ONE* 14:e0219850. doi: 10.1371/journal.pone.0219850

Frei, K. M., and Frei, R. (2011). The geographic distribution of strontium isotopes in Danish surface waters base for provenance studies in archaeology, hydrology and agriculture. *Appl. Geochem.* 26, 326–340. doi: 10.1016/j.apgeochem.2010.12.006

Frei, K. M., Mannering, U., Kristiansen, K., Allentoft, M. E., Wilson, A. S., Skals, I. S., et al. (2015). Tracing the dynamic life story of a Bronze Age Female. *Sci. Rep.* 5:10431. doi: 10.1038/srep10431

Frei, K. M., Mannering, U., Van den Berghe, I., and Kristiansen, K. (2017a). Bronze age wool: provenance and dye investigations of Danish textiles. *Antiquity* 91, 640–654. doi: 10.15184/aqy.2017.64

Frei, K. M., and Price, T. D. (2012). Strontium isotopes and human mobility in prehistoric Denmark. *Archaeol. Anthropol Sci.* 4, 103–114. doi: 10.1007/s12520-011-0087-7

Frei, K. M., Villa, C., Jørkov, M. L., Allentoft, M. E., Kaul, F., Ethelberg, P., et al. (2017b). A matter of months: High precision migration chronology of a Bronze Age female. *PLoS ONE* 12:e0178834. doi: 10.1371/journal.pone.0178834

Frei, R., and Frei, K. M. (2013). The geographic distribution of Sr isotopes from surface waters and soil extracts over the island of Bornholm (Denmark) – a base for provenance studies in archaeology and agriculture. *Appl. Geochem* 38, 147–160. doi: 10.1016/j.apgeochem.2013.09.007

Frei, R., Frei, K. M., and Jessen, S. (2020). Shallow retardation of the strontium isotope signal of agricultural liming – implications for isoscapes used in provenance studies. *Sci. Total Environ.* 706:135710. doi: 10.1016/j.scitotenv.2019.135710

Goulding, K. W. T. (2016). Soil acidification and the importance of liming agricultural soils with particular reference to the United Kingdom, *Soil Use Manag.* 32, 390–399. doi: 10.1111/sum.12270

Grimstead, D., Nugent, S., and Whipple, J. (2017). Why a standardization of strontium isotope baseline environmental data is needed and recommendations for methodology. *Advan. Archaeol. Practice* 5, 184–195. doi: 10.1017/aap.2017.6

Guede, I., Ortega, L. A., Cruz Zuluaga, M., Alonso-Olazabal, A., Murelaga, X., Pina, M., et al. (2017). Isotope analyses to explore diet and mobility in a medieval Muslim population at Tauste (NE Spain). *PLoS ONE* 12:e0176572. doi: 10.1371/journal.pone.0176572

Håkansson, E., and Pedersen, S. A. S (1992). *Geologisk kort over den Danske* Undergrund, Varv.

Høje Målebordsblade (1842–1899). Available online at: http://miljoegis.mim.dk/spatialmap

Hoogewerff, J. A., Reimann, C., Ueckermann, H., Frei, R., Frei, K. M., van Aswegen, T., et al. (2019). Bioavailable $^{87}Sr/^{86}Sr$ in European soils: a baseline for provenancing studies. *Sci. Total Environ.* 672, 1033–1044. doi: 10.1016/j.scitotenv.2019.03.387

Houmark-Nielsen, M. (1987). Pleistocene stratigraphy and glacial history of the central part of Denmark. *Bull. Geol. Soc. Denmark* 36, 1–189.

Houmark-Nielsen, M. (2003). Signature and timing of the Kattegat Ice Stream: onset of the LGM-sequence in the southwestern part of the Scandinavian Ice Sheet. *Boreas* 32, 227–241. doi: 10.1111/j.1502-3885.2003.tb01439.x

Houmark-Nielsen, M., Krüger, J., and Kjær, K. H. (2005). De seneste 150.000 år i Danmark. *Geoviden* 2, 1–19. Available online at: https://www.geocenter.dk/wp-content/uploads/2018/07/Geoviden_2_2005.pdf

Jessen, S., Jakobsen, R., Postma, D., Looms, M., and Larsen, F. (2014a). *Carbon Transfer Across the Vadose Zone: Inhibition by 20th Century Acid Rain?* Available online at: https://co2gs.geus.net/xpdf/WP5-Carbon_transfer_across_the_vadose_zone.pdf

Jessen, S., Postma, D., Jakobsen, R., Looms, M. C., and Larsen, F. (2014b). Inhibition of carbon transfer across the vadose zone by 20th century rain. *Geophys. Res. Abstracts* 16:EGU2014-6340.

Kjær, K. H., Houmark-Nielsen, M., and Richardt, N. (2003). Ice-flow patterns and dispersal of erratics at the southwestern margin of the last Scandinavian ice sheet: imprint after palaeo-ice streams. *Boreas* 32, 130–148. doi: 10.1111/j.1502-3885.2003.tb01434.x

Knipper, C., Mittnik, A., Massy, K., Kociumaka, C., Kucukkalipci, I., Maus, M., et al. (2017). Female exogamy and gene pool diversification at the transition from the Final Neolithic to the Early Bronze Age in central Europe. *PNAS* 114, 10083–10088. doi: 10.1073/pnas.1706355114

Kootker, L. M., Van Lanen, R. J., Kars, H., and Davies, G. R. (2016). Strontium isoscapes in the Netherlands. Spatial variations in $^{87}Sr/^{86}Sr$ as a proxy for paleomobility. *J. Archaeol. Sci. Rep.* 6:15. doi: 10.1016/j.jasrep.2016.01.015

Krüger, J. (1983). "Glacial morphology and deposits in Denmark," in *Glacial Deposits in North-west Europe*, eds J. Ehlers and A. A. Balkema (Rotterdam), 181–191.

Larsen,. G., and Kronborg, C. (1994). Geologisk set. *Det mellemste Jylland. Miljøministeriet, Skov og Naturstyrelsen og Geografforlaget*, 1–272.

Madgwick, R., Lamb, A. L., Sloane, H., Nederbragt, A. J., Albarella, U., Pearson, M. P., et al. (2019). Multi-isotope analysis reveals that feasts in the Stonehenge environs and across Wessex drew people and animals from throughout Britain. *Sci. Adv.* 5:eaau6078. doi: 10.1126/sciadv.aau6078

Madsen, H. B., Nørr, A. H., and Holst, K., Aa. (1992). *Atlas over Danmark, S.1, B.3*, Copenhagen: C. A. Reitzel Publisher.

Maurer, A. -F., Galer, S. J. G., Knipper, C., Beierlein, L., and Nunn, E. V., Peters, D. et al. (2012). Bioavailable $^{87}Sr/^{86}Sr$ in different environmental samples. Effects of anthropogenic contamination and implications for isoscapes in past migration studies. *Sci. Total Environ.* 233, 216–229. doi: 10.1016/j.scitotenv.2012.06.046

Milthers, V. (1931). Israndens Tilbagerykning fra Østjylland til Sjælland-Fyn, belyst ved Ledeblokke. *Medd. Dansk Geol. Foren.* 8, 1–70.

Montgomery, J. (2010). Passports from the past: investigating human dispersals using strontium isotope analysis of tooth enamel. *Ann. Hum. Biol.* 37, 325–346. doi: 10.3109/03014461003649297

Montgomery, J., Evans, J. A., and Cooper, R. E. (2007). Resolving archaeological populations with Sr-isotope mixing models. *Appl. Geochem.* 22, 1502–1514. doi: 10.1016/j.apgeochem.2007.02.009

Nielsen, B. H., Christensen, T. E., Moltsen, C., Frei, A. K., Reiter,. S., Mortensen, M. F., et al. (2020). Late Neolithic Stenildgård grave: Re-excavated re-analysed and re-interpreted. *Acta Archaeologica* 9, 121–145. doi: 10.1111/j.1600-0390.2020.12224.x

Oh, N. H., and Raymond,. P. A. (2006). Contribution of agricultural liming to riverine bicarbonate export and CO2 sequestration in the Ohio River basin. *Global Biogeochem. Cycles* 20: GB3012. doi: 10.1029/2005GB002565

Poszwa, A., Ferry, B., Dambrine, E., Pollier, B., Wickman, T., Loubet, M., et al. (2004). Variations of bioavailable Sr concentration and $^{87}Sr/^{86}Sr$ ratio in boreal forest ecosystems. Role of biocycling, mineral weathering and depth of root uptake. *Biogeochemistry* 67, 1–20. doi: 10.1023/B:BIOG.0000015162.12857.3e

Price, T. D., Burton, J. H., and Bentley, R. A. (2002). The characterization of biologically available strontium isotope ratios for the study of prehistoric migration. *Archaeometry* 44, 117–135. doi: 10.1111/1475-4754.00047

Price, T. D., Frei, K., M., Dobat, A. S., Lynnerup, N., and Bennike, P. (2011). Who was in Harold Bluetooth's army? Stronium isotope investigation of the cemetary

at the Viking Age fortress at Trelleborg, Denmark. *Antiquity* 85, 476–489. doi: 10.1017/S0003598X00067880

Price, T. D., Meiggs, D., Weber, M. -J., and Pike-Tay, A. (2017). The migration of Late Pleistocene reindeer: Isotopic evidence from northern Europe. *Archaeol. Anthropol. Sci.* 9, 371–394. doi: 10.1007/s12520-015-0290-z

Price, T. D., Nielsen, J. N., Frei, K. M., and Lynnerup, N. (2012). Sebbersund: isotopes and mobility in an 11^{th}-12^{th} c. AD Danish churchyard. *J. Archaeological Sci.* 39, 3714–3720. doi: 10.1016/j.jas.2012.06.015

Refsgaard, J. C., Henriksen, H. J., Nilsson, B., Rasmussen, P., Kronvang, B., Skriver, J., et al. (2002). Vidensstatus for sammenhængen mellem tilstanden i grundvand og overfladevand. *Arbejdsrapport fra Miljøstyrelsen* 21, 1–110. Available online at: https://www2.mst.dk/udgiv/publikationer/2002/87-7972-157-5/pdf/87-7972-158-3.pdf

Slovak, N. M., and Paytan, A. (2011). "Applications of Sr isotopes in archaeology," in *Handbook of Environmental Isotope Geochemistry*. ed M. Baskaran (Berlin; Heidelberg: Springer-Verlag), 743–768. doi: 10.1007/978-3-642-10637-8_35

Smed, P. (1978). *Landskabskort Over Danmark*. Geografforlaget: Brenderup.

Smed, P. (2013). *Weichsel istiden på Sjælland*. Geologisk Tidsskrift 1–42, ISSN 2245-7097, Copenhagen.

Thomsen, E., and Andreasen, R. (2019). Agricultural lime disturbs natural strontium isotope variations: implications for provenance and migration studies. *Sci. Adv.* 5:eaav8083. doi: 10.1126/sciadv.aav8083

Tjelldén, A. K. E., Matthiesen, H., Petersen, L. M. M., Søe, N. E., and Kristiansen, S. M. (2016). *In situ* preservation solutions for deposited Iron Age human bones in Alken Enge, Denmark. *Conservat. Manage. Archaeol. Sites* 18, 126–138. doi: 10.1080/13505033.2016.1182768

Van der Sluis, L. G., Daly, J. S., Frei, K. M., and Reimer, P. J. (2020). Mobility and diet in Prehistoric Denmark: strontium isotope analysis and incremental stable isotope analysis of human remains from the Limfjord area. *Danish J. Archaeol.* 9, 1–29. doi: 10.7146/dja.v9i0.116301

Widga, C. J., Walker, J. D., and Boehm, A. (2017). Variability in Bioavailable $^{87}Sr/^{86}Sr$ in the North American Midcontinent. *Open Quaternary* 3, 1–7. doi: 10.5334/oq.32

Willmes, M., Bataille, C. P., James, H. F., Moffat, I., McMorrow, L., Kinsley, L., et al. (2018). Mapping of bioavailable strontium isotope ratios in France for archaeological provenance studies. *Appl. Geochem.* 90, 75–86. doi: 10.1016/j.apgeochem.2017.12.025

Conflict of Interest: The authors declare that the research was conducted in the absence of any commercial or financial relationships that could be construed as a potential conflict of interest.

frontiers in Ecology and Evolution

ORIGINAL RESEARCH
published: 22 January 2021
doi: 10.3389/fevo.2020.590837

Historical Landscape Use of Migratory Caribou: New Insights From Old Antlers

Joshua H. Miller[1], Brooke E. Crowley[1,2], Clément P. Bataille[3], Eric J. Wald[4†], Abigail Kelly[1], Madison Gaetano[1], Volker Bahn[5] and Patrick Druckenmiller[6]*

[1] Department of Geology, University of Cincinnati, Cincinnati, OH, United States, [2] Department of Anthropology, University of Cincinnati, Cincinnati, OH, United States, [3] Department of Earth and Environmental Sciences, University of Ottawa, Ottawa, ON, Canada, [4] Arctic National Wildlife Refuge, U.S. Fish and Wildlife Service, Fairbanks, AK, United States, [5] Department of Biological Sciences, Wright State University, Dayton, OH, United States, [6] Department of Geosciences, University of Alaska Fairbanks and University of Alaska Museum, Fairbanks, AK, United States

Accumulations of shed caribou antlers *(Rangifer tarandus)* are valuable resources for expanding the temporal scope with which we evaluate seasonal landscape use of herds. Female caribou shed their antlers within days of giving birth, thus marking calving ground locations. Antler geochemistry ($^{87}Sr/^{86}Sr$) reflects the isotopic signature of regions used during antler growth, thereby providing data on a second component of seasonal landscape use. Here, we evaluate shed caribou antlers from the Coastal Plain of the Arctic National Wildlife Refuge, Alaska. The Central and Eastern regions of the Coastal Plain are calving grounds for the Porcupine Caribou Herd, while the Western Coastal Plain supports calving by the Central Arctic Herd. We found that antler $^{87}Sr/^{86}Sr$ from the Central and Eastern Coastal Plain were isotopically indistinguishable, while antler $^{87}Sr/^{86}Sr$ from the Western Coastal Plain was significantly smaller. For each region, we compared isotopic data for "recent" antlers, which overlap the bulk of standardized state and federal caribou monitoring (early 1980s and younger), with "historical" antlers shed in years predating these records (from the 1300s to the 1970s). For Porcupine Herd females calving in the Arctic Refuge, comparisons of antler $^{87}Sr/^{86}Sr$ through time indicate that summer ranges have been consistent since at least the 1960s. However, changes between historical and recent antler $^{87}Sr/^{86}Sr$ for the Central Arctic Herd indicate a shift in summer landscape use after the late 1970s. The timing of this shift is coincident with multiple factors including increased infrastructural development in their range related to hydrocarbon extraction. Accumulations of shed caribou antlers and their isotope geochemistry extend modern datasets by decades to centuries and provide valuable baseline data for evaluating potential anthropogenic and other influences on caribou migration and landscape use.

Keywords: conservation paleobiology, historical ecology, seasonal landscape use, strontium isotope ratios, ANWR

OPEN ACCESS

Edited by:
Jennifer Leonard, Consejo Superior de Investigaciones Científicas (CSIC), Spain

Reviewed by:
James Schaefer, Trent University, Canada
Pam Groves, University of Alaska Fairbanks, United States

****Correspondence:***
Joshua H. Miller
josh.miller@uc.edu

†Present address:
Eric J. Wald, Inventory and Monitoring Program, National Park Service, Fairbanks, AK, United States

Specialty section:
This article was submitted to Paleoecology, a section of the journal Frontiers in Ecology and Evolution

Received: *03 August 2020*
Accepted: *16 December 2020*
Published: *22 January 2021*

Citation:
Miller JH, Crowley BE, Bataille CP, Wald EJ, Kelly A, Gaetano M, Bahn V and Druckenmiller P (2021) Historical Landscape Use of Migratory Caribou: New Insights From Old Antlers. Front. Ecol. Evol. 8:590837. doi: 10.3389/fevo.2020.590837

INTRODUCTION

Seasonal landscape use is a core component of animal ecology and population biology and is influenced by a variety of factors including population size, climate, and anthropogenic impacts (Fryxell and Sinclair, 1988; Dingle, 2006; Avgar et al., 2014). Many of these drivers operate on decadal timescales or longer, but datasets rarely have the temporal depth to capture their

underlying long-term variability, trends, or oscillations (Vors and Boyce, 2009; Magurran et al., 2010; Mihoub et al., 2017). Additionally, the scale of ecological changes due to natural and anthropogenic influences is often masked because wildlife monitoring programs generally start after populations had been subjected to significant perturbations (Terry, 2009; Tomasovych and Kidwell, 2017). The need for datasets that extend beyond the temporal restrictions of available biomonitoring data is particularly critical for species living in regions with high rates of climate-related environmental change (e.g., the Arctic) or dependent on ecological strategies, such as migration, that are particularly threatened by anthropogenic impacts (Berger, 2004; Festa-Bianchet et al., 2011; Tucker et al., 2018). While historical ecology remains mostly lost to time, an increasing number of ecological proxies can help quantify the magnitude and directions of otherwise cryptic biological changes, including aspects of landscape use and migration (Morneau and Payette, 1998, 2000; Zalatan et al., 2006; Kidwell, 2007; Froyd and Willis, 2008; Behrensmeyer and Miller, 2012; Kidwell and Tomasovych, 2013; Miller et al., 2013; Dietl et al., 2015; Barnosky et al., 2017; Grace et al., 2019).

Bones are one such proxy, as they can persist on landscape surfaces for decades, centuries, or longer and can faithfully record data on their source populations (Behrensmeyer, 1978; Andrews, 1995; Sutcliffe and Blake, 2000; Western and Behrensmeyer, 2009; Miller, 2011; Behrensmeyer and Miller, 2012; Miller et al., 2013). In addition to data on species presence and relative abundances through time, some skeletal materials are capable of recording patterns of seasonal landscape use. Antlers of deer (Cervidae) are grown and shed following seasonal schedules (Espmark, 1971; Bergerud, 1976; Hall, 2005). After decades, shed antlers can accumulate into measurable densities on landscape surfaces (e.g., 10^2-10^3 antlers/km^2), with regions of relatively high or low antler densities faithfully recording the herd's patterns of seasonal landscape use (Miller and Barry, 1992; Miller, 2012; Miller et al., 2013).

Caribou (*Rangifer tarandus*) are unique among cervids in that both females and males can annually grow and shed antlers (Espmark, 1971; Bergerud, 1976). Differences in antler size and morphology enable sex determination (Høymork and Reimers, 1999; Miller et al., 2013), opening opportunities to evaluate patterns of sex-specific landscape use. In caribou, timing of antler shedding depends on maturity, sex, and other hormonal drivers. Mature males, for example, shed antlers shortly after fall mating, while immature males may keep them until spring (Bergerud, 1976; Blake et al., 1998). Females that do not become pregnant either shed their antlers following the fall mating season or keep them until early spring (several weeks or more before pregnant caribou give birth; Espmark, 1971; Bubenik et al., 1997). Notably, pregnant female caribou retain their antlers until the spring calving season and only shed them within a few days before or after giving birth (Espmark, 1971; Bergerud, 1976; Whitten, 1995). The calving period is highly conserved annually, with peak calving date for individual herds varying on the scale of days (Griffith et al., 2002). Tens-of-thousands of pregnant females may visit calving grounds each year, resulting in large accumulations of shed female antlers (10^2-10^3 antlers/km^2) that can be used as a geographic proxy for mapping both recent and historical calving grounds (Miller et al., 2013).

While locations of shed antlers document landscape use during the shedding period, antler isotope geochemistry can provide complementary ecological information on landscape use during antler growth. Strontium isotope ratios ($^{87}Sr/^{86}Sr$) of bone, tooth, hair, and antlers are a broadly used tool in forensic science, ecology, archeology, and paleoecology to help track the geographic origins of biological tissues (reviewed by Bentley, 2006; Hobson et al., 2009; Makarewicz and Sealy, 2015; Crowley et al., 2017). This is possible because bioavailable $^{87}Sr/^{86}Sr$ varies across landscapes primarily in response to changes in surface geology (Capo et al., 1998; Crowley et al., 2017; Bataille et al., 2020). As strontium ions can replace calcium during the formation of biological tissues, $^{87}Sr/^{86}Sr$ can be sequestered in bones, teeth, and other calcium-rich structures (Koch et al., 1995; Capo et al., 1998; Hobson et al., 2009). Developing tissue can record the isotopic signatures of the strontium source because this replacement occurs with negligible, and correctable, fractionation (Flockhart et al., 2015; Lewis et al., 2017). By first establishing how strontium isotope ratios change across space, the $^{87}Sr/^{86}Sr$ in biological materials (modern and fossil) can provide geographic context to specimens including deciphering patterns of landscape use and migration (Hoppe and Koch, 2007; Britton et al., 2009; Gigleux et al., 2017; Widga et al., 2017; Bataille et al., 2018, 2020).

In this study, we tested the capacity of antler $^{87}Sr/^{86}Sr$ to discriminate between two caribou herds (Porcupine and Central Arctic) that calve on different regions of the Coastal Plain within the Arctic National Wildlife Refuge, Alaska (USA, **Figure 1**). Alaskan caribou calve primarily in early June (Cameron et al., 2002; Griffith et al., 2002; Nicholson et al., 2016), and subsequent re-growth of female antlers occurs following calving and during the summer (Bergerud, 1976; Bubenik et al., 1997). Thus, antler $^{87}Sr/^{86}Sr$ should primarily reflect bioavailable $^{87}Sr/^{86}Sr$ from a caribou's post-calving spring and summer ranges. Based on mapped geological differences between summer ranges of the Porcupine and Central Arctic Herds (**Figure 1**; Wilson et al., 2015), we predict that antlers collected from the Central and Eastern Coastal Plain (calving grounds of the Porcupine Herd) will be isotopically distinct from antlers collected from the Western Coastal Plain (Central Arctic Herd calving grounds).

We also used antler $^{87}Sr/^{86}Sr$ to test for changes in summer landscape use for the Porcupine and Central Arctic Herds. Because bone weathering is slow in arctic settings (Meldgaard, 1986; Sutcliffe and Blake, 2000), it is likely that some antlers lying on the calving grounds were shed hundreds of years ago. We used antler weathering characteristics and radiocarbon dating to identify antlers from different time periods and test for changes in landscape use ($^{87}Sr/^{86}Sr$) through time. Since surveys of the Central Arctic Herd began in the 1970s, there have been dramatic increases in petroleum-related infrastructure in portions of their calving, summer, and winter ranges (Fancy, 1983; Fancy et al., 1989; Cameron et al., 1992; Nicholson et al., 2016) as well as dramatic changes in herd size (Lenart, 2015; Curl, 2020; Johnson et al., 2020). Both of these factors could have impacted patterns of seasonal landscape use (Bergerud,

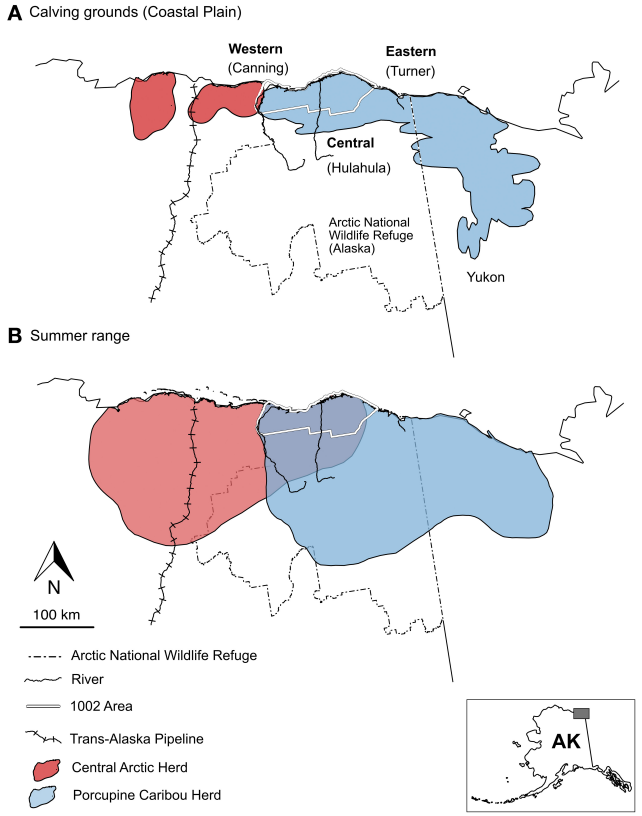

FIGURE 1 | Seasonal ranges for caribou of the Arctic National Wildlife Refuge, AK. Ranges of the Central Arctic (red) and Porcupine Herds (blue) are distinct during **(A)** calving periods, but there is greater spatial overlap across their **(B)** summer ranges. Antler surveys were conducted along the Coastal Plain calving grounds, accessed by major river systems; Canning River (Western Coastal Plain), Hulahula River (Central Coastal Plain), and Turner River (Eastern Coastal Plain). The Trans-Alaska Pipeline (cross-hatched line) was completed in 1977. Herd range boundaries from Trammell et al. (2015).

1996; Boertje and Gardner, 2000; Hinkes et al., 2005; Vistnes and Nellemann, 2008; Nicholson et al., 2016). Across a similar time period, the Porcupine Herd experienced relatively limited anthropogenic development of their range and comparatively less dramatic changes in population size (Griffith et al., 2002; Caikoski, 2020). We therefore expect that landscape use of the Porcupine Herd has been more consistent through time.

MATERIALS AND METHODS

The Caribou Study System

The Arctic National Wildlife Refuge (Arctic Refuge) is ideally suited to evaluate the geographic and seasonal data recorded in antlers of migratory caribou. The Coastal Plain of the Arctic Refuge is a broad, flat, tussock-tundra-rich landscape used as a caribou calving ground by the Porcupine Herd and the Central Arctic Herd (**Figure 1**; Cameron et al., 2002; Griffith et al., 2002; Jorgenson et al., 2002; Jorgenson and Walker, 2018). Most calving activity in the Arctic Refuge is by Porcupine Herd females, which generally enter the Coastal Plain from the east and south (Fancy et al., 1989; Griffith et al., 2002). Caribou that calve along the western margin of the Arctic Refuge's Coastal Plain are mostly from the Central Arctic Herd, whose calving grounds are predominately west of the Arctic Refuge (**Figure 1**; Fancy et al., 1989; Cameron et al., 2002; Nicholson et al., 2016; Prichard et al., 2020). While geographically separated during calving, the current ranges of the Porcupine and Central Arctic Herds partially overlap during summers (on the Coastal Plain) and winters (generally south of the Brooke Range; Lenart, 2015; Nicholson et al., 2016; Prichard et al., 2020). Yet even with this overlap, the overall geology of summer ranges is distinct, which is important for differentiating herds using antler $^{87}Sr/^{86}Sr$. The summer ranges of both herds overlay unconsolidated Quaternary sediments, but the range of the Porcupine Herd extends east and south into regions dominated by metasediments, mafic rocks, and Neoproterozoic siliciclastic rocks (Wilson et al., 2015; Colpron et al., 2016), while the range of the Central Arctic Herd extends west into areas richer in Mesozoic carbonates as well as Mesozoic and Cenozoic siliciclastic rocks (Wilson et al., 2015).

The Central Arctic and Porcupine Herds have been studied for decades by state, territorial, and federal offices of the US and Canada (Russell et al., 1993, 2005; Cameron et al., 2002; Griffith et al., 2002; Russell and Gunn, 2019; Caikoski, 2020). The long history of evaluation is due, in part, to Alaska's rich oil reserves and mandates to consider the consequences of petroleum development on caribou ecology and herd sizes across Alaska (USA-Canada, 1987; Whitten, 1994; Griffith et al., 2002; Cameron et al., 2005; Russell and Gunn, 2019). Within the Arctic Refuge, significant work has focused on a region of the Coastal Plain referred to as the "1002 Area" (**Figure 1**), which includes the majority of the Porcupine Herd's Alaskan Coastal Plain calving grounds (Griffith et al., 2002; Caikoski, 2020). In 1980, the United States Congress excluded this region from many long-term protections bestowed on most wildlife refuge lands and it was established as a region for possible hydrocarbon development (Udall, 1980). Lease sales for hydrocarbon development were mandated by the U.S. Congress in 2017 (Brady, 2017). In this context, many management questions related to the Arctic Refuge's Coastal Plain have focused on assessing the potential ecological consequences of developing the 1002 Area (Cameron and Whitten, 1980; Cameron et al., 1992, 2005; Griffith et al., 2002; Arthur and Del Vecchio, 2009; Pearce et al., 2018; Russell and Gunn, 2019). Thus, a pertinent question for this study is whether antler records provide new information on how caribou use this region.

The size and location of caribou ranges are determined by endogenous and exogenous drivers, including herd size and anthropogenic stressors (Skoog, 1968; Russell et al., 1993; Bergerud, 1996; Cameron et al., 2005; Hinkes et al., 2005). Human infrastructural developments can produce clear and sustained impacts on caribou landscape use (Vistnes and Nellemann, 2008; Johnson and Russell, 2014). This is most clearly seen as avoidance of developed areas such as tourist lodging and infrastructure supporting petroleum exploration (Klein, 1971; Helle and Särkelä, 1993; Vors et al., 2010; Wilson et al., 2016). Roads, particularly when they run perpendicular

to the direction of migration, can also represent significant barriers to caribou movement and delay the arrival of females to calving grounds (Bolger et al., 2008; Wilson et al., 2016). Caribou may also shift or functionally abandon portions of seasonal ranges due to development (Cameron et al., 1992, 2005; Joly et al., 2006). Population size and climate also impact caribou landscape use, but do so more cyclically. For example, caribou populations can fluctuate decadally by tens- to hundreds-of-thousands of individuals (Vors and Boyce, 2009), often influenced by hemispheric climate cycles (Griffith et al., 2002; Joly et al., 2011). Large changes in population can lead to changes in overall geographic range and even influence whether caribou undergo annual migrations at all or become more sedentary (Bergerud, 1996; Baltensperger and Joly, 2019).

The Central Arctic Herd was first identified in 1975, but the herd's range has been subjected to petroleum development since the 1960s (Bergerud, 1996; Hinkes et al., 2005). This development includes the Trans-Alaska Pipeline (completed in 1977), and scores of subsequent drill sites and roadways connecting oil fields across calving and summer ranges (**Figure 1**; Fancy et al., 1989; Arthur and Del Vecchio, 2009). There has been widespread interest in evaluating herd impacts from economic development, including changes in landscape use in response to oil fields and other developments, and reduced body weight for calves in closer proximity to roads and drilling operations (Dau and Cameron, 1986; Cameron et al., 1992; Lawhead and Prichard, 2003; Arthur and Del Vecchio, 2009; Nicholson et al., 2016). The population of the Central Arctic Herd has also changed dramatically across the available timeseries, increasing from ca. 5,000–6,000 to 28,000 individuals during the 1970s and 1990s, before increasing again to 68,000 in 2010 and subsequently falling to 23,000 in 2016 (Cameron and Whitten, 1979; Whitten and Cameron, 1983; Cameron et al., 2005; Lenart, 2015; Curl, 2020; Johnson et al., 2020). In 2019, the herd was estimated at 30,000 individuals (Curl, 2020). The Central Arctic Herd calving grounds are concentrated in two core regions on the Coastal Plain, one of which overlaps the western margin of the Arctic Refuge. The summer range of the herd incorporates a broad section of the Coastal Plain and Brooks Range foothills within the Arctic Refuge and extends to the west (**Figure 1**; Cameron et al., 2002; Nicholson et al., 2016).

The Porcupine Herd has been monitored since the 1960s and 1970s, with particular emphasis on population size, patterns of landscape use, the geographic covariates of calf survivorship, and other core components of population biology (Skoog, 1968; Whitten et al., 1984, 1992; Fancy et al., 1989; Fancy and Whitten, 1991; Bergerud, 1996; Griffith et al., 2002; PCMB, 2016). Population estimates show that the Porcupine Herd increased from 100,000 to 178,000 individuals between the 1970s and 1989, before falling to 123,000 in 2001 (Caikoski, 2020). The herd then increased from 168,000 to 218,000 between 2010 and 2017 (Caikoski, 2020). Unlike the Central Arctic Herd, the annual range of the Porcupine Herd has been subjected to less infrastructural and economic activity (Fancy et al., 1989; Griffith et al., 2002; PCMB, 2016). For both herds, data on seasonal landscape use and migration have become more robust with increased numbers of radio-collared (and now GPS-collared) caribou and the standardization of survey and data processing protocols starting in the 1980s (Griffith et al., 2002; Caikoski, 2020). The calving grounds of the Porcupine Herd encompass nearly the entire Coastal Plain of the Arctic Refuge and extend into Yukon, Canada. The summer range extends from the Coastal Plain to the Brooks Range in both Alaska and Yukon (**Figure 1**; Fancy et al., 1989; Russell et al., 1993; Griffith et al., 2002).

Specimen Collection and Selection

Antlers for this study were selected from collections for a larger study on arctic bone weathering and caribou landscape use (e.g., Miller et al., 2013). Shed caribou antlers were collected from tundra surfaces along the Arctic Refuge Coastal Plain in the summers of 2010–2012, 2014, and 2015 (**Figure 1**). We used major river systems to collect antlers from three regions of the Coastal Plain: Western (Canning River), Central (Hulahula and Jago Rivers), and Eastern (Turner and Kongakut Rivers). From west to east, this sampling extends across 100 km. The river systems extend northward from the Brooks Range to the Arctic Ocean, and thus provide opportunities to sample across the width of the Coastal Plain (ca. 10–70 km; **Figure 1**).

Antlers were collected by walking across tundra surfaces using standardized surveys of well-drained tundra habitats rich in the low-growing evergreen flowering plant, *Dryas* (*Dryas* river terraces, sensu Jorgenson et al., 2002; Jorgenson and Walker, 2018). *Dryas* terraces are generally found within a few kilometers of river channels. Survey sites were accessed by fixed-wing aircraft or by rafting down rivers to survey locations. On *Dryas* terraces, the ground is not visually obstructed by tussocks, willows, or other vegetation that would hamper antler observation; this makes antlers highly visible and readily sampled (Miller et al., 2013). Surveys and collections were done with permission from, and in collaboration with, the Arctic National Wildlife Refuge (United States Fish and Wildlife Service).

While distinguishing female antlers from much larger and more palmated adult male antlers is straightforward, differentiating antlers of adult females from similarly sized and shaped young males requires careful evaluation (Høymork and Reimers, 1999; Miller et al., 2013). To categorize antlers by sex, we used museum reference collections and measurements of the major and minor axis of the roughly elliptical pedicle attachment surface (Miller et al., 2013). For each specimen, calculations provide a mean probability and 95% confidence interval that the antler is female (Miller et al., 2013). Female antlers dominate our dataset ($n = 57$), but to provide preliminary $^{87}Sr/^{86}Sr$ comparisons between the sexes, we also included a small number of males from the Central and Eastern Coastal Plain ($n = 7$). One antler could not be confidently assigned to either sex and is excluded from comparisons between males and females.

Shed antlers can be identified by the presence of an exposed antler-skull attachment surface. All but two antlers reported here were shed. The first exception (T01-20-14 09) is the proximal portion of a female antler that is still attached to a fragment of the cranium. This specimen shows clear bone resorption along the antler attachment surface, which we interpret as strong evidence that shedding was underway and that this individual died during the calving season. The second antler (ANWR-120) is a male that

includes a section of the antler pedicle and is also interpreted as a mortality. Both specimens were included because they are heavily weathered and likely predate available biomonitoring data by at least several decades. While some antlers were partially obscured in tundra or moss, all were at least partially exposed. One antler (T01-14-12 14) was found fully exposed, but almost entirely covered in root etching and was likely previously buried. This specimen was also included for its likely antiquity.

To test for change in seasonal landscape use through time, we selected antlers from our collection that spanned a potentially wide range of ages; methods for discriminating antler age categories are described below ("dating antlers"). Antlers were categorized as "recent" or "historical" depending on whether they were shed in years that overlapped the best-available caribou management records and/or following infrastructure development on herd ranges. This distinction is separately evaluated for the Porcupine and Central Arctic Herds due to their different management histories. For antlers from the Central and Eastern Coastal Plain (calving grounds of the Porcupine Herd), the dividing date between historical and recent was 1983. This division corresponds to standardization of calving surveys for the Porcupine Herd and when the numbers of radio-collared females began to substantially increase (Griffith et al., 2002). For antlers from the Western Coastal Plain (calving grounds of the Central Arctic Herd), the dividing date between historical and recent was 1980 to coincide with the completion of many infrastructural development projects and the onset of several others (Fancy et al., 1989; Cameron et al., 1992). Results were consistent when using the same cutoff for both regions (i.e., 1980 or 1983). We selected equivalent samples of "recent" ($n = 34$) and "historical" ($n = 31$) antlers from each of the three regions of the Coastal Plain ($n_{\text{median}} = 10$; $n_{\text{range}} = [9, 13]$, female only: $n_{\text{median}} = 10$, $n_{\text{range}} = [8, 10]$).

Dating Antlers

To assign antlers as either historical or recent, we estimated growth year using a combination of antler weathering analysis and Accelerator Mass Spectrometry (AMS) radiocarbon dating. Historical antlers were first identified by their advanced weathering and confirmed by AMS dates. To identify recent antlers without needing to directly date all specimens, we calibrated the progression of early weathering using a second series of AMS dates.

Bones in many environments progress beyond initial stages of weathering (weathering stages 0 and 1; sensu Behrensmeyer, 1978) within a few years (Behrensmeyer, 1978; Miller, 2009). However, bone weathering rates are dramatically slowed in arctic settings (results below; Meldgaard, 1986; Sutcliffe and Blake, 2000). By observing antler weathering patterns, it became apparent that the progressive loss of original bone textures was a potential indicator of initial weathering duration. We defined original bone textures as smooth, unmodified bone surfaces that may or may not maintain a glossy shine. The simplicity of the definition means antler surfaces can be readily assessed as original or modified. This definition is also non-ambiguous and highly restrictive as to which surfaces are considered original. Small cracks, slight roughening of external cortical surfaces, and other subtle, yet easily identified deviations from original bone textures are all recognized as modifications.

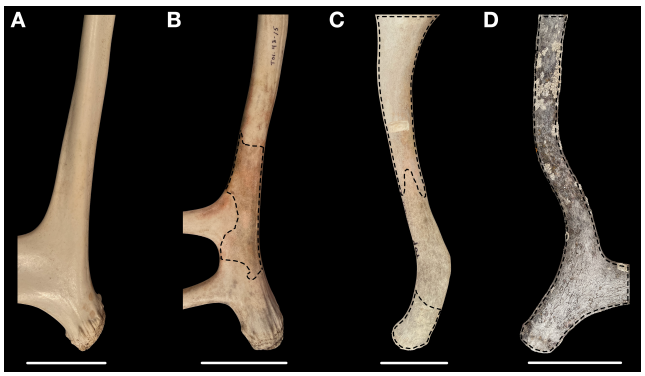

FIGURE 2 | Examples of antlers in the four weathering categories of original bone texture. **(A)** Bone texture score 0: preservation of more than two-thirds of original bone texture. **(B)** Score 1: between one- and two-thirds original bone texture preserved. **(C)** Score 2: less than one-third original bone texture preserved. **(D)** Score 3: no original bone texture preserved. Dashed lines outline regions of modified bone. In **(C)**, unmodified bone is difficult to visually differentiate due to discoloration, but these areas are smooth to the touch. Region sampled for $^{87}Sr/^{86}Sr$ is visible as a light colored area in the upper half of **(C)**. After evaluating the skyward and groundward sides of each antler, scores are added to create a Composite Score of bone texture ranging from 0 (supermajority of original bone texture preserved) to 6 (no original bone texture preserved). Scale bars are 5 cm. Photographed specimens are **(A)** ANWR-133, **(B)** T01-43-15 01, **(C)** T01-16-12 12, and **(D)** T01-32-14 15.

To evaluate initial weathering, we visually and tactilely assessed the coverage of preserved original bone texture for all antlers and scored them using four categories (**Figure 2**): 0 = more than two-thirds original bone texture preserved, 1 = between one- and two-thirds preserved, 2 = less than one-third preserved, and 3 = no original bone texture remaining. We also recorded whether lichens were present or absent. Because lichens lead to pocked bone surfaces (Hospitaleche et al., 2011), antler surfaces covered in lichens were scored as 3. For each antler, we separately evaluated skyward and ground-facing sides, because these surfaces can experience different weathering microhabitats (Behrensmeyer, 1978; Andrews and Whybrow, 2005). To standardize our assessments, we focused on the proximal portion of the main beam (**Figure 3**, shaded area of antler schematic). This region has fairly even thickness of dense cortical bone, which is important for consistently estimating bone weathering duration (Behrensmeyer, 1978). Focusing on this anatomical region is also appropriate because it must be at least partially preserved to identify the antler as shed. After evaluating original bone texture, we added scores from the skyward and groundward sides into a Composite Score of bone texture, ranging from 0 (supermajority of all original bone texture preserved) to 6 (no original bone texture preserved).

To calibrate Composite Scores of bone texture to weathering duration, we AMS dated antlers with Scores of 3 ($n = 3$), 4 ($n = 1$), 5 ($n = 2$), and 6 ($n = 29$; includes all antlers previously identified as "historical"). Antlers with no or limited signs of weathering (Composite Scores 0–2) were not dated to maximize

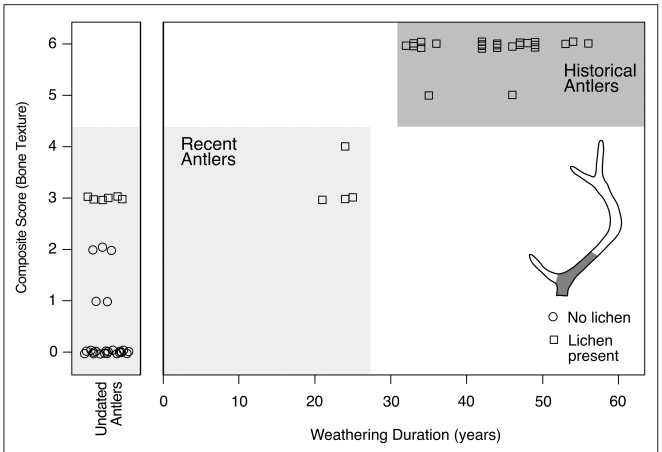

FIGURE 3 | Composite Scores of original bone texture calibrated to weathering duration. Weathering durations are calculated as the antler collection date minus the calibrated AMS date. Composite Scores range from 0 (super-majority of original bone textures preserved) to 6 (no original bone textures preserved). Composite Scores focus on the preservation of original surface textures of antlers. Composite Scores 0–5 characterize antlers in Weathering Stages 0 and 1 (Behrensmeyer, 1978). Antlers were evaluated along the proximal portion of the main beam (shaded area of antler schematic). Lichen presence or absence (squares or circles) is also indicated.

dates nearest the temporal divisions between "recent" and "historical." Further, progressions of bone weathering observed elsewhere instill confidence that antlers with no or minimal weathering have experienced the shortest weathering durations and are confidently "recent" (Behrensmeyer, 1978; Andrews and Whybrow, 2005; Miller, 2009; Western and Behrensmeyer, 2009).

For AMS dating, antlers were sampled from the proximal portion of the main beam. This region has dense cortical bone, which is resistant to contamination. Antlers were cut using a low-speed Dremel with a diamond wheel. Samples were cut into small chips and sent to the Keck-Carbon Cycle AMS Facility at the University of California, Irvine or the Center for Accelerator Mass Spectrometry at the Lawrence Livermore National Lab for chemical pretreatment and AMS dating. Collagen was prepared using standard treatments for demineralization and humic acid removal (Beaumont et al., 2010; Crowley et al., 2010), ultra-filtered, and lyophilized. For the 29 samples sent to the Keck-Carbon Cycle AMS Facility (**Supplementary Table 1**), lipids were removed by sonicating antler chips in a 2:1 chloroform/methanol solution for 30 min prior to demineralization. This was repeated with a fresh chloroform/methanol solution until the solution was no longer cloudy. Samples were then sonicated for 30 min in methanol, and 30 min in Milli-Q water. The sonicator bath was cooled to keep the temperature below 60°C. Of the six antlers dated at Lawrence Livermore, we only removed lipids from one (T03-02-11 28) by repeatedly sonicating in petroleum ether for 15 min until fat bubbles were no longer visible, and then rinsing with ultrapure water. There was no difference in $\delta^{13}C$ values for antlers with ($n = 30$) or without ($n = 5$) lipid removal (Wilcoxon $U = 78$, $p = 0.81$), suggesting this should be of negligible concern for date corrections.

Radiocarbon dates were calibrated to calendar years using IntCal13 or BombNH13, depending on whether the antlers were grown before or after atmospheric nuclear weapons testing in the 1950s and 1960s (Hua et al., 2013; Reimer et al., 2013). We used the *clam* package in R to convert conventional ^{14}C dates into calendar years from which we report all date ranges and associated posterior probabilities within the 95% confidence interval of the calibrated date (Blaauw, 2019). From those probability distributions, we categorized antlers as "recent" (post 1980 or 1983 depending on location) or "historical" (pre 1980 or 1983) based on the age with the highest probability. While dating errors can be as small as a few years for antlers grown after the 1950s, dating uncertainties are greater for antlers grown prior to the 1950s (Uno et al., 2013). For these older antlers, we summarized their ages by calculating the weighted-mean of the age probability distribution, the 1-sigma variance around the mean, and the range of the 95% confidence interval (Telford et al., 2004; Blaauw, 2010).

Because of the swift spike and subsequent protracted decay of atmospheric radiocarbon produced by nuclear weapons testing in the 1950's, antlers grown after weapons testing can often be calibrated to two different sets of years (e.g., the 1960s and the 1980s; Reimer et al., 2004). Furthermore, even if antlers were grown during the earlier period of the post-bomb era (e.g., 1960s), the quick initial pulse of radiocarbon relative to slow subsequent decay can mean that antler radiocarbon may have more expansive overlap with later parts of the calibration curve (e.g., 1980s). Ultimately, this means that the most supported calibrated date may not always correctly identify whether an antler was grown in historical or recent times. Fortunately, antler weathering features can add meaningful independent data with which to evaluate the AMS calibration. When antler weathering was inconsistent with the most supported age-range of a bifurcated set of dates, we used weathering to inform which date range should be used.

Strontium Isotope ($^{87}Sr/^{86}Sr$) Preparation and Analysis

Antler samples were prepared for $^{87}Sr/^{86}Sr$ analysis following estalished protocols (Crowley and Wheatley, 2014; Baumann and Crowley, 2015; Crowley et al., 2018). Ca. 20 mg of powder was milled from each antler using a low-speed Dremel with a burr attachment. We focused on a region of dense cortical bone roughly 15 cm from the base of the antler pedicle attachment and removed exterior bone surfaces in order to exclude weathered bone or other surface contaminants. Samples were soaked in 30% hydrogen peroxide (H_2O_2) at room temperature for 72 h and then rinsed five times with ultrapure water. Samples were agitated frequently, and H_2O_2 was refreshed after roughly 40 h. Samples were then reacted with 1M acetic acid (CH_3COOH) buffered with calcium acetate ($Ca(C_2H_3O_2)_2$) at 4°C for 24 h, rinsed five times with ultrapure water, and freeze dried.

Three to 5 mg of each pretreated sample were sent to the Multicollector ICPMS Laboratory at the University of Illinois, Urbana-Champaign for strontium extraction and analysis. Samples were dissolved in 3M nitric acid (H_2NO_3) and filtered

through Eichrom Sr-specific resin, followed by sequential rinsing with 0.05, 3, and 8M H_2NO_3 to isolate strontium. Strontium was eluted from the resin with 3 mL of ultrapure water and 1 mL of 0.05 M H_2NO_3 into 4 mL autosampler vials. Samples were analyzed on a Nu Plasma high-resolution multi-collector inductively-coupled plasma mass spectrometer. Data were corrected for drift using the international standard NBS 987 while two internal laboratory references ("Coral" and "E&A") were used to monitor accuracy and precision.

Analytical Framework

To test if antler accumulations faithfully differentiate the Porcupine and Central Arctic Herds, we compared female antler $^{87}Sr/^{86}Sr$ from the Western, Central, and Eastern Coastal Plain using Levene tests for homogeneity of variance and pairwise Mann-Whitney *U*-tests with a Bonferroni correction. Comparisons were evaluated separately for historical and recent female antlers. To test for changes in female antler $^{87}Sr/^{86}Sr$ through time, we used Mann-Whitney U and Levene tests to compare recent and historical antlers from the same Coastal Plain region. We also tested whether male and female antler $^{87}Sr/^{86}Sr$ provides similar spatial information (Mann Whitney-U). To make our Bonferroni corrections more intuitive, our reported *p*-values have been multiplied by the number of comparisons; thus our target alpha value remains 0.05. This is equivalent to adjusting the target alpha level itself by dividing by the number of comparisons. We used non-parametric tests in all analyses because the $^{87}Sr/^{86}Sr$ data deviate from normality (Sokal and Rohlf, 2011).

To estimate bioavailable $^{87}Sr/^{86}Sr$ on the Coastal Plain and surrounding regions, we used a modeled $^{87}Sr/^{86}Sr$ isoscape (Bataille et al., 2020). This model combines a global compilation of bioavailable $^{87}Sr/^{86}Sr$ in local plants, soils and animals, as well as geoenvironmental maps into a machine-learning regression to predict bioavailable $^{87}Sr/^{86}Sr$ at the global scale (1 km resolution). The model should work well for our purposes because the training data included soil, plant, and animal samples from Alaska. We used the latitude and longitude of each collected antler to extract the expected bioavailable $^{87}Sr/^{86}Sr$ at each collection site. To assess where antlers were grown, we applied a continuous-surface assignment framework available in the *assignR* package in R (Ma et al., 2020). This method compares the observed $^{87}Sr/^{86}Sr$ values (x^*) with those predicted by the isoscape. We used the function *assignR* to calculate the likelihood (z^*) that any given cell of the isoscape (c) represents a potential origin for an antler [$f(z^*|c)$] using a normal probability density function:

$$f(z^*|c) = \left(\frac{1}{\sqrt{2\pi}}\right) \exp\left[-\frac{z^{*2}}{2}\right]$$

with $z^* = \frac{x^* - \mu_C}{\sigma}$

where μ_c and σ represents the mean and uncertainty at each pixel of the isoscape. We started by calculating probability surfaces for each female antler. We then summarized probabilities for each herd by summing the probability maps and dividing by the number of antlers sampled. These summary maps represent the average probabilities for each pixel. Map probabilities range from 0.0 (extremely low probability) to 1.0 (very high probability). Given this framework, we used female antler $^{87}Sr/^{86}Sr$ from the Western Coastal Plain to estimate regions of possible summer landscape use for the Central Arctic Herd and female antler $^{87}Sr/^{86}Sr$ from the Central and Eastern Coastal Plain to estimate regions of possible summer landscape use for the Porcupine Herd. All analyses were scripted in R version 3.4.1 (R Core Team, 2017).

RESULTS

Antler Weathering and Radiocarbon Dating

Composite Scores of original bone texture for all antlers and AMS dating results are available in **Supplementary Tables 1**, **2**. As a reminder, our antler weathering analysis focused on the progressive loss of original bone textures, which only evaluates initial patterns of weathering. Antlers with Composite Scores 0–5 generally corresponded to antlers in the earliest weathering stages (WS 0–1; Behrensmeyer, 1978). Antlers that have lost all original bone textures (Composite Score 6) may be in any of the more advanced weathering stages (WS 2–5).

Weathering durations overlap for antlers that have lost most or all of their original bone texture (Composite Scores 5 and 6, **Figure 3**). Such antlers have been weathering for at least 32 years. Antlers with modestly better preservation (Composite Scores 3 and 4) have overlapping and tightly clustered weathering durations between 21 and 25 years. There is no overlap between Composite Score 3–4 antlers and those showing more advanced weathering (Composite Scores 5–6). We also found that lichens colonize antlers by the time antlers weather to Composite Score 3 (ca. 20 years; **Figure 3**, squares), after which they are a constant presence on subaerially exposed antlers.

All undated antlers had Composite Scores between 0 and 3 (**Figure 3**); the majority of which (21 of 30) exhibited only minimal weathering (Composite Scores 0–1). Clear distinction in weathering duration between more-weathered (Composite Scores 5–6) and less-weathered antlers (Composite Scores 4 and less) indicates that undated antlers have all been weathering for less than ∼25 years. We thus conclude that antlers with Composite Scores 0–4, including all undated specimens, came from generations of caribou that overlap available management records, and are thus considered "recent" (**Figure 3**).

Two antlers had calibrated radiocarbon dates for which the most supported date range was inconsistent with antler weathering. These were T01-16-12 06 (Western Coastal Plain) and T01-42-15 78 (Eastern Coastal Plain). Both antlers have lost all original bone texture (Composite Score 6). T01-16-12 06 has substantial bone surface cracking and flaking (akin to a shallowly developed Weathering Stage 2, Behrensmeyer, 1978). The calibrated age range for T01-16-12 06, which was collected in 2012, included dates in both the 1960s and 1980s (**Table 1**). Higher posterior probability support for candidate ages between 1984 and 1988 indicated ca. 24–28 years of weathering. However, our weathering calibration indicates that antlers would likely still have some preserved original bone textures after this weathering duration, or display weathering features more

TABLE 1 | Antlers with conflicts between weathering features and most-supported ranges of post-bomb (BombNH13) calibrated AMS dates.

Antler	Original bone texture (Composite Score)	Calibrated date range (calendar years)	Posterior probability
T01-16-12 06	6	1959.14–1961.75	27.1%
		1984.08–1987.68	67.8%
T01-42-15 78	6	1958.77–1961.13	9.9%
		1984.97–1988.64	85.1%

Antler weathering is summarized by the Composite Score of original bone texture. Date ranges and associated posterior probability support is based on the 95% confidence interval of the calibration.

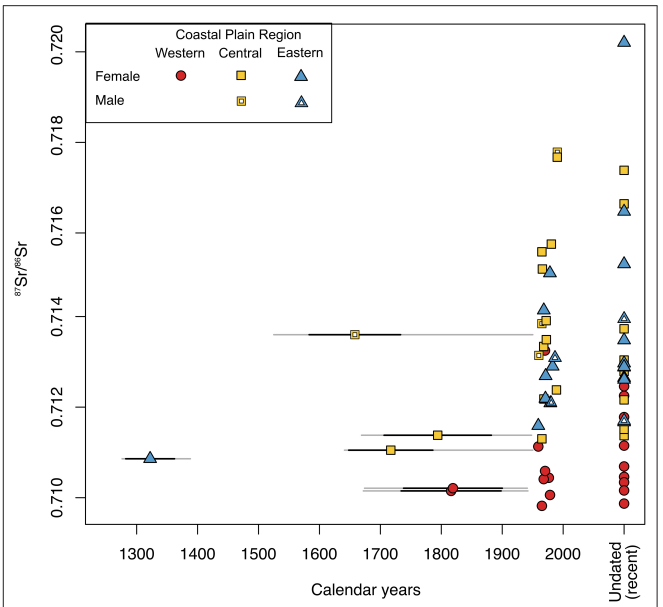

FIGURE 4 | Timeseries of $^{87}Sr/^{86}Sr$ for female and male caribou antlers from the Western, Central, and Eastern Coastal Plain. Antler ages (calendar years) are calibrated AMS dates. For antlers shed prior to the 1950s, calibrated radiocarbon ages are illustrated as the weighted mean (points), total age range (gray horizontal lines), and 1-sigma around the mean (black horizontal lines) of the 95% confidence interval. For antlers shed after the 1950s, calibrated dates are summarized as the year with the highest posterior probability of the calibration (points); dating errors for these antlers are too small to be shown but are available in **Supplementary Table 2**.

consistent with their recent loss. Thus, the highly weathered surfaces of T01-16-12 06 indicate it is an historical antler from ca. 1960. Antler T01-42-15 78 was collected in 2015 and has a similarly structured calibrated date showing support for either ca. 1960 or ca. 1986 (**Table 1**). However, T01-42-15 78 is more weathered than T01-16-12 06 (advanced form of Behrensmeyer's Weathering Stage 2; Behrensmeyer, 1978), including widening longitudinal cracks. Again, the highly weathered surfaces of T01-42-15 78 are inconsistent with other antlers dating to the 1980s and early 1990s (**Figure 3**). Thus, we determined T01-42-15 78 is an historical antler from the late 1950s to early 1960s.

Radiocarbon dates revealed that six antlers were shed prior to the 1900s. Each region of the Coastal Plain included at least one antler over 100 years old (**Figure 4**). Among these antlers, the oldest is ca. 700 years old (T03-02-11 28, **Supplementary Tables 1**, **2**) and shows no indication of previous burial. Only one of the antlers with a calibrated date prior to the 1900s exhibited taphonomic indications of previous burial (T01-14-12 14, **Supplementary Tables 1**, **2**).

Antler $^{87}Sr/^{86}Sr$ Across Space and Time

For both the Western and Central Coastal Plain, female antler $^{87}Sr/^{86}Sr$ (median and variance) differed significantly from bioavailable $^{87}Sr/^{86}Sr$ at the sites of antler collection (**Figure 5**, **Table 2**). For the Eastern Coastal Plain, antler and bioavailable $^{87}Sr/^{86}Sr$ had similar medians, but the variance of antler $^{87}Sr/^{86}Sr$ was significantly larger (**Table 4**). Overall, bioavailable $^{87}Sr/^{86}Sr$ increased across the study area from west to east (**Figure 5**). While antler $^{87}Sr/^{86}Sr$ also increased between the Western ($n = 19$) and Central Coastal Plain ($n = 20$; $U = 41$, $p << 0.01$), there was no change in antler $^{87}Sr/^{86}Sr$ between the Central and Eastern Coastal Plain ($n = 20$, $U = 173$, $p = 0.85$; **Figure 5**).

Comparing recent female antlers among regions, we found that antler $^{87}Sr/^{86}Sr$ was indistinguishable between the Central and Eastern Coastal Plain (Porcupine Caribou calving grounds; **Figure 6**, **Table 3A**). However, antlers from both regions had significantly larger $^{87}Sr/^{86}Sr$ than the Western Coastal Plain (Central Arctic calving ground). This pattern was repeated for historical antlers; Central and Eastern Coastal Plain antlers were statistically indistinguishable, but Western Coastal Plain antlers had significantly smaller $^{87}Sr/^{86}Sr$ (**Table 3B**).

Comparing female antlers through time in each region, we found no differences between historical and recent antler $^{87}Sr/^{86}Sr$ in either the Central or Eastern Coastal Plain (**Table 4**). However, comparisons between historical and recent antlers from the Western Coastal Plain revealed multiple differences (**Table 4**). First, the distribution of $^{87}Sr/^{86}Sr$ for nearly all historical Western Coastal Plain antlers was more constrained than all other datasets (**Figure 6**). The one antler outside of this cluster (T01-18-12 05, grown ca. 1970; **Supplementary Tables 1**, **2**) had a strontium isotope ratio more than six times the interquartile range larger than the median and was beyond the 95th percentile of the dataset, both satisfying common thresholds for identifying outliers (Gotelli and Ellison, 2004). Further, $^{87}Sr/^{86}Sr$ for this outlier exceeds that for any other antler from the Western Coastal Plain (historical or recent) and is close to the median for historical female antler $^{87}Sr/^{86}Sr$ for the Central Coastal Plain. Based on these characteristics, it is possible that this antler came from a rare Porcupine Herd female calving on the Western Coastal Plain. After removing this outlier, we find that recent antlers from the Western Coastal Plain have significantly larger variance and marginally larger $^{87}Sr/^{86}Sr$ compared to historical antlers (**Table 4**). Increased variance of recent antlers persists after the analysis is limited to

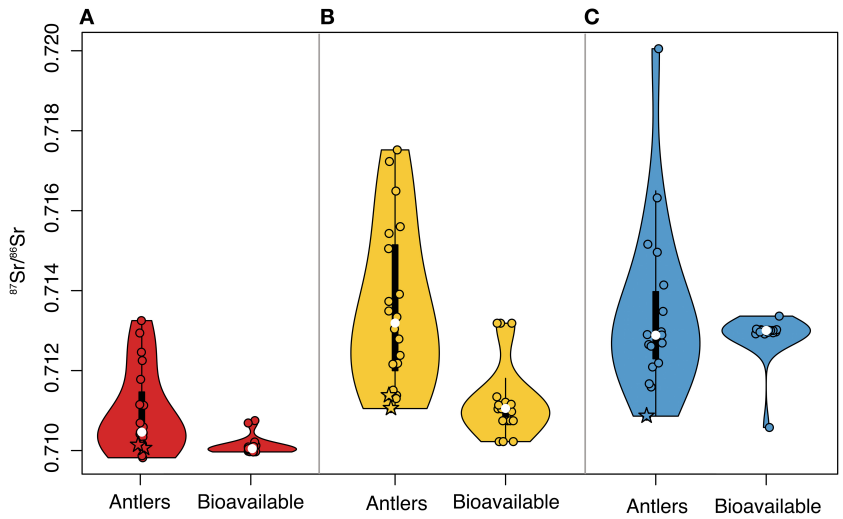

FIGURE 5 | Violin plots showing distributions of female antler $^{87}Sr/^{86}Sr$ and estimated bioavailable $^{87}Sr/^{86}Sr$ of each antler location for the **(A)** Western, **(B)** Central, and **(C)** Eastern Coastal Plain. Plots illustrate kernel density estimates (violin boundaries), interquartile range (thick vertical bars), 1.5 times the interquartile range (thin vertical line), and median (white point). Antler and bioavailable $^{87}Sr/^{86}Sr$ (points) are offset to aid visibility. Stars identify $^{87}Sr/^{86}Sr$ for antlers grown prior to 1900 CE.

TABLE 2 | Mann-Whitney U and Levene tests between female antler $^{87}Sr/^{86}Sr$ and bioavailable $^{87}Sr/^{86}Sr$ at collection sites.

Region ($n_{antlers}$)	Mann-Whitney U	Levene test
Western (19)	***U* = 296, *p* < 0.01**	**10.42, *p* < 0.01**
Central (20)	***U* = 362, *p* << 0.01**	**11.54, *p* < 0.01**
Eastern (18)	$U = 126$, $p = 0.26$	**6.82, *p* = 0.013**

For each Coastal Plain region, sample size corresponds to the number of female antlers evaluated, which equals the number of estimated bioavailable $^{87}Sr/^{86}Sr$ values from the isoscape (Bataille et al., 2020). Significant comparisons are in bold.

antlers grown after 1900 CE, which approximately equalizes the temporal extents of the datasets (**Table 4**).

Differences between historical and recent antler $^{87}Sr/^{86}Sr$ from the Western Coastal Plain (Central Arctic Herd) correspond to shifts in modeled landscape use (**Figures 7A,C**). Modeled landscape use for recent antlers (**Figure 7A**) overlaps the documented summer range of the Central Arctic Herd (**Figure 7A** dashed line; Arthur and Del Vecchio, 2009; Nicholson et al., 2016). Strong correspondence between antler $^{87}Sr/^{86}Sr$ and biomonitoring records suggests the method is appropriate for extrapolating beyond known management conditions. Historical reconstructions show that regions of possible landscape use are more uniform (probabilities closer to 1.0) and concentrated within a smaller geographic region of the current summer range (**Figure 7C**). Data for historical antlers from the Central Arctic Herd also indicate that areas used today as calving grounds had previously been likely regions of summer range. We also found support for more focused historical use of the Arctic Refuge's 1002 Area during summer months (**Figure 7C**).

For the Porcupine Herd, modeled areas of potential landscape use (**Figures 7B,D**) are less focused than the Central Arctic Herd; a pattern that holds for both historical and recent periods. Modeled landscape use based on recent antlers overlaps the documented summer range of the Porcupine Herd (**Figure 7B**, dashed line), though probability surfaces also show support outside of the Porcupine Herd's summer range.

Antlers from the Central and Eastern Coastal Plain that were grown prior to 1900 CE ("antique" antlers) generally have small $^{87}Sr/^{86}Sr$, and in some cases the smallest $^{87}Sr/^{86}Sr$ for their respective regions (**Figure 4**). This is not universal, however, as the oldest Western Coastal Plain antlers do not have unusually small $^{87}Sr/^{86}Sr$ compared to historical antlers younger than 1900 CE (**Figure 4**). Further, the single antique male antler from the Central Coastal Plain (**Figure 4**, open square, $^{87}Sr/^{86}Sr = 0.71360$) has larger $^{87}Sr/^{86}Sr$ than antique females from the same region (mean $female_{antique}$ $^{87}Sr/^{86}Sr = 0.71122$) but is consistent with the mean for Central Coastal Plain historical antlers grown after 1900 CE (male-only = 0.71349, female + male = 0.71373; female-only = 0.71379). Thus, $^{87}Sr/^{86}Sr$ is not explicitly linked to time.

Male and female antlers from the Central and Eastern Coastal Plain show broad overlap in $^{87}Sr/^{86}Sr$ (**Figure 4**). After pooling all female ($n = 38$) and male antlers ($n = 7$), we do not find evidence for isotopic distinction between sexes ($U = 117$, $p = 0.63$).

DISCUSSION

Expanding Ecological Timeseries

Our results demonstrate that antlers on the Arctic Refuge Coastal Plain can predate management records by centuries. Because slow weathering processes enable long-term survival of bone

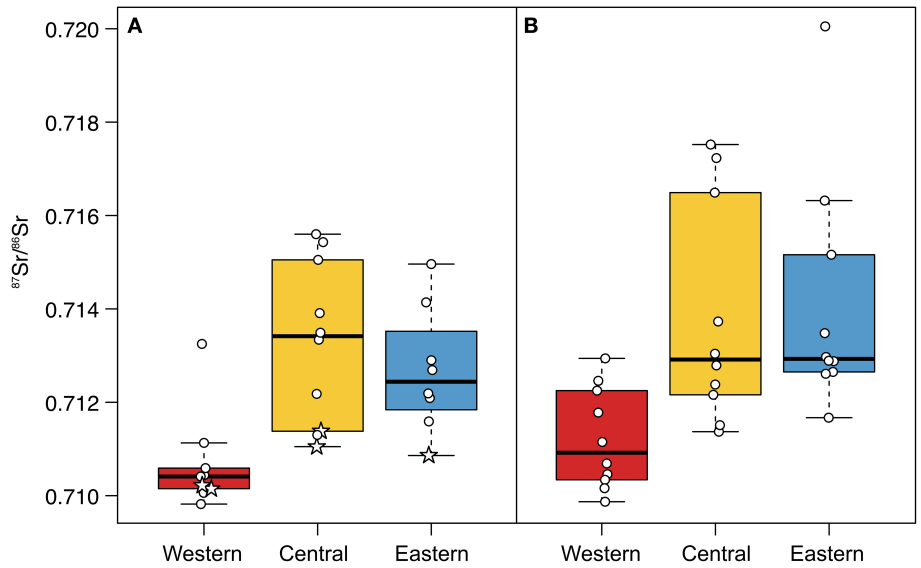

FIGURE 6 | Distributions of $^{87}Sr/^{86}Sr$ for **(A)** historical and **(B)** recent female antlers from the Western, Central, and Eastern Coastal Plain. Stars identify $^{87}Sr/^{86}Sr$ for antlers grown prior to 1900 CE. Boxplots illustrate the interquartile range (box), 1.5 times the interquartile range (dashed whiskers), and median (thick black bar). Points (female antler $^{87}Sr/^{86}Sr$) are offset to aid visibility.

TABLE 3 | Pairwise Mann-Whitney *U*-tests among female antler $^{87}Sr/^{86}Sr$ in the Western, Central, and Eastern Coastal Plain.

	Central	Eastern
A. Recent antlers		
Western	***U* = 14, *p* = 0.016**	***U* = 8, *p* = 0.0022**
Eastern	$U = 55$, $p > 0.05$	
B. Historical antlers		
Western	***U* = 5, *p* = 0.0012**	***U* = 7, *p* = 0.011**
Eastern	$U = 32$, $p > 0.05$	

*Separate tests are provided for comparisons among **(A)** recent antlers and **(B)** historical antlers. Sample sizes for recent antlers are Western (10), Central (10), Eastern (10). Sample sizes for historical antlers are Western (9), Central (10), Eastern (8). To maintain an alpha value of 0.05, all p-values were multiplied by 3 to correct for the number of comparisons. Significant results are in bold.*

TABLE 4 | Mann-Whitney U and Levene tests between historical and recent female antlers from the Western, Central, and Eastern Coastal Plain.

Region ($n_{Historical}$, n_{Recent})	Mann-Whitney U	Levene test
Western (8, 10)	$U = 19$, $p = 0.068$ •	**7.63, *p* = 0.014**
$Western_{1900s-2000s}$ (6, 10)	$U = 16$, $p = 0.15$	**5.26, *p* = 0.038**
Central (10, 10)	$U = 44$, $p = 0.68$	0.82, $p = 0.38$
Eastern (8, 10)	$U = 24$, $p = 0.17$	0.95, $p = 0.34$

Comparisons among Western Coastal Plain antlers are calculated with the outlier removal. Western Coastal Plain antlers grown after 1900 are compared in $Western_{1900s-2000s}$. Significant results are in bold. Marginally significant comparison ($p < 0.1$) indicated as •. $n_{Historical}$ = sample size of historical antlers. n_{Recent} = sample size of recent antlers.

(Meldgaard, 1986; Sutcliffe and Blake, 2000), antlers lying on tundra surfaces can dramatically extend the temporal window with which we assess caribou landscape use. The simple presence of shed female antlers from hundreds of years ago lying on the same landscapes as antlers of caribou that recently gave birth provides the first physical evidence of the longstanding use of the Arctic Refuge Coastal Plain as a calving ground. This finding is consistent with accounts of caribou herd behaviors in the 1800s and traditional ecological knowledge of the Gwich'in (Burch, 2012; Benson, 2019). Furthermore, because antlers are still being deposited on arctic landscapes, antler surveys simultaneously yield data on contemporary and distantly historical populations, contributing unique data for evaluating ecological responses to long-term environmental changes (Mihoub at al., 2017) for a highly mobile and long-lived mammal at increasing risk due to climate change and anthropogenic disturbance (Festa-Bianchet et al., 2011; Tucker et al., 2018).

Slow bone weathering on the Coastal Plain is likely caused by multiple factors, with below-freezing mean annual temperatures likely being of central importance (Fiorillo, 1995; Douglas et al., 2002; Todisco and Monchot, 2008; Miller, 2011; Pokines et al., 2016). Additionally, while summers bring 24-h sun and prolonged exposure to ultraviolet (UV) radiation, UV intensity is low at arctic latitudes and Coastal Plain summers are often cloudy or blanketed in dense fog for weeks at a time (U.S. Fish Wildlife Service, 2015; Miller, personal obs.). Bone weathering rates may also be slowed through limited summer rainfall, and reduced wet-dry cycles (shrinkage-expansion) that damage bone, particularly on well-drained *Dryas* terraces (Behrensmeyer, 1978; U.S. Fish Wildlife Service, 2015; Pokines et al., 2018). Under such conditions, it is perhaps unsurprising that antlers are well-preserved for extended durations, including maintaining original bone texture for decades. Similar or more extreme conditions in the Canadian High Arctic and Greenland support the persistence of unburied antlers on landscape surfaces for

millennia (Meldgaard, 1986; Sutcliffe and Blake, 2000). This is in stark contrast to tropical settings, where bones of large mammals are unlikely to persist beyond several decades (Behrensmeyer, 1978; Tappen, 1994), or temperate settings where bones may only survive on landscape surfaces for up to two centuries (Miller, 2011). The need for historical references is particularly acute in arctic populations, as these ecosystems have already been and will continue to be subjected to some of the most extreme environmental perturbations due to global warming (ACIA, 2004; Graversen et al., 2008; IPCC, 2014). Unfortunately, data access and integration from arctic ecosystems are often hampered by challenges in consistently accessing remote areas as well as changes in survey methodologies (but see Magurran et al., 2010). Even under such constraints, bones, teeth, and antlers lying on landscape surfaces can faithfully record diverse aspects of community ecology and seasonal landscape use and allow us to reclaim components of lost ecological history (Behrensmeyer et al., 1979; Western and Behrensmeyer, 2009; Miller, 2011, 2012; Miller et al., 2013, 2014).

Antler $^{87}Sr/^{86}Sr$ vs. Bioavailable $^{87}Sr/^{86}Sr$

Mismatch between female antler $^{87}Sr/^{86}Sr$ and bioavailable $^{87}Sr/^{86}Sr$ across the Coastal Plain indicated that antlers were not grown locally (**Figure 5**, **Table 2**). As both herds are migratory, this was an expected finding and is consistent with previous work showing that differences between skeletal materials and local bioavailable $^{87}Sr/^{86}Sr$ can identify mobile individuals (e.g., Hoppe et al., 1999; Hoppe and Koch, 2007; Baumann and Crowley, 2015). We also showed that broad spatial sampling (here, across 100 km) and evaluating multiple summary statistics (e.g., median and variance) can be important for evaluating differences between focal specimens and regional changes in bioavailable $^{87}Sr/^{86}Sr$. For example, median values of antler and bioavailable $^{87}Sr/^{86}Sr$ on the Eastern Coastal Plain were not statistically different, though antler $^{87}Sr/^{86}Sr$ had larger variance (**Figure 5**, **Table 2**). Antler $^{87}Sr/^{86}Sr$ also did not follow the west-to-east gradient of increasing bioavailable $^{87}Sr/^{86}Sr$ across the study area, further indicating antlers were not grown where they were shed.

Antler $^{87}Sr/^{86}Sr$ Can Differentiate Caribou Populations

Shed female antlers track two components of seasonal landscape use: ranges used during antler growth (antler $^{87}Sr/^{86}Sr$) and the subsequent spring calving ground (shed antler locations). Herd-specific patterns of landscape use by the Central Arctic Herd (Western Coastal Plain) and Porcupine Herd (Central and Eastern Coastal Plain) can be differentiated using $^{87}Sr/^{86}Sr$ of female antlers lying on tundra surfaces. When multiple herds are contributing antlers to a region, differentiating herd-specific inputs is an important step before using spatial variability in antler densities (antlers/km^2) to evaluate preferences in landscape use (Miller and Barry, 1992; Miller, 2012; Miller et al., 2013). While the discriminatory power of this method relies on the variability and distinctiveness of bioavailable $^{87}Sr/^{86}Sr$ among herd ranges (Beard and Johnson, 2000; Britton et al., 2011; Crowley et al., 2017), differences in $^{87}Sr/^{86}Sr$ between antlers on Central Arctic and Porcupine Herd calving grounds indicate that even herds with partially overlapping ranges (**Figure 1**) can be distinguished when geologic conditions are favorable.

Landscape Use Through Time: The Porcupine Caribou Herd

Antler $^{87}Sr/^{86}Sr$ indicates that for caribou calving on the Central and Eastern Coastal Plain, overall patterns of landscape use during the previous summer have been consistent since at least the 1960s (**Figures 6**, **7**). These data augment biomonitoring records that also suggest large-scale continuity in seasonal calving and summer ranges (Russell et al., 1993; Griffith et al., 2002; McFarland et al., 2017).

Herd size is an important contributor to changes in caribou landscape use, including shifts in the fidelity of seasonal ranges, migratory distances, and the tendency of individuals to migrate or remain more sedentary (Skoog, 1968; Fancy et al., 1989; Schaefer and Mahoney, 2003, 2013; Hinkes et al., 2005; Couturier et al., 2010; Taillon et al., 2012; Peters et al., 2017; Joly et al., 2019). Climate cycles such as the Pacific Decadal Oscillation and the North Atlantic Oscillation can also influence landscape ecology and population size (Griffith et al., 2002; Joly et al., 2011). Yet, even amidst changes in climate and herd size, we find continuity between shed Porcupine Herd antler locations (calving grounds) and their antler geochemistry (summer landscape use). An important component of this consistency may be the relatively small extent of anthropogenic development across the Porcupine Herd range, permitting populations to fluidly adapt their landscape use to changes in climate and population size. Expanded sampling of antler $^{87}Sr/^{86}Sr$ from calving areas in the Arctic Refuge and neighboring Yukon will provide important tests for how ubiquitous this stability is between summer and calving ranges. If infrastructural development increases in Porcupine Herd ranges, it will be important to track the degree to which the links between calving grounds and summering areas stay within the range of multidecadal variability established here.

While antler $^{87}Sr/^{86}Sr$ for the Central and Eastern Coastal Plain portrays a degree of ecological consistency across relatively recent history, antique antlers (grown prior to 1900 CE) from this region have comparatively small $^{87}Sr/^{86}Sr$ (**Figures 4**, **6** stars). Our small datasets preclude a full evaluation, but there are two potential reasons why antique Central and Eastern Coastal Plain antlers could have small $^{87}Sr/^{86}Sr$: (1) diagenetic alternation, or (2) different patterns of landscape use during the Little Ice Age (1250 to as late as 1900 CE; Solomina et al., 2015; Gaglioti et al., 2019).

Overall excellent preservation of antlers suggests that subtle differences in antique antler $^{87}Sr/^{86}Sr$ of the Central and Eastern Coastal Plain most likely reflect changes in landscape use. Antlers have generally undergone limited taphonomic modification, the most obvious of which includes gnawing, UV-exposure, freeze-thaw, and root etching (one buried specimen). Cutting the specimens for AMS dating also revealed that weathering features are generally limited to a thin patina near the surface without penetrating deeply into the antler. Consistent with

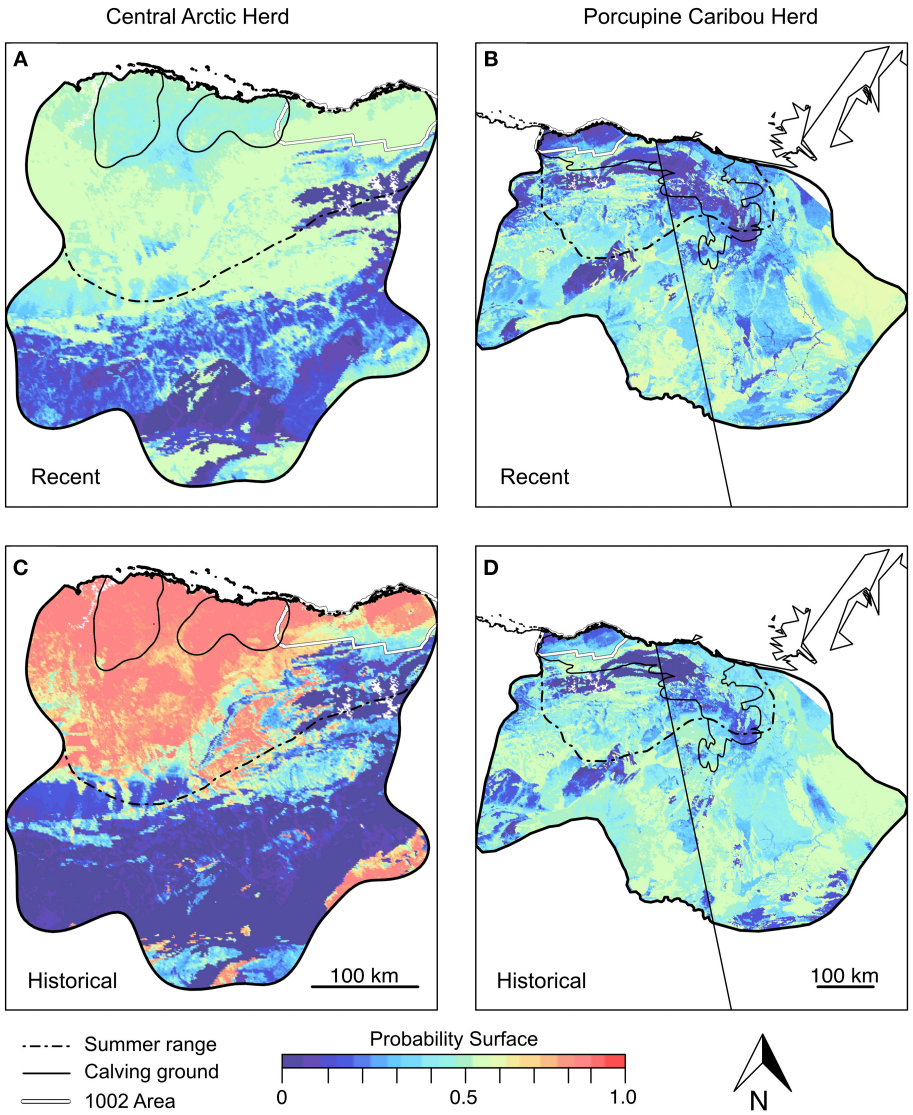

FIGURE 7 | Modeled Coastal Plain landscape use calculated from female antler $^{87}Sr/^{86}Sr$. Recent **(A,B)** and historical **(C,D)** landscape use is estimated separately for the Central Arctic **(A,C)** and Porcupine Caribou Herds **(B,D)**. Historical landscape use for the Central Arctic Herd is estimated after removing the outlier. The Porcupine Herd is modeled by pooling female antlers from the Central and Eastern Coastal Plain. Sample sizes for calculations in panels **(A–D)** are $n = 10$, 20, 8, and 18, respectively. Outlines of modern summer ranges (dashed) and calving grounds (solid lines) are provided for reference within the annual range of each herd (black outline of probability surface). Herd range boundaries from Trammell et al. (2015).

well-preserved bone, antlers do not show steady shifts in $^{87}Sr/^{86}Sr$ with time, which would be expected for early diagenetic obfuscation of primary isotope values. For example, after over 50 years of weathering, there is no change in median $^{87}Sr/^{86}Sr$ between recent and historical antlers on the Central and Eastern Coastal Plain (**Figure 6**). If alteration was driving antique antler $^{87}Sr/^{86}Sr$, we would also expect to see similar values for similarly aged antlers. Instead, similarly-aged antique antlers from the Central Coastal Plain have highly variable $^{87}Sr/^{86}Sr$ (**Figure 4**, yellow squares). Additionally, $^{87}Sr/^{86}Sr$ for the oldest Eastern Coastal Plain antler (T03-02-11 28; **Figure 5C**), is smaller than bioavailable $^{87}Sr/^{86}Sr$. Thus, even after hundreds of years of weathering, we do not see strong evidence that antique antler $^{87}Sr/^{86}Sr$ was altered. Strontium ratios of antique antlers from the Western Coastal Plain (Central Arctic Herd, discussed more below) are also not abnormally small relative to more recently shed antlers in that region (**Figures 4**, **6**). In the absence of a clear diagenetic explanation, the alternative explanation is that smaller $^{87}Sr/^{86}Sr$ of antique female antlers from the Central and Eastern Coastal Plain reflect a shift in summer landscape use for caribou calving in these regions during the Little Ice Age. Robustly evaluating this hypothesis will require larger sample sizes of antique antlers, but our results provide a first glimpse into possible differences in caribou landscape use during a time

when northeastern Alaska was significantly cooler and perhaps drier (Sikorski et al., 2009).

Landscape Use Through Time: The Central Arctic Herd

The Western Coastal Plain offers an excellent opportunity to sample antlers from Central Arctic Herd calving grounds while minimizing the distance to Porcupine Herd calving grounds. This close proximity makes comparing Western Coastal Plain antlers with antlers from the Central and Eastern Coastal Plain a strong test of whether antler $^{87}Sr/^{86}Sr$ can differentiate herd identity. At the same time, because the Western Coastal Plain is only one edge of the Central Arctic Herd calving grounds, sampling antler $^{87}Sr/^{86}Sr$ across the remainder of their calving grounds will be important for assessing the full scope of changes in summer landscape use through time.

For antlers collected along the Western Coastal Plain, those shed in the 1980s and more recently show a shift in median $^{87}Sr/^{86}Sr$ and greater variability than historical antlers. These changes manifest as greater overlap in recent $^{87}Sr/^{86}Sr$ between Western Coastal Plain antlers ($n = 4$ of 10) and those of the Central and Eastern Coastal Plain (**Figure 6**). There are two plausible explanations for these changes: (1) increased calving by the Porcupine Herd on the Western Coastal Plain; and (2) shifts in landscape use by the Central Arctic Herd.

The first possibility seems unlikely because the Porcupine Herd rarely calve near the Western Coastal Plain and there is no spatial overlap between our antler surveys and known Porcupine Herd calving areas. While the Porcupine Herd calved nearest our antler surveys in the early 1990s (Griffith et al., 2002; McFarland et al., 2017), antlers from this time-period are not well-represented in our dataset. Antlers were surveyed on the Western Coastal Plain in 2012, so antlers shed in the mid-1990s would mostly likely have original bone texture with Composite Scores of 3 or 4 (**Figure 3**). Instead, the majority of recent antlers from the Western Coastal Plain ($n = 6$ of 10) are nearly pristine (Composite Score 0), including half the Western Coastal Plain $^{87}Sr/^{86}Sr$ values (2 of 4) that overlap recent Central and Eastern Coastal Plain antlers. While Composite Score 0 has not been calibrated to weathering duration, comparisons to bone weathering observed elsewhere (Miller, 2011) suggest that these antlers were likely shed in the preceding decade. Thus, it is unlikely that the shift in Western Coastal Plain antler $^{87}Sr/^{86}Sr$ between historical and recent times was driven by antlers from Porcupine Herd females.

We consider the second possibility as the most probable scenario: differences in historical and recent antler $^{87}Sr/^{86}Sr$ from the Western Coastal Plain are best explained as a shift in summer landscape use by the Central Arctic Herd after the 1970s. Comparisons of modeled recent and historical summer landscape use (**Figures 7A,C**) indicate that range shifts were non-trivial. Historical summer landscape use (**Figure 7C**) was more consistent among individuals (probabilities closer to 1.0) with increased summer activity in what is currently spring calving grounds of the Central Arctic Herd. Reconstructions also indicate more concentrated summer use in the northeast and northwest portions of the Arctic Refuge's 1002 Area. While our dataset does not have the temporal resolution to pinpoint the onset of changes, the observed isotopic shifts roughly coincide with three factors known to alter patterns of landscape use in caribou: (1) population growth, (2) climate change, and (3) increased anthropogenic disturbances to their summer and calving ranges.

Since modern biomonitoring surveys were initiated in the 1970s, the Central Arctic Herd experienced some of the largest proportional population swings of any of Alaska's northern caribou herds, including an over 10-fold increase in population size between 1978 and 2010 (Cameron et al., 2005; Lenart, 2015). Most "recent" antlers come from this period of dramatic population increase, though some minimally weathered antlers (Composite Score 0) may come from the initial period of population reduction following 2010. It is possible that increased variance of $^{87}Sr/^{86}Sr$ in recent antlers and the marginal shift toward larger $^{87}Sr/^{86}Sr$ (**Table 4**) is a reflection of changes in landscape use associated with population expansion (Boertje and Gardner, 2000; Bergerud et al., 2008; Nicholson et al., 2016). However, similarity in antler $^{87}Sr/^{86}Sr$ across the historical antler timeseries is intriguing as it includes two antlers from the 1800s that may also have come from larger populations. Knowledge of caribou populations from this time are limited, but reports from travelers in northeast Alaska indicate that the historical equivalent of the Central Arctic Herd had population highs ca. 1840 and between the 1880s and 1890s (Burch, 2012). Uncertainties in calibrated AMS dates are high for the two antique antlers (T01-14-12 14, T01-16-12 10), but the most supported date ranges overlap these periods of past population highs (1832–1893 and 1833–1891, respectively; **Supplementary Table 2**). Thus, through time, relationships between antler $^{87}Sr/^{86}Sr$ and herd size may be complex and should be explored with a more complete timeseries.

Environmental and ecological changes due to global climate change are particularly acute in the arctic, where surface temperature anomalies have been consistently increasing since the 1980s or earlier (ACIA, 2004; Graversen et al., 2008; IPCC, 2014). Climate can influence ungulate population size and landscape ecology (Post and Stenseth, 1998; Joly et al., 2011) and is an obvious candidate driver of recent shifts in Central Arctic Herd antler $^{87}Sr/^{86}Sr$. However, antler $^{87}Sr/^{86}Sr$ of the Porcupine Herd showed no response across the same interval, even though landscapes of the Arctic Coastal Plain and the Porcupine Herd itself are known to respond strongly to climate and environmental change (Griffith et al., 2002; Joly et al., 2011). While testing the role of climate in structuring recent shifts in Central Arctic Herd landscape use requires further exploration, the lack of response by the Porcupine Herd to recent warming is noteworthy and suggests other factors may be contributing to the shift in Central Arctic Herd landscape use.

Increased human developments during the 1970s and 1980s are a likely alternative driver of shifts in summer landscape use for the Central Arctic Herd. Infrastructural development supporting oil exploration and recovery has been occurring in Central Arctic Herd ranges since the 1960s. However, the scale and scope of development increased in the mid 1970s and 1980s, including oil field expansion, construction of the

Trans-Alaska Pipeline, and road networks built through portions of the Central Arctic Herd's calving, summer, and winter ranges (Fancy, 1983; Arthur and Del Vecchio, 2009; Nicholson et al., 2016). There are known behavioral responses to infrastructure, including avoidance of pipelines and roads by pregnant females and reduced calf birth weight in areas with more intense anthropogenic impacts and barriers (Cameron and Whitten, 1980; Cameron et al., 2002, 2005; Arthur and Del Vecchio, 2009; Nicholson et al., 2016). Multiple anthropogenic disturbances to movement and habitat access can also compound into regional-scale impacts on caribou landscape use (Johnson and Russell, 2014; Johnson et al., 2020). Thus, a shift between historical and recent Central Arctic Herd summer range is not surprising. An important future area of research will be to test this shift in preferred summer landscapes using an expanded sampling of antlers across the herd's calving grounds. Of particular interest is to compare modeled summer landscape use between the two epicenters of Central Arctic Herd calving (**Figure 1**). If anthropogenic pressures are driving changes in summer landscape use of the Central Arctic Herd, one would expect greater differences between historical and recent shifts for caribou calving within the western calving ground, which has undergone more intense development. Antler data could also test the longevity of the two calving centers, and if calving was more geographically continuous prior to major development projects. A combined approach linking Traditional Ecological Knowledge of caribou with antler proxy studies could be a valuable strategy for synthesizing available information on historical patterns of seasonal landscape use.

Future Directions for Modeling Bioavailable $^{87}Sr/^{86}Sr$

When working across the spatial scales of caribou ranges, translating changes in antler $^{87}Sr/^{86}Sr$ through time into estimated shifts in landscape use requires a modeled $^{87}Sr/^{86}Sr$ isoscape. An important assumption in using such a model is that caribou diet echoes local bioavailable $^{87}Sr/^{86}Sr$ (as defined by exchangeable $^{87}Sr/^{86}Sr$ in soils that are incorporated into local plants). While this is a reasonable assumption for most consumers, caribou are somewhat unusual in their consumption of lichens, which incorporate the bulk of their nutrients from atmospheric sources (Nash, 2008). Consequently, caribou $^{87}Sr/^{86}Sr$ may be influenced by atmospherically available $^{87}Sr/^{86}Sr$ more than many mammals. However, while caribou consume large amounts of lichens during fall and winter, summer diets (coincident with the bulk of antler growth) are dominated by herbaceous browse that more likely reflects modeled bioavailable $^{87}Sr/^{86}Sr$ (Thompson and McCourt, 1981; Boertje, 1984). Another possible caveat is that while the model used to estimate bioavailable $^{87}Sr/^{86}Sr$ includes soil and plant data from Alaska, it does not incorporate samples from our exact study area. We do not think this is a large issue. The isoscape, which is intended for global applications, is generally accurate even in regions distant from directly sampled points, and this is particularly true for North America and Europe (Bataille et al., 2020). Nevertheless, future work will focus on sampling plants, soils, lichens, and small mammals from the Coastal Plain to develop a more nuanced $^{87}Sr/^{86}Sr$ isoscape for the Arctic Refuge and surrounding regions.

Place-Based Baselines of Ecological Variability From Bones on the Landscape

Today, naturally continuous landscapes are divided by invisible boundaries controlled by different countries, government entities, and private landowners, each with differing management mandates and stakeholder interests. Because of these divisions, many conservation and management questions focus on specific regions. The Arctic Refuge is no exception, where the 1002 Area is the focus of many management questions and ecological studies (Cameron and Whitten, 1980; Cameron et al., 1992, 2005; Arthur and Del Vecchio, 2009; Pearce et al., 2018; Russell and Gunn, 2019). Yet, particularly for highly mobile species, it can be challenging to discriminate the ecological "value" of one area relative to another, or the overall breadth of habitats and geographies needed to maintain a population or species. Bone surveys provide data that are inherently local. For caribou and other highly mobile taxa, bone geochemistry may also identify regions of additional ecological significance. Perhaps most importantly, beyond a snapshot of current ecological conditions, surveys of skeletal materials can establish biological variability through time and highlight when populations and communities have shifted beyond decadal-, centennial-, or even millennial-scale baselines (Terry, 2009; Rowe and Terry, 2014; Kidwell, 2015; Tomasovych and Kidwell, 2017). Slow bone weathering rates in Arctic settings may produce particularly time-rich datasets, but bones and their spatiotemporal records are ubiquitous in a wide variety of climatic settings and habitats (Behrensmeyer et al., 1979; Tappen, 1995; Andrews and Armour-Chelu, 1998; Andrews and Whybrow, 2005; Western and Behrensmeyer, 2009; Miller, 2011). Where gaps in historical ecological knowledge persist, those landscapes may be covered in skeletal data that are both spatially explicit and time-rich.

CONCLUSIONS

Accumulations of shed caribou antlers lying on calving grounds of the Arctic National Wildlife Refuge, Alaska, provide data on seasonal landscape use that complement more traditional wildlife surveys. Shed female antlers also extend our records of seasonal landscape use and caribou activity on Arctic Refuge calving grounds by over 700 years. Our findings support that antler $^{87}Sr/^{86}Sr$ can discriminate caribou herds and establish historical contexts for modern patterns of seasonal landscape use. Female antler $^{87}Sr/^{86}Sr$ from the Arctic Refuge's Central and Eastern Coastal Plain (a calving ground of the Porcupine Herd) has been consistent since the 1960s, indicating continuity in patterns of summer landscape use (when females grow antlers). Conversely, antler $^{87}Sr/^{86}Sr$ from the Western Coastal Plain (a calving ground of the Central Arctic Herd) reveals meaningful shifts in caribou landscape use after the 1970s, a time of significant changes in herd size, climate, and infrastructural development within the herd's calving and summer ranges. The decadal-to-centennial-scale

perspectives provided by accumulations of shed antlers and their isotope geochemistry provide important baselines for evaluating variability in caribou migration and landscape use prior to the initiation of traditional biomonitoring efforts. The long-term perspectives available from antlers are likely ubiquitous on arctic caribou calving grounds and can be acquired from relatively limited sampling. Emerging toolkits for decoding the records preserved in accumulations of antlers and other bones are producing historical ecological data that were once considered lost to time.

DATA AVAILABILITY STATEMENT

The original contributions presented in the study are included in the **Supplementary Materials**. Further inquiries can be directed to the corresponding author.

ETHICS STATEMENT

Ethical review and approval was not required for this study because no living animals were used.

AUTHOR CONTRIBUTIONS

JM designed the project, conducted fieldwork, analyzed data, and wrote the manuscript. BC and AK prepared specimens for isotope analysis. CB analyzed the combined surface probabilities. EW conducted fieldwork. MG wrote part of the manuscript. VB contributed to the analytical framework. PD provided logistical and field support in Alaska. All authors contributed to and edited the manuscript.

FUNDING

This research was supported by the U.S. Fish and Wildlife Service (Arctic National Wildlife Refuge), the National Geographic Society (grant 9133-12 to JM), a Christine Stevens Wildlife Award from the Wildlife Society (to JM), and the University of Cincinnati.

ACKNOWLEDGMENTS

We are grateful to the many people who helped make this work possible, including Dave Payer, Steve Arthur, and Greta Burkart. We are indebted to pilots Hollis Twitchell, Dave Sowards, and Roger Kaye who always got us home safely, even when the weather had other plans. We thank Lucinda Lawson for helpful discussions related to this work and our two reviewers for comments that improved the manuscript.

SUPPLEMENTARY MATERIAL

The Supplementary Material for this article can be found online at: https://www.frontiersin.org/articles/10.3389/fevo.2020.590837/full#supplementary-material

REFERENCES

ACIA (Arctic Climate Impact Assessment). (2004). *Impacts of a Warming Arctic: Arctic Climate Impact Assessment*. New York, NY: Cambridge University Press.

Andrews, P. (1995). Experiments in taphonomy. *J. Archaeol. Sci.* 22, 147–153. doi: 10.1006/jasc.1995.0016

Andrews, P., and Armour-Chelu, M. (1998). Taphonomic observations on a surface bone assemblage in a temperate environment. *Bull. Soc. Géologique France* 169, 433–442.

Andrews, P., and Whybrow, P. (2005). Taphonomic observations on a camel skeleton in a desert environment in Abu Dhabi. *Palaeontol. Electron.* 8, 1–17.

Arthur, S. M., and Del Vecchio, P. A. (2009). *Effects of oil field development on calf production and survival in the Central Arctic herd. Alaska Department of Fish and Game*, Final Research Technical Report. Grants W-27-5 and W-33-1 through W-33-4. Project 3.46. Juneau, AK: Federal Aid in Wildlife Restoration.

Avgar, T., Street, G., and Fryxell, J. M. (2014). On the adaptive benefits of mammal migration. *Can. J. Zool.* 92, 481–490. doi: 10.1139/cjz-2013-0076

Baltensperger, A. P., and Joly, K. (2019). Using seasonal landscape models to predict space use and migratory patterns of an arctic ungulate. *Movement Ecol.* 7:18. doi: 10.1186/s40462-019-0162-8

Barnosky, A. D., Hadly, E. A., Gonzalez, P., Head, J., Polly, P. D., Lawing, A. M., et al. (2017). Merging paleobiology with conservation biology to guide the future of terrestrial ecosystems. *Science* 355:eaah4787. doi: 10.1126/science.aah4787

Bataille, C. P., Crowley, B. E., Wooller, M. J., and Bowen, G. J. (2020). Advances in global bioavailable strontium isoscapes. *Palaeogeogr. Palaeoclimatol. Palaeoecol.* 555:109849. doi: 10.1016/j.palaeo.2020.109849

Bataille, C. P., von Holstein, I. C. C., Laffoon, J. E., Willmes, M., Liu, X.-M., and Davies, G. R. (2018). A bioavailable strontium isoscape for Western Europe: a machine learning approach. *PLoS ONE* 13:e0197386. doi: 10.1371/journal.pone.0197386

Baumann, E. J. Jr., and Crowley, B. E. (2015). Stable isotopes reveal ecological differences amongst now-extinct proboscideans from the Cincinnati region, USA. *Boreas* 44, 240–254. doi: 10.1111/bor.12091

Beard, B. L., and Johnson, C. M. (2000). Strontium isotope composition of skeletal material can determine the birth place and geographic mobility of humans and animals. *JFS* 45, 1049–1061. doi: 10.1520/JFS14829J

Beaumont, W., Beverly, R., Southon, J., and Taylor, R. E. (2010). Nuclear instruments and methods in physics research B. *Nuclear Inst. Methods Phys. Res. B* 268, 906–909. doi: 10.1016/j.nimb.2009.10.061

Behrensmeyer, A. K. (1978). Taphonomic and ecologic information from bone weathering. *Paleobiology* 4, 150–162. doi: 10.1017/S0094837300005820

Behrensmeyer, A. K., and Miller, J. H. (2012). "Building links between ecology and paleontology using taphonomic studies of recent vertebrate communities," in *Paleontology in Ecology and Conservation*, ed J. Louys (Berlin: Springer), 69–91. doi: 10.1007/978-3-642-25038-5_5

Behrensmeyer, A. K., Western, D., and Boaz, D. E. D. (1979). New perspectives in vertebrate paleoecology from a recent bone assemblage. *Paleobiology* 5, 12–21. doi: 10.1017/S0094837300006254

Benson, K. (2019). *Gwich'in Knowledge of Porcupine Caribou: State of Current Knowledge and Gaps Assessment*. Fort McPherson, NT: Department of Cultural Heritage, Gwich'in Tribal Council.

Bentley, A. R. (2006). Strontium isotopes from the Earth to the archaeological skeleton: a review. *J. Archaeol. Method Theor.*13, 135–187. doi: 10.1007/s10816-006-9009-x

Berger, J. (2004). The last mile: how to sustain long-distance migration in mammals. *Conserv. Biol.* 18, 320–331. doi: 10.1111/j.1523-1739.2004.00548.x

Bergerud, A. T. (1976). The annual antler cycle in Newfoundland caribou. *Can. Field Natural.* 90, 449–463.

Bergerud, A. T. (1996). Evolving perspectives on caribou population dynamics, have we got it right yet? *Rangifer* 16, 95–116. doi: 10.7557/2.16.4.1225

Bergerud, A. T., Luttich, S. N., and Camps, L. (2008). *The Return of Caribou to Ungava*. Montreal, QC: McGill Queens University Press. doi: 10.2307/j.ctt817j4

Blaauw, M. (2010). Methods and code for 'classical' age-modelling of radiocarbon sequences. *Quat. Geochronol.* 5, 512–518. doi: 10.1016/j.quageo.2010.01.002

Blaauw, M. (2019). *Clam: Classical Age-Depth Modelling of Cores from Deposits*. R package version 2.3.2. Available online at: https://cran.r-project.org/web/packages/clam/index.html (accessed August 10, 2020).

Blake, J. E., Rowell, J. E., and Suttie, J. M. (1998). Characteristics of first-antler growth in reindeer and their association with seasonal fluctuations in steroid and insulin-like growth factor 1 levels. *Can. J. Zool.* 76, 2096–2102. doi: 10.1139/z98-130

Boertje, R. D. (1984). Seasonal diets of the Denali caribou herd, Alaska. *Arctic* 37, 161–165. doi: 10.14430/arctic2182

Boertje, R. D., and Gardner, C. L. (2000). The Fortymile caribou herd: novel proposed management and relevant biology, 1992-1997. *Rangifer* 17–37. doi: 10.7557/2.20.5.1622

Bolger, D. T., Newmark, W. D., Morrison, T. A., and Doak, D. F. (2008). The need for integrative approaches to understand and conserve migratory ungulates. *Ecol. Lett.* 11, 63–77. doi: 10.1111/j.1461-0248.2007.01109.x

Brady, K. (2017). "H.R.1. An Act to provide for reconciliation pursuant to titles II and V of the concurrent resolution on the budget for fiscal year 2018," in *115th Congress of the United States of America* (Washington, DC).

Britton, K., Britton, K., Grimes, V., Grimes, V., Niven, L., Niven, L., et al. (2011). Strontium isotope evidence for migration in late Pleistocene *Rangifer*: implications for neanderthal hunting strategies at the middle Palaeolithic site of Jonzac, France. *J. Hum. Evol.* 61, 176–185. doi: 10.1016/j.jhevol.2011.03.004

Britton, K., Grimes, V., Dau, J., and Richards, M. P. (2009). Reconstructing faunal migrations using intra-tooth sampling and strontium and oxygen isotope analyses: a case study of modern caribou (*Rangifer tarandus granti*). *J. Archaeol. Sci.* 36, 1163–1172. doi: 10.1016/j.jas.2009.01.003

Bubenik, G. A., Schams, D., White, R. J., and Rowell, J. (1997). Seasonal levels of reproductive hormones and their relationship to the antler cycle of male and female reindeer (*Rangifer tarandus*). *Comparat. Biochem. Physiol. B* 116B, 269–277. doi: 10.1016/S0305-0491(97)00183-1

Burch, E. S. Jr. (2012). "Chapter 5. The northern district," in *Caribou Herds of Northwest Alaska 1850-2000*, eds I. Krupnik and J. Dau (Fairbanks, AK: University of Alaska Press).

Caikoski, J. (2020). *Porcupine Caribou Herd Management Report and Plan, Game Management Units 25A, 25B, 25D, and 26C: Report Period 1 July 2012–30 June 2017, and Plan Period 1 July 2017–30 June 2022*. Alaska Department of Fish and Game, Species Management Report and Plan ADF&G/DWC/SMR&P-2020–22, Juneau, AK, United States.

Cameron, R. D., Reed, D. J., Dau, J., and Smith, W. (1992). Redistribution of calving caribou in response to oil field development on the Arctic Slope of Alaska. *Arctic* 45, 338–342. doi: 10.14430/arctic1412

Cameron, R. D., Smith, W. T., White, R. G., and Griffith, B. (2005). Central Arctic Caribou and petroleum development: distributional, nutritional, and reproductive implications. *Arctic* 58, 1–9. doi: 10.14430/arctic382

Cameron, R. D., and Whitten, K. R. (1979). Seasonal movements and sexual segregation of caribou determined by aerial survey. *Arctic* 43, 626–633. doi: 10.2307/3808740

Cameron, R. D., and Whitten, K. R. (1980). *Effects of the Trans-Alaska Pipeline on Caribou Movements*. Juneau, AK: Department of Fish and Game.

Cameron, R. D., Smith, W. T., White, R. G., and Griffith, B. (2002). "Section 4: the Central Arctic caribou herd," in *Arctic Refuge Coastal Plain Terrestrial Wildlife Research Summaries. Biological Science Report USGS/BRD/BSR-2002-0001*, eds D. C. Douglas, P. E. Reynolds, and E. Rhode (Reston, VA: United States Geological Survey), 38–45.

Capo, R. C., Stewart, B. W., and Chadwick, O. A. (1998). Strontium isotopes as tracers of ecosystem processes: theory and methods. *Geochem. Cosmochim. Acta* 82, 197–225. doi: 10.1016/S0016-7061(97)00102-X

Colpron, M., Israel, S., Murphy, D., Pagage, L., and Moynihan, D. (2016). *Yukon Bedrock Geology Map and Legend*. Available online at: http://data.geology.gov.yk.ca/Reference/69477#InfoTab (accessed November 14, 2020).

Couturier, S., Otto, R. D., Côté, S. D., Luther, G., and Mahoney, S. P. (2010). Body size variations in caribou ecotypes and relationships with demography. *J. Wildlife Manage.*74, 395–404. doi: 10.2193/2008-384

Crowley, B. E., Carter, M. L., Karpanty, S. M., Zihlman, A. L., Koch, P. L., and Dominy, N. J. (2010). Stable carbon and nitrogen isotope enrichment in primate tissues. *Oecologia* 164, 611–626. doi: 10.1007/s00442-010-1701-6

Crowley, B. E., Castro, I., Soarimalala, V., and Goodman, S. M. (2018). Isotopic evidence for niche partitioning and the influence of anthropogenic disturbance on endemic and introduced rodents in central Madagascar. *Sci. Nat.* 105:44. doi: 10.1007/s00114-018-1564-y

Crowley, B. E., Miller, J. H., and Bataille, C. P. (2017). Strontium isotopes ($^{87}Sr/^{86}Sr$) in terrestrial ecological and palaeoecological research: empirical efforts and recent advances in continental-scale models. *Biol. Rev.* 92, 43–59. doi: 10.1111/brv.12217

Crowley, B. E., and Wheatley, P. V. (2014). To bleach or not to bleach? Comparing treatment methods for isolating biogenic carbonate. *Chem. Geol.* 381, 234–242. doi: 10.1016/j.chemgeo.2014.05.006

Curl, J. A. (2020). *Central Arctic Caribou Herd News, Summer 2020*. Fairbanks, AK: Alaska Department of Fish and Game, Division of Wildlife Conservation.

Dau, J. R., and Cameron, R. D. (1986). Effects of a road system on caribou distribution during calving. *Rangifer* 6, 95–101. doi: 10.7557/2.6.2.588

Dietl, G. P., Kidwell, S. M., Brenner, M., Burney, D. A., Flessa, K. W., Jackson, S. T., et al. (2015). Conservation paleobiology: leveraging knowledge of the past to inform conservation and restoration. *Annu. Rev. Earth Planet. Sci.* 43, 79–103. doi: 10.1146/annurev-earth-040610-133349

Dingle, H. (2006). Animal migration: is there a common migratory syndrome? *J. Ornithol.* 147, 212–220. doi: 10.1007/s10336-005-0052-2

Douglas, D. C., Reynolds, P. E., and Rhode, E. (2002). *Arctic Refuge Coastal Plain Terrestrial Wildlife Research Summaries*. Reston, VA: U.S. Geological Survey Biological Science Report USGS/BRD/BSR-2002–R-0001.

Espmark, Y. (1971). Antler shedding in relation to parturition in female reindeer. *J. Wild Manage* 35, 175–177. doi: 10.2307/3799887

Fancy, S. G. (1983). Movements and activity budgets of caribou near oil drilling sites in the Sagavanirktok River floodplain, Alaska. *Arctic* 36, 193–197. doi: 10.14430/arctic2262

Fancy, S. G., Pank, L. F., Whitten, K. R., and Regelin, W. L. (1989). Seasonal movements of caribou in arctic Alaska as determined by satellite. *Can. J. Zool.* 67, 644–650. doi: 10.1139/z89-093

Fancy, S. G., and Whitten, K. R. (1991). Selection of calving sites by Porcupine Herd Caribou. *Can. J. Zool.* 69, 1736–1743. doi: 10.1139/z91-242

Festa-Bianchet, M., Ray, J. C., Boutin, S., Côté, S. D., and Gunn, A. (2011). Conservation of caribou (*Rangifer tarandus*) in Canada: an uncertain future. *Can. J. Zool.* 89, 419–434. doi: 10.1139/z11-025

Fiorillo, A. R. (1995). The possible influence of low temperature on bone weathering in curecanti National recreation area, southwest Colorado. *Curr. Res. Pleistocene* 12, 69–71.

Flockhart, D. T. T., Kyser, T. K., Chipley, D., Miller, N. G., and Norris, D. R. (2015). Experimental evidence shows no fractionation of strontium isotopes ($^{87}Sr/^{86}Sr$) among soil, plants, and herbivores: implications for tracking wildlife and forensic science. *Isotopes Environ. Health Stud.* 51, 37–381. doi: 10.1080/10256016.2015.1021345

Froyd, C. A., and Willis, K. J. (2008). Emerging issues in biodiversity & conservation management: the need for a palaeoecological perspective. *Quat. Sci. Rev.* 27, 1723–1732. doi: 10.1016/j.quascirev.2008.06.006

Fryxell, J. M., and Sinclair, A. R. E. (1988). Causes and consequences of migration by large herbivores. *Trends Ecol. Evol.* 3, 237–241. doi: 10.1016/0169-5347(88)90166-8

Gaglioti, B. V., Mann, D. H., Wiles, G. C., Jones, B. M., Charlton, J., Wiesenberg, N., et al. (2019). Timing and potential causes of 19th-century glacier advances in coastal Alaska based on tree-ring dating and historical accounts. *Front. Earth Sci.* 7:122. doi: 10.3389/feart.2019.00082

Gigleux, C., Grimes, V., Tütken, T., Knecht, R., and Britton, K. (2017). Reconstructing caribou seasonal biogeography in Little Ice Age (late Holocene) Western Alaska using intra-tooth strontium and oxygen isotope analysis. *J. Archaeol. Sci. Rep.* 23, 1043–1054. doi: 10.1016/j.jasrep.2017.10.043

Gotelli, N. J., and Ellison, A. M. (2004). *A Primer of Ecological Statistics*. Sunderland, MA: Sinauer Associates, Inc.

Grace, M., Akçakaya, H. R., Bennett, E., Hilton-Taylor, C., Long, B., Milner-Gulland, E. J., et al. (2019). Using historical and palaeoecological data to inform ambitious species recovery targets. *Phil. Trans. R. Soc. B* 374:20190297. doi: 10.1098/rstb.2019.0297

Graversen, R. G., Mauritsen, T., Tjernström, M., Källén, E., and Svensson, G. (2008). Vertical structure of recent Arctic warming. *Nature* 541, 53–56. doi: 10.1038/nature06502

Griffith, B., Douglas, D. C., Walsh, N. E., Young, D. D., McCabe, T. R., Russell, D. E., et al. (2002). "Section 3: the porcupine caribou herd," in *Arctic Refuge Coastal Plain Terrestrial Wildlife Research Summaries. Biological Science Report USGS/BRD/BSR-2002-0001*, eds D. C. Douglas, P. E. Reynolds, and E. Rhode (Reston, VA: United States Geological Survey), 8–37.

Hall, B. K. (2005). *Bones and Cartilage: Developmental and Evolutionary Skeletal Biology*. 2nd ed. Halifax, NS: Academic Press. doi: 10.1016/B978-0-12-319060-4.50065-8

Helle, T., and Särkelä, M. (1993). The effects of outdoor recreation on range use by semi-domesticated reindeer. *Scand. J. For. Res.* 8, 123–133. doi: 10.1080/02827589309382761

Hinkes, M. T., Collins, G. H., and van Daele, L. J. (2005). Influence of population growth on caribou herd identity, calving ground fidelity, and behavior. *J. Wildlife Manage.* 69, 1147–1162. doi: 10.2193/0022-541X(2005)069[1147:IOPGOC]2.0.CO;2

Hobson, K. A., Barnett-Johnson, R., and Cerling, T. E. (2009). "Using isoscapes to track animal migration," in *Understanding movement, pattern, and process on Earth through isotope mapping*, eds J. B. West, G. J. Bowen, T. E. Dawson, and K. P. Tu (New York, NY: Springer), 273–298. doi: 10.1007/978-90-481-3354-3_13

Hoppe, K. A., and Koch, P. L. (2007). Reconstructing the migration patterns of late Pleistocene mammals from northern Florida, USA. *Quat. Res.* 68, 347–352. doi: 10.1016/j.yqres.2007.08.001

Hoppe, K. A., Koch, P. L., Carlson, R. W., and Webb, S. D. (1999). Tracking mammoths and mastodons: reconstruction of migratory behavior using strontium isotope ratios. *Geology* 27, 439–442. doi: 10.1130/0091-7613(1999)027<0439:TMAMRO>2.3.CO;2

Hospitaleche, C. A., Márquez, G., Pérez, L. M., Rosato, V., and Cione, A. L. (2011). Lichen bioerosion on fossil vertebrates from the Cenozoic of Patagonia and Antarctica. *Ichnos* 18, 1–8. doi: 10.1080/10420940.2011.552577

Høymork, A., and Reimers, E. (1999). Antler development in reindeer in relation to age and sex. *Rangifer* 22, 75–82. doi: 10.7557/2.22.1.692

Hua, Q., Barbetti, M., and Rakowski, A. Z. (2013). Atmospheric radiocarbon for the period 1950–2010. *Radiocarbon* 55, 2059–2072. doi: 10.2458/azu_js_rc.v55i2.16177

IPCC (Intergovernmental Panel on Climate Change). (2014). "Climate change 2014: synthesis report," in *Contribution of Working Groups I, II and III to the Fifth Assessment Report of the Intergovernmental Panel on Climate Change,* eds R. K. Pachauri and L. A. Meyer (Geneva: Intergovernmental Panel on Climate Change). doi: 10.1017/CBO9781107415416

Johnson, C. J., and Russell, D. E. (2014). Long-term distribution responses of a migratory caribou herd to human disturbance. *Biol. Conserv.* 177, 52–63. doi: 10.1016/j.biocon.2014.06.007

Johnson, H. E., Golden, T. S., Adams, L. G., Gustine, D. D., and Lenart, E. A. (2020). Caribou use of habitat near energy development in Arctic Alaska. *J. Wild. Mgmt.* 84, 401–412. doi: 10.1002/jwmg.21809

Joly, K., Gurarie, E., Sorum, M. S., Kaczensky, P., Cameron, M. D., Jakes, A. F., et al. (2019). Longest terrestrial migrations and movements around the world. *Sci. Rep.* 9:15333. doi: 10.1038/s41598-019-51884-5

Joly, K., Klein, D. R., Verbyla, D. L., Rupp, T. S., and Chapin, F. S. (2011). Linkages between large-scale climate patterns and the dynamics of Arctic caribou populations. *Ecography* 34, 345–352. doi: 10.1111/j.1600-0587.2010.06377.x

Joly, K., Nellemann, C., and Vistnes, I. (2006). A reevaluation of caribou distribution near an oilfield road on Alaska's North Slope. *Wildl. Soc. Bull.* 34, 866–869. doi: 10.2193/0091-7648(2006)34[866:AROCDN]2.0.CO;2

Jorgenson, J. C., and Walker, D. A. (2018). *Land Cover and Vegetation Map, Arctic National Wildlife Refuge*. Oak Ridge, TN: ORNL DAAC.

Jorgenson, J. C., Joria, P. E., and Douglas, D. C. (2002). "Section 2: land cover," in *Arctic Regufe Coastal Plain Terrestrial Wildlife Research Summaries. Biological Science Report USGS/BRD/BSR-2002-0001*, eds D. C. Douglas, P. E. Reynolds, and E. Rhode (Reston, VA: United States Geological Survey), 4–7.

Kidwell, S. M. (2007). Discordance between living and death assemblages as evidence for anthropogenic ecological change. *Proc. Natl. Acad. Sci. U.S.A.* 104, 17701–17706. doi: 10.1073/pnas.0707194104

Kidwell, S. M. (2015). Biology in the Anthropocene: challenges and insights from young fossil records. *Proc. Natl. Acad. Sci U.S.A.* 112, 4922–4929. doi: 10.1073/pnas.1403660112

Kidwell, S. M., and Tomasovych, A. (2013). Implications of time-averaged death assemblages for ecology and conservation biology. *Annu. Rev. Ecol. Evol. Syst.* 44, 539–563. doi: 10.1146/annurev-ecolsys-110512-135838

Klein, D. R. (1971). Reaction of reindeer to obstructions and disturbances. *Science* 173, 393–398. doi: 10.1126/science.173.3995.393

Koch, P. L., Heisinger, J., Moss, C. J., Carlson, R. W., Fogel, M. L., and Behrensmeyer, A. K. (1995). Isotopic tracking of change in diet and habitat use in African elephants. *Science* 267, 1340–1343. doi: 10.1126/science.267.5202.1340

Lawhead, B. E., and Prichard, A. K. (2003). *Surveys of Caribou and Muskoxen in the Kuparuk-Colville Region, Alaska, 2002.* Fairbanks, AK: Final Report prepared for ConocoPhillips Alaska, Inc. ABR, Inc.

Lenart, E. A. (2015). "Chapter 18: units 26B and 26C caribou," in *Caribou Management Report of survey and Inventory Activities 1 July 2012–30 June 2014*, eds P. Harper and L. A. McCarthy (Juneau, AK: Alaska Department of Fish and Game, Species Management Report ADF&G/DWC/SMR-2015-4), 1–38.

Lewis, J., Pike, A. W. G., Coath, C. D., and Evershed, R. P. (2017). Strontium concentration, radiogenic ($^{87}Sr/^{86}Sr$) and stable ($\delta^{88}Sr$) strontium isotope systematics in a controlled feeding study. *STAR Sci. Tech. Archaeol. Res.* 3, 45–57. doi: 10.1080/20548923.2017.1303124

Ma, C., Vander Zanden, H. B., Wunder, M. B., and Bowen, G. J. (2020). assignR: an R package for isotope-based geographic assignment. *Methods Ecol. Evol.* 111, 996–1001. doi: 10.1111/2041-210X.13426

Magurran, A. E., Baillie, S. R., Buckland, S. T., Dick, J. M., Elston, D. A., Scott, E. M., et al. (2010). Long-term datasets in biodiversity research and monitoring: assessing change in ecological communities through time. *Trends Ecol. Evol.* 25, 574–582. doi: 10.1016/j.tree.2010.06.016

Makarewicz, C. A., and Sealy, J. (2015). Dietary reconstruction, mobility, and the analysis of ancient skeletal tissues: expanding the prospects of stable isotope research in archaeology. *J. Archaeol. Sci.* 56, 146–158. doi: 10.1016/j.jas.2015.02.035

McFarland, H. R., Caikoski, J., Lenart, E., and Taras, M. (2017). *Porcupine Caribou News, Summer 2017*. Fairbanks, AK: Alaska Department of Fish and Game; Division of Wildlife Conservation.

Meldgaard, M. (1986). The Greenland caribou - zoogeography, taxonomy, and population dynamics. *Meddelelser Gronland* 20, 1–89.

Mihoub, J.-B., Henle, K., Titeux, N., Brotons, L., Brummitt, N. A., and Schmeller, D. S. (2017). Setting temporal baselines for biodiversity: the limits of available monitoring data for capturing the full impact of anthropogenic pressures. *Sci. Rep.* 7:41591. doi: 10.1038/srep41591

Miller, F. L., and Barry, S. J. (1992). Nonrandom distribution of antlers cast by Peary caribou bulls, Melville Island, Northwest Territories. *Arctic* 45, 252–257. doi: 10.14430/arctic1399

Miller, J. H. (2009). *The Large-Mammal Death Assemblage of Yellowstone National Park: Historical Ecology, Conservation Biology, Paleoecology* (Ph.D. Dissertation). University of Chicago, Chicago, IL.

Miller, J. H. (2011). Ghosts of yellowstone: multi-decadal histories of wildlife populations captured by bones on a modern landscape. *PLoS ONE* 6:e18057. doi: 10.1371/journal.pone.0018057

Miller, J. H. (2012). Spatial fidelity of skeletal remains: elk wintering and calving grounds revealed by bones on the Yellowstone landscape. *Ecology* 93, 2474–2482. doi: 10.1890/12-0272.1

Miller, J. H., Behrensmeyer, A. K., Du, A., Lyons, S. K., Patterson, D., Tóth, A., et al. (2014). Ecological fidelity of functional traits based on species presence-absence in a modern mammalian bone assemblage (Amboseli, Kenya). *Paleobiology* 40, 560–583. doi: 10.1666/13062

Miller, J. H., Druckenmiller, P., and Bahn, V. (2013). Antlers on the Arctic Refuge: capturing multi-generational patterns of calving ground use from bones on the landscape. *Proc. R. Soc. B* 280:20130275. doi: 10.1098/rspb.2013.0275

Morneau, C., and Payette, S. (1998). A dendroecological method to evaluate past caribou (*Rangifer tarandus* L.) activity. *Écoscience* 5, 64–76. doi: 10.1080/11956860.1998.11682446

Morneau, C., and Payette, S. (2000). Long-term fluctuations of a caribou population revealed by tree-ring data. *Can. J. Zool.* 78, 1784–1790. doi: 10.1139/z00-122

Nash, T. H. III. (2008). *Lichen Biology*. 2nd ed. Cambridge: Cambridge University Press. doi: 10.1017/CBO9780511790478

Nicholson, K. L., Arthur, S. M., Horne, J. S., Garton, E. O., and Del Vecchio, P. A. (2016). Modeling caribou movements: seasonal ranges and migration routes of the Central Arctic Herd. *PLoS ONE* 11:e0150333. doi: 10.1371/journal.pone.0150333

PCMB (Porcupine Caribou Management Board). (2016). *Porcupine Caribou Annual Summary Report 2016*. Whitehorse, YT: Porcupine Caribou Management Board.

Pearce, J. M., Flint, P. L., Atwood, T. C., Douglas, D. C., Adams, L. G., Johnson, H. E., et al. (2018). *Summary of Wildlife-Related Research on the Coastal Plain of the Arctic National Wildlife Refuge, Alaska, 2002–17*. Reston, VA: U.S. Department of the Interior. doi: 10.3133/ofr20181003

Peters, W., Hebblewhite, M., Mysterud, A., Spitz, D., Focardi, S., Urbano, F., et al. (2017). Migration in geographic and ecological space by a large herbivore. *Ecol. Monogr.* 87, 297–320. doi: 10.1002/ecm.1250

Pokines, J. T., Faillace, K., Berger, J., Pirtle, D., Sharpe, M., Curtis, A., et al. (2018). The effects of repeated wet-dry cycles as a component of bone weathering. *J. Arch. Sci. Rep.* 17, 433–441. doi: 10.1016/j.jasrep.2017.11.025

Pokines, J. T., King, R. E., Graham, D. D., Costello, A. K., Adams, D. M., Pendray, J. M., et al. (2016). The effects of experimental freeze-thaw cycles to bone as a component of subaerial weathering. *JASREP* 6, 594–602. doi: 10.1016/j.jasrep.2016.03.023

Post, E., and Stenseth, N. C. (1998). Large-scale climatic fluctuation and population dynamics of moose and white-tailed deer. *J. Anim. Ecol.* 67, 537–543. doi: 10.1046/j.1365-2656.1998.00216.x

Prichard, A. K., Parrett, L. S., Lenart, E. A., Caikoski, J. R., Joly, K., and Person, B. T. (2020). Interchange and overlap among four adjacent arctic caribou herds. *J. Wildlife Manage.* 84, 1500–1514. doi: 10.1002/jwmg.21934

R Core Team. (2017). *R: A language and environment for statistical computing*. Vienna: R Foundation for Statistical Computing. Available online at: https://www.R-project.org/ (accessed June 30, 2017).

Reimer, P. J., Bard, E., Bayliss, A., Beck, J. W., Blackwell, P. G., Ramsey, C. B., et al. (2013). IntCal13 and marine13 radiocarbon age calibration curves 0–50,000 years cal BP. *Radiocarbon* 55, 1869–1887. doi: 10.2458/azu_js_rc.55.16947

Reimer, P. J., Brown, T. A., and Reimer, R. W. (2004). Discussion: reporting and calibration of post-bomb ^{14}C data. *Radiocarbon* 46, 1299–1304. doi: 10.1017/S0033822200033154

Rowe, R. J., and Terry, R. C. (2014). Small mammal responses to environmental change: integrating past and present dynamics. *J. Mammal.* 95, 1157–1174. doi: 10.1644/13-MAMM-S-079

Russell, D., and Gunn, A. (2019). *Vulnerability Analysis of the Porcupine Caribou Herd to Potential Development of the 1002 lands in the Arctic National Wildlife Refuge, Alaska*. Report prepared for: Environment Yukon, Canadian Wildlife Service, and GNWT Department of Environment and Natural Resources, 143.

Russell, D. E., Martell, A. M., and Nixon, W. A. C. (1993). Range ecology of the Porcupine Caribou Herd in Canada. *Rangifer Special Issue* 8, 1–168. doi: 10.7557/2.13.5.1057

Russell, D. E., White R. G., and Daniel, C. J. (2005). *Energetics of the Porcupine Caribou Herd: A Computer Simulation Model*. Technical Report Series No. 431. Ottawa, ON: Canadian Wildlife Service.

Schaefer, J. A., and Mahoney, S. P. (2003). Spatial and temporal scaling of population density and animal movement: a power law approach. *Ecoscience* 10, 496–501. doi: 10.1080/11956860.2003.11682797

Schaefer, J. A., and Mahoney, S. P. (2013). Spatial dynamics of the rise and fall of caribou (*Rangifer tarandus*) in Newfoundland. *Can. J. Zool.* 91, 767–774. doi: 10.1139/cjz-2013-0132

Sikorski, J. J., Kaufman, D. S., Manley, W. F., and Nolan, M. (2009). Glacial-geologic evidence for decreased precipitation during the Little Ice Age in the Brooks Range, Alaska. *Arct. Antarct. Alp. Res.* 41, 138–150. doi: 10.1657/1523-0430-41.1.138

Skoog, R. O. (1968). *Ecology of the caribou (Rangifer tarandus granti) in Alaska* (Ph.D. Dissertation). Berkeley, CA: University of California Berkeley.

Sokal, R. R., and Rohlf, F. J. (2011). *Biometry*. 3rd ed. New York, NY: W. H. Freeman and Company.

Solomina, O. N., Bradley, R. S., Hodgson, D. A., Ivy-Ochs, S., Jomelli, V., Mackintosh, A. N., et al. (2015). Holocene glacier fluctuations. *Quat. Sci. Rev.* 111, 9–34. doi: 10.1016/j.quascirev.2014.11.018

Sutcliffe, A. J., and Blake, W. (2000). Biological activity on a decaying caribou antler at Cape Herschel, Ellesmere Island, Nunavut, high Arctic Canada. *Polar Record.* 233–246. doi: 10.1017/S0032247400016491

Taillon, J., Festa-Bianchet, M., and Côté, S. D. (2012). Shifting targets in the tundra: protection of migratory caribou calving grounds must account for spatial changes over time. *Biol. Conserv.* 147, 163–173. doi: 10.1016/j.biocon.2011.12.027

Tappen, M. (1994). Bone weathering in the tropical rain forest. *J. Archaeol. Sci.* 21, 667–673. doi: 10.1006/jasc.1994.1066

Tappen, M. (1995). Savanna ecology and natural bone deposition: implications for early hominid site formation, hunting, and scavenging. *Curr. Anthropol.* 36, 223–260. doi: 10.1086/204353

Telford, R. J., Heegaard, E., and Birks, H. J. B. (2004). The intercept is a poor estimate of a calibrated radiocarbon age. *Holocene* 14, 296–298. doi: 10.1191/0959683604hl707fa

Terry, R. C. (2009). The dead do not lie: using skeletal remains for rapid assessment of historical small-mammal community baselines. *Proc. R Soc. B* 324, 1061–1064. doi: 10.1098/rspb.2009.1984

Thompson, D. C., and McCourt, K. H. (1981). Seasonal diets of the Porcupine Caribou Herd. *Am. Midl. Nat.* 105:70. doi: 10.2307/2425011

Todisco, D., and Monchot, H. (2008). Bone weathering in a periglacial environment: the Tayara Site (KbFk-7), Qikirtaq Island, Nunavik (Canada). *Arctic* 61, 87–101. doi: 10.14430/arctic9

Tomasovych, A., and Kidwell, S. M. (2017). Nineteenth-century collapse of a benthic marine ecosystem on the open continental shelf. *Proc. R. Soc. B* 284:20170328. doi: 10.1098/rspb.2017.0328

Trammell, E. J., Carlson, M. L., Fresco, N., Gotthardt, T., McTeague, M. L., and Vadapalli, D. (eds.). (2015). *North Slope Rapid Ecoregional Assessment*. Prepared for the Bureau of Land Management. Anchorage, AK: U.S. Department of the Interior.

Tucker, M. A., Böhning-Gaese, K., Fagan, W. F., Fryxell, J. M., van Moorter, B., Alberts, S. C., et al. (2018). Moving in the Anthropocene: global reductions in terrestrial mammalian movements. *Science* 359, 466–469. doi: 10.1126/science.aam9712

U.S. Fish and Wildlife Service. (2015). "Chapter 4: affected environment," in *Arctic National Wildlife Refuge Revised Comprehensive Conservation Plan* (Fairbanks, AK: U.S. Fish and Wildlife Service), 255.

Udall, M. (1980). "H.R.39. Alaska national interest lands conservation act," in *96th Congress of the United States of America* (Washington, DC).

Uno, K. T., Quade, J., Fisher, D. C., Wittemyer, G., Douglas-Hamilton, I., Andanje, S., et al. (2013). Bomb-curve radiocarbon measurement of recent biologic tissues and applications to wildlife forensics and stable isotope (paleo)ecology. *Proc. Natl. Acad. SciU.S.A.* 110, 11736–11741. doi: 10.1073/pnas.1302226110

USA-Canada. (1987). *Agreement Between the Government of Canada and the Government of the United States of America on the Conservation of the Porcupine Caribou Herd*. Washington, DC: Government of the United States of America.

Vistnes, I., and Nellemann, C. (2008). The matter of spatial and temporal scales: a review of reindeer and caribou response to human activity. *Polar Biol.* 31, 399–407. doi: 10.1007/s00300-007-0377-9

Vors, L., Schaefer, J., Pond, B., Rodgers, A., and Patterson, B. (2010). Woodland caribou extirpation and anthropogenic landscape disturbance in Ontario. *J. Wild. Manage* 71, 1249–1256. doi: 10.2193/2006-263

Vors, L. S., and Boyce, M. S. (2009). Global declines of caribou and reindeer. *Glob. Chang. Biol.* 15, 2626–2633. doi: 10.1111/j.1365-2486.2009.01974.x

Western, D., and Behrensmeyer, A. K. (2009). Bone assemblages track animal community structure over 40 years in an African savanna ecosystem. *Science* 324, 1061–1064. doi: 10.1126/science.1171155

Whitten, K. R. (1994). "International cooperation in managing the Porcupine Caribou Herd," in *74th Annual Conference Westen Association of Fish and Wildlife Agencies* (Alaska), 64–68.

Whitten, K. R. (1995). Antler loss and udder distention in relation to parturition in caribou. *J. Wild Manage* 59, 273–277. doi: 10.2307/3808940

Whitten, K. R., and Cameron, R. D. (1983). Population dynamics of the Central Arctic Herd, 1975-1981. *Acta Zool. Fennica* 175, 159–161.

Whitten, K. R., Garner, G. W., and Mauer, F. J. (1984). "Calving distribution, initial productivity, and neonatal mortality of the Porcupine Caribou Herd, 1983," in *Arctic National Wildlife Refuge Coastal Plain Resource Assessment, 1983 Update Report Baseline Study of the Fish, Wildlife, and Their Habitats*, eds G. W. Garner and P. E. Reynolds (Anchorage, AK: United States Fish and Wildlife Service), 359–420.

Whitten, K. R., Garner, G. W., Mauer, F. J., and Harris, R. B. (1992). Productivity and early calf survival in the Porcupine caribou herd. *J. Wild Manage*. 201–212. doi: 10.2307/3808814

Widga, C., Walker, J. D., and Boehm, A. (2017). Variability in bioavailable $^{87}Sr/^{86}Sr$ in the North American midcontinent. *Open Quat*. 3, 4–7. doi: 10.5334/oq.32

Wilson, F. H., Hultz, C. P., Mull, C. G., and Karl, S. M. (2015). *Geologic Map of Alaska*. U.S.: Geological Survey Scientific Investigations Map 3340. doi: 10.3133/sim3340

Wilson, R., Parrett, L., Joly, K., and Dau, J. (2016). Effects of roads on individual caribou movements during migration. *Biol. Conserv*. 195, 2–8. doi: 10.1016/j.biocon.2015.12.035

Zalatan, R., Gunn, A., and Henry, G. H. R. (2006). Long-term abundance patterns of barren-ground caribou using trampling scars on roots of *Picea mariana* in the Northwest Territories, Canada. *Arct. Antarct. Alp. Res.* 38, 624–630. doi: 10.1657/1523-0430(2006)38[624:LAPOBC]2.0.CO;2

Conflict of Interest: The authors declare that the research was conducted in the absence of any commercial or financial relationships that could be construed as a potential conflict of interest.

frontiers in Ecology and Evolution

ORIGINAL RESEARCH
published: 05 February 2021
doi: 10.3389/fevo.2020.588422

Strontium Is Released Rapidly From Agricultural Lime–Implications for Provenance and Migration Studies

Rasmus Andreasen and Erik Thomsen*

Department of Geoscience, Aarhus University, Aarhus, Denmark

The use of strontium isotopes in pre-historic mobility studies requires accurate isoscapes for evaluating whether pre-historic individuals are local to the areas in which they were buried or not. Isoscapes are often based on modern-day samples, commonly surface waters. There is, however, growing evidence that modern-day farming has a significant impact on the strontium isotopic composition of surface waters and farmed soils, mainly due to the use of agricultural lime for soil improvement. In this paper, we investigate the fate of strontium from agricultural lime in an experimentally-manipulated field in central Jutland, Denmark. Agricultural limestone was added to this field at very high rates in 2012 and 2013 to investigate CO_2 storage in soils. Strontium was first measured from the site in 2014. In 2019 we reevaluated strontium concentrations and found that 80–100% of the strontium from the agricultural lime had leached out of the organic-rich topsoil, and likely seeped into the underlying groundwater and nearby surface waters. In both the sandy soils of the liming test site and farmed soils and heathland in the adjacent area, Sr exhibits a degree of mobility similar to that of calcium, which is in agreement with data for other soil types and what is predicted by the size of its hydrated ions. Strontium isotopic compositions of unfarmed heathland samples show much higher $^{87}Sr/^{86}Sr$ ratios, and so are not influenced by carbonates, suggesting that the limestone $^{87}Sr/^{86}Sr$ signature seen in the farmland and in streams and rivers in contact with this comes from agricultural lime, and not from natural carbonate relicts occasionally found in the area. This suggests that the $^{87}Sr/^{86}Sr$ signatures of the area were higher in pre-historic times, and that an isoscape map based on samples from modern-day farmland is inappropriate for application to provenance and mobility studies of pre-historic people. Thus, it is critical that the possible impact of farming is evaluated when conducting provenance and mobility studies, especially in areas with Sr-poor soils and where agricultural lime is used for soil improvement. Overlooking this can result in significant overestimation of the degree of pre-historic mobility.

Keywords: $^{87}Sr/^{86}Sr$, agricultural lime, pre-historic human mobility, element mobility, glacial deposit, soil profile

OPEN ACCESS

Edited by:
Joshua H. Miller,
University of Cincinnati, United States

Reviewed by:
Lihai Hu,
University of Ottawa, Canada
Chris Widga,
East Tennessee State University, United States

****Correspondence:***
Rasmus Andreasen
rasmus.andreasen@geo.au.dk

Specialty section:
This article was submitted to Paleoecology, a section of the journal Frontiers in Ecology and Evolution

Received: *28 July 2020*
Accepted: *29 December 2020*
Published: *05 February 2021*

Citation:
Andreasen R and Thomsen E (2021) Strontium Is Released Rapidly From Agricultural Lime–Implications for Provenance and Migration Studies. Front. Ecol. Evol. 8:588422. doi: 10.3389/fevo.2020.588422

INTRODUCTION

For the past 35 years, strontium isotopes have been used to elucidate the histories of our pre-historic ancestors, from analyses of their remains, food, tools and other artifacts (e.g., Ericson, 1985; Müller et al., 2003; Haak et al., 2008; Knipper et al., 2017; Madgwick et al., 2019). The strontium (Sr) method is based on the observation that $^{87}Sr/^{86}Sr$ ratios in soils vary geographically, reflecting the compositions of the soil and the underlying geology (e.g., Faure et al., 1967; Capo et al., 1998; Blum et al., 2000; Montgomery et al., 2007). Strontium is released from the substrate to the groundwater and surface waters, and becomes bioavailable, so that it is taken up in plants and animals, with no change to the average $^{87}Sr/^{86}Sr$ ratio (Blum et al., 2000; Bentley, 2006; Montgomery, 2010), making Sr a powerful tracer of the origin and migration history of people and animals during pre-historic times. In order to interpret measured $^{87}Sr/^{86}Sr$ ratios of archeological artifacts from such pre-historic individuals, these must be compared to a reference map showing the $^{87}Sr/^{86}Sr$ ratios of the bioavailable Sr in the area in which the artifacts were found. Thus, the success of the Sr method hinges on the accuracy of the reference map or *isoscape*. In the absence of contemporaneous samples of known geographical origin, construction of a given isoscape is based on data measured on present-day samples of surface waters, plants, animal bones, or soils (e.g., Grimstead et al., 2017; Bataille et al., 2018, 2020). A key assumption of the Sr method is that the $^{87}Sr/^{86}Sr$ signatures measured in the environment today is the same as those that would have been imparted to people during pre-historic times.

Yet there is growing evidence that modern-day farming can impact the $^{87}Sr/^{86}Sr$ ratios of the surface environment to such an extent that $^{87}Sr/^{86}Sr$ signatures measured today may be radically different than those that existed in preindustrial times, especially due to the use of agricultural lime in farming (Böhlke and Horan, 2000; Oh and Raymond, 2006; Aquilina et al., 2012; Maurer et al., 2012; Thomsen and Andreasen, 2019). This can lead to erroneous conclusions regarding the origin and mobility of pre-historic individuals, as the application of agricultural lime to low-calcareous soils can significantly lower the $^{87}Sr/^{86}Sr$ ratio of an entire watershed (Thomsen and Andreasen, 2019). In the cases of iconic Bronze Age females, The Egtved Girl and The Skrydstrup Woman, buried in central Jutland, Denmark, this effect was shown to lower the $^{87}Sr/^{86}Sr$ signatures of the local, modern watersheds from around 0.713 to 0.709, making it appear that these individuals must have come from afar, though there is no chemical or archaeological evidence to suggest that they came from anywhere other than the areas in which they were buried (Thomsen and Andreasen, 2019). Recently, the fate of Sr from agricultural lime was questioned in an article by Frei et al. (2020a), who hypothesize that Sr from agricultural lime is retained indefinitely in organic-rich farmed topsoils, and that the lime-influenced Sr isotopic signatures observed in surface waters—including lakes and rivers, comes predominantly from the dissolution of naturally-occurring carbonates in the deeper, less organic-rich parts of the soil (Frei et al., 2020a).

However, it is challenging to chemically distinguish agricultural lime from naturally-occurring limestone in a soil, as agricultural lime is nothing more than pulverized, naturally-occurring limestone, and thus is very similar to other naturally-occurring limestones. Marine limestones have the $^{87}Sr/^{86}Sr$ signature of seawater at the time that the lime was deposited (Edmond, 1992), and though the $^{87}Sr/^{86}Sr$ compositions of the oceans have changed significantly though geologic time, the variations of $^{87}Sr/^{86}Sr$ signatures in marine carbonates are very small (0.7067–0.7094—Veizer et al., 1999) compared to the variations in siliciclastic sediments and bedrock (0.703–>0.725—e.g., Hoogewerff et al., 2019; Bataille et al., 2020). One approach to studying the release of Sr from agricultural lime into the environment is using test fields where known quantities of agricultural lime have been applied to parts of the field, while other parts of the fields are used as control sites. One such test field is located in Voulund, south of the town of Ikast in central Jutland, Denmark, where the Geological Survey of Denmark and Greenland (GEUS) conducted CO_2 storage in soil experiments from 2010 to 2014, by applying massive quantities of agricultural lime to farmland soil, in an attempt to increase the CO_2 binding capacity of the soil. This test field was later used by Frei et al. (2020a) as "a representative site in the West Jutland sandy outwash plain" in their paper concluding that Sr from agricultural lime is retained in topsoils indefinitely, and does not contribute to the $^{87}Sr/^{86}Sr$ ratios of surface waters in contact with these. We reinvestigated this site 5 years later to study the fate of the Sr in the soils.

METHODS

Massive quantities of agricultural lime were applied to parts of the test field at Voulund (56, 02, 06 N; 9, 10, 24 E) in 2012 and 2013 by Jessen et al. (2014a), as part of their experiments on CO_2 storage in soils. The test field is located on a glacial outwash plain from the Weichsel ice age (**Figure 1**), and has been farmed for at least 100 years. The site was split into 4 quadrants (A,B,C, and D) (Jessen et al., 2014a,b), and agricultural lime was supplied at a rate of 32 t/ha to quadrants B and C in 2013, and at a rate of 4 and 16 t/ha to B & C, respectively, in 2012, for a total 36 t/ha lime added to B, and 48 t/ha lime to C. Quadrants B and C differed, in that the topsoil in C was later homogenized through tillage, while quadrant B was no-till farmed, during the course of the experiment. Quadrants A and D were used as control sites. For the duration of the experiment, barley (*Hordeum vulgare*) was grown in quadrants A, B, & C, and maize (*Zea mays*) in quadrant D. After the experiments ended in 2014, all quadrants were planted with Christmas trees (*Picea abies*), which are still growing in the field today. These trees have received only a minimal amount of NPK fertilizer by hand, and no agricultural lime, according to the farmer. The test field site was split from a larger field in 2010, and the rest of this field (**Figure 1**) has remained actively-farmed, with crop rotation every 2 years between barley (*Hordeum vulgare*) and potatoes (*Solanum tuberosum*). North of the field lies a forest and heathland (**Figure 1**), which has not been farmed in historical times.

Quadrants A, B, and C were selected for analysis in this study, along with a site in the currently-farmed field F, due to

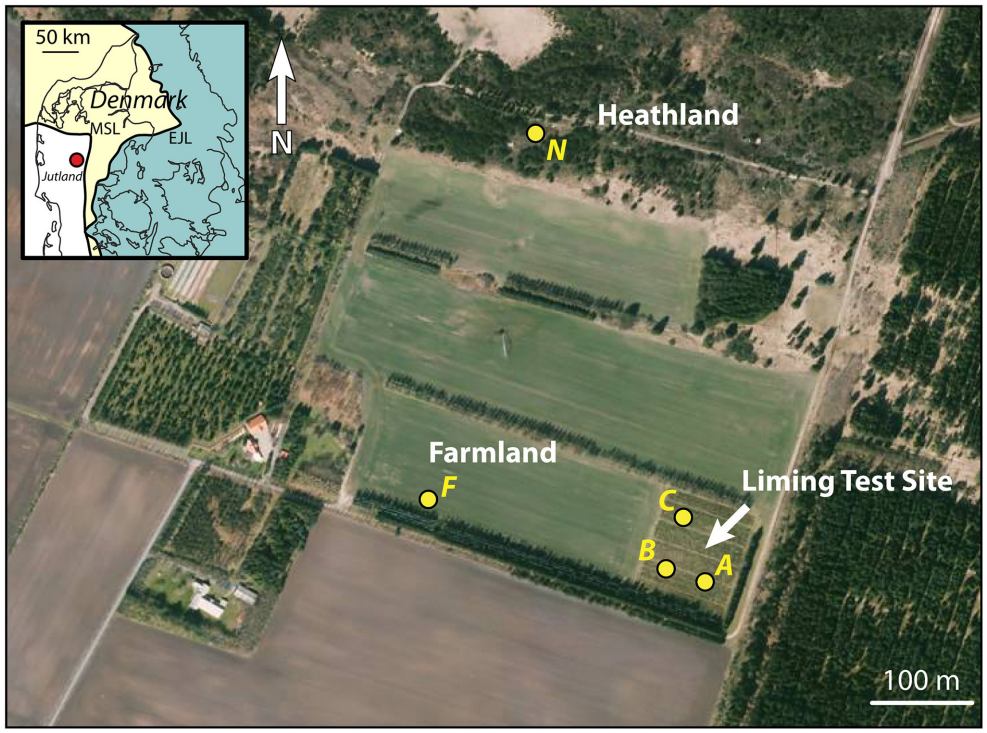

FIGURE 1 | Orthophoto from the spring of 2019 of the liming test site at Voulund with surrounding farm- and heathland. The locations of soil profiles (A, B, & C) within the liming test site, and F & N on farm- and heathland are indicated with yellow dots. Map insert shows the locality relative to the two major ice front locations during the Weichselian Ice Age (Houmark-Nielsen, 2003). Orthophoto from *Styrelsen for Dataforsyning og Effektivisering*—Denmark.

the similarities in soil use. Additionally, a site on the unfarmed heathland, N was selected for comparison (**Figure 1**). As the CO_2 storage experiments focused on the mobility of major cations, Sr was not monitored continuously, but soil samples taken in March 2014 from quadrant C—the most intensively limed quadrant—was measured for Sr concentrations and $^{87}Sr/^{86}Sr$ compositions by Frei et al. (2020a), though this site certainly cannot be described as typical farmland, as is implied in Frei et al. (2020a), as the liming rates employed over the duration of the CO_2 storage experiments were ca. 48 times higher than those of currently-farmed site, F, which receives around 2 t/ha every 4 years, according to the farmer. The data presented in Frei et al. (2020a) show that Sr concentrations are very low in soils below the organic-rich topsoil. This is an expected finding, as the substratum is a glacial meltwater sand, consisting predominantly of quartz, and thus has a very low cation exchange capacity. The layer of meltwater sand starts at a depth of 40–50 cm and continues to the groundwater table at a depth of around 6 m and beyond. Thus, rapid transfer of cations to the groundwater is expected, from the point that cations enter the meltwater sand in the unsaturated zone. Consequently, the depth of the soil pits in this study were limited to around 70 cm, in order to capture the transition from the organic-rich topsoil to the meltwater sand, as well as the compositions of the topmost layers of meltwater sand, whilst avoiding unnecessary large scale excavation.

A schematic drawing of the soil profiles and a photo of profile A is shown in **Figure 2**. Profiles A, B, C, and F each have an organic-rich topsoil layer of ca. 40 cm thickness, with a sharp boundary to the quartz-rich meltwater sand below. Profiles A and B contain slivers of meltwater sand within the organic-rich topsoil, which stem from plowing. Profile N is the only profile with developed soil horizons, consisting of a thin very organic-rich O-horizon, underlain by a bleached E-horizon of bluish-gray sand, and a B-horizon with reddish sand, and signs of iron-oxy-hydroxide accumulation, underlain by meltwater-sand at a depth of 34 cm.

The soil profiles were sampled every 5–10 cm (**Figure 2**), and were sampled carefully, to avoid sampling the boundaries between units. A total of 49 samples were collected from the five profiles. These were supplemented by 8 soil samples from four of the locations (7 from non-farmed soils and 1 from farmed soil) in central and eastern Jutland, including the Vallerbæk Tributary of the Karup River studied in Thomsen and Andreasen (2019), such that in all, 57 samples were obtained for analysis. Samples were collected in plastic bags and dried for 2 days at 40°C. In order to examine the budget of bioavailable and easily-leachable major and trace elements from the soils, 3 aliquots of around 5 grams each were weighed out from each sample, after the samples had been dried. To the first of the 3 aliquots, 10 ml of 1.0 M ammonium nitrate (NH_4NO_3) were added for 2 h to extract the bioavailable fraction of cations (Willmes et al., 2018; Hoogewerff et al., 2019). To the second fraction, 10 ml of 0.2 M acetic acid (CH_3COOH) was added for 1 h to extract easily leachable cations and dissolve any limestone present in

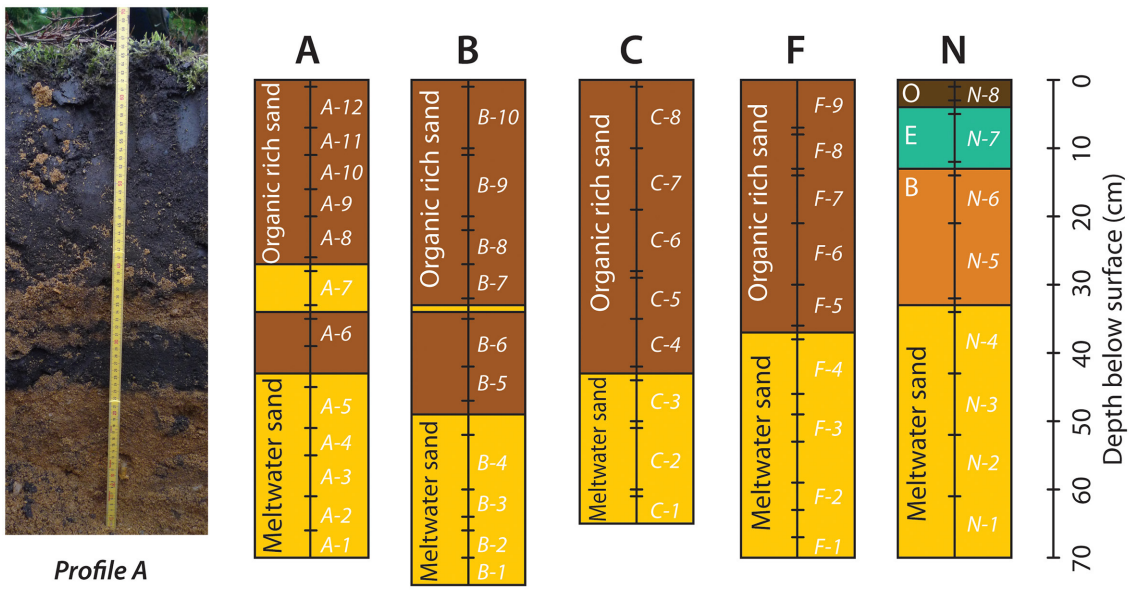

FIGURE 2 | Photograph of soil profile A, and schematic drawings of the 5 soil profiles with lithologies and sampling depth. See **Figure 1** for the position of the soil profiles. Photo by Claus Heilmann Clausen.

the soil (Frei et al., 2020a). To the last fraction, 10 ml of MQ-water (18.2 MΩ) was added for 3 weeks to simulate rainwater percolating through the soil. All three fractions were agitated at regular intervals (every 15 min for the samples in ammonium nitrate and acetic acid, and daily for the samples in water) for the duration of the extraction. Following extraction, the leachate was pipetted from each sample, centrifuged, and analyzed for trace element analyses by quadruple ICP-MS. In addition, Sr isotopic analyses were conducted by MC-ICP-MS for soil samples from the unfarmed, heathland (Profile N), and on soil samples taken adjacent to the Vallerbæk tributary of the Karup River, where water samples had been analyzed by Thomsen and Andreasen (2019), in order to compare these with existing soil and water data, and with the data from the Voulund test site. Three soil samples were analyzed from the Vallerbæk tributary, two from either side of the brook, from where it leaves the mixed heath and forest, and enters the farmland, and one (Sample VS1) from the forest, a little removed from the brook—a site selected in order to sample an area shielded by trees from the dust blown from the farmed fields, by the predominantly westerly winds. The two samples from either side of the brook were obtained <5 m apart—one from the farmed field (Sample KF), the other from the shrubland immediately opposite the field (Sample KM).

Trace Element Analysis

The centrifuged soil leachate samples were diluted with 2% HNO_3 and analyzed for selected major and trace elements by solution quadrupole ICP-MS on an Agilent 7900, at the Department of Geoscience, Aarhus University. Each set of soil leachates, ammonium nitrate, acetic acid, and water were run independently with matrix-matched multi-element standards and NIST 1643-F for calibration and quality control. Concentrations of Li, Be, Na, Mg, Al, K, Ca, V, Cr, Mn, Fe, Co, Ni, Cu, Zn, Ga, As, Rb, Sr, Ag, Cd, Cs, Ba, Tl, Pb, and U were determined. The concentrations of Li, Be, V, Cr, Cu, Ga, As, Ag, Cs, and U were generally below detection level for all samples. The concentration of Na, Mg, Al, K, Ca, Mn, Fe, Co, Ni, Zn, Rb, Sr, Cd, Ba, Tl, and Pb are given in **Supplementary Table 1** as ppm or ppb (mg/kg or μg/kg) normalized to the dry weight of the soil sample.

Strontium Isotope Analyses

The centrifuged soil leachate samples and two samples of rainwater were dried down and digested overnight in 2 ml of aqua regia, dried down again, and dissolved in nitric acid for Sr separation chemistry. Strontium was separated from the sample matrix using Eichrom (TrisKem International) Sr spec resin and analyzed for isotopic composition using a Nu Plasma II multicollector ICP-MS (inductively coupled plasma mass spectrometer) at the Department of Geoscience, Aarhus University. The four stable isotopes of strontium (^{84}Sr, ^{86}Sr, ^{87}Sr, and ^{88}Sr) were measured simultaneously, as were isotopes of Kr, Rb, Y, and doubly charged REE, to monitor and correct for interferences. Masses 82, 83, 84, 85, 86, 87, 88, and 89 were measured simultaneously, as were half-masses 83.5, 84.5, 85.5, 86.5, and 87.5. Baselines were determined by on-peak zero, and each sample run consisted of 400 s of peak time. Data were fractionation-corrected using the exponential law and normalized to NBS SRM 987 ($^{87}Sr/^{86}Sr = 0.71025$). Samples of Holocene foraminifera (*Baculogypsina sphaerulata*), expected to give a modern-day seawater Sr isotope value ($^{87}Sr/^{86}Sr = 0.70917$—Dia et al., 1992) were processed along with the

samples as a secondary standard. Three samples of foraminifera analyzed throughout the analytical campaign gave $^{87}Sr/^{86}Sr = 0.709173 \pm 5$ (7 ppm, 2σ). The reproducibility of individual measurements of samples is estimated at 25 ppm (2σ), based on repeat measurements of standards and samples. The Sr isotopic compositions of the analyzed samples are given in **Table 1**. Strontium isotopic compositions from Profile C have been found to be dominated by limestone (Frei et al., 2020a). It was therefore deemed unnecessary to repeat Sr isotopic measurements on the soils from the liming test site. The results of the strontium isotope measurements are presented in **Table 1**.

RESULTS

The concentrations of most trace elements are highest in the (bioavailable) ammonium nitrate leach (see **Supplementary Table 1**), which is in good agreement with the assumption that this is the most aggressive of the leaches applied in this study (Willmes et al., 2018). Notable exceptions are the concentrations of Ca and Sr in the topmost sample from Profile B, which contained visible pieces of agricultural lime that reacted vigorously with the acetic acid. There, the Ca and Sr concentrations in the acetic acid leach are higher than in the ammonium nitrate leach. Concentrations of alkali metals and alkaline earth metals (Groups I and II of the periodic table) are generally higher in the extracts from organic-rich soils than in the extracts from sandy soils, whereas the concentrations of transition elements are similar in the organic-rich soils and the sandy ones. Calcium concentrations range from 0.3 ppm to nearly 2,300 ppm in the ammonium nitrate extracts, from 0.3 ppm to nearly 5,800 ppm in the acetic acid extracts, and 0.1 ppm to 100 ppm in the water extracts. Strontium concentrations range from 7 ppb to 8.5 ppm in the ammonium nitrate extracts, from 4 ppb to 15.5 ppm in the acetic acid extracts, and from 1 ppb to 0.4 ppm in the water extracts. The heathland profile, N exhibits the largest gradients in elemental concentrations, with high concentrations in the O-horizon, intermediate concentrations in the E- and B-horizons, and very low concentrations in the meltwater sand below the B-horizon. This is an unsurprising result, as these are the only soils that have not been mechanically mixed by tilling. The strontium isotopic compositions of the heathland soils show much greater variation than those seen in the test site soils. The $^{87}Sr/^{86}Sr$ ratios of the ammonium nitrate extracts of the heathland soils, Profile N, increase systematically with depth—from 0.7122 in the O-horizon to 0.7270 in the meltwater sand at a depth of 70 cm (**Table 1**). This variation is much greater than that found for the liming test site, Profile C, where the $^{87}Sr/^{86}Sr$ ratios in ammonium nitrate leachates from the meltwater sand range from 0.7081 to 0.7108 (Frei et al., 2020a), though (near total dissolution) aqua regia extracts from Profile C have strontium ratios up to 0.7267 (Frei et al., 2020a), similar to what is found in Profile N samples leached in ammonium nitrate.

DISCUSSION

The Mobility of Strontium

When comparing the degrees of mobility for different elements in soils, it is useful looking at elemental ratios rather than concentrations, as this allows for a direct comparison of the relative mobility of pairs of elements, while avoiding the issue of dilution with inert or mostly inert phases, such as quartz in these sandy soils. In **Figure 3**, ratios for the mobile alkali metals and alkaline earth metals are plotted for the water and acetic acid leachates against those of the ammonium nitrate leachate for the same sample. The relative strength of the three extracts are: water < acetic acid < ammonium nitrate, such that when compared to the ammonium nitrate leach, the greatest enrichment of a more mobile element (relative to a less mobile one) is expected in the water leach. Such an enrichment is also expected in the acetic acid leach, though to a lesser degree than in the water leach. This effect is exhibited by the period 3 and 4 alkali metals, sodium (Na) and potassium (K) (**Figure 3A**), where the 1:1 line represents ammonium nitrate. The slope of the water extracts is significantly lower than that of the acetic acid extracts, which is significantly lower than that of the ammonium nitrate ones. Slopes <1:1 indicate that the element in the denominator is more mobile than the element in the numerator. In this case, Na is more mobile than K. The same is the case for the period 3 and 4 alkaline earth metals, magnesium (Mg) and calcium (Ca), (**Figure 3B**), where the slopes for the water- and acetic acid extracts are also below the 1:1 line, expressing the fact that Mg is more mobile than Ca. For the alkali metals of group 4 and 5, potassium and rubidium (Rb) (**Figure 3C**), the slopes for the water and acetic acid extracts are above the 1:1 line, and the slope for the water extracts is the steepest. Thus, K is more mobile than Rb. The high degree of scatter is primarily caused by the samples from Profile F—the only currently-farmed soil, and likely reflect the farmer's use of water-soluble NPK fertilizer, which has high K/Rb ratios.

The relationship between period 4 and 5 alkaline earth metals, calcium and strontium (**Figure 3D**) is different, however, in that all three extracts have the same relationship. This implies that the mobility of calcium and strontium is very similar. A few samples fall off the 1:1 line—the N-7 and N-6 samples, which represent the E- and part of the B-horizons from the Profile N heathland soil. These all have lower Ca/Sr in the water- and acetic acid extracts than in the ammonium nitrate extract, implying that Sr is released preferentially to Ca from these soils. Interestingly, this is not the case for the O-horizon, which falls on the 1:1 line. Samples containing pieces of agricultural lime fall above the 1:1 line in **Figure 3D**, as the acetic acid preferentially dissolves the lime, which is richer in Ca relative to Sr. Overall, the slopes for the water- and acetic acid extracts are within error of 1, showing that Sr is as mobile as Ca in the soils studied here (**Figure 3E**). For period 5 and 6 alkaline earth metals, strontium and barium (Ba), the slopes of the water- and acetic acid extracts are both above the 1:1 line, and the slope of the water extract is the steepest, showing that Sr is more mobile than Ba.

The retention of cations in the soil is a function of ionic charge, ionic size of the hydrated ions, the cation exchange

TABLE 1 | Strontium isotopic compositions and concentrations of analyzed soil samples and samples of rainwater and samples of modern day foraminifera analyzed for quality control.

Sample	°N	°E	Horizon	Depth (cm)	Sr (ppm)	1/Sr	$^{87}Sr/^{86}Sr$
N-8 AN	56.03874	9.07170	O	0–4	5.09	0.20	0.71222 ± 2
N-8 AA	–	–	–	–	0.35	2.8	0.71219 ± 2
N-7 AN	–	–	E	4–13	0.36	2.8	0.71363 ± 2
N-6 AN	–	–	B	13–21	0.11	9.3	0.71577 ± 2
N-5 AN	–	–	B	21–33	0.03	31.1	0.71747 ± 2
N-4 AN	–	–	MW	33–43	0.03	37.1	0.71898 ± 2
N-3 AN	–	–	MW	43–52	0.01		
N-2 AN	–	–	MW	52–61	0.01	77.3*	0.72735 ± 2*
N-1 AN	–	–	MW	61–70	0.01		
KF AN	56.26960	9.23059		10–20	6.62	0.15	0.70790 ± 2
KF AA	–	–		–	3.67	0.27	0.70775 ± 2
KM AN	56.26958	9.23055		10–20	0.32	3.1	0.71369 ± 2
KM AA	–	–		–	0.21	4.7	0.71304 ± 2
VS1 AN	56.26670	9.23410		10–20	0.28	3.5	0.71692 ± 2
VS1 AA	–	–		–	0.15	6.7	0.71613 ± 2
Rain (Sept. 11, 2019)#	56.16360	10.20856			0.0005	2146	0.70980 ± 2
Rain (Sept. 13, 2019)	55.97281	10.14569			0.0001	12591	0.70917 ± 10
Baculogypsina sphaerulata 1§						0.70917 ± 2	
Baculogypsina sphaerulata 2						0.70917 ± 2	
Baculogypsina sphaerulata 3						0.70917 ± 2	

AN denotes ammonium nitrate extract. AA denotes acetic acid extract. MW denotes meltwater sand without discernible soil horizon development. Samples N-3 AN, N-2 AN, N-1 AN were combined before separation of Sr due to the similarity between samples their low strontium concentrations. Strontium concentrations of rain samples were calculated based on recovery of strontium in the isotopic measurement. Strontium concentrations of other samples were measured by Q-ICP-MS.

** Sample N-1 AN, N-2 AN, and N-3 AN were combined for Sr isotope analysis.*

 # This rainstorm was the remnants of Hurrican Dorian.

§ Holocene Foraminifera (Okinawa, Japan). Has the Sr isotopic composition of Modern Day Seawater.

capacity of the soil, and the redox conditions of the soil (Marcus, 2016), in a complex relationship that is also dependent on the composition of porewater and organic matter in the soils, the compositions of which may change with time. There is a strong correlation between the observed mobility in the sandy soils and the limiting ionic conductivity for the alkali metals and alkaline earth metals, which are not redox sensitive; and this is also an indicator for element mobility (Burgess, 2011). The soils studied here are from 3 different glacial outwash plains and 2 samples from a moraine; and these soils exhibit a wide range of organic content, from nearly nothing to around 5%, which is common for farmland located on glacial outwash plains in Europe and North America (Krüger et al., 2013). Otherwise, these soils can be seen as a common matrix, such that the relative mobilities of elements determined here are valid for such soils of similar types. Strontium is as mobile as calcium, and more mobile than barium in the very soils studied by Frei et al. (2020a) (**Figure 3**), such that there is certainly no reason to suspect that the Sr from agricultural lime will accumulate in the topsoil over time, as hypothesized by those authors, and in spite of the fact that calcium is widely regarded as a highly mobile element (e.g., Burgess, 2011). This is supported both by other studies that find significant Sr mobility in waters (e.g., Solecki, 2005; Wallace et al., 2012), and by the very similar behavior of Ca and Sr in most soil types (Smičiklas et al., 2015). The adsorbtion of Ca and Sr on DNA also appear to be similar to each other and different from the other alkaline earth metals (Long et al., 2020), which could explain the behavior observed in the organic-rich soils, where Ca and Sr appear to be equally mobile, though more work is needed to see whether this relationship is common for alkaline earth metal complexes with organic material.

The Fate of Strontium From Agricultural Lime

The liming test site in Voulund presents a unique opportunity to estimate the rate at which Sr from agricultural lime is mobilized from a soil. Frei et al. (2020a) speculated that the majority of Sr from agricultural lime is retained in the soil indefinitely, though did not provide any calculations showing how much of the Sr they measured in 2014 was there before the massive additions of agricultural lime in 2012 and 2013. By comparing the amounts and distribution of Sr within the soils of the five profiles, the rates of liming in 2012 and 2013 (Jessen et al., 2014a), and the Sr concentrations in Profile C in 2014 (Frei et al., 2020a) it is

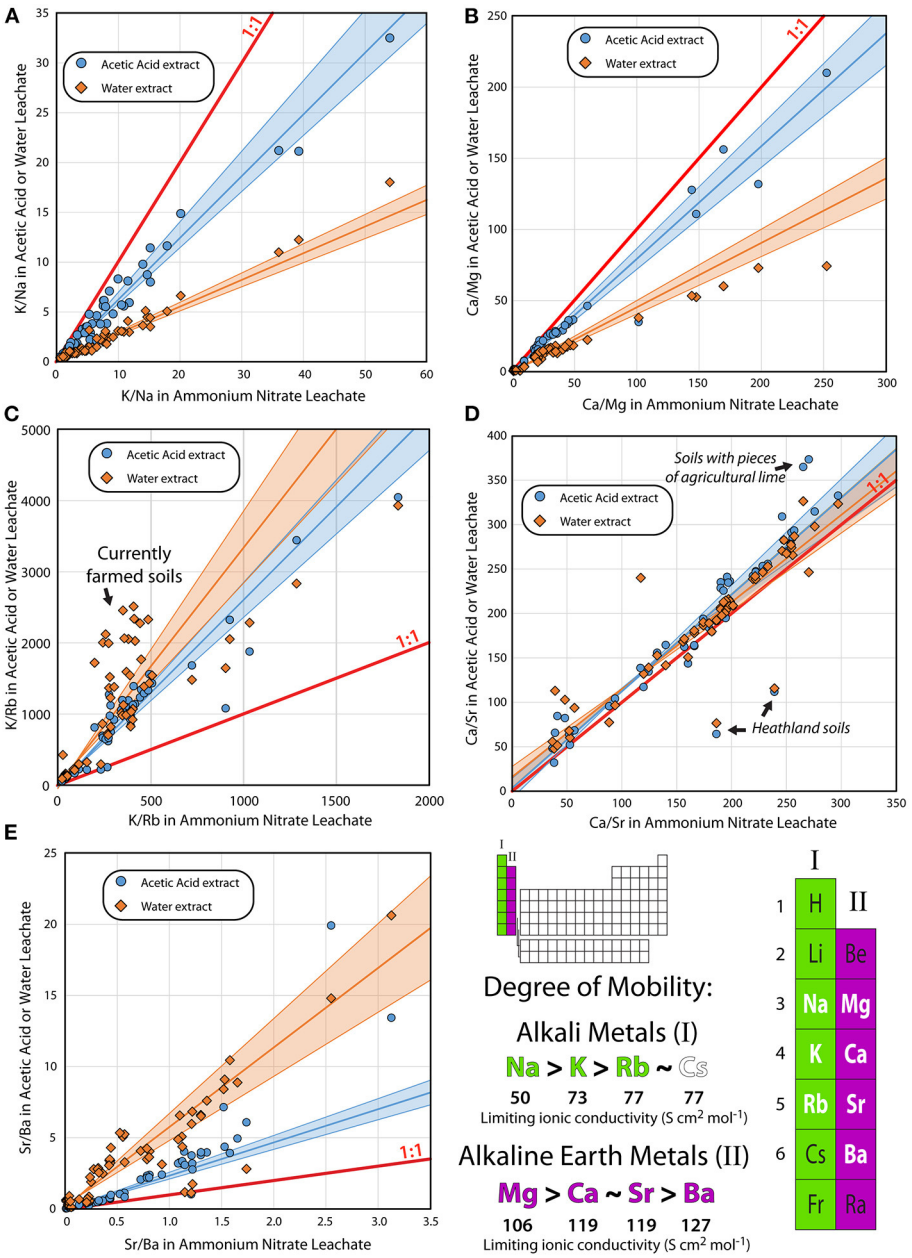

FIGURE 3 | Relative mobility of the major alkali metals and alkaline earth metals (groups I and II in the periodic table). **(A–E)** Ratios in leachates of water (orange diamonds) and 0.2 M acetic acid (light blue circles) on the y-axis compared with the ratios of 1.0 M ammonium nitrate leachates of the same soil sample. Also shown are 1:1 and best fit regression lines and 95% confidence intervals [calculated using IsoplotR—Vermeesch (2018)] for the data. Slopes shallower than 1:1 indicate that the element in the numerator is more mobile in the weaker water- and acetic acid leachates than in the ammonium nitrate leach. Slopes steeper than 1:1 indicate that the element in the denominator is more mobile, whereas slopes following 1:1—including the slope of Ca/Sr—indicate that the two elements are equally mobile. Limiting ionic conductivities are from Burgess (2011).

possible to construct a mass balance for the Sr in the agricultural lime applied to the liming test site in 2012 and 2013.

In **Figure 4**, the Sr concentrations in the five soil profiles from Voulund are shown for both the ammonium nitrate- and acetic acid leaches. Apart from the topmost part of Profile B, which contains residual agricultural lime, the Sr concentration is higher for all samples in the ammonium nitrate leach. The Sr concentration in Profile N—the heathland, is highest in the O-horizon, and decreases rapidly and systematically with depth. Perhaps surprisingly, the Sr concentration of the O-horizon in Profile N is the same as the topsoil in the heavily-limed Profile C. Profile A—the control site, and Profile F—the currently-farmed

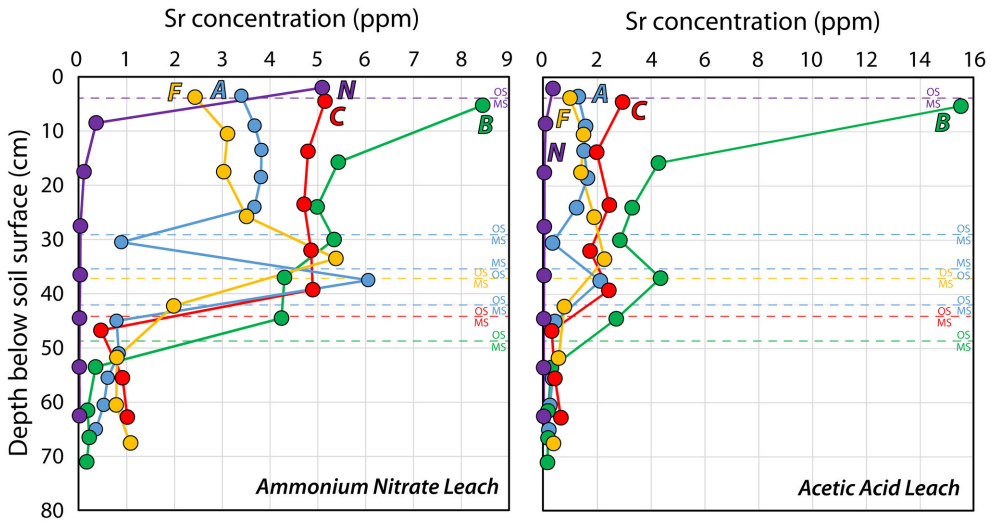

FIGURE 4 | Strontium concentrations in ammonium nitrate- and acetic acid leachates from the five soil profiles; (A, B, C) from the liming test site, the farmland Profile F and the heathland Profile N. See **Figure 1** for locations of soil profiles.

soil, exhibit similar patterns of Sr concentrations, which increase with depth in the organic-rich topsoil and decline sharply in the meltwater sand. This is indicative of Sr leaching from the uppermost topsoil. In Profile C—the limed test site with tilling, the Sr concentration is constant throughout the organic-rich topsoil, but only slightly higher than in Profiles A and F. As in the other profiles, this is followed by a sharp decrease in Sr concentration in the meltwater sand. For Profile B—the untilled, limed test site, the Sr concentration is highest at the top and decreases with depth. This is unsurprising, as there are still pieces of agricultural lime at the surface in Profile B, dissolving and releasing Sr. The differences between Profiles B and C show the effectiveness of tilling in redistributing and breaking down the agricultural lime for the release of Ca (and thus also Sr) for soil improvement. In Profile C, there are no visible pieces of agricultural lime left 6–7 years after the test site was limed with the equivalent of around 96 years' worth of agricultural lime (i.e., 48 t/ha over 2 years compared to the average rate of 2 t/ha every 4 years). The Sr and Ca are homogenously distributed within the organic-rich soil, and the Sr and Ca concentrations in the acetic acid extracts are much lower than those in the ammonium nitrate, suggesting the complete dissolution of the agricultural lime.

So where did the Sr go? **Figure 5** shows the concentrations of Sr in ammonium nitrate- and acetic acid leaches of Profiles A, B, and C in 2019 and in Profile C in 2014 (Frei et al., 2020a). The Sr concentration in the ammonium nitrate leach was higher in the topmost layer of soil (0–10 cm) in 2014 than it was in 2019, and then was similar to that in the untilled Profile B sampled in 2019, but higher in the rest of the organic-rich soil (10–40 cm) in 2019 than it was in 2014. This again demonstrates the effectiveness of tilling in redistributing Sr in soils. For the acetic acid extracts, the concentration of Sr was much higher in 2014 than in 2019, showing that agricultural lime was present in the soil in significant quantities. Unfortunately, the resolution in the acetic acid extract data is limited for 2014, but a simple mass balance can be constructed for comparing the soil profiles, using an estimated soil density (r), which for simplicity's sake is kept constant at 1.5 g/cm^3 for all depths at all profiles, the soil thickness (h), and the strontium concentration at each sampled interval (i) down to a depth of 65 cm, which is the depth of the shallowest profile (Equation 1).

$$\sum_{i=1}^{n} \rho(\mathrm{g/m^3}) \cdot \mathrm{h\,(m)} \cdot \mathrm{Sr\ conc.\ (mg/g)} \qquad (1)$$

Table 2 shows the weighted averages of the amounts of Sr extractable by ammonium nitrate and acetic acid for each of the five profiles measured here, to 65 cm depth, and Profile C in 2014 (Frei et al., 2020a). The control profile, A and the currently-farmed Profile F have nearly the same amount of extractable Sr by both ammonium nitrate and acetic acid. The heathland Profile N, has a much smaller amount of extractable Sr, despite having the same Sr concentration in the top of the profile. This is due to the thin O-horizon in the heathland soil, compared to that in the farmland. The heathland also has by far the smallest fraction of Sr extractable by acetic acid, which is unsurprising, as the soil has never been improved by liming or marling. The untilled Profile B has the most extractable Sr, where more is extractable with acetic acid than ammonium nitrate, due to the presence of agricultural lime. Profile C has the same amount of Sr extractable by ammonium nitrate in 2019 as it did in 2014; on the other hand, the amount of extractable Sr by acetic acid was much greater in 2014 than in 2019. The amount of extractable Sr in 2014 is based on the two available measurements from Frei et al. (2020a), and is listed here as a minimum estimate, as any attempt to inter- and/or extrapolate to the rest of the soil profile is likely to result in a severe overestimation. Based on the amount of agricultural lime

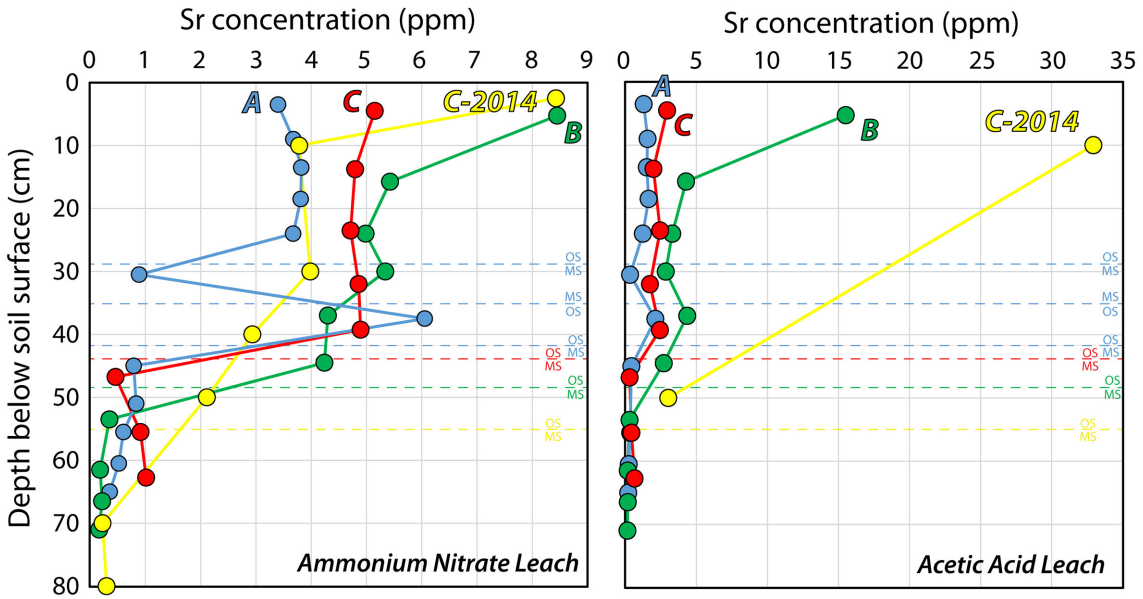

FIGURE 5 | Strontium concentration in the three soil profiles (A, B, C) from the liming test site in ammonium nitrate- and acetic acid leaches. C (2014) shows the concentrations of Sr measured for samples from quadrant C taken in March 2014, about 6 months after the last application of agricultural lime at a rate of 32 t/ha, and 18 months after the first application of agricultural lime at a rate of 16 t/ha, in the course of CO_2 storage experiments (Frei et al., 2020a).

TABLE 2 | The amount of Sr in the top 65 cm of one square meter of each soil profile that is extractable with ammonium nitrate and acetic acid, and the ratio between the two.

Soil profile	Extractable Sr by NH_4NO_3 in the top 65 cm (mg/m^2)	Extractable Sr by CH_3COOH in the top 65 cm (mg/m^2)	Ratio of Sr in soil extracts NH_4NO_3/CH_3COOH
A	2,675	1,030	2.6
B	4,228	4,612	0.9
C	3,402	1,642	2.1
C (2014)	3,390	>5,500	<0.6
F	2,448	1,145	2.1
N	381	46	8.3

Also listed are values measured for Profile C in 2014 by Frei et al. (2020a).

added to Profile C—48 t/ha (i.e., 4.8 kg/m^2–Jessen et al., 2014a) and an estimated Sr concentration in the agricultural lime of 800–1,000 mg/kg (Thomsen and Andreasen, 2019), it is calculated that Profile C received ~3.8–4.8 g/m^2 of Sr in 2012 and 2013, as part of the CO_2-storage experiment. The difference in Sr extractable by acetic acid between Profile C in 2014, the control site, Profile A, and the currently-farmed Profile F in 2019 is more than 4,400 mg/m^2, suggesting that nearly the entire amount of Sr added during the liming experiment was bound up in the lime in March of 2014, when the samples for Frei et al. (2020a) were obtained. This is reasonable, as most of the agricultural lime was added in the fall of 2013, and the soil sampling in March 2014 was likely done before plowing and seeding that year. The difference in the amount of Sr extractable by acetic acid between Profile C in 2014 and 2019 is more than 3,900 mg/m^2, suggesting that 80–100% of the Sr from the agricultural lime has been leached out of the soil, during these 5 years, as the amount of bioavailable Sr remained constant during that period. The Sr leached from the soil has very likely exchanged with bioavailable Sr in the soil, but as both have Sr isotope compositions dominated by limestone signatures, the extent of this exchange is difficult to determine. This likely occurs in a dynamic equilibrium, where amount of the input is roughly equal to that of the output, though with exchange in the inventory of Sr in the soil. Once the Sr from the agricultural lime enters the meltwater sand, it quickly ends up in the groundwater, due to the very low ion exchange capacity of the quartz-rich sand. From there, most of the Sr enters the surface waters in contact with the groundwater, including streams and rivers, imparting a lime Sr isotopic signature to these surface waters, as determined by Thomsen and Andreasen (2019).

From the shallow groundwater, some of the Sr may be transported to deeper groundwater reservoirs (i.e., >60 m depth) and may impact the Sr isotopic composition of deeper groundwaters. Shallow groundwaters at the CO_2-storage test

site at Voulund have high Sr concentrations and low $^{87}Sr/^{86}Sr$ ratios (Frei et al., 2020a) dominated by lime, whereas shallow groundwaters in the vicinity of the test site (Thomsen et al., 2021) and nearby areas unaffected by farming (Jørgensen et al., 1999; Thomsen and Andreasen, 2019) have low Sr concentrations and high $^{87}Sr/^{86}Sr$ ratios, indicating that the Sr isotopic composition of the shallow groundwater at the test site is almost certainly dominated by agricultural lime. Meanwhile, deeper groundwaters have higher Sr concentrations and lower $^{87}Sr/^{86}Sr$ ratios likely dominated by natural limestone (Jørgensen et al., 1999), as do drinking water wells located 10-15 km from the test site (Frei et al., 2020b). However, as the drinking water in this area is pumped from depths of nearly 200 m, this does not reflect the surface geology, as has been argued by Frei et al. (2020b). This combined with high-degrees of lateral movement of groundwater (Danapour et al., 2019), thus renders Sr from present-day drinking waters a very poor choice for creating isoscapes for provenance studies, including pre-historic mobility studies, as has been proposed by Frei et al. (2020b), even if such waters have not been limed or otherwise treated for water hardness by municipal water works.

Strontium isotopic investigation of Profile C by Frei et al. (2020a), from samples obtained in 2014, yielded a mixing trend between a silicate endmember (having a low Sr concentration and a high $^{87}Sr/^{86}Sr$ ratio) and a lime endmember (having a high Sr concentration and a low $^{87}Sr/^{86}Sr$ ratio), but it was not possible to distinguish whether the lime endmember was agricultural lime, or whether it was residual natural of limestone found in one of the soil horizons, due to the fact that the Cretaceous Age agricultural lime, and the residual Silurian Age limestone remnants—likely deposited in the meltwater sand during the Weichselian ice age, as ice rafted material from Gotland, Sweden—have very similar Sr isotopic signatures (Frei et al., 2020a). The fact that the Sr isotopic composition of the porewaters in Frei et al. (2020a) are both lime-dominated and constant throughout the profile, suggests that the lime signature is imparted from the top of the soil through agricultural lime, rather than from occasional limestone remnants at depth. Likewise, the Silurian limestone pieces tend to be very erosion resistant (Kjær et al., 2003), and thus are unlikely to contribute much to the Sr budget. This is attested by their presence in the soil 22,000 years after deposition, compared to the agricultural lime, which dissolves in these soils within a few years. Nonetheless, Sr isotopes cannot be used to discriminate between the two sources of lime (where $^{87}Sr/^{86}Sr$ of the Cretaceous limestone = 0.7078 and $^{87}Sr/^{86}Sr$ of the local Silurian limestone = 0.7081), but an investigation of Profile N, which has never been treated with agricultural lime could resolve whether the mixing trend is due to agricultural lime or to residual natural lime.

In **Figure 6**, the $^{87}Sr/^{86}Sr$ compositions and reciprocal Sr concentrations are plotted for the ammonium nitrate extracts of pristine Profile N (this study) and intensively-limed Profile C (Frei et al., 2020a). The mixing trend observed for Profile N exhibits the same silicate endmember as that of Profile C, but it does not approach a limestone endmember. Rather, the $^{87}Sr/^{86}Sr$ ratio of the O-horizon (N8) is 0.7122, a value far higher than that of limestone (0.708). The linearity of the mixing line for

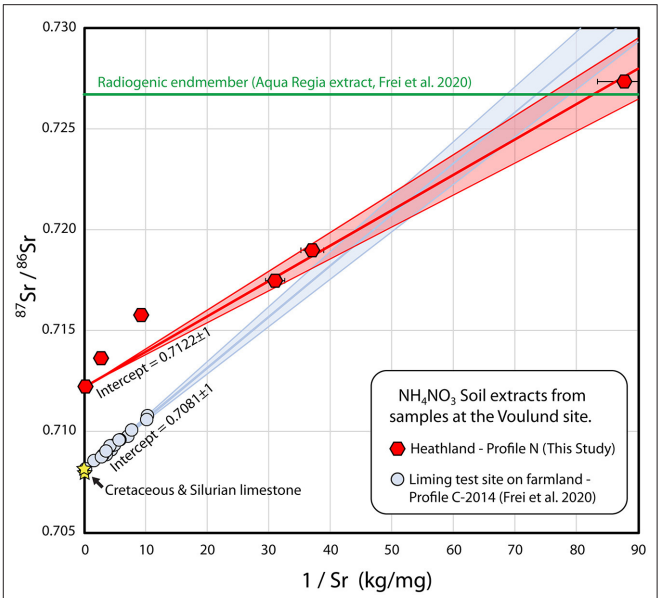

FIGURE 6 | Strontium mixing diagram with Sr isotopic compositions of ammonium nitrate leachates from Voulund soils as a function of the reciprocal Sr concentrations. Samples from soil profile N (heathland), this study, are shown as red hexagons, and samples from soil profile C—liming test site (Frei et al., 2020a), are shown as light blue circles. Also shown is the aqua regia extract of the deepest meltwater sand sample from Profile C in 2014, Frei et al. (2020a) (shown as a green line), as the Sr concentration of this is not directly comparable to the ammonium nitrate leachate samples. The compositions of the Cretaceous limestone that sources agricultural lime, and the Silurian limestone, sporadically found locally in the glacial outwash sands are shown as yellow stars. Regression lines were calculated with IsoplotR (Vermeesch, 2018), and shaded areas indicate 2σ uncertainty envelopes.

Profile N is not perfect. In the regression, the E- and topmost sample of the B-horizon (N7 & N6) have been omitted, as these are the two samples that fall far below the 1:1 line in **Figure 3D**. It is unclear whether their relatively higher Sr concentration compared to $^{87}Sr/^{86}Sr$ is due to the ammonium nitrate extracts not reaching equilibrium or to mineralogical differences amongst the samples. Regardless of whether or not these samples are included, a regression of this profile that includes the O-horizon gives an intercept of 0.7122. There is no indication that there is any natural residual limestone in the heathland soil, and unsurprisingly, it is therefore also highly likely that the lime endmember in the heavily-limed Profile C is agricultural lime. One reason for the mixing relationship in the pristine Profile N could be the accumulation of Sr from rainwater in the upper parts of the soil. It would require full retention of 3,000–4,000 years of Sr from rainwater to explain the mixing, or more realistically, ca. 15% retention of Sr from rainwater for the 22,000 years since the outwash plain was formed, assuming that the Sr concentrations of rainwater determined in the course of this study and Thomsen and Andreasen (2019) are representative for the concentration of Sr in rainwater since the end of the Weichselian ice age. Alternatively, it could be that the top of Profile N is affected by windblown dust from the nearby frequently limed farmed fields,

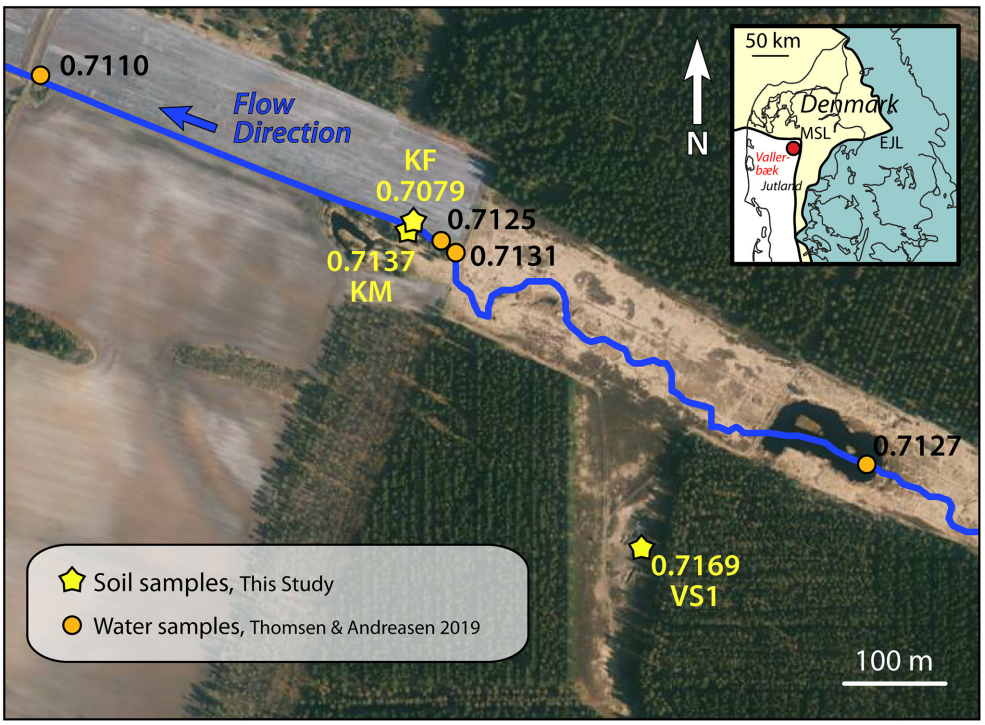

FIGURE 7 | Orthophoto from Spring 2019 of the Vallerbæk tributary of the Karup River, where the stream enters farmland. Measurements of Sr isotopic composition in the stream water (Thomsen and Andreasen, 2019) are shown with orange dots. Measurements of the Sr isotopic composition of ammonium nitrate leachate of soil samples are shown with yellow stars. The flow direction of the stream is SE to NW. The white bands in the fields are varying proportions of quartz in the soil. Map insert shows the locality relative to the two major ice front locations during the Weichselian Ice Age (Houmark-Nielsen, 2003). Orthophoto from *Styrelsen for Dataforsyning og Effektivisering*—Denmark.

which is carried by the predominantly westerly winds. Profile N was selected for this study, due to its proximity to the liming test site; a heathland site more isolated from farmland would be useful in order to determine the relative contributions of Sr from rainwater and windblown dust from the farmland.

Comparison With the Vallerbæk Tributary of the Karup River

In order to see whether the large variation in Sr isotopic compositions of the soils in Voulund is an isolated phenomenon, ammonium nitrate extracts of several soil samples from the Vallerbæk tributary of the Karup River were also analyzed. Water samples from this stream had been analyzed by Thomsen and Andreasen (2019); and $^{87}Sr/^{86}Sr$ ratios for both soil and water samples are presented in **Figure 7**. These samples show very different $^{87}Sr/^{86}Sr$ isotopic signatures—the sample from the field (KF) shows a signature identical to that of agricultural lime (0.7079), whereas the shrubland sample (KM) is unaffected by agricultural lime, with an $^{87}Sr/^{86}Sr$ ratio of 0.7137. This latter value is identical to that of the brook at that point. The sample from the forest (VS1) gives a much higher $^{87}Sr/^{86}Sr$ ratio of 0.7169, a signature that is not seen in the water samples of the brook, nor in the local groundwater (Thomsen and Andreasen, 2019).

This, and the large variations seen in the Sr isotopic compositions of the soils at Voulund highlight one of the difficulties of using soil samples for the construction of Sr baselines—namely that a very detailed sampling grid is required to characterize each area. Conversely, the use of surface water samples (Thomsen and Andreasen, 2019; Thomsen et al., 2021) or perhaps plant samples reflects a weighted average of an area, which can be used to assess the bioavailable Sr in pre-historic times, provided agricultural areas are avoided, especially in places where soils are naturally low- to non-calcareous.

CONCLUSIONS

Our investigation into the fate of Sr from agricultural lime at a test field site on a glacial outwash plain confirms that Sr is as highly mobile as Ca is, and little is retained in organic-rich topsoils, such that Sr seeps into the underlying groundwater and nearby surface waters. In both the sandy soils of the an intensively-limed CO_2 storage test site and farmed- and heathland soils adjacent to the test site, Sr exhibits a degree of mobility similar to that of Ca, as is expected, given data for other soil types (Smičiklas et al., 2015) and is what is predicted by the size of strontium's hydrated ions (Burgess, 2011). $^{87}Sr/^{86}Sr$ values from samples obtained from the pristine heathland next to the test site are

significantly higher than those obtained from the test site, so the test site is unlikely to be influenced by natural relict carbonates occasionally found in the area, as was proposed by Frei et al. (2020a), confirming that the lime $^{87}Sr/^{86}Sr$ signature of farmland soils, and streams and rivers in contact with the farmland almost certainly comes from agricultural lime. This indicates that the $^{87}Sr/^{86}Sr$ signatures of the area were likely much higher, during pre-historic times, and that isoscapes based on samples from modern-day farmland or from surface waters in contact with these—like Frei and Frei's (2011) isoscape of Denmark are inappropriate for use in provenance and mobility studies of pre-historic people. And this can have significant consequences for the interpretation of pre-historic archaeological finds, as it has in these areas, including the iconic Bronze Age females, The Egtved Girl, The Skrydstrup Woman Frei et al. (2015, 2017), Thomsen and Andreasen (2019) and other individuals, discussed in Thomsen et al. (2021). Thus, it is critical that the possible impact of farming is evaluated when conducting provenance and mobility studies, especially in areas with Sr-poor soils and where agricultural lime is used for soil improvement, including the glacial outwash plains covering large parts of Europe and North America (Gillespie et al., 2003; Böse et al., 2012; Reimann et al., 2014). Overlooking this can result in significant overestimation of the degree of pre-historic mobility in an area, as it has in Denmark, where the overall mobility during pre-historic times was likely significantly lower than recently proposed (Frei et al., 2019).

DATA AVAILABILITY STATEMENT

The original contributions presented in the study are included in the article/**Supplementary Material**, further inquiries can be directed to the corresponding author/s.

AUTHOR CONTRIBUTIONS

ET selected the soil pits locations. RA did soil sampling in the Vallerbæk area, sample processing, and analyses as well as the initial geochemical interpretation, and drafted the manuscript. All authors did initial sampling at the Voulund site, additional sampling there was done by ET. All authors devised the study, contributed to the interpretations and the manuscript, and approved the submitted version.

FUNDING

This work was supported by AUFF (Aarhus University Research Foundation) NOVA grant E-2019-9-27.

ACKNOWLEDGMENTS

Claus Heilmann Clausen is thanked for his expertise and tireless efforts in digging soil pits. Discussions on organic geochemistry with Hamed Sanei and Arka Rudra are greatly appreciated, as are discussions with Søren Munch Kristiansen on soil chemistry. Sincere thanks to Benjamin C. Bostick for sharing his insight into element mobility. The authors are grateful to Erin J. Rosenberg, who improved the manuscript. Insightful comments from two reviewers and associate guest editor Joshua Miller were very helpful in improving the presentation of the data and refining the discussion of these.

SUPPLEMENTARY MATERIAL

The Supplementary Material for this article can be found online at: https://www.frontiersin.org/articles/10.3389/fevo.2020.588422/full#supplementary-material

REFERENCES

Aquilina, L., Poszwa, A., Walter, C., Vergnaud, V., Pierson-Wickmann, A.-C., and Ruiz, L. (2012). Long-term effects of high nitrogen loads on cation and carbon riverine export in agricultural catchments. *Environ. Sci. Technol.* 46, 9447–9455 doi: 10.1021/es301715t

Bataille, C. P., Crowley, B. E., Wooller, M. J., and Bowen, G. J. (2020). Advances in global bioavailable strontium isoscapes. *Palaeogeogr. Palaeoclimatol. Palaeoecol.* 555:109849. doi: 10.1016/j.palaeo.2020.109849

Bataille, C. P., von Holstein, I. C. C., Laffoon, J. E., Willmes, M., Liu, X.-M., and Davies, G. R. (2018). A bioavailable strontium isoscape for Western Europe: a machine learning approach. *PLoS ONE* 13:e0197386. doi: 10.1371/journal.pone.0197386

Bentley, R. A. (2006). Strontium isotopes from the earth to the archaeological skeleton: a review. *J. Archaeol. Meth. Theor.* 13, 135–187. doi: 10.1007/s10816-006-9009-x

Blum, J. D., Taliaferro, E. H., Wiesse, M. T., and Holmes, R. T. (2000). Changes in Sr/Ca, Ba/Ca and 87Sr/86Sr ratios between trophic levels in two forest ecosystems in the northeastern U.S.A. *Biogeochemistry* 49, 87–101. doi: 10.1023/A:1006390707989

Böhlke, J. K., and Horan, M. F. (2000). Strontium isotope geochemistry of groundwaters and streams affected by agriculture, Locust Grove, MD. *Appl. Geochem.* 15, 599–609. doi: 10.1016/S0883-2927(99)00075-X

Böse, M., Lüthgens, C., Lee, J. R., and Rose, J. (2012). Quaternary glaciations of northern Europe. *Quat. Sci. Rev.* 44, 1–25. doi: 10.1016/j.quascirev.2012.04.017

Burgess, J. (2011). *Ions in Solution, Basic Principles of Chemical Interactions.* Ellis Horwood Limited. Cambridge: Woodhead Publishing Limited.

Capo, R. C., Stewart, B. W., and Chadwick, O. A. (1998). Strontium isotopes as tracers of ecosystem processes: theory and methods. *Geoderma* 82, 197–225. doi: 10.1016/S0016-7061(97)00102-X

Danapour, M., Højberg, A. L., Jensen, K. H., and Stisen, S. (2019). Assessment of regional inter-basin groundwater flow using both simple and highly parameterized optimization schemes. *Hydrogeol. J.* 27, 1929–1947. doi: 10.1007/s10040-019-01984-3

Dia, A. N., Cohen, A. S., O'Nions, R. K., and Shackleton, N. J. (1992). Seawater Sr isotope variation over the past 300 kyr and influence of global climate cycles. *Nature* 356, 786–788. doi: 10.1038/356786a0

Edmond, J. T. (1992). Himalayantectonics, weathering processes, and the strontium isotope record in marine limestones. *Science* 258, 1594–1597. doi: 10.1126/science.258.5088.1594

Ericson, J. E. (1985). Strontium isotope characterization in the study of prehistoric human ecology. *J. Hum. Evol.* 14, 503–514. doi: 10.1016/S0047-2484(85)80029-4

Faure, G., Crockett, J. H., and Hurley, P. M. (1967). Some aspects of strontium and calcium in the Hudson Bay and the great Lakes. *Geochim. Cosmochim. Acta* 81, 451–461. doi: 10.1016/0016-7037(67)90053-1

Frei, K. M., Bergerbrant, S., Sjögren, K. -G., Jørkov, M. L., Lynnerup N, Harvig, L., et al. (2019). Mapping human mobility during the third and second millennia BC in present-day Denmark. *PLoS ONE* 14:e0219850. doi: 10.1371/journal.pone.0219850

Frei, K. M., and Frei, R. (2011). The geographic distribution of strontium isotopes in Danish surface waters – a base for provenance studies in archaeology, hydrology and agriculture. *Appl. Geochem.* 26, 326–340. doi: 10.1016/j.apgeochem.2010.12.006

Frei, K. M., Mannering, U., Kristiansen, K., Allentoft, M. E., Wilson, A. S., Skals, I., et al. (2015). Tracing the dynamic life story of a Bronze age female. *Sci. Rep* 5:10431. doi: 10.1038/srep10431

Frei, K. M., Villa, C., Jørkov, M. L., Allentoft, M. E., and Kaul, F., Ethelberg, et al. (2017). A matter of months: high precision migration chronology of a Bronze age female. *PLoS ONE* 12:e0178834. doi: 10.1371/journal.pone.0178834

Frei, R., Frei, K. M., and Jessen, S. (2020a). Shallow retardation of the strontium isotope signal of agricultural liming - implications for isoscapes used in provenance studies. *Sci. Total Environ.* 706:135710. doi: 10.1016/j.scitotenv.2019.135710

Frei, R., Frei, K. M., Kristiansen, S. M., Jessen, S., Schullehner, J., and Hansen, B. (2020b). The link between surface water and groundwater-based drinking water – strontium isotope spatial distribution patterns and their relationships to Danish sediments. *Appl. Geochem.* 121:104698. doi: 10.1016/j.apgeochem.2020.104698

Gillespie, A. R., Porter, S. C., and Atwater, B. F. (2003). *The Quaternary Period in the United States, Vol. 1.* Amsterdam: Elsevier Science.

Grimstead, D. N., Nugent, S., and Whipple, J. (2017). Why a standardization of strontium isotope baseline environmental data is needed and recommendations for methodology. *Adv. Archaeol. Pract.* 5, 184–195. doi: 10.1017/aap.2017.6

Haak, W., Brandt, G., de Jong, H. N., Meyer, C., Ganslmeier, R., Heyd, V., et al. (2008). Ancient DNA, strontium isotopes, and osteological analyses shed light on social and kinship organization of the later stone age. *Proc. Natl. Acad. Sci. U.S.A.* 105, 18226–18231. doi: 10.1073/pnas.0807592105

Hoogewerff, J. A., Reimann, C., Ueckermann, H., Frei, R., Frei, K. M., van Aswegen, T., et al. (2019). Bioavailable 87Sr/86Sr in European soils: a baseline for provenancing studies. *Sci. Total Environ.* 672, 1033–1044. doi: 10.1016/j.scitotenv.2019.03.387

Houmark-Nielsen, M. (2003). Signature and timing of the kattegat ice stream: onset of the LGM-sequence in the southwestern part of the scandinavian ice sheet. *Boreas* 32, 227–241. doi: 10.1111/j.1502-3885.2003.tb01439.x

Jessen, S., Jakobsen, R., Postma, D., Looms, M., and Larsen, F. (2014a). *Carbon Transfer Across the Vadose Zone: Inhibition by 20th Century Acid Rain?.* Available online at: https://co2gs.geus.net/xpdf/WP5-Carbon_transfer_across_the_vadose_zone.pdf

Jessen, S., Postma, D., Jakobsen, R., Looms, M. C., and Larsen, F. (2014b). *Inhibition of Carbon Transfer Across the Vadose Zone by 20th Century Acid Rain.* Vienna: EGU General Assembly.

Jørgensen, N. O., Morthorst, J., and Holm, P. M. (1999). Strontium-isotope studies of "brown water" (organic-rich groundwater) from Denmark. *Hydrogeol. J.* 7, 533–539. doi: 10.1007/s100400050226

Kjær, K. H., Houmark-Nielsen, M., and Richardt, N. (2003). Ice-flow patterns and dispersal of erratics at the southwestern margin of the last scandinavian ice sheet: imprint after palaeo-ice streams. *Boreas* 32, 130–148. doi: 10.1111/j.1502-3885.2003.tb01434.x

Knipper, C., Mittnik, A., Massy, K., Kociumaka, C., Kucukkalipci, I., Maus, M., et al. (2017). Female exogamy and gene pool diversification at the transition from the final neolithic to the early bronze age in central Europe. *Proc. Natl. Acad. Sci. U.S.A.* 114, 10083–10088. doi: 10.1073/pnas.17063 55114

Krüger, J., Jensen, N. H., and Greve, M. H. (2013). A statistically based mapping of the influence of geology and land use on soil pH. A case study from Denmark. *Geoderma* 192, 453–462. doi: 10.1016/j.geoderma.2012. 08.024

Long, M. P., Alland, S., Martin, M. E., and Isborn, C. M. (2020). Molecular dynamics simulations of alkaline earth metal ions binding to DNA reveal ion size and hydration effects. *Phys. Chem. Chem. Phys.* 22:5584. doi: 10.1039/C9CP06844A

Madgwick, R., Lamb, A. L., Sloane, H., Nederbragt, A. J., Albarella, U., Pearson, M. P., et al. (2019). Multi-isotope analysis reveals that feasts in the stonehenge environs and across wessex drew people and animals from throughout Britain. *Sci. Adv.* 5:eaau6078. doi: 10.1126/sciadv.aau6078

Marcus, Y. (2016). *Ions in Solution and Their Solvation*. Hoboken, NJ: John Wiley & Sons, Inc.

Maurer, A. -F., Galer, S. J. G., Knipper, C., Beierlein, L., Nunn, E. V., Peters, D., et al. (2012). Bioavailable 87Sr/86Sr in different environmental samples. Effects of anthropogenic contamination and implications for isoscapes in past migration studies. *Sci. Total Environ.* 233, 216–229. doi: 10.1016/j.scitotenv.2012.06.046

Montgomery, J. (2010). Passports from the past: investigating human dispersals using strontium isotope analysis of tooth enamel. *Ann. Hum. Biol.* 37, 325–346. doi: 10.3109/03014461003649297

Montgomery, J., Evans, J. A., and Cooper, R. E. (2007). Resolving archaeological populations with Sr-isotope mixing models. *Appl. Geochem.* 22, 1502–1514. doi: 10.1016/j.apgeochem.2007.02.009

Müller, W., Fricke, H., Halliday, A. N., McCulloch, M. T., and Wartho, J. A. (2003). Origin and migration of the Alpine Iceman. *Science* 302, 862–866. doi: 10.1126/science.1089837

Oh, N. H., and Raymond, P, A. (2006). Contribution of agricultural liming to riverine bicarbonate export and CO sequestration in the Ohio river basin. *Global Biogeochem. Cycles* 20:3. doi: 10.1029/2005GB002565

Reimann, C., Birke, M., Demetriades, A., Filzmoser, P., and O'Connor, P (eds). (2014). Chemistry of Europe's agricultural soils – part A: methodology and interpretation of the GEMAS data set. Geologisches Jahrbuch (Reihe B 102). Hannover: Schweizerbarth

Smičiklas, I., Jović, M., Šljivić-Ivanović, M., Mrvić, V., Cakmak, D., and Dimović, S. (2015). Correlation of Sr2+ retention and distribution with properties of different soil types. *Geoderma* 253–254, 21–29. doi: 10.1016/j.geoderma.2015.04.003

Solecki, J. (2005). Investigation of ^{85}Sr adsorption on selected soils of different horizons. *J. Environ. Radioact.* 82 303–320. doi: 10.1016/j.jenvrad.2005.02.001

Thomsen, E., and Andreasen, R. (2019). Agricultural lime disturbs natural strontium isotope variations: implications for provenance and migration studies. *Sci. Adv.* 5:eaav8083. doi: 10.1126/sciadv.aav8083

Thomsen, E., Andreasen, R., and Rasmussen, T. L. (2021). Homogenous Glacial Landscapes can have high local variability of strontium isotope signatures: implications for prehistoric migration studies. *Front. Ecol. Evol.* 8:588318. doi: 10.3389/fevo.2020.588318

Veizer, J., Ala, D., Azmy, K., Bruckschen, P., Buhl, D., Bruhn, F., et al. (1999). Sr-87/Sr-86, delta C-13 and delta O-18 evolution of phanerozoic seawater. *Chem. Geol.* 161:59–88. doi: 10.1016/S0009-2541(99)00081-9

Vermeesch, P. (2018). IsoplotR: a free and open toolbox for geochronology. *Geosci. Front.* 9, 1479–1493. doi: 10.1016/j.gsf.2018.04.001

Wallace, S. H., Shaw, S., Morris, K., Small, J. S., Fuller, A. J., and Burke, I. T. (2012). Effect of groundwater pH and ionic strength on strontium sorption in aquifer sediments: implications for 90Sr mobility at contaminated nuclear sites. *Appl. Geochem.* 27, 1482–1491. doi: 10.1016/j.apgeochem.2012.04.007

Willmes, M., Bataille, C. P., James, H. F., Moffat, I., McMorrow, L., Kinsley, L., et al. (2018). Mapping of bioavailable strontium isotope ratios in France for archaeological provenance studies. *Appl. Geochem.* 90, 75–86. doi: 10.1016/j.apgeochem.2017.12.025

Conflict of Interest: The authors declare that the research was conducted in the absence of any commercial or financial relationships that could be construed as a potential conflict of interest.

frontiers in Ecology and Evolution

PERSPECTIVE
published: 17 February 2021
doi: 10.3389/fevo.2021.632681

$^{87}Sr/^{86}Sr$ in Archeological and Paleobiological Research: A Perspective

*Andrew Sillen**

Department of Anthropology, Rutgers University, New Brunswick, NJ, United States

The stable isotope ratio $^{87}Sr/^{86}Sr$ has been shown to have extraordinary potential for documenting the movement and life-histories of humans and other animals, both in history and prehistory. Thirty years of expanding applications has taken the method from a niche (if not fringe) approach to a normal part of archeological and paleobiological enquiry; indeed a "Golden Age." The technique is inherently interdisciplinary, because in addition to those archeologists and paleobiologists wishing to apply it, most applications require informed input from ecologists, geochemists, and calcified tissue biologists. This perspective explores how such interdisciplinarity is both a strength and an impediment to further advancement.

Keywords: strontium isotopes, paleodiet, paleohabitat, paleoecology, life-history

OPEN ACCESS

Edited by:
Clement Pierre Bataille,
University of Ottawa, Canada

Reviewed by:
Judith Sealy,
University of Cape Town, South Africa
Jane Evans,
The Lyell Centre, United Kingdom

***Correspondence:**
Andrew Sillen
andrew.sillen@rutgers.edu

Specialty section:
This article was submitted to Paleoecology, a section of the journal Frontiers in Ecology and Evolution

Received: *23 November 2020*
Accepted: *04 January 2021*
Published: *17 February 2021*

Citation:
Sillen A (2021) $^{87}Sr/^{86}Sr$ in Archeological and Paleobiological Research: A Perspective. Front. Ecol. Evol. 9:632681. doi: 10.3389/fevo.2021.632681

Thirty-five years ago, back in the paleolithic, archeologists and paleobiologists were just beginning to appreciate the potential of strontium isotope research for biological source-tracing, and the attendant implications for reconstructing landscape use and transhumance. A seminal article by Jonathon E. Ericson, who was then Professor of Environmental Health Science and Policy at UC Irvine, captured the attention of those few archeologists and physical anthropologists at the time who were interested in bone and fossil chemistry for any other purpose than radiocarbon dating (Ericson, 1985).

In those days, you could count on one hand the scientists whose primary interest was the past, and who were prepared to use biogeochemical phenomena to study it, and there were significant impediments for all of us. Those of us trained in Anthropology Departments already did not fit in any convenient departmental pigeon hole: we were using the material conventionally studied by physical anthropologists (skeletons) to address questions conventionally asked by archeologists (behavior): we were neither fish nor fowl.

An even bigger problem was the inherently interdisciplinary nature of isotope research in bioarcheology. Very few individuals could confidently – and competently – apply environmental chemical phenomena and methods to biological tissues that have undergone geochemical alteration, for the purpose of reconstructing ancient animal and human behavior! At the time, everyone involved in this kind of thing was undertrained in at least one aspect of what was necessary to navigate that vast terrain of diverse disciplines. And it always seemed like an amusing, albeit frustrating irony that, in drawing from the diverse disciplines of biogeochemistry, calcified tissue biology, paleobiology, and archeology, our work was thought of as "specialized."

By 1989, these issues were becoming better understood, when my colleagues at the University of Cape Town and I wrote "*Chemistry and Paleodietary Research: No More Easy Answers*" (Sillen et al., 1989). Strontium isotopes were just beginning to draw our attention and were included almost as an afterthought (the article focused on $\delta^{13}C$, $\delta^{15}N$, and Sr/Ca); and yet the conclusions were applicable to all of the techniques, and bear repeating:

> *"With few exceptions, basic research that has addressed the techniques themselves (rather than explicit applications) has consisted of manipulating the available archeological and modern faunal and floral specimens . . . While necessary, this research strategy no longer suffices. Most of the stumbling blocks . . . call for a more aggressively experimental approach . . . Expanding the experimental basis of the research presents a formidable barrier mainly because the necessary intermediate research fits no convenient academic pigeon hole".*

The point has been taken up and re-emphasized in an important review article by Makarewicz and Sealy (2015) (see also Britton, 2017). As these authors emphasize, the need for foundational and proof-of-concept studies has become somewhat more urgent as the applications of isotopes to archeology and paleobiology (including strontium isotope analysis) have exploded. Strontium isotope analysis has been applied to ancient materials on every inhabited continent, from mammals and mollusks (Vanhaeren et al., 2004); and for just about every age from the Pleistocene (Hoppe et al., 1999; Britton et al., 2011; Copeland et al., 2011; Sillen and Balter, 2018), to changes in human and animal lifeways with the onset of agriculture (Bentley et al., 2005; Bentley, 2013), to the forced relocations of both Indonesian and African slaves (Schroeder et al., 2009; Bastos et al., 2016; Kootker et al., 2016).

For paleoanthropologists (a term I am using to include both archeologists and physical anthropologists), studies centered on isotopic techniques represented a methodological departure from approaches that depended on skeletal morphology or from indirect inference drawn from contextual contemporaneous archeological residues. For paleontologists, it represented a shift away from attempts aimed purely at characterizing or describing fossil bones (exemplified in Wyckoff's, 1972 volume The Biochemistry of Animal Fossils), and toward focused applications of chemical phenomena to archeological problems.

In the early days, those who came together from different scientific backgrounds to undertake this new type of research understandably made many mistakes and had a habit of talking right past each other. The anthropologists, always seeking new tools and anticipating an avalanche of new insight, sometimes applied new techniques somewhat indiscriminately, and there were more than a few unfortunate rabbit-holes. There were endless squabbles with geochemists who approached fossils as if they were rocks. Geochemists had a point to make about diagenesis, but rarely articulated a useful archeological question.

There were no texts or guideposts. The closest thing to a text was Wyckoff's, 1972 book, written before anybody ever contemplated looking for any kind of isotope in a fossil.

After an initial burst of enthusiasm, it was clear there was a further problem – that there was not always a good fit between the proposed technique and a paleontological or archeological problem researchers sought to address. When the questions posed by one discipline are addressed with techniques and methodologies grafted from another, there are bound to be difficulties. There are the rare instances when the information provided by an analytical technique seamlessly addresses a narrative archeological or paleontological theme – the application of $\delta^{13}C$ to early maize cultivation comes to mind (Vogel and van der Merwe, 1977) – but, but such instances are the exception rather than the rule, and the danger comes when, in the pursuit of easy answers, techniques are force-fitted onto issues to which they are really not suited. Beyond strontium isotopes, the issues and opportunities around grafting new scientific techniques onto classical archeological problems have been reviewed by Killick (2015).

The classic example in archeology was the early adoption of radiocarbon dating. When the technique was first developed in the early 1950s, there was an explosive initial period of obvious applications and easy pickings, where rough approximations of age were sufficient. Subsequently, complications in the application of radiocarbon became apparent – such as the De Vries and Suess effects, the resolution of which, while no less heroic, was somewhat less glorious. Hard, highly technical work was required, both to explore the more subtle ramifications of the new development, and also to clean-up after some of the uncritical assumptions, excess, and errors of the earlier period (Damon and Peristykh, 2000).

With very few exceptions, the background data necessary to fully explore strontium isotope analysis to archeological and fossil materials are not available from the hard sciences. The gaps are not unpredictable, however, and derive from the different priorities which set the stage for the background research in the first place. This can be illustrated with the literature on elemental strontium, which was the focus of my research in the 1980s (Sillen and Kavanagh, 1982). Until then, virtually all literature on biological strontium focused on understanding and mitigating the health consequences of atmospheric fallout (especially ^{89}Sr and ^{90}Sr) from above-ground nuclear testing.

Figure 1 is the amount of ^{90}Sr and ^{89}Sr fallout which found its way into milk marketed in New York City during the early 1960s, which became a major public health concern. **Figure 2** taken from the bibliography of that review article, shows the frequency of articles on strontium in the biochemical literature from the 1950s to the 1970s. The dotted line in both graphs depicts the summer of 1963, when John F Kennedy and Nikita Kruschev signed the above-ground nuclear test-ban treaty. **Figure 1** shows that radiogenic Sr in milk increased dramatically as both countries accelerated atomic testing in anticipation of the treaty. The short-lived isotope ^{89}Sr is highest immediately before the treaty. Research into radiogenic Sr in food webs was similarly high during this period, and after a rush to get into print, published biochemical research on Sr declined.

The graphs illustrate that strontium research, like any other research, was conducted for a reason, in this case concern over the ubiquity of a radioactive isotope in food. What emerges as a

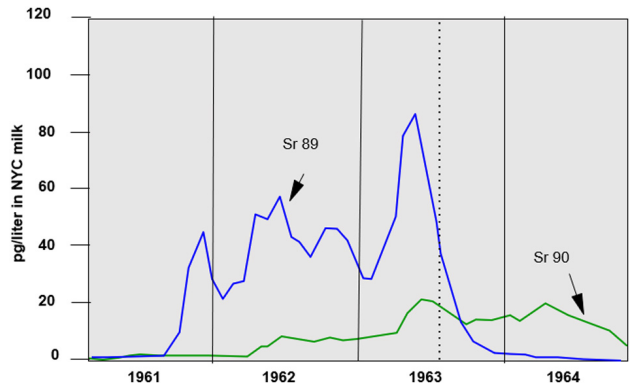

FIGURE 1 | Radioisotopes marketed in milk in New York City, 1960–1965.

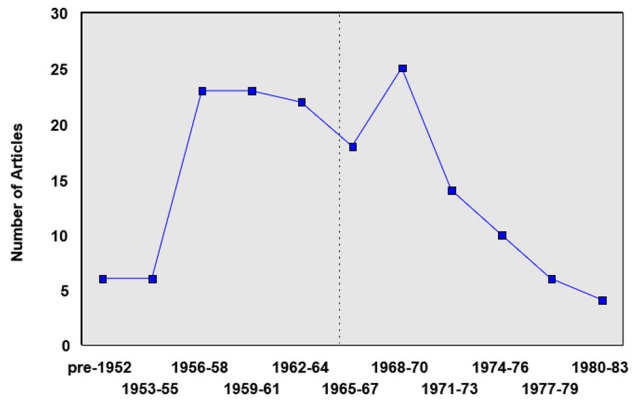

FIGURE 2 | Frequency of articles published on strontium in the biochemical literature, 1952–1983.

point of great importance is what the research was *not* aimed at: the development of dietary, mobility, and environmental markers for paleobiologists and archeologists. As a direct result, there were, at the time of the first applications of elemental strontium to archeology, significant gaps in background data necessary to apply these new methods appropriately.

To take just one example from my own experience, in the early days of $^{87}Sr/^{86}Sr$ research, well before ecologist J. B. West et al. (2010) coined the term "isoscape," a lot of people thought that all you had to do was look at a geological map to infer meaning to observed differences in $^{87}Sr/^{86}Sr$ isotopes in archeological materials. From my dissertation research on elemental strontium, I was aware that total and available soil Sr/Ca could differ enormously, so suggested an empirical approach at the Pleistocene site of Swartkrans, in the Sterkfontein Valley. The discoveries available in $^{87}Sr/^{86}Sr$ plants in this region bore little resemblance to that of whole rock substrates, and that $^{87}Sr/^{86}Sr$ varied more with hydrology (riparian vs. dry habitats) than geological maps may have been lucky accidents (Sillen et al., 1998), but illustrated rather profoundly the potential distance between existing theory and the real world which in many cases may not be serious, but in others might fatally undermine the unwary.

Over 20 years later, we may indeed think of strontium isotopic research as entering a "Golden Age" firstly because the number of actual and potential applications in archeology and paleobiology is ever increasing, but perhaps more importantly that there is a full appreciation of the basic research necessary to realize more fully the archeological and paleobiological potentials of these methods. The problem remains that by no stretch of the imagination could this basic research be considered to be archeology or paleobiology.

For my own home discipline, it is exciting to see the evolution of $^{87}Sr/^{86}Sr$ applications (along with light isotopes) from a somewhat exotic untested approach on the margins, to one fully embedded in the discipline. It is hard to imagine a single modern archeological monograph that does not include isotopic analysis as a key element of past behavioral reconstruction. Wow.

It is similarly satisfying to see a continued and growing emphasis on basic research, notably an emphasis on isoscape mapping, modeling, and *in vivo* feeding studies. It seems obvious, as well, that it has finally been established beyond any doubt that research depending on the wide diversity of knowledge outlined in the beginning of this short essay (and that featured in the field at its outset), is perhaps best conducted in interdisciplinary teams. In addition to archeologists, paleoecologists and geochemists, to fully explore the potential for elucidating life-histories (of both humans and other animals), my sense is there will need to be a far greater participation of calcified tissue biochemists and micromorphologists going forward.

To whom does the responsibility fall to provide such basic studies – mapping, modeling, feeding – and of course studies of tissue formation and diagenetic alteration? Very few scientists have both the proper training and motivation to undertake these: those with the greatest motivation are not necessarily the best qualified to do so, while those most familiar with the necessary methods have little motivation to make a contribution. As a result, it can often prove difficult to attract funding for such issues (as opposed to eye-catching applications).

Ultimately it must be those who have a stake in their application: while those outside our disciplines may have the instrumentation and essential expertise, few will have the inclination, funds – or most importantly – the sense of problem. Therefore, excursions into unfamiliar terrain will require the continued indulgence of established disciplines prepared to invest in their future, and the active participation of those best equipped to help us with the problems and questions we articulate. A powerful case exists to pursue the necessary basic research, and experience shows that well-conceived projects with the potential to materially advance eventual applications can attract funding, as they should.

This volume demonstrates that the questions addressed by strontium isotopic research are inherently cross-disciplinary, are essentially limitless, and may profoundly advance our understanding of both history and prehistory. Here, we have a special issue about strontium in which the nominally different fields of archeology and paleoecology are blurred almost to the point of fusion. From this it is apparent that the question-asking

stage of strontium paleobiology has reached maturity; indeed the cusp of a golden age. The task now is to explicitly recognize that interdisciplinarity is both a strength and an impediment, and to address the impediment.

DATA AVAILABILITY STATEMENT

The original contributions presented in the study are included in the article/supplementary material, further inquiries can be directed to the corresponding author/s.

AUTHOR CONTRIBUTIONS

The author confirms being the sole contributor of this work and has approved it for publication.

ACKNOWLEDGMENTS

I am grateful to the editors of this volume for the opportunity to provide this perspective. Kate Britton and JS supplied helpful comments on earlier drafts of this text.

REFERENCES

Bastos, M. Q. R., Santos, R. V., de Souza, S. M. F., Rodrigues-Carvalho, C., Tykot, R. H., Cook, D. C., et al. (2016). Isotopic study of geographic origins and diet of enslaved Africans buried in two Brazilian cemeteries. *J. Archaeol. Sci.* 70, 82–90. doi: 10.1016/j.jas.2016.04.020

Bentley, R. A. (2013). Mobility and the diversity of Early Neolithic lives: Isotopic evidence from skeletons. *J. Anthropol. Archaeol.* 32, 303–312. doi: 10.1016/j.jaa.2012.01.009

Bentley, R. A., Pietrusewsky, M., Douglas, M. T., and Atkinson, T. C. (2005). Matrilocality during the prehistoric transition to agriculture in Thailand? *Antiquity* 79, 865–881. doi: 10.1017/s0003598x00115005

Britton, K. (2017). A stable relationship: isotopes and bioarchaeology are in it for the long haul. *Antiquity* 91, 853–864. doi: 10.15184/aqy.2017.98

Britton, K., Grimes, V., Niven, L., Steele, T., McPherron, S., Soressi, M., et al. (2011). Strontium isotope evidence for migration in late Pleistocene Rangifer: Implications for Neanderthal hunting strategies at the Middle paleolithic site of Jonzac. *France. J. Hum. Evol.* 61, 176–185. doi: 10.1016/j.jhevol.2011.03.004

Copeland, S. R., Sponheimer, M., de Ruiter, D. J., Lee-Thorp, J. A., Codron, D., le Roux, P. J., et al. (2011). Strontium isotope evidence for landscape use by early hominins. *Nature* 474, 76–78. doi: 10.1038/nature10149

Damon, P. E., and Peristykh, A. (2000). Radiocarbon calibration and application to geophysics, solar physics, and astrophysics. *Radiocarbon* 42, 137–150. doi: 10.1017/s0033822200053108

Ericson, J. (1985). Strontium isotope characterization in the study of prehistoric human ecology. *J. Hum. Evol.* 14, 503–514. doi: 10.1016/s0047-2484(85)80029-4

Hoppe, K. A., Koch, P. L., Carlson, R. W., and Webb, D. S. (1999). Tracking mammoths and mastodons: reconstruction of migratory behaviour using strontium isotope ratios. *Geology* 27, 439–442. doi: 10.1130/0091-7613(1999)027<0439:tmamro>2.3.co;2

Killick, D. (2015). "Using evidence from natural sciences in archaeology," in *Material Evidence; Learning from Archaeological Practice*, eds R. Chapman and A. Wylie (London: Routledge), 161–172.

Kootker, L. M., Mbeki, L., Morris, A. G., Kars, H., and Davies, G. R. (2016). Dynamics of Indian ocean slavery revealed through isotopic data from the colonial era cobern street burial site, Cape Town, South Africa (1750-1827). *PLoS One* 11:e0157750. doi: 10.1371/journal.pone.0157750

Makarewicz, C. A., and Sealy, J. (2015). Dietary reconstruction, mobility, and the analysis of ancient skeletal tissues: expanding the prospects of stable isotope research in archaeology. *J. Archaeol. Sci.* 56, 146–158. doi: 10.1016/j.jas.2015.02.035

Schroeder, H., O'Connell, T. C., Evans, J. A., Shuler, K. A., and Hedges, R. E. M. (2009). Trans-atlantic slavery: isotopic evidence for forced migration to barbados. *Am. J. Phys. Anthropol.* 139, 547–557. doi: 10.1002/ajpa.21019

Sillen, A., and Balter, V. (2018). Strontium isotopic aspects of Paranthropus robustus teeth; implications for habitat, residence, and growth. *J. Hum. Evol.* 114, 118–130. doi: 10.1016/j.jhevol.2017.09.009

Sillen, A., Hall, G., Richardson, S., and Armstrong, R. (1998). $^{87}/^{86}$Sr ratios in modern and fossil food-webs of the sterkfontein valley: implications for early hominid habitat preference. *Geochim. Cosmochim. Acta* 62, 2463–2473. doi: 10.1016/s0016-7037(98)00182-3

Sillen, A., and Kavanagh, M. (1982). Strontium and paleodietary research: a Review. *Yearb. Phys. Anthropol.* 25, 67–90. doi: 10.1002/ajpa.1330250505

Sillen, A., Sealy, J. C., Nikolaas, J., and van der Merwe, N. J. (1989). Chemistry and paleodietary research: no more easy answers. *Am. Antiq.* 54, 504–512. doi: 10.2307/280778

Vanhaeren, M., d'Errico, F., Billy, I., and Grousset, F. (2004). Tracing the source of Upper paleolithic shell beads by strontium isotope dating. *J. Archaeol. Sci.* 31, 1481–1488. doi: 10.1016/j.jas.2004.03.011

Vogel, J. C., and van der Merwe, N. J. (1977). Isotopic evidence for early maize cultivation in New York State. *Am. Antiq.* 42, 238–242. doi: 10.2307/278984

West, J. B., Bowen, G. J., Dawson, T. E., and Tu, K. P. (eds) (2010). *Isoscapes: Understanding Movement, Pattern and Process on Earth Through Isotope Mapping*. Netherlands: Springer.

Wyckoff, R. W. G. (1972). *The Biochemistry of Animal Fossils*. United Kingdom: Scientechnica.

Conflict of Interest: The author declares that the research was conducted in the absence of any commercial or financial relationships that could be construed as a potential conflict of interest.

frontiers in Ecology and Evolution

ORIGINAL RESEARCH
published: 19 February 2021
doi: 10.3389/fevo.2021.583301

The Circulation of Ancient Animal Resources Across the Yellow River Basin: A Preliminary Bayesian Re-evaluation of Sr Isotope Data From the Early Neolithic to the Western Zhou Dynasty

Xueye Wang[1,2,3]*, *Patrick Roberts*[3], *Zihua Tang*[1,4], *Shiling Yang*[1,4,5], *Michael Storozum*[3,6], *Marcus Groß*[3] *and Ricardo Fernandes*[3,7,8]*

[1] Key Laboratory of Cenozoic Geology and Environment, Institute of Geology and Geophysics, Chinese Academy of Sciences, Beijing, China, [2] University of Chinese Academy of Sciences, Beijing, China, [3] Department of Archaeology, Max Planck Institute for the Science of Human History, Jena, Germany, [4] CAS Center for Excellence in Life and Paleoenvironment, Beijing, China, [5] College of Earth and Planetary Sciences, University of Chinese Academy of Sciences, Beijing, China, [6] Institute of Archaeological Science, Fudan University, Shanghai, China, [7] School of Archaeology, University of Oxford, Oxford, United Kingdom, [8] Faculty of Arts, Masaryk University, Brno, Czechia

Many questions still remain regarding the acquisition and circulation of ancient domesticated animals across the Yellow River Basin, one of the key areas for the development of complex societies in ancient China. Here, we re-evaluate previously published strontium isotope data ($^{87}Sr/^{86}Sr$, $n = 167$) from tooth enamel of domesticated animals at 10 archaeological sites in the Yellow River Basin to shed new light on the transition between the Neolithic (7000–5000 BCE) and the Western Zhou Dynasty (1046–771 BCE). The results show that from the Late Neolithic to the Western Zhou Dynasty, some domesticated animals, mostly cattle and sheep, were increasingly sourced from non-local areas. We employed Bayesian methods to define an isoscape of bioavailable Sr for the Yellow River Basin and to show the considerable diversity in the origins of non-local domesticated animals, some of which may have come from locations hundreds of kilometers away from the site as early as the Late Neolithic. The increasingly variable $^{87}Sr/^{86}Sr$ ratios of domesticated animals from the Neolithic to the Western Zhou Dynasty are consistent with that of associated human remains, and also match the archaeological and zooarchaeological evidence for increased circulation of animal products in the Yellow River Basin. Therefore, we infer that local economies increasingly incorporated non-local animals as part of wider circulation networks that emerged with the development of complex societies since the Late Neolithic.

Keywords: strontium isotopes, isoscape, zooarchaeology, Yellow River Basin, animal mobility

OPEN ACCESS

Edited by:
Kate Britton,
University of Aberdeen,
United Kingdom

Reviewed by:
Joshua Wright,
University of Aberdeen,
United Kingdom
Yaowu Hu,
University of Chinese Academy of Sciences, China

***Correspondence:**
Xueye Wang
wangxueye@mail.iggcas.ac.cn
Ricardo Fernandes
fernandes@shh.mpg.de

Specialty section:
This article was submitted to Paleoecology, a section of the journal Frontiers in Ecology and Evolution

Received: *14 July 2020*
Accepted: *08 January 2021*
Published: *19 February 2021*

Citation:
Wang X, Roberts P, Tang Z, Yang S, Storozum M, Groß M and Fernandes R (2021) The Circulation of Ancient Animal Resources Across the Yellow River Basin: A Preliminary Bayesian Re-evaluation of Sr Isotope Data From the Early Neolithic to the Western Zhou Dynasty. Front. Ecol. Evol. 9:583301. doi: 10.3389/fevo.2021.583301

INTRODUCTION

The Yellow River Basin is often considered the birthplace of ancient Chinese civilization, making this area the focus of archaeological research for decades (e.g., Liu and Chen, 2012; Chen et al., 2016; Dong et al., 2017; Li et al., 2020). As the geographic and cultural center of China, the Yellow River Basin hosted increasingly complex societies dating from the Neolithic to the Bronze Age, including the first agricultural villages and the earliest state-level and urban societies in China (Liu and Chen, 2003; Liu, 2009). Archaeological evidence from these periods revealed that settlement patterns, subsistence practices, mortuary customs, and circulation networks dramatically changed from the Early Neolithic (7000–5000 BCE) to the Western Zhou Dynasty (1046–771 BCE), laying the foundation for the subsequent development of ancient civilizations in China (Chang, 1986; Liu and Chen, 2012; Underhill, 2013; Shelach-Lavi and Jaffe, 2014; Zhang et al., 2020).

Through these different time periods, animals remained a consistent and essential part of the subsistence, ritual, and economic lifeways of past societies living within the Yellow River Basin (Yuan, 2002, 2015; Yuan and Flad, 2005; Dong and Yuan, 2020). As a result, information from zooarchaeological remains related to changes in animal communities, management, and origins can be immensely important indicators of economic and societal changes, providing a major contribution to our growing understanding of the societal transitions in the Yellow River Basin. Previous zooarchaeological research within the Yellow River Basin has mainly focused on the history of animal domestication and exploitation strategies. This revealed that pigs were domesticated independently in China (Cucchi et al., 2011; Dong et al., 2020), while sheep and goats were introduced into the middle and lower Yellow River Basin from West Asia during the Early Longshan period (ca. 2500 BCE, Flad et al., 2007; Cai et al., 2011), quickly being distributed within the basin during the Late Longshan period (2500–1900 BCE) and the Bronze Age (1900–500 BCE, Liu and Ma, 2017). Domesticated cattle firstly appeared in northern China between 3000 and 2000 BCE, and later was widely dispersed through the entire Yellow River Basin (Cai et al., 2014; Liu and Ma, 2017). Horses were introduced to China by the second millennium BCE and were adopted by the Shang elite as a prestige animal used in sacrificial activities (Yuan and Flad, 2005). With increasing social complexity and political centralization within northern China starting at the Late Neolithic, sheep/goats and cattle not only complemented pigs and dogs for meat consumption and ritual activities, but also provided secondary products, such as transportation of goods, wool, milk, and traction (Owlett et al., 2018; Yuan et al., 2020). Evidence of sheep kill-off patterns at Taosi and Erlitou suggested that sheep were used as a source of traded secondary products, such as wool exploitation (Li, 2014; Li et al., 2014; Brunson et al., 2016). The increasingly important use of these animals lead to a marked rise in the number of animals buried in sites from the Late Neolithic. For instance, the number of sheep bones clearly increased (almost in equal proportion with pigs) at Taosi between the middle and late periods (Tao, 2007; Brunson, 2008). During the early periods of Erlitou, cattle and sheep accounted for more than 25% of the zooarchaeological assemblage, and by the late periods rose to more than 42%, a trend that continued throughout the Bronze Age within the basin (Li et al., 2014).

Zooarchaeological evidence can also provide useful insights into ancient networks of circulation, here understood as the human behaviors associated with the acquisition, trade, and exchange, of animals between and among different villages and communities (Yuan and Flad, 2005; Liu and Chen, 2012). With an increase in the demand for animal resources to be employed in more diverse set of roles during the Late Neolithic and Bronze Age, long-distance circulation of animal resources are believed to have led to an increase in imports from areas surrounding and beyond the Yellow River Basin (Flad et al., 2007; Liu and Chen, 2012; Cao, 2014; Yuan, 2015). However, zooarchaeological evidence for mobility may be insufficient (e.g., Shimao, Owlett et al., 2018) and unlikely to offer a precise geographical origin for animals within vast regions such as those managed by past human societies across China.

Strontium isotope ($^{87}Sr/^{86}Sr$) analysis has been widely used to identify and source non-local animals in prehistoric and historical zooarchaeological assemblages (Ericson, 1985; Bentley, 2006; Britton et al., 2011). Strontium has four stable isotopes ^{84}Sr, ^{86}Sr, ^{87}Sr, and ^{88}Sr. Among them, ^{87}Sr is radiogenic, as it is produced by the β-decay of rubidium (^{87}Rb). The relative abundance of ^{87}Sr compared to ^{86}Sr varies across geologic materials, according to their age and the original bedrock $^{87}Rb/^{86}Sr$ ratios (Faure, 1986). Since strontium has an electron configuration similar to calcium, strontium released from weathered rocks enters into the soil, water, and plants, and becomes incorporated into animal skeletal tissues. Once absorbed into plant and animal tissues, strontium acts as a substitute for calcium and has a small mass-dependent fractionation which can be corrected during mass spectrometric analysis (Bentley, 2006; Moynier et al., 2012). In the case of human teeth, $^{87}Sr/^{86}Sr$ of tooth enamel which formed during childhood does not change over the course of a lifetime, meaning that the method can be employed to assess the geological location of an individual's early childhood (Montgomery, 2010; Thornton, 2011). Although the underlying geology predominately determines the Sr isotopic compositions of biosphere materials, there are many factors that influence the $^{87}Sr/^{86}Sr$ of the biosphere, including atmospheric deposition, different weathering rates of minerals within rocks, anthropogenic disturbances to the environment and general topographic processes (Graustein and Armstrong, 1983; Evans et al., 2009; Hartman and Richards, 2014; Thomsen and Andreasen, 2019). Therefore, when establishing $^{87}Sr/^{86}Sr$ ratios for a given area, it is necessary to measure bioavailable $^{87}Sr/^{86}Sr$ ratios in biosphere materials instead of predicting ratios exclusively based on bedrock geology.

Strontium isotopes have been used to investigate early hominin landscape use and to examine the influence of climate change on early human mobility strategies (e.g., Copeland et al., 2011; Lugli et al., 2019). In later time periods, strontium isotopes have been used to inform archaeological perspectives on different modes of social organization in the ancient world (e.g., Knipper et al., 2017; Mittnik et al., 2019) and to assess the movement

patterns in different animal species within paleoecological and archaeological studies (e.g., Pleistocene extinct megafauna, bird and fish species, domesticated animals such as pig mobility at Stonehenge) (Hoppe et al., 1999; Brennan et al., 2019; Madgwick et al., 2019).

To date, thousands of sites with abundant faunal materials have been excavated across the Yellow River Basin (Campbell et al., 2011; Bao, 2014). Previous strontium isotopic studies preliminarily distinguished between non-local and local animals at a given site (Yin, 2008; Zhao et al., 2011a,b; Zhao et al., 2015, 2016a,b; Lan, 2017; Fang, 2018; Wu, 2018; Zhao, 2018; Zhao et al., 2018; Wu et al., 2019). Although these studies provided useful insights it is also relevant to notice that:

(1) Most of the studies were published in local Chinese journals and rarely translated into English;
(2) The studies are often focused on a single site and lack a discussion on the acquisition and circulation of animals across time;
(3) The studies lack an in-depth discussion of the geographic origins of exotic animals as there is no baseline map available for the Yellow River Basin.

In this paper, we re-evaluate previously published animal strontium isotope data to investigate animal resource circulation from the Neolithic until the Western Zhou Dynasty across the Yellow River Basin. We establish a bioavailable Sr baseline map for the Yellow River Basin using a novel Bayesian modeling method (AverageR) which, in turn, allow us to employ another Bayesian model (LocateR) to determine the place of origin of animals and thus offer insights into their movements and circulation across the landscape.

MATERIALS AND METHODS

Archaeological Sites

In this study, we compiled $^{87}Sr/^{86}Sr$ data from 167 animal enamel samples (including pig, cattle, sheep/goat, horses, and dogs) from 10 archaeological sites distributed across the Yellow River Basin (**Supplementary Table 1**) and dating from the Early Neolithic until the Western Zhou Dynasty. Investigated sites cover Jiahu, an Early Neolithic (7000–5000 BCE) village, a series of sites dating to the Middle to the Late Neolithic (5000–2000 BCE), Qingliangsi, Lajia, Jiaojia, Taosi, and Shimao, Erlitou and Wangjinglou dating to the Erlitou-Erligang periods (1900/1800–1250 BCE), Yinxu dating to the Late Shang Dynasty (1250–1046 BCE), and finally, Zaoshugounao dating to the Predynastic-Zhou and Western Zhou Dynasty (1046–771 BCE). Most of these sites are located along the middle reaches of the Yellow River (**Figure 1**), while Lajia is the only site from the upper course of the river and Jiaojia is located in the lower reaches of the river. Most of the sites are located in areas with similar geological backgrounds. Information concerning the excavation of these sites is given in **Supplementary Information**.

Modeling Methods for $^{87}Sr/^{86}Sr$ Baseline and Place of Origin

Within isotopic studies of past mobility, when the $^{87}Sr/^{86}Sr$ ratios for ancient human or animal tooth enamel formed during early lifetime differ from an established $^{87}Sr/^{86}Sr$ baseline at the location of their burial, it is assumed that this likely indicates that investigated human and animals migrated from regions with different isotopic signatures for bioavailable $^{87}Sr/^{86}Sr$ ratios (Evans et al., 2010; Montgomery, 2010). However, distinguishing

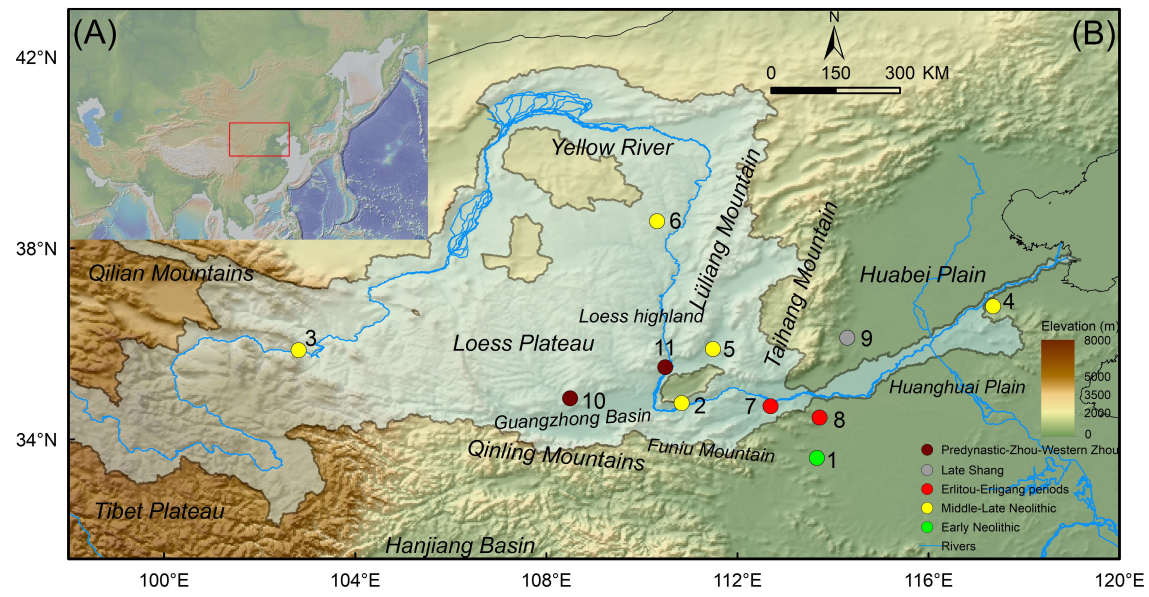

FIGURE 1 | (A,B) shows the current Yellow River drainage basin (blue shaded area) and its surroundings, as well as the archaeological sites referred in the study. (1) Jiahu; (2) Qingliangsi; (3) Lajia; (4) Jiaojia; (5) Taosi; (6) Shimao; (7) Erlitou; (8) Wangjinglou; (9) Yinxu; (10) Zaoshugounao; (11) Ruicheng. **(A)** was created using the software GeoMapApp (http://www.geomapapp.org) (Ryan et al., 2009).

non-locals from locals and identifying their possible geographic place of origin are challenging and require an accurate baseline map showing the distribution of bioavailable $^{87}Sr/^{86}Sr$ across a wide region (Bataille et al., 2020; Wang and Tang, 2020). In practice, directly sampled environmental materials, such as soil leachates, surface and groundwater, plants, and animal skeletons, form the basis of bioavailable $^{87}Sr/^{86}Sr$ maps (Bentley and Knipper, 2005; Maurer et al., 2012; Ventresca Miller et al., 2017; Snoeck et al., 2020). Recent advances in computational modeling, such as multi-source mixing models and random forest regression models employed a combination of baseline data and geological information to produce large-scale $^{87}Sr/^{86}Sr$ maps for the USA, Europe, the circum-Caribbean region, and also to assess global scale $^{87}Sr/^{86}Sr$ variability (e.g., Bataille and Bowen, 2012; Bataille et al., 2012, 2014, 2018, 2020; Willmes et al., 2018; Hoogewerff et al., 2019).

Unfortunately, the absence of a bioavailable $^{87}Sr/^{86}Sr$ map for the Yellow River Basin has hindered the use of strontium isotope methods for archaeological provenance studies in the region. To remedy this situation, we relied on previously published measurements on biosphere samples (**Supplementary Table 2**), including surface water, shallow groundwater, plants, snail shells, loess leachates, and low-mobility animals. From this data we employed Bayesian modeling to generate a $^{87}Sr/^{86}Sr$ baseline map across the Yellow River Basin and probability density maps to identify possible spatial origins for archaeological animals. This baseline map and assignment of animal origins are highly dependent on the density and types of analyzed samples that are currently available for the Yellow River Basin (Maurer et al., 2012; Willmes et al., 2018). To improve the reliability of spatial modeling, some samples were removed prior to analysis: (1) if measurement standards deviated considerably from reference values (>0.00003) or these were not reported; (2) if river samples may have been influenced of modern pollution; (3) using spatial statistical analysis to detect outliers. We calculated the global spatial autocorrelation (Moran's I) to test the spatial autocorrelation of $^{87}Sr/^{86}Sr$ data, which revealed a positive spatial autocorrelation (z-scores: 29.27, p-value < 0.05). A cluster/outlier analysis using Anselin's Local Moran's I was applied to test for local spatial autocorrelation to remove outliers (Anselin, 1995) following the method described by Pellegrini et al. (2016) and Scaffidi and Knudson (2020). Spatial statistical analysis was conducted using ESRI ArcMAP 10.2.

We produced a Bayesian spatial $^{87}Sr/^{86}Sr$ isoscape from 477 published samples using the Bayesian model AverageR available as an R-based (R Core Team, 2013) Open Access app, developed within the Pandora & IsoMemo initiatives (https://www.isomemoapp.com/). AverageR is a generalized additive mixed model that uses a thin plate regression spline (Wood, 2003). This spline smoother uses a Bayesian smoothing parameter governing the smoothness of the surface which is estimated from the data and a trade-off bias against variance to make the optimal prediction for new, unseen data (Wood, 2003; Groß, 2016; Rosenstock et al., 2019). By introducing a random intercept for the site, intra-site as well as the inter-site variation was employed in estimating uncertainty, expressed as a standard error of the mean. More specifically, we employ the following modeling formula:

$$Y_{ij} = s\left(\text{longitude, latitude}\right) + u_i + \varepsilon_{ij}$$

where:

Y_{ij}: independent variable for site i and individual j
s (longitude, latitude): spline smoother (Wood, 2003)
$u_i \sim N\ (0, \sigma_u)$: random intercept for site i.
$\varepsilon_{ij} \sim N\ (0, \sigma_\varepsilon)$: residual error for individual j in site i

The posterior distribution (P_x) generated by AverageR is given as:

$$P_x(y|\text{long, lat}) \sim N(\mu\left(\text{long, lat}\right), \sigma(\text{long, lat}))$$

To identify the place of origin for archaeological animals, we employed the Bayesian model LocateR, also developed within the Pandora & IsoMemo initiatives (https://www.isomemoapp.com/). Let x^* be an observed measurements with unknown location. Within the model LocateR, a measure of likelihood that a certain value x^* originates from a specific location is then the density of the posterior distribution P_x at point x^*:

$$P_x(x^*|\text{long, lat})$$

If the value x^* inherits some uncertainty σ_x^*, i.e., $x^* \sim N\ (\mu^*, \sigma^*)$, then we look for the overlap of both distributions, i.e., area of overlap. In practice this can be computed by simulating from $N\ (\mu^*, \sigma^*)$ and averaging over the corresponding posterior distribution values. This similarity index is then computed for each location of interest, giving a spatial map of similarity or locational likelihood for the observed measures.

RESULTS

Strontium Isotope Variations Across the Yellow River Basin

The resulting baseline map shows significant geographical variation in $^{87}Sr/^{86}Sr$ between the Yellow River Basin and surrounding areas (**Figure 2A**), with relatively homogeneous ratios (~0.7108–0.7118) within the basin and higher ratios (>0.712) distributed in the Qilian and Qinling Mountains, largely reflecting the influence of the underlying geology. Thick deposits of Quaternary loess cover the Loess Plateau of China (Liu, 1985; Ding et al., 2002), and much of this sediment is carried down into the Yellow River Basin. Since these areas are covered in thick deposits of loess or reworked loess, the $^{87}Sr/^{86}Sr$ signature for the region is relatively homogenous, with $^{87}Sr/^{86}Sr$ ratios slightly lower in the drainage basin than in the surrounding mountains. This hinders the identification of animals transported within most areas of the Yellow River Basin and from other areas: as far north as Yinshan Mountain, as far south as the Guanzhong Basin, as far west as the northeast of the Tibet Plateau, and as far east as the Huanghuai Plain. However, the underlying geologies and bioavailable $^{87}Sr/^{86}Sr$ ratios for the regions outside this area are sufficiently varied to enable the detection of animal and human movements into the Yellow River Basin.

The Qilian Mountains, close to the northwest of the upper Yellow River Basin, exhibit higher $^{87}Sr/^{86}Sr$ ratios (>0.712) than

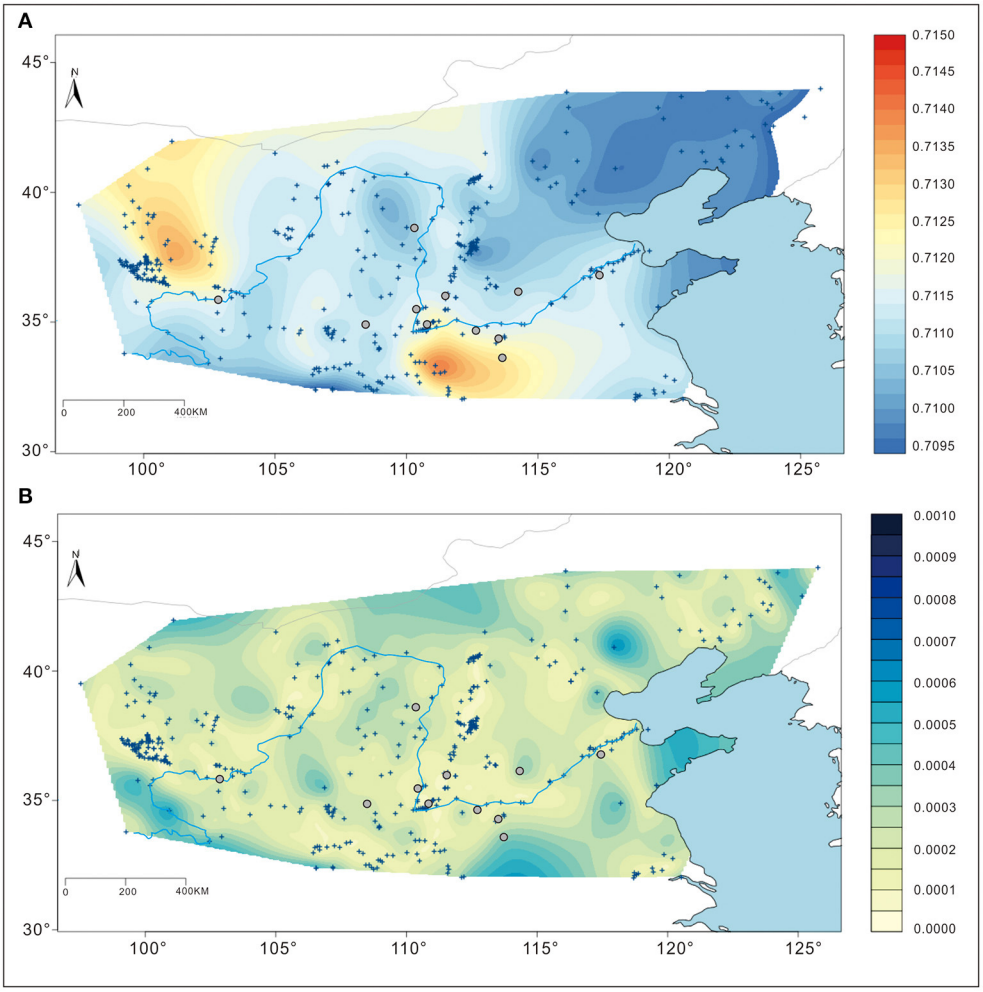

FIGURE 2 | (A) Bayesian mapping of bioavailable $^{87}Sr/^{86}Sr$ ratios for the Yellow River Basin and its surrounding areas; **(B)** Map of standard error of the mean map for predicted $^{87}Sr/^{86}Sr$ ratios.

the basin. This is mainly due to the presence of the Archean and Paleoproterozoic metamorphic rocks and granites (**Figure 3**) (Wu et al., 2010). In the south, the $^{87}Sr/^{86}Sr$ ratios in the Qinling Mountains, near the middle and lower reaches of the Yellow River, also show higher $^{87}Sr/^{86}Sr$. These ratios are likely the results of the presence of the Mesozoic granites and Precambrian rocks in the Qinling Mountains (Wang et al., 2013). Thus, long-distance movements of animals between Qilian or the Qinling Mountains and sites within the Yellow River Basin should be distinguishable using $^{87}Sr/^{86}Sr$ analysis (**Figure 2A**).

The baseline map (**Figure 2A**) also shows differences in the $^{87}Sr/^{86}Sr$ ratios for investigated archaeological sites. Most locations (Jiaojia, Qingliangsi, Shimao, Taosi, Lajia, Yinxu, and Zaoshugounao) have lower ratios (~0.7108–0.7118), probably due to the influence of the underlying loess and other Cenozoic sediments. The remaining three other sites, located adjacent to the northern edge of the Qinling Mountains (Wangjinglou, Erlitou, and Jiahu) exhibit slightly higher $^{87}Sr/^{86}Sr$ ratios (>0.7118), probably influenced by the geology of the Qinling Mountains. The standard error of the mean for predicted $^{87}Sr/^{86}Sr$ (**Figure 2B**) obtained through Bayesian modeling are generally lower than 0.0006 across the mapped region.

Defining the Local $^{87}Sr/^{86}Sr$ Signature

While having great potential, methods for establishing local Sr isotopic signature still vary and remain complex. In general, two methods have been suggested (Scaffidi and Knudson, 2020). The commonly used method is to measure the $^{87}Sr/^{86}Sr$ ratio of enamel or bones in archeological low-mobility animal species (e.g., snail shells, rodents, and pigs) which will likely average Sr isotopes within their dwelling area (Bentley et al., 2004). However, different low-mobility animal species may vary in $^{87}Sr/^{86}Sr$ ratios given a variability in dietary preferences, species-specific dwelling ranges, trade, animal husbandry and herding practices (Price et al., 2002; Montgomery, 2010). The second approach is to use the $^{87}Sr/^{86}Sr$ of various types of local environmental samples, such as bedrock, soil leachate, plants, and water (Evans et al., 2010; Lugli et al., 2019). In this

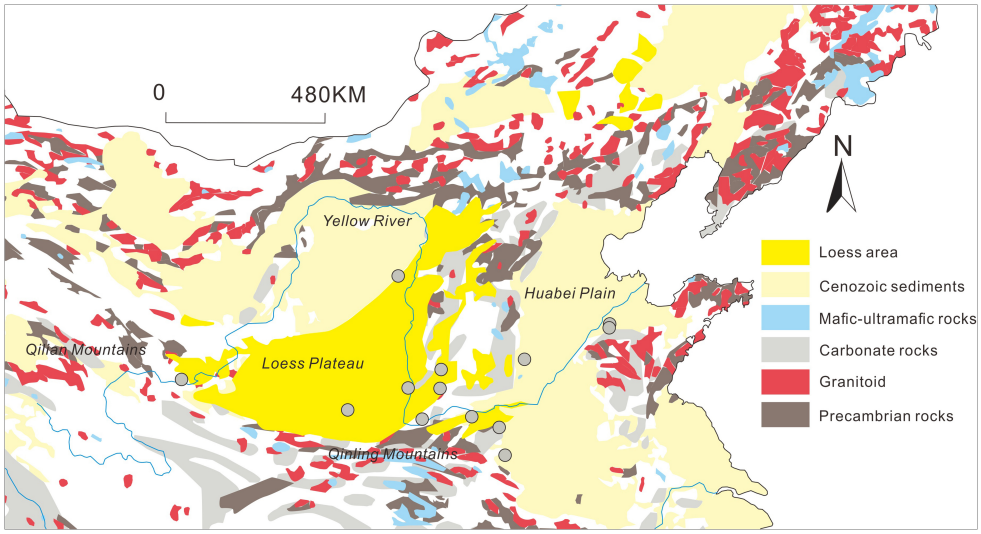

FIGURE 3 | Geological map of the study area (Modified after Ma et al., 2002).

case, comparisons of $^{87}Sr/^{86}Sr$ measurements on environmental samples revealed variations among materials since these are the results of different depositional and biochemical process, and thus may not match with the $^{87}Sr/^{86}Sr$ ratios for tissues of local animals and humans (Maurer et al., 2012). Therefore, it is recommended that reliable local $^{87}Sr/^{86}Sr$ reference ratios should be established by extensive field collections (Grimstead et al., 2017; Britton et al., 2020). In our study area, published $^{87}Sr/^{86}Sr$ ratios for local samples (especially plants) are scarce and unevenly distributed around most of the archaeological sites for which $^{87}Sr/^{86}Sr$ animal data are available. Here, we define local ranges for $^{87}Sr/^{86}Sr$ ratios by taking the mean and two standard deviations (2SD) of $^{87}Sr/^{86}Sr$ ratios measured in local low-mobility animals.

Pigs may be employed as a good reference for local $^{87}Sr/^{86}Sr$ ranges in migration studies as they are often raised near settlements and consume human by-products such as table scraps and crop wastes which can average bioavailable Sr isotope signals for the areas within which local residents utilize food resources (Bentley and Knipper, 2005). Previous zooarchaeological studies have shown that domesticated pigs in China were present at the Jiahu site as early as the Early Neolithic period and played an important role in food consumption and sacrificial activities in ancient China in both prehistorical and historical times (Cucchi et al., 2011; Yuan, 2015; Brunson et al., 2016). In contrast, some studies have shown that pigs were also subject to trade by past societies and thus can possibly originate from areas distant from their burial location (Shaw et al., 2009; Madgwick et al., 2019). In view of this, we compared the $^{87}Sr/^{86}Sr$ ratios measured on pigs with those from bioavailable baseline map. The $^{87}Sr/^{86}Sr$ ratios of pigs obtained from the 10 sites range from 0.710842 to 0.712388, and fall within the ranges for the Yellow River Basin and Qinling Mountains. Furthermore, the variability of $^{87}Sr/^{86}Sr$ ratios for archaeological sites is relatively small, suggesting that they moved within a narrow geographic area. Thus, the local $^{87}Sr/^{86}Sr$ ranges for each site in this study is defined by the mean ratio (± 2SD) for pig tooth enamel, providing the local ranges for Jiahu (0.71220–0.71242), Qingliangsi (0.71118–0.71171), Lajia (0.71080–0.71106), Jiaojia (0.71097–0.71173), Taosi (0.71103–0.71133), Shimao (0.71107–0.71129), Erlitou (0.71189–0.71227), Wangjinglou (0.71182–0.71203), Yinxu (0.71132–0.71174), and Zaoshugounao (0.71085–0.71161).

Identifying Non-local Domesticated Animals

Domesticated animals other than pigs ($n = 93$, mostly cattle and sheep/goats) have $^{87}Sr/^{86}Sr$ ranging from 0.709431 to 0.712844. The presence of non-local domesticated animals appears as early as the Late Neolithic with three sheep found at Shimao and Taosi as well as a cattle sample from Lajia (**Figure 4**). The most radiogenic ratios are observed in a Late Shang horse from Yinxu (0.712844) and a cattle sample from Erlitou (0.712593), and the lowest ratios are present in a separate horse from Yinxu (0.709431) and a predynastic Zhou-Western Zhou sheep from Zaoshugounao (0.709995), all of which have ratios well-beyond the local range defined by pigs for each of these sites.

Although the majority of the non-pig domesticated animals yielded strontium isotope ratios that are consistent with the baseline map (**Figure 4**), 24 animal samples are classified as isotopic outliers. These outliers include three sheep and one cattle from sites dating to the Middle to Late Neolithic (4/25), five sheep and six cattle recovered from the Erlitou-Erligang period sites (11/30), five horses from Yinxu during the Late Shang Dynasty (5/10), as well as two sheep, one dog and one cattle from a predynastic Zhou-Western Zhou site (4/18), which shows a slight increase in the percentage of non-local animals after the Late Neolithic. These "outliers" plot on both sides of

the strontium isotope baseline at sites dating from the Erlitou-Erligang periods to the West Zhou Dynasty, suggesting that these non-local animals may have diverse geographic origins.

Excluding pigs, the variability in $^{87}Sr/^{86}Sr$ ratios for domesticated animals increases through time (**Figure 5**, 1 SD for sites dating to the Middle-Late Neolithic: 0.000087–0.000296;

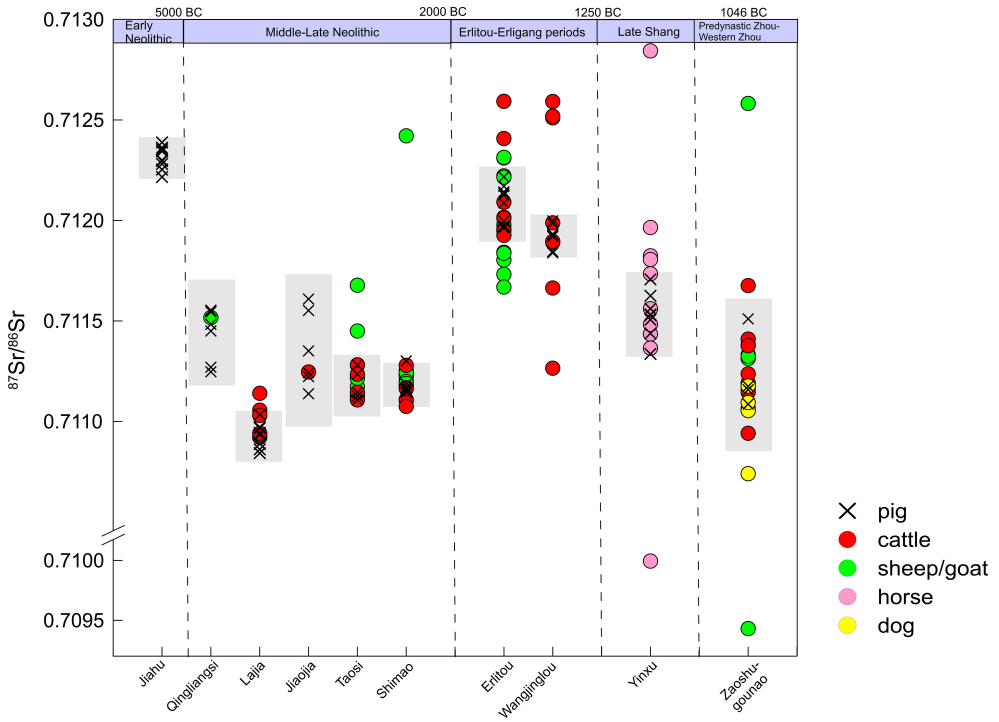

FIGURE 4 | $^{87}Sr/^{86}Sr$ ratios for animal tooth samples from 12 archaeological sites. Gray intervals represent the $^{87}Sr/^{86}Sr$ range for pigs at each site.

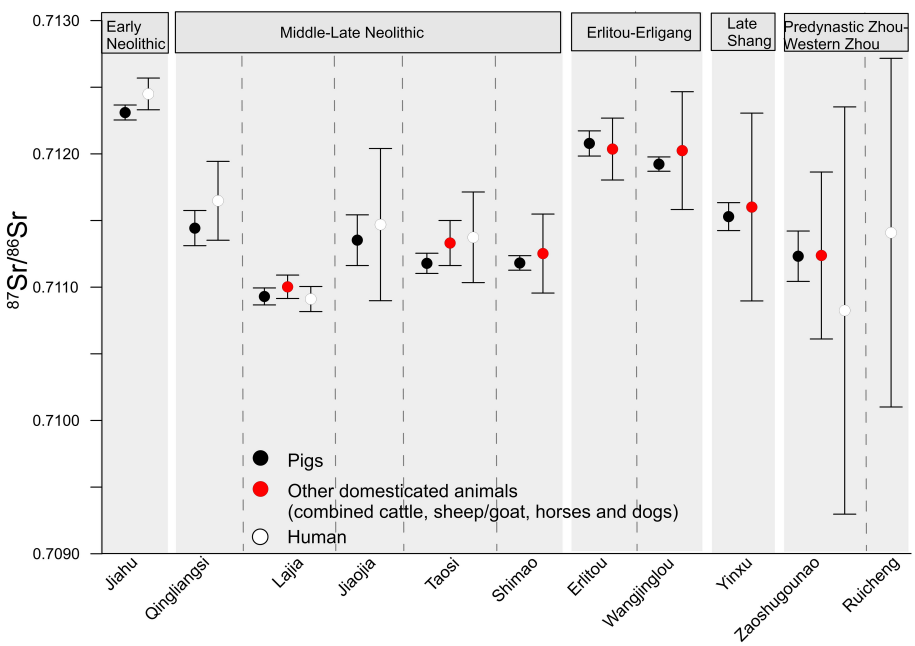

FIGURE 5 | Mean and standard deviation of $^{87}Sr/^{86}Sr$ ratios for pigs, other domesticated animals, and human samples from archaeological sites across different periods within the Yellow River Basin.

Erlitou-Erligang: 0.000232–0.000442; Late Shang: 0.000704; Predynastic Zhou-Western Zhou: 0.000626). Notwithstanding the limited sample size for some periods, there is a clear increase in the variability of animal circulation from the Middle-Late Neolithic to the Western Zhou Dynasty. Particularly at sites dating to the Late Neolithic (Shimao), the Late Shang Dynasty (Yinxu), and the Predynastic Zhou-Western Zhou Dynasty (Zaoshugounao), two sheep (0.709431 and 0.712421, respectively) and two horse teeth (0.709995 and 0.712884, respectively) have $^{87}Sr/^{86}Sr$ ratios that are significantly different from the local isotopic signature and that are rarely observed within the Yellow River Basin.

The high variability in $^{87}Sr/^{86}Sr$ ratios for animals, excluding pigs, may also result from the herding of animals across areas showing large $^{87}Sr/^{86}Sr$ variation within relatively short distances which may occur in vertical transhumance (Montgomery, 2010). The Yellow River Basin is located at a transitional zone between agriculturalist and agro-pastoralist lifeways (Cao et al., 2020). This transitional zone shifted northward or southward as a result of climate change and/or human adaptions (e.g., establishing irrigation farming such as Tuntian (屯田) in the north or due to territorial changes arising from conflicts with nomadic populations) (Han, 2012). Ancient local populations within the region relied primarily on production activities such as crop farming or livestock husbandry albeit with temporal variations. Therefore, we cannot exclude the possibility of animal herding within the basin, which could have resulted in $^{87}Sr/^{86}Sr$ signatures differing from local site ranges. To further investigate this possibility, intra-tooth sequential sampling work could be performed. Additionally, the larger variability in $^{87}Sr/^{86}Sr$ ratios in cattle, goats and sheep compared to that of pigs can also result from different human feeding practices involving cultivated millets and C_3-based plants within the Yellow River Basin. Previous research employing carbon and nitrogen isotopes have suggested that pigs were mainly fed on C_4-based foods (e.g., millets) while other domesticated animals consumed a mix of C_3 and C_4 foods from the Late Neolithic onward (Chen et al., 2016; Dai et al., 2016; Wang et al., 2018). In this respect, different types of plants within a certain region may show variable $^{87}Sr/^{86}Sr$ ratios as a result of different physiologies and water utilization strategies (e.g., depth of the root uptake) or growth in different landscape (e.g., valleys vs. foothills) (Poszwa et al., 2004; Montgomery, 2010; Reynolds et al., 2012), it is possible that non-local pigs with more diverse fodders yield larger variations. However, several examples of extreme $^{87}Sr/^{86}Sr$ outliers in Shimao, Zaoshugounao and Yinxu are well-beyond the isotopic ranges observed within the basin, indicating that people were circulating animals between and among different remote regions.

Human vs. Animal Mobility

Strontium isotope analysis in the Yellow River Basin was also previously carried out on human teeth (Yin, 2008; Chen, 2012; Zhao et al., 2016b; Lan, 2017; Fang, 2018; Wu, 2018). Human samples from the Early Neolithic indicate that their ratios are mostly similar to their local baseline reference and show little variability (**Figure 5**). A larger variation of $^{87}Sr/^{86}Sr$ in human samples is observed during the Middle-Late Neolithic compared to the Early Neolithic, and an even larger variation in human $^{87}Sr/^{86}Sr$ ratios is found at the two archaeological sites dating to the Predynastic Zhou-Western Zhou Dynasty (1 SD of humans for sites dating to the Neolithic: 0.000094–0.000571; Predynastic Zhou-Western Zhou: 0.001308–0.001527), a result that is consistent with the variability observed in animals. This suggests that the introduction of animals into these sites from a wider geographic range during the later periods is likely related with shifts in human mobility.

Origins of Non-local Domesticated Animals

We took as reference the $^{87}Sr/^{86}Sr$ baseline map and employed the model LocateR to map the probability of origin at different locations for outlier animals, that is, those that had the most extreme $^{87}Sr/^{86}Sr$ ratios when compared to the two-sigma range observed at the different sites (**Figure 6**). As mentioned previously, 24 outliers are identified from all sites and most of these ($n = 19$) have $^{87}Sr/^{86}Sr$ ratios similar to those found in or near the surroundings of the Yellow River Basin. In this case, we cannot identify if these animals were raised nearby the site or brought from afar within the basin or the Loess Plateau. For example, the six non-local cattle and five non-local sheep that date to the Erlitou-Erligang periods have $^{87}Sr/^{86}Sr$ ratios between 0.711265 and 0.712593. The likely geographical sources for these extreme ratios are all found in vicinity to the site or within the larger basin region for which similar baseline $^{87}Sr/^{86}Sr$ ratios are observed (**Figure 6**). Future research should employ a multi-proxy approach (e.g., $^{87}Sr/^{86}Sr$ in combination with oxygen or sulfur isotopes) under which it will likely be possible, using LocateR, to achieve a higher spatial constraint for place of origin.

For some extreme outliers ($n = 5$), the Bayesian modeling results suggest a place of origin which can be at large distances from the archaeological sites where the animal remains were found. For instance, one sheep sample from the Late Neolithic site of Shimao has a $^{87}Sr/^{86}Sr$ ratio (0.712421) similar to those observed at the Qinling or Qilian Mountains, located at a distance larger than 400 km from the site. Two horse samples from the Late Shang Dynasty have extreme $^{87}Sr/^{86}Sr$ ratios (0.712844 and 0.709995) which differ considerably from the site reference. The likely source for the horse with the upper extreme ratio is within areas located at least 200 km from the site (e.g., northern Qinling Mountains). For the horse with the low extreme ratio, the place of origin is likely the northern part of the Huabei Plain and northeastern China at a distance of over 150 km from the site. From the Zaoshugounao site, which dates to the predynastic Zhou-Western Zhou Dynasty, the likely origins of the high $^{87}Sr/^{86}Sr$ ratio from a sheep (0.712582) are the Qinling or the Qilian Mountains, while the low ratio of another sheep (0.709431) fits well with the $^{87}Sr/^{86}Sr$ ratios observed within the Hanjiang Basin located in the south of the Qinling Mountains, as well as extended sections of northern part of the Huabei Plain and northeastern China, around 150 km distant from the site.

DISCUSSION

$^{87}Sr/^{86}Sr$ Evidence for Animal Circulation

The statistical analysis of the animal isotopic data and the modeling results demonstrate the circulation of animal resources

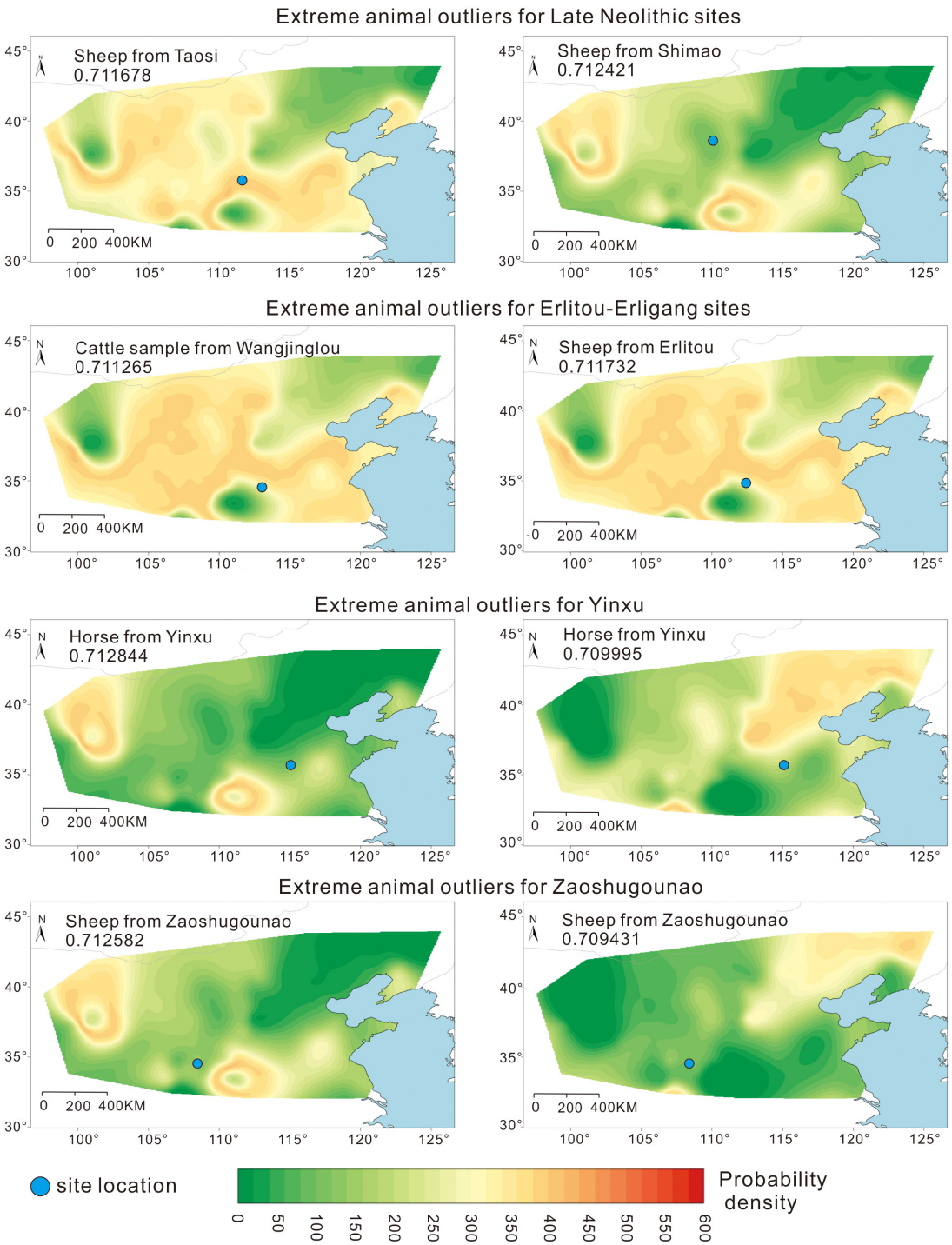

FIGURE 6 | Probability density map for Bayesian estimates on the possible geographical origins for extreme outlier $^{87}Sr/^{86}Sr$ ratios observed in animals at different archaeological sites. Points show the site location and a color scale is used to represent the probability of origin across the map.

from the Late Neolithic onwards that could have been driven by inter-regional networks that extended beyond the Yellow River Basin. From the Late Shang to the Western Zhou Dynasty, an increasingly higher number of animal resources may have arrived at investigated sites through long-distance circulation networks. This temporal pattern revealed by animal $^{87}Sr/^{86}Sr$ data matches the zooarchaeological evidence which shows an increase of the regional exchange of animal resources after the Neolithic (see discussion below). With more socially complex societies and stronger hierarchical systems emerging after the

Neolithic, domesticated animals filled an increasingly diverse set of roles, not only as food sources and ritual goods, but also as sources of secondary products (e.g., traction, dairy products) for humans. This rise in the demand for domesticated animals led to a temporal increase in the number of animals imported into the basin through various means, such as war, trade, tribute, and different animal management strategies.

During the Early-Middle Neolithic period, domesticated pigs served as a main source of meat and were frequently sacrificed for ritual purposes (Kim et al., 1994; Yuan, 2015; Dong and Yuan, 2020). After pigs, dogs were the second most important sacrificial offering and were also used as a hunting aid during the Neolithic period (Dong et al., 2020) and later were more routinely sacrificed in ritual ceremonies during the Shang Dynasty, particularly in the lower Yellow River Basin. Following the introduction of sheep/goats and cattle into north China during the Middle-Late Neolithic, these domesticated animals were frequently used in social and economic activities complemented with pigs and dogs (Flad et al., 2007; Yuan, 2010; Lu et al., 2017). During the Shang and Zhou Dynasties, with the increase in social complexity and the consolidation of social hierarchies, cattle and sheep replaced the pig dominated zooarchaeological assemblages that typified the Neolithic in some regions (Li, 2012; Brunson, 2015; Ren, 2019). As for animal consumption, the contribution from cattle increased from the Erlitou period onward, growing from 5 to 20% between 1850 and 1400 BCE and jumping to 50% after only a century before stabilizing during the Shang Dynasty (Cao, 2014). During ritual activities, the Zhou king established a hierarchical system of animal sacrifice, revealing that cattle and sheep were only represented at the top two hierarchical systems (Sun, 1989). A large number of cattle and sheep were required for sacrifice in ancestral worship ceremonies and according to *Yizhoushu·Shifujie*, the Zhou king sacrificed about 500 cattle to the heavens and about 2,700 sheep, dogs, and pigs to nature (Huang, 2007). Therefore, it is possible that these early states secured external supplies to meet the huge demand for consumption and ritual activities involving animals within cities.

Unlike other domesticated animals, people deemed horses a prestige animal throughout the Bronze Age, particularly during the Late Shang period when this kind of animal had just been introduced to China and were used in warfare and as sacrifices in the tombs of kings (Xie, 1959; Yuan and Flad, 2005). Many adult horses were found in excavations at Yinxu, but were rarely found in the surrounding regions, indicating that, except for locally raised horses, some of these horses were probably brought to Yinxu from distant regions. Based on zooachaeological evidence and on unearthed mortuary goods (e.g., chariots and horse fittings) some outposts were likely sources of horses, such as Gaohong (Shanxi, $^{87}Sr/^{86}Sr \sim 0.7110$), Zhangying (Beijing, $^{87}Sr/^{86}Sr \sim 0.7100$) and northeastern China ($^{87}Sr/^{86}Sr < 0.7100$) (Yang, 2006a; Cao, 2014). From the probability density map (**Figure 6**), the nearest sources for the $^{87}Sr/^{86}Sr$ ratios observed for Late Shang horses are the north and west parts of the Huabei Plain (including Shanxi and Zhangying), about 100 km way from the site, indicating that Yinxu had interregional interactions with these regions, a hypothesis supported by the presence of trade goods like bronze vessels, gold ornaments, and bronze weapons also from this region (Cao, 2014). Beyond consumption and sacrifice, these animals were used by the military, for agriculture, the transportation of goods, and as a source of traded secondary products (e.g., wool exploitation) since the Late Neolithic (Li, 2014; Li et al., 2014).

Written Evidence for Animal Circulation

Written records (e.g., oracle bone inscriptions, see Guo, 1978–1983) dating to the Late Shang Dynasty are a useful source of information regarding ancient animal circulation networks. Although these are ritual texts from high-ranking elites, it is evident that animals were imported to the capital city by trade, tribute, or as the spoils of war during the Late Shang (Yang, 1999). For instance, high-ranking elite Zi (子) sent envoys to inquire among professional traders, who usually traveled long distances, on the source of horses which were considered valuable exotic animals in ancient China (Guo, 2010). However, these written records contain few details on the locations or distances to the sources of exotic animals. One oracle bone inscription mentioned that to "get" cattle from Cha, the western outpost probably in the Linfen Basin, was about a 10 days' journey away from the capital city Anyang (*HJ* 8977). Another inscription recorded that Cha and Zhi Guo (probably persons or places from modern Shanxi) delivered horses to Anyang (*HJ 8797*), and some Shang vassal states (e.g., Weifang, modern Shandong) also supplied cattle to the capital city (*HJ* 32896, Cao, 2014). Yet another inscription mentions that the Shang court ordered an inspection of sheep/goats in the western land where they might intend to import sheep/goats from west (*HJ* 8777).

Additionally, there are multiple oracle bone inscriptions referring to animals as tribute. One group mentions that someone "offers" (供or 登), "turns in" (入) and "presents" (见,similar to 献) animals to the Shang king (e.g., *HJ* 10405, *HJ* 19875, *HJ* 1606, *HJ* 5685, and *HJ* 102). The other group shows that the Shang king ordered his subjects to "get" (取), "bring" (来) animals (e.g., horse) for him (e.g., *HJ* 945, *HJ* 8979, and *HJ* 8966). The described animals include cattle, horse, sheep, dog, pig and other wild animals. The largest number of cattle for tribute mentioned in inscriptions is once about four hundred (e.g., *HJ* 8965), followed by sheep at three hundred (e.g., *HJ* 8959), dogs at two hundred, horse at thirty (e.g., *HJ* 500), (e.g., *HJ* 8979), and for pig only two (e.g., *HJ* 11432). Those who gave offerings included professional traders, foreign statelets, vassals, or elite-officials. Additionally, in the records from the early Western Zhou bronze *Xiao Yu Ding* (小盂鼎), a commander *Yu* is said to have captured a large number of domesticated animals (355 cattle and 28 sheep/goats) and chariots in two campaigns against the Guifang (in northern Shaanxi and Shanxi), and presented them to the king (Li, 2006).

Animal Circulation and Social Complexity

The $^{87}Sr/^{86}Sr$ evidence presented in this study offered detailed insights into changes in animal mobility and circulation networks from the Early Neolithic to the Western Zhou Dynasty. Domesticated animals showed a temporal increase in non-local origins starting with the Late Neolithic. A greater number of

outliers for later periods also observed for humans, probably indicates that human movement expanded the use of animal resources across wider geographic areas. This shift was probably not only a consequence of increased social complexity but also it reflected the increased network of linkages between China's different regions.

During the Neolithic, most domesticated animals have $^{87}Sr/^{86}Sr$ ratios indicating that these resided within the Yellow River Basin. Animals that have ratios which are extreme outliers are found only at large Late Neolithic sites, indicating that the initial period of extensive animal circulation might have begun during the Late Neolithic. The Early Neolithic reveals a mixed economy that combined hunting and gathering, raising domesticated animals (pig and dog), and cultivating domesticated plants (millet and rice) in the Yellow River Basin (Liu et al., 2005; Hu et al., 2006; Underhill and Habu, 2006). During this period, the settlement pattern of the region consisted of small villages scattered within the major river valleys and ceramics were hand molded into relatively simple shapes (Underhill, 2013; Shelach-Lavi, 2015).

However, during the Middle-Late Neolithic (e.g., Late Yangshao and Longshan periods), particularly the Late Neolithic, Neolithic society witnessed an increase in social complexity and developed early forms of urbanism with political, religious, and economic functions: mortuary goods showing remarkable signs of social hierarchy (Underhill, 2002; Liu and Chen, 2012), regional centers built with walled enclosures (Liu and Chen, 2012), an increase in population density, settlement numbers, and size (Liu et al., 2005), the introduction of sheep and cattle (Barnes, 1999; Flad et al., 2007), more elaborate shapes and production techniques of ceramics and jade and their long-distance circulations (Shelach-Lavi, 2015), exotic trade and exchange items (e.g., turtle shells and ivory artifacts) (Barnes, 1999; Li, 2015), the use of bronze and copper artifacts (Liu, 2004), greater inter-polity conflict and warfare, and early writing system (Liu, 2004). Painted potteries were developed around the middle region of the Yellow River during the Yangshao period and later spread into other regions, such as the Wei River region, northeast China, and into the lower region of the Yellow River (Underhill, 2002). High quality eggshell and fine black ceramics typical of sites in the Shandong area during the Longshan period were found in some large sites in the middle region of the Yellow River, such as Wangchenggang (Shelach-Lavi, 2015). Jade artifacts provide further evidence for interactions among societies with many sites in the Yellow River Basin revealing the presence of Liangzhu-style jades such as *cong* 琮 and *bi* 璧 (from the lower Yangtze Basin), probably representing the elite-controlled exchange of prestige items (Liu and Chen, 2012; Shelach-Lavi, 2015).

Larger variability in $^{87}Sr/^{86}Sr$ ratios for animals from the Erlitou-Erligang periods indicates that animal resources were increasingly transported from more diverse regions, consistent with political and economic shifts documented at this time. As suggested by Liu (2009), the Erlitou period is often described as exhibiting the earliest state-level societies in China based on a mono-centered and highly integrated political system that spread across a wide region. However, some opposing archaeological views hold that the first state-level states in China emerged during the Late Neolithic which may have included the Liangzhu and Taosi cultures (e.g., Allan, 2007; Shelach-Lavi and Jaffe, 2014; Renfrew and Liu, 2018). The peripheral regions provided the dominant center (Erlitou and Erligang) with raw materials and exotic goods as tribute to support urban growth and technological production, contributing to the formation and maintenance of hierarchical social and political structures. Many goods and natural resources, such as timber for building palaces, kaolinic clay for making white pottery, salt for daily use, lead, tin, and copper for making bronzes, lithic materials for stones tools, were imported into Erlitou (Liu, 2003) which is located on alluvial plains and is poor on natural resources (Liu and Chen, 2001; Chen et al., 2010; Li, 2011). However, most of these resources could have been acquired from the surrounding regions within radii of 20 to 200 km (Liu and Chen, 2003). For instance, stone resources were abundant in the Mangling Hills (200 km to the southwest of the site) and Sangshan Mountains (40 km to southeast of the site) (Liu and Chen, 2003). The Hedong Salt Lake, located ∼160 km to the northeast of Erlitou, was the only salt source for Erlitou (Liu and Chen, 2012). Considering that other goods and resources were moved from exotic locales as well (Yang, 2006b), it is unsurprising that the $^{87}Sr/^{86}Sr$ signatures of the domesticated animals reveal that some of these were imported from regions far off from the Yellow River Basin.

The Late Shang was characterized by a multicentre political landscape and multiple overlapping regional economies (Liu and Chen, 2012; Dreyer, 2015). The forms of interaction between the Shang state and its surroundings became more complex through exchange, warfare, and tribute (Chang, 1980; Yang, 1999). According to the historical records and archaeological evidence, a number of exotic goods, raw materials, animals for sacrifice and other resources were imported from the peripheries, or, in some cases, remote locations (Bagley, 1999; Chen et al., 2019). A remarkable development during the Late Shang Dynasty was the introduction of horses. Unlike other animals such as cattle or sheep/goats commonly used for consumption and sacrifice, horses were an important means of transport for both people and goods, in long distance trade, warfare, and as a prestige animal sacrificed for royal tombs (Yuan and Flad, 2005). High-quality horses, in particular, were always desirable to the elite class and were often obtained from remote regions and thus it is unspringing that the horses at Yinxu have extreme $^{87}Sr/^{86}Sr$ ratios (Cao, 2014).

A chronological comparison reveals that the largest variability in animal $^{87}Sr/^{86}Sr$ ratios took place during the Western Zhou Dynasty. The Western Zhou adopted a feudal political system 分封制 in which the king enfeoffed his relatives and non-cognate meritorious generals and leaders by granting them land and these in returned had to heed the king's commands and pay a regular tribute (Li, 2008). The kings strengthened royal rule over nearby territories, established strict relationships with feudal lords, and increased the kingdom's territory through military conquest. This contributed to the multi-directional flow and re-distribution of materials and resources through trade, tribute and war (e.g., bronze vessels, jades, and animals;

Underhill, 2002; Shelach-Lavi, 2015). New technologies, such as bronze or iron casting, and religious innovations easily crossed political boundaries and were commonly adopted throughout the Zhou world (von Falkenhausen, 2006; Chastain, 2019). Bronze vessels became ornate artistic products during the Western Zhou Dynasty. In comparison to the Late Shang Dynasty, there was a larger production of bronze vessels and also a greater diversity in shapes and styles (Chastain, 2019). Bronze vessels are commonly found in elite burials and caches from the early Western Zhou Dynasty onward. A later development was the adoption of the sumptuary system known as *lie ding* (列鼎), in which the types and quantities of bronze vessels buried with the deceased were strictly prescribed by rank. This system was used throughout the Zhou territory (Shelach-Lavi, 2015; Jaffe, 2016).

CONCLUSIONS

Our study builds on previous archaeological and zooarchaeological discussions on the circulation of animal resources within the Yellow River Basin from the Neolithic until the Bronze Age. We address outstanding questions regarding the interconnectedness of animal circulation networks by mapping bioavailable $^{87}Sr/^{86}Sr$ across China. In our meta-analysis, we employed previously reported strontium isotopes measured in tooth enamel from domesticated animals (cattle, sheep/goats, horses, and dogs) to investigate animal movement and circulation across the Yellow River Basin over extended time periods. A few strontium isotope ratios outliers for animals from large Late Neolithic sites reveals the initial expansion of animal circulation systems which likely took place during Late Neolithic and Erlitou-Erligang periods. Our data also revealed that from the Late Shang period until the Western Zhou Dynasty there was an increase in the proportion of animals originating from regions with a higher degree of social complexity. This was likely the result of the adoption, at later time periods, of considerably more complex and interconnected economic and social systems. Nonetheless, the huge time span and area covered in our study plus the relatively small size of the presented dataset hinders a deeper discussion on the factors that influenced animal circulation. To overcome these limitations, future work is necessary to systematically increase the size of animal samples from across different periods plus the employment of multi-isotope methods. Nonetheless, our study provides a solid foundation for the use of strontium isotopes as a powerful tool in animal mobility studies within China.

DATA AVAILABILITY STATEMENT

The original contributions presented in the study are included in the article/**Supplementary Material**, further inquiries can be directed to the corresponding author/s.

AUTHOR CONTRIBUTIONS

XW, PR, ZT, and RF conceived the project. RF and XW conducted data analysis. All authors shared ideas, contributed to the interpretation of the results, and to the writing of the manuscript.

FUNDING

This work was funded by the Chinese Academy of Sciences (Grant Nos. XDA19050104, XDB26020401, and IGGCAS-201905) and the National Natural Science Foundation of China (Grant Nos. 41672177 and 42072210). PR and RF would like to thank the Max Planck Society for funding.

ACKNOWLEDGMENTS

We thank Ms. Lauren Kancle from Durham University for her assistance in the preparation of this manuscript. We also thank the editor Dr. Kate Britton and three reviewers for their constructive comments which greatly improved the manuscript.

SUPPLEMENTARY MATERIAL

The Supplementary Material for this article can be found online at: https://www.frontiersin.org/articles/10.3389/fevo.2021.583301/full#supplementary-material

REFERENCES

Allan, S. (2007). Erlitou and the formation of Chinese civilization: toward a new paradigm. *J. Asian Stud.* 80, 461–496. doi: 10.1017/S002191180700054X

Anselin, L. (1995). Local indicators of spatial association-LISA. *Geogr. Anal.* 27, 93–115. doi: 10.1111/j.1538-4632.1995.tb00338.x

Bagley, R. (1999). "Shang archaeology," in *The Cambridge History of Ancient China: from the Origins of Civilization to 221 BC*, eds M. Loewe and E. L. Shaughnessy (Cambridge: Cambridge University Press), 124–231. doi: 10.1017/CHOL9780521470308.005

Bao, S. G. 包曙光(2014). *Study on the animal sacrifices of Xia Dynasty to Warring States in Northern Region of China* 中国北方地区夏至战国时期的殉牲研究 (Ph.D. Thesis). Jilin University, Changchun, China (In Chinese).

Barnes, G. (1999). *China Korea and Japan: The Rise of Civilisation in East Asia*. New York, NY: Thames and Hudson.

Bataille, C. P., and Bowen, G. J. (2012). Mapping $^{87}Sr/^{86}Sr$ variations in bedrock and water for large scale provenance studies. *Chem. Geol.* 304–305, 39–52. doi: 10.1016/j.chemgeo.2012.01.028

Bataille, C. P., Brennan, S. R., Hartmann, J., Moosdorf, N., Wooller, M. J., and Bowen, G. J. (2014). A geostatistical framework for predicting variations in strontium concentrations and isotope ratios in Alaskan rivers. *Chem. Geol.* 389, 1–15. doi: 10.1016/j.chemgeo.2014.08.030

Bataille, C. P., Crowley, B. E., Wooller, M. J., and Bowen, G. J. (2020). Advances in global bioavailable strontium isoscapes. *Palaeogeogr. Palaeoclimatol. Palaeoecol.* 555:109849. doi: 10.1016/j.palaeo.2020.109849

Bataille, C. P., Laffoon, J., and Bowen, G. J. (2012). Mapping multiple source effects on the strontium isotopic signatures of ecosystems from the circum-Caribbean region. *Ecosphere* 3, 1–24. doi: 10.1890/es12-00155.1

Bataille, C. P., von Holstein, I. C. C., Laffoon, J. E., Willmes, M., Liu, X. M., and Davies, G. R. (2018). A bioavailable strontium isoscape for Western Europe: a machine learning approach. *PLoS ONE* 13:e0197386. doi: 10.1371/journal.pone.0197386

Bentley, R. A., and Knipper, C. (2005). Geographical patterns in biologically available strontium, carbon and oxygen isotope signatures in prehistoric SW Germany*. *Archaeometry* 47, 629–644. doi: 10.1111/j.1475-4754.2005.00223.x

Bentley, R. A., Price, T. D., and Stephan, E. (2004). Determining the 'local' $^{87}Sr/^{86}Sr$ range for archaeological skeletons: a case study from Neolithic Europe. *J. Archaeol. Sci.* 31, 365–375. doi: 10.1016/j.jas.2003.09.003

Bentley, R. A. (2006). Strontium isotopes from the earth to the archaeological skeleton: a review. *J. Archaeol. Method Theor.* 13, 135–187. doi: 10.1007/s10816-006-9009-x

Brennan, S. R., Schindler, D. E., Cline, T. J., Walsworth, T. E., Buck, G., and Fernandez, D. P. (2019). Shifting habitat mosaics and fish production across river basins. *Science* 364, 783–786. doi: 10.1126/science.aav4313

Britton, K., Grimes, V., Niven, L., Steele, T. E., McPherron, S., Soressi, M., et al. (2011). Strontium isotope evidence for migration in late Pleistocene Rangifer: implications for Neanderthal hunting strategies at the Middle Palaeolithic site of Jonzac, France. *J. Hum. Evol.* 61, 176–185. doi: 10.1016/j.jhevol.2011.03.004

Britton, K., Le Corre, M., Willmes, M., Moffat, I., Grün, R., Mannino, M. A., et al. (2020). Sampling plants and malacofauna in $^{87}Sr/^{86}Sr$ bioavailability studies: implications for isoscape mapping and reconstructing of past mobility patterns. *Front. Ecol. Evol.* 8:579473. doi: 10.3389/fevo.2020.579473

Brunson, K., He, N., and Dai, X. (2016). Sheep, cattle, and specialization: new zooarchaeological perspectives on the Taosi Longshan. *Int. J. Osteoarchaeol.* 26, 460–475. doi: 10.1002/oa.2436

Brunson, K. (2008). *Shifting animal exploitation strategies in Late Neolithic China: a zooarchaeological analysis of the longshan culture site of Taosi* (BA Thesis). Harvard University, Cambridge, MA, United States.

Brunson, K. (2015). *Craft specialization and animal products at the longshan period sites of Taosi and Zhoujiazhuang, Shanxi Province, China* (Ph.D. Thesis). University of California, United States.

Cai, D. W., Sun, Y., Tang, Z. W., Hu, S. M., Li, W. Y., Zhao, X. B., et al. (2014). The origins of Chinese domestic cattle as revealed by ancient DNA analysis. *J. Archaeol. Sci.* 41, 423–434. doi: 10.1016/j.jas.2013.09.003

Cai, D. W., Tang, Z. W., Yu, H. X., Han, L., Ren, X. Y., Zhao, X. B., et al. (2011). Early history of Chinese domestic sheep indicated by ancient DNA analysis of Bronze Age individuals. *J. Archaeol. Sci.* 38, 896–902. doi: 10.1016/j.jas.2010.11.019

Campbell, R. B., Li, Z., He, Y., and Jing, Y. (2011). Consumption, exchange and production at the Great Settlement Shang: bone-working at Tiesanlu, Anyang. *Antiquity* 85, 1279–1297. doi: 10.1017/s0003598x00062050

Cao, Q., Wu, J. G., Yu, D. Y., Wang, R. Q., and Qiao, J. M. (2020). Regional landscape futures to moderate projected climate change: a case study in the agro-pastoral transitional zone of North China. *Reg. Environ. Change* 20, 66. doi: 10.1007/s10113-020-01661-2

Cao, D. (2014). *The loess highland in a trading network (1300–1050 BC)* (Ph.D. Thesis). Princeton University, Princeton, NJ, United States.

Chang, K. C. (1980). *Shang Civilization*. New Haven, CT: Yale University Press.

Chang, K. C. (1986). *The Archaeology of Ancient China*. New Haven, CT: Yale University Press.

Chastain, M. L. (2019). *The ceramic technology of bronze-casting molds in Ancient China: production practices at three Western Zhou foundry sites in the Zhouyuan area* (Ph.D. Thesis). Massachusetts Institute of Technology, Cambridge, MA, United States.

Chen, X. L., Fang, Y. M., Hu, Y. W., Hou, Y. F., Lü, P., Yuan, J., et al. (2016). Isotopic reconstruction of the Late Longshan period (ca. 4200–3900 BP) dietary complexity before the onset of state-level societies at the Wadian site in the Ying River Valley, Central Plains, China. *Int. J. Osteoarchaeol.* 26, 808–817. doi: 10.1002/oa.2482

Chen, X. C., Liu, L., and Zhao, C. Y. (2010). "Salt from southern Shanxi and the development of early states in China," in *Salt Production in China in a Comparative Perspective, Salt Archaeology in China, Vol. 2*, eds S. C. Li and L. Falkenhausen (Beijing: Science Press), 42–65.

Chen, K. L., Mei, J. J., Rehren, T., Liu, S. R., Yang, W., Martinón-Torres, M., et al. (2019). Hanzhong bronzes and highly radiogenic lead in Shang period China. *J. Archaeol. Sci.* 101, 131–139. doi: 10.1016/j.jas.2018.11.010

Chen, X. 陈曦(2012). *The isotopic analysis of human bone unearthed in the Rui State cemetery in the Late Xi Zhou Dynasty* 梁带村芮国墓地出土西周时期人骨的骨化学特征研究 (Master Thesis). Northwest University, Xi'an, China (In Chinese).

Copeland, S. R., Sponheimer, M., de Ruiter, D. J., Lee-Thorp, J. A., Codron, D., le Roux, P. J., et al. (2011). Strontium isotope evidence for landscape use by early hominins. *Nature* 474, 76–78. doi: 10.1038/nature10149

Cucchi, T., Hulme-Beaman, A., Yuan, J., and Dobney, K. (2011). Early Neolithic pig domestication at Jiahu, Henan Province, China: clues from molar shape analyses using geometric morphometric approaches. *J. Archaeol. Sci.* 38, 11–22. doi: 10.1016/j.jas.2010.07.024

Dai, L. L., Balasse, M., Yuan, J., Zhao, C. Q., Hu, Y. W., and Vigne, J. D. (2016). Cattle and sheep raising and millet growing in the Longshan age in central China: stable isotope investigation at the Xinzhai site. *Quat. Int.* 426, 145–157. doi: 10.1016/j.quaint.2016.02.035

Ding, Z. L., Derbyshire, E., Yang, S. L., Yu, Z. W., Xiong, S. F., and Liu, T. S. (2002). Stacked 2.6-Ma grain size record from the Chinese loess based on five sections and correlation with the deep-sea $\delta^{18}O$ record. *Paleoceanography* 17, 5–21. doi: 10.1029/2001pa000725

Dong, N. N., and Yuan, J. (2020). Rethinking pig domestication in China: regional trajectories in central China and the Lower Yangtze Valley. *Antiquity* 94, 864–879. doi: 10.15184/aqy.2020.122

Dong, G. H., Du, L. Y., and Wei, W. Y. (2020). The impact of early trans-Eurasian exchange on animal utilization in northern China during 5000–2500 BP. *Holocene*. doi: 10.1177/0959683620941169

Dong, Y., Morgan, C., Chinenov, Y., Zhou, L. G., Fan, W. Q., Ma, X. L., et al. (2017). Shifting diets and the rise of male-biased inequality on the Central Plains of China during Eastern Zhou. *Proc. Natl. Acad. Sci. U.S.A.* 114, 932–937. doi: 10.1073/pnas.1611742114

Dreyer, J. T. (2015). *China's Political System*. New York, NY: Routledge. doi: 10.4324/9781315664613

Ericson, J. E. (1985). Strontium isotope characterization in the study of prehistoric human ecology. *J. Hum. Evol.* 14, 503–514. doi: 10.1016/S0047-2484(85)80029-4

Evans, J. A., Montgomery, J., and Wildman, G. (2009). Isotope domain mapping of $^{87}Sr/^{86}Sr$ biosphere variation on the Isle of Skye, Scotland. *J. Geol. Soc.* 166, 617–631. doi: 10.1144/0016-76492008-043

Evans, J. A., Montgomery, J., Wildman, G., and Boulton, N. (2010). Spatial variations in biosphere $^{87}Sr/^{86}Sr$ in Britain. *J. Geol. Soc.* 167, 1–4. doi: 10.1144/0016-76492009-090

Fang, S. Y. 房书玉(2018). *Strontium isotope analysis of human migration of Jiaojia Site* 焦家遗址人口迁移的锶同位素研究 (Master Thesis). Shandong University, Jinan, China (In Chinese).

Faure, G. (1986). *Principles of Isotope Geology*. New York, NY: Wiley.

Flad, R. K., Yuan, J., and Li, S. C. (2007). Zooarcheological evidence for animal domestication in northwest China. *Dev. Quat. Sci.* 9, 167–203. doi: 10.1016/S1571-0866(07)09012-4

Graustein, W., and Armstrong, R. (1983). The use of strontium-87/strontium-86 ratios to measure atmospheric transport into forested watersheds. *Science* 219, 289–292. doi: 10.1126/science.219.4582.289

Grimstead, D. N., Nugent, S., and Whipple, J. (2017). Why a standardization of strontium isotope baseline environmental data is needed and recommendations for methodology. *Adv. Archaeol. Pract.* 5, 184–195. doi: 10.1017/aap.2017.6

Groß, M. (2016). Modeling body height in prehistory using a spatio-temporal Bayesian errors-in variables model. *AStA Adv. Stat. Anal.* 100, 289–311. doi: 10.1007/s10182-015-0260-x

Guo, M. R. 郭沫若(1978–1983). *Jiaguwen Heji* 甲骨文合集. Beijing: Zhonghuashuju (In Chinese).

Guo, X. D. 郭旭东(2010). *Study of oracle inscriptions and rules of rites in Shang Dynasty* 卜辞与殷礼研究 (Ph.D. Thesis). Shaanxi Normal University, Xi'an, China (In Chinese).

Han, M. L. 韩茂莉(2012). *Historical Agricultural Geography of China* 中国历史时期农业地理. Beijing: Peking University Press (In Chinese).

Hartman, G., and Richards, M. (2014). Mapping and defining sources of variability in bioavailable strontium isotope ratios in the Eastern Mediterranean. *Geochim. Cosmochim. Acta* 126, 250–264. doi: 10.1016/j.gca.2013.11.015

Hoogewerff, J. A., Reimann, C., Ueckermann, H., Frei, R., Frei, K. M., Van Aswegen, T., et al. (2019). Bioavailable $^{87}Sr/^{86}Sr$ in European soils: a baseline for provenancing studies. *Sci. Total Environ.* 672, 1033–1044. doi: 10.1016/j.scitotenv.2019.03.387

Hoppe, K. A., Koch, P. L., Carlson, R. W., and Webb, S. D. (1999). Tracking mammoths and mastodons: reconstruction of migratory behavior using strontium isotope ratios. *Geology* 27, 439–442. doi: 10.1130/0091-7613(1999)027<0439:TMAMRO>2.3.CO;2

Hu, Y. W., Ambrose, S. H., and Wang, C. S. (2006). Stable isotopic analysis of human bones from Jiahu site, Henan, China: implications for the transition to agriculture. *J. Archaeol. Sci.* 33, 1319–1330. doi: 10.1016/j.jas.2006.01.007

Huang, H. X. 黄怀信(2007). *Yizhoushu Huijiao Jizhu* 逸周书汇校集注. Shanghai: Shanghaiguji Press (In Chinese).

Jaffe, Y. (2016). *The continued creation of communities of practice – Finding variation in the Western Zhou Expansion (1046–771 BCE)* (Ph.D. Thesis). Harvard University, Cambridge, MA, United States.

Kim, S. O., Antonaccio, C. M., Lee, Y. K., Nelson, S. M., Pardoe, C., Quilter, J., et al. (1994). Burials, pigs, and political prestige in Neolithic China [and Comments and Reply]. *Curr. Anthropol.* 35, 119–141. doi: 10.1086/204251

Knipper, C., Mittnik, A., Massy, K., Kociumaka, C., Kucukkalipci, I., Maus, M., et al. (2017). Female exogamy and gene pool diversification at the transition from the Final Neolithic to the Early Bronze Age in central Europe. *Proc. Natl. Acad. Sci. U.S.A.* 114, 10083–10088. doi: 10.1073/pnas.1706355114

Lan, D. 兰栋(2017). *Isotope analysis on human and animal's bone unearthed from Zaoshugounao Site in Chunhua County, Shaanxi Province* 陕西枣树沟脑遗址出土人和动物骨骼的同位素分析 (Master Thesis). Northwest University, Xi'an, China (In Chinese).

Li, Z. P., Campbell, R., Brunson, K., Yang, J., and Tao, Y. (2014). "The exploitation of domestic animal products from the Late Neolithic Age to the Early Bronze Age in the heartland of ancient China," in *Animal Secondary Products: Domestic Animal Exploitation in Prehistoric Europe, the Near East and the Far East*, ed H. Greenfield (Oxford: Oxbow), 56–79. doi: 10.2307/j.ctvh1dr4j.8

Li, X., Zhang, S. J., Lü, M. X., Qiu, M. H., Wen, S. Q., and Ma, M. M. (2020). Dietary shift and social hierarchy from the Proto-Shang to Zhou Dynasty in the Central Plains of China. *Environ. Res. Lett.* 15:035002. doi: 10.1088/1748-9326/ab6783

Li, F. (2006). *Landscape and Power in Early China: the Crisis and Fall of the Western Zhou 1045–771 BC*. Cambridge: Cambridge University Press.

Li, F. (2008). *Bureaucracy and the State in Early China: Governing the Western Zhou*. Cambridge: Cambridge University Press.

Li, J. X. 李建西(2011). *Jinnan Zaoqi Tongkuangye Yizhi Kaocha Yanjiu* 晋南早期铜矿冶遗址考察研究 (Ph.D. Thesis). University of Science and Technology Beijing, Beijing, China (In Chinese).

Li, Z. P. (2012). The consumption, utilization and supply of sheep and goats at the late Shang Dynasty capital: a zooarchaeological study on the sheep and goat remains unearthed in the Yinxu area. *Chinese Archaeol.* 12, 195–200. doi: 10.1515/char-2012-0024

Li, Z. P. 李志鹏(2014). The Zooarchaeogical study of wool explotation from the Neolithic Age to the early Bronze Age in the Central Plains 中原地区新石器时代到青铜时代早期羊毛开发的动物考古学研究. *Quat. Sci.* 34, 149–158 (In Chinese).

Li, X. W. 李新伟(2015). Zhongguo Shiqian Shehui Shangceng Yuanjuli Jiaoliuwang de Xingcheng 中国史前社会上层远距离交流网的形成. *Wenwu* 4, 51–58 (In Chinese).

Liu, L., and Chen, X. C. (2001). Cities and town: the contral of natural resources in early states, China. *Bull. Museum Far East. Anti.* 73, 5–47.

Liu, L., and Chen, X. C. (2003). *State Formation in Early China*. London: Duckworth.

Liu, L., and Chen, X. C. (2012). *The Archaeology of China: From the Late Paleolithic to the Early Bronze Age*. Cambridge: Cambridge University Press. doi: 10.1017/CBO9781139015301

Liu, L., and Ma, X. L. (2017). "The zooarchaeology of Neolithic China," in *The Oxford Handbook of Zooarchaeology*, eds U. Albarella, M. Rizzetto, H. Russ, K. Vickers, and S. Viner-Daniels (Oxford: Oxford University Press), 304–318. doi: 10.1093/oxfordhb/9780199686476.013.20

Liu, L., Chen, X. C., Lee, Y. K., Wright, H., and Rosen, A. (2005). Settlement patterns and development of social complexity in the Yiluo region, North China. *J. Field Archaeol.* 29, 75–100. doi: 10.1179/jfa.2004.29.1-2.75

Liu, T. S. 刘东生(1985). *Loess and Environment in China* 黄土与环境. Beijing: Science Press (In Chinese).

Liu, L. (2003). Production of prestige goods in the Neolithic and early state periods of China. *Asian Perspect.* 42, 1–40. doi: 10.1353/asi.2003.0025

Liu, L. (2004). *The Chinese Neolithic: Trajectories to Early States*. Cambridge: Cambridge University Press. doi: 10.1017/CBO9780511489624

Liu, L. (2009). State emergence in early China. *Annu. Rev. Anthropol.* 38, 217–232. doi: 10.1146/annurev-anthro-091908-164513

Lu, P., Brunson, K., Yuan, J., and Li, Z. P. (2017). Zooarchaeological and genetic evidence for the origins of domestic cattle in ancient China. *Asian Perspect.* 56, 92–120. doi: 10.1353/asi.2017.0003

Lugli, F., Cipriani, A., Capecchi, G., Ricci, S., Boschin, F., Boscato, P., et al. (2019). Strontium and stable isotope evidence of human mobility strategies across the Last Glacial Maximum in southern Italy. *Nat. Ecol. Evol.* 3, 905–911. doi: 10.1038/s41559-019-0900-8

Ma, L. F., Qiao, X. F., and Liu, N. L. (2002). *Geological Atlas of China*. Beijing: Geological Publishing House (In Chinese).

Madgwick, R., Lamb, A. L., Sloane, H., Nederbragt, A. J., Albarella, U., Pearson, M. P., et al. (2019). Multi-isotope analysis reveals that feasts in the Stonehenge environs and across Wessex drew people and animals from throughout Britain. *Sci. Adv.* 5:eaau6078. doi: 10.1126/sciadv.aau6078

Maurer, A. F., Galer, S. J., Knipper, C., Beierlein, L., Nunn, E. V., Peters, D., et al. (2012). Bioavailable $^{87}Sr/^{86}Sr$ in different environmental samples-effects of anthropogenic contamination and implications for isoscapes in past migration studies. *Sci. Total Environ.* 433, 216–229. doi: 10.1016/j.scitotenv.2012.06.046

Mittnik, A., Massy, K., Knipper, C., Wittenborn, F., Friedrich, R., Pfrengle, S., et al. (2019). Kinship-based social inequality in Bronze Age Europe. *Science* 366, 731–734. doi: 10.1126/science.aax6219

Montgomery, J. (2010). Passports from the past: investigating human dispersals using strontium isotope analysis of tooth enamel. *Ann. Hum. Biol.* 37, 325–346. doi: 10.3109/03014461003649297

Moynier, F., Day, J. M. D., Okui, W., Yokoyama, T., Bouvier, A., Walker, R. J., et al. (2012). Planetary-scale strontium isotopic heterogeneity and the age of volatile depletion of early Solar System materials. *Astrophys. J.* 758, 45–52. doi: 10.1088/0004-637X/758/1/45

Owlett, T. E., Hu, S. M., Sun, Z. Y., and Shao, J. (2018). Food between the country and the city: the politics of food production at Shimao and Zhaimaoliang in the Ordos Region, northern China. *Archaeol. Res. Asia* 14, 46–60. doi: 10.1016/j.ara.2017.10.002

Pellegrini, M., Pouncett, J., Jay, M., Pearson, M. P., and Richards, M. P. (2016). Tooth enamel oxygen "isoscapes" show a high degree of human mobility in prehistoric Britain. *Sci. Rep.* 6:34986. doi: 10.1038/srep34986

Poszwa, A., Ferry, B., Dambrine, E., Pollier, B., Wickman, T., Loubet, M., et al. (2004). Variations of bioavailable Sr concentration and $^{87}Sr/^{86}Sr$ ratio in boreal forest ecosystems. *Biogeochemistry* 67, 1–20. doi: 10.1023/B:BIOG.0000015162.12857.3e

Price, T. D., Burton, J. H., and Bentley, R. A. (2002). The characterization of biologically available strontium isotope ratios for the study of prehistoric migration. *Archaeometry* 44, 117–135. doi: 10.1111/1475-4754.00047

R Core Team (2013). *R: A Language and Environment for Statistical Computing*. Vienna: R Foundation for Statistical Computing.

Ren, W. J. 任文洁(2019). *Research on the Function of "Liu-chu" during the pre-qin period in Northern China* 中国北方地区先秦时期"六畜"功能研究. (Master Thesis). Northwest AandF University, Xianyang, China.

Renfrew, C., and Liu, B. (2018). The emergence of complex society in China: the case of Liangzhu. *Antiquity* 92, 975–990. doi: 10.15184/aqy.2018.60

Reynolds, A. C., Quade, J., and Betancourt, J. L. (2012). Strontium isotopes and nutrient sourcing in a semi-arid woodland. *Geoderma* 189, 574–584. doi: 10.1016/j.geoderma.2012.06.029

Rosenstock, E., Ebert, J., Martin, R., Hicketier, A., Walter, P., and Groß, M. (2019). Human stature in the Near East and Europe ca. 10,000–1000 BC: its spatiotemporal development in a Bayesian errors-in-variables model. *Archaeol. Anthropol. Sci.* 11, 5657–5690. doi: 10.1007/s12520-019-00850-3

Ryan, W. B., Carbotte, S. M., Coplan, J. O., O'Hara, S., Melkonian, A., Arko, R., et al. (2009). Global multi-resolution topography synthesis. *Geochem. Geophys. Geosyst.* 10:Q03014. doi: 10.1029/2008GC002332

Scaffidi, B. K., and Knudson, K. J. (2020). An archaeological strontium isoscape for the prehistoric Andes: understanding population mobility through a geostatistical meta-analysis of archaeological $^{87}Sr/^{86}Sr$ values from humans, animals, and artifacts. *J. Archaeol. Sci.* 117:105121. doi: 10.1016/j.jas.2020.105121

Shaw, B. J., Summerhayes, G. R., Buckley, H. R., and Baker, J. A. (2009). The use of strontium isotopes as an indicator of migration in human and pig Lapita populations in the Bismarck Archipelago, Papua New Guinea. *J. Archaeol. Sci.* 36, 1079–1091. doi: 10.1016/j.jas.2008.12.010

Shelach-Lavi, G., and Jaffe, Y. (2014). The earliest states in China: a long-term trajectory approach. *J. Archaeol. Res.* 22, 327–364. doi: 10.1007/s10814-014-9076-6

Shelach-Lavi, G. (2015). *The Archaeology of Early China: From Prehistory to the Han Dynasty*. Cambridge: Cambridge University Press. doi: 10.1017/CBO9781139022682

Snoeck, C., Ryan, S., Pouncett, J., Pellegrini, M., Claeys, P., Wainwright, A. N., et al. (2020). Towards a biologically available strontium isotope baseline for Ireland. *Sci. Total Environ.* 712:136248. doi: 10.1016/j.scitotenv.2019.136248

Sun, X. D. 孙希旦(1989). *Li Ji Ji Jie* 礼记集解. Beijing: Zhonghuashuju (In Chinese).

Tao, Y. (2007). *Taosi Yizhi Chutu Dongwu Guge Yicun Yanjiu* 陶寺遗址出土动物骨骼遗存研究 (Master Thesis). Chinese Academy of Social Sciences, Beijing, China (In Chinese).

Thomsen, E., and Andreasen, R. (2019). Agricultural lime disturbs natural strontium isotope variations: Implications for provenance and migration studies. *Sci. Adv.* 5:eaav8083. doi: 10.1126/sciadv.aav8083

Thornton, E. K. (2011). Reconstructing ancient Maya animal trade through strontium isotope ($^{87}Sr/^{86}Sr$) analysis. *J. Archaeol. Sci.* 38, 3254–3263. doi: 10.1016/j.jas.2011.06.035

Underhill, A. P., and Habu, J. (2006). "Early communities in East Asia: economic and sociopolitical organization at the local and regional levels," in *Archaeology of Asia*, ed M. T. Stark (Malden, MA: Blackwell), 121–148. doi: 10.1002/9780470774670.ch7

Underhill, A. P. (2002). *Craft Production and Social Change in Northern China*. New York, NY: Kluwer Academic/Plenum Publishers. doi: 10.1007/978-1-4615-0641-6

Underhill, A. P. (2013). *A Companion to Chinese Archaeology*. Malden, MA: Wiley-Blackwell. doi: 10.1002/9781118325698

Ventresca Miller, A. R., Winter-Schuh, C., Usmanova, E. R., Logvin, A., Shevnina, I., and Makarewicz, C. A. (2017). Pastoralist mobility in bronze age landscapes of Northern Kazakhstan: $^{87}Sr/^{86}Sr$ and $\delta^{18}O$ analyses of human dentition from Bestamak and Lisakovsk. *Environ. Archaeol.* 23, 352–366. doi: 10.1080/14614103.2017.1390031

von Falkenhausen, L. (2006). *Chinese Society in the Age of Confucius (1000–250 BC): the Archaeological Evidence*. Los Angeles, CA: Cotsen Institute of Archaeology, UCLA. doi: 10.2307/j.ctvdmwwt6

Wang, X. Y., and Tang, Z. H. (2020). The first large-scale bioavailable Sr isotope map of China and its implication for provenance studies. *Earth Sci. Rev.* 210:103353. doi: 10.1016/j.earscirev.2020.103353

Wang, X., Fuller, B. T., Zhang, P. C., Hu, S. M., Hu, Y. W., and Shang, X. (2018). Millet manuring as a driving force for the Late Neolithic agricultural expansion of north China. *Sci. Rep.* 8:5552. doi: 10.1038/s41598-018-23315-4

Wang, X. X., Wang, T., and Zhang, C. L. (2013). Neoproterozoic, Paleozoic, and Mesozoic granitoid magmatism in the Qinling Orogen, China: constraints on orogenic process. *J. Asian Earth Sci.* 72, 129–151. doi: 10.1016/j.jseaes.2012.11.037

Willmes, M., Bataille, C. P., James, H. F., Moffat, I., McMorrow, L., Kinsley, L., et al. (2018). Mapping of bioavailable strontium isotope ratios in France for archaeological provenance studies. *Appl. Geochem.* 90, 75–86. doi: 10.1016/j.apgeochem.2017.12.025

Wood, S. N. (2003). Thin plate regression splines. *J. R. Stat. Soc. Ser. B Stat. Methodol.* 65, 95–114. doi: 10.1111/1467-9868.00374

Wu, W. H., Xu, S. J., Yang, J. D., Yin, H. W., Lu, H. Y., and Zhang, K. J. (2010). Isotopic characteristics of river sediments on the Tibetan Plateau. *Chem. Geol.* 269, 406–413. doi: 10.1016/j.chemgeo.2009.10.015

Wu, X. T., Zhang, X. X., Jin, Z. Y., Song, Y. B., Luan, F. S., and Xue, X. M. (2019). Strontium isotope analysis of Yangtze alligator remains from Late Neolithic North China. *Archaeol. Anthropol. Sci.* 11, 1049–1058. doi: 10.1007/s12520-017-0589-z

Wu, X. T. 吴晓桐(2018). *Human migration and material circulation in Yellow River Valley during Longshan Period* 龙山时期黄河流域的人群迁移与资源流通 (Ph.D. Thesis). University of Science and Technology of China, Hefei, China (In Chinese).

Xie, C. X. 谢成侠(1959). *Zhongguo Yangma Shi* 中国养马史. Beijing: Science Press (In Chinese).

Yang, S. N. 杨升南(1999). Jiaguwenzhong Suojian Shangdai De Gongna Zhidu 甲骨文中所见商代的贡纳制度. *Yindu Xuekan* 2, 27–32 (In Chinese).

Yang, C. 杨春(2006a). *Neimenggu Xicha Yizhi Dongwu Yicun Yanjiu* 内蒙古西岔遗址动物遗存研究 (Master Thesis). Jilin University, Changchun, China (In Chinese).

Yang, J. 杨杰(2006b). *Zoological archaeology of Erlitou Site in Yanshi, Henan Province* 河南偃师二里头遗址的动物考古学研究 (Ph.D. Thesis). Graduate School of Chinese Academy of Social Sciences, Beijing, China (In Chinese).

Yin, R. C. 尹若春(2008). *Prehistoric human migration study based on Sr isotope analysis from Jiahu relics* 锶同位素分析技术在贾湖遗址人类迁移行为研究中的应用 (Ph.D. Thesis). University of Science and Technology of China, Hefei, China (In Chinese).

Yuan, J., and Flad, R. (2005). New zooarchaeological evidence for changes in Shang Dynasty animal sacrifice. *J. Anthropol. Archaeol.* 24, 252–270. doi: 10.1016/j.jaa.2005.03.001

Yuan, J., Roderick, C., Lorenzo, C., and Chen, X. L. (2020). Subsistence and persistence: agriculture in the Central Plains of China through the Neolithic to Bronze Age transition. *Antiquity* 94, 900–915. doi: 10.15184/aqy.2020.80

Yuan, J. (2002). The formation and development of Chinese zooarchaeology: a preliminary review. *Archaeofauna* 11, 205–212.

Yuan, J. 袁靖(2010). Zooarchaeological study on the domestic animals in ancient China 中国古代家养动物的考古动物学研究. *Quat. Sci.* 30, 298–306 (In Chinese).

Yuan, J. (2015). *Zooarchaeology of China* 中国动物考古学. Beijing: Cultural Relics Press (In Chinese).

Zhang, G. W., Zhang, J. H., Zhao, L. Y., Tao, D. W., Zhou, Y. W., Han, G. H., et al. (2020). Reconstructing diets and subsistence strategies of the Bronze Age humans from the Central Plains of China: a stable isotopic study on the Nanwa site. *Int. J. Osteoarchaeol.* 30, 362–374. doi: 10.1002/oa.2865

Zhao, C. Y. 赵春燕, Li, Z. P. 李志鹏, Yuan, J. 袁靖, Zhao, H. T. 赵海涛, Chen, G. L. 陈国梁, and Xu, H. 许宏(2011a). Preliminary explorations on the resources of the cattle, sheep and goat in Erlitou Site — Based on the strontium isotope analyses to their tooth enamels 二里头遗址出土动物来源初探—根据牙釉质的锶同位素比值分析. *Kaogu* 7, 68–75 (In Chinese).

Zhao, C. Y. 赵春燕, Yuan, J., 袁靖, and He, N. 何努(2011b). Strontium isotope analysis of archaeological fauna from the Taosi site, Xiangfen county, Shanxi Province 山西省襄汾县陶寺遗址出土动物牙釉质的锶同位素比值分析. *Quat. Sci.* 31, 23–28 (In Chinese).

Zhao, C. Y. 赵春燕, Li, Z. P. 李志鹏, and Yuan, J. 袁靖(2015). Sr isotopic analysis of horses and pig enamel unearthed in the Yinxu Site, Henan Province 陕西石峁遗址后阳湾地点出土动物牙釉质的锶同位素比值分析. *Nanfang Guwu* 3, 77–80 (In Chinese).

Zhao, C. Y. 赵春燕, Hu, S. M. 胡松梅, Sun, Z. Y. 孙周勇, Shao, J. 邵晶, and Yang, M. M. 杨苗苗(2016a). Strontium isotopic analysis of teeth dental tissues from the Houyangwan at the Shimao site in Shenmu, Shaanxi 陕西石峁遗址后阳湾地点出土动物牙釉质的锶同位素比值分. *Kaogu Yu Wenwu* 4, 128–133 (In Chinese).

Zhao, C. Y. 赵春燕, Wang, M. H. 王明辉, and Ye, M. L. 叶茂林(2016b). Strontium isotope analysis of human teeth and bones from the Lajia site in Qinghai Province 青海喇家遗址人类遗骸的锶同位素比值分析. *Acta Anthrop. Sin.* 35, 212–222 (In Chinese).

Zhao, C. Y. 赵春燕, Lu, P. 吕鹏, Yuan, J. 袁靖, and Ye, M. L. 叶茂林(2018). Strontium isotopic ratios in animal remains at the Lajia site, Qinghai Province 青海喇家遗址动物遗骸的锶同位素比值分析. *Sci. Archaeol.* 5, 67–76 (In Chinese).

Zhao, C. Y. 赵春燕(2018). The origins of cattle and sheep during the Erlitou period in Songshan region 嵩山地区二里头文化时期牛和羊来源蠡测. *Huaxia Kaogu* 6, 77–84 (In Chinese).

Conflict of Interest: The authors declare that the research was conducted in the absence of any commercial or financial relationships that could be construed as a potential conflict of interest.

frontiers in Ecology and Evolution

ORIGINAL RESEARCH
published: 17 March 2021
doi: 10.3389/fevo.2021.584325

Bioavailable Strontium, Human Paleogeography, and Migrations in the Southern Andes: A Machine Learning and GIS Approach

Ramiro Barberena[1,2], Marcelo Cardillo[3], Gustavo Lucero[4], Petrus J. le Roux[5]*, Augusto Tessone[6], Carina Llano[7], Alejandra Gasco[1,2], Erik J. Marsh[1], Amalia Nuevo-Delaunay[8], Paula Novellino[9], Cecilia Frigolé[1], Diego Winocur[10], Anahí Benítez[10], Luis Cornejo[11], Fernanda Falabella[12], Lorena Sanhueza[12], Francisca Santana Sagredo[13], Andrés Troncoso[12], Valeria Cortegoso[1,2], Víctor A. Durán[1,2] and César Méndez[8]**

[1] Laboratorio de Paleoecología Humana, Instituto Interdisciplinario de Ciencias Básicas (ICB), Consejo Nacional de Investigaciones Científicas y Técnicas (CONICET), Facultad de Ciencias Exactas y Naturales, Universidad Nacional de Cuyo, Mendoza, Argentina, [2] Facultad de Filosofía y Letras, Universidad Nacional de Cuyo, Mendoza, Argentina, [3] Instituto Multidisciplinario de Historia y Ciencias Humanas, Consejo Nacional de Investigaciones Científicas y Técnicas (CONICET), Ciudad Autónoma de Buenos Aires, Argentina, [4] Departamento de Antropología, Facultad de Ciencias Sociales y Humanidades, Universidad Católica de Temuco, Temuco, Chile, [5] Department of Geological Sciences, University of Cape Town, Cape Town, South Africa, [6] Instituto de Geocronología y Geología Isotópica, Universidad de Buenos Aires, Consejo Nacional de Investigaciones Científicas y Técnicas (CONICET), Ciudad Autónoma de Buenos Aires, Argentina, [7] Facultad de Ciencias Aplicadas a la Industria, Universidad Nacional de Cuyo, Consejo Nacional de Investigaciones Científicas y Técnicas (CONICET), San Rafael, Argentina, [8] Centro de Investigación en Ecosistemas de la Patagonia (CIEP), Coyhaique, Chile, [9] Museo de Ciencias Naturales y Antropológicas Juan C. Moyano, Consejo Nacional de Investigaciones Científicas y Técnicas (CONICET), Mendoza, Argentina, [10] Departamento de Ciencias Geológicas, Facultad de Ciencias Exactas y Naturales, Instituto de Estudios Andinos (IDEAN), Universidad de Buenos Aires, Ciudad Autónoma de Buenos Aires, Argentina, [11] Departamento de Antropología, Universidad Alberto Hurtado, Santiago, Chile, [12] Departamento de Antropología, Universidad de Chile, Santiago, Chile, [13] Pontificia Universidad Católica de Chile, Santiago, Chile*

OPEN ACCESS

Edited by:
Clement Pierre Bataille, University of Ottawa, Canada

Reviewed by:
Omar Reyes, Universidad de Magallanes, Chile
Matthew Wooller, University of Alaska Fairbanks, United States

***Correspondence:**
Ramiro Barberena
rbarberena@mendoza-conicet.gob.ar
César Méndez
cesar.mendez@ciep.cl
Petrus J. le Roux
petrus.leroux@uct.ac.za

Specialty section:
This article was submitted to Paleoecology, a section of the journal Frontiers in Ecology and Evolution

Received: *16 July 2020*
Accepted: *12 February 2021*
Published: *17 March 2021*

Citation:
Barberena R, Cardillo M, Lucero G, le Roux PJ, Tessone A, Llano C, Gasco A, Marsh EJ, Nuevo-Delaunay A, Novellino P, Frigolé C, Winocur D, Benítez A, Cornejo L, Falabella F, Sanhueza L, Santana Sagredo F, Troncoso A, Cortegoso V, Durán VA and Méndez C (2021) Bioavailable Strontium, Human Paleogeography, and Migrations in the Southern Andes: A Machine Learning and GIS Approach. Front. Ecol. Evol. 9:584325. doi: 10.3389/fevo.2021.584325

The Andes are a unique geological and biogeographic feature of South America. From the perspective of human geography, this mountain range provides ready access to highly diverse altitudinally arranged ecosystems. The combination of a geologically and ecologically diverse landscape provides an exceptional context to explore the potential of strontium isotopes to track the movements of people and the conveyance of material culture. Here we develop an isotopic landscape of bioavailable strontium (87Sr/86Sr) that is applied to reconstruct human paleogeography across time in the southern Andes of Argentina and Chile (31°–34°S). These results come from a macro-regional sampling of rodents (N = 65) and plants (N = 26) from modern and archeological contexts. This "Southern Andean Strontium Transect" extends over 350 km across the Andes, encompassing the main geological provinces between the Pacific coast (Chile) and the eastern lowlands (Argentina). We follow a recently developed approach to isoscape construction based on Random Forest regression and GIS analysis. Our results suggest that bioavailable strontium is tightly linked with bedrock geology and offers a highly resolved proxy to track human paleogeography involving the levels of territories or daily mobility and anomalous events that disrupt home ranges, such as migration. The

southern Andes provide an ideal geological setting to develop this approach, since the geological variation in rock age and composition produces distinctive isotopic signatures for each main biogeographical region. Finally, we apply this framework to a set of results from human remains from the Uspallata Valley in Mendoza (Argentina), to assess the incidence of migration in the key period of the consolidation of agropastoral economies between AD 800 and 1400. The application of the isoscape to the values from human remains confirms the persistence of human groups with relatively restricted territories encompassing Uspallata and the adjacent Precordillera between AD 800 and 1500. We also identify a pulse of human migration between AD 1280 and 1420, shortly preceding the Inka conquest. Looking forward, we expect to converge with ongoing efforts in South America to build a continental research framework to track the movement of people, animals, and artifacts across space and time.

Keywords: bioavailable strontium, archeology, Andes, machine learning, human paleomobility, migrations, radiogenic strontium isotope

INTRODUCTION

Strontium isotopes ($^{87}Sr/^{86}Sr$) in human teeth and bone remains average the biologically available strontium in the landscape(s) inhabited in the past (Price et al., 2002; Bentley, 2006), providing a proxy of the geographic place of origin of an individual and the spatial scale of the territories occupied (Price et al., 2000; Montgomery, 2010; Knudson et al., 2014a; Laffoon et al., 2017). Since first applied in archeology (Ericson, 1985), strontium isotopes ($^{87}Sr/^{86}Sr$) have widened the scope of archeological enquiry across analytical scales, from small-scale aspects of human life-history and identity construction (Kutschera and Müller, 2003; Montgomery, 2010; Andrushko et al., 2011; Knudson et al., 2012; Torres-Rouff and Knudson, 2017) to large-scale group migration processes (Borić and Price, 2013; Yu et al., 2020). In addition, convergent interdisciplinary efforts from geology, ecology, paleoecology, forensics, and archeology have resulted in increasingly more sophisticated approaches to assess the mobility of the organisms under study and, building on this, to identify non-local residence and migration on different spatial and social scales (Price et al., 2002; Bentley, 2006; Montgomery et al., 2007; Bataille et al., 2014, 2020; Kootker et al., 2016; Tipple et al., 2018; Willmes et al., 2018; Scaffidi and Knudson, 2020; Snoeck et al., 2020). Thus, resulting from the combination of growing frames of scientific enquiry, robust methodological approaches, and extensive databases, we consider it is fair to describe the present time as a "golden age" of strontium isotopes to geographically source materials across space and time. However, this advance is highly heterogeneous in the different continents (Bataille et al., 2020). In South America, strontium isotopic research has been largely focused in the Central and South-Central Andes encompassing Peru, western Bolivia and northern Chile (Knudson et al., 2014a,b; Dantas and Knudson, 2016; Chala-Aldana et al., 2018; Mader et al., 2018; Slovak et al., 2018; Standen et al., 2018; Takigami et al., 2019; Santana-Sagredo et al., 2021). We have recently started a project with the goal of extending the bioavailable strontium framework to the southern Andes in Central Argentina and Chile (Barberena et al., 2017, 2019, 2020; Durán V. et al., 2018). From a comparative perspective, this project allows incorporating Andean regions with different archeological trajectories of socio-economic change, complexity, and possibly diverse incidence of migrations compared to the more systematically studied Central Andes.

The general objective of this project is to develop a multidisciplinary approach to human scale of mobility, role of migration, and trans-Andean interaction since the initial human peopling in the Pleistocene-Holocene transition (García, 2003), with a focus on the period witnessing the evolution of agropastoral economies in the last 2,000 years (Gil et al., 2014; Falabella et al., 2016; Llano et al., 2017; Durán V. et al., 2018; Gasco, 2018). In this agenda, the specific goal of this paper is to present the strontium isotope ($^{87}Sr/^{86}Sr$) results for plant and rodent samples from a trans-Andean transect encompassing from the Pacific Ocean in Central Chile to the eastern lowlands in Argentina (31°–34°S) (**Figure 1**). The "Southern Andean Strontium Transect" (SAST, from now onward) samples the main geological provinces across the Andes that span the last ca. 450 my, between the lower Paleozoic and the late Quaternary. From a methodological perspective, we apply an innovative and robust approach based on Random Forest regression designed to assess which biophysical variables predict the observed strontium isotope variation with the highest resolution (Bataille et al., 2014, 2018, 2020; see also Serna et al., 2020). Our results demonstrate that the southern Andes provide an ideal geological setting for the development of this approach, since there is an impressive geological variation in rock age and composition that produces distinctive isotopic signatures for each biogeographical region of archeological relevance. Finally, we apply this geostatistical framework to a recently published archeological case-study from the Uspallata montane Valley in northwestern Mendoza, Argentina (**Figure 1**). The specific archeological goal consists in assessing the spatial scale of mobility of human remains buried in five archeological cemeteries spanning the key period between the consolidation of agropastoral economies and the regional conquest by the Inka

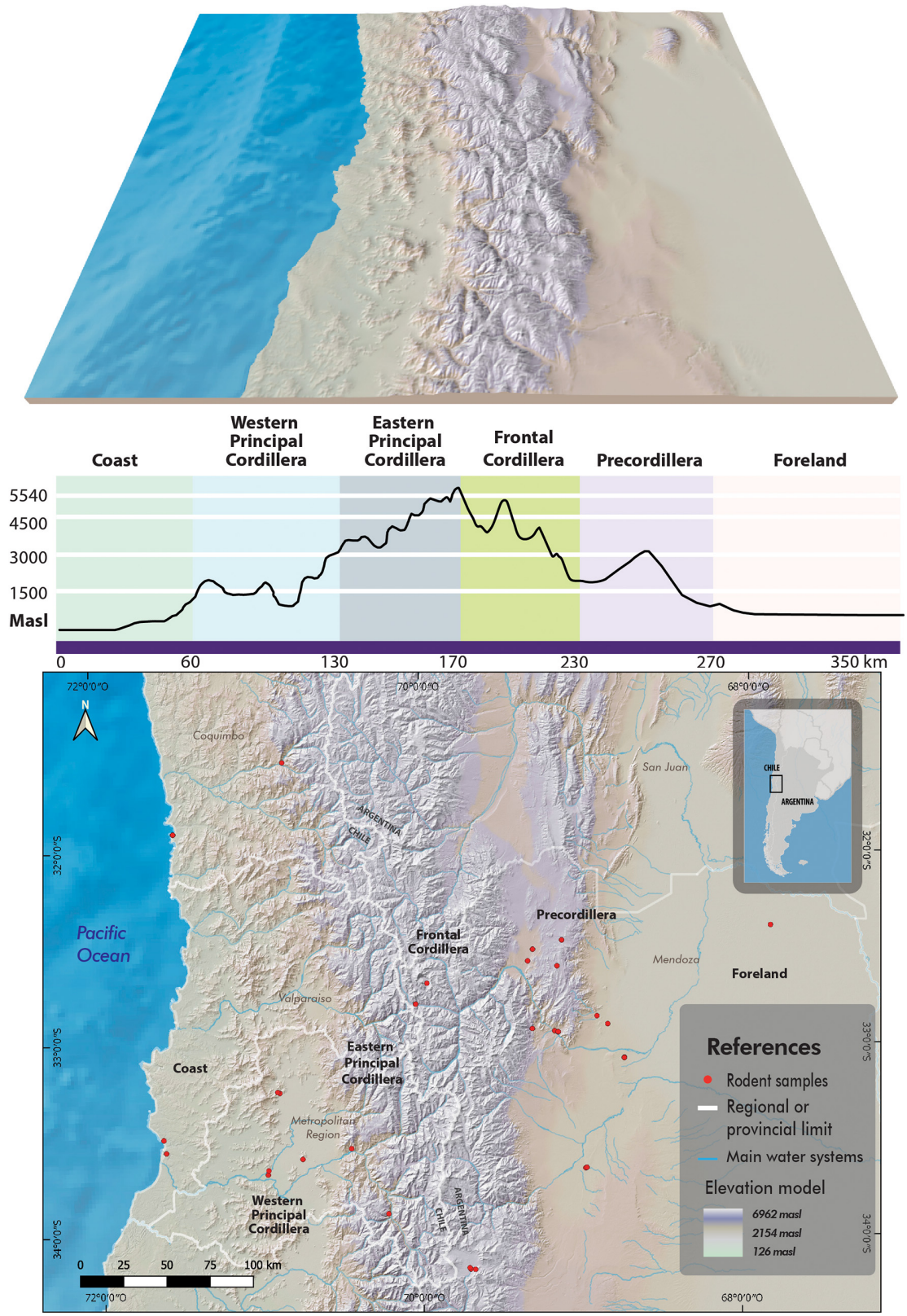

FIGURE 1 | Study area and location of the samples for isotopic analysis.

Empire (AD 800–1400) (Barberena et al., 2020). Building on this, we assess the incidence of migration in the conformation of these human groups through time.

GEOLOGICAL, ECOLOGICAL, AND ARCHEOLOGICAL BACKGROUND

Geological Framework for the Analysis of Bioavailable Strontium

The southern Andes of Argentina and Chile is a mountain belt formed at the convergent margin between the Nazca and South American plates. Our study area encompasses Central Argentina and Chile and is located in the transition zone between the Pampean flat slab, characterized by a shallow subduction angle resulting in a volcanic gap, and the normal subduction zone of central Chile and Argentina (Ramos and Folguera, 2009). This segment corresponds to the northernmost active volcanism of the Southern Volcanic Zone of the Andean belt. In this latitudinal block, the Andes are composed of seven major morpho-structural provinces that provide our framework for the sampling and analysis of bioavailable strontium. Since it represents a particular strontium biozone in terms of human diet and mobility (Banner, 2004; Standen et al., 2018), we also include the Pacific Ocean as the first unit along the west to east SAST, as follows: (1) Pacific Ocean; (2) Coastal Cordillera; (3) Central Depression-Central Chilean Valley; (4) Western Principal Cordillera; (5) Eastern Principal Cordillera; (6) Frontal Cordillera; (7) Precordillera; and (8) Active Foreland or Quaternary lowlands (**Figure 2**).

The first unit is the (1) *Pacific Ocean* that was sampled in coastal settings between the modern towns of Los Vilos in the north (31°55′S) and San Antonio in the south (33°40′S) (**Figure 1**). Eastwards from the Pacific coast follows the *Coastal Cordillera* (2), which has a Paleozoic-Triassic basement in the west and Jurassic-Cretaceous clastic and volcanoclastic intra-arc sequences in the east. These units are intruded by Upper Cretaceous igneous rocks of dioritic to monzodioritic composition. The *Central Depression* (3) is an extensional basin developed since late Eocene-Oligocene times and filled by volcanic and volcanoclastic rocks (Charrier et al., 2002). During the early to mid-Miocene, calc-alkaline andesitic lava, and acid pyroclastic flows of the Farellones Formation were deposited in the central part of the basin (Kurtz et al., 1997). From the eastern flank of the Central Depression develops the *Cordillera Principal*, divided into two geological provinces with different rock ages and compositions: the *Western Cordillera Principal* (4), formed by Oligocene and Miocene volcanic and intrusive rocks, and the *Eastern Cordillera Principal* (5), constituted by sedimentary Mesozoic rocks deformed into the Aconcagua fold and thrust belt (Giambiagi et al., 2009). The Jurassic to middle Cretaceous sedimentary rocks of the Eastern Cordillera Principal include marine evaporites, sandstones, clay-stones, and limestones. Immediately eastwards lies the *Cordillera Frontal* (6), containing a Paleozoic basement constituted by sedimentary, metamorphic and igneous rocks intruded by Upper Paleozoic granitoids unconformably covered by Permo-Triassic igneous rocks. The *Precordillera* unit (7) is emplaced eastwards of the Cordillera Frontal and has a southern limit at ∼33°S. It is composed of Lower and Upper Paleozoic (Cambrian to Permian) sedimentary rocks intruded by Paleozoic calc-alkaline granitoids (Furque and Cuerda, 1979; Astini et al., 1995; Giambiagi et al., 2003). Finally, late Quaternary clastic deposits occur in the *Active Foreland* (8), to the east of the Frontal Cordillera and Precordillera. This foreland basin results from the progressive erosion of the rocks forming the different morpho-structural Andean units. Synthesizing these trends, rock age increases eastwards from the Pacific coast, hence leading to low $^{87}Sr/^{86}Sr$ in the west and increasingly higher values eastwards (Barberena et al., 2017).

Ecology Across the Southern Andean Strontium Transect

This latitudinal band of the Andes presents the highest average altitude separating the Pacific and Atlantic slopes of South America (Clapperton, 1993). The interaction between the Andean topography and the prevailing westerly storm tracks bringing humidity to the continent from the Pacific Ocean produces marked spatial variation in temperature, precipitation, and ecology (Garreaud, 2009; Oyarzabal et al., 2018; Masiokas et al., 2020). These communities are dominated by shrubs in the lowlands and by an increase in the herbaceous stratum up to 3,300 masl (Muñoz-Schick et al., 2000). There is a succession of vegetation communities by altitude (from east to west): open scrubland (1,000–1,500 masl), sub-Andean and Andean scrubland (1,500–2,700 masl), Andean steppe (2,700–3,300 masl), and Andean desert (>3,300 masl). Andean steppe and scrubland associated with the Patagonia phytogeographical province (3,300–1,400 masl) are followed to the east by the dry scrublands of the Monte phytogeographical province (Abraham et al., 2009).

The Andean highlands are characterized by large amounts of precipitation occurring mostly during winter as snow and, as altitude decreases, ecosystems become increasingly dry east and westwards. In this geographical context, the SAST between the Pacific Ocean and the eastern Andean lowlands connects a succession of tightly packed altitudinally arranged ecosystems (**Figure 3**). This is a highly seasonal landscape where large areas above 2,500 masl would only be available for systematic occupation and circulation during the summer months (Durán V. et al., 2018). This is a fundamental landscape feature that would have conditioned patterns of trans-Andean human movement and social interaction (Cornejo and Sanhueza, 2011; Cortegoso et al., 2016).

Archeological Background

The archeological record from the southern Andes provides a window to study diachronic socio-demographic processes spanning the early human dispersion and colonization of the continent beginning in the late Pleistocene, the effective occupation of available spaces within socially defined territories, processes of economic intensification and reduction of mobility, development of agropastoral economies, and socio-political complexity ending with the successive annexation by the Inka

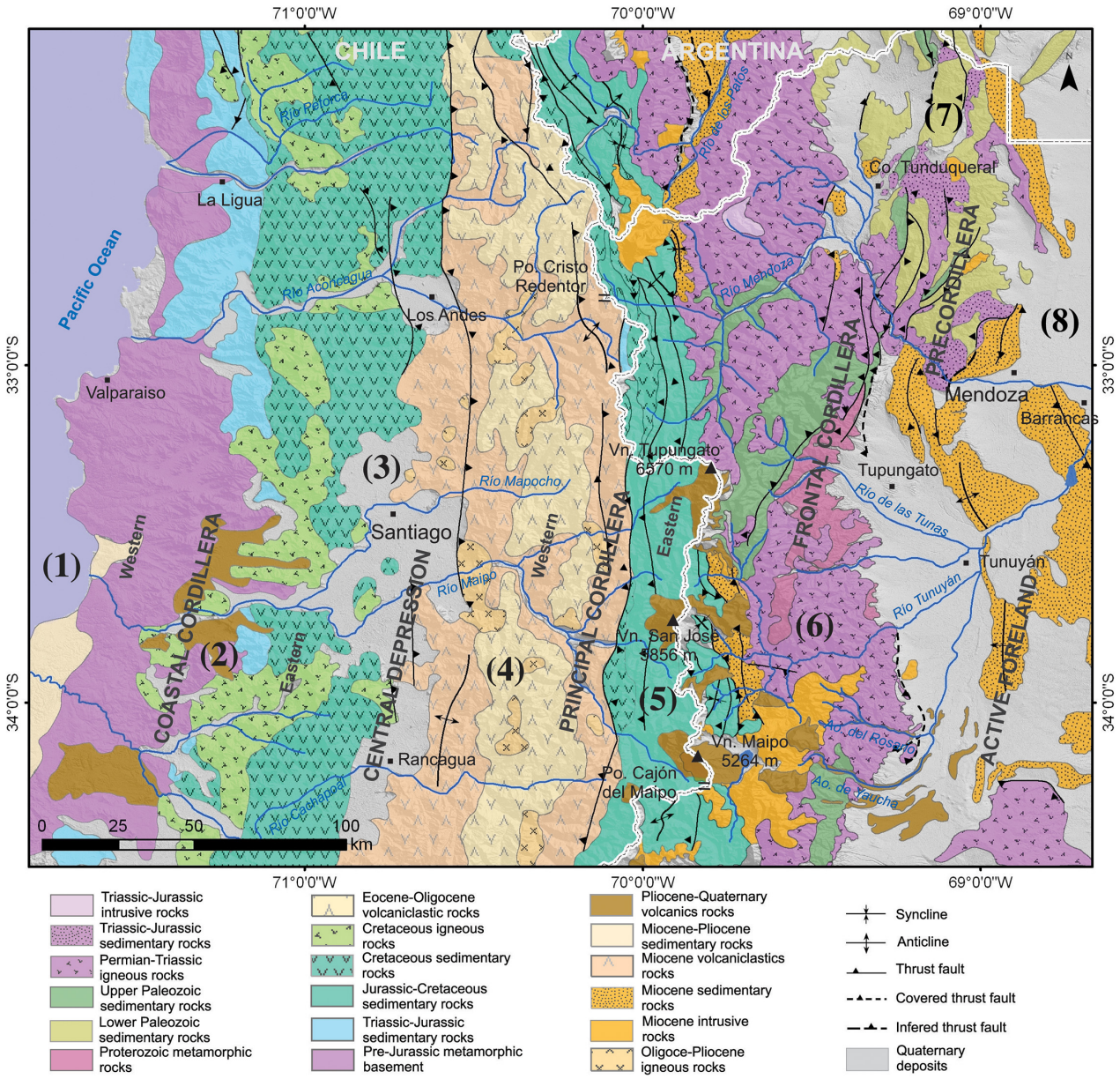

FIGURE 2 | Main morpho-structural units of the southern Andes between 32° and 34°S in Argentina and Chile (modified from Barberena et al., 2017). *Key*: (1) Pacific Ocean; (2) Coastal Cordillera; (3) Central Depression-Central Chilean Valley; (4) Western Principal Cordillera; (5) Eastern Principal Cordillera; (6) Frontal Cordillera; (7) Precordillera; and (8) Active Foreland.

and Spanish empires. The scale(s) of human paleomobility and the role of migration through time would have been key components of the trajectories of these and other historical processes.

Humans have occupied the coastal and mountain environments of the southern Andes of Argentina and Chile since the late Pleistocene (García, 2003; Méndez Melgar, 2013; Méndez et al., 2018). For most of the Holocene, mobile foraging was the dominant way of life, documented by a variety of hunting weapon systems, the consumption of diverse plant taxa such as algarrobo (*Prosopis* sp.) and molle (*Schinus polygamus*), and the wild camelid guanaco as some of the main staples (Bárcena, 2001; Llano, 2015; Cornejo et al., 2016). There are indications of a major regional shift in human adaptations and economic practices starting before 2,000 years BP. Domestic plants are recorded, including maize (*Zea mays*), quinoa (*Chenopodium quinoa*), beans (*Phaseolus* sp.), and squash (*Cucurbita* sp.) (Planella et al., 2015; Llano et al., 2017), as well as the earliest pottery (Sanhueza and Falabella, 1999; Marsh, 2017). Burial practices became more elaborate and some of the first formal cemeteries in central-western Argentina are dated to these centuries (Rusconi, 1962; Novellino et al., 2013; Menéndez et al.,

FIGURE 3 | Main regions incorporated in the Southern Andean Transect. *Key*: **(a)** Bahía La Cachina, Pacific Coast (Chile). **(b)** El Manzano, Western Cordillera Principal (Chile). **(c)** Cogotí, Western Cordillera Principal (Chile). **(d)** Laguna del Diamante, Eastern Principal Cordillera (Argentina). **(e)** Uspallata Valley, transition between Frontal Cordillera and Precordillera (Argentina). **(f)** Corsemar, Active Foreland (Argentina).

2014). The llama domestic camelid (*Lama glama*) would have been present in areas within this region (Gasco, 2018). For at least a millennium, people had an agropastoral lifeway that would have combined hunting, gathering, farming, and herding in diverse proportions. The Inka Empire arrived in central Argentina and Chile immediately after AD 1400 (Cornejo, 2014; Marsh et al., 2017).

MATERIALS AND METHODS

Sampling Strategy

The SAST extends for over 350 km between the Pacific Ocean (Chile) and the eastern lowlands in Mendoza Province (Argentina) (**Figure 1**). In order to build an isoscape of bioavailable strontium across the southern Andes we sampled small rodents—with restricted home ranges—and plants (Price et al., 2002; Copeland et al., 2016; Snoeck et al., 2018; Scaffidi and Knudson, 2020). Our strategy was initially designed to target rodents as the main proxy for bioavailable strontium (Barberena et al., 2017), and we turned to plant samples for areas where rodent samples were not readily available. Accordingly, the sampling was not designed to formally compare these two substrates. However, since we detected important differences for rodents and plants coming from some of the geological regions, we develop two alternative Random Forest models, respectively, analyzing rodents, on the one hand, and rodents and plants, on the other hand. We then explore the robustness of the resulting models and the main biophysical variables that explain the observed isotopic variation.

The rodent samples include modern and archeological specimens (Barberena et al., 2019, 2020) and the plant samples

are all modern. Two strategies for sampling plants were applied: the plant samples from Argentina combine five near-located individuals from the same species in each sampling locality and the samples from Chile correspond to only one plant in each case. It is not expected that this may cause any significant difference in the results obtained. Whenever possible, native taxa were selected (**Table 2**). Considering the wide altitudinal (∼0–3,400 masl), climatic, and ecological variation in the SAST, three different plant types were sampled: in the Monte of the dry lowlands of eastern Argentina we sampled shrubs such as *Larrea, Prosopis, Schinus,* and *Adesmia*, with deep rooting systems reaching the groundwater at beyond 20 m-depth; in the dry highlands of the Patagonian phytogeographical Province we selected grasses (Poaceae) with low-depth root systems; and finally in the more mesic lowland settings west of the Andes we sampled evergreen trees (*Quillaja saponaria, Peumus boldus, Eucalyptus robusta*), where a large part of the roots providing the soil nutrients are located near the surface (Díaz et al., 1999; Jobbágy et al., 2011). Considering that plant physiology conditions the sources of strontium uptake within the same landscape (Capo et al., 1998; English et al., 2001; Reynolds et al., 2012; Grimstead et al., 2017), we will augment our current sampling in order to account for possible inter-specific differences within geological regions.

The geological provinces described above were used as the units of analysis for the bioavailable strontium sampling. However, the samples are not randomly distributed within these regions since in many cases work focused in areas of archeological interest, such as Los Vilos, Combarbalá, and the Maipo River in Chile and the Uspallata Valley and Laguna del Diamante in Argentina. However, these are representative of the geologic areas from which the samples were gathered. The plant and rodent samples are distributed in the spatial units of analysis as follows: Pacific coast, $n = 15$; Coastal Cordillera, $n = 10$; Western Principal Cordillera, $n = 10$; Eastern Principal Cordillera, $n = 10$; Frontal Cordillera $n = 8$; Precordillera, $n = 24$; and Active Foreland, $n = 14$.

Laboratory Methods

Strontium isotope analysis was performed in the Department of Geological Sciences, University of Cape Town, following routine chemical and MC-ICP-MS methods (Copeland et al., 2010, 2016; Scott et al., 2020). Plant sample material was cut into <1 cm pieces and subsamples of plants from each sampling locality where placed in a pure quartz silica crucible. The crucibles were placed in a muffle furnace set at 300°C, and the temperature ramped by 100°C/h to 650°C and held at that temperature overnight. Once cooled, the ashed plant material was transferred to a 7 ml Savillex Teflon beaker. For digestion, 2 ml of a 4:1 mixture of 48% HF: 65% HNO_3 was added, the beaker closed and placed overnight on a hotplate set at 140°C. Following two stages of dry down and re-dissolving in 1 ml 65% HNO_3, 1.5 ml 2 M HNO_3 was added and allowed to settle overnight to be ready for strontium separation chemistry. Powdered bone and enamel samples were weighed into 7 ml Savillex Teflon beakers, 2–3 ml of 65% HNO_3 added and the closed beakers placed on a hotplate at 140°C for an hour. Following complete sample dissolution, the beakers were opened, and the samples dried. Once dry, the samples were redissolved in 1.5 ml 2 M HNO_3 to be for strontium separation chemistry.

Strontium separation chemistry for all samples followed the same method (Pin et al., 1994) and used Triskem Sr. Spec resin. The separated strontium fraction for each sample was dried down, dissolved in 2 ml 0.2% HNO_3 and diluted to 200 ppb Sr concentrations for Sr isotope ratio analysis using a Nu Instruments NuPlasma HR MC-ICP-MS. Analyses were referenced to bracketing analyses of NIST SRM987, using a $^{87}Sr/^{86}Sr$ reference value of 0.710255. All strontium isotope data are corrected for isobaric rubidium interference at 87 amu using the measured signal for ^{85}Rb and the natural $^{85}Rb/^{87}Rb$ ratio. Instrumental mass fractionation was corrected using the measured $^{86}Sr/^{88}Sr$ ratio, the exponential law, and an accepted $^{86}Sr/^{88}Sr$ value of 0.1194. An in-house carbonate reference material processed and measured with the batches of unknown samples in this study yielded results ($^{87}Sr/^{86}Sr$ 0.708914 ± 0.000045 2σ; $n = 12$) in agreement with long-term results for this reference material from this facility ($^{87}Sr/^{86}Sr$ 0.708911 ± 0.000040 2σ; $n = 414$). Total procedural blanks processed with these samples yielded background Sr levels <250 pg, and therefore negligible.

Random Forest, GIS, and Strontium Isoscapes

The Random Forest approach is based in a bootstrapping procedure that generates an ensemble (or forest) of trees resulting in different combinations of the target variable ($^{87}Sr/^{86}Sr$) and its biophysical predictors (Breiman, 2001; Bataille et al., 2018). Compared to other classification or regression methods, the average of the Random Forest trees has smaller variance and a higher predictive performance. In addition, compared with other machine learning methods it is less prone to overfitting (Kuhn, 2013). As has been robustly demonstrated (Bataille et al., 2018, 2020), this method allows combining quantitative and categorical variables and has a remarkable versatility to generate $^{87}Sr/^{86}Sr$ isoscapes.

In order to determine the most parsimonious subset of variables with the highest predictive power, the Variable Selection using Random Forest (VSURF) package was used (Genuer et al., 2019). We incorporate spatial, geological, and bioclimatic variables in the model (**Table 1**). We also utilize as a predictor variable the "bedrock model" (Bataille et al., 2018, 2020) that predicts the median, Quartile 1 and Quartile 3 of $^{87}Sr/^{86}Sr$ values for bedrock in a global scale. This will expand the recent application developed by Serna et al. (2020) for northern Patagonia. The variables are introduced in a stepwise manner in order to detect the combination of predictors that reduces the mean "Out-of-Bag Error" (see details in **Supplementary Data**).

The Random Forest approach divides the total isotopic sample into a *training phase* of the model, encompassing 80% ($n = 72$) of the results, while the remaining 20% ($n = 19$) was used in a *testing phase* to assess the predictive capacity of new data of the model produced (see script in **Supplementary Material**).

TABLE 1 | List of locational, geological, and bioclimatic variables used in the model.

Name	Variable	Type	Scale	Source
Latitude	Latitude	C	90 m	
Longitude	Longitude	C	90 m	
r.elevation	Altitude (SRTM masl)	C	90 m	Jarvis et al., 2008
Distance	Distance to the nearest coast	C		
Geological province	Geological region	D		Barberena et al., 2017
r.m1	Median bedrock model	D	1 km	Bataille et al., 2020
Glim_UTM	Lithological classification	D	1 km	Hartmann and Moosdorf, 2012
r.meanage_geol	GLiM age attribute (Myrs)	D	1 km	Hartmann and Moosdorf, 2012
r.clay	Clay (weight%)	C	250 m	Hengl et al., 2017
r.pH	Soil pH in H_2O solution	C	250 m	Hengl et al., 2017
r.dust.t	Multi-models average	C	1° × 1°	Mahowald et al., 2006
r.salt.t	CCSM.3 simulation	C	1.4° × 1.4°	Hengl et al., 2017
Vapr_01	Evapotranspiration January (kPa)	C	30 arc s	Fick and Hijmans, 2017
Vapr_07	Evapotranspiration July (kPa)	C	30 arc s	Fick and Hijmans, 2017
Bio15	Seasonality based on temperature	C	30 arc s	Fick and Hijmans, 2017
Bio4	Seasonality based on precipitation	C	30 arc s	Fick and Hijmans, 2017
Prec_01	Precipitation January (mm)	C	30 arc s	Fick and Hijmans, 2017
Prec_07	Precipitation July (mm)	C	30 arc s	Fick and Hijmans, 2017
Tavg_01	Average temperature January (°C)	C	30 arc s	Fick and Hijmans, 2017
Tavg_07	Average temperature July (°C)	C	30 arc s	Fick and Hijmans, 2017
Tmax_01	Maximum temperature January (°C)	C	30 arc s	Fick and Hijmans, 2017
Tmax_07	Maximum temperature July (°C)	C	30 arc s	Fick and Hijmans, 2017
Tmin_01	Minimum temperature January (°C)	C	30 arc s	Fick and Hijmans, 2017
Tmin_07	Minimum temperature July (°C)	C	30 arc s	Fick and Hijmans, 2017
wc2 1_5m_01	Evapo-transpiration January (kPA)	C	30 arc s	Fick and Hijmans, 2017
wc2 1_5m_07	Evapo-transpiration July (kPA)	C	30 arc s	Fick and Hijmans, 2017

C, continuous; D, discrete.

The full dataset is first randomized to avoid any structure resulting from record or sampling order. The Random Forest was first passed through a tuning phase in order to find the optimal number of variable combinations with respect to the Out-of-Bag error estimate, by using only the subset of variables automatically selected by VSURF. Afterward, we selected the model showing the smaller Mean Squared Error (MSE) between predicted and observed $^{87}Sr/^{86}Sr$ values. The relative weight of each variable in reducing the overall error in the Random Forest model was measured by the "variable importance impurity measure," graphically represented by the partial dependence of $^{87}Sr/^{86}Sr$ values on those variables. The $^{87}Sr/^{86}Sr$ values predicted by the Random Forest model in relation to the predictor variables were then used to produce the isoscapes, while the residuals between the predicted and observed values provide the uncertainty associated with the isoscape. In addition, the uncertainty in the prediction for each case was measured using the standard error generated by the data used to generate the model. Finally, we used a Mantel correlogram (Legendre and Fortin, 1989) to assess the existence of remaining spatial structuration in the $^{87}Sr/^{86}Sr$ values unaccounted for by the covariables of the model, that would indicate that unknown variables have a weight in structuring the observed variation. To accomplish this, we utilized the residuals of the Random Forest model with 10,000 permutations on two distance-matrices produced on the basis of the residuals and the spatial coordinates on the training model (80% of the sample).

The Random Forest model was adjusted with the software Ranger (Wright and Ziegler, 2017) and tuneRanger (Probst et al., 2019) that implement quantile regression for Random Forest, and with VSURF (Genuer et al., 2019). The graphs of partial dependence were produced with the pdp package (Greenwell, 2017) and the analysis of spatial structure in the residuals was conducted with the packages ncf (Bjornstad and Cai, 2020) and ecodist (Goslee and Urban, 2007). All the analyses were performed in R Core Team (2020). For the geostatistical analysis, we compiled a georeferenced database incorporating the results of the Random Forest model. This information was processed in the platform QGIS 3.14 in order to build the isoscapes of bioavailable strontium using the Inverse Distance Weighing—IDW—function (Kootker et al., 2016; Bataille et al., 2018).

RESULTS

Strontium Isotopes in Plant and Rodent Samples

We present new $^{87}Sr/^{86}Sr$ results for modern plant samples ($n = 26$) (**Table 2**), which are combined with previously published

TABLE 2 | $^{87}Sr/^{86}Sr$ results for plant samples from the southern Andes of Argentina and Chile (source: this paper).

Sampling site	Geological province	Taxon	Latitude (S)	Longitude (W)	$^{87}Sr/^{86}Sr$	±2s
Cartagena Bay	Pacific Coast	*Quillaja saponaria* (native)	33°30.451′	71°36.411′	0.708132	0.000012
Rocas de Santo Domingo	Pacific Coast	Unknown	33°37.903′	71°38.058′	0.707697	0.000012
Cartagena	Coastal Cordillera	Unknown	33°33.037′	71°33.987′	0.705779	0.000014
El Membrillo	Coastal Cordillera	*Eucalyptus robusta* (non-native)	33°28.569′	71°36.265′	0.707543	0.000012
Malvilla	Coastal Cordillera	*Acacia caven* (native)	33°34.823′	71°30.224′	0.706011	0.000014
Las Palmas	Coastal Cordillera	Unknown	33°37.204′	71°25.091′	0.705627	0.000013
Puangue	Coastal Cordillera	*Eucalyptus robusta* (non-native)	33°38.620′	71°21.936′	0.705894	0.000013
Yeso River	W Principal C.	*Peumus boldus* (native)	33°43.848′	70°8.341′	0.704203	0.000012
Maipo River	W Principal C.	*Peumus boldus* (native)	33°46.530′	70°15.562′	0.705419	0.000016
Maipo River	W Principal C.	*Quillaja saponaria* (native)	33°34.906′	70°'24.093′	0.705654	0.000014
La Reina	W Principal C.	*Ligustrum lucidum* (non-native)	33°26.946′	70°31.640′	0.704452	0.000011
Yeso River	E Principal Cordillera	Unknown	33°37.330′	69°57.770′	0.70665	0.000028
Laguna del Diamante	E Principal Cordillera	Poaceae (native)	34°10.802′	69°39.502′	0.705656	0.000011
Paramillos Ignimbrite	Frontal Cordillera	*Schinus* spp. (native)	34°14.951′	69°19.411′	0.706885	0.000016
Road to Laguna del Diamante	Frontal Cordillera	*Adesmia* sp. (native)	34°13.456′	69°25.874′	0.711841	0.000010
Cerro Tunduqueral	Precordillera	*Prosopis* aff. *Alpataco* (native)	32°31.967′	69°18.572′	0.706689	0.000012
Cerro Tunduqueral	Precordillera	*Larrea cuneifolia* (native)	32°31.970′	69°18.468′	0.706818	0.000014
San Alberto-Tambillos	Precordillera	*Larrea nitida* (native)	32°23.772′	69°23.398′	0.707777	0.000014
San Alberto-Tambillos	Precordillera	*Larrea divaricata* (native)	32°23.911′	69°23.595′	0.707598	0.000013
Uspallata-Usina Sur	Precordillera	*Larrea nitida* (native)	32°38.055′	69°22.467′	0.70754	0.000008
Uspallata-Usina Sur	Precordillera	*Fabiana denudata* (native)	32°37.951′	69°22.541′	0.707014	0.000012
Paramillos	Precordillera	*Larrea nitida* (native)	32°28.518′	69°11.593	0.707572	0.000010
Road to Canota	Precordillera	*Mulinum spinosum* (native)	32°30.740′	69°2.845′	0.707747	0.000014
Cruz de Paramillos	Precordillera	Poaceae (native)	32°29.592′	69°7.050′	0.70815	0.000011
Pampa de Canota	Precordillera	Poaceae (native)	32°38.427′	69°8.081′	0.707834	0.000013
Corsemar	Active Foreland	*Larrea cuneifolia* (native)	32°40.241′	68°52.860′	0.707036	0.000015

results for rodent samples (n = 65) (**Table 3**). While this sample can be considered as preliminary given the large size of the study-area, the results offer a first characterization of the geological provinces across the southern Andes.

The $^{87}Sr/^{86}Sr$ values are normally distributed (W = 0.98094, p = 0.2039) ranging between 0.70393 and 0.71184 with an average of 0.70723 ± 0.00177. When considering the plant and rodent samples separately, the 26 plant samples have a mean $^{87}Sr/^{86}Sr$ value of 0.70689 ± 0.00149, a maximum value of 0.71184 (Frontal Cordillera), and a minimum value of 0.7042 (Western Principal Cordillera). The 65 rodent samples have a mean $^{87}Sr/^{86}Sr$ value of 0.70736 ± 0.00187, a maximum value of 0.7109 (Precordillera), and a minimum value of 0.70393 (Western Principal Cordillera).

Particularly for the Precordillera geological province, that includes the key archeological locality of the Uspallata Valley discussed here (**Figure 1**), we have adequate sample sizes for plant and rodent samples to allow a first comparison. Unexpectedly, the respective isotopic ranges do not overlap. Plants have a mean value of 0.70747 ± 0.00047 and rodents of 0.70964 ± 0.00082. Interestingly, not only rodents but also wild herbivore camelids from Uspallata-Precordillera fail to reproduce the signal for modern plants (Barberena et al., 2019). While this sampling was not designed to compare the performance of different substrates to build strontium isoscapes, these differences are considered large and they would have implications for the reconstruction of human paleomobility and migration. Accordingly, we explore next if there are differences in the main predictor variables of $^{87}Sr/^{86}Sr$ values in two alternative Random Forest models: one combining values for plants and rodents (n = 91) and another one including only rodents (n = 65). Based on this comparison we assess the predictive capacity of the two alternative models.

Random Forest Modeling and Strontium Isoscape

In the "Plants + Rodents" dataset, the selected Random Forest model explains a 76% of the variation in the observed OOB values with an MSE of 0.00000008 ($^{87}Sr/^{86}Sr$ RMSE = 0.0003), suggesting a good power of the predictive variables utilized and a low error. The variables with the highest predictive power are—in decreasing order of importance—Geological Province, Bio15 (temperature seasonality), and Mean-age, with a subordinate role by six other bioclimatic variables (**Figure 4A**). In the case of the "Rodents" sample, the selected Random Forest model accounts for 85% of the observed values with an OOB MSE = 0.0000007 ($^{87}Sr/^{86}Sr$ RMSE = 0.0007). The variables with a high predictive power are only three: Geological Province, Mean-age, and Distance to coast (**Figure 4B**). In sum, the "Rodents" model has a higher predictive capacity than the "Plants + Rodents" model (85 vs. 76%). Additionally, in the "Rodent" model this variation is accounted for by only three predictor variables, two of which are tightly connected with the geological substrate

TABLE 3 | $^{87}Sr/^{86}Sr$ results for rodent samples from the southern Andes (Argentina and Chile).

N	Site	Geological unit	Taxon	Latitude (S)	Longitude (W)	$^{87}Sr/^{86}Sr$	Source
1	Los Vilos	Pacific Coast	Rodentia	31°54.692′	71°30.616′	0.708395	Barberena et al., 2020
2	Los Vilos	Pacific Coast	Rodentia	31°54.692′	71°30.616′	0.708706	Barberena et al., 2020
3	Los Vilos	Pacific Coast	Rodentia	31°54.692′	71°30.616′	0.709022	Barberena et al., 2020
4	Los Vilos	Pacific Coast	Rodentia	31°54.692′	71°30.616′	0.708593	Barberena et al., 2020
5	Los Vilos	Pacific Coast	Rodentia	31°54.692′	71°30.616′	0.708885	Barberena et al., 2020
6	Los Vilos	Pacific Coast	Rodentia	31°54.692′	71°30.616′	0.708999	Barberena et al., 2020
7	Los Vilos	Pacific Coast	Rodentia	31°54.692′	71°30.616′	0.708898	Barberena et al., 2020
8	Los Vilos	Pacific Coast	Rodentia	31°54.692′	71°30.616′	0.709019	Barberena et al., 2020
9	LEP-C	Pacific Coast	*Myocastor coipus*	33°30.222′	71°36.580′	0.708572	Barberena et al., 2020
10	LEP-C	Pacific Coast	*Octodon* sp.	33°30.222′	71°36.580′	0.708197	Barberena et al., 2020
11	LEP-C	Pacific Coast	*Octodon* sp.	33°30.222′	71°36.580′	0.708566	Barberena et al., 2020
12	Arévalo 2	Pacific Coast	*Octodon* sp.	33°34.305′	71°35.675′	0.707365	Barberena et al., 2020
13	Arévalo 2	Pacific Coast	*Octodon* sp.	33°34.305′	71°35.675′	0.707754	Barberena et al., 2020
14	RML-015	Coastal Cordillera	*Octodon* sp.	33°16.154′	70°52.995′	0.704151	Barberena et al., 2020
15	E-101-3	Coastal Cordillera	Rodentia	33°41.661′	70°57.884′	0.706320	Barberena et al., 2020
16	RML-008	Coastal Cordillera	*Octodon* sp.	33°15.852′	70°53.816′	0.704150	Barberena et al., 2020
17	Cerro Chena	Coastal Cordillera	*Myocastor coipus*	33°36.926′	70°44.814′	0.705305	Barberena et al., 2020
18	E-101-1	Coastal Cordillera	*Myocastor coipus*	33°40.340′	70°57.627′	0.705072	Barberena et al., 2020
19	Combarbalá	W. Principal Cordillera	Rodentia	31°11.372′	70°59.793′	0.704083	Barberena et al., 2020
20	Combarbalá	W. Principal Cordillera	Rodentia	31°11.372′	70°59.793′	0.704131	Barberena et al., 2020
21	Alero Paulino González	W. Principal Cordillera	Rodentia	31°32.756′	70°50.195′	0.704249	Barberena et al., 2020
22	Los Azules 1	W. Principal Cordillera	Rodentia	33°36.906′	70°24.762′	0.70393	Barberena et al., 2017
23	Manzano 1	W. Principal Cordillera	Rodentia	33°33.806′	70°26.568′	0.70396	Barberena et al., 2017
24	Los Queltehues	W. Principal Cordillera	Rodentia	33°54.110′	70°11.333′	0.70401	Barberena et al., 2017
25	Las Cuevas	E. Principal Cordillera	Rodentia	32°48.803′	70°2.148′	0.705557	Barberena et al., 2020
26	Las Cuevas	E. Principal Cordillera	Rodentia	403034.84	70°2.148′	0.705566	Barberena et al., 2020
27	Las Cuevas	E. Principal Cordillera	Rodentia	403034.84	70°2.148′	0.705276	Barberena et al., 2020
28	Laguna del Diamante	E. Principal Cordillera	*Ctenomys* sp.	34°11.835′	69°42.318′	0.707028	Barberena et al., 2020
29	Laguna del Diamante	E. Principal Cordillera	Rodentia	34°11.953′	69°40.579′	0.706000	Barberena et al., 2020
30	Las Cuevas 1	E. Principal Cordillera	*Eligmodontia* sp.	32°48.804′	70°2.150′	0.70567	Barberena et al., 2019
31	Las Cuevas 2	E. Principal Cordillera	*Eligmodontia* sp.	32°48.804′	70°2.150′	0.70567	Barberena et al., 2019
32	Aconcagua 1	E. Principal Cordillera	Rodentia	32°42.301′	69°57.921′	0.70557	Barberena et al., 2019
33	Gendarmería. L. Diamante	Frontal Cordillera	Rodentia	34°11.429′	69°42.685′	0.70655	Barberena et al., 2017
34	Quebrada de La Manga	Frontal Cordillera	Rodentia	32°56.650′	69°18.984′	0.707626	Barberena et al., 2020
35	Quebrada de La Manga	Frontal Cordillera	Rodentia	32°56.650′	69°18.984′	0.707750	Barberena et al., 2020
36	Quebrada de La Manga	Frontal Cordillera	*Ctenomys* sp.	32°56.650′	69°18.984′	0.70799	Barberena et al., 2019
37	Paramillos	Frontal Cordillera	Rodentia	32°28.931′	69°8.099′	0.707288	Barberena et al., 2020
38	Paramillos	Frontal Cordillera	Rodentia	32°28.931′	69°8.099′	0.707579	Barberena et al., 2020
39	Alero Tunduqueral	Precordillera (Uspallata)	Rodentia	32°31.819′	69°18.837′	0.70864	Barberena et al., 2017
40	Alero Tunduqueral	Precordillera (Uspallata)	*Ctenomys* sp.	32°31.819′	69°18.837′	0.70849	Barberena et al., 2019
41	Barrio Ramos	Precordillera (Uspallata)	Rodentia	32°35.480′	69°20.653′	0.709194	Barberena et al., 2020
42	San Ignacio	Precordillera	*Galea* sp.	32°57.367′	69°10.700′	0.70910	Barberena et al., 2019
43	San Ignacio	Precordillera	Rodentia	32°57.367′	69°10.700′	0.708230	Barberena et al., 2020
44	San Ignacio	Precordillera	Rodentia	32°57.367′	69°10.700′	0.710457	Barberena et al., 2020
45	Los Conitos	Precordillera	Rodentia	32°57.697′	69°9.409′	0.710907	Barberena et al., 2020
46	Los Conitos	Precordillera	Rodentia	32°57.697′	69°9.409′	0.709528	Barberena et al., 2020
47	Los Conitos 1	Precordillera	*Galea* sp.	32°57.657′	69°9.403′	0.71026	Barberena et al., 2019
48	Los Conitos 2	Precordillera	*Phyllotis* sp.	32°57.657′	69°9.403′	0.70950	Barberena et al., 2019
49	Agua de la Cueva	Precordillera	*Phyllotis* sp.	32°37.017′	69°9.818′	0.71008	Barberena et al., 2019
50	Agua de la Cueva	Precordillera	*Ctenomys* sp.	32°37.017′	69°9.818′	0.71016	Barberena et al., 2019
51	Agua de la Cueva	Precordillera	Rodentia	32°37.017′	69°9.818′	0.710480	Barberena et al., 2020
52	Agua de la Cueva	Precordillera	Rodentia	32°37.017′	69°9.818′	0.710039	Barberena et al., 2020
53	COINCE. San Carlos	Active foreland	Rodentia	33°40.271′	68°59.139′	0.70732	Barberena et al., 2017

(Continued)

TABLE 3 | Continued

N	Site	Geological unit	Taxon	Latitude (S)	Longitude (W)	$^{87}Sr/^{86}Sr$	Source
54	Barrancas B61	Active foreland	Rodentia	33°5.720′	68°44.820′	0.70666	Barberena et al., 2017
55	Barrancas B61	Active foreland	*Galea* sp.	33°5.720′	68°44.820′	0.70692	Barberena et al., 2019
56	Barrancas B61	Active foreland	*Galea* sp.	33°5.720′	68°44.820′	0.70681	Barberena et al., 2019
57	Natania	Active foreland	*Galea* sp.	32°55.148′	68°51.013′	0.70704	Barberena et al., 2019
58	Divisadero	Active foreland	*Ctenomys* sp.	32°52.640′	68°55.022′	0.70747	Barberena et al., 2019
59	Natania	Active foreland	Rodentia	32°55.148′	68°51.013′	0.706979	Barberena et al., 2020
60	Natania	Active foreland	Rodentia	32°55.148′	68°51.013′	0.706986	Barberena et al., 2020
61	Lavalle	Active foreland	Rodentia	32°23.782′	67°51.077′	0.707564	Barberena et al., 2020
62	Lavalle	Active foreland	Rodentia	32°23.782′	67°51.077′	0.707494	Barberena et al., 2020
63	Capiz Alto	Active foreland	Rodentia	33°40.134′	68°58.702′	0.707015	Barberena et al., 2020
64	Capiz Alto	Active foreland	Rodentia	33°40.134′	68°58.702′	0.707507	Barberena et al., 2020
65	Barrancas B6	Active foreland	Rodentia	33°5.595′	68°44.785′	0.706543	Barberena et al., 2020

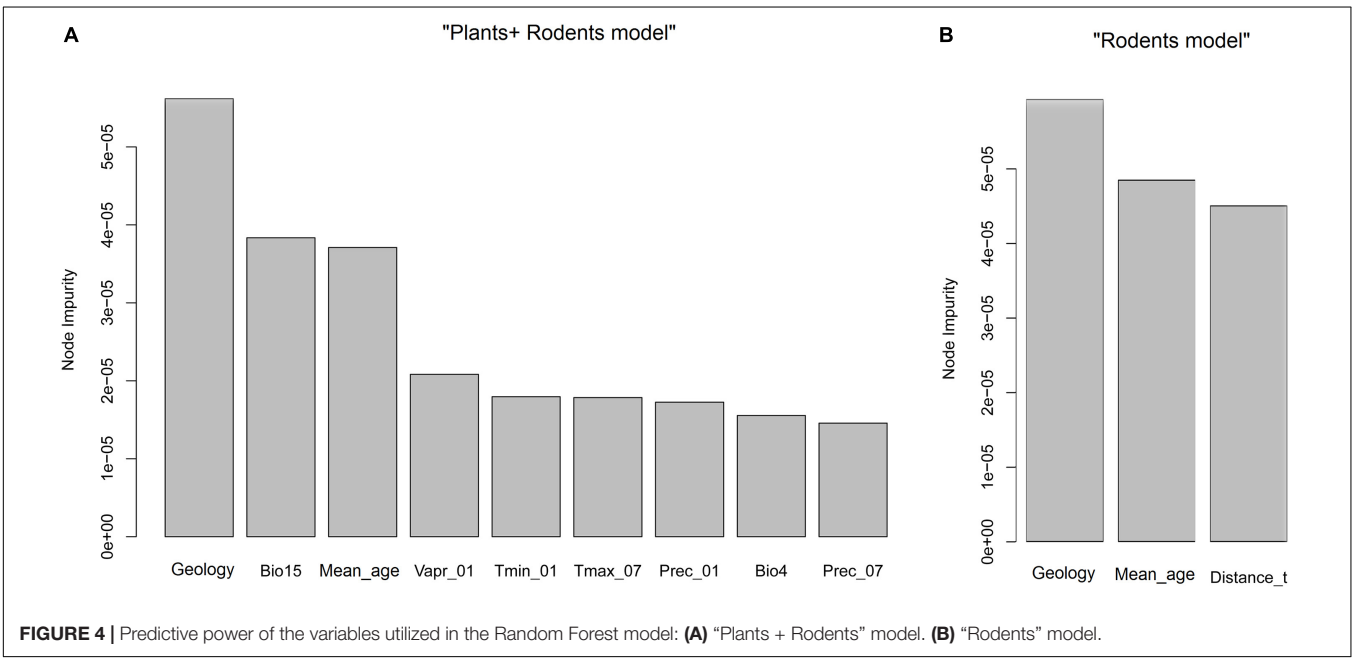

FIGURE 4 | Predictive power of the variables utilized in the Random Forest model: **(A)** "Plants + Rodents" model. **(B)** "Rodents" model.

(Geological Province and Mean-age), while the third (Distance to coast) would be related with the decreasing incidence of marine strontium—0.709202 ± 0.000003—(Kuznetsov et al., 2012) with increasing distance from the coast (Alonzi et al., 2020). Importantly, in the "Plants + Rodents" model several bioclimatic variables contribute to structure variation with a substantial role of temperature seasonality (Bio15).

The analysis of the linear fit between the predicted and observed $^{87}Sr/^{86}Sr$ values shows that the plant samples have a larger estimation error than the rodent samples, likely affecting the amount of variation, respectively, explained by the two Random Forest models presented, as well as the number of variables selected by each model (9 in the "Plants + Rodents" model vs. 3 in the "Rodents" model, **Figure 4**). In the "Plants + Rodents" model the validation of the Random Forest model with the new cases from the test set (20% of the sample) accounts for 72% of the variation (R-squared = 0.72) with a RMSE = 0.0008. The Mantel test produces a value of $r = -0.07$, $p > 0.05$, suggesting that there is no significant remaining spatial structure in the residuals, although a low autocorrelation was detected in two distance intervals (**Supplementary Figure 1A**). While the linear regression between the values included in the training and testing sets for the "Plants + Rodents" samples shows a good overall fit, there is a larger dispersion of the residuals in the area of the most radiogenic values—between 0.709 and 0.710—(**Figures 5A,B**). In the SAST, these samples are located adjacent or within the Precordillera highlands (including the Uspallata Valley), formed by Lower Paleozoic rocks that are the oldest present (**Figure 2**). This increase in the magnitude of residual values in contexts with higher $^{87}Sr/^{86}Sr$ ratios has been shown to be a global phenomenon (Bataille et al., 2020) and explains the existence of considerably higher residuals in the "Plants + Rodents" model compared to the "Rodents" model (**Figures 5B,D**).

The regression between the predicted and observed results for the "Rodents" sample shows a high fit between predicted

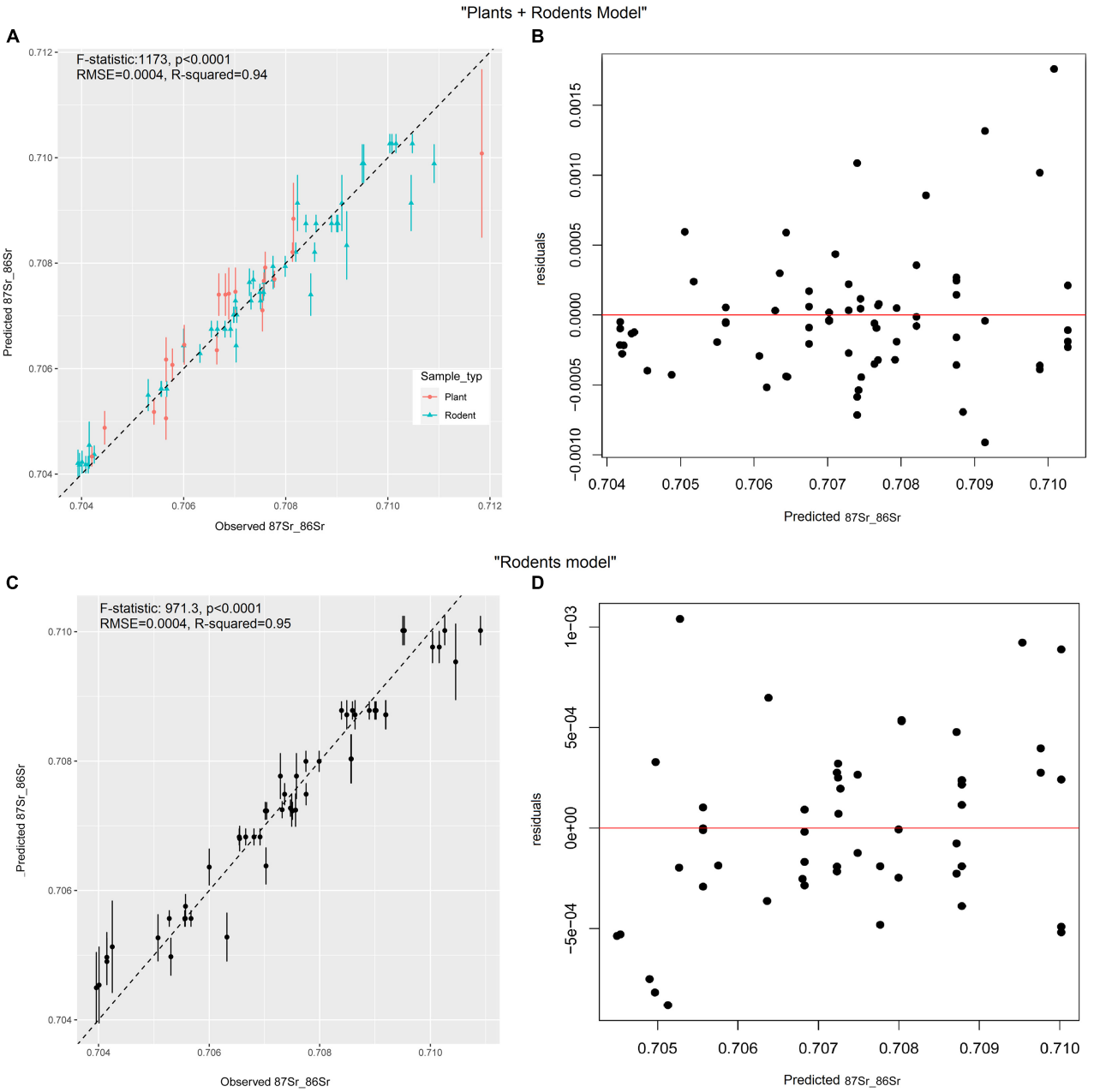

FIGURE 5 | Linear regression between predicted and observed $^{87}Sr/^{86}Sr$ values and associated residuals: **(A,B)** "Plants + Rodents" model. **(C,D)** "Rodents" model.

and observed $^{87}Sr/^{86}Sr$ values (**Figure 5C**) and the validation of the Random Forest model with the new cases from the test set (20% of the sample) accounts for 95% of the variation (*R*-squared = 0.95, RMSE = 0.003) (**Figures 5C,D**). The Mantel test produces a value of $r = 0.005$, $p > 0.05$, suggesting that there is no remaining spatial structure in the residuals (**Supplementary Figure 1B**). In **Supplementary Figure 1** we present the isoscapes with the Standard Error, Quartile 1 (25%), Quartile 3 (median), and Quartile 3 (75%). In the **Supplementary Materials** file we also present the results for all the covariates analyzed in this model.

The analysis of partial dependence between the predictor variables and $^{87}Sr/^{86}Sr$ values for the "Plants + Rodents" model suggests an eastwards exponential increase of the values beyond 150 km from the Pacific coast, reaching the highest values at a distance of 250 km from the coast (**Figure 6**). This is compatible with the underlying trends in bedrock age from west to east, characterized by the succession of increasingly older rocks: Western Principal Cordillera (Oligocene-Pliocene), Eastern Principal Cordillera (Cretaceous-Jurassic), Frontal Cordillera (Permian-Triassic), and Precordillera (Lower Paleozoic) (**Figure 2**). Eastwards from

Precordillera, there is a decrease in $^{87}Sr/^{86}Sr$ values in the Active Foreland, a Quaternary basin that averages sediments from Precordillera and younger formations such as the Cordillera Frontal and Cordillera Principal (**Figure 6A**). While sampling is small in these Quaternary deposits, it is expected that spatial resolution will be lower compared to the Andes (see below).

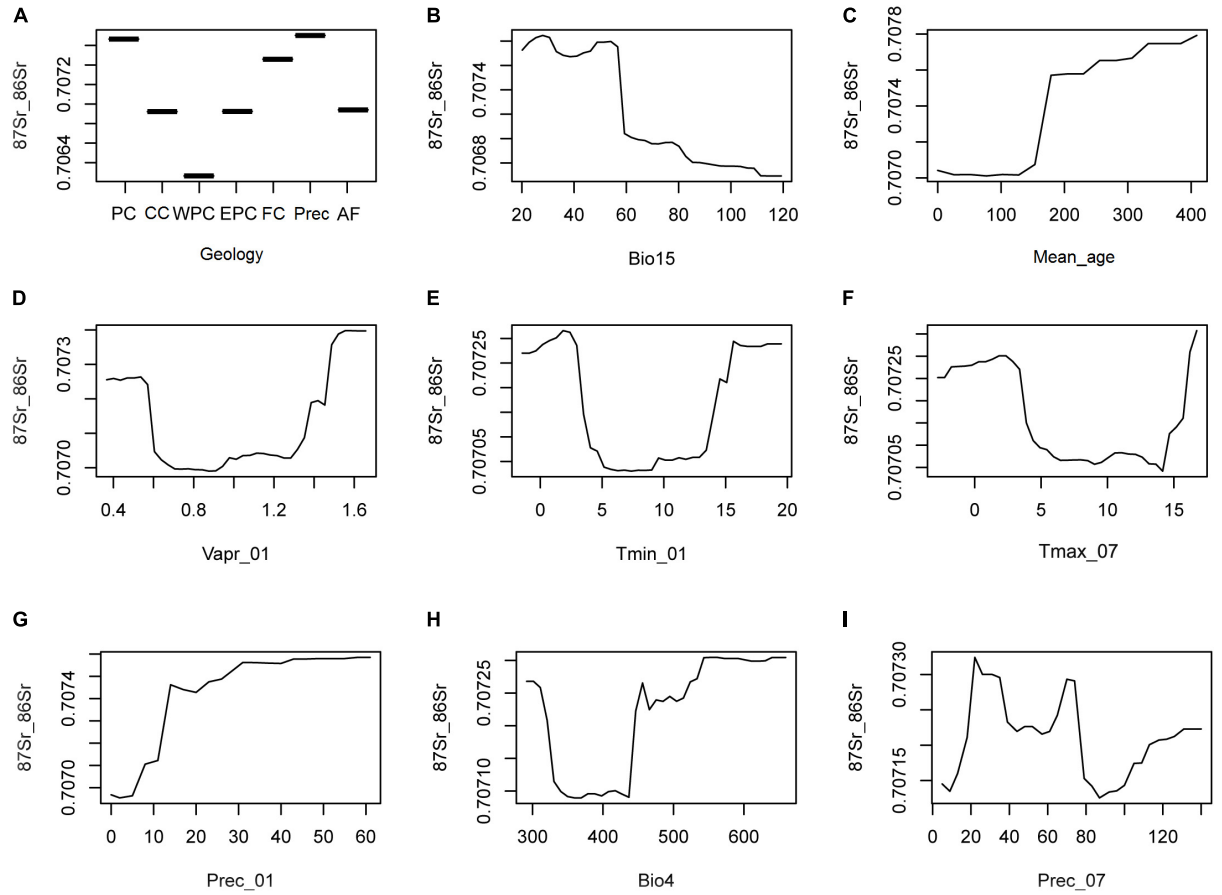

FIGURE 6 | Analysis of partial dependence between the variables of the Random Forest models and $^{87}Sr/^{86}Sr$ values for the "Plants + Rodents" model. Key: **(A)** geological province, **(B)** temperature seasonality, **(C)** mean rock age (years), **(D)** evapotranspiration January, **(E)** minimum temperature January, **(F)** maximum temperature July, **(G)** precipitations January, **(H)** precipitation seasonality, and **(I)** precipitation July.

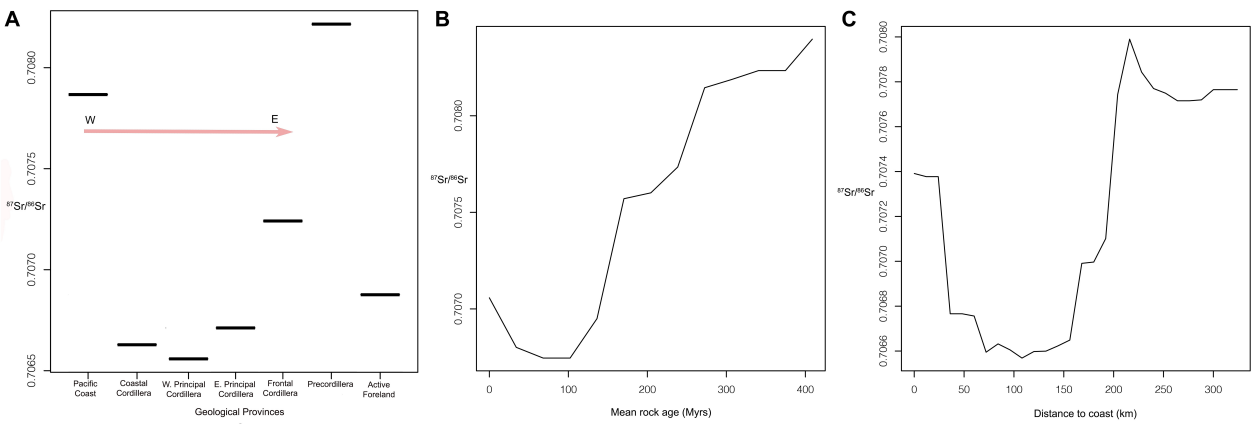

FIGURE 7 | Analysis of partial dependence between the variables of the Random Forest models and $^{87}Sr/^{86}Sr$ values for the "Rodents" model. Key: **(A)** geological province, **(B)** mean rock age (years), and **(C)** distance to coast (km).

The most important bioclimatic variable identified is *Bio15*, a coefficient of Seasonality based on temperature, followed by *Tmin07*—Minimum July temperature.

The "Rodents" model, on the other hand, is accounted for in a much more simplified fashion by only three predictor variables: Geology, Mean-age, and Distance to coast (**Figure 7**), indicating that the rodent samples track the geological variation more closely than the "Plants + Rodents" model, where several bioclimatic variables contribute significantly.

Isoscape for the Southern Andean Strontium Transect

We have presented the results for bioavailable strontium across the SAST connecting the Pacific Ocean in Chile and the eastern lowlands in Argentina. The application of the Random Forest approach pioneered by Bataille et al. (2018) has allowed comparing two substrates that can be used to build frames of reference for the interpretation of $^{87}Sr/^{86}Sr$ values in archeological remains. The "Rodents" model presents the best fit between predicted and observed values (85%) in association with a small error (RMSE = 0.0007). This large amount of variation can be accounted for with a simpler model where only the predictors Geological province, Mean rock age, and Distance to coast explain the observed variation, whereas in the "Plants + Rodents" model several bioclimatic variables—particularly seasonality of precipitation (Bio15)—contribute to explain variation in addition to geological province and Mean-age (**Figures 6**, **7**). Considering that the plant samples analyzed are modern, an issue that will need to be explored in the future is the possible incidence of modern mining activities in the $^{87}Sr/^{86}Sr$ values in plants (Burger and Lichtscheidl, 2019; Thomsen and Andreasen, 2019).

While this project was not formally designed to compare alternative substrates to build strontium isoscapes, we suggest that by its higher fidelity to bedrock geology, rock age, and distance to coast, rodents provide a more accurate proxy for the interpretation of values in human remains in our study area (Price et al., 2002; Bentley, 2006). In **Figure 8A** we present the strontium isoscape and the associated residual values (**Figure 8B**) to assess the uncertainty of the isoscape across the SAST.

SCALE OF HUMAN MOBILITY AND MIGRATION IN THE SOUTHERN ANDES: A REGIONAL CASE-STUDY

We have recently reported $^{87}Sr/^{86}Sr$ values for 38 human samples (12 teeth and 26 bones) from 30 individuals from seven archeological sites in the Andean Uspallata Valley in Northwestern Mendoza province, Argentina, which span the period between AD 800–1500 and encompass the conquest by the Inka Empire starting ca. AD 1410 (Barberena et al., 2020; **Table 4**). The economic basis during this period would have been highly variable across space and time with multiple combinations of wild plants, the wild camelid guanaco—*Lama guanicoe*—, the domestic llama—*Lama glama*—, and several cultivated plants including maize, squash, chinoa, and beans (Frigolé and Gasco, 2016; Ots et al., 2016; Gil et al., 2020). In this context, the spatial scale of human territories was likely variable through time and remains as an issue of considerable debate. In order to tackle this issue directly, we next apply the newly presented strontium isoscape derived from the Random Forest approach to reconstruct the geographic range of the individuals analyzed from the inter-mountain Uspallata Valley (see location **Figure 1** and landscape in **Figure 3e**).

The results have a bimodal distribution with two non-overlapping groups determined by mixture analysis: the first one is composed of 27 samples with a mean of 0.7090 ± 0.0003 (range: 0.7083–0.7095) and the second group is composed of 11 samples with a mean of 0.7073 ± 0.0001 (range: 0.7072–0.7075). These groups are significantly different statistically (Mann-Whitney z = 4.7637, p = 0.0001). The geographic allocation produced with the random forest strontium isoscape indicates that the first

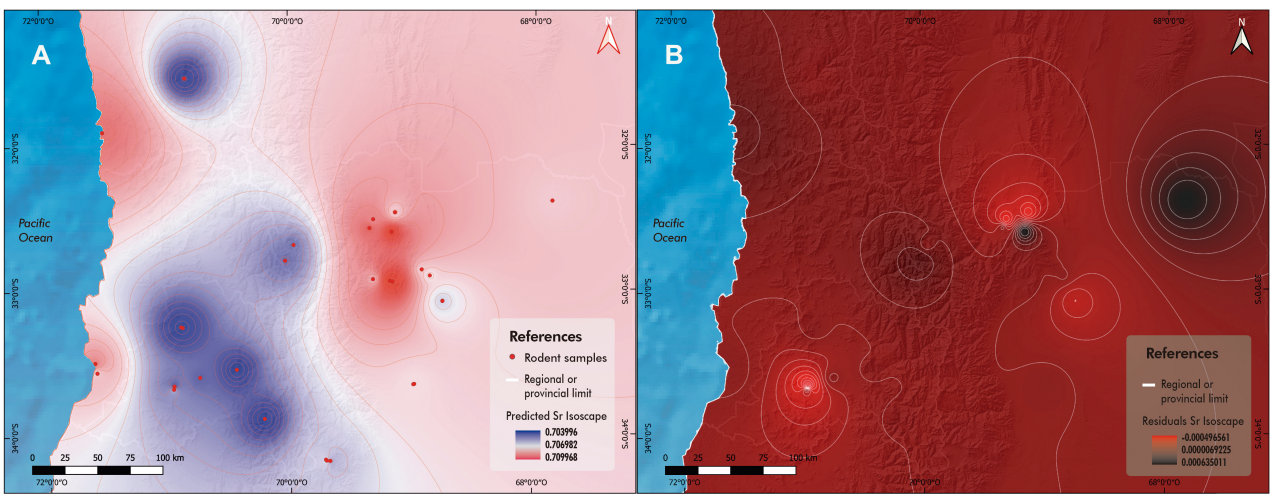

FIGURE 8 | "Rodents" model: **(A)** Random Forest bioavailable strontium isoscape. **(B)** Associated uncertainty.

TABLE 4 | $^{87}Sr/^{86}Sr$ results and contextual information for human remains from the Uspallata Valley, northwestern Mendoza, Argentina (from Barberena et al., 2020).

Site	Individual	Latitude (S)	Longitude (W)	^{14}C age (BP)	Calibrated range (AD)	Sex	Age (years)	Tissue	$^{87}Sr/^{86}Sr$
Barrio Ramos I	1	32°35.480′	69°20.653′	583 ± 43	1310–1450	M?	35–40	rib	0.709582
Barrio Ramos I	1	32°35.480′	69°20.653′	583 ± 43	1310–1450	M?	35–40	I	0.709333
Barrio Ramos I	2	32°35.480′	69°20.653′	583 ± 43	1310–1450	M	40–50	LC	0.70901
Barrio Ramos I	2	32°35.480′	69°20.653′	583 ± 43	1310–1450	M	40–50	rib	0.70953
Barrio Ramos I	3	32°35.480′	69°20.653′	583 ± 43	1310–1450	F	>40	I2	0.70865
Barrio Ramos I	3	32°35.480′	69°20.653′	583 ± 43	1310–1450	F	>40	rib	0.70922
Monte de Algarrobos	1219	32°36.345′	69°20.932′	298 ± 28	1500–1800	F	Adult	rib	0.70757
Monte de Algarrobos	1219	32°36.345′	69°20.932′	298 ± 28	1500–1800	F	Adult	I^2 right	0.709128
Usina Sur 2	1	32°38.055′	69°22.467′	772 ± 25	1220–1380	ND	Adult	rib	0.707462
Usina Sur 2	2	32°38.055′	69°22.467′	772 ± 25	1220–1380	ND	Adult	Molar	0.707504
Túmulo I	n/n 1	32°35.23′	69°21.61′	977 ± 35	1020–1190	ND	Adult	1st metatarsal	0.709443
Túmulo I	n/n 2	32°35.23′	69°21.61′	977 ± 35	1020–1190	ND	Young adult	1st metatarsal	0.709378
Túmulo I	n/n 3	32°35.23′	69°21.61′	977 ± 35	1020–1190	ND	Adult	1st metatarsal	0.709528
Túmulo I	n/n 4	32°35.23′	69°21.61′	977 ± 35	1020–1190	ND	Adult	1st metatarsal	0.709156
Túmulo II	237	32°35.23′	69°21.61′			N/D	2.5–4	rib	0.708931
Túmulo II	238	32°35.23′	69°21.61′			F?	8–9	I dentine-enamel	0.709073
Túmulo II	239	32°35.23′	69°21.61′	1269 ± 35	680–890	F	>50	rib	0.709188
Túmulo II	239	32°35.23′	69°21.61′	1269 ± 35	680–890	F	>50	I_2/M2	0.708635
Túmulo II	240	32°35.23′	69°21.61′			M	40–49	rib	0.709019
Túmulo II	240	32°35.23′	69°21.61′			M	40–49	I_2 right	0.708342
Túmulo II	241	32°35.23′	69°21.61′			ND	35–45	rib	0.709164
Túmulo II	242	32°35.23′	69°21.61′			M	18–23	rib	0.709002
Túmulo II	242	32°35.23′	69°21.61′			M	18–23	I^2 right dentine-enamel	0.708639
Túmulo II	243	32°35.23′	69°21.61′	1178 ± 41	770–1020	F	40–49	calcaneous	0.709098
Túmulo II	243	32°35.23′	69°21.61′	1178 ± 41	770–1020	F	40–49	I dentine/M3	0.708497
Túmulo II	244	32°°35.23′	69°21.61′			F	39–45	molar	0.709026
Túmulo II	245	32°35.23′	69°21.61′			M	35–45	rib	0.709038
Túmulo II	245	32°35.23′	69°21.61′			M	35–45	I_2 right	0.709035
Túmulo III	n/n 1	32°35.23′′	69°21.61′	671 ± 40	1290–1400	ND	Adult	1st metatarsal	0.708955
Túmulo III	n/n 2	32°35.23′	69°21.61′	671 ± 40	1290–1400	ND	Adult	1st metatarsal	0.70879
Túmulo III	n/n 3	32°35.23′	69°21.61′	671 ± 40	1290–1400	ND	Adult	1st metatarsal	0.707267
Potrero Las Colonias	n/n 1	32°36.555′	69°21.724′	568 ± 38	1320–1450	ND	Sub-adult	1st metatarsal	0.707251
Potrero Las Colonias	n/n 2	32°36.555′	69°21.724′	634 ± 28	1300–1420	ND	Adult	1st metatarsal	0.70732
Potrero Las Colonias	n/n 3	32°36.555′	69°21.724′	682 ± 25	1290–1400	ND	Adult	1st metatarsal	0.707343
Potrero Las Colonias	n/n 4	32°36.555′	69°21.724′	682 ± 25	1290–1400	ND	Adult	1st metatarsal	0.707252
Potrero Las Colonias	n/n 5	32°36.555′	69°21.724′	682 ± 25	1290–1400	ND	Adult	1st metatarsal	0.707407
Potrero Las Colonias	n/n 6	32°36.555′	69°21.724′	682 ± 25	1290–1400	ND	Adult	1st metatarsal	0.707243
Potrero Las Colonias	n/n 7	32°36.555′	69°21.724′	682 ± 25	1290–1400	ND	Adult	1st metatarsal	0.707401

group of individuals—from the sites Túmulo I, Túmulo II, and Barrio Ramos I—had a relatively restricted range of paleomobility which includes the Uspallata Valley and immediately adjacent areas of Precordillera and Cordillera Frontal (**Figure 9**). While the isoscape also points to the Pacific coast as a possible area of residence, this alternative can be ruled out on the basis of paleodietary information that does not suggest any intake of marine foods (Gil et al., 2014; Barberena et al., 2020). In addition, the organization of lithic and ceramic technology offer evidence compatible with restricted human territories for the period between AD 500 and 1000 in the inter-mountain Potrerillos Valley, adjacent to the Precordillera and close to Uspallata (Cortegoso, 2006; Frigolé and Gasco, 2016). While it certainly cannot be inferred that these groups were sedentary, we suggest that this first group of analyzed individuals had a local scale of mobility centered around Uspallata and not systematically connecting with the eastern lowlands nor the western Andean shed. Building on this, and also supported by the presence of multiple cemeteries, it can be suggested that Uspallata witnessed a sustained occupation by groups tethered to the valley (Barberena et al., 2017, 2020).

Regarding the second group of individuals—from the sites Potrero Las Colonias, Usina Sur 2, and Túmulo III—, the isoscape suggests that they had a disjunct geographic range and did not reside in Uspallata for a significant amount of time. While the precise geographic area of origin of these individuals cannot be precisely determined yet, the geographic analysis identifies some possible—if not the only—sources. Hence, we

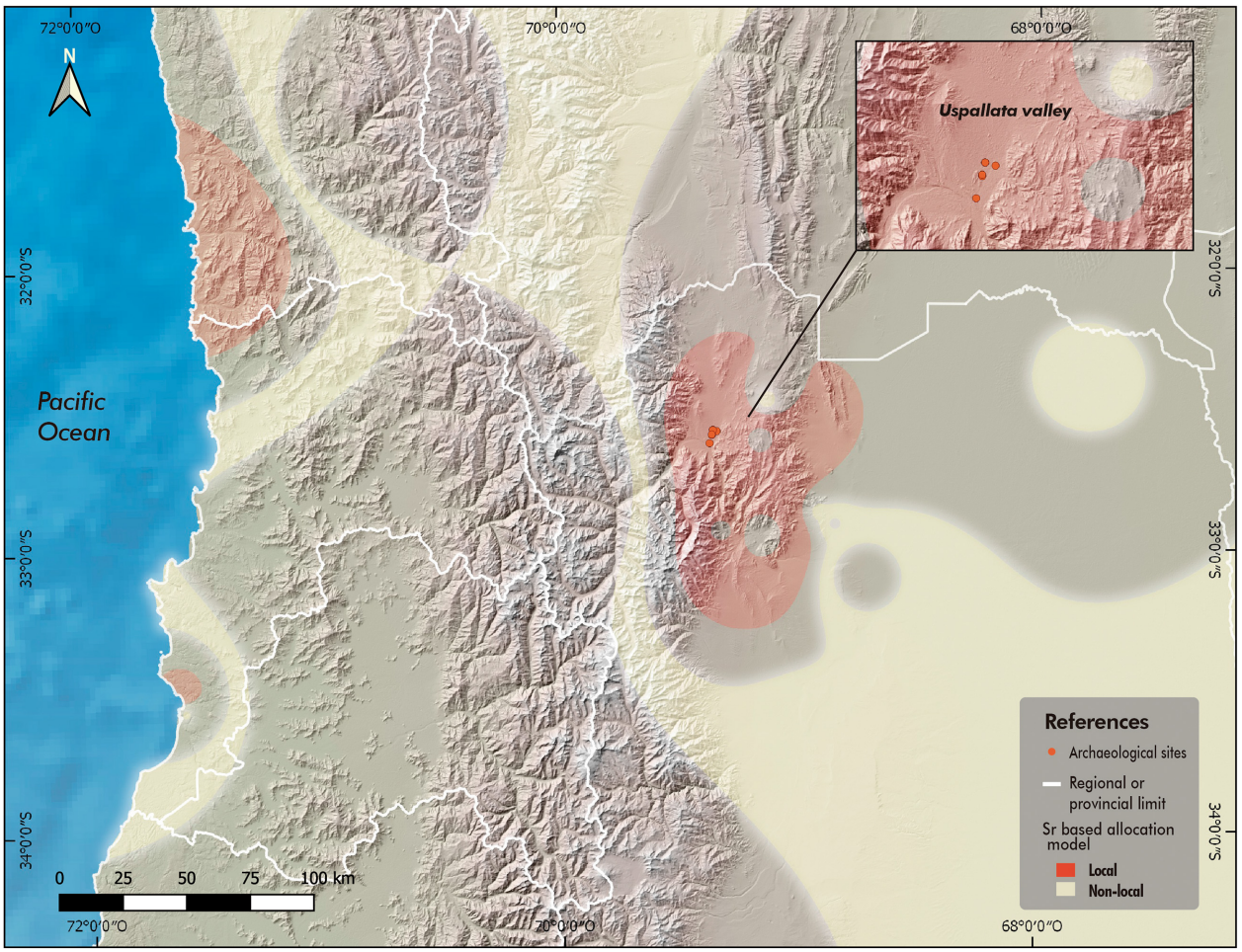

FIGURE 9 | Geographical allocation of local and non-local individuals from the Uspallata Valley (Mendoza Province, Argentina).

argue that these individuals, tough buried in Uspallata, can be interpreted as migrants.

Interestingly, there is a patterned temporal trend in the distribution of these two isotopic groups. The 27 local samples come from four sites spanning AD 800–1500, which indicates the continuous presence of locals in the Valley until the Inka arrival ∼AD 1410 (Marsh et al., 2017). On the other hand, the non-local individuals are temporally clustered between AD 1280 and 1420, a brief phase that includes 10 of the 11 non-local individuals. This immigration pulse shortly precedes the initial presence of the Inka in Uspallata, leading us to suggest that there was a multicultural social setting when the Empire arrived. This entails a more complex dynamic of interaction between the Inka and the diverse preexisting local societies in the southern periphery (Garrido, 2016; Durán V. A. et al., 2018; Troncoso, 2018; Pavlovic et al., 2019).

CONCLUSION AND PERSPECTIVES

The bioavailable strontium isoscape reconstructed for the SAST by means of Random Forest can be compared with recent macro-regional results presented for northern Patagonia (Serna et al., 2020), southwards from our study area. Serna et al. (2020) record limited strontium isotopic variation which is not strongly related to bedrock geology. Specifically, they identify a gradual increase in $^{87}Sr/^{86}Sr$ eastwards inversely correlated with elevation and positively correlated with the rate of dust deposition, which are selected by the model as the main variables accounting for the observed variation. Building on these finds, the authors suggest that the deposition and reworking of unradiogenic volcanic sediments by aeolian, fluvial, and glacial erosion homogenized the isotopic landscape, decoupling to some extent bioavailable variation from underlying bedrock geology. This study indicates that recent geomorphic processes have an impact in the spatial resolution in terms of that can be achieved by means of bioavailable $^{87}Sr/^{86}Sr$ data to assess past landscape use (Crowley and Godfrey, 2019; Scaffidi and Knudson, 2020; Scaffidi et al., 2020; Serna et al., 2020; Snoeck et al., 2020; Miller et al., 2021).

Our results for the southern Andes of Argentina and Chile show a different picture, particularly regarding rodent values, where there is large isotopic variation and a very tight correlation with bedrock geology, mean rock age, and

distance to coast, which altogether allow building a robust model accounting for 85% of the observed variation with little associated uncertainty across space—as measured by the residuals between predicted and observed values. Our results suggest that bioavailable strontium is tightly linked with bedrock geology and offers a highly resolved proxy to track human paleogeography involving the complementary levels of territories or daily mobility anomalous events that disrupt home ranges, such as migration (Barberena et al., 2020). By combining these different studies guided by the Random Forest approach we can learn about the geological and biophysical variables that contribute to structure the observed isotopic variation, thus calibrating the spatial resolution that can be achieved for each study area. The global bedrock model of expected strontium values (Bataille et al., 2020) is not selected as a strong predictor variable in these two studies. As Bataille et al. (2020) suggest, this model has a larger associated error for regions that are data-poor, have geologies that fall outside of the calibration dataset originally employed, or have outdated geology maps in the GLiM database utilized by the model. South America is one of the world regions that can be considered as still under-studied in this regard (Bataille et al., 2020).

At a regional scale of archeological analysis, the application of the southern Andean isoscape to geographically allocate archeological human remains from the Uspallata Valley shows promising results at two complementary levels: first, it confirms the persistence of human groups with relatively restricted territories encompassing Uspallata-Precordillera between the period AD 800 and 1,500. This reduced mobility is well-grounded in the isoscape-based analysis and goes against previous interpretations of high residential mobility across altitudinal regions developed on the basis of $\delta^{18}O$ values (Ugan et al., 2012). Secondly, we have identified a pulse of migration from a still undetermined region that shortly precedes the Inka conquest of the southern frontier of the Empire. Stable carbon isotopes results suggest that these migrants were intensive maize-farmers (Barberena et al., 2020). In synthesis, we have been able to analyze the daily (territories) and anomalous (migration) spheres of mobility making up human paleogeography in the southern Andes in all its complexity. Based on this first large-scale approach to bioavailable strontium across the southern Andes of Argentina and Chile, it will be possible to move forward in comparing the spatial resolution offered by different isotopic proxies of human paleomobility in diverse geographic and climatic contexts (Ugan et al., 2012; Knudson et al., 2014b; Barberena et al., 2017; Grimstead et al., 2017; Bataille et al., 2018; Willmes et al., 2018; Serna et al., 2019; Snoeck et al., 2020). Finally, we expect that the project presented here will converge with other ongoing efforts in the South-Central Andes (Scaffidi and Knudson, 2020) and northern Patagonia (Serna et al., 2020) to build a pan-Andean frame of research to track the movement of people, animals and artifacts across space and time in South America.

DATA AVAILABILITY STATEMENT

The isotopic, Random Forest results, and the R code produced in this study are fully included in the article/**Supplementary Material**. Further inquiries can be directed to the corresponding authors.

AUTHOR CONTRIBUTIONS

RB designed research. RB, CL, AG, AN-D, EM, CF, LC, FF, LS, AT, FS, VC, VD, and CM collected samples for analysis. RB, AT, CL, and AG prepared the samples for lab analyses. PL was in charge of isotopic analyses. MC conducted the Machine Learning analysis. GL developed the GIS construction of isoscapes. DW and AB built the geological framework. RB, MC, GL, and CM wrote the manuscript with contributions from all authors.

FUNDING

This research was funded by the National Geographic Society (Project HJ-136R-17), ANID-FONDECYT 1170408, Programa Regional ANID 20F0002 (Chile), and PIP-CONICET 0301 (Argentina).

ACKNOWLEDGMENTS

We acknowledge Consejo Nacional de Investigaciones Científicas y Técnicas (CONICET), the Insrtituto Interdisciplinario de Ciencias Básicas (ICB), and the Universidad Nacional de Cuyo for their continuous support, and the Comisión Nacional de Energía Atómica (San Rafael) for the help with sample preparation. Clement P. Bataille kindly offered his advice regarding the Random Forest models. Finally, we acknowledge the insightful comments provided by the two reviewers and the guest editors of the volume.

SUPPLEMENTARY MATERIAL

The Supplementary Material for this article can be found online at: https://www.frontiersin.org/articles/10.3389/fevo.2021.584325/full#supplementary-material

REFERENCES

Abraham, E., del Valle, H. F., Roig, F., Torres, L., Ares, J. O., Coronato, F., et al. (2009). Overview of the geography of the monte desert biome (Argentina). *J. Arid Environ.* 73, 144–153. doi: 10.1016/j.jaridenv.2008.09.028

Alonzi, E., Pacheco-Forés, S. I., Gordon, G. W., Kuijt, I., and Knudson, K. J. (2020). New understandings of the sea spray effect and its impact on bioavailable radiogenic strontium isotope ratios in coastal environments. *J. Archaeol. Sci. Rep.* 33:102462. doi: 10.1016/j.jasrep.2020.102462

Andrushko, V. A., Buzon, M. R., Gibaja, A. M., McEwan, G. F., Simonetti, A., and Creaser, R. A. (2011). Investigating a child sacrifice event from the Inca heartland. *J. Archaeol. Sci.* 38, 323–333. doi: 10.1016/j.jas.2010.09.009

Astini, R. A., Benedetto, J. L., and Vaccari, N. E. (1995). The early paleozoic evolution of the argentine precordillera as a laurentian rifted, drifted, and collided terrane: a geodynamic model. *Geol. Soc. Am. Bull.* 107, 253–273. doi: 10.1130/0016-7606(1995)107<0253:tepeot>2.3.co;2

Banner, J. L. (2004). Radiogenic isotopes: systematics and applications to earth surface processes and chemical stratigraphy. *Earth Sci. Rev.* 65, 141–194. doi: 10.1016/s0012-8252(03)00086-2

Barberena, R., Durán, V. A., Novellino, P., Winocur, D., Benítez, A., Tessone, A., et al. (2017). Scale of human mobility in the southern Andes (Argentina and Chile): a new framework based on strontium isotopes. *Am. J. Phys. Anthropol.* 164, 305–320. doi: 10.1002/ajpa.23270

Barberena, R., Menéndez, L., Novellino, P., Lucero, G., Luyt, J., Sealy, J., et al. (2020). Multi-isotopic and morphometric evidence for the migration of farmers leading up to the Inka conquest of the southern Andes. *Sci. Rep.* 10:21171.

Barberena, R., Tessone, A., Cagnoni, M., Gasco, A., Durán, V., Winocur, D., et al. (2019). Bioavailable strontium in the southern andes (argentina and chile): a tool for tracking human and animal movement. *Environ. Archaeol. in press*. doi: 10.1080/14614103.2019.1689894

Bárcena, J. R. (2001). "Prehistoria del centro-oeste argentino," in *Historia Argentina Prehispánica*, eds E. Berberian and A. E. Nielsen (Córdoba: Brujas), 561–634.

Bataille, C. P., Brennan, S. R., Hartmann, J., Moosdorf, N., Wooller, M. J., and Bowen, G. J. (2014). A geostatistical framework for predicting variations in strontium concentrations and isotope ratios in Alaskan rivers. *Chem. Geol.* 389, 1–15. doi: 10.1016/j.chemgeo.2014.08.030

Bataille, C. P., Crowley, B. E., Wooller, M. J., and Bowen, G. J. (2020). Advances in global bioavailable strontium isoscapes. *Palaeogeogr. Palaeoclimatol. Palaeoecol.* 555:109849. doi: 10.1016/j.palaeo.2020.109849

Bataille, C. P., von Holstein, I. C. C., Laffoon, J. E., Willmes, M., Liu, X.-M., and Davies, G. R. (2018). A bioavailable strontium isoscape for Western Europe: a machine learning approach. *PLoS One* 13:e0197386. doi: 10.1371/journal.pone.0197386

Bentley, R. A. (2006). Strontium Isotopes from the Earth to the Archaeological skeleton: a review. *J. Archaeol. Method Theory* 13, 135–187. doi: 10.1007/s10816-006-9009-x

Bjornstad, O. N., and Cai, J. (2020). *ncf: Spatial Covariance Functions*. Available online at: https://CRAN.R-project.org/package=ncf [accessed July 14, 2020].

Borić, D., and Price, T. D. (2013). Strontium isotopes document greater human mobility at the start of the Balkan Neolithic. *Proc. Natl. Acad. Sci. U.S.A.* 110, 3298–3303. doi: 10.1073/pnas.1211474110

Breiman, L. (2001). Random forests. *Mach. Learn.* 45, 5–32.

Burger, A., and Lichtscheidl, I. (2019). Strontium in the environment: review about reactions of plants towards stable and radioactive strontium isotopes. *Sci. Total Environ.* 653, 1458–1512. doi: 10.1016/j.scitotenv.2018.10.312

Capo, R. C., Stewart, B. W., and Chadwick, O. A. (1998). Strontium isotopes as tracers of ecosystem processes: theory and methods. *Geoderma* 82, 197–225. doi: 10.1016/s0016-7061(97)00102-x

Chala-Aldana, D., Bocherens, H., Miller, C., Moore, K., Hodgins, G., and Rademaker, K. (2018). Investigating mobility and highland occupation strategies during the early holocene at the cuncaicha rock shelter through strontium and oxygen isotopes. *J. Archaeol. Sci. Rep.* 19, 811–827. doi: 10.1016/j.jasrep.2017.10.023

Charrier, R., Baeza, O., Elgueta, S., Flynn, J. J., Gans, P., Kay, S. M., et al. (2002). Evidence for cenozoic extensional basin development and tectonic inversion south of the flat-slab segment, southern central andes. Chile (33°–36°S.L.). *J. S. Am. Earth Sci.* 15, 117–139. doi: 10.1016/s0895-9811(02)00009-3

Clapperton, C. (1993). *Quaternary Geology and Geomorphology of South America*. Amsterdam: Elsevier.

Copeland, S. R., Cawthra, H. C., Fisher, E. C., Lee-Thorp, J. A., Cowling, R. M., le Roux, P. J., et al. (2016). Strontium isotope investigation of ungulate movement patterns on the pleistocene paleo-agulhas plain of the greater cape floristic region, South Africa. *Quat. Sci. Rev.* 141, 65–84. doi: 10.1016/j.quascirev.2016.04.002

Copeland, S. R., Sponheimer, M., Lee-Thorp, J. A., De Ruiter, D. J., Le Roux, P. J., Grimes, V., et al. (2010). Using strontium isotopes to study site accumulation processes. *J. Taphonomy* 8, 115–127.

Cornejo, L. (2014). Sobre la cronología de la imposición cuzqueña en Chile. *Estudios Atacameños* 47, 101–116.

Cornejo, L. E., Jackson, D., and Saavedra, M. (2016). "Cazadores-rccolectores arcaicos al sur del desierto (ca. 11.000 a 300 años a.C.)," in *Prehistoria en Chile. Desde sus Primeros Habitantes Hasta Los Incas*, eds F. Falabella, M. Uribe, L. Sanhueza, C. Aldunate, and J. Hidalgo (Santiago de Chile: Sociedad Chilena de Arqueología), 285–317.

Cornejo, L., and Sanhueza, L. (2011). Caminos que cruzan la cordillera: el rol del paso del maipo en la ocupación de la cordillera en chile central. *Revista Chilena de Antropología*. 23, 101–122.

Cortegoso, V. (2006). Comunidades agrícolas en el Valle de Potrerillos (NO de Mendoza) durante el Holoceno tardío: organización de la tecnología y vivienda. *Intersecciones en Antropología* 7, 77–94

Cortegoso, V., Barberena, R., Durán, V., and Lucero, G. (2016). Geographic vectors of human mobility in the Andes (34–36° S): comparative analysis of 'minor' obsidian sources. *Quat. Int.* 422, 81–92. doi: 10.1016/j.quaint.2015.11.133

Crowley, B. E., and Godfrey, L. R. (2019). Strontium isotopes support small home ranges for extinct lemurs. *Front. Ecol. Evol.* 7:490.

Dantas, M., and Knudson, K. J. (2016). Isótopos de estroncio: cría, circulación y apropiación de camélidos en Aguada de Ambato (Catamarca. Argentina). *Intersecciones en Antropología* 17, 239–250.

Díaz, S., Cabido, M., Zak, M., Carretero, E. M., and Araníbar, J. (1999). Plant functional traits, ecosystem structure and land-use history along a climatic gradient in central-western Argentina. *J. Veg. Sci.* 10, 651–660. doi: 10.2307/3237080

Durán, V. A., Cortegoso, V., Barberena, R., Frigolé, C., Novellino, P., Lucero, G., et al. (2018). 'To and fro' the southern Andean highlands (Argentina and Chile): archaeometric insights on geographic vectors of mobility. *J. Archaeol. Sci. Rep.* 18, 668–678. doi: 10.1016/j.jasrep.2017.05.047

Durán, V., Novellino, P., Menéndez, L., Gasco, A., Marsh, E., and Barberena, R. (2018). Barrio ramos i. funebria y modos de vida en el inicio del período de dominación inca del valle de Uspallata (Mendoza, Argentina). *Relaciones de la Sociedad Argentina de Antropología* XLIII(1), 55–86. doi: 10.31819/9783954871704-004

English, N. B., Betancourt, J. L., Dean, J. S., and Quade, J. (2001). Strontium isotopes reveal distant sources of architectural timber in Chaco Canyon, New Mexico. *Proc. Natl. Acad. Sci. U.S.A.* 98, 11891–11896. doi: 10.1073/pnas.211305498

Ericson, J. E. (1985). Strontium isotope characterization in the study of prehistoric human ecology. *J. Hum. Evol.* 14, 503–514. doi: 10.1016/s0047-2484(85)80029-4

Falabella, F., Pavlovic, D., Planella, M. T., and Sanhueza, L. (2016). "Diversidad y heterogeneidad cultural y social en Chile Central durante los períodos Alfarero temprano e Intermedio Tardío (300 años a.C. a 1450 años d.C.)," in *Prehistoria en Chile*, eds F. Falabella, M. Uribe, L. Sanhueza, C. Aldunate, and J. Hidalgo (Santiago de Chile: Sociedad Chilena de Antropología), 365–400.

Fick, S. E., and Hijmans, R. J. (2017). WorldClim 2: new 1-km spatial resolution climate surfaces for global land areas. *Int. J. Climatol.* 37, 4302–4315. doi: 10.1002/joc.5086

Frigolé, C., and Gasco, A. (2016). Potters and herders at the southern edge of the Andean world: risk management and mobility in Northwestern Mendoza. Argentina. *Quat. Int.* 422, 152–162. doi: 10.1016/j.quaint.2016.02.032

Furque, G., and Cuerda, A. J. (1979). Precordillera de la rioja, san juan y mendoza. *Geol. Regional Argentina* 1, 455–522.

García, A. (2003). La ocupación temprana de los Andes centrales argentinos (ca. 11.000-8.000 años C14 AP). *Relaciones de la Sociedad Argentina de Antropología* 28, 153–165.

Garreaud, R. D. (2009). The andes climate and weather. *Adv. Geosci.* 22, 3–11. doi: 10.5194/adgeo-22-3-2009

Garrido, F. (2016). Rethinking imperial infrastructure: a bottom-up perspective on the Inca road. *J. Anthropol. Archaeol.* 43, 94–109. doi: 10.1016/j.jaa.2016.06.001

Gasco, A. (2018). Cazadores y pastores desde el 2000 AP en el límite sur del área Andina: estado de la cuestión y perspectivas futuras. *Cuadernos del Instituto Nacional de Antropología y Pensamiento Latinoamericano* 6, 15–38.

Genuer, R., Poggi, J.-M., and Tuleau-Malot, C. (2019). *VSURF Function | R Documentation*. Available online at: https://www.rdocumentation.org/packages/VSURF/versions/1.1.0/topics/VSURF [accessed July 14, 2020]

Giambiagi, L. B., Ramos, V. A., Godoy, E., Alvarez, P. P., and Orts, S. (2003). Cenozoic deformation and tectonic style of the andes, between 33\circ$ and 34\circ$ south latitude. *Tectonics* 22, n/a–n/a.

Giambiagi, L. B., Tunik, M., Ramos, V. A., and Godoy, E. (2009). The high andean cordillera of central argentina and chile along the piuquenes pass-cordon del portillo transect: darwin's pioneering observations compared eith modern geology. *Revista de la Asociación Geológica Argentina* 64, 43–54.

Gil, A. F., Villalba, R., Franchetti, F. R., Otaola, C., Abbona, C. C., Peralta, E. A., et al. (2020). Between foragers and farmers: climate change and human strategies in northwestern patagonia. *Quaternary* 3:17. doi: 10.3390/quat3020017

Gil, A. F., Villalba, R., Ugan, A., Cortegoso, V., Neme, G., Michieli, C. T., et al. (2014). Isotopic evidence on human bone for declining maize consumption during the little ice age in central western Argentina. *J. Archaeol. Sci.* 49, 213–227. doi: 10.1016/j.jas.2014.05.009

Goslee, S. C., and Urban, D. L. (2007). The ecodist package for dissimilarity-based analysis of ecological data. *J. Stat. Softw.* 22, 1–9.

Greenwell, B. M. (2017). Pdp: an r package for constructing partial dependence plots. *R J.* 9, 421–436 doi: 10.32614/rj-2017-016

Grimstead, D. N., Nugent, S., and Whipple, J. (2017). Why a standardization of strontium isotope baseline environmental data is needed and recommendations for methodology. *Adv. Archaeol. Pract.* 5, 184–195. doi: 10.1017/aap.2017.6

Hartmann, J., and Moosdorf, N. (2012). The new global lithological map database GLiM: a representation of rock properties at the Earth surface. *Geochem. Geophys. Geosyst.* 13:Q12004.

Hengl, T., de Jesus, J. M., Heuvelink, G. B. M., Gonzalez, M. R., Kilibarda, M., Blagotiæ, A., et al. (2017). SoilGrids250m: global gridded soil information based on machine learning. *PLoS One* 12:e0169748. doi: 10.1371/journal.pone.0169748

Jarvis, A., Reuter, A., Nelson, A., and Guevara, E. (2008). *Hole-Filled SRTM for the Globe Version 4*.

Jobbágy, E. G., Nosetto, M. D., Villagra, P. E., and Jackson, R. B. (2011). Water subsidies from mountains to deserts: their role in sustaining groundwater-fed oases in a sandy landscape. *Ecol. Appl.* 21, 678–694. doi: 10.1890/09-1427.1

Knudson, K. J., Goldstein, P. S., Dahlstedt, A., Somerville, A., and Schoeninger, M. J. (2014a). Paleomobility in the Tiwanaku diaspora: biogeochemical analyses at Rio Muerto. Moquegua Peru. *Am. J. Phys. Anthropol.* 155, 405–421. doi: 10.1002/ajpa.22584

Knudson, K. J., Pestle, W. J., Torres-Rouff, C., and Pimentel, G. (2012). Assessing the life history of an andean traveller through biogeochemistry: stable and radiogenic isotope analyses of archaeological human remains from Northern Chile. *Int. J. Osteoarchaeol.* 22, 435–451. doi: 10.1002/oa.1217

Knudson, K. J., Webb, E., White, C., and Longstaffe, F. J. (2014b). Baseline data for Andean paleomobility research: a radiogenic strontium isotope study of modern Peruvian agricultural soils. *Archaeol. Anthropol. Sci.* 6, 205–219. doi: 10.1007/s12520-013-0148-1

Kootker, L. M., van Lanen, R. J., Kars, H., and Davies, G. R. (2016). Strontium isoscapes in the Netherlands. spatial variations in 87Sr/86Sr as a proxy for palaeomobility. *J. Archaeol. Sci. Rep.* 6, 1–13. doi: 10.1016/j.jasrep.2016.01.015

Kuhn, M. (2013). *The Caret Package*. Available online at: http://topepo.github.io/caret/index.html [accessed July 14, 2020]

Kurtz, A. C., Kay, S. M., Charrier, R., and Farrar, E. (1997). Geochronology of Miocene plutons and exhumation history of the El Teniente region, Central Chile (34-35°8). *Andean Geol.* 24, 75–90.

Kutschera, W., and Müller, W. (2003). "Isotope language" of the Alpine Iceman investigated with AMS and MS. *Nucl. Instrum. Methods Phys. Res. B* 204, 705–719. doi: 10.1016/s0168-583x(03)00491-9

Kuznetsov, A. B., Semikhatov, M. A., and Gorokhov, I. M. (2012). The Sr isotope composition of the world ocean, marginal and inland seas: implications for the Sr isotope stratigraphy. *Stratigr. Geol. Correl.* 20, 501–515. doi: 10.1134/s0869593812060044

Laffoon, J. E., Sonnemann, T. F., Shafie, T., Hofman, C. L., Brandes, U., and Davies, G. R. (2017). Investigating human geographic origins using dual-isotope (87Sr/86Sr, δ18O) assignment approaches. *PLoS One* 12:e0172562. doi: 10.1371/journal.pone.0172562

Legendre, P., and Fortin, M. J. (1989). Spatial pattern and ecological analysis. *Vegetatio* 80, 107–138.

Llano, C. (2015). On optimal use of a patchy environment: archaeobotany in the Argentinean Andes (Argentina). *J. Archaeol. Sci.* 54, 182–192. doi: 10.1016/j.jas.2014.12.002

Llano, C., Cortegoso, V., and Marsh, E. (2017). Producción hortícola a baja escala en el límite continental del desarrollo andino: un aporte desde la arqueobotánica. *Darwiniana Nueva Serie* 5, 109–125. doi: 10.14522/darwiniana.2017.52.757

Mader, C., Hölzl, S., Heck, K., Reindel, M., and Isla, J. (2018). The llama's share: highland origins of camelids during the Late Paracas period (370 to 200 BCE) in south Peru demonstrated by strontium isotope analysis. *J. Archaeol. Sci. Rep.* 20, 257–270. doi: 10.1016/j.jasrep.2018.04.032

Mahowald, N. M., Muhs, D. R., Levis, S., Rasch, P. J., Yoshioka, M., Zender, C. S., et al. (2006). Change in atmospheric mineral aerosols in response to climate: last glacial period, preindustrial, modern, and doubled carbon dioxide climates: dust response to climate. *J. Geophys. Res.* 111, n/a–n/a.

Marsh, E. J. (2017). La fecha de la cerámica más temprana en los Andes sur. Una perspectiva macrorregional mediante modelos bayesianos. *Revista del Museo de Antropología Supl. Especial* 1, 83–94. doi: 10.31048/1852.4826.v10.n0.13501

Marsh, E. J., Kidd, R., Ogburn, D., and Durán, V. (2017). Dating the expansion of the inca empire: bayesian models from Ecuador and Argentina. *Radiocarbon* 59, 117–140. doi: 10.1017/rdc.2016.118

Masiokas, M. H., Rabatel, A., Rivera, A., Ruiz, L., Pitte, P., Ceballos, J. L., et al. (2020). A review of the current state and recent changes of the andean cryosphere. *Front. Earth Sci.* 8:99.

Méndez Melgar, C. (2013). Terminal pleistocene/early holocene 14C dates form archaeological sites in Chile: critical chronological issues for the initial peopling of the region. *Quat. Int.* 301, 60–73. doi: 10.1016/j.quaint.2012.04.003

Méndez, C., Nuevo Delaunay, A., Seguel, R., Maldonado, A., Murillo, I., Jackson, D., et al. (2018). Late pleistocene to early holocene high-quality quartz crystal procurement from the Valiente quarry workshop site (32°S, Chile, South America). *PLoS One* 13:e0208062. doi: 10.1371/journal.pone.0208062

Menéndez, L., Novellino, P., D'Addona, L. A., Brachetta Aporta, N., Béguelin, M., and Bernal, V. (2014). "El registro bioarqueológico y la incorporación de las prácticas agrícolas en el Centro– Norte de Mendoza," in *Arqueología de Ambientes de Altura de Mendoza y San Juan (Argentina)*, eds V. Cortegoso, V. A. Durán, and A. Gasco (Mendoza: EDIUNC), 99–123.

Miller, J. H., Crowley, B. E., Bataille, C. P., Wald, E. J., Kelly, A., Gaetano, M., et al. (2021). Historical landscape use of migratory caribou: new insights from old antlers. *Front. Ecol. Evol.* 8:590837.

Montgomery, J. (2010). Passports from the past: investigating human dispersals using strontium isotope analysis of tooth enamel. *Ann. Hum. Biol.* 37, 325–346. doi: 10.3109/03014461003649297

Montgomery, J., Evans, J. A., and Cooper, R. E. (2007). Resolving archaeological populations with Sr-isotope mixing models. *Appl. Geochem.* 22, 1502–1514. doi: 10.1016/j.apgeochem.2007.02.009

Muñoz-Schick, M., Moreira-Muñoz, A., Villagrán, C., and Luebert, F. (2000). Caracterización florística y pisos de vegetación en los Andes de Santiago, Chile Central. *Bol. Mus. Natl. Hist. Nat.* 49, 9–50.

Novellino, P. S., Aporta, N. B., D'Addona, L. A., Estrella, D., Bernal, V., Devincenzi, S., et al. (2013). Sitios de entierro de la localidad arqueológica Barrancas, Maipú (Mendoza, Argentina). *Intersec. Antropol.* 14, 271–277.

Ots, M. J., Garcia Llorca, J., and Cahiza, P. (2016). Recursos y estrategias de consumo en el Centro de Mendoza entre los siglos X-XVI AD. *Intersecciones en Antropología* 17, 375–387.

Oyarzabal, M., Clavijo, J., Oakley, L., Biganzoli, F., Tognetti, P., Barberis, I., et al. (2018). Unidades de vegetación de la Argentina. *Ecol. Austral* 28, 040–063.

Pavlovic, D., Sánchez, R., Pascual, D., Martínez, A., and Cortés, C. (2019). Rituales de la vida y de la muerte: dinámicas de interacción entre el Tawantinsuyu y las poblaciones locales en la cuenca del Maipo-Mapocho. *Chile Central. Estud. Atacameños.* 63, 43–80. doi: 10.2307/j.ctvf3w3k5.6

Pin, C., Briot, D., Bassin, C., and Poitrasson, F. (1994). Concominant separation of strontium and samarium–neodymium for isotopic analysis in silicate samples, based on specific extraction chromatography. *Analytica Chimica Acta* 298, 209–217. doi: 10.1016/0003-2670(94)00274-6

Planella, M. T., Falabella, F., Belmar, C., and Quiroz, L. (2015). Huertos, chacras y sementeras. *Plantas cultivadas* y su participación en los desarrollos culturales de Chile central. *Rev. Esp. Antropol. Am.* 44, 495–522.

Price, T. D., Burton, J. H., and Bentley, R. A. (2002). The characterization of biologically available strontium isotope ratios for the study of

prehistoric migration. *Archaeometry* 44, 117–135. doi: 10.1111/1475-4754.00047

Price, T. D., Manzanilla, L., and Middleton, W. D. (2000). Immigration and the ancient city of teotihuacan in mexico: a study using strontium isotope ratios in human bone and teeth. *J. Archaeol. Sci.* 27, 903–913. doi: 10.1006/jasc.1999.0504

Probst, P., Wright, M. N., and Boulesteix, A.-L. (2019). Hyperparameters and tuning strategies for random forest. *WIREs Data Min. Knowl. Discov.* 9:e1301.

R Core Team (2020). *R: a Language and Environment for Statistical Computing*. Vienna: R Foundation for Statistical Computing.

Ramos, V. A., and Folguera, A. (2009). Andean flat-slab subduction through time. *Geol. Soc. London Spec. Publ.* 327, 31–54. doi: 10.1144/sp327.3

Reynolds, A. C., Quade, J., and Betancourt, J. L. (2012). Strontium isotopes and nutrient sourcing in a semi-arid woodland. *Geoderma* 18, 574–584. doi: 10.1016/j.geoderma.2012.06.029

Rusconi, C. (1962). *Poblaciones Pre y Post Hispánicas de Mendoza. Arqueología*, Vol. III. Mendoza.

Sanhueza, L., and Falabella, F. (1999). Las comunidades alfareras iniciales en Chile central. *Revista Chilena de Antropología* 15, 29–47.

Santana-Sagredo, F., Schulting, R. J., Méndez-Quiros, P., Vidal-Elgueta, A., Uribe, M., Loyola, R., et al. (2021). White gold' guano fertilizer drove agricultural intensification in the Atacama desert from ad 1000. *Nature Plants* 7, 152–158

Scaffidi, B. K., and Knudson, K. J. (2020). An archaeological strontium isoscape for the prehistoric andes: understanding population mobility through a geostatistical meta-analysis of archaeological 87Sr/86Sr values from humans, animals, and artifacts. *J. Archaeol. Sci.* 117:105121. doi: 10.1016/j.jas.2020.105121

Scaffidi, B. K., Tung, T. A., Gordon, G., Alaica, A. K., González, La Rosa, L. M., et al. (2020). Drinking locally: a water 87Sr/86Sr isoscape for geolocation of archeological samples in the peruvian andes. *Front. Ecol. Evol.* 8:281.

Scott, M., le Roux, P., Sealy, J., and Pickering, R. (2020). Lead and strontium isotopes as palaeodietary indicators in the Western Cape of South Africa. *S. Afr. J. Sci.* 116, 1–8. doi: 10.15700/saje.v38ns2a1416

Serna, A., Prates, L., Mange, E., Salazar-García, D. C., and Bataille, C. P. (2020). Implications for paleomobility studies of the effects of quaternary volcanism on bioavailable strontium: a test case in North Patagonia (Argentina). *J. Archaeol. Sci.* 121:105198. doi: 10.1016/j.jas.2020.105198

Serna, A., Prates, L., Valenzuela, L. O., and Salazar-García, D. C. (2019). Back to the bases: building a terrestrial water δ18O baseline for archaeological studies in North Patagonia (Argentina). *Quat. Int.* 548, 4–12. doi: 10.1016/j.quaint.2019.06.008

Slovak, N. M., Paytan, A., Rick, J. W., and Chien, C.-T. (2018). Establishing radiogenic strontium isotope signatures for Chavín de Huántar, Peru. *J. Archaeol. Sci. Rep.* 19, 411–419. doi: 10.1016/j.jasrep.2018.03.014

Snoeck, C., Pouncett, J., Claeys, P., Goderis, S., Mattielli, N., Parker Pearson, M., et al. (2018). Strontium isotope analysis on cremated human remains from stonehenge support links with west wales. *Sci. Rep.* 8:10790.

Snoeck, C., Ryan, S., Pouncett, J., Pellegrini, M., Claeys, P., Wainwright, A. N., et al. (2020). Towards a biologically available strontium isotope baseline for Ireland. *Sci. Total Environ.* 712:136248. doi: 10.1016/j.scitotenv.2019.136248

Standen, V. G., Santoro, C. M., Arriaza, B., and Coleman, D. (2018). Hunting, gathering, and fishing on the coast of the atacama desert: chinchorro population mobility patterns inferred from strontium isotopes. *Geoarchaeology* 33, 162–176. doi: 10.1002/gea.21594

Takigami, M., Uzawa, K., Seki, Y., Chocano, D. M., and Yoneda, M. (2019). Isotopic evidence for camelid husbandry during the formative period at the pacopampa site, peru. *Environ. Archaeol.* 25, 262–278. doi: 10.1080/14614103.2019.1586091

Thomsen, E., and Andreasen, R. (2019). Agricultural lime disturbs natural strontium isotope variations: implications for provenance and migration studies. *Sci. Adv.* 5:eaav8083. doi: 10.1126/sciadv.aav8083

Tipple, B. J., Valenzuela, L. O., and Ehleringer, J. R. (2018). Strontium isotope ratios of human hair record intra-city variations in tap water source. *Sci .Rep.* 8:3334.

Torres-Rouff, C., and Knudson, K. J. (2017). Integrating identities: an innovative bioarchaeological and biogeochemical approach to analyzing the multiplicity of identities in the mortuary record. *Curr. Anthropol.* 58, 381–409. doi: 10.1086/692026

Troncoso, A. (2018). "Inca landscapes of domination," in *The Oxford Handbook of the Incas*, eds S. Alconini and A. Covey (Oxfort: Oxford University Press).

Ugan, A., Neme, G., Gil, A., Coltrain, J., Tykot, R., and Novellino, P. (2012). Geographic variation in bone carbonate and water δ18O values in Mendoza, Argentina and their relationship to prehistoric economy and settlement. *J. Archaeol. Sci.* 39, 2752–2763. doi: 10.1016/j.jas.2012.04.013

Willmes, M., Bataille, C. P., James, H. F., Moffat, I., McMorrow, L., Kinsley, L., et al. (2018). Mapping of bioavailable strontium isotope ratios in France for archaeological provenance studies. *Appl. Geochem.* 90, 75–86. doi: 10.1016/j.apgeochem.2017.12.025

Wright, M. N., and Ziegler, A. (2017). Ranger: a fast implementation of random forests for high dimensional data in C++ and R. *J. Statist. Softw.* 77, 1–17. doi: 10.18637/jss.v077.i01

Yu, H., Spyrou, M. A., Karapetian, M., Shnaider, S., Radzevičiūtė, R., and Nägele, K. (2020). Paleolithic to bronze age siberians reveal connections with first americans and across Eurasia. *Cell* 181, 1232–1245.e20.

Conflict of Interest: The authors declare that the research was conducted in the absence of any commercial or financial relationships that could be construed as a potential conflict of interest.

frontiers in Ecology and Evolution

PERSPECTIVE
published: 15 October 2021
doi: 10.3389/fevo.2021.748938

Silver Linings at the Dawn of a "Golden Age"

Kate Britton[1,2], Brooke E. Crowley[3,4], Clément P. Bataille[5,6], Joshua H. Miller[3] and Matthew J. Wooller[7,8]*

[1] Department of Archaeology, University of Aberdeen, Aberdeen, United Kingdom, [2] Department of Human Evolution, Max-Planck-Institute for Evolutionary Anthropology, Leipzig, Germany, [3] Department of Geology, University of Cincinnati, Cincinnati, OH, United States, [4] Department of Anthropology, University of Cincinnati, Cincinnati, OH, United States, [5] Department of Earth and Environmental Sciences, University of Ottawa, Ottawa, ON, Canada, [6] Department of Biology, University of Ottawa, Ottawa, ON, Canada, [7] Alaska Stable Isotope Facility, University of Alaska Fairbanks, Fairbanks, AK, United States, [8] Department of Marine Biology, University of Alaska Fairbanks, Fairbanks, AK, United States

Nearly four decades after the first applications of strontium isotope analyses in archaeology and paleoecology research, it could be said that we are entering a "Golden Age". Here, we reflect on major past developments and current strengths in strontium isotope research, as well as speculate on future directions. We review (1) the currently limited number of (but much needed) controlled feeding experiments, (2) recent advances in isoscape mapping and spatial assignment, and (3) the strength of multi-proxy approaches (including both the integration of strontium isotopes with other isotope systems and complementary techniques such as ancient DNA analyses). We also explore the integration of strontium isotope research with other types of paleoecological or archaeology data, as well as with evidence and interpretative frameworks from other fields (such as conservation ecology, conservation paleobiology or history). This blending is critical as we seek to advance the field beyond simply distinguishing local or relatively sedentary individuals from those that were non-local or highly mobile. We finish with a call for future research centered on balancing methodological developments and novel applications with critical self-reflection, deeper theoretical considerations and cross-disciplinarity.

Keywords: mobility, provenance, migrations, landscape use, $^{87}Sr/^{86}Sr$

OPEN ACCESS

Edited by:
Florent Rivals, Catalan Institution for Research and Advanced Studies (ICREA), Spain

Reviewed by:
Kathryn Hoppe, Green River College, United States
Patrick Roberts, Max Planck Institute for the Science of Human History (MPI-SHH), Germany

****Correspondence:***
Kate Britton
k.britton@abdn.ac.uk

Specialty section:
This article was submitted to Paleoecology, a section of the journal Frontiers in Ecology and Evolution

Received: *28 July 2021*
Accepted: *24 September 2021*
Published: *15 October 2021*

Citation:
Britton K, Crowley BE, Bataille CP, Miller JH and Wooller MJ (2021) Silver Linings at the Dawn of a "Golden Age". Front. Ecol. Evol. 9:748938. doi: 10.3389/fevo.2021.748938

INTRODUCTION

Almost 40 years have passed since the earliest uses of strontium isotopes ($^{87}Sr/^{86}Sr$) for evaluating provenance and mobility in paleoanthropology (Sillen and Kavanagh, 1982; Ericson, 1985). Today, strontium isotope investigations are increasingly common in studies of past human mobility and in applications to zooarchaeological remains. Analyses of other biogenic materials (such as wood, keratin and shell) are now also on the rise in archaeology. These trends are mirrored in the field of paleoecology. From large-scale studies of population movement histories of different species, to tracking the individual life-histories of single animals, strontium isotope research is proving a valuable means of reconstructing the spatial behaviors of humans and other species, as well as the geographical tracking of cultural objects in the past (see recent reviews in Crowley et al., 2017; Bataille et al., 2020; Britton, 2020). In archaeology in particular, the study of movement beyond the "fact of mobility" (Aldred, 2021: preface) is also vital to shaping our understanding of the past,

illuminating relationships between people and place, moving bodies, and material culture (Aldred, 2021). In the past, as in contemporary society, place is potent.

HISTORY OF RESEARCH AND CURRENT STATUS

As with other "new" tools for studying ancient remains, strontium isotope research saw a blossoming of early applications built on fundamental research, later to be tempered with more sobering explorations of the complexities and pitfalls of sample selection, data generation, environmental variability, diagenetic influences, and data treatment and analysis. For example, early archaeological research commonly utilized bone (Ericson, 1985; Price et al., 1994), but tooth enamel is now far more commonly (but not always) the favored analyte in studies of past human or faunal movement due to the issue of diagenesis—the consequence of more than 30 years of experimental research and lively debate (e.g., Nelson et al., 1986; Price et al., 1992; Budd et al., 2000; Montgomery, 2002; Hoppe et al., 2003). Despite these attentions, strontium isotope analysis has been relatively underutilized in both archaeology and paleoecology (as well as ecology) compared to other isotope systems (e.g., carbon, nitrogen, oxygen, hydrogen). This has largely been due to analytical costs and the need for robust empirical reference datasets. However, recent technical advances have lowered costs, accelerated sample throughput, and minimized destructive sampling. Other advances, such as predictively modeled spatially explicit isotope maps (isoscapes), are also contributing to rapidly moving the field forward. These improvements, coupled with a growing awareness of sampling issues, diagenesis and other limitations, are allowing for more widespread and nuanced application of strontium isotope analysis in archaeological and paleoecological enquiries. After nearly four decades of investigation, experimentation and application in archaeology, and more recently in paleoecology, strontium isotope research can perhaps finally be said to be entering a golden age.

UNDERSTANDING *IN VIVO* "INPUTS" AND TISSUE "OUTPUTS"

As demonstrated in the various works in this research topic, and by many recent papers in the field, there are developing trends and recent directions in strontium isotope research in archaeology and paleoecology. There is an emerging emphasis on experimental work, which has been missing from strontium isotope research for some time. For example, the recent publication of controlled feeding studies (Lewis et al., 2017; Anders et al., 2019; Weber et al., 2020, this research topic), provides important datasets on intra-group variability and the influences of factors such as dietary composition and nutritional content, drinking water, and dust on mammalian mineralized tissues from controlled settings. While other isotope systems, such as carbon and nitrogen, benefited from controlled feeding investigations as early as the 1970s (e.g., DeNiro and Epstein, 1978, 1981), such studies are only a very recent addition to strontium isotope research. These studies are, however, very welcome as they urge us to consider further caveats in archaeological and paleoecological applications, and also, conversely, can permit more confidence in data interpretations. On a related note, while the issue of diagenesis received some early attention (e.g., Nelson et al., 1986; Price et al., 1992; Budd et al., 2000; Montgomery, 2002; Hoppe et al., 2003), there has been relatively little interest in this topic for the past two decades. One exception is experimental research on calcined (burnt) bone (e.g., Snoeck et al., 2015), which is significant in that it permits mobility studies on cremated human remains, such as those from Stonehenge (Snoeck et al., 2018). Experiments on dental tissues using chemical tracers (combined with multi-element mapping) also mark an important methodological advance in understanding and quantifying diagenetic stability and change (Weber et al., 2021). Specimen alteration continues to be relevant to both archaeology and paleoecology, and additional research into how strontium isotope signatures in living tissues may be modified (or preserved) after death and in the burial environment is needed, especially as we seek to extend applications further into deep-time (e.g., Wallace et al., 2019; Terrill et al., 2020). These methodological considerations concerning the vital links between behavior in life, the isotope chemistry of tissues *in vivo*, and that of tissues recovered long after death are vital as we all seek to better understand and apply these approaches with confidence.

RECENT ADVANCES IN ISOSCAPE MAPPING AND SPATIAL ASSIGNMENT

One rapidly growing area of strontium isotope research, especially over the last 5 years, has been the advancement and use of computational approaches both to develop and refine strontium isoscapes (e.g., Bataille et al., 2018, 2020; Funck et al., 2021; Holt et al., 2021). The methodological considerations of isoscape mapping, especially in terms of appropriate data and sample selection, have been the subject of a number of recent papers. Spatial assignment tools targeted at identifying the origins of archaeological people, animals, and goods (e.g., the Biosphere Isotope Domains tool for the United Kingdom, see Evans et al., 2018) highlight the ways in which isoscape mapping is intersecting with the desire for empirical and probabilistic assignments of geographical origin in archaeological case studies. However, significant challenges remain in relating tissues values to (predicted) landscape variability in order to infer movements. In many deep-time paleontological applications, for example, establishing high-resolution isoscapes of contemporary strontium isotope ratios may be deeply challenging due to subsequent erosion, changes in sea-level and patterns of atmospheric strontium deposition, and even mountain building and other changes in strontium sources. Yet, even in such cases, assuming diagenetic alternation is controlled for, variability in strontium isotope ratios may still provide meaningful insight into seasonal movement histories, niche differentiation, and other aspects of paleoecology (e.g., Wallace et al., 2019; Terrill et al., 2020).

Moving forward, it is also clear that strontium isotope research is critically lacking controlled studies that link isoscapes with empirical isotope data to reconstruct individual movements. Although unsuccessful for strontium isotopes, Hu et al. (2020) provide an example in this special issue of such a "controlled movement" study. There is a serious need for designing such controlled movement studies linking isoscapes and isotope values from an individual with known travel history. These records of movement from free ranging organisms could come from the application of GPS, radio collars, satellite tracking, and drones which are also rapidly advancing technologies. For example, expected $^{87}Sr/^{86}Sr$ of GPS-collared animals could be reconstructed and compared to isotope profiles recorded in the same individuals' teeth, tusks, antlers, or possibly hair (e.g., Lazzerini et al., 2021). Integration of these approaches with movement models, such as those borrowed from spatial ecology, is perhaps the next natural step in reconstructing the movement of people and animals in the past (e.g., see discussion in Britton, 2017, and the PleistoHERD project webpage[1]).

IMPORTANCE OF MULTI-PROXY APPROACHES

Integrating strontium isotope data within multi-proxy frameworks will be another important future research direction. A logical first step would be to better combine strontium isotopes with other isotope systems. The benefit of multi-isotope research is not new, but researchers are only beginning to combine multiple isotopes in isoscape mapping and spatial assignments (see Bataille et al., 2021 for an example and discussion). Depending on what underpins spatial variability in other isotope systems (e.g., geology, anthropogenic emissions, and coastal proximity for sulfur, or climate and topography for oxygen or hydrogen), multi-isotope approaches can reinforce (or alternatively, challenge) inferences made from strontium isotopes alone (e.g., Leach et al., 2009; Crowley et al., in press; Czére et al., in press; Neil et al., 2020; Colleter et al., 2021; Funck et al., 2021; Reich et al., 2021; Wooller et al., 2021). Trace element studies, such as those using lead, can also provide more nuanced insights (e.g., Shaw et al., 2016; Moore et al., 2020; Walser et al., 2020). Ultimately, with analytical advances in "non-traditional" isotopes (e.g., zinc, copper) and the development of new isotope tools, multi-isotope studies will become increasingly common and powerful (Jaouen and Pons, 2017).

An additional key step in both archaeology and paleoecology will be the continued integration of $^{87}Sr/^{86}Sr$ analysis with other cross-disciplinary tools. For example, strontium isotope studies focused on human or animal remains will greatly benefit from further integration with ancient DNA (aDNA) analysis. In paleoecology, aDNA often provides a "broad brush" biogeographic context that can form the basis for testable hypotheses of faunal and human movement using strontium isotopes (e.g., Funck et al., 2020; Vershinina et al., 2021). Genetic data can also provide important information about individual samples, such as sex, which may be highly relevant to movement studies (e.g., Wooller et al., 2021). In archaeology, isotope and aDNA analyses can be combined to approach ancestry in a more holistic sense, particularly when material cultural, funereal, or other archaeological evidence is taken into account. Of course, strontium isotope and aDNA analyses provide evidence of movement histories on very different scales. However, integrated approaches provide the best opportunities to explore the life histories of individuals or groups of individuals beyond simply reconstructing patterns of movement, landscape use, or geographical location of an individual during childhood and allow us to infer "origin" on multiple levels. Significantly, such studies also lead us to question preconceived notions of whom might be considered "non-local" on the basis of either geographical provenance or biogeographical ancestry in the past, and to examine our own biases. The recent isotopic, genetic and forensic evidence for ethnic diversity in both Roman and Tudor Britain (Leach et al., 2009, 2015; Martiniano et al., 2016; Scorrer et al., 2021), and the negative reception of these findings by some (largely anti-immigration) factions of the British media and public, highlights the value of such studies in illuminating past societies, and also the part such research can play in helping to dispel dangerous myths of racial or cultural homogeneity in past populations. The field must, however, also acknowledge, anticipate, and challenge narratives that attempt to draw on isotopic studies that may show a lack of past population mobility, for example, to support nationalist agendas, as recently called for with ancient DNA studies (e.g., Hakenbeck, 2019).

TOWARD AN INTEGRATED, CROSS-DISCIPLINARY FUTURE

Strontium isotope studies in archaeology and paleoecology not only benefit from fuller integration with other techniques, but also with other disciplines. For example, historically-focused research is one area to which ecologists, historians, archaeologists and isotope scientists can all contribute. Themes in historical archaeology, such as agricultural intensification, urbanism, and industrialization, are just now beginning to receive attention by isotope bioarchaeologists as researchers seek to better understand changes in animal and human diet that characterized these major transitions (see discussion in Britton and Guiry, 2020). Not only are strontium isotope studies in archaeology now increasingly focusing on historic periods, researchers are also increasingly employing truly interdisciplinary approaches (see Colleter et al., 2021 for an example). Future work in historical isotope archaeology must continue to go beyond just referring to historical sources or documents and remain on this trajectory of cross-disciplinary collaboration, where studies are co-designed, and interpretations made within frameworks meaningful for all fields involved. This should include evaluating and embracing diverse (and sometimes

[1]https://www.leverhulme.ac.uk/research-project-grants/pleistoherd-integrative-approaches-late-pleistocene-herbivore-ecology

contradictory) evidence types, as opposed to simply pitting isotopic evidence ("hard science") against current historical discourse (Britton and Guiry, 2020).

Although currently underused in historical and contemporary ecology, strontium isotopes are now beginning to be increasingly employed (for example, to explore the historical movements of North American caribou; Gigleux et al., 2019; Miller et al., 2021, this research topic). Against a backdrop of dramatically changing patterns of seasonal movements and migration for a variety of populations and species (Berger, 2004; Tucker et al., 2018), there is a clear need to more fully understand the ecological impacts on landscape use and movement associated with climate change, human encroachment, and other modern ecological stressors. Subfossil, archaeological, and fossil collections provide unique opportunities to fill in temporal gaps in available ecological data. These are critical resources for reconstructing animal behaviors and their variability prior to human disturbances, as well as building more holistic strategies for successfully managing populations into the future (i.e., Conservation Paleobiology: Dietl and Flessa, 2011; Behrensmeyer and Miller, 2012; Dietl et al., 2015; Barnosky et al., 2017). Such research would be further strengthened by incorporating some of the other factors mentioned above (e.g., multi-isotope approaches, DNA, ecological niche models, etc.), and other useful spatial data to refine historical movement reconstructions.

Finally, it must be noted that applications of strontium isotopes in both archaeology and paleoecology will continue to benefit from advances in other fields. For example, numerous advances have been, and are continuing to be made in the field of fisheries science, both in terms of isoscape development and technical improvements, such as laser ablation of small samples like otoliths (fish ear bones). Fish otoliths are a particularly attractive target for studying the lifetime movement patterns of anadromous and other highly mobile fish due to the high temporal resolution they preserve. Interpreting $^{87}Sr/^{86}Sr$ records preserved in otoliths has also necessitated the development of sophisticated modeling approaches to relate fish $^{87}Sr/^{86}Sr$ to the $^{87}Sr/^{86}Sr$ in their environment (e.g., Brennan et al., 2015, 2019; Brennan and Schindler, 2017). Laser ablation technology is continuing to advance and is now becoming more readily available to investigators. The same approaches can be used to analyze larger specimens, including teeth or tusks, provided potential interferences from other elements are taken into account and strontium concentrations are adequately high (Irrgeher et al., 2016; Wooller et al., 2021). Both archaeology and paleoecology will also benefit from (but also have great potential to contribute to) developments in forensic science and food source authentication, as these fields, too, seek to better understand strontium isotope systematics for geographic tracing and provenance studies (e.g., Almeida and Vasconcelos, 2001; Coelho et al., 2017; Techer et al., 2017; Bartelink and Chesson, 2019). Identifying cross-disciplinary challenges and common goals, as well as exchanging of ideas, data and best practices will maximize the value of strontium isotope analysis to researchers in a wide number of allied fields.

CONCLUDING THOUGHTS

As explored above, it can perhaps now be said that we are at the dawn of a golden age of strontium isotope research in both archaeology and paleoecology—and yet much work lays ahead. Current research is addressing significant practical and methodological concerns, alongside novel applications. Scrutiny in research design, experimental studies (*sensu stricto*) and analytical innovation must continue along with research that addresses fundamental queries for isotope research in all fields, including tissue formation processes and diagenesis. Now is perhaps also the time for revisiting some theoretical concerns, leaning on the epistemologies of fields such as ecology but also on the frameworks of humanities research. While documenting and characterizing the "fact of mobility" may be a primary goal in most archaeological and paleoecological strontium isotope research, the use of $^{87}Sr/^{86}Sr$ data—particularly in the study of past human societies—necessitates such introspection. These silver linings will increase the confidence in our data and interpretations but will also serve to influence the theoretical frameworks within which we interpret these data and may even serve to change the questions we ask of the past.

DATA AVAILABILITY STATEMENT

The original contributions presented in the study are included in the article/supplementary material, further inquiries can be directed to the corresponding author/s.

AUTHOR CONTRIBUTIONS

KB and BEC planned out the manuscript. KB wrote the complete initial draft with input from BEC, CPB, JHM, and MJW who all made written contributions, comments, and edits. KB had oversight of integration of changes and edits. All authors contributed to the article and approved the submitted version.

FUNDING

KB would like to thank the Leverhulme Trust for support during the production of this perspective piece (PLP-2019-284). Open access publication costs were provided by the University of Alaska Fairbanks (MJW).

ACKNOWLEDGMENTS

We would like to thank the editors at Frontiers for their support and patience, and the careful consideration two reviewers gave to this manuscript. MJW would like to acknowledge that, at Fairbanks, he is working on the ancestral land of Troth Yeddha', home of the Lower Tanana people. He would also like to acknowledge that the lands on which he does his work are the ancestral lands of the Dené people who stewarded those lands for thousands of years and continue to steward those lands, further he would like to thank them and respect their enduring relationship to their homelands.

REFERENCES

Aldred, O. (2021). *The Archaeology of Movement*. London: Routledge.

Almeida, C. M., and Vasconcelos, M. T. S. D. (2001). ICP-MS determination of strontium isotope ratio in wine in order to be used as a fingerprint of its regional origin. *J. Anal. Atomic Spectrom.* 16, 607–611.

Anders, D., Osmanovic, A., and Vohberger, M. (2019). Intra- and inter-individual variability of stable strontium isotope ratios in hard and soft body tissues of pigs. *Rapid Commun. Mass Spectrom.* 33, 281–290. doi: 10.1002/rcm.8350

Barnosky, A. D., Hadly, E. A., Gonzalez, P., Head, J., Polly, P. D., Lawing, A. M., et al. (2017). Merging paleobiology with conservation biology to guide the future of terrestrial ecosystems. *Science* 355:eaah4787. doi: 10.1126/science.aah4787

Bartelink, E. J., and Chesson, L. A. (2019). Recent applications of isotope analysis to forensic anthropology. *Forensic Sci. Res.* 4, 29–44. doi: 10.1080/20961790.2018.1549527

Bataille, C. P., Crowley, B. E., Wooller, M. J., and Bowen, G. J. (2020). Advances in global bioavailable strontium isoscapes. *Palaeogeogr. Palaeoclimatol. Palaeoecol.* 555:109849. doi: 10.1016/j.palaeo.2020.109849

Bataille, C. P., Jaouen, K., Milano, S., Trost, M., Steinbrenner, S., Crubezy, E., et al. (2021). Triple sulfur-oxygen-strontium isotopes probabilistic geographic assignment of archaeological remains using a novel sulfur isoscape of western Europe. *PLoS One* 16:e0250383. doi: 10.1371/journal.pone.0250383

Bataille, C. P., von Holstein, I. C. C., Laffoon, J. E., Willmes, M., Liu, X.-M., and Davies, G. R. (2018). A bioavailable strontium isoscape for Western Europe: a machine learning approach. *PLoS One* 13:e0197386. doi: 10.1371/journal.pone.0197386

Behrensmeyer, A. K., and Miller, J. H. (2012). "Building Links Between Ecology and Paleontology Using Taphonomic Studies of Recent Vertebrate Communities," in *Paleontology in Ecology and Conservation. Springer Earth System Sciences*, ed. J. Louys (Berlin: Springer).

Berger, J. (2004). The Last Mile: How to Sustain Long-Distance Migration in Mammals. *Conserv. Biol.* 18, 320–331. doi: 10.1111/j.1523-1739.2004.00548.x

Brennan, S. R., Cline, T. J., and Schindler, D. E. (2019). Quantifying habitat use of migratory fish across riverscapes using space-time isotope models. *Methods Ecol. Evol.* 10, 1036–1047. doi: 10.1111/2041-210X.13191

Brennan, S. R., and Schindler, D. E. (2017). Linking otolith microchemistry and dendritic isoscapes to map heterogeneous production of fish across river basins. *Ecol. Appl.* 27, 363–377. doi: 10.1002/eap.1474

Brennan, S. R., Zimmerman, C. E., Fernandez, D. P., Cerling, T. E., McPhee, M. V., and Wooller, M. J. (2015). Strontium isotopes delineate fine-scale natal origins and migration histories of Pacific salmon. *Sci. Adv.* 1:e1400124. doi: 10.1126/sciadv.1400124

Britton, K. (2017). A stable relationship: isotopes and bioarchaeology are in it for the long haul. *Antiquity* 91, 853–864. doi: 10.15184/aqy.2017.98

Britton, K. (2020). "Isotope Analysis for Mobility and Climate Studies," in *Archaeological Science: An Introduction*, eds K. Britton and M. Richards (Cambridge: Cambridge University Press), 99–124.

Britton, K., and Guiry, E. J. (2020). "Isotope Bioarchaeology in Historical Archaeology," in *The Routledge Handbook of Global Historical Archaeology*, eds C. Orser, A. S. Zarankin, J. Symonds, P. Funari, and S. Lawrence (London: Routledge), 423–442.

Budd, P., Montgomery, J., Barreiro, B., and Thomas, R. G. (2000). Differential diagenesis of strontium in archaeological human dental tissues. *Appl. Geochem.* 15, 687–694.

Coelho, I., Castanheira, I., Bordado, J. M., Donard, O., and Silva, J. A. L. (2017). Recent developments and trends in the application of strontium and its isotopes in biological related fields. *TrAC Trends Anal. Chem.* 90, 45–61. doi: 10.1016/j.trac.2017.02.005

Colleter, R., Bataille, C. P., Dabernat, H., Pichot, D., Hamon, P., Duchesne, S., et al. (2021). The last battle of Anne of Brittany: Solving mass grave through an interdisciplinary approach (paleopathology, biological anthropology, history, multiple isotopes and radiocarbon dating). *PLoS One* 16:e0248086. doi: 10.1371/journal.pone.0248086

Crowley, B. E., Bataille, C. P., Haak, B., and Sommer, K. M. (in press). Identifying nesting grounds for migratory birds with dual isotope provenancing: A test with North American raptors. *Ecosphere*

Crowley, B. E., Miller, J. H., and Bataille, C. P. (2017). Strontium isotopes (87Sr/86Sr) in terrestrial ecological and palaeoecological research: empirical efforts and recent advances in continental-scale models. *Biol. Rev.* 92, 43–59. doi: 10.1111/brv.12217

Czére, O., Fawcett, J., Evans, J., Sayle, K. L., Müldner, G., Hall, M., et al. (in press). Multi-isotope analysis of the human skeletal remains from Blair Atholl, Perth & Kinross, Scotland: insights into the diet and lifetime mobility of an early medieval individual. *Tayside Fife Archaeol. J.*

DeNiro, M. J., and Epstein, S. (1978). Influence of diet on the distribution of carbon isotopes in animals. *Geochim. Cosmochim. Acta* 42, 495–506.

DeNiro, M. J., and Epstein, S. (1981). Influence of diet on the distribution of nitrogen isotopes in animals. *Geochim. Cosmochim. Acta* 45, 341–351.

Dietl, G. P., and Flessa, K. W. (2011). Conservation paleobiology: putting the dead to work. *Trends Ecol. Evol.* 26, 30–37. doi: 10.1016/j.tree.2010.09.010

Dietl, G. P., Kidwell, S. M., Brenner, M., Burney, D. A., Flessa, K. W., Jackson, S. T., et al. (2015). Conservation paleobiology: leveraging knowledge of the past to inform conservation and restoration. *Ann. Rev. Earth Planet. Sci.* 43, 79–103. doi: 10.1146/annurev-earth-040610-133349

Ericson, J. E. (1985). Strontium isotope characterization in the study of prehistoric human ecology. *J. Human Evol.* 14, 503–514.

Evans, J., Mee, K., Chenery, C., Cartwright, C., Lee, K., and Marchant, A. (2018). *User guide for the Biosphere Isotope Domains GB (Version 1) dataset and web portal*.

Funck, J., Bataille, C., Rasic, J., and Wooller, M. (2021). A bio-available strontium isoscape for eastern Beringia: a tool for tracking landscape use of Pleistocene megafauna. *J. Quater. Sci.* 36, 76–90. doi: 10.1002/jqs.3262

Funck, J., Heintzman, P. D., Murray, G. G. R., Shapiro, B., McKinney, H., Huchet, J.-B., et al. (2020). A detailed life history of a pleistocene steppe bison (Bison priscus) skeleton unearthed in Arctic Alaska. *Quaternary Sci. Rev.* 249:106578. doi: 10.1016/j.quascirev.2020.106578

Gigleux, C., Grimes, V., Tütken, T., Knecht, R., and Britton, K. (2019). Reconstructing caribou seasonal biogeography in Little Ice Age (late Holocene) Western Alaska using intra-tooth strontium and oxygen isotope analysis. *J. Archaeol. Sci. Rep.* 2019:43. doi: 10.1016/j.jasrep.2017.10.043

Hakenbeck, S. E. (2019). Genetics, archaeology and the far right: an unholy Trinity. *World Archaeol.* 51, 517–527.

Holt, E., Evans, J. A., and Madgwick, R. (2021). Strontium (87Sr/86Sr) mapping: A critical review of methods and approaches. *Earth Sci. Rev.* 216:103593. doi: 10.1016/j.earscirev.2021.103593

Hoppe, K. A., Koch, P. L., and Furutani, T. T. (2003). Assessing the preservation of biogenic strontium in fossil bones and tooth enamel. *Int. J. Osteoarchaeol.* 13, 20–28.

Hu, L., Chartrand, M. M. G., St-Jean, G., Lopes, M., and Bataille, C. P. (2020). Assessing the Reliability of mobility interpretation from a multi-isotope hair profile on a traveling individual. *Front. Ecol. Evol.* 8:568943. doi: 10.3389/fevo.2020.568943

Irrgeher, J., Galler, P., and Prohaska, T. (2016). 87Sr/86Sr isotope ratio measurements by laser ablation multicollector inductively coupled plasma mass spectrometry: Reconsidering matrix interferences in bioapatites and biogenic carbonates. *Spectrochim. Acta Part B: Atomic Spectrosc.* 125, 31–42. doi: 10.1016/j.sab.2016.09.008

Jaouen, K., and Pons, M.-L. (2017). Potential of non-traditional isotope studies for bioarchaeology. *Archaeol. Anthropol. Sci.* 9, 1389–1404. doi: 10.1007/s12520-016-0426-9

Lazzerini, N., Balter, V., Coulon, A., Tacail, T., Marchina, C., Lemoine, M., et al. (2021). Monthly mobility inferred from isoscapes and laser ablation strontium isotope ratios in caprine tooth enamel. *Sci. Rep.* 11:2277. doi: 10.1038/s41598-021-81923-z

Leach, S., Eckardt, H., Chenery, C., Müldner, G., and Lewis, M. (2015). A Lady of York: migration, ethnicity and identity in Roman Britain. *Antiquity* 84, 131–145. doi: 10.1017/S0003598X00099816

Leach, S., Lewis, M., Chenery, C., Muldner, G., and Eckardt, H. (2009). Migration and diversity in Roman Britain: a multidisciplinary approach to the identification of immigrants in Roman York. *Eng. Am. J. Phys. Anthropol.* 140, 546–561. doi: 10.1002/ajpa.21104

Lewis, J., Pike, A. W. G., Coath, C. D., and Evershed, R. P. (2017). Strontium concentration, radiogenic (87Sr/86Sr) and stable (δ88Sr) strontium isotope

systematics in a controlled feeding study. *STAR: Sci. Technol. Archaeol. Res.* 3, 45–57. doi: 10.1080/20548923.2017.1303124

Martiniano, R., Caffell, A., Holst, M., Hunter-Mann, K., Montgomery, J., Muldner, G., et al. (2016). Genomic signals of migration and continuity in Britain before the Anglo-Saxons. *Nat. Commun.* 7:10326. doi: 10.1038/ncomms10326

Miller, J. H., Crowley, B. E., Bataille, C. P., Wald, E. J., Kelly, A., Gaetano, M., et al. (2021). Historical landscape use of migratory caribou: new insights from old antlers. *Front. Ecol. Evol.* 8:590839. doi: 10.3389/fevo.2020.590837

Montgomery, J. (2002). *Lead and strontium isotope compositions of human dental tissues as an indicator of ancient exposure and population dynamics: The application of isotope source-tracing methods to identify migrants among British archaeological burials and a consideration of ante-mortem uptake, tissue stability and post-mortem diagenesis.* Doctoral Thesis. Bradford: The University of Bradford.

Moore, J., Rose, A., Anderson, S., Evans, J., Nowell, G., Grocke, D. R., et al. (2020). A multi-isotope (C, N, O, Sr, Pb) study of Iron Age and Roman period skeletons from east Edinburgh, Scotland exploring the relationship between decapitation burials and geographical origins. *J. Archaeol. Sci. Rep.* 29:102075. doi: 10.1016/j.jasrep.2019.102075

Neil, S., Evans, J., Montgomery, J., and Scarre, C. (2020). Isotopic evidence for human movement into central england during the early neolithic. *Eur. J. Archaeol.* 23, 512–529. doi: 10.1017/eaa.2020.22

Nelson, D. E., DeNiro, M. J., Schoeninger, M. J., DePaolo, D. J., and Hare, P. E. (1986). Effects of diagenesis on strontium, carbon, nitrogen, and oxygen concentration and isotopic composition of bone. *Geochimt. Cosmochim. Acta* 50, 1941–1949.

Price, T. D., Blitz, J., Burton, J. H., and Ezzo, J. A. (1992). Diagenesis in prehistoric bone: Problems and solutions. *J. Archaeol. Sci.* 19, 513–529.

Price, T. D., Grupe, G., and Schroter, P. (1994). Reconstruction of migration patterns in the Bell Beaker period by stable strontium analysis. *Appl. Geochem.* 9, 413–417.

Reich, M. S., Flockhart, D. T. T., Norris, D. R., Hu, L., and Bataille, C. P. (2021). Continuous-surface geographic assignment of migratory animals using strontium isotopes: A case study with monarch butterflies. *Methods Ecol. Evol.* 2021:13707. doi: 10.1111/2041-210X.13707

Scorrer, J., Faillace, K. E., Hildred, A., Nederbragt, A. J., Andersen, M. B., Millet, M.-A., et al. (2021). Diversity aboard a Tudor warship: investigating the origins of the Mary Rose crew using multi-isotope analysis. *Royal Soc. Open Sci.* 8:202106. doi: 10.1098/rsos.202106

Shaw, H., Montgomery, J., Redfern, R., Gowland, R., and Evans, J. (2016). Identifying migrants in Roman London using lead and strontium stable isotopes. *J. Archaeol. Sci.* 66, 57–68. doi: 10.1016/j.jas.2015.12.001

Sillen, A., and Kavanagh, M. (1982). Strontium and paleodietary research: a review. *Am. J. Phys. Anthropol.* 25, 67–90. doi: 10.1002/ajpa.1330250505

Snoeck, C., Lee-Thorp, J., Schulting, R., de Jong, J., Debouge, W., and Mattielli, N. (2015). Calcined bone provides a reliable substrate for strontium isotope ratios as shown by an enrichment experiment. *Rapid Commun. Mass Spectrom.* 29, 107–114. doi: 10.1002/rcm.7078

Snoeck, C., Pouncett, J., Claeys, P., Goderis, S., Mattielli, N., Parker Pearson, M., et al. (2018). Strontium isotope analysis on cremated human remains from Stonehenge support links with west Wales. *Sci. Rep.* 8:10790. doi: 10.1038/s41598-018-28969-8

Techer, I., Medini, S., Janin, M., and Arregui, M. (2017). Impact of agricultural practice on the Sr isotopic composition of food products: Application to discriminate the geographic origin of olives and olive oil. *Appl. Geochem.* 82, 1–14. doi: 10.1016/j.apgeochem.2017.05.010

Terrill, D. F., Henderson, C. M., and Anderson, J. S. (2020). New application of strontium isotopes reveals evidence of limited migratory behaviour in Late Cretaceous hadrosaurs. *Biol. Lett.* 16:20190930. doi: 10.1098/rsbl.2019.0930

Tucker, M. A., BohningGaese, K., Fagan, W. F., Fryxell, J. M., VanMoorter, B., Alberts, S. C., et al. (2018). Moving in the Anthropocene: Global reductions in terrestrial mammalian movements. *Science* 359, 466–469. doi: 10.1126/science.aam9712

Vershinina, A. O., Heintzman, P. D., Froese, D. G., Zazula, G., Cassatt-Johnstone, M., Dalén, L., et al. (2021). Ancient horse genomes reveal the timing and extent of dispersals across the Bering Land Bridge. *Mol. Ecol.* 2021:15977. doi: 10.1111/mec.15977

Wallace, J. P., Crowley, B. E., and Miller, J. H. (2019). Investigating equid mobility in Miocene Florida, USA using strontium isotope ratios. *Palaeogeogr. Palaeoclimatol. Palaeoecol.* 516, 232–243. doi: 10.1016/j.palaeo.2018.11.036

Walser, J. W. III, Kristjansdottir, S., Grocke, D. R., Gowland, R. L., Jakob, T., Nowell, G. M., et al. (2020). At the world's edge: Reconstructing diet and geographic origins in medieval Iceland using isotope and trace element analyses. *Am. J. Phys. Anthropol.* 171, 142–163. doi: 10.1002/ajpa.23973

Weber, K., Weber, M., Menneken, M., Kral, A. G., Mertz-Kraus, R., Geisler, T., et al. (2021). Diagenetic stability of non-traditional stable isotope systems (Ca, Sr, Mg, Zn) in teeth – An in-vitro alteration experiment of biogenic apatite in isotopically enriched tracer solution. *Chem. Geol.* 572:120196. doi: 10.1016/j.chemgeo.2021.120196

Weber, M., Tacail, T., Lugli, F., Clauss, M., Weber, K., Leichliter, J., et al. (2020). Strontium Uptake and Intra-Population 87Sr/86Sr Variability of Bones and Teeth—Controlled Feeding Experiments With Rodents (Rattus norvegicus, Cavia porcellus). *Front. Ecol. Evol.* 8:569940. doi: 10.3389/fevo.2020.569940

Wooller, M. J., Bataille, C., Druckenmiller, P., Erickson, G. M., Groves, P., Haubenstock, N., et al. (2021). Lifetime mobility of an Arctic woolly mammoth. *Science* 373, 806–808. doi: 10.1126/science.abg1134

Conflict of Interest: The authors declare that the research was conducted in the absence of any commercial or financial relationships that could be construed as a potential conflict of interest.

Advantages of publishing in Frontiers

OPEN ACCESS
Articles are free to read for greatest visibility and readership

FAST PUBLICATION
Around 90 days from submission to decision

HIGH QUALITY PEER-REVIEW
Rigorous, collaborative, and constructive peer-review

TRANSPARENT PEER-REVIEW
Editors and reviewers acknowledged by name on published articles

Frontiers
Avenue du Tribunal-Fédéral 34
1005 Lausanne | Switzerland

Visit us: www.frontiersin.org
Contact us: frontiersin.org/about/contact

REPRODUCIBILITY OF RESEARCH
Support open data and methods to enhance research reproducibility

DIGITAL PUBLISHING
Articles designed for optimal readership across devices

FOLLOW US
@frontiersin

IMPACT METRICS
Advanced article metrics track visibility across digital media

EXTENSIVE PROMOTION
Marketing and promotion of impactful research

LOOP RESEARCH NETWORK
Our network increases your article's readership